NUREG/CR-4110
SAND84-2668

Repository Site Data Report for Unsaturated Tuff, Yucca Mountain, Nevada

NUREG/CR--4110

TI86 003566

Manuscript Completed: August 1985
Date Published: November 1985

Prepared by
Pei-Lin Tien, C. D. Updegraff, K. K. Wahi, Science Applications International Corporation
M. D. Siegel, Sandia National Laboratories
R. V. Guzowski, Remote Sensing System, Inc.

Sandia National Laboratories
Albuquerque, NM 87185

Subcontractors:
Science Applications International Corporation
505 Marquette Avenue, NW
Suite 1200
Albuquerque, NM 87102
and
Remote Sensing System, Inc.
2101 San Pedro Boulevard, NE
Suite A
Albuquerque, NM 87110

Prepared for
Division of Waste Management
Office of Nuclear Material Safety and Safeguards
U.S. Nuclear Regulatory Commission
Washington, D.C. 20555
NRC FIN A1158

NOTICE

This report was prepared as an account of work sponsored by an agency of the United States Government. Neither the United States Government nor any agency thereof, or any of their employees, makes any warranty, expressed or implied, or assumes any legal liability of responsibility for any third party's use, or the results of such use, of any information, apparatus, product or process disclosed in this report, or represents that its use by such third party would not infringe privately owned rights.

NOTICE

Availability of Reference Materials Cited in NRC Publications

Most documents cited in NRC publications will be available from one of the following sources:

1. The NRC Public Document Room, 1717 H Street, N.W.
   Washington, DC 20555
2. The Superintendent of Documents, U.S. Government Printing Office, Post Office Box 37082, Washington, DC 20013-7082
3. The National Technical Information Service, Springfield, VA 22161

Although the listing that follows represents the majority of documents cited in NRC publications, it is not intended to be exhaustive.

Referenced documents available for inspection and copying for a fee from the NRC Public Document Room include NRC correspondence and internal NRC memoranda; NRC Office of Inspection and Enforcement bulletins, circulars, information notices, inspection and investigation notices; Licensee Event Reports; vendor reports and correspondence; Commission papers, and applicant and licensee documents and correspondence.

The following documents in the NUREG series are available for purchase from the NRC/GPO Sales Program: formal NRC staff and contractor reports, NRC-sponsored conference proceedings, and NRC booklets and brochures. Also available are Regulatory Guides, NRC regulations in the *Code of Federal Regulations*, and *Nuclear Regulatory Commission Issuances.*

Documents available from the National Technical Information Service include NUREG series reports and technical reports prepared by other federal agencies and reports prepared by the Atomic Energy Commission, forerunner agency to the Nuclear Regulatory Commission.

Documents available from public and special technical libraries include all open literature items, such as books, journal and periodical articles, and transactions. *Federal Register* notices, federal and state legislation, and congressional reports can usually be obtained from these libraries

Documents such as theses, dissertations, foreign reports and translations, and non NRC conference proceedings are available for purchase from the organization sponsoring the publication cited.

Single copies of NRC draft reports are available free, to the extent of supply, upon written request to the Division of Technical Information and Document Control, U S. Nuclear Regulatory Commission, Washington, DC 20555.

Copies of industry codes and standards used in a substantive manner in the NRC regulatory process are maintained at the NRC Library, 7920 Norfolk Avenue, Bethesda, Maryland, and are available there for reference use by the public. Codes and standards are usually copyrighted and may be purchased from the originating organization or, if they are American National Standards, from the American National Standards Institute, 1430 Broadway, New York, NY 10018.

ABSTRACT

The U. S. Department of Energy is currently considering the thick sequences of unsaturated, fractured tuff at Yucca Mountain, on the southwestern boundary of the Nevada Test Site, as a possible candidate host rock for a nuclear-waste repository. Yucca Mountain is in one of the most arid areas in the United States. The site is within the south-central part of the Great Basin section of the Basin and Range physiographic province and is located near a number of silicic calderas of Tertiary age. Although localized zones of seismic activity are common throughout the province, and faults are present at Yucca Mountain, the site itself is basically aseismic.

No data are available on the composition of ground water in the unsaturated zone at Yucca Mountain. It has been suggested that the composition is bounded by the compositions of water from wells USW-H3, UE25p-1, J-13, and snow or rain. There are relatively few data available from Yucca Mountain on the moisture content and saturation, hydraulic conductivity, and characteristic curves of the unsaturated zone. The available literature on thermomechanical properties of tuff does not always distinguish between data from the saturated zone and data from the unsaturated zone. Geochemical, hydrologic, and thermomechanical data available on the unsaturated tuffs of Yucca Mountain are tabulated in this report. Where the data are very sparse, they have been supplemented by data from the saturated zone or from areas other than Yucca Mountain.

TABLE OF CONTENTS

* There are no appendixes for Chapters 4, 6, 7, or 8.

FIGURES

TABLES

ACKNOWLEDGEMENTS

The authors want to especially acknowledge the assistance of Dr. Regina Hunter of Sandia National Laboratories Division 6431. Without Dr. Hunter's careful review and attention to detail, the quality of this report would have certainly suffered; without the many evening and weekend hours that she spent on this document, the report might not have been produced.

Dr. Douglas Smith, of the University of New Mexico, wrote Sections 5.4.1 through 5.4.3. Anna Trujillo, of SAI, helped to compile Appendix 5.2. Dr. William Olsson, of Sandia Division 1542, reviewed the manuscript. Neil Coleman of NRC NMSS was the Program Manager for the project.

INTRODUCTION

This report documents work performed for the U. S. Nuclear Regulatory Commission (NRC) by Sandia National Laboratories in Albuquerque, New Mexico (SNLA). The work is related to a geologic repository for high-level nuclear waste in unsaturated tuff. The primary purpose of the work is to provide data that the NRC can use as input to codes that will be used to assess the performance of a geologic repository in unsaturated tuff. The data will also support future preliminary performance modeling.

This report is part of a continuing program of data compilation for possible repository sites in various geologic media, funded under NRC FIN No. A-1158. Three media--bedded salt, saturated tuff, and basalt--have been investigated and the studies published. Repository site descriptions are an integral part of the NRC program at SNLA to develop performance assessment methodologies for the geological disposal of high-level waste. By preparing repository site descriptions, SNLA develops an understanding of the natural systems and a familiarity with the data to be used in risk assessment.

Data on a high-level nuclear-waste repository site in tuff at Yucca Mountain, Nevada, previously have been documented by SNLA for the NRC (Guzowski and others, 1983). Recently, the unsaturated tuff in Yucca Mountain is being considered as a candidate host rock for a high-level nuclear-waste repository by the U.S. Department of Energy (Dudley and Erdal, 1982). The NRC expects to receive a Site Characterization Plan from the DOE for the Yucca Mountain site. An understanding of the natural systems of the unsaturated zone and a data base, therefore, are essential for the development of performance assessment methodologies.

This report is a compilation of the published information available from the Yucca Mountain site, with emphasis on data derived from or applicable to the unsaturated zone. Discussions of the regional setting, geomorphology, geology, hydrology, geochemistry, thermomechanical properties of unsaturated tuff, and natural resources of southern Nevada are included. When the published information on Yucca Mountain site did not supply sufficient data for a particular parameter, the data base was supplemented with data from outside the study area. In order to fulfill the characterization requirements of a high-level nuclear-waste repository site in the unsaturated zone, relevant data already documented in the report by Guzowski and others (1983) are also included.

Because of the technical nature of this report, the readers are assumed to be familiar with the general concepts and common nomenclature of various geotechnical disciplines.

This report does not address all siting concerns. For the most part, the information presented is data that will be of use in the modeling of long-term, far-field transport of waste through hydrogeological mechanisms.

CHAPTER 1 - REGIONAL SETTING

Yucca Mountain lies on the southwest boundary of the Nevada Test Site (NTS) in south-central Nevada, between approximately 36°40' and 37°00' north latitude and 116°25' and 116°35' west longitude (Figure 1-1). The regional setting of the study area is documented in this chapter.

1.1 Climate

Yucca Mountain is within the most arid part of Nevada, the most arid state in the United States (Winograd and Thordarson, 1975). The arid climate in this part of Nevada is caused partly by the latitude and partly by the rain shadow effect of the Sierra Nevada Range in eastern California (Plummer and McGeary, 1979). Local variation in climate, however, is governed by the topography (Bertram and Everett, 1982).

1.1.1 Temperature

Detailed temperature information for Yucca Mountain is not available, but sporadic temperature data from the general area are in the literature. Bertram and Everett (1982) state that the daily high temperature in the valleys of the Yucca Mountain area is 10°C in January and 35°C in July. At Las Vegas (station altitude 2,162 feet, or 659 meters), approximately 90 miles (145 kilometers) southeast of Yucca Mountain, the daily maximum temperature ranges from 13°C in January to 40.5°C in July; the daily minimum temperatures for the same months ranges from 0.5°C to 24.5°C. In general, temperatures in the high valleys, such as central Yucca Flat (station altitude 4,076 feet, or 1,242 meters), approximately 27 miles (43.5 kilometers) northeast of Yucca Mountain, are as much as 3°C to 8.5°C lower than those at Las Vegas (Winograd and Thordarson, 1975).

1.1.2 Precipitation

According to Weedfall (1963) and Quiring (1965), precipitation in southern Nevada is a function of altitude and longitude. The mean annual precipitation ranges from 3 to 6 inches (7.7 to 15.4 centimeters) in the valleys and averages less than 10 inches (25.6 centimeters) on the ridges and mesas (Figure 1-2). Precipitation in the region also varies with the season. Most precipitation occurs in the winter and summer. Monthly precipitation at Las Vegas and NTS is shown in Figure 1-3.

1.1.3 Evaporation

Meyers (1962) has estimated an annual rate of about 70 inches (179.5 centimeters) of potential evaporation from the basins of southern Nevada. South of the study area, Death Valley, California, has an average annual precipitation of 1.7 inches (4.4 centimeters) and a measured annual rate of 155.05 inches (397.6 centimeters) of pan evaporation (Winograd and Thordarson, 1975). This large annual water-budget deficit in the region causes all, or nearly all, precipitation to return to the atmosphere, rather than to infiltrate to the regional water table (Sinnock, 1982).

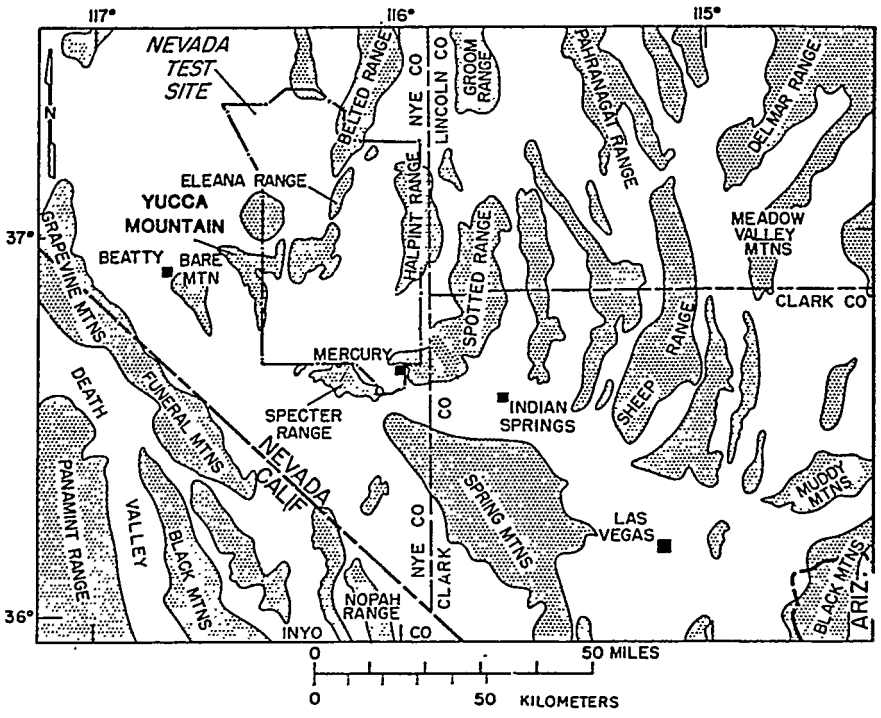

Figure 1-1. Location map of Yucca Mountain (after Gordon and Poole, 1968).

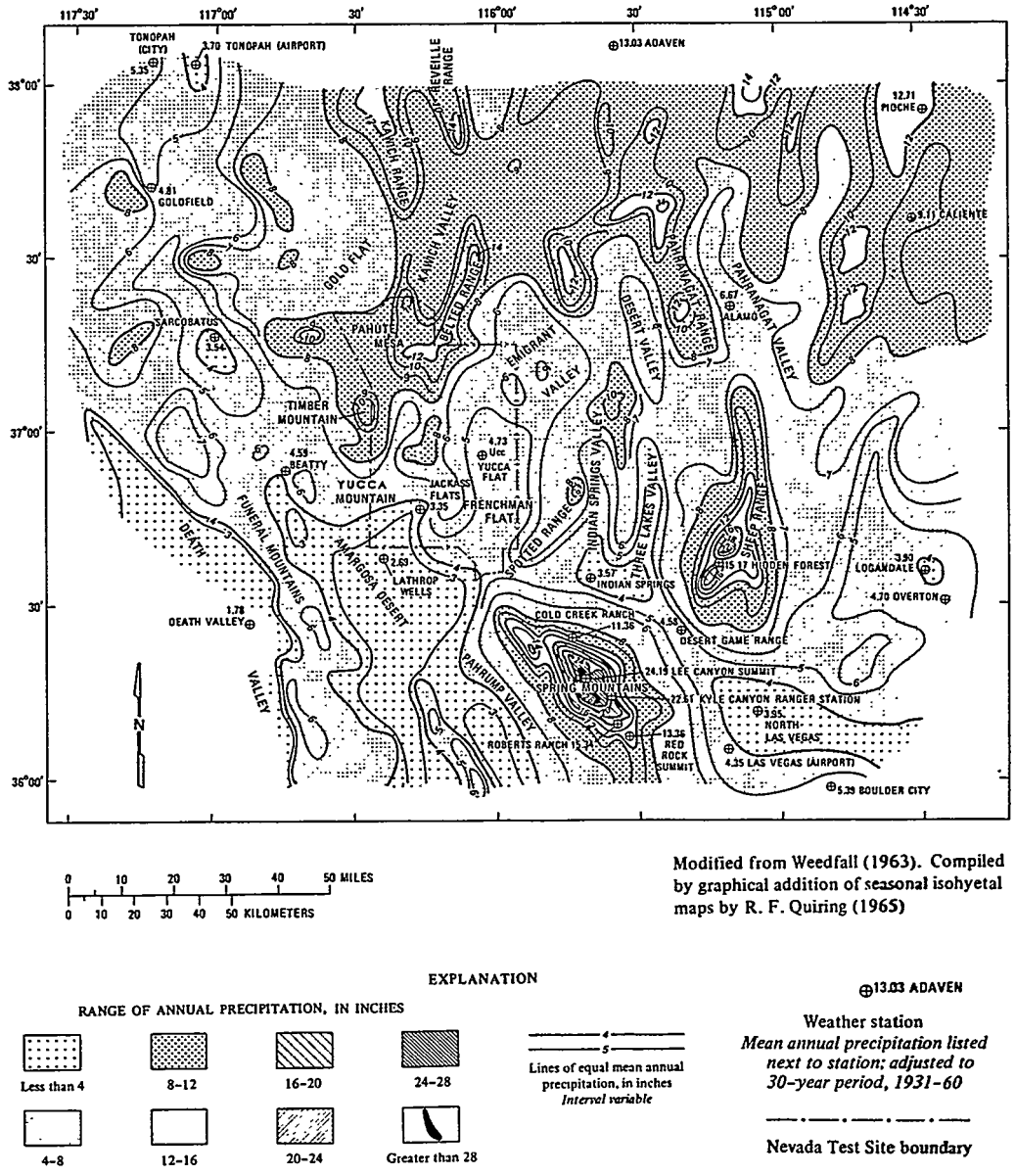

Figure 1-2. Mean annual precipitation (after Winograd and Thordarson, 1975).

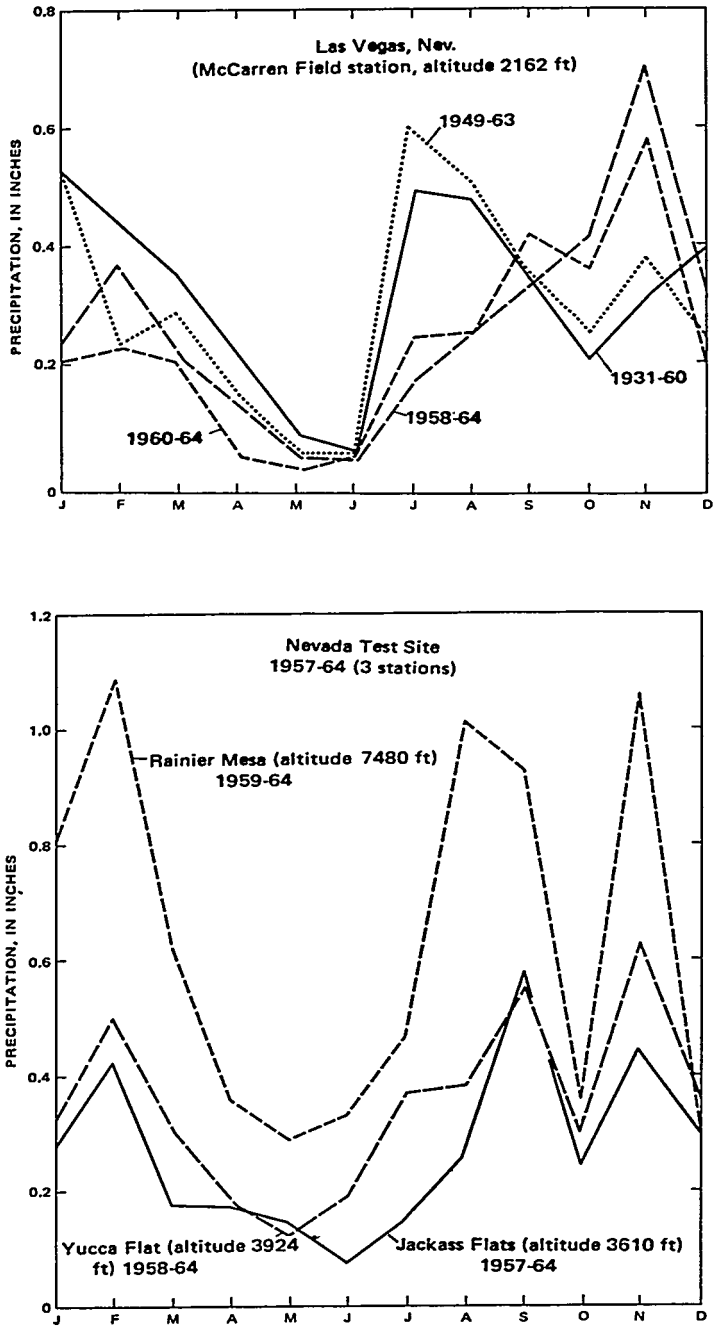

Figure 1-3. Means of monthly precipitation (after Winograd and Thordarson, 1975).

1.1.4 Paleoclimate

No continental or alpine glaciation during the Pleistocene Epoch is evident in the Yucca Mountain area (Guzowski and others, 1983). Geological, paleontological, paleoclimatological and paleoecological studies indicate, however, that the region was significantly wetter and cooler during the Pleistocene Epoch, approximately 10,000 to 1.8 million years ago (Winograd and Thordarson, 1975; Winograd and Doty, 1980). Especially during middle-to-late Wisconsin time (between 40,000 and 10,000 years ago), some of the topographically closed basins in the region intermittently had lakes and woodland plants (Winograd and Doty, 1980). The flora in these basins occurred at altitudes as much as 1,968 feet (600 meters) lower than today (Wells and Berger, 1967). Wells and Jorgensen (1964) examined plant remains in fossilized packrat middens and concluded that during the glacial maximum of approximately 18,000 years ago, annual precipitation in the Mojave Desert was only about 35 percent greater than at present (Dudley and Erdal, 1982). During the last pluvial period in the northern two-thirds of Nevada, where the most pluvial lakes occurred, the mean annual temperature was 3° lower and precipitation 65 percent higher than at present (Mifflin and Wheat, 1979). In Spring Valley in east-central Nevada, Snyder and Langbein (1962) estimated that annual precipitation was 20.1 inches or 51 centimeters (12.2 inches or 31 centimeters at present) and evaporation was 31.1 inches or 79 centimeters (43.3 inches or 110 centimeters at present). Water infiltration rates during the Pleistocene were probably no more than twice those today (a few millimeters per year). In addition, because of the increase of transpiration from a denser vegetation cover, vertical percolation was probably not significantly greater than at present (Wollenberg and others, 1982). No evidence indicates that precipitation exceeded evapotranspiration during the last pluvial period in the region (Geotechnical Engineers, Inc., 1979). Furthermore, if future pluvial periods are similar to those of the Pleistocene, the future water table will not be affected significantly because of the low gradient and relatively high transmissivity of the regional carbonate aquifer (Wollenberg and others, 1982). Detailed evidence and discussions on paleoclimate in the region during the Pleistocene Epoch are given by Broecker and Kaufman (1965), Mehringer (1965, 1967), Miller (1948), Ore and Warren (1971), Smith (1968, 1979), Snyder and Langbein (1962), Spaulding (1977, 1980), Van Devender (1977), Van Devender and Spaulding (1979), Weide and Weide (1977), Wells (1979), Wells and Jorgensen (1964), and Winograd and Doty (1980).

1.2 Physiographic Setting

Yucca Mountain is within the south-central part of the Great Basin section of the Basin and Range physiographic province (Fenneman, 1931) and is one of the major highlands along the western edge of the NTS (Spengler and others, 1979). It is bounded by Crater Flat on the west and the Amargosa Desert on the south. It is separated from Timber Mountain caldera by Beatty Wash on the north, from Shoshone Mountain and Calico Hills by Fortymile Canyon, and from Jackass Flat by Fortymile Wash on the east (Figure 1-4).

A series of predominantly north-trending volcanic ridges and valleys characterizes Yucca Mountain (Sinnock, 1982). The highest peak of Yucca

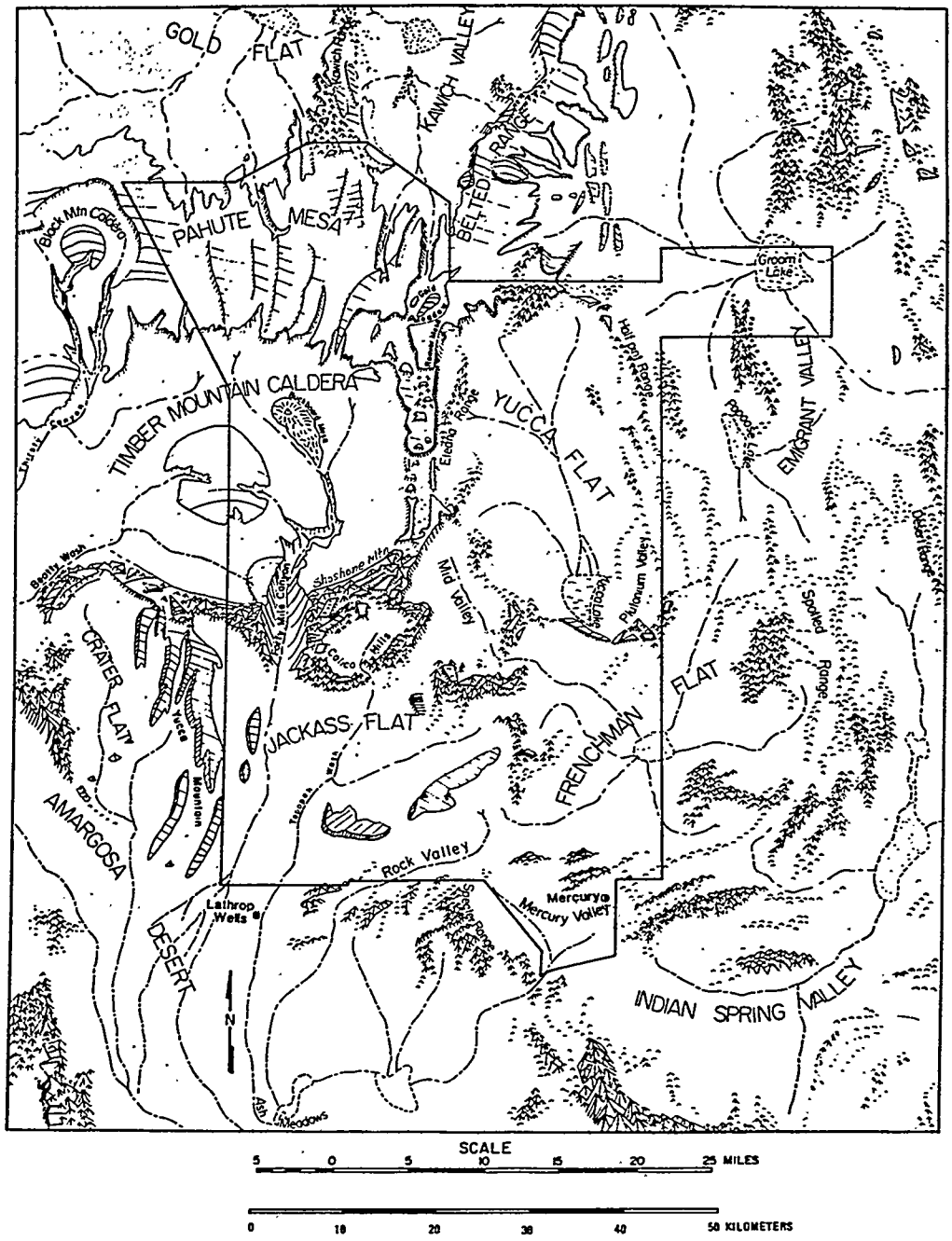

Figure 1-4. Physiographic diagram of Yucca Mountain and vicinity (after Sinnock, 1982).

Mountain reaches 6,708 feet (2,044.5 meters) above mean sea level. Along its northern limits, Yucca Mountain extends northwestward to include Chocolate Mountain and low-lying hills southeast of Beatty Wash (Spengler and others, 1979). Yucca Mountain is formed by relatively flat-lying strata, the dips of which at the surface are, in general, 10° or less (Sinnock and others, 1984). Most of the Yucca Mountain area has moderate slopes, generally more than ten percent, and is characterized by deeply carved and widely spaced canyons (Sinnock, 1982; Sinnock and others, 1984).

The Amargosa Desert is a southeast-trending valley approximately 50 miles (80.5 kilometers) long and as much as 20 miles (32.2 kilometers) wide. The valley floor generally ranges in altitude from 2,000 to 3,000 feet (608.2 to 914.4 meters). Both Crater Flat and Jackass Flat are small intermontane valleys with north and northeast trends, respectively. The floors of these two alluvial valleys range in altitude from 2,800 to 4,000 feet (853.4 to 1,219.1 meters). Fortymile Canyon incises a 2,500 feet (762 meters) gorge through the southeastern rim of the Timber Mountain caldera (Sinnock, 1982). All the valleys around the Yucca Mountain drain to the Death Valley drainage sink (Sinnock, 1982) via ephemeral or intermittent tributaries of the Amargosa River.

Timber Mountain is a structural dome produced by resurgence of magma beneath the center of the Timber Mountain caldera (Byers and others, 1964, 1976b). The dome is about 9 by 7 miles (14.5 by 12.3 kilometers), elongate in a northwest direction (Carr and Quinlivan, 1968). North of the Timber Mountain caldera is Pahute Mesa, a large volcanic plateau that is bounded on the north by Kawich Valley, Kawich Range, and Gold Flat and on the northeast by the Belted Range. To the west, Pahute Mesa is flanked by the Black Mountain caldera (Figure 1-4). Northeast of the Timber Mountain caldera is Rainier Mesa, south of which is the Eleana Range. Rainier Mesa and the Eleana Range form the eastern edge of Pahute Mesa and separate the Timber Mountain caldera from Yucca Flat. The Calico Hills are located southwest of Yucca Flat. Along the northern edge of Jackass Flat, the Calico Hills form a structural and topographic dome with Paleozoic rocks exposed at the center (Sinnock, 1982).

1.3 Surface Geologic Processes

In arid regions such as the study area, heavy rains and storms play an important role in shaping the regional landscape. Because of the sparsity of vegetative cover, heavy rains and storms cause rapid erosion and resulting slope retreat, especially of the steep mountain fronts, and deposition on the valley floors. Sediments picked up by flash floods and mudflows are deposited on alluvial fans where the stream channels widen as they flow out of the narrow gorges onto the open valley floors (Plummer and McGeary, 1979). Because the heavy rains and storms are of short duration and infrequent, slope retreat and denudation rates are expected to be low. Denudation rates for the Yucca Mountain area are not available. Calculated denudation rates ranging from 3.5 to 7.0 inches (9 to 18 centimeters) per 1,000 years for small drainage basins in arid and semiarid climates (Schumm, 1963), however, can be used in assessing the integrity of a potential repository site in Yucca Mountain. Winograd (1974), after reviewing the literature, has given the same range of denudation rates in similar climates.

1.4 Tectonic Setting

The study area is located within the Basin and Range province, a subdivision of the Cordillera of North America (Eardley, 1951). The Basin and Range province is bounded on the east by the Wasatch Mountains and High Plateau of Utah, on the north by the Malheur plateau and Snake River lava plains, and on the west by the Sierra Nevada. The narrowing southern end of the Basin and Range province has been arbitrarily defined by Nolan (1943) to have the San Andreas fault on the west and the Colorado River on the east.

Both ranges and basins are tilted fault blocks (Leet and Judson, 1971). Most of these ranges are bordered on one or both sides by normal faults, along which the ranges have been uplifted and tilted (Gilluly and others, 1959). The intervening basins, on the other hand, are downfaulted with respect to the ranges. According to Eardley (1951), the range front is bordered by a fault zone in which individual faults may be relatively short, and both en echelon relationships and step or distribution faults are commonly found within this zone. The amount or degree of tilting reaches a maximum close to the faults. The location of some of the faults has been determined by pre-existing structural features, especially older faults. Recurrent movement along these faults appears to be quite common. One of the major crustal features of the Basin and Range province is the Walker Lane and Las Vegas Valley shear zone (Locke and others, 1940; Longwell, 1960), where right-lateral deformation has occurred (Spengler and others, 1979). Yucca Mountain lies along the projected trend of this zone (Figure 1-5).

The geologic history of the Basin and Range province is complex and much debated (Judson and others, 1976). A generalized conclusion, however, can be made. During late Mesozoic and early Tertiary time, a variety of geosynclinal sediments has been subjected to compressive stress, as evidenced by the folds and thrust and strike-slip faults in outcrops. Thrust faulting has laterally displaced pre-Tertiary rocks a few thousand feet to several miles (Winograd and Thordarson, 1975). Strike-slip faults and shear zones cut and offset the thrust faults in many places. The presence of the Sevier Arch in western Utah and probably much of southeastern Nevada from late Jurassic to late Cretaceous time has resulted in nondeposition of Mesozoic sediments in southeastern Nevada (Harris 1959). Extensive volcanic and plutonic activity occurred in the region from Miocene through Quaternary time (Winograd and Thordarson, 1975). In Miocene and later time, the region underwent extensional stress on a very large scale (Judson and others, 1976). As a result, the entire region was up-lifted and faulted. Accordingly, not all of the faults, even in the same range, are of the same age. The maximum movement along an individual fault may have been earlier or later than that on a neighboring fault (Eardley, 1951). The faults, which are dominantly normal, are thought to have been produced when the earth's crust became extended as it was arched upward. The uplift was probably caused from overriding of a portion of the East Pacific Rise by the North American plate (Birkeland and Larson, 1978; Seyfert and Sirkin, 1973). The pattern of magnetic anomalies in the floor of the northeastern Pacific Ocean also indicates that a section of the East Pacific Rise may now lie under eastern Nevada and western Utah (Figure 1-6). Heating and expansion of the mantle under the Basin and Range province would have

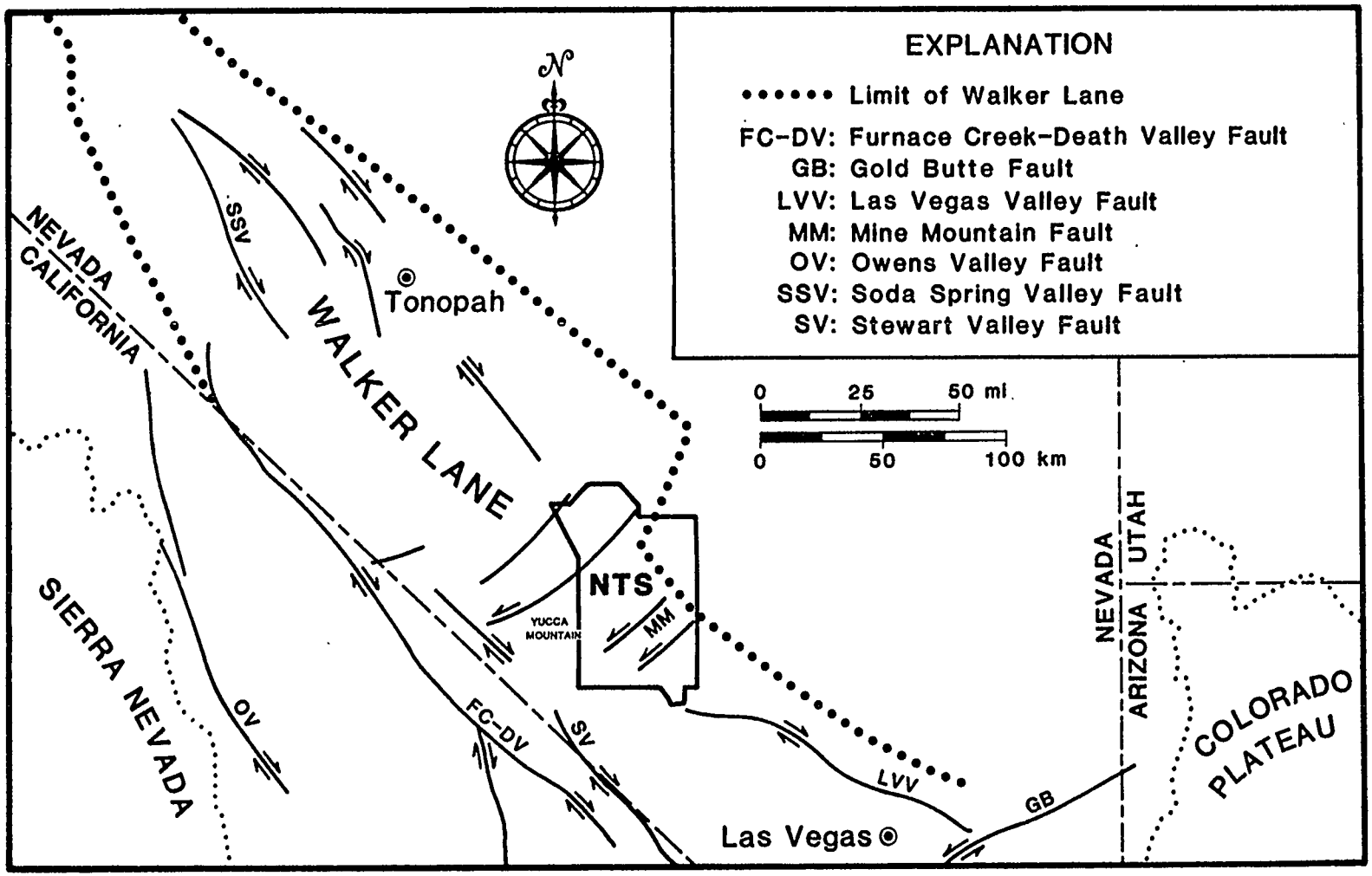

Figure 1-5. Distribution of major strike-slip faults in southern Nevada and adjacent California (after U.S. Geological Survey, 1974).

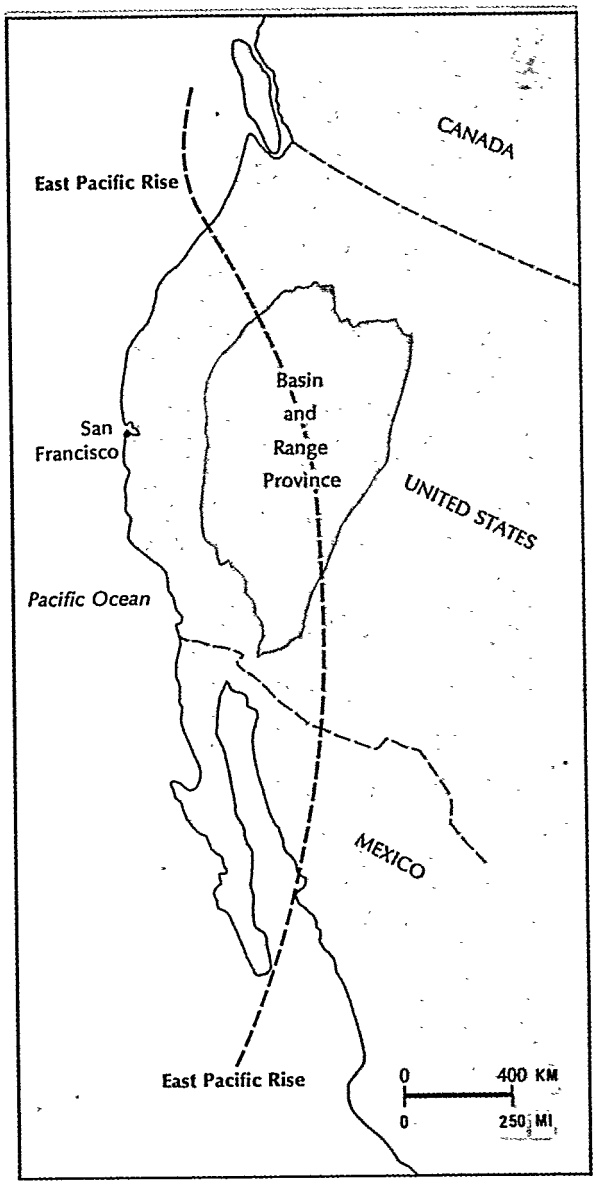

Figure 1-6. Location of Basin and Range province, and the possible location at depth of the East Pacific Rise divergence zone (after Birkeland and Larson, 1978). (From Putnum's Geology, Third Edition by Peter W. Birkeland and Edwin E. Larson. Copyright © 1978 by Oxford University Press, Inc. Reprinted by permission.

resulted in large-scale arching of the overlying crust (Seyfert and Sirkin, 1973). During the past 10 million years, the tectonic flux of the region has decreased, especially in southeastern Nevada, where deformation tends to be concentrated in zones such as the relatively narrow structural depressions of Crater and Yucca Flats. Localization and slowing of tectonic activity has allowed areas such as Yucca Mountain to remain relatively stable during the past few million years (Carr, 1982a).

1.5 Igneous Activities

Both intrusive and extrusive rocks occur in the region. Three pre-Tertiary intrusions, Gold Meadows, Climax, and Twin Ridge Stocks, are located in the northwestern part of the NTS, approximately 35 to 40 miles (56.4 to 64.4 kilometers) northeast of Yucca Mountain (Figure 1-7). Radiometric dates for Gold Meadows and Climax Stocks indicate that these two plutons are Mesozoic in age, although their absolute ages are variably reported (Table 1-1). No age data are available for Twin Ridge Stock; however, it may be genetically related to Climax Stock (Maldonado, 1981).

Intrusive bodies of Tertiary age (Figure 1-7) include small granitic stocks exposed in south-central NTS (Ekren and Sargent, 1965) and along the southeastern and northern edges of the Timber Mountain resurgent dome (Byers and others, 1976a). According to Orkild and others (1969), granite intruded into volcanic rocks occurs in a drill hole at a depth of approximately 9,000 feet (2,743 meters) at the northwestern corner of the NTS. Other Tertiary granitic intrusions have been inferred by many workers at different locations in the region (Daniels and Scott, 1980), notably below Calico Hills (Christiansen and others, 1977; Snyder and Oliver, 1981), and the Timber Mountain caldera (Byers and others, 1976b; Carr and Quinlivan, 1968; Kane and others, 1981). Outcrops of Tertiary dikes, sills, and plugs (Figure 1-7) of rhyolitic and basaltic compositions are numerous throughout the region (Sinnock, 1982).

Table 1-1. Reported ages of Gold Meadows and Climax Stocks

Stock	Age (m.y.)	Source
Gold Meadows	130-140	Gibbons and others (1963)
	91	Marvin and others (1970)
Climax	89-97	Marvin and others (1970)
	93	Maldonado (1977)
	93	Naeser and Maldonado (1981)

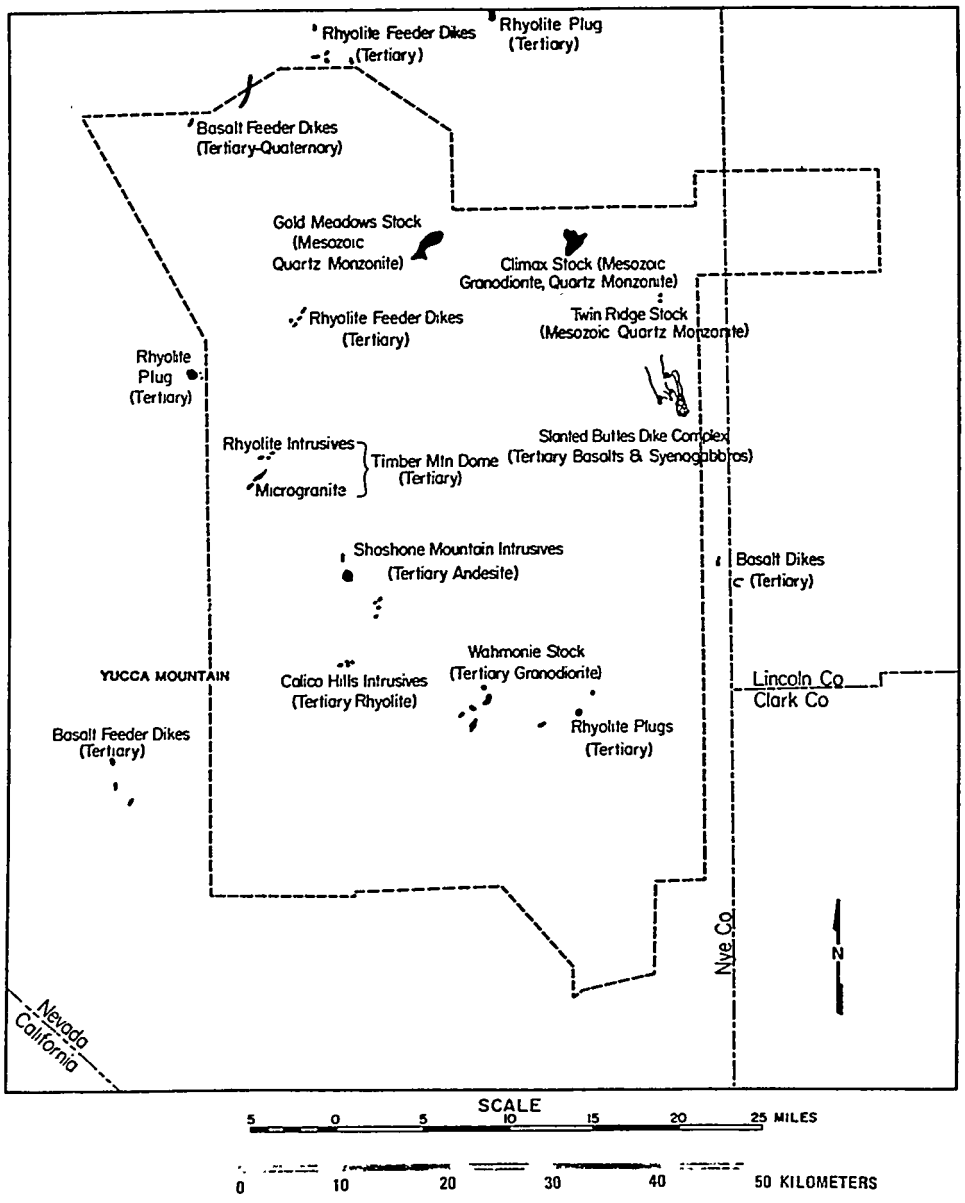

Figure 1-7. Distribution of intrusive outcrops in the NTS area (compiled by Sinnock, 1982, from Cornwall, 1972a; Tschanz and Pampeyan, 1970; Longwell and others, 1965; and USGS GQ Map Series of the NTS region).

Extrusive rocks in the region include tuffs and lava flows. The distribution of these rocks in the NTS area is illustrated in Figures 1-8, 1-9, and 1-10.

In Eocene time, volcanic activity began in northern Nevada (Armstrong, 1970; Snyder and others, 1976; Stewart and others, 1977). In Miocene time, volcanic activity started in the study area and the immediate vicinity (Kistler, 1968). As a result, lava piles, dikes, sills, laccolith-like masses, plugs, and stocks of intermediate composition were formed. The age of these rocks is bracketed by the major ash flow tuff units dated radiometrically at 22.3 and 17.8 million years (Anderson and Ekren, 1968). Since then, much volcanic activity has taken place, as indicated by the results of radiometric dating (Appendix 1.1). The location of known and inferred eruptive centers in the NTS vicinity is shown in Figure 1-11.

Volcanic activities prior to the end of Thirsty Canyon time were predominantly silicic phase (Figures 1-8 and 1-9), accompanied by minor basaltic extrusions (Armstrong, 1970; Byers and others, 1976b; Luft, 1964). After the eruption of the Thirsty Canyon Tuff, 6.2 to 6.5 million years ago (Kistler, 1968), silicic volcanism was succeeded by relatively minor basaltic activities, which dominated late Pliocene and Pleistocene time. Basaltic magma was erupted in belts along the western and eastern margins of the Great Basin (Best and Hamblin, 1978; Stewart and Carlson, 1978) and along a northeast-trending belt that extends through NTS (Crowe and Carr, 1980). The young volcanic rocks are alkali-olivine basalts with minor basaltic-andesite differentiates (Best and Brimhall, 1974; Hausel and Nash, 1977; Leeman and Rogers, 1970; Vaniman and others, 1980). They occur in Crater Flat (Carr, 1982b; Cornwall and Kleinhampl, 1961; Crowe and Carr, 1980), the Timber Mountain moat (Byers and others, 1976a; Christiansen and others, 1977), Kawich Valley (Ekren and others, 1971), the southern end of the Halfpint Range (Byers and Barnes, 1967), and along Rocket Wash (Lipman and others, 1966b). The distribution of late Tertiary and Quaternary basalt flows in the NTS area is shown in Figure 1-10. Potassium-argon dating indicates that these young basalts range in age from about 5 million years to 0.25 million years old (Sinnock and Easterling, 1982). The youngest eruptive center is Lathrop Wells cone, located less than 12.4 miles (20 kilometers) from the southern end of Yucca Mountain (Vaniman and Crowe, 1981).

1.6 Seismicity

The majority of the earthquakes in the Yucca Mountain region are concentrated within two seismic zones (Carr and Rogers, 1982), the California-Nevada seismic zone and the "East-West" seismic zone (Figure 1-12). Outside these zones, much of the region is experiencing a low level of seismicity (Suppe and others, 1975). Yucca Mountain is within the "East-West" seismic zone and lies within an area of relatively low-level seismicity (Rogers and others, 1983).

The California-Nevada seismic zone is one of the major seismic zones in the western United States. It arises near the San Andreas zone in southern California and runs along the northern margin of the Mojave Desert. This

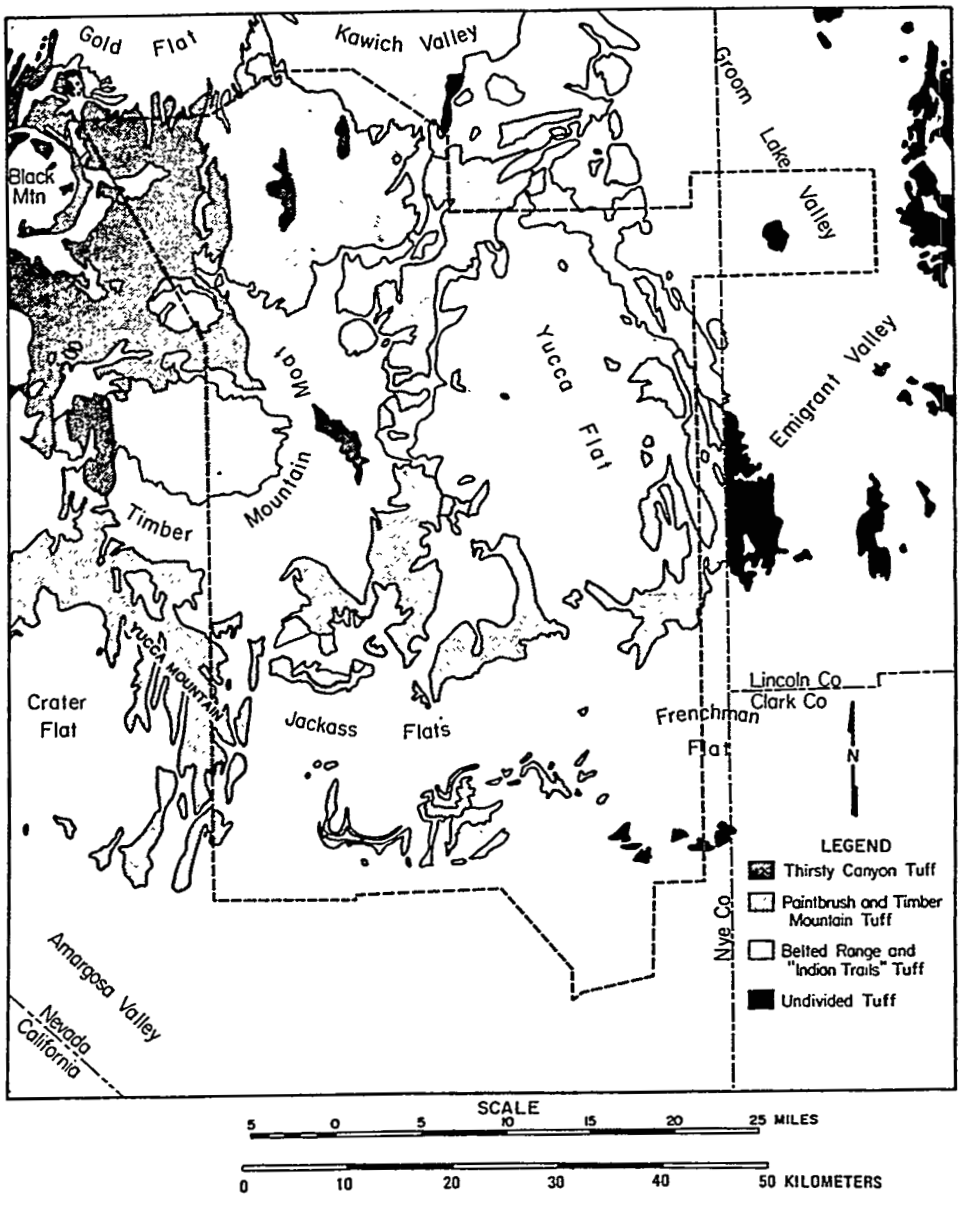

Figure 1-8. Distribution of silicic tuff and related rock outcrops in the NTS Area (compiled by Sinnock, 1982, from Cornwall, 1972a; Tschanz and Pampeyan, 1970; Longwell and others, 1965; and USGS GQ Map Series of the NTS region).

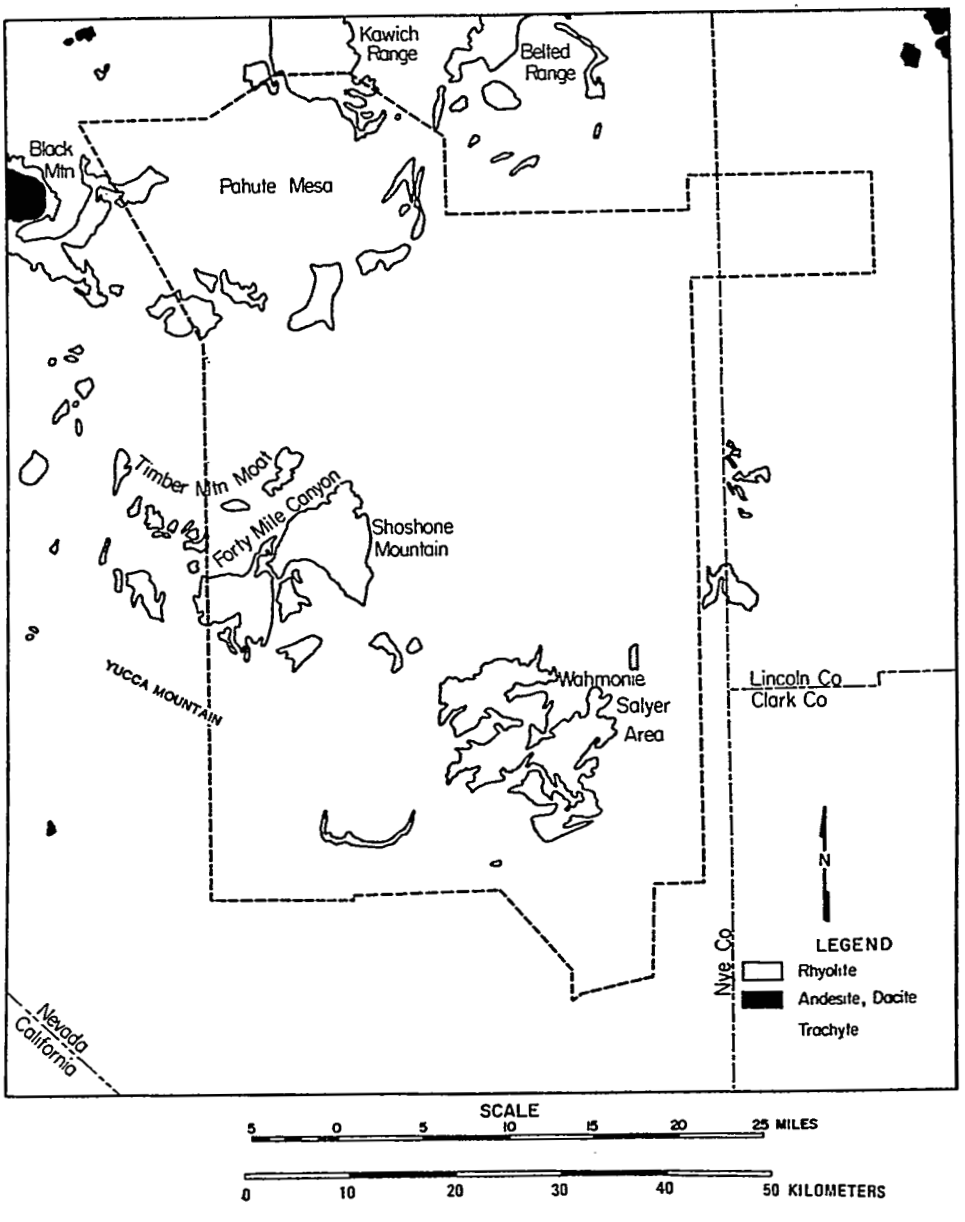

Figure 1-9. Distribution of silicic and intermediate composition lava flows in the NTS area (compiled by Sinnock, 1982, from Cornwall, 1972a; Tschanz and Pampeyan, 1970; Longwell and others, 1965; and USGS GQ Map Series of the NTS region).

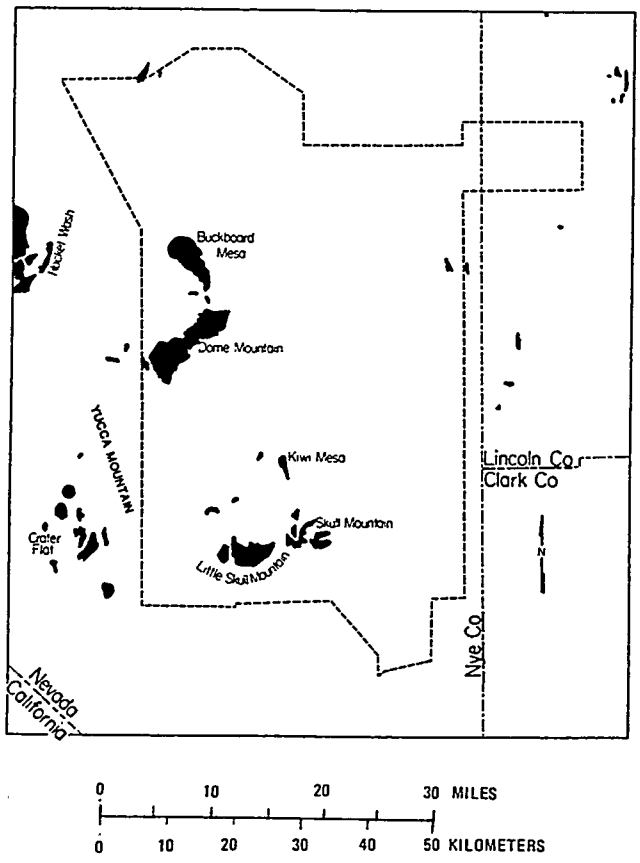

Figure 1-10. Distribution of late Tertiary and Quaternary basalt flows in the NTS area (compiled by Sinnock, 1982, from Cornwall, 1972a; Tschanz and Pampeyan, 1970; Stewart and Carlson, 1976; and USGS GQ Map Series of the NTS region).

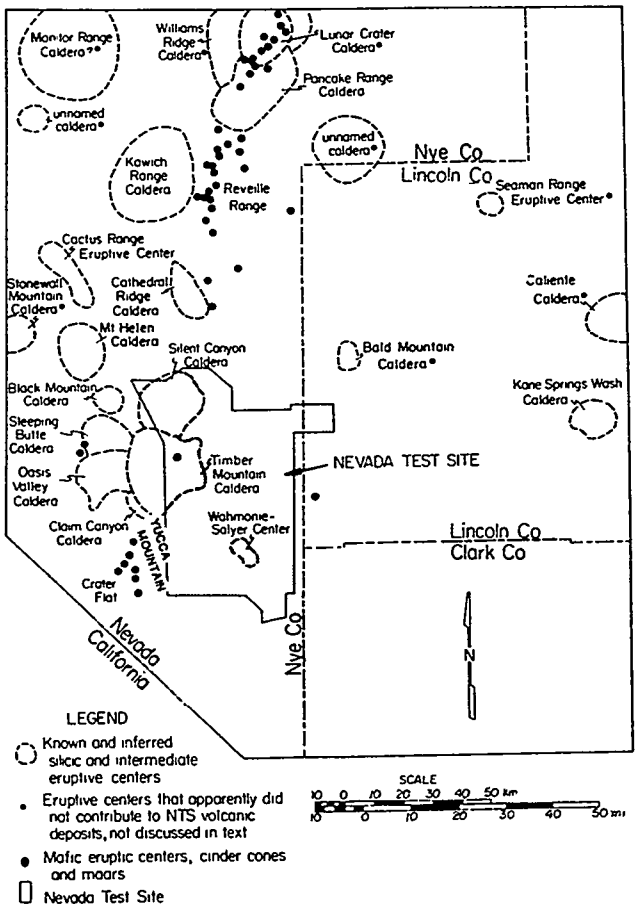

Figure 1-11. General location of known and inferred eruptive centers in the NTS vicinity (after Stewart, 1980).

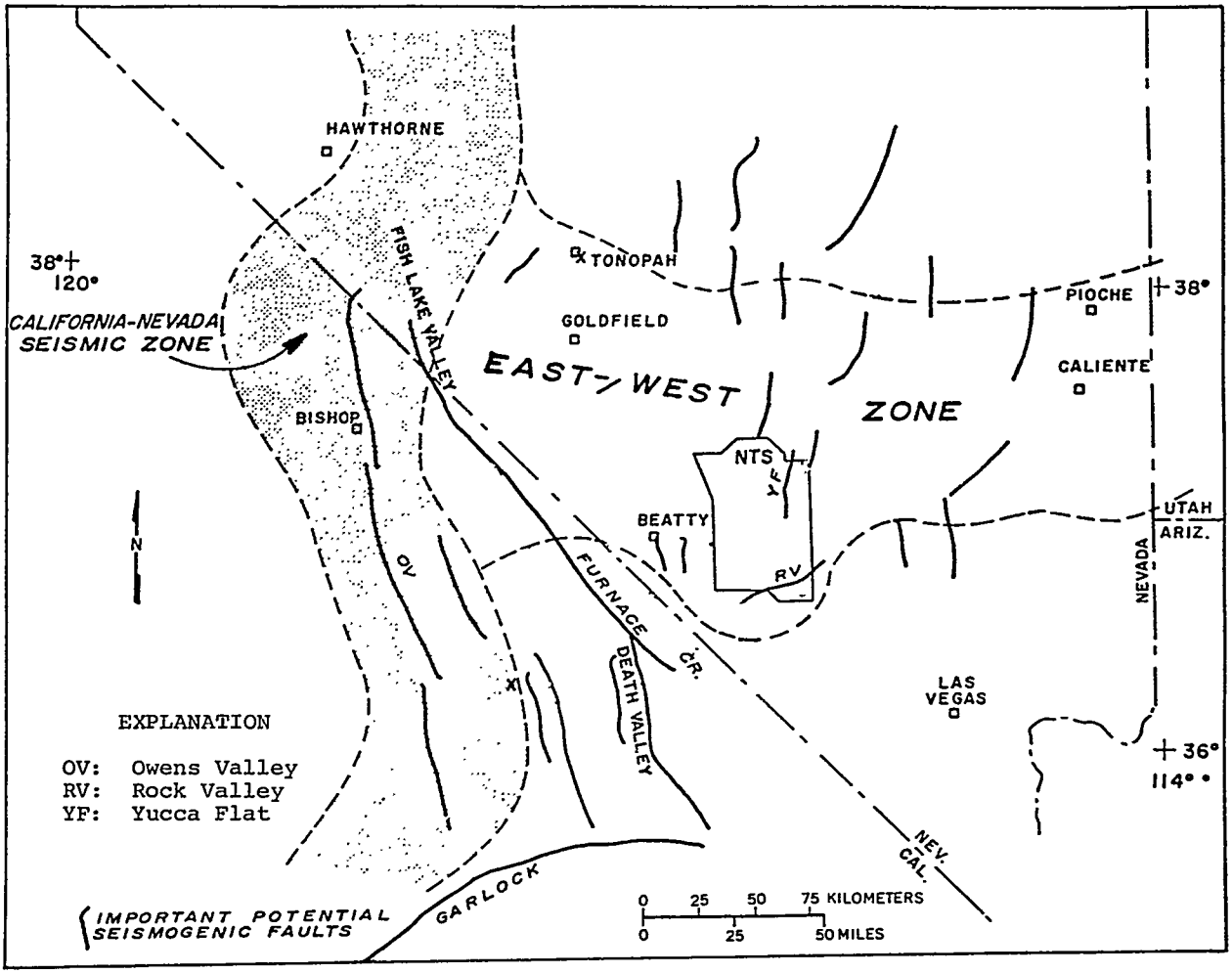

Figure 1-12. Seismic zones and important potentially seismogenic faults in the NTS region (after Carr and Rogers, 1982).

seismic zone then splits into two zones. The California-Nevada seismic zone continues approximately northward along the east flank of the Sierra Nevada and across the California-Nevada border. The "East-West" zone runs from west to east across southeastern Nevada. Locations of historic earthquake epicenters within 248 miles (400 kilometers) of the NTS are depicted in Figure 1-13. This historic record of seismicity for the past 200 years (Rogers and others, 1976) yields a pattern (Figure 1-13) in agreement with the 12-year record (Figure 1-14), and serves further to emphasize the trends of these two seismic zones (Figure 1-12).

Based upon the preliminary mapping, seismicity, and fault studies, Carr (1979) interprets that a possible paleoseismic belt with moderate earthquake activity existed in southern Nye and westernmost Lincoln Counties in early to middle Quaternary time. This possible belt extended northeastward across the Amargosa Desert and southeastern NTS and northward through Emigrant and Sand Spring Valleys, and coincides in a general way with a belt of Pliocene and Pleistocene basaltic lava. Only one fault system in the seismic belt shows evidence of important late Pleistocene movement; however, low-level seismicity elsewhere in the belt indicates that many other faults in the belt may be active.

The record of historic earthquakes between 1769 and 1974 (Rogers and others, 1976, 1977) indicates that no earthquakes with MM intensity greater than or equal to V or magnitude greater than or equal to 4.0 have been recorded at Yucca Mountain. Figure 1-15 shows all the known earthquakes of magnitude 3.0 or greater within the NTS and vicinity. The largest events within this area are about magnitude 5, but some of these events may be unannounced nuclear explosions (Rogers and others, 1977). According to Rogers and others (1977), a large proportion of the events near the NTS may be nuclear-explosion aftershocks, because only 17 of these events had occurred before the nuclear testing began in 1960. Dudley and Erdal (1982) report that only one small earthquake has been detected at Yucca Mountain in more than two years. This event, with a magnitude of 1.7 (Rogers and others, 1983) occurred in the second quarter of 1981 at an estimated depth of 4.8 miles (7.7 kilometers) below sea level under Yucca Mountain (NNWSI, 1981).

Within the NTS and vicinity, earthquakes of magnitude 6.0 or greater are rare (Wallenberg and others, 1983). Rogers and others (1977) have assessed the seismic hazard of the NTS region and conclude that the mean expected peak accelerations range from 0.2 to 0.7 g at various locations at the NTS, for a maximum magnitude of 7. Geologic evidence indicates that recurrence intervals for these magnitudes average several thousand years. The predicted accelerations in the Yucca Mountain area range from 0.3 to 0.5 g (Sinnock and others, 1984). The predictions of peak acceleration by Rogers and others (1977) and Sinnock and others (1984) are preliminary. New data from the recently installed seismograph network in southern Nevada and the adjacent California (Carr and Rogers, 1982) are being accumulated by the U.S. Geological Survey. It is expected that a new assessment of the seismic hazard in the NTS region or the Yucca Mountain area will be available to the public in the near future.

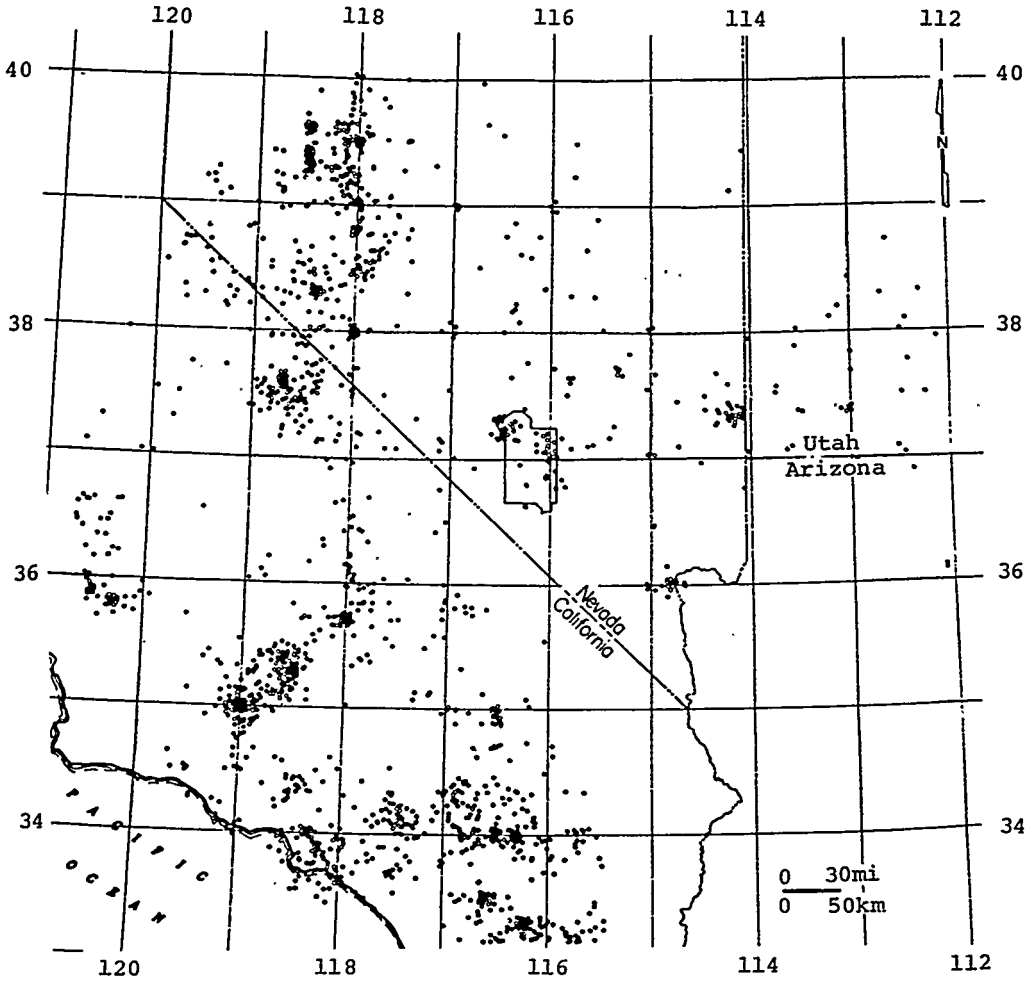

Figure 1-13. Location of historic earthquakes (1,959 events) within 400 kilometers of the study area with Modified Mercalli Intensity ≥V (5) and/or Magnitude ≥ 4.0 from 1769 through 1974 (after Rogers and others, 1977).

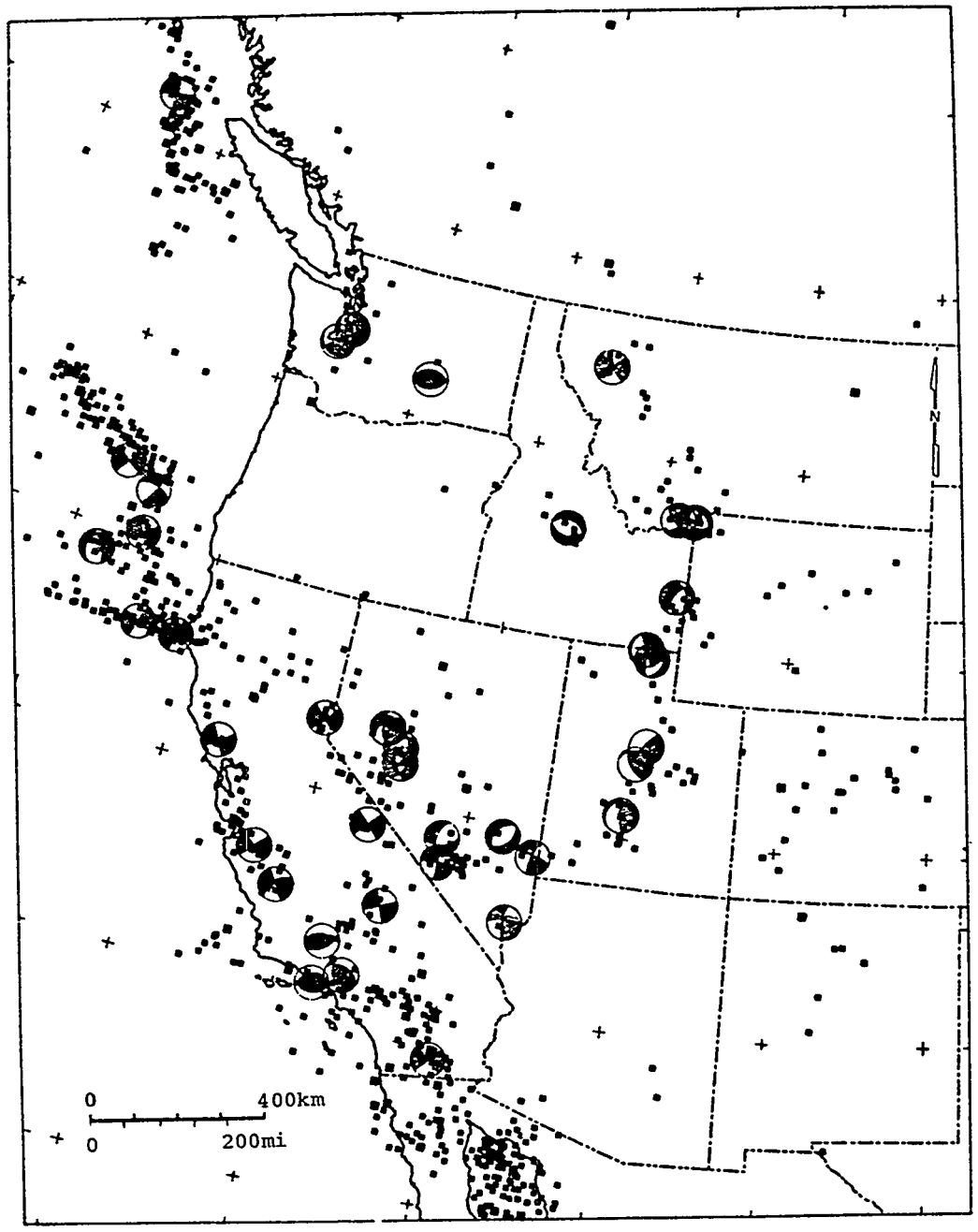

Figure 1-14. Seismicity of the western United States, showing epicenters for earthquakes of magnitudes greater than 4.0 for the years 1960-1972 (after Suppe and others, 1975).

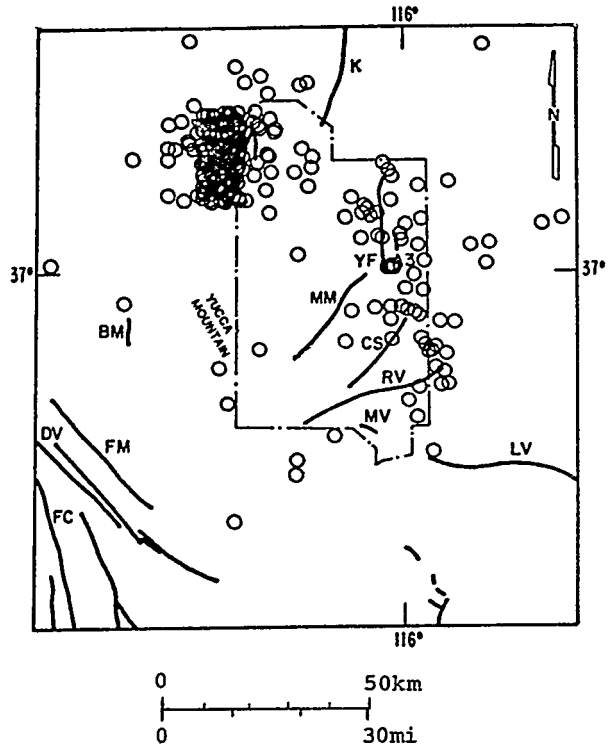

EXPLANATION

MM: Mine Mt. fault
YF: Yucca fault
CS: Cane Spring fault
RV: Rock Valley fault
MV: Mercury Valley fault
LV: Las Vegas fault
K: Kawich fault
BM: Bare Mt. fault
FM: Funeral Mts. fault
DV: Death Valley fault
FC: Furnace Creek fault

O: Earthquake location
fault

Figure 1-15. Locations of all historic earthquakes in NTS and vicinity ($M \geq 3.0$) (modified from Rogers and others, 1977).

1.7 Geothermal Gradient

Temperature measurements from 60 drill holes in and around the NTS, including Yucca Mountain, have been used for geothermal-gradient determination (Dudley and Erdal, 1982; Sass and Lachenbruch, 1982). One of these drill holes, located in the northwestern corner of the NTS, is selected as representative, because it is believed to provide the most reliable results (Guzowski and others, 1983). Within this particular drill hole, three zones of geothermal gradient can be recognized. The geothermal gradient of the upper 0.9 mile (1.5 kilometers) is linear at approximately 1.4°F/100 feet (26°C/kilometer). Between 0.9 and 1.9 miles (1.5 and 3.0 kilometers), the geothermal gradient is highly erratic as a result of both vertical and horizontal ground-water flow. At depths greater than 1.9 miles (3 kilometers) the geothermal gradient is also linear at 2.0°F/100 feet (37°C/kilometer) (Sass and Lachenbruch, 1982).

At and near Yucca Mountain, 16 drill holes have been studied by Sass and Lachenbruch (1982). In those drill holes where thermal equilibrium has been reached, the unsaturated zone has extreme variations in the geothermal gradient. These variations are probably caused by two-phase water flow; the ratio between liquid and vapor phases changes with depth (Lachenbruch, 1981). Based upon data from these drill holes at Yucca Mountain, deeper drill holes seem to have more consistent thermal profiles. For example, within drill hole USW-G1, the average geothermal gradient is approximately 1.35°F/100 feet (24.6°C/kilometer) (Smyth and Caporuscio, 1981). The geothermal gradient within the unsaturated zone penetrated by deeper drill holes averages 1.1°F/100 feet (20°C/kilometer); within the saturated zone, the geothermal gradient averages 1.6°F/100 feet (29°C/kilometer) (Sass and Lachenbruch, 1982).

1.8 Energy and Mineral Resources

Even though the Yucca Mountain area does not show any evidence of significant mineralization or occurrences of known economic resources (Sinnock and others, 1984), exploration activity along the western boundary of the Yucca Mountain area has been intense, and very large areas of land have been placed under mining claims during the past few years (Bell and Larson, 1982). Furthermore, energy and mineral resources, especially those in association with Tertiary volcanic rocks, do occur and have been reported from many locations in southern Nevada (Anderson, 1968; Bell and Larson, 1982; Cornwall, 1972b; Cornwall and Kleinhampl, 1961; Ekren, 1968). The identification of these resources in the region and their levels of potential are necessary in assessing the feasibility of a candidate repository site at Yucca Mountain. In addition to Guzowski and others (1983), who reviewed the natural resources of potentially high economic value in the Yucca Mountain region, Bell and Larson (1982) documented the energy and mineral resources of southwestern NTS, including Yucca Mountain and vicinity. Except as otherwise noted, the following descriptions are based upon the work of Bell and Larson (1982).

Energy resources in the Yucca Mountain region appear to be limited. Low-to-moderate-temperature geothermal resources are considerable in quantity, but not suitable for power generation. No occurrences of oil, natural gas, oil shale, or coal have been reported in the literature (Garside and Papki, 1980;

Horton, 1964). Occurrences of these resources at depth are highly unlikely because of the unfavorable geologic setting. Mines and prospects for radioactive energy resources are unknown within the region (Garside, 1973, 1979; Lovering, 1954); however, minor amounts of uranium have been reported in association with fluorite from the Crowell mine and the Butler Bluebird prospect immediately west of Yucca Mountain (Garside, 1973, 1979). To the north of Yucca Mountain, the Silent Canyon caldera is characterized by peralkaline comenditic ash and lava flows (Byers and others, 1976b; Crowe and Sargent, 1979), the petrologies of which are similar to those of the volcanic rocks of the McDermitt caldera complex (Sheridan and Burt, 1979) located along the Nevada-Oregon border. These volcanic rocks are known to host uranium mineralization (Rytuba and Conrad, 1981; Wallace and Roper, 1981) of potential commercial value. However, no published information is available to indicate the radioactive-element content of the volcanic rocks associated with the Silent Canyon caldera.

Deposits of precious and base metals and associated mineral resources are known to occur in the region in association with altered igneous rocks of intermediate composition (Anderson and Ekren, 1968). Gold, fluorite, and mercury were or are mined in the Bare Mountain district (Kral, 1951; Cornwall, 1972b), including Bare Mountain and the northwestern part of Yucca Mountain (Cornwall and Kleinhampl, 1961). Historical production of gold and silver from Hornsilver mine of the Wahmonie district (Heikes, 1931) within the NTS, and from Gold Reed, Cactus Range, and Silver Bow within Nellis Air Force Range has also been reported (Ekren, 1968). A possible buried mineralization of gold- and silver-bearing rock extending southward from Goldfield to Timber Mountain underlying the Thirsty Canyon Tuff was identified by Anderson and others (1965). For the few locations where information is available, mineralization appears to be structurally controlled.

Within the Bare Mountain district, both mercury and gold mineralizations occur along steep fissures in the Devonian dolomite at the Harvey or Telluride mine (Gianella, 1940; Kral, 1951). The mineralization at the only active precious metal mining operation in the district, the Stirling mine, is believed to be fine-grained gold in weathered, oxidized parts of quartzite along the irregular trace of a low-angle thrust fault. At the Crowell, Mary, and Diamond Queen mines and several fluorite prospects, the fluorite is associated with quartz, calcite, and clay and is found replacing and cementing carbonate rock fragments in irregular pipe-like breccia bodies developed along east-dipping faults. According to Papke (1979), both Mary and Diamond Queen deposits are hydrothermal in origin and are possibly related to rhyolitic rocks present north of these mines (Cornwall, 1972a). At the Thompson and Curly Wright mines and prospects of northwest Yucca Mountain, mercury occurs as cinnabar in pods, lenses, and veinlets within silicified tuffs and flows of Tertiary age (Holmes, 1965).

At the northern end of Yucca Mountain, veins of precious metal are in various tuffs and other volcanic rocks related to the Timber Mountain caldera (Byers and others, 1968). Many prospects appear to be associated with fracture zones along the margin of the caldera. In drill hole USW-G1, gold and silver were encountered in the lower Tram Member of the Crater Flat Tuff

at the 3,515.1-foot (1,071.7-meter) level (Spengler and others, 1981). Chemical analysis indicates that the sample contains 0.5 ppm (or 0.16 oz/ton eq.) of gold, and 20 ppm (or 0.64 oz/ton eq.) of silver.

The location, mineralization, and production of selected mines and prospects are summarized in Appendix 1.2. Production information in the literature appears to be guess-work rather than data-based estimates. It is useful, however, for depicting the general level of the potential resources in the region.

Deposits of industrial-material resources, including clay (Kral, 1951; Papke, 1970; Smith, 1977), sand, gravel (Smith, 1977), volcanic cinders (Elevatorski, 1973), perlite (Cornwall, 1972b; Cornwall and Kleinhampl, 1961; Smith, 1977), silica (Cornwall, 1972b; Kral, 1951), limestone/dolomite, zeolite, and diatomite (Kral, 1951), are widely distributed in the region. Occurrences of alunite (Hall, 1978; McKay, 1963; Smith, 1977), magnesite, and brucite (Gildersleeve, 1962; Smith, 1977) are also reported. Because of their low unit value or low grade, if they are mined, these deposits are only locally significant.

CHAPTER 2 - STRATIGRAPHY

The water table is more than 1,600 feet (487.5 meters) deep beneath central Yucca Mountain. As a result, members of the Paintbrush Tuff and most of the bedded tuff of Calico Hills are in the unsaturated zone (Dudley and Erdal, 1982). Stratigraphic data, especially subsurface data, are mainly from drill hole logs, core descriptions, stratigraphic cross sections, and a variety of geophysical surveys available when this report was prepared. Most of the drill holes are located within, or close to, an area where extensive exploration has taken place. This area, a potential candidate site for a nuclear-waste repository (Dudley and Erdal, 1982), is located within the northeastern part of Yucca Mountain (Spengler and others, 1981). Drill holes J-12 and J-13 were drilled on the east side of Fortymile Wash in Jackass Flat, and are outside the area of interest. These two drill holes, however, have provided convenient anchors for cross sections through Yucca Mountain (Byers and Warren, 1983). A generalized geologic map with drill hole locations is presented in Figure 2-1. A fence diagram of the general area is shown in Figure 2-2. The following sections describe the stratigraphic features of the major lithologic units within the unsaturated zone. The thicknesses of these units encountered in each drill hole are summarized in Table 2-1. In descending order, the stratigraphic units within the unsaturated zone are

Alluvium and colluvium
Paintbrush Tuff
  Tiva Canyon Member
  Yucca Mountain Member
  Pah Canyon Member
  Topopah Spring Member
Bedded Tuff of Calico Hills

Detailed lithologic descriptions of the stratigraphic units and thickness variations of the internal subunits at different drill hole locations are given in Appendix 2.1.

2.1 Alluvium and Colluvium

Surficial deposits of Quaternary age, including gravel, sand, and silt, occur as valley fillings. They are made predominantly of ash flow and bedded tuff debris of the Paintbrush Tuff (Spengler and Rosenbaum, 1980; Spengler and others, 1979, 1981). Because no detailed descriptions on these deposits are available, separation of alluvium from colluvium at most locations is not possible. The only exception is in drill hole UE25a-7, where about 65 feet (19.8 meters) of core interval consisting of colluvium of cobble- to boulder-size tuff fragments of variable lithology (Appendix 2.1, Table A2.1-11) are reported (Spengler and Rosenbaum, 1980). The known thicknesses of these undifferentiated Quaternary deposits in the wash vary from 20 feet (6.1 meters) in drill hole UE25a-6 to 150 feet (45.7 meters) in UE25b-1. Alluvium from drill hole J-13, located approximately 4 miles (6.4 kilometers) to the southeast of drill hole UE25a-1, is reported to reach 435 feet (132.5 meters) in thickness (Byers and Warren, 1983). In general, these deposits are

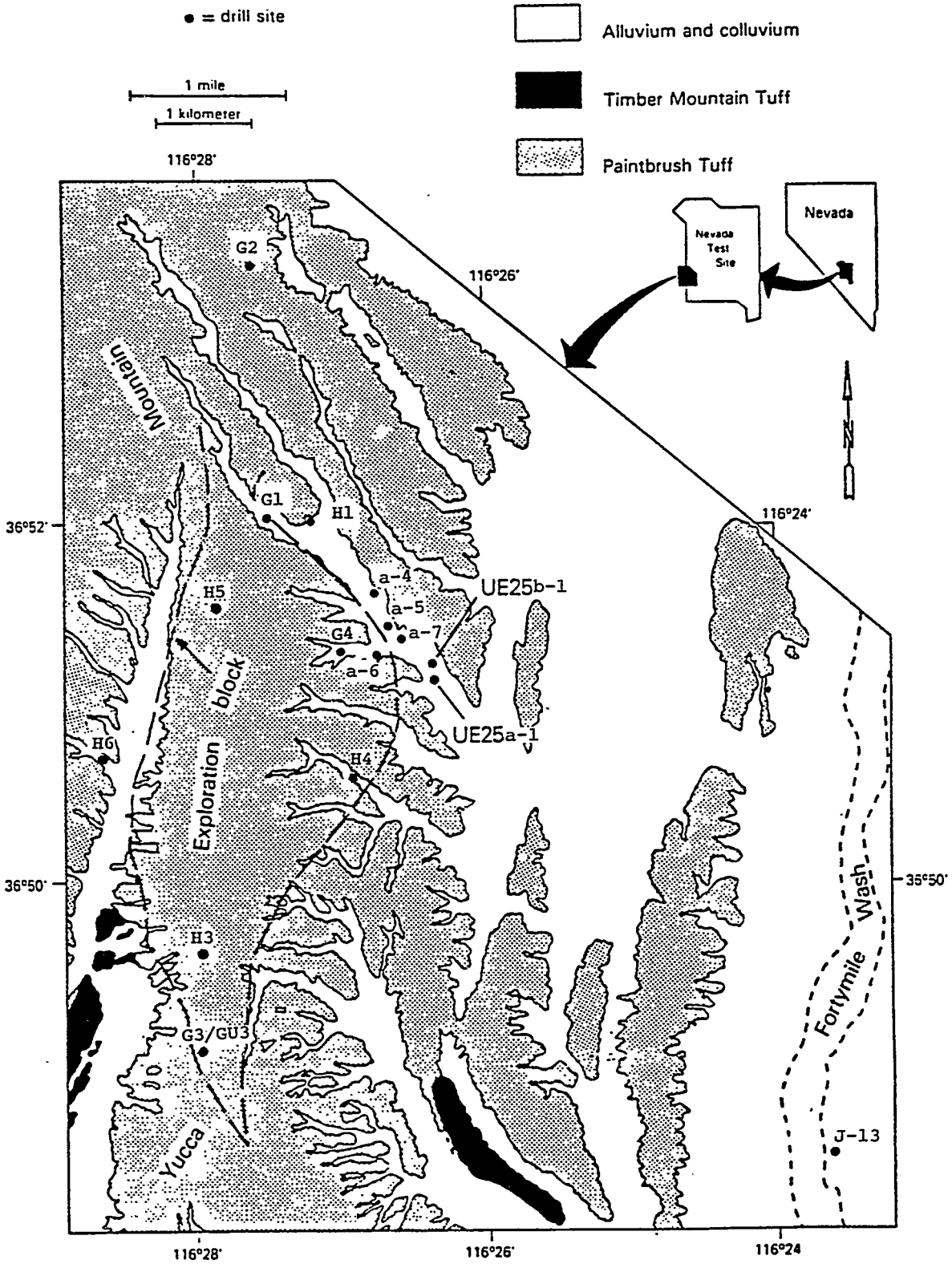

Figure 2-1. Generized geologic map of Yucca Mountain area, with some drill hole locations and an outline of the exploration block for the NNWSI program (geology after Bish and others, 1982).

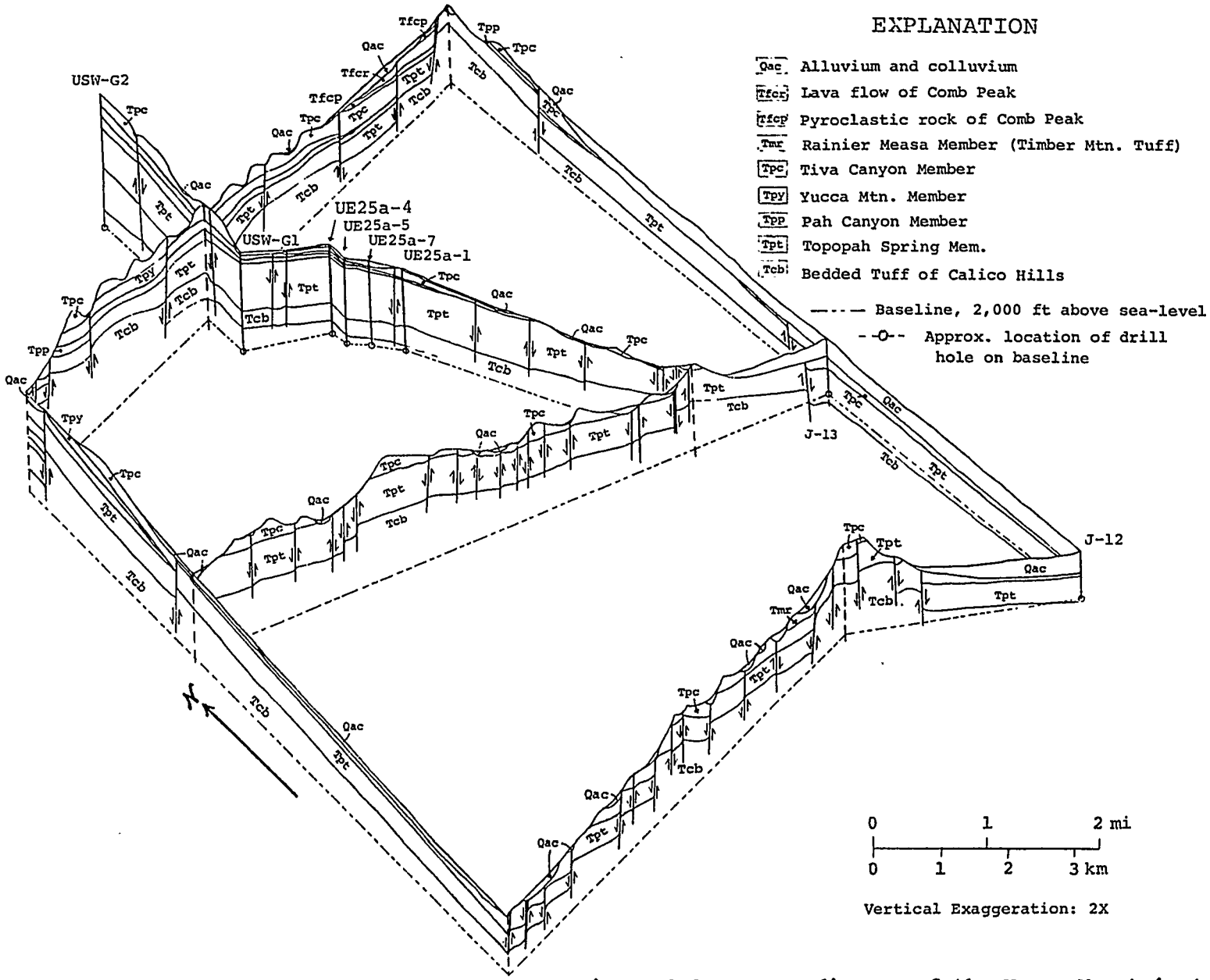

Figure 2-2. Fence diagram of the Yucca Mountain Area.

Table 2-1. Summary of thickness variation of stratigraphic units in drill holes, Yucca Mountain area

Stratigraphic Unit	Depth to Base of Unit		Thickness of Unit		Elevation of Base of Unit	
	Feet	Meter	Feet	Meter	Feet	Meter
Well no. USW-G1, Ground Elevation 4,349.6 ft (1,325.7 m) [3,10]						
Alluvium	60.0	18.3	60.0	18.3	4,289.3	1,307.4
Paintbrush Tuff						
Tiva Canyon	–	–	0	0	–	–
Yucca Mountain	135.0	41.2	75.0	22.9	4,214.3	1,284.5
Pah Canyon	235.0	71.6	100.0	30.4	4,114.3	1,254.1
Topopah Spring	1,403.9	427.9	1,168.9	356.3	2,945.4	897.8
Calico Hills	1,801.5	549.1	397.6	121.2	2,547.8	776.6
Well no. USW-G2, Ground Elevation 5,098.0 ft (1,553.9 m) [8]						
Alluvium	–	–	0	0	–	–
Paintbrush Tuff						
Tiva Canyon	245.0	74.7	245.0	74.7	4,853.0	1,479.2
Yucca Mountain	498.0	151.8	253.0	77.1	4,600.0	1,402.1
Pah Canyon	759.4	231.5	261.4	79.7	4,338.6	1,322.4
Topopah Spring	1,701.0	518.5	941.6	287.0	3,397.0	1,035.4
Calico Hills	2,704.0	824.2	1,003.0	305.7	2,394.0	729.7
Well no. USW-G3, Ground Elevation not available [13]						
Alluvium	–	–	0	0	–	–
Paintbrush Tuff						
Tiva Canyon	423.9	129.2	423.9	129.2		
Yucca Mountain	–	–	0	0	–	–
Pah Canyon	–	–	0	0	–	–
Topopah Spring	1,406.3	428.6	982.4	299.4		
Calico Hills	1,560.2	475.6	153.9	47.0		
Well no. USW G-4, Ground Elevation 4,166.9 ft (1,270 m) [1]						
Alluvium	22.0	6.7	22.0	6.7	4,144.9	1,263.3
Paintbrush Tuff						
Tiva Canyon	148.0	45.1	126.0	38.4	4,018.9	1,224.9
Yucca Mountain	168.3	51.3	20.3	6.2	3,998.6	1,218.7
Pah Canyon	228.0	69.5	59.7	18.2	3,938.9	1,200.5
Topopah Spring	1,409.5	429.6	1,181.5	360.1	2,757.4	840.4
Calico Hills	1,761.6	536.9	352.1	107.3	2,405.3	733.1

Table 2-1. Summary of thickness variation of stratigraphic units in drill holes, Yucca Mountain area--continued

Stratigraphic Unit	Depth to Base of Unit		Thickness of Unit		Elevation of Base of Unit	
	Feet	Meter	Feet	Meter	Feet	Meter
Well no. USW-H1, Ground Elevation 4,272.5 ft (1,302.2 m) [9]						
Alluvium	–	–	0	0	–	–
Paintbrush Tuff						
Tiva Canyon	95.0	25.0	95.0	25.0	4,177.5	1,273.2
Yucca Mountain	190.0	58.0	95.0	33.0	4,082.5	1,244.2
Pah Canyon	278.6	85.0	88.6	27.0	3,993.9	1,217.2
Topopah Spring	1,505.6	459.0	1,227.0	374.0	2,766.9	843.2
Calico Hills	1,856.6	566.0	351.0	107.0	2,415.9	736.2
Well no. USW-H3, Ground Elevation not available [5]						
Alluvium	–	–	0	0	–	–
Paintbrush Tuff						
Tiva Canyon	404.0	123.1	404.0	123.1		
Yucca Mountain	–	–	0	0	–	–
Pah Canyon	–	–	0	0	–	–
Topopah Spring	1,392.0	424.3	988.0	301.2		
Calico Hills	1,487.0	453.2	95.0	28.9		
Well no. USW-H4, Ground Elevation not available [5]						
Alluvium	–	–	0	0	–	–
Paintbrush Tuff						
Tiva Canyon	214.0	65.2	214.0	65.2		
Yucca Mountain	–	–	0	0	–	–
Pah Canyon	–	–	0	0	–	–
Topopah Spring	1,312.0	399.9	1,098.0	334.0		
Calico Hills	1,627.0	495.9	315.0	96.0		
Well no. USW-H5, Ground Elevation 4,851.0 ft (1,478.5 m) [2]						
Alluvium	–	–	0	0	–	–
Paintbrush Tuff						
Tiva Canyon	490.2	149.4	490.2	149.4	5,345.1	1,629.1
Yucca Mountain	–	–	0	0	–	–
Pah Canyon	542.0	165.2	51.8	15.8	5,293.2	1,613.3
Topopah Spring	1,710.0	521.2	1,168.0	356.0	4,125.2	1,257.3
Calico Hills	1,945.0	592.8	235.0	71.6	3,892.2	1,186.3

Table 2-1. Summary of thickness variation of stratigraphic units in drill holes, Yucca Mountain area--continued

Stratigraphic Unit	Depth to Base of Unit		Thickness of Unit		Elevation of Base of Unit	
	Feet	Meter	Feet	Meter	Feet	Meter
Well no. USW-H6, Ground Elevation 4,271.9 ft (1,302 m) [4]						
Alluvium	29.9	9.1	29.9	9.1	4,242.0	1,292.9
Paintbrush Tuff						
Tiva Canyon	270.0	82.3	240.1	73.2	4,001.9	1,219.7
Yucca Mountain	-	-	0	0	-	-
Pah Canyon	300.2	91.5	30.2	9.2	3,971.7	1,210.5
Topopah Spring	1,376.4	419.5	1,076.2	328.0	2,895.5	882.5
Calico Hills	1,504.0	458.4	127.6	38.9	2,767.9	843.6
Well no. UE25a-1, Ground Elevation 3,932.9 ft (1,198.7 m) [3,12]						
Alluvium	30.0	9.1	30.0	9.1	3,902.9	1,189.6
Paintbrush Tuff						
Tiva Canyon	218.2	66.4	188.2	57.3	3,714.7	1,132.3
Yucca Mountain	-	-	0	0	-	-
Pah Canyon	271.2	82.6	53.0	16.2	3,661.7	1,116.1
Topopah Spring	1,361.2	414.8	1,090.0	332.2	2,571.7	783.9
Calico Hills	1,836.9	559.8	475.7	145.0	2,096.0	638.9
Well no. UE25a-4, Ground Elevation 4,101.7 ft (1,249.8 m) [12, a]						
Alluvium	30.0	9.1	30.0	9.1	4,071.7	1,240.7
Paintbrush Tuff						
Tiva Canyon	152.7	46.5	122.7	37.4	3,949.0	1,203.3
Yucca Mountain	191.0	58.2	38.3	11.7	3,910.7	1,191.6
Pah Canyon	280.0	85.3	89.0	27.1	3,821.7	1,164.5
Topopah Spring			220+	67+		
Calico Hills						
Well no. UE25a-5, Ground Elevation 4,055.6 ft (1,235.7 m) [11, a]						
Alluvium	90.0	27.4	90.0	27.4	3,965.6	1,208.3
Paintbrush Tuff						
Tiva Canyon	138.6	42.2	48.6	14.8	3,917.0	1,193.5
Yucca Mountain	185.3	56.4	46.7	14.2	3,870.3	1,179.3
Pah Canyon	237.1	72.2	51.8	15.8	3,818.5	1,163.5
Topopah Spring			249.9+	76.1+		
Calico Hills						

Table 2-1. Summary of thickness variation of stratigraphic units in drill holes, Yucca Mountain area--continued

Stratigraphic Unit	Depth to Base of Unit		Thickness of Unit		Elevation of Base of Unit	
	Feet	Meter	Feet	Meter	Feet	Meter
Well no. UE25a-6, Ground Elevation 4,056.3 ft (1,235.9 m) [11, a]						
Alluvium	20.0	6.1	20.0	6.1	4,036.3	1,229.9
Paintbrush Tuff						
Tiva Canyon	149.3	45.5	129.3	39.4	3,907.0	1,190.5
Yucca Mountain	188.2	57.3	38.9	11.8	3,868.1	1,178.7
Pah Canyon	227.0	69.1	38.8	11.8	3,829.3	1,166.9
Topopah Spring			287+	87.4+		
Calico Hills						
Well no. UE25a-7, Ground Elevation 4,008.5 ft (1,221.4 m) [11, a]						
Alluvium	137.5	41.9	137.5	41.9	3,871.0	1,179.5
Paintbrush Tuff						
Tiva Canyon	174.5	53.2	37.0	11.3	3,834.0	1,168.2
Yucca Mountain	197.9	60.0	22.4	6.8	3,811.6	1,161.4
Pah Canyon	245.1	74.8	48.6	14.8	3,763.0	1,146.6
Topopah Spring			204.3+	62.2+		
Calico Hills						
Well no. UE25b-1, Ground Elevation 3,938.2 ft (1,200.3 m) [7]						
Alluvium	149.9	45.7	149.9	45.7	3,788.3	1,154.6
Paintbrush Tuff						
Tiva Canyon	239.8	73.1	89.9	27.4	3,698.4	1,127.1
Yucca Mountain	–	–	0	0	–	–
Pah Canyon	274.9	83.8	35.1	10.7	3,663.3	1,116.4
Topopah Spring	1,385.2	422.2	1,110.3	338.4	2,553.0	778.0
Calico Hills	1,869.2	569.7	484.0	147.5	2,069.0	630.5
Well no. J-12, Ground Elevation 3,125.0 ft (952.2 m) [6]						
Alluvium	515.0	156.9	515.0	156.9	2,610.0	795.2
Paintbrush Tuff						
Tiva Canyon	580.0	176.7	65.0	19.8	2,545.0	775.4
Yucca Mountain	–	–	0	0	–	–
Pah Canyon	–	–	0	0	–	–
Topopah Spring	1,140.0	347.3	560.0[b]	170.6	1,985.0	604.8
Calico Hills						

Table 2-1. Summary of thickness variation of stratigraphic units in drill holes, Yucca Mountain area--concluded

Stratigraphic Unit	Depth to Base of Unit		Thickness of Unit		Elevation of Base of Unit	
	Feet	Meter	Feet	Meter	Feet	Meter
Well no. J-13, Ground Elevation 3,318.1 ft (1,011.3 m) [3]						
Alluvium	435.0	132.5	435.0	132.5	2,883.0	878.8
Paintbrush Tuff						
Tiva Canyon	680.0	207.7	245.0	74.8	2,638.0	803.6
Yucca Mountain	-	-	0	0	-	-
Pah Canyon	-	-	0	0	-	-
Topopah Spring	1,475.0	449.6	795.0	242.3	1,843.0	561.7
Calico Hills	1,740.0	530.4	265.0	80.8	1,578.0	480.9

(1) Bentley, 1984
(2) Bentley and others, 1983
(3) Bish and others, 1982
(4) Craig and others, 1983
(5) Levy, 1984
(6) Lipman and McKay, 1965
(7) Lobmeyer and others, 1983
(8) Maldonado and Koether, 1983
(9) Rush and others, 1983
(10) Sinnock, 1982
(11) Smith and Ross, 1979
(12) Spengler and Rosenbaum, 1980
(13) Vaniman and others, 1984

a. Calculated from base elevation of Tiva Canyon Member.
b. Measured from cross section.

relatively thin along the margin of the wash, as indicated by those in drill holes UE25a-4 and UE25a-6. They increase in thickness substantially, however, toward the middle of the wash, as indicated by those in drill holes UE25a-5 and UE25a-7 (Table 2-1). The contact relationship between these deposits and the bedrocks apparently is unconformable owing to the V-shaped configuration of the valley (Spengler and Rosenbaum, 1980).

2.2 Paintbrush Tuff

The first bedrock tuff encountered in outcrops and drill holes within the area of interest is the Paintbrush of Miocene age (Byers and others, 1976a, 1976b; Dudley and Erdal, 1982; Spengler and others, 1979, 1981; Spengler and Rosenbaum, 1980). The Paintbrush Tuff includes, in descending order, the Tiva Canyon, Yucca Mountain, Pah Canyon, and Topopah Spring Members.

The Paintbrush Tuff probably originated from the source areas located within Claim Canyon and Oasis Valley calderas (Figure 2-3) (Christiansen and others, 1977). According to Kistler (1968) and Marvin and others (1970), the Paintbrush Tuff was deposited about 12 to 13 million years ago.

The thickest section of the Paintbrush Tuff is reported to be 6,500 feet (1,980 meters) within the Claim Canyon caldera (Byers and others, 1976b). In the study area, this formation thins in a south to southeasterly direction with thickness ranging from 1,710 feet (521.2 meters) in drill hole USW-H5 (Bentley and others, 1983) to 1,235.3 feet (376.5 meters) in drill hole UE25b-1 (Lobmeyer and others, 1983). Farther southeast from drill hole UE25a-1, the Paintbrush Tuff encountered by drill hole J-13 has a thickness of 1,040 feet (317 meters) (Byers and Warren, 1983). Among the four members of the Paintbrush Tuff, only the Topopah Spring Member covers the entire study area; the distribution of the upper three members is discontinuous (Bish and others, 1982). Generalized maps of areal and thickness distribution for each member of the Paintbrush Tuff are in Appendix 2.2.

2.2.1 Tiva Canyon Member

At most of the locations in the study area, the Paintbrush Tuff that is exposed on the surface is part of the Tiva Canyon Member, with a slope gradient of approximately 10 percent. The base of the Tiva Canyon Member is generally inclined to the east and southeast (Figure 2-4). In washes or on gentle slopes, the Tiva Canyon Member is directly beneath the alluvium and/or colluvium covers except at the location of drill hole USW-G1, where the Tiva Canyon Member is absent (Spengler and others, 1981). Because the upper part of the Tiva Canyon Member may be removed in places by erosion, the thickness of this unit varies greatly (Appendix 2.2, Figure A2.2-1). The maximum known thickness of the Tiva Canyon Member in the Yucca Mountain area is approximately 490 feet (149.3 meters) (Bentley and others, 1983). In general, however, the Tiva Canyon Member is much thinner under the alluvium and colluvium covers (Table 2-1). A composite stratigraphy and lithology of the Tiva Canyon Member is summarized, in descending order, in Table 2-2.

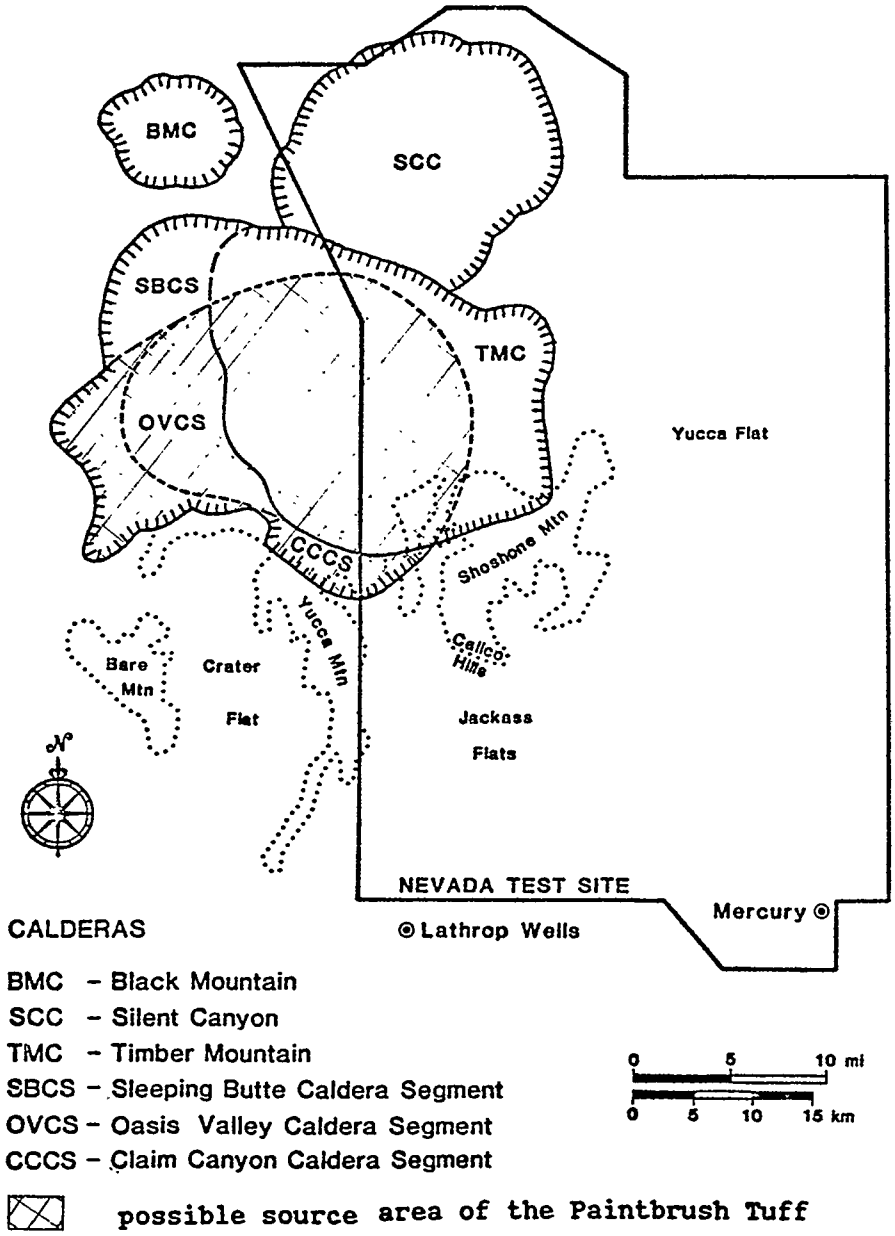

Figure 2-3. Caldera complex north of Yucca Mountain showing possible source area of the Paintbrush Tuff (after Byers and others, 1976b).

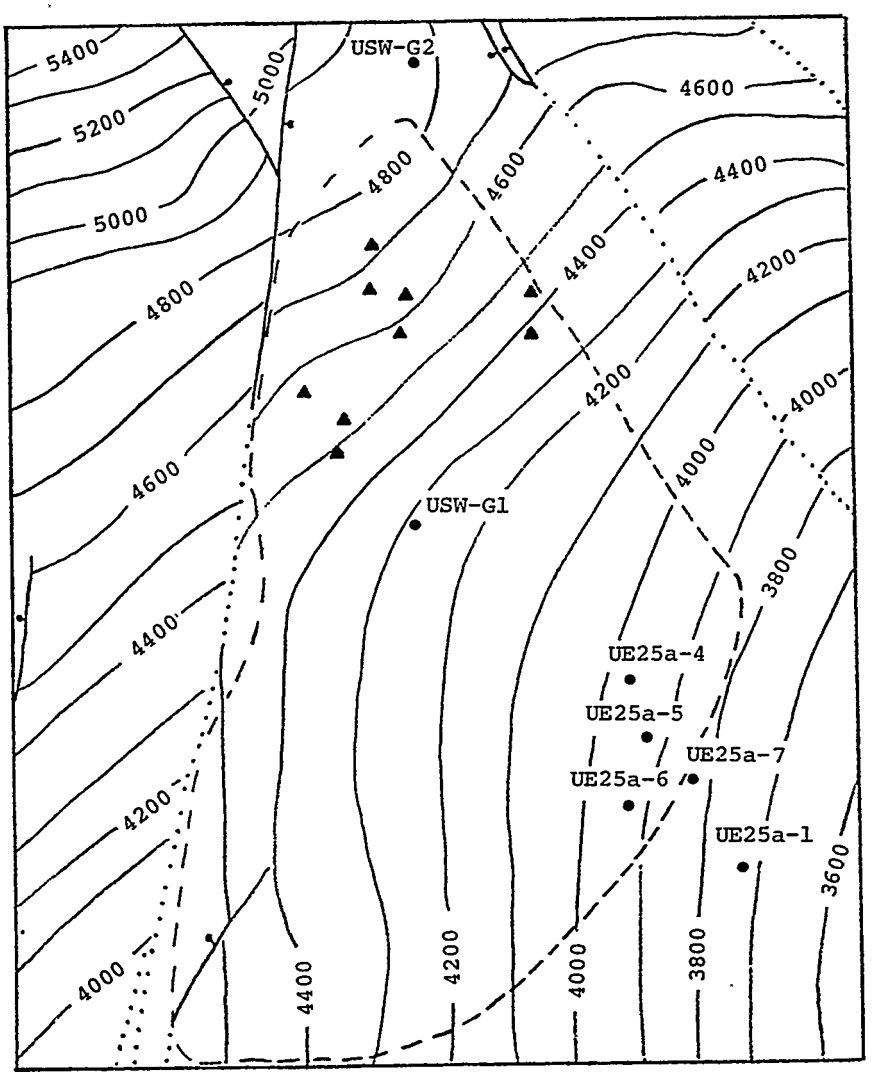

EXPLANATION

——— — — —····	Fault-ball and bar on downthrown side Dashed where inferred Dotted where concealed
USW-G2 ●	Approximate location of drill hole
▲	Surveyed stations at base of Tiva Canyon
——— 4000 ———	Contour on base of Tiva Canyon (contour interval - 100 feet)

Figure 2-4. Structure contour map of base of Tiva Canyon Member at northern Yucca Mountain (after Spengler and Rosenbaum, 1980).

Table 2-2. Summary of stratigraphy and lithology of the Tiva Canyon Member, Yucca Mountain area

Lithology	Thickness (feet)	Thickness (meters)
Tuff, nonwelded to partly welded, vitric or vapor-phase crystallized, gray, pumiceous	<10	<3.1
Tuff, densely welded, vitric, red and black	5	1.5
Tuff, densely welded, vitric, red and black	50-100	15.2-30.5
Tuff, welded, purple-grey, lithophysal	100-200	30.5-61.0
Tuff, densely welded, devitrified, purple-gray, closely spaced conchoidal fractures subparallel to foliation	75-150	22.9-45.7
Tuff, moderately welded, vapor-phase crystallized, commonly grey, crudely columnar-jointed	15-30	4.6-9.1
Tuff, partly welded vitric shards, brown or orange-brown	10-20	3.1-6.1
Tuff, nonwelded, vitric, gray or white, poorly-bedded	15-30	4.6-9.1
Tuff, nonwelded, bedded	5-10	1.5-3.1

2.2.2 Yucca Mountain Member

The distribution of the Yucca Mountain Member is discontinuous in the study area. In drill hole USW-G1, this unit is directly under the alluvium and colluvium. Elsewhere in the study area, if it is present, the Yucca Mountain Member is overlain by Tiva Canyon Member. The Yucca Mountain Member gradually thins toward the south and southeast (Appendix 2.2, Figure A2.2-2). It ranges in thickness from 253 feet (77.1 meters) in drill hole USW-G2 to 20.3 feet (6.2 meters) in drill hole USW-G4 (Table 2-1). According to Byers and others (1976b) the thinning rate for Yucca Mountain Member in the study area is approximately 16 feet/1,000 feet, or 1.76 meters/100 meters. Based upon the borehole data, Spengler and Rosenbaum (1980) calculated a thinning rate for the Yucca Mountain Member of only 5 feet/1,000 feet or 0.5 meter/100 meters. The absence of the Yucca Mountain Member in drill holes UE25a-1, USW-G3, -H3, -H4, and -H5 indicates that the Yucca Mountain Member is limited to the northern part of the study area (Appendix 2.2, Figure A2.2-2).

2.2.3 Pah Canyon Member

In most drill holes within the study area, the Pah Canyon Member is overlain by the Yucca Mountain Member, except in drill hole UE25a-1 where the Yucca Mountain Member is absent, and the Pah Canyon Member is overlain by the Tiva Canyon Member (Table 2-1). The Pah Canyon Member thins toward the south and southeast, and completely wedges out before reaching the locations of drill holes J-13, USW-H3, and -H4 (Appendix 2.2, Figure A2.2-3) (Byers and Warren, 1983; Levy, 1984; Spengler and Rosenbaum, 1980). Using borehole data, Spengler and Rosenbaum (1980) calculated a thinning rate of 17 feet/1,000 feet or approximately 1.7 meters/100 meters for Pah Canyon Member in the Yucca Mountain area. This figure is close to that of 18 feet/1,000 feet or 1.8 meters/100 meters given by Byers and others (1976b). Thicknesses of the Pah Canyon Member range from 261.4 feet (79.7 meters) in drill USW-G2 to 30.2 feet (9.2 meters) in drill hole USW-H6 (Table 2-1).

2.2.4 Topopah Spring Member

The Topopah Spring Member is the lowermost member of the Paintbrush Tuff and occurs directly below the Pah Canyon Member in the northern part of the study area. In the southern and southeastern parts of the study area, the Topopah Spring Member lies directly under the Tiva Canyon Member (Figure 2-2). This unit is the thickest and most widespread member of the Paintbrush Tuff (Lipman and others, 1966a). Thicknesses of the Topopah Spring Member range from approximately 1,227 feet (374 meters) in drill hole USW-H1 to 795 feet (242.3 meters) in drill hole J-13 (Table 2-1). An isopach map for the Topopah Spring Member is provided in Appendix 2.2, Figure A2.2-4.

2.3 Bedded Tuff of Calico Hills

At Yucca Mountain, tuffs occupying the stratigraphic interval between the Paintbrush Tuff and the Crater Flat Tuff have been informally named the tuffaceous beds of Calico Hills (Spengler and others, 1979, 1981). The name Bedded Tuff of Calico Hills for this informal stratigraphic unit was used by Dudley and Erdal (1982) and is adopted in this report.

According to Dudley and Erdal (1982), the Bedded Tuff of Calico Hills is Miocene in age. The rhyolites that occur outside of the study area in the same stratigraphic interval as the tuffs have been dated by Kistler (1968) as 13.4 million years old. Within the study area, 16 units of relatively massive, homogeneous, nonwelded ash-flow tuff have been recognized in the Bedded Tuff of Calico Hills. Each of the 16 ash-flow units is separated by thin, bedded to massive reworked air-fall tuffs (Spengler and others, 1981). A relatively thick sequence of reworked tuff, air-fall tuff, and tuffaceous sandstone makes up the basal unit of the formation (Appendix 2.1). Thickness of the Bedded Tuff of Calico Hills varies from drill hole to drill hole, and ranges from 1,003 feet (305.7 meters) in USW-G2 to 95 feet (28.9 meters) in USW-H3 (Table 2-1). Because the number of drill holes that penetrate the Bedded Tuff of Calico Hills is limited, and most of the available geologic cross sections do not include the base of this formation, the isopach map (Appendix 2.2, Figure A2.2-5) for the Bedded Tuff of Calico Hills is tentative at the present time.

2.4 Stratigraphic Units older than the Bedded Tuff of Calico Hills

The Bedded Tuff of Calico Hills is underlain by the Crater Flat Tuff, which includes rhyolitic, nonwelded to moderately welded ash-flow sheets of Miocene age (Dudley and Erdal, 1982). The Crater Flat Tuff and the stratigraphic units below it are under the static water table in the study area, and therefore, beyond the scope of this report. For a general description of these units in the Yucca Mountain area, the reader is advised to refer to the work of Guzowski and others (1983).

CHAPTER 3 - PETROLOGY AND MINERALOGY

3.1 Petrologic Characteristics

3.1.1 Terminology and classification of tuffs

The unsaturated zone in the Yucca Mountain area consists predominantly of tuffs that are referred to in this report, in a broad sense, as consolidated pyroclastic deposits, without reference to Fisher's (1961) classification by particle size. The definition for tuff recommended by Schmid (1981, p. 43), "a tuff is a pyroclastic rock whose average pyroclast size is less than 2 mm," therefore, is not restrictively applied in this report.

Tuffs have been classified in many ways. Guzowski and others (1983) briefly reviewed chemical, petrological, and depositional aspects of the classification of tuffs. The following descriptions are based partly on their work.

3.1.1.1 Classification based on mode of occurrence

An ash-flow tuff is a consolidated deposit resulting from an ash flow (Ross and Smith, 1961, p. 3), a turbulent mixture of high-temperature gas and unsorted, mostly fine grained pyroclastics ejected explosively and emplaced rapidly from fissures or a crater.

An ash-fall tuff is a consolidated deposit resulting from an ash fall, the descent of volcanic ash from an eruptive cloud by air-fall deposition. An ash-fall tuff commonly occurs at the base of an ash-flow deposit. Ash-fall tuffs are generally well sorted, highly permeable, and low in density and have low thermal conductivity relative to ash-flow tuff (Smyth and others, 1978). Ash-fall tuffs are commonly zeolitized.

Either an ash-flow tuff or an ash-fall tuff may be eroded and redeposited by streams and ponds or by volcaniclastic mudflows. Such processes give rise to sorted, bedded deposits called bedded or reworked tuff (Johnstone and Wolfsberg, 1980, p. 26). The term "bedded tuff" refers to tuff that is distinctly stratified (Byers and others, 1976a, p. 2). Accordingly, both ash-fall tuff and reworked tuff are bedded tuffs.

3.1.1.2 Classification based on petrography

Williams and others (1954, p. 149) subdivide tuffs into vitric tuff, crystal tuff, and lithic tuff based on the content of glass (including pumice), crystals (including crystal fragments), or rock fragments (Figure 3-1). Cook (1965), in a study of Tertiary volcanic rocks in eastern Nevada, used the same parameters, but adopted a more detailed classification (Figure 3-2). Glass and crystals were also used by Pettijohn (1975) as end members in differentiation of tuff types, with vitric tuff consisting of 100-75 percent glass and 0-25 percent crystals; vitric crystal tuff consisting of 75-50 percent glass and 25-50 percent crystals; crystal vitric tuff consisting of

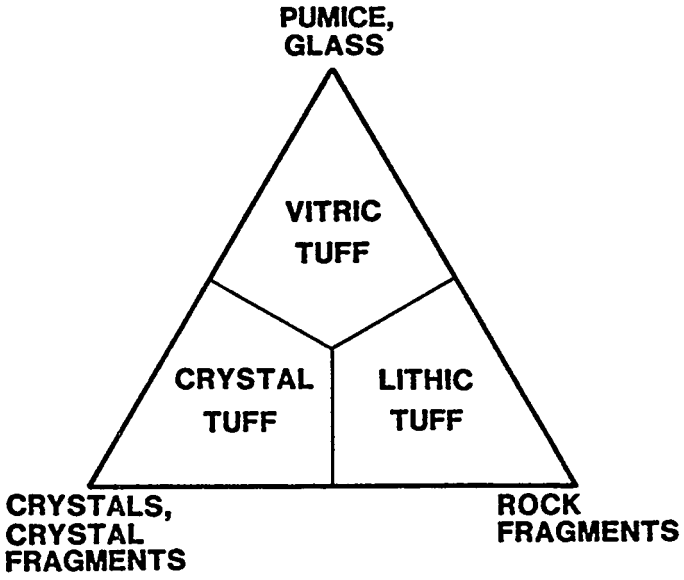

Figure 3-1. Subdivision of tuffs according to their fragmental composition (after Schmid, 1981).

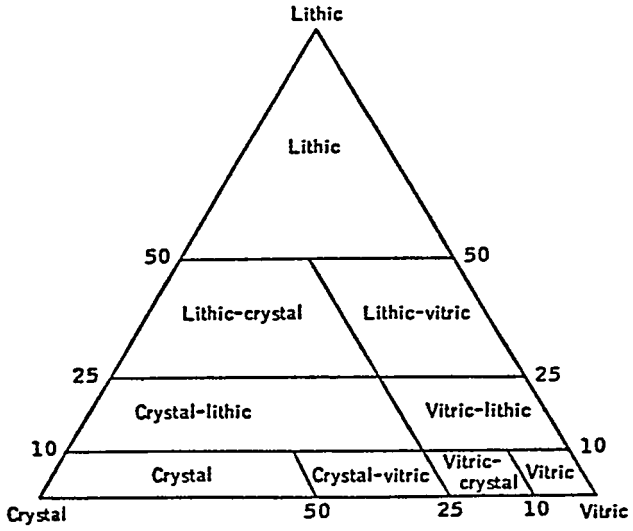

Figure 3-2. Cook's (1965) classification of volcanic rocks.

50-25 percent glass and 50-75 percent crystals; and crystal tuff consisting of 25-0 percent glass and 75-100 percent crystals.

3.1.1.3 Classification based on chemistry and mineralogy

Chemical and mineralogical classification for tuffs is the same as for other volcanic rocks. If the tuff has glass as the major constituent, the differentiation of the types is dependent solely on chemical analysis. According to Ross and Smith (1961), ash-flow tuffs in the western U.S. are generally rhyolites, dacites and rhyodacites, or quartz latites.

Rhyolite in general consists of more than 70 percent SiO_2 by weight. Quartz and alkali feldspar (sanidine, plagioclase, and anorthoclase) are major constituents with minor amounts of mafic minerals such as biotite and clinopyroxene. Dacite contains approximately 61 percent SiO_2 by weight. Typical minerals are andesine, biotite, and hornblende with or without the presence of pyroxene. Quartz and K-feldspar may be present as phenocrysts or in the groundmass. Rhyodacite or quartz latite is intermediate in composition between rhyolite and dacite, with quartz, plagioclase, and biotite as the principal phenocryst minerals. Fine-grained to glassy groundmasses of the rhyodacites are composed of alkali-feldspar and silica minerals. Tuffs in the Yucca Mountain area are mainly rhyolites and rhyodacites (Scott and others, 1983).

3.1.2. Ash-flow tuff

According to Smith (1960b), ash-flow tuffs can be subdivided, on the basis of their cooling history, into simple cooling units and compound cooling units. The following descriptions are mainly abridged from the work of Smith (1960a, 1960b). Ash-flow tuff may be deposited at variable temperatures (less than 100°C to as great as 800°C). Initial magmatic temperatures, mechanism of eruption, and transport distance from the source are controlling factors for the emplacement temperature.

3.1.2.1 Simple cooling unit

A simple cooling unit is the result of a single eruption or several closely-timed eruptions that are emplaced in rapid succession and cooled as a single unit. Tuff deposits above the minimum welding temperature, approximately 550°C in the presence of water vapor (Smith, 1960a), will weld. Welding is the process of compaction and cohesion of glassy fragments by viscous deformation (Smyth and others, 1978, p. 7). Ash-flow tuff when initially deposited varies vertically with respect to temperature and lithostatic load. Consequently, vertical variations in degrees of welding give rise to distinct welded zones. Based upon the degree of welding and crystallization, under ideal conditions, a simple cooling unit can be subdivided, from top to bottom, into five distinct zones (Figure 3-3): (1) upper nonwelded zone; (2) upper partially welded zone; (3) densely welded zone; (4) lower partially welded zone; and (5) lower nonwelded zone. The contacts of these zones are gradational. Welding zones within a cooling unit vary in porosity and bulk density (Figure 3-4). The degree of welding in part

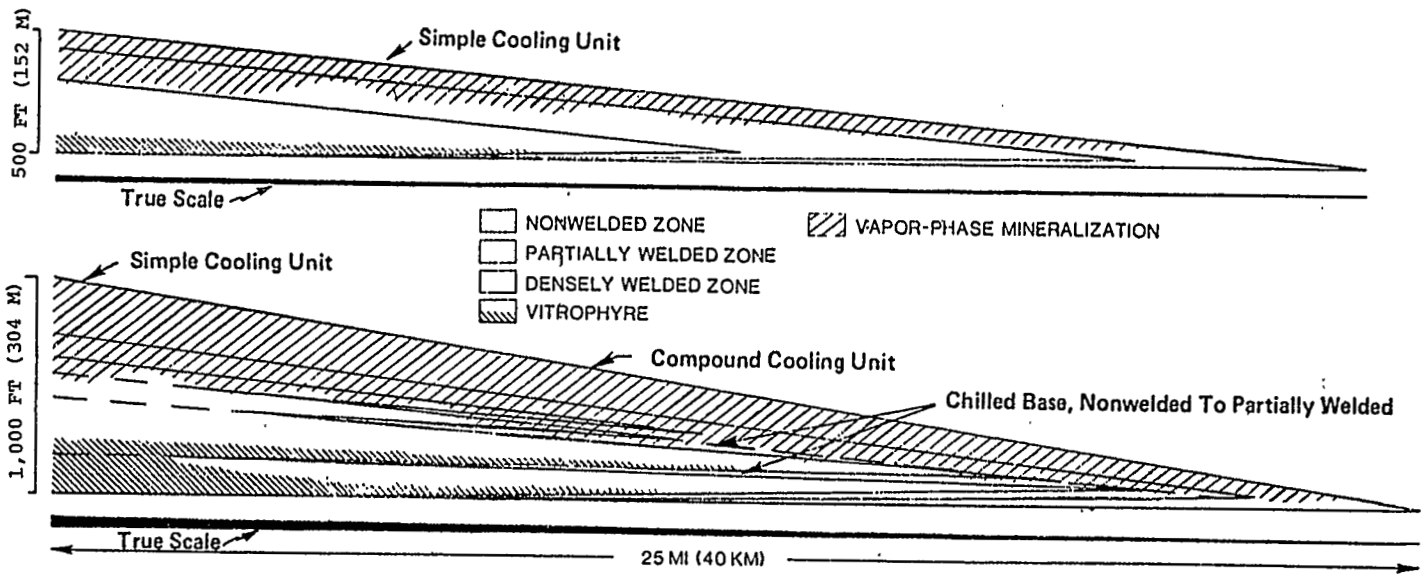

Figure 3-3. Zones of ash-flow cooling units (after Smith, 1960b).

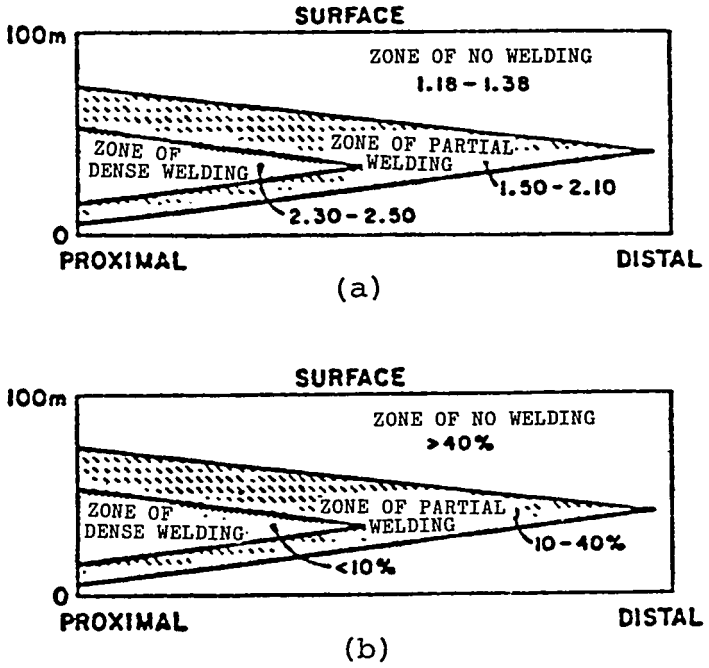

Figure 3-4. Representative values of (a) bulk dry density (gm/cm^3) and (b) percent porosity by volume with respect to the welding zones of a cooling unit. Data are compiled by Smyth and others (1978) from Ratte and Steven (1967), Sheridan (1970), and Smith and Bailey (1968).

determines the type and degree of crystallization, which includes devitrification of glass shards and formation of vapor-phase minerals in pore spaces. Welding is dependent on composition of the ash, composition of the volatiles, emplacement temperature, and overburden (French and Freeman, 1979).

The upper nonwelded and partially welded zones are absent in places because of erosion, alteration to clay by weathering, or possibly hurricane sandblasting that occurred during a later eruption (Mackin, 1960). In the nonwelded zone, pumice will exist as undeformed fragments. With increased welding, pumice becomes progressively flattened normal to the compaction.

The densely welded zone is usually several times thicker than the underlying partially welded and nonwelded zones. If the emplacement temperature is high enough, the densely welded zone in a thick flow may extend to the base and remain glassy after cooling, except for a narrow interior zone that is devitrified. Pumice in the densely welded zone is generally flattened into discoidal glassy bodies that are usually darker than the surrounding matrix. Phenocrysts such as biotite are often present with a preferred orientation, roughly normal to the plane of compaction. Extreme welding in an ash flow results in a vitrophyre in which all porosity has been eliminated, and ash and pumice have been essentially homogenized into a dense obsidian-like rock. Vitrophyres usually occur at the base of the densely welded zone as dense glass layers that are useful marker beds (Smith, 1960b). In a densely welded zone, well developed cooling joints are present. These joints are usually in a rectangular pattern spaced from a few inches to a few feet apart, and generally normal to the layering of a flow. The cooling joints may deviate from this general orientation over buried topographic irregularities (Ross and Smith, 1961).

The lower partially welded and nonwelded zones have the same characteristics as their upper counterparts, but under ideal conditions these lower zones are thinner. The lower zones represent the chilled lower margin of the ash flow.

Within a simple cooling unit, individual ash flows may have slight differences in their chemical and physical properties. Ash flows are usually separated by partings that may be marked by concentrations of lump pumice; fine- to coarse-bedded air-fall ash, lapilli, or blocks; bedded ash from a reworking of the surface of the ash flow by wind or water; and minor erosional unconformities. In some densely welded tuffs, however, the partings between two ash flows may be obscured.

3.1.2.2. Compound cooling unit

A compound cooling unit (Figure 3-3) is the result of successive eruptions from the same source that were in close enough succession to interrupt the cooling history of a simple ash flow (Smith, 1960a). Factors contributing to compound cooling are unequal areal distribution of individual ash flows; degree of development of phenomena that cause the partings; successive emplacement of ash flows of radically different temperatures; and periodicity of eruptions.

Compound cooling units are characterized by pronounced deviations in the pattern of zones described for simple cooling units. The following features may be indicative of compound cooling: (1) reversal of relative thickness of upper and lower zones of partial welding; (2) extensive development of a vapor-phase zone below a devitrified zone of dense welding with a transitional contact between the two zones; (3) a basal nonwelded zone that is many times thicker than overlying zones; (4) visible reversals in density or porosity within the zones of welding, exclusive of those related to differing mineral facies; and (5) extensive development of columnar joints below a zone of dense welding.

3.2 Mineralogic Characteristics

3.2.1 General properties

Minerals in the ash-flow tuffs can be grouped into the vapor-phase, the groundmass phase, and the phenocryst phase. Quartz, sanidine, plagioclase, and biotite are common phenocryst minerals in an ash-flow tuff. Other less common phenocryst minerals include pyroxene, hornblende, apatite, zircon, and magnetite. Lithic fragments, pieces of country rock picked up during eruptions, are found near the base of an ash-flow tuff. The groundmass of an ash-flow tuff consists of ash material of less than 0.25 millimeter in size, and is often devitrified into cristobalite and feldspar (Ross and Smith, 1961). The vapor-phase minerals, usually concentrated in the upper part of an ash-flow tuff, commonly result from the presence of gasses. Zeolites, cristobalite, tridymite, and sanidine are the most common vapor-phase minerals.

Glass shards and pumice are the main constituents of bedded or reworked tuff. Zeolites and smectites are common secondary minerals.

Mineral abundance in selected drill holes within the interval of interest is included in Appendices 3.1 and 3.2.

3.2.2 Secondary mineralization

Alteration of tuff is important to assessing a candidate respository site in tuff. This is because some of the secondary minerals, especially some of the zeolite and smectite minerals, have high sorptive coefficients for large-radius cations (Smyth and others, 1978) and can aid in the long-term isolation of high-level nuclear waste (Bish and others, 1983b). There are two types of alteration in tuff, devitrification and zeolitization. Devitrification is the conversion of the glassy texture of the rock to a crystalline texture. Zeolitization involves the introduction of or replacement by a mineral (or minerals) of the zeolite group. The minerals that result from both types of alteration include anhydrous phases such as quartz, calcite, and feldspar, or hydrous phases such as zeolites, smectites and manganese minerals (Bish and others, 1983b).

Bish and others (1983a) studied zeolite samples from USW-H3, -H4, and -H5 (Levy, 1984) and suggested three episodes of zeolitization in the upper Crater Flat Tuff and the overlying units. The earliest episode was shallow buried

diagenesis of the Tuff of Calico Hills and the upper Crater Flat Tuff, before the emplacement of the overlying Paintbrush Tuff. The second episode involved crystallization of heulandite and smectite during the late stage devitrification of the lower vitrophyre in the Topopah Spring Member (Levy, 1983). According to Levy (1983), the distribution of heulandite and smectite in the vitrophyre appears to be controlled mainly by the location of the devitrified tuff-glassy tuff transition zone in the Topopah Spring Member. A third episode of zeolitization occurred after the Paintbrush Tuff and older units of Yucca Mountain were displaced downward to the east.

In general, the distribution of zeolitized and nonzeolitized tuff is related to present and former elevations of the static water level (Levy, 1984). Zeolitization in the southern part of Yucca Mountain is sparse in the upper Crater Flat Tuff and the overlying tuff units. In the northern part of Yucca Mountain, heavy zeolitization occurs in the Tuff of Calico Hills and the nonwelded base of Topopah Spring Member (Bish and others, 1983a). The amount and nature of alteration deeper in vitrophyre is highly variable. According to Levy (1983), the variation may be related to factors influenced by thickness of the tuff units or proximity to the volcanic source. Some variation in amount of alteration is probably also related to local conditions such as fracture abundance.

Beneath the exploration block at Yucca Mountain, four intervals of zeolitization have been recognized (Table 3-1) (Bish and others, 1983a). The first interval is a zeolite- and clay-rich zone that commonly occurs at the top of the lower Topopah Spring vitrophyre. Zeolitization in this interval may result from alteration concentrated along the devitrified front at the top of the vitrophyre. Heulandite is the common zeolite in this inverval. This interval tends to be thin (less than 3 meters) except in drill hole UE25a-1 (Sykes and others, 1979), where it passes directly into the second interval. The second interval is a relatively thick zeolitized zone that may occur in the bedded, nonwelded, and poorly welded tuffs that form the base of Topopah Spring Member and in the underlying Tuff of Calico Hills. In some locations, this interval is in the lower vitrophyre of the Topopah Spring Member. Clinoptilolite is the dominant zeolite in this interval. In places, mordenite may also occur. Lateral distribution of zeolitization is inconsistent in the second interval. It is complete vitric and unzeolitized in drill holes USW-G3 (Vaniman and others, 1984) and USW-H3 (Levy, 1984); elsewhere the zeolitized zone ranges in thickness from 29.5 feet (9 meters) in drill hole USW-H5 (Levy, 1984) to approximately 492 feet (150 meters) in drill hole UE25a-1. The wide range in thickness indicates that the second interval is thin or absent along the crest of Yucca Mountain and thickens dramatically downdip to the east and toward Drill Hole Wash. The third and fourth intervals occur in the Crater Flat Tuff, which is below the static water level in the area of interest. Clinoptilolite is the dominant zeolite with minor occurrence of mordenite in the third interval. The thickness of this interval ranges from 111.6 feet (34 meters) to 298.6 feet (91 meters). Clinoptilolite is the dominant zeolite in the fourth interval except in drill hole UE25a-1, where mordenite is dominant. The thickness of the fourth interval varies from 88.6 feet (27 meters) to 144.4 feet (44 meters).

Table 3-1. Depth, thickness, and zeolite abundances in commonly zeolitized intervals beneath Yucca Mountain (after Vaniman and others, 1984)

	USW-G1 SWL=1,893 ft (577 m) deep*	UE25a-1 UE25b-1 SWL=1,542.0 ft (470 m) deep	USW-G4 SWL=1,775.0 ft (541 m) deep	USW-H4 SWL=1,702.8 ft (519 m) deep
Interval I: above the lower Topopah Spring vitrophyre	depth: 1,286.1 - 1,288.4 ft (392 - 392.7 m) 15% cpt*	depth: 1,263.2 - 1,273.0 ft (385 - 388 m) 7% cpt	depth: 1,299.2 - 1,314.0 ft (396 - 400.5 m) 10% (±12) cpt	depth: 1,171 - 1,184.4 ft (357 - 365 m) no analyses
Interval II: base of the Topopah Spring unit, Tuff of Calico Hills	depth: 1,394.4 - 1,857.0 ft (425 - 566 m) 52% (±17) cpt	depth: 1,326.5 - 1,824.2 ft (404 - 556 m) 67% (±6) cpt 17% (±20) mord*	depth: 1,378.0 - 1,788.1 ft (420 - 545 m) 50% (±19) cpt 5% (±7) mord	depth: 1,312.4 - 1,653.6 ft (400 - 504 m) 63% (±13) cpt 8% (±12) mord
Interval III: between the Prow Pass and Bullfrog units	depth: 2,040.8 - 2,316.4 ft (622 - 706 m) 45% (±12) cpt 18% (±18) mord	depth: 2,086.7 - 2,329.5 ft (636 - 710 m) 60% cpt and mord	depth: 1,968.6 - 2,237.6 ft (600 - 682 m) 32% (±12) cpt 19% (±10) mord	depth: 1,955.5 - 2,290.1 ft (596 - 698 m no analyses
Interval IV: between the Bullfrog and Tram units	depth: 2,555.9 - 2,700.3 ft (779 - 823 m) 37% (±6) 15% (±11) mord	depth: 2,838.5 - 2,920.1 ft (863 - 890 m) 4% (±4) cpt 16% (±10) mord	depth: 2,716.7 - 2,821.7 ft (828 - 860 m) 8% (±8) cpt 38% (±32) mord	depth: 2,510.0 - 2,539.5 ft (765 - 774 m) no analyses

Table 3-1. Depth, thickness, and zeolite abundances in commonly zeolitized intervals beneath Yucca Mountain--concluded

	USW-H5 SLW=2,309.8 ft (704 m) deep	USW-H3 SLW=2,473.9 ft (754 m) deep	USW-GU3 USW-G3 SWL (see USW-H3)
Interval I: above the lower Topopah Spring vitrophyre	depth: 1,591.3 ft (485 m) 10% cpt	depth: 1,204.1 - 1,317.2 ft (367 - 371 m) no anlayses	depth: 1,181.2 - 1,194.3 ft (360 to 364 m) trace cpt
Interval II: base of the Topopah Spring unit, Tuff of Calico Hills	depth: 1,916.1 - 1,948.9 ft (584 - 594 m) 37% cpt	VITRIC (nonzeolitized)	VITRIC (nonzeolitized)
Interval III: between the Prow Pass and Bullfrog units	depth: 2,149.1 - 2,260.6 ft (655 - 689 m) 60% cpt	depth: 2,801.3 - 2,001.4 ft (549 - 610 m) 68% cpt	depth: 1,827.5 - 2,011.3 ft (557 - 613 m) 58% (±8) cpt
Interval IV: between the Bullfrog and Tram units	no samples	depth: 2,401.7 - 2,493.6 ft (732 - 760 m) 52% (±17) cpt 18% (±13) mord	depth: 2,546.1 - 2,697.0 ft (776 - 822 m) 36% (±8) cpt

* SWL = static water level, cpt = clinoptilolite and heulandite, and mord = mordenite.

3.2.3 Mineral stability

As mentioned above, zeolites and smectites are common secondary minerals in tuffs. Their cation exchange and sorptive properties allow these minerals to retard the migration of various radionuclides in aqueous solution (Bish and others, 1983b; Smyth, 1982; Smyth and Caporuscio, 1981). On the other hand, zeolite and smectite minerals dehydrate at elevated temperatures and at low water-vapor pressures, and the cation exchange capacity in general diminishes with loss of water (Deer and others, 1971). Furthermore, under unsaturated conditions dehydration of these minerals can cause contraction of the unit cell (Boles, 1971, 1972; Greene-Kelly, 1957; Grim, 1968) and evolution of fluids. Thus, they may provide both a pathway (shrinkage fractures) and a driving force (fluid pressure) for release of radionuclides to the biosphere, and may completely alter the physical and chemical properties of the host rocks (Bish and others, 1983; Smyth, 1982; Smyth and Caporuscio, 1981). In addition to zeolite and smectite minerals, hydrated volcanic glasses are also present in some of the tuff units as a major constituent. Much of the hydrated volcanic glass has been transformed to zeolites and one or another silicates (Bish and others, 1983; Levy, 1983).

Major mineralogic changes have occurred in the tuffs at temperatures below 100°C (Smyth, 1982). If nuclear waste is placed in these rocks, further changes are expected. These changes include dehydration and crystallization of zeolites and smectites. Understanding the stability of these minerals is essential for performance assessment of a geologic site in tuffs.

The principal zeolite phases in the tuffs of Yucca Mountain area are heulandite, clinoptilolite, mordenite, and analcime. According to Smyth (1982), two types of reaction in these tuffs may occur at temperatures below 200°C; (1) simple reversible dehydration, and (2) complex mineralogic phase changes. Dehydration involves the loss of loosely bound water of hydration in the zeolites and the development and propagation of fractures. It results in loss of mechanical strength of the host rocks. Complex mineralogic phase changes involve complete recrystallization and exchange of cations and/or water with the environment. Such reactions may evolve or incorporate significant quantities of water and result in volume changes in large quantities of rock and incorporated fluids.

When heulandite is slowly heated, part of its initial water is lost rapidly at first and then slowly up to 200°C, at which temperature the mineral again begins to dehydrate rapidly (Figure 3-5). According to Breger and others (1970), the structural transformation of heulandite begins at 55°C, above the temperature at which loss of tightly bound water starts. This transition is in part accompanied by an irreversible structural change. There are contracted phases that appear at temperatures as low as 202°$\pm$ 3°C (Boles, 1972). In general, however, the higher temperatures are required to contract the sample. The molar volume decrease of heulandite is approximately 3.6 percent below 300°C.

The dehydration behavior of clinoptilolite (Figure 3-6) is similar to that of heulandite except that loss of tightly bound water begins at a somewhat

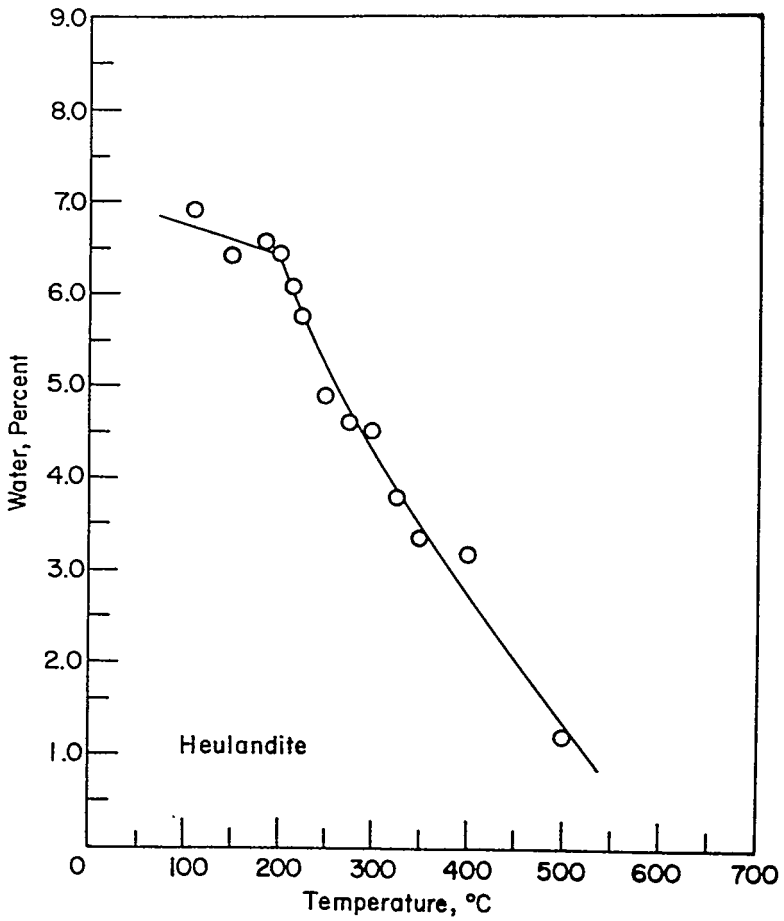

Figure 3-5. Water content of heulandite after heating to various temperatures (Breger and others, 1970).

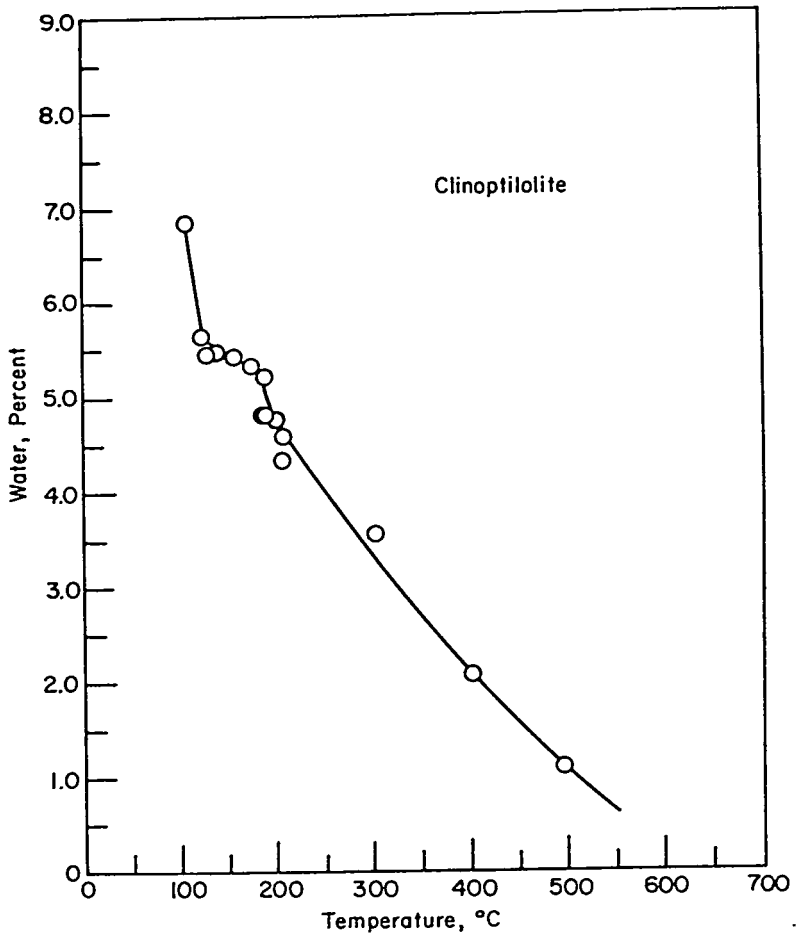

Figure 3-6. Water content of clinoptilolite after heating to various temperatures (Breger and others, 1970).

lower temperature (185° to 190°). Upon heating in a dry atmosphere between 200° to 300° C, followed by cooling, clinoptilolite dehydrates into two contracted phases (Alietti, 1972; Boles, 1971, 1972; Breger and others, 1970). The more alkalic and silicic the clinoptilolite, the higher is the temperature at which the contracted phases appear. The contracted phase decreases its volume by as much as 10 percent (Smyth, 1982). Bish (1984) examined six natural and three cation exchanged clinoptilolites and found that the unit cell of all samples decreased in volume between 20° to 300°. Among these samples, Na-saturated clinoptilolite had the greatest volume reduction (8.4 percent) and K-saturated clinoptilolite had the smallest volume reduction (1.6 percent). The volume decrease for the Ca-saturated clinoptilolite was 3.6 percent. It is apparent that the effects of heating on volume depend strongly on the exchangeable cation content. Directionally, the highest percentage decrease for every sample was along the b axis, generally making up 80 to 90 percent of the total volume decrease. The change along the a axis was the smallest, usually less than 5 percent, although 26.5 percent of the contraction of the Na-exchanged clinoptilolite was along the a axis.

Mordenite behaves similarly to clinoptilolite on dehydration, as indicated by the studies of Schlenker and others (1979a, 1979b). It loses loosely bound water on increased temperatures up to 300°C. Water loss is accompanied by a reduction in unit cell volume of as much as 8 percent (Smyth, 1982).

No detailed information on the dehydration behavior of analcime has been found in the open literature. Because analcime contains substantially smaller amounts of water than clinoptilolite and mordenite, dehydration effects on this mineral are likely less pronounced (Smyth and Caporuscio, 1981).

Under repository conditions, Smyth and Caporuscio (1981) reported preliminary data outlining potential effects of dehydration reactions in clinoptilolite and analcime tuffs. They concluded that major dehydration (loss more than 3 percent by weight) does not occur at temperatures less than 100°C if the zeolites remain equilibrated with liquid water. Minor dehydration (loss of 2 percent or less water by weight), however, is likely to occur. As pointed out earlier, clinoptilolite and mordenite have limited thermal stability and tend to form denser, less hydrous phases at elevated temperatures. It is likely under the repository conditions the reactions have the potential to release large amounts of water, to cause significant volume reduction with development and propagation of fractures, and to alter the physical and chemical properties of the host rocks. The reaction of clinoptilolite to analcime appears to take place at relatively low temperatures and, hence, has the greatest potential to constrain thermal loadings. This reaction has been observed in the labortatory in pore fluids that consist of approximately 5,000 ppm of sodium (pH = 11) at 100°C in 21 days (Boles, 1971). In the field, analcime is reported to form at temperatures as low as 85°C in sodic pore fluids with concentration approximately 10,000 ppm (pH = 8.5) (Figure 3-7).

Figure 3-8 is a plot of the observed geothermal gradient in drill hole USW-G1. Also plotted are the maximum paleogeothermal gradient, as inferred from the first appearance of analcime and albitized tuffs in drill hole

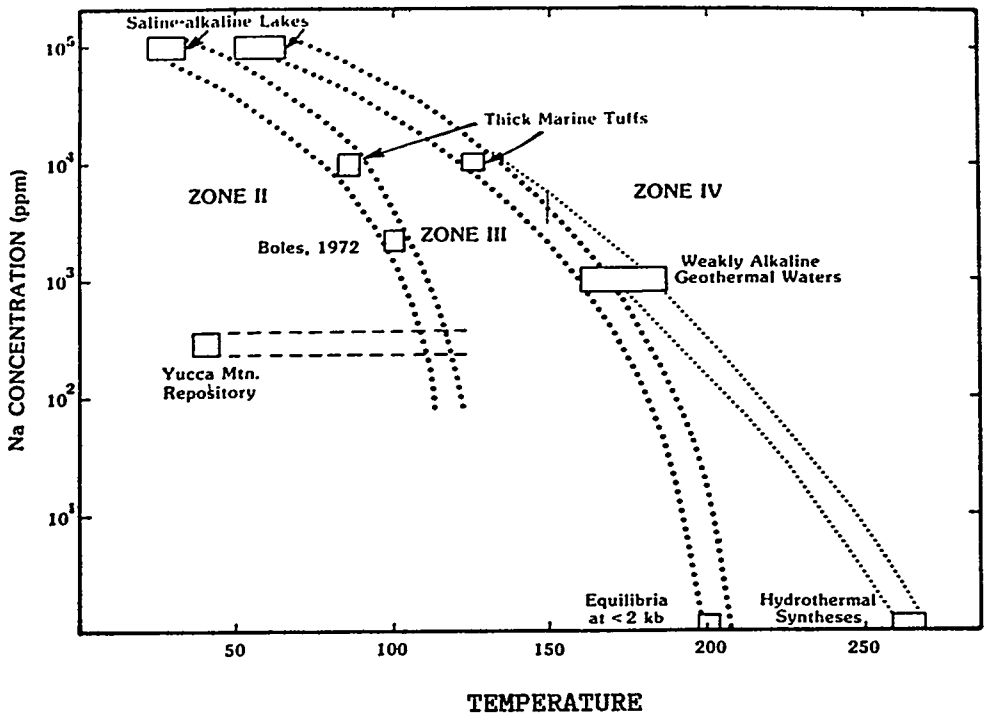

Figure 3-7. Na concentration vs. temperature for reactions bounding zeolite zones (after Iijima, 1975). The lowest temperature and concentration field is for the assemblage alkali clinoptilolite + silica + H_2O and corresponds to Zone II (see Appendix 3.4). The reaction of the assemblage to analcime + quartz + H_2O is delineated by three data points: temperatures of saline alkaline lakes, those of thick marine tuffs, and the laboratory experiment of Boles (1972). The reaction of the assemblage analcime + quartz + H_2O (Zone III) to albite + quartz + H_2O is bounded by four data points: saline alkaline lakes (e.g., Mariner and Surdam, 1970), thick marine tuffs (Iijima and Ohwa, 1980), weakly alkaline geothermal waters (e.g., Honda and Muffler, 1970), and some laboratory experiments (e.g., Liou, 1971; Saha, 1959). The composition of water from drill hole J-13 in Jackass Flat is plotted at the approximate ambient temperature of possible repository horizons at Yucca Mountain (Smyth, 1982).

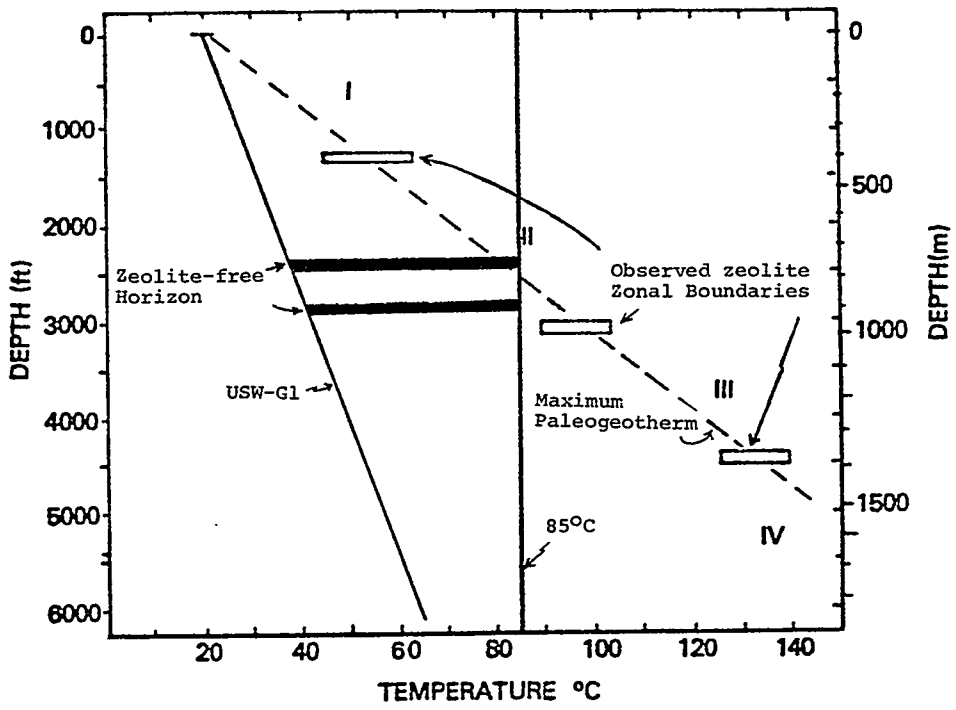

Figure 3-8. Approximate temperatures vs. depth from drill hole USW-G1 (after Smyth and Caporuscio, 1982). Possible repository locations are in the center of the two zeolite-free horizons 197 to 328 feet (60 to 100 m) thick. The length of the horizontal bars corresponds to the maximum allowable induced temperature increases resulting from emplaced wastes.

USW-G1, and the temperature of clinoptilolite-analcime transition. From Figure 3-8, it appears that maximum temperature rises in zeolitic zones adjacent to these potential repository host zones will be limited to about 50°C (Smyth, 1982). According to Smyth (1982), preliminary thermal conduction models for a repository located at 2,625-foot (800-meter) depths in Yucca Mountain indicated that temperatures in clinoptilolite zones will not exceed 85° if reprocessed high-level waste is emplaced at a gross thermal loading of 75 Kw/acre (Tyler and Langkopf, 1980). Calculations for spent fuel emplaced at the same loading, however, indicated that temperatures in zeolite zones may reach 110° to 120°C.

Smectites comprise up to 50 percent of individual tuff units and occur both as discrete layers and along perlitic fractures in vitrophyres. In the unsaturated zone, these minerals are Na-Ca-K-saturated smectites with slightly higher-than-normal layer charge (Bish and others, 1983). There is little, if any, interstratified illite occurring at depths shallower than about 3,000 feet (900 meters) in the tuffs below the surface of the Yucca Mountain area (Bish, 1983; Bish and others, 1982). Smectites have the ability to rapidly and reversibly expand and collapse in response to minor changes in temperature and humidity (Norrish, 1972; Tien and others, 1975). Upon heating, smectites begin to dehydrate at temperatures less than 50°C. In general, the dehydration at temperatures below 200°C results from the loss of sorbed water (Greene-Kelly, 1957), the amount of which is contingent upon the hydration energy of the adsorbed cations (Mackenzie, 1964). Therefore, the weight loss at a given temperature for smectites of different composition varies (Figure 3-9). Smectites will undergo volume reduction along the c axis in response to dehydration. Rehydration of smectites after preheating to temperatures in the 200° to 500°C region has been investigated in detail (Greene-Kelly, 1957). The maximum temperature from which a hydrated smectite mineral can be rehydrated depends upon the saturation of cation species, particle size, and crystallinity. Hofmann and Endell (1939) reported that Li-saturated smectite loses its power to re-expand with moisture after heating to temperatures in the 105° to 125°C range, while H-saturated and Ca-saturated samples can be heated to 300° to 390°C, and a Na-saturated sample can be heated to 390° to 490°C before dehydration becomes irreversible. Various heat-treatments on smectites and observation of their changes in the laboratory are short in duration of time. It is likely that a complete dehydration of smectites can take place at much lower temperatures over extended periods of time.

3.3 Petrology and Mineralogy of Individual Stratigraphic Units

This section provides a description of the petrology and mineralogy of each of the stratigraphic units within the unsaturated zone at Yucca Mountain. Because of their potential use as repository host units, special emphasis is on the Topapah Spring Member of the Paintbrush Tuff and the Bedded Tuff of Calico Hills. The lithology and mineral zones of the tuffs from selected drill holes are illustrated in Appendix 3.3. Except as otherwise noted, the following descriptions are based on the work of Bish and others (1981, 1982), Daniels and others (1981), Hagstrum and others (1980), Levy (1983, 1984), Lipman and McKay (1965), Maldonado and Koether (1983), Spengler and Rosenbaum,

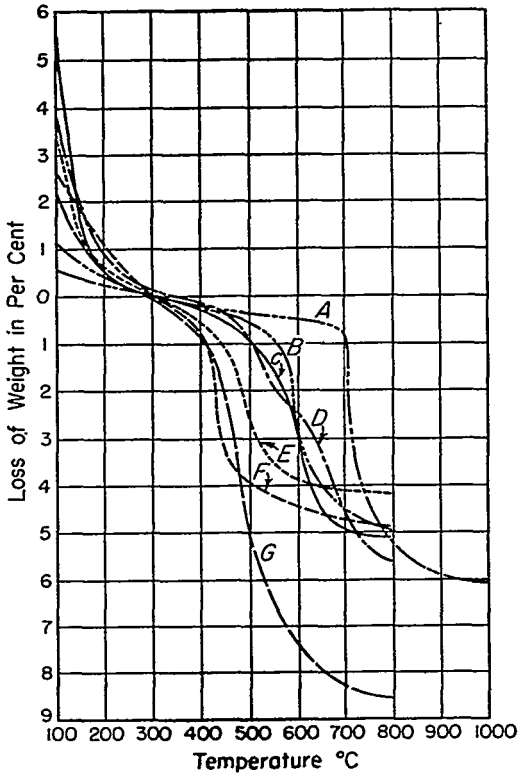

Figure 3-9. Dehydration curves of smectites (after Ross and Hendricks, 1945). (A) Hectorite, Hector, California; (B) montmorillonite, Belle Fourche, South Dakota; (c) montmorillonite, Tatatilla, Mexico; (D) montmorillonite, Montmorillon, France; (E) nontronite, Spokane, Washington; (F) nontronite, Sandy Ridge, South Carolina; (G) montmorillonite, Pontotoc, Mississippi.

(1980), Spengler and others (1979, 1981), Sykes and others (1979), Vaniman and Crowe (1981), and Vaniman and others (1984). For detailed descriptions on mineralogy and petrology, the reader is encouraged to refer to their reports.

3.3.1 Alluvium and colluvium

As mentioned above, the alluvium and colluvium consist of gravel, sand, and silt that are composed predominantly of ash-flow and ash-fall tuff debris. Petrologically, this nonwelded to densely-welded, vitric to devitrified debris is derived from the Paintbrush Tuff and is classified as sandy to pebbly gravel or submature volcanic arenite. The deposits are locally cemented by secondary calcium carbonate (caliche) that forms thin coatings on the gravels up to boulder-size. Spengler and others (1981) report the occurrence of such secondary calcium carbonate from drill hole USW-G1. The same description has also been given by Spengler and Rosenbaum (1980) for surfacial deposits at drill hole UE25a-7. In drill hole J-13, sand grains are coated with detrital clay (Heiken and Bevier, 1979). The presence of caliche in the alluvial deposits indicates that precipitation of calcium carbonate took place at shallow depths by evaporation and transpiration of downward solution.

3.3.2 Paintbrush Tuff

All four members of the Paintbrush Tuff represent ash-flow tuff units separated by thin ash-fall tuff and tuffaceous sediments (Spengler and others, 1981). The members are genetically, chemically, and petrographically related (Orkild, 1965). The uppermost and lowermost members of the Paintbrush Tuff are compound cooling units. The intervening members are simple cooling units (Spengler and others, 1981).

3.3.2.1 Tiva Canyon Member

Petrologically, the Tiva Canyon Member can be divided into a multiple-flow compound cooling unit overlying a bedded tuff unit (Lipman and McKay, 1965). The multiple-flow compound cooling unit consists of a vitric ash-flow sheet of moderately to densely welded tuff that progressively grades downward to a nonwelded base unit. The bedded tuff unit consists of reworked tuff and forms the lower unit of the Tiva Canyon Member (Spengler and Rosenbaum, 1980).

Within the multiple-flow compound cooling unit, both vitric and vapor phases are present. The vitric phase has been replaced by authigenic K-feldspar and silica minerals. Vapor-phase crystallization occurs most often as crystalline rims of fillings of vugs (Bish and others, 1982).

Phenocrysts, usually alkaline-feldspar (andesine/oligoclase), sanidine, hornblende, orthopyroxene, biotite, magnetite, and some titanite, are present in various quantities depending upon the stratigraphic and geographic locations, but are commonly less than 14 percent by volume (Bish and others, 1982). At drill hole UE25a-1, the densely welded upper zone is poor in phenocrysts (Spengler and others, 1979), which include less than 5 percent of sanidine, magnetite, plagioclase, honrblende, and titanite. The nonwelded base of the compound cooling unit is relatively crystal-rich, consisting of

approximately 14 percent oligoclase, sanidine, biotite, magnetite, and orthopyroxene. In the bedded tuff unit, a total of 11 percent of alkaline feldspar (andesine/oligoclase), sanidine, biotite, magnetite, and orthopyroxene is counted as phenocrysts. At drill hole J-13 the phenocrysts range from approximately 9 percent near the top of the compound cooling unit to a trace near the nonwelded base. In general, the pumice clasts in a cooling unit decrease downward from about 15 to 2 to 5 percent (Heiken and Bevier, 1979). At drill hole USW-GU3, the Tiva Canyon Member is characterized by the predominance of sanidine phenocrysts (5 to 10 % of the rock), with minor amounts of titanite, and trace amounts of zircon, perrierite, and titanomagnetite throughout the unit. Locally, biotite, hornblende, oligoclase, clinopyroxene, and quartz are also present (Vaniman and others, 1984).

The matrix of the vitric tuff consists predominantly of cristobalite and alkali-feldspar with minor amounts of tridymite and biotite. Analysis of glasses from drill hole UE25a-1 indicates rhyolitic and dacitic compositions for the nonwelded base of the cooling unit and for the bedded tuff unit, respectively.

Zeolites are rare in the Tiva Canyon Member. According to Levy (1984), the bedded air-fall tuff in drill hole USW-H3 may be partly zeolitic. Other secondary minerals, such as calcite, have been reported from drill holes USW-G3 (Vaniman and others, 1984), and USW-H5 (Levy, 1984). Opaque Fe-Ti oxide minerals show a wide range of oxidation throughout the Tiva Canyon Member (Vaniman and others, 1984).

3.3.2.2 Yucca Mountain Member

The only report that provides a complete description of the petrology and mineralogy of the Yucca Mountain Member is that by Caporuscio and others (1982). The following summary is mainly from their report. The Yucca Mountain Member is subdivided petrologically into a simple cooling ash-flow tuff unit overlying a bedded tuff unit.

The ash-flow tuff is vitric nonwelded and partially welded (Bish and others, 1982; Spengler and Rosenbaum, 1980). It rests on bedded tuff that separates the ash-flow tuff from the underlying Pah Canyon Member. The bedded tuff includes air-fall and reworked tuffs and tuffaceous sand, most of which are thick bedded and vitric (Spengler and Rosenbaum, 1980).

In general, the cooling unit comprises a moderately to densely welded central core that is sandwiched by partly welded to nonwelded ash-flow tuff. Where the cooling unit is less than 50 feet (15.2 meters) thick, the unit is pink to gray, and the entire unit is nonwelded to partly welded vitric shard tuff. Where the unit is thicker, the welded central portions are purple-brown, and are thoroughly devitrified to either cristobalite-alkali feldspar intergrowths or mixtures of smectites and alkali-feldspars. Minor vapor-phase crystallization of tridymite occurs in cavities of the partly welded tuff in the upper part of the unit. Well-preserved shard structures have been observed in the lower nonwelded portions, but the groundmass and the outer margins of the glass shards are altered to authigenic smectites. In the

welded portions, the Fe-Ti oxide minerals are essentially unoxidized. The low oxidation state of the Fe-Ti oxides and the presence of unaltered glass in central portions of the large shards indicate that little, if any, movement of ground water occurs in this unit.

The phenocrysts, mostly sanidine and oligoclase with rare biotite and quartz, range from less than 1 to 3 percent. Approximately 3 to 10 percent of pumice lapilli are in the tuff. Small lithic inclusions of angular red-brown aphanitic volcanic rock have been observed rarely. Some of the tuffs of the Yucca Mountain Member are highly altered and contain from 30 percent to as high as 60 percent of smectites. Minor amounts of calcite in the tuffs have also been reported.

3.3.2.3 Pah Canyon Member

The Pah Canyon Member consists of a thin-bedded and reworked air-fall tuff unit overlain by a sequence of ash-flow tuffs that form a simple cooling unit. In drill holes UE25a-4 and -5, the base of the bedded tuff is marked by about a foot (0.3 meter) of light-red to moderate-red clay of a high degree of plasticity. This interval, however, is represented only by iron-staining in drill hole UE25a-7 (Spengler and Rosenbaum, 1980). The ash-flow tuff is vitric and mostly nonwelded with a moderately welded central zone (Bish and others, 1982). Because Caporuscio and others (1982) provide the only complete report on petrology and mineralogy of the Pah Canyon Member, and because the discussions by Bish and others (1982) are based on that report, their work forms the basis of the following descriptions.

On the basis of petrologic and mineralogic properties of the simple cooling unit, it is subdivided into upper nonwelded vitric, central moderately welded, and lower nonwelded vitric zones. At drill hole USW-G2, a heavily zeolitized unit occurs between the lower nonwelded vitric zone and the bedded and reworked air-fall tuff unit (Bish and others, 1982). Elsewhere, the bedded and reworked air-fall tuff is directly in contact with the lower nonwelded vitric zone.

In the upper nonwelded vitric zone, glass, smectites, and alkali-feldspar are major constituents. Groundmass glass has altered to smectite, but glass shards and pumice clasts remain unaltered. Iron-titanium oxide minerals in this zone are slightly to moderately oxidized.

The central moderately welded zone is characterized by devitrification and zeolitization. As a result of devitrification, growth of cristobalite and sanidine in some glass shards has occurred. Zeolitization followed the devitrification, and the remaining glass was replaced by heulandite, smectite, and minor amounts of opal. The dominant constituent of the groundmass is smectite, which may reach amounts up to 30 to 50 percent. Vapor-phase crystallization of cristobalite and sanidine occurred as thin linings along the fracture walls and, later, heulandite and opal filled in the fractures. Iron-titanium oxides in the central zone are in moderately high oxidation states.

In the lower nonwelded vitric zone, glass shards, pumice clasts, and groundmass are unaltered; however, the glass content in this zone is less than that in the upper nonwelded vitric zone. Zeolitization has not been observed in this zone. Other constituents include smectite, alkali-feldspar, and calcite. Calcite occurs in a significant amount in the open portions of the groundmass and pumice. Smectite in this zone is higher than it is in the upper nonwelded vitric zone, and may reach as high as 50 percent. Iron-titanium oxides are slightly to moderately oxidized.

The heavily zeolitized pumice unit encountered in drill hole USW-G2 contains predominantly heulandite and calcium-clinoptilolite with minor amounts of tridymite. Pumice in this unit is large and undeformed, with zeolite and smectite pseudomorphs.

Glass shards and pumices are the main constituents of the bedded tuff unit. A significant amount of calcite occurs in the open portions of the pumices.

Tuffs of the Pah Canyon Member contain 1 to 6 percent phenocrysts that mainly are alkali feldspar with minor amounts of biotite, augite, and quartz. In general, the phenocryst content is higher in the upper portions than in the lower portions of the sections. Small lithic fragments of volcanic rocks measuring 0.1 to 0.3 inch (0.25 to 0.76 centimeter) compose 1 to 2 percent of the Pah Canyon Member.

The presence of unaltered glass and the slight to moderate oxidation states of Fe-Ti oxides in both upper and lower vitric zones may indicate that these two zones have not been saturated by ground water for any significant period of time. On the other hand, the significant amounts (up to 30%) of heulandite and relatively high oxidation states of Fe-Ti oxides in the central moderately welded zone at drill hole USW-G2 may be significant and indicative that this central zone has been partly or completely saturated by ground water. Because this zone is far above the present static water table at drill hole USW-G2, and no zeolite occurrences are reported in the lower nonwelded vitric zone, Bish and others (1982) interpret that a local perched water table over the densely welded Topopah Spring caprock may cause this anomaly, and the porous areas in the lower nonwelded zone were sealed by calcium-carbonate before zeolitization took place.

3.3.2.4 Topopah Spring Member

The Topopah Spring Member is the lowermost and thickest stratigraphic unit of the Paintbrush Tuff. It comprises a major compound cooling, multiple flow unit and a minor thin bedded and reworked tuff unit at the base of the member. The compound cooling, multiple flow unit represents a typical ignimbrite sheet in which both the nonwelded upper and lower parts progressively grade into the densely welded central part, wherein the innermost zone is characterized by lithophysae (Spengler and others, 1981). As in the other members of the Paintbrush Tuff, the ash-flow tuff of the Topopah Spring Member rests on a sequence of bedded air-fall and reworked tuffs that separate it from the underlying bedded tuff of Calico Hills.

Based upon the lithologic properties, the compound cooling unit is subdivided into five zones. In descending order, they are the upper ash flow, the upper vitrophyre, the central crystallized interior, the lower vitrophyre, and the lower ash flow.

The upper ash flow is a phenocryst-poor (less than 2%) pumiceous tuff. It is poorly bedded and nonwelded to moderately welded. Commonly, the tuff is partly silicified or otherwise altered. At drill holes USW-G1 and UE25a-1, the glass is unaltered, but at drill hole USW-G2, 70 to 90 percent of the glass has been replaced by heulandite and calcium-rich clinoptilolite. The upper ash-flow zone grades downward, by increasing the degree of welding, into the upper vitrophyre zone.

The upper vitrophyre zone comprises red and black, densely welded, partially devitrified, crystal-rich ash-flows. Disseminated hematite and rutile are found in association with vitric pumice lapilli that measure greater than 0.28 inch (0.7 centimeter). Along the margins of pumice walls and perlitic fractures, smectites are found. Patches of devitrified cristobalite and alkali feldspar are minor constituents locally within the pumice clasts. Groundmass in the upper vitrophyre zone is altered to clay partly by partial devitrification and authigenic crystallization. Some of the shards are clear and glassy. Others have devitrified to sheaves of cristobalite and alkali feldspar oriented parallel to the long axis of the shards. Phenocrysts are common, making up 20 percent of the rock. The phenocrysts are mainly sanidine, plagioclase, and anorthoclase with minor amounts of quartz, biotite, clinopyroxene, and Fe-Ti oxides. The upper vitrophyre zone grades downward into the central crystallized interior zone.

The central crystallized interior zone is the thickest subunit within the Topopah Spring Member, and consists of moderately to densely welded crystal tuff. The uppermost portion of this subunit is red-brown, devitrified, densely welded ash flow characterized by distinctive gray-white eutaxitic pumice. The presence of tridymite along the walls of vugs indicates that the vapor phase crystallization has caused extreme alteration of the tuff. Veins in the tuff are partly to wholly filled by tridymite, calcite, and clays. Primary structures of the flat pumice lapilli have been obscured by devitrification. The open areas within the pumice have been filled by spherulite and granular aggregates of cristobalite and alkali feldspar. Multiple growth of spherulites is common. The final infill materials in some tridymite pockets that overprint on the pumice are clays and oxides. The groundmass is dark brown and consists of smectite and devitrified shards. The textures of the shards are axiolitic and granular. The middle portions of the crystallized interior zone are purple-gray, lithophysal, welded tuffs. Distinctive angular lithic inclusions of red-brown porphyritic volcanic rocks are characteristics near the top. The lower portions of this interior zone consist of brown devitrified, densely welded tuffs. Vapor-phase alteration is common in both middle and lower portions. In general, between the densely welded individual cooling units, there are tuffs of moderate welding. According to Bish and others (1982), four stages of devitrification and vapor-phase crystallization can be recognized in pumice lapilli within the middle and lower portions of the interior zone. At the very beginning, small spherulites, sheaves of

cristobalite and/or axiolitic minerals nucleate on the outer margins of the pumice and grow inwards. The second stage is that interlocking, mottled spherulites partially fill open spaces in the pumice. That is followed by vapor-phase crystallization of tridymite and alkali feldspar. Finally, granophyric crystallization takes place in interstitial spaces in which the groundmass is characterized by high clay contents, spherulites, granular quartz, and alkali feldspar. Plumose asymmetrical spherulites across the relict pyroclast boundaries are common in some samples from these intervals. Abundant lithophysal cavities occur in areas of intense vapor-phase development. Crystals of alkali feldspar and quartz (retrograded from tridymite) up to 1 millimeter grow into partially opened cavities. Fractures are also common in the middle and lower portions of the interior zone. Some of the fractures have been sealed by silica phases or calcium-carbonate; others are open. Chronologically, there are three types of fracture recognized. Those filled by silicates are contraction fraction fractures formed during cooling of the ash flows. These silicates are products of vapor-phase crystallization. Fractures of the second type are those filled by calcite and are younger than those filled by silicates. The open fractures are younger than those of the other two types. Areas with open fractures and abundant lithophysae may be significant in providing pathways for ground-water movement. Heiken and Bevier (1979) have reported a zone bearing zeolites over a 89.9-foot (27.4-meter) interval in densely welded tuffs of the interior zone at drill hole J-13. The occurrence of zeolite in the interior zone has not been reported at other drill-hole locations. The central crystallized interior zone grades downward into lower vitrophyre zone.

The lower vitrophyre zone consists of predominantly unaltered, densely welded glass of rhyolitic composition. At drill hole USW-G2, the glass, groundmass, and pumice in densely welded intervals have been partially replaced by clinoptilolite. At other drill-hole locations, however, the glass in shards and groundmass are unaltered, though veins of clinoptilolite and/or heulandite are common associations. Pumice clasts in the vitrophyre from these drill holes are partially altered to clay and possibly to minor clinoptilolite. Perlitic fractures are common throughout the vitrophyre, and consist principally of plagioclase and alkali feldspar with trace amounts of Fe-Ti oxides, quartz, and biotite.

The lower ash flow of the Topopah Spring Member consists of olive-brown, vitric, poorly bedded, partly welded to nonwelded ash-flows. The tuffs are heavily zeolitized. In general, shards in the nonwelded portions are largely undeformed, and are completely pseudomorphed by zeolites. Shard boundaries are often rimmed by clays. Phenocrysts in this lower ash flow are similar in abundance and composition to these in the lower vitrophyre zone. Pumice lapilli are also normally undeformed but completely replaced by zeolites and clays. Clays are also found as coatings on the entire walls of vesicles. The tubes are filled with zeolites. Clinoptilolite is found in drill holes USW-G1, USW-G2, and J-13 as the dominant authigenic mineral; however, the important authigenic phases at drill hole UE25a-1 are mordenite, clinoptilolite-heulandite, and clays.

3.3.3 Bedded Tuff of Calico Hills

The Bedded Tuff of Calico Hills comprises nonwelded, vitric, and zeolitized ash-flow units that, in general, are interbedded with thin bedded to massive, reworked air-fall tuff units. The interlayered nature of the Calico Hills indicates that the volcanic eruptions were temporarily interrupted with the deposition of reworked air-fall ash. Because of the intensive zeolitization in the tuffs, only clinoptilolite pseudomorphs after shards can be recognized; other original glass textures are obscured. Furthermore, the permeability of zeolitized tuffs is also drastically reduced in comparison with that of unzeolitized tuffs. Authigenic minerals in the cores of the Calico Hills tuffs are mainly clinoptilolite and mordenite, with lesser amounts of quartz, cristobalite, and alkali feldspar, though the distribution of clinoptilolite and mordenite differs substantially from location to location. Minor amounts of smectite have also been observed as rims on pumice clasts and shards, thin coatings of vesicle walls, and fracture fillings in pumices. Highly oxidized Fe-Ti oxides are abundant in the tuffs. The presence of abundant zeolites and highly oxidized Fe-Ti oxides may indicate extensive interaction between ground water and the country rock, and the variation of zeolite distribution may be reflected by variation of groundwater flow and chemistry.

In the groundmass, clinoptilolite and mordenite are also major constituents with minor amounts of smectite. Terminated crystals of clinoptilolite are frequently observed in small vugs within the groundmass, but rare mordenite. Bish and others (1982) have reported that clinoptilolite is often associated with euhedral crystals of adularia. Quartz and smectite have been reported as fracture fillings at drill hole USW-G2. In general, vapor-phase crystallization and fractures are not too frequently noted in the Tuff of Calico Hills. Lithic fragments are primarily clasts of moderately to densely welded vapor-phase-altered ash-flow tuffs, rhyolites, and older pumices. The amount of lithic fragments increases downward in sections ranging from 1 to 13 percent of the tuffs.

Based upon the abundance, size, and mineral composition of the phenocrysts, the Bedded Tuff of Calico Hills is subdivided into two major units (Caporuscio and others, 1982). The upper unit contains less than 2 percent phenocrysts including quartz, sanidine, plagioclase, and biotite. The lower unit, recognized only at drill hole USW-G2, consists of approximately 6 to 9 percent of phenocrysts near the top. The amounts of phenocrysts increase systematically downward to 15 to 25 percent near the base. The principal phenocrysts are quartz, sanidine, plagioclase, and biotite. Quartz and sanidine are the dominant phases near the top. Plagioclase and quartz are more abundant at depth. Biotite is present in trace amounts at the top and increases to 10 percent near the base of the lower unit. The size of phenocrysts within the lower unit also increases downward; they are two to three times larger in the lower portions than in the upper portions. Mineral composition of the phenocrysts changes with depth; the Fe:Mg ratios in biotite decrease downward from 0.60 to 0.64 near the top to 0.51 to 0.55 at the base; and the Or in sanidine ranges from 66 to 69 near the top to 71 to 77 at the base.

CHAPTER 4 - GEOLOGIC STRUCTURES

At the location being considered for a repository, Yucca Mountain trends roughly north and south and is bounded on the east and west by west-dipping normal faults. Other fault systems that trend northwest and northeast are present. Yucca Mountain lies northeast of the Crater Flat volcanic center and south of the Timber Mountain - Oasis Valley caldera complex. The stratigraphic sequence is a thick accumulation of generally east-dipping silicic volcanic rocks underlain by undetermined but most probably Paleozoic sedimentary rocks similar to those exposed at Bare Mountain and the Calico Hills. Because the present plans are for the subsurface facility to be in the unsaturated zone of the volcanic rocks, the emphasis of this chapter will be on the structures observed and inferred to be present in this zone. Only passing reference will be made to the structures expected in the Paleozoic rocks beneath the silicic volcanic rocks.

4.1 Layering

The recognition of structural features is based on the observed bending, faulting, and fracturing of layering inherent to the rock sequence. For tuffs, this layering can be defined by large-scale lithologic and compositional variations, structural differences, and textures and flow structures within an ash flow.

Along the crest of Yucca Mountain, the layering generally dips east or southeast at 6° to 12° (Christiansen and Lipman, 1965; Lipman and McKay, 1965). In the vicinity of Abandoned Wash (Figure 4-1), the dip of the layering increases to 40° and locally to 70°, although the steep dips are absent north of this wash (Scott and others, 1983). Local steepening is associated with faulting.

4.2 Faults

4.2.1 Dip-slip faults

Faults in the Yucca Mountain area can be divided into three groups. The most prominent group of faults are those with dip-slip displacement. These faults generally strike from N5°E to N35°E, although locally, as at Abandoned Wash (Figure 4-2), the strikes are to the north-northwest (Lipman and McKay, 1965; Scott and others, 1983). Dips are steeply to the west or northwest with the hanging wall down. Displacements on these faults commonly are in the range of tens to hundreds of meters of vertical offset. Both the abundance and amount of displacement along the faults decrease north of Drill Hole Wash. The orientation of these faults and the sense of displacement along them are typical of basin and range faults throughout the region.

4.2.2 Strike-slip faults

A second group of faults has strike-slip displacements. The strike of these faults ranges from N15°W to N40°W, and the dip ranges from 60° to 90° to

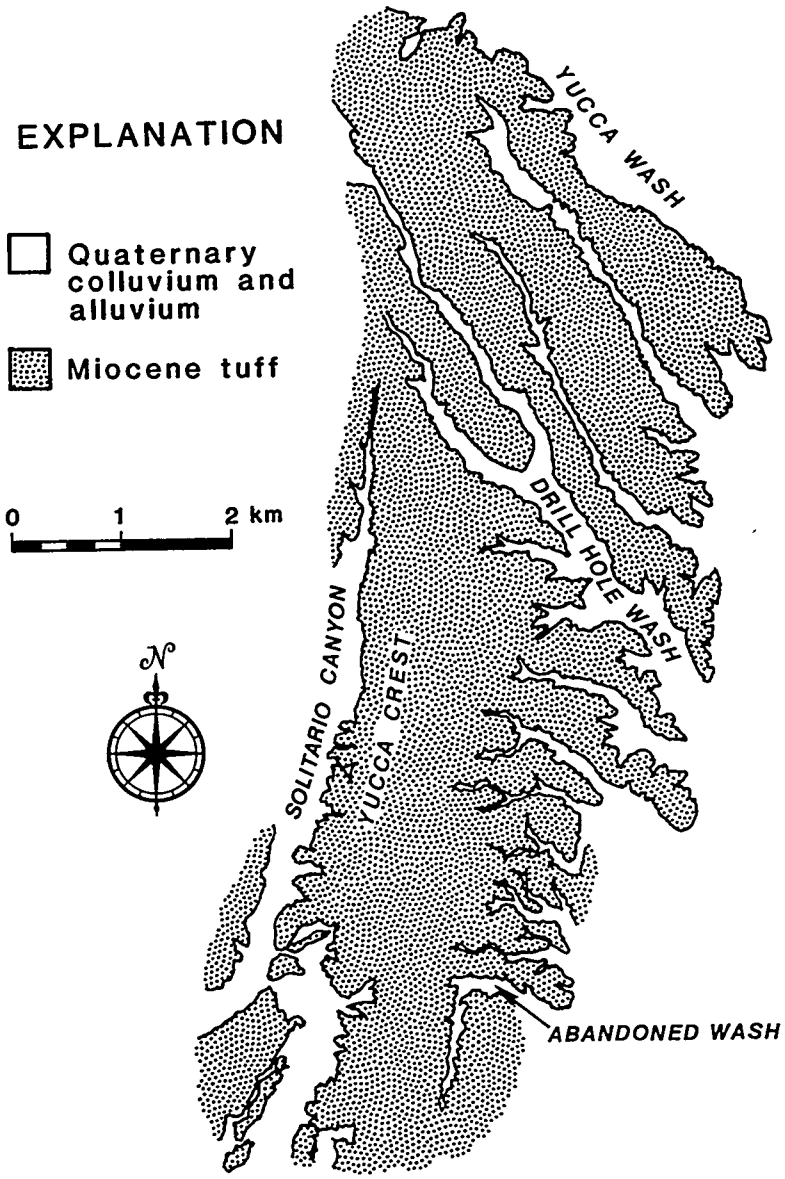

Figure 4-1. Location map of topographic features at Yucca mountain (after Scott and others, 1983).

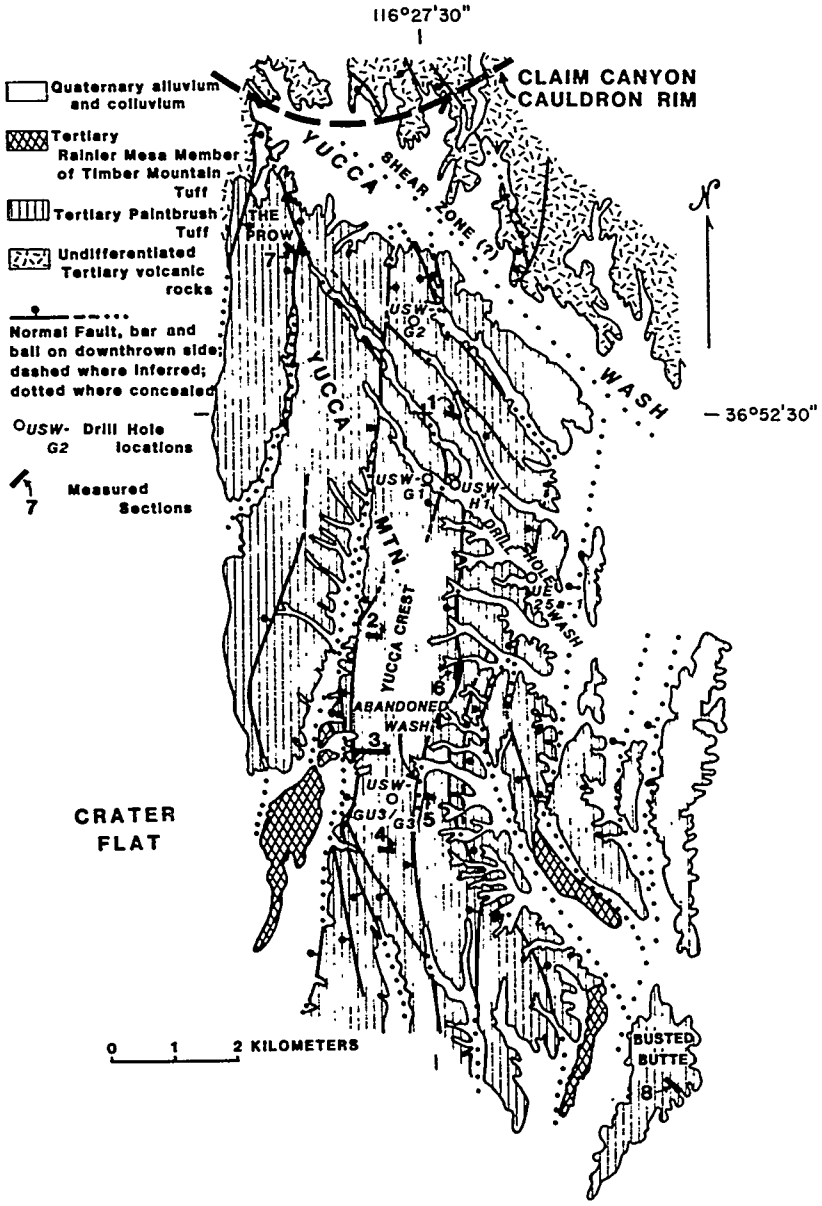

Figure 4-2. Geologic map of central Yucca mountain (after Scott and others, 1983). From Mercer, Rao, and Marine, Role of the Unsaturated Zone in Radioactive and Hazardous Waste Disposal. Copyright 1983 Ann Arbor Science Publishers. Used with permission of the publisher.

the west and southwest. South of Drill Hole Wash, the strike-slip faults generally strike north-northwest. North of Drill Hole Wash the faults strike northwest parallel to or within the northwest-trending (N25° - 40°W) washes. The sense of movement on these faults generally is right lateral, although near the major north-northeast- trending faults, displacement may be dip-slip. Displacement on the faults commonly is too small to be measured, but at one locality west of drill hole USW-G2, a displacement of 10 to 30 meters was observed (Scott and others, 1983).

4.2.3 Volcanotectonic faults

Volcanic activity in the Yucca Mountain region produced the faults that are in the third group. Complex faulting is associated with areas of eruption, caldera collapse, and resurgent domes. The Timber Mountain-Oasis Valley caldera complex has been identified north of Yucca Mountain (Byers and others, 1976a, 1976b). Results from a recent gravity survey suggest that segments of older calderas adjacent to the Timber Mountain-Oasis Valley caldera complex may extend southward into the northern part of Crater Flat and may underlie part of the repository site (Snyder and Carr, 1982) (Figure 4-3). In addition, a caldera with a resurgent dome was postulated for central and western Crater Flat (Snyder and Carr, 1982). Because the features postulated from geophysical data are not exposed at the surface, the structures associated with these features are not known.

4.3 Fractures

Tuff ranges from a nonwelded, bedded rock to a brittle, densely welded rock. This range in rock type results in a wide range of mechanical response to imposed stresses. Whereas nonwelded to partially welded tuff can dissipate stresses by intergranular movement with little or no fracturing, the brittle densely welded tuff responds to sufficiently large stresses by extensive fracturing. The result is a gradation in fracture density that has a direct relationship to the degree of welding. An exception to this scheme is densely welded vitrophyre that has an intermediate fracture density (Scott and others, 1983).

As an ash flow cools, the resultant cooling fractures would be expected to form in a random or polygonal pattern similar to the way basaltic magma cools. For reasons not understood at present, the fractures in tuff at Yucca Mountain tend to have a preferred orientation (Figure 4-4). Because the fractures have an orientation similar to the basin-and-range faults, a tectonic origin for the fractures is indicated (Scott and others, 1983). Another possible reason for this preferred orientation is deposition and cooling of the ash flows on a slope not steep enough to allow flow but sufficiently steep to impose an extensional stress field or fracturing of the rocks as a result of large-scale deformation.

In order to indicate the abundance of fractures at a location, fracture density generally is reported as fractures per unit length. For accuracy, the fractures must be perpendicular to the line along which the count is made or a

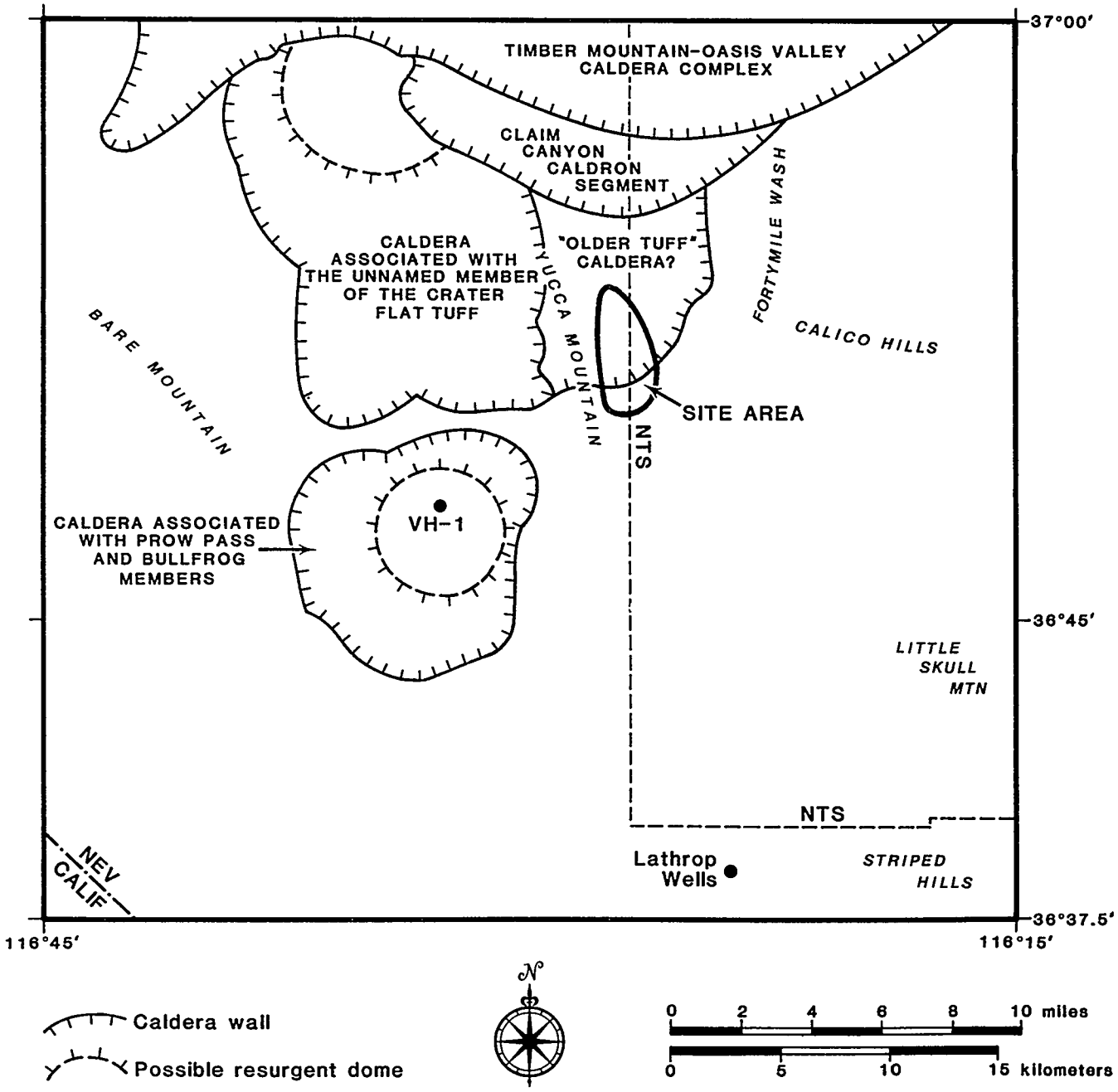

Figure 4-3. Location of calderas in the Yucca Mountain area (after Snyder and Carr, 1982).

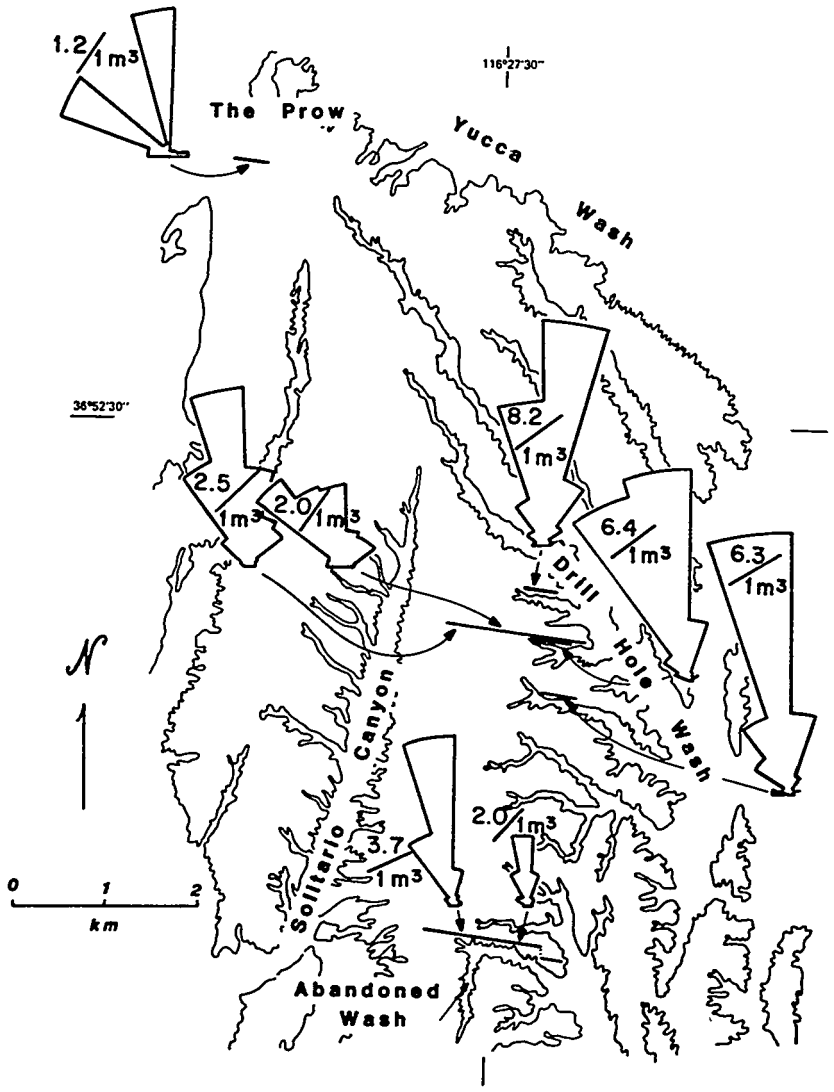

Figure 4-4. Rose diagrams of strikes of fractures along traverses at Yucca Mountain. Northernmost rose is for the tuffaceous beds of Calico Hills. All other traverses are for the Tiva Canyon Member. For the two long traverses (one north of Abandoned Wash, one south of Drill Hole Wash), the eastern roses are for areas mostly underlain by moderately welded tuff, whereas the western roses are for densely welded tuff. (after Scott and others, 1983). From Mercer, Rao, and Marine, Role of the Unsaturated Zone in Radioactive and Hazardous Waste Disposal.

correction must be applied. The correction for fracture frequency along a length of core is

$$F_c = (\sin A)^{-1} F_m \qquad (4\text{-}1)$$

where F_c = corrected fracture frequency
A = angle between core axis and fracture set
F_m = apparent fracture frequency measured along core (Scott and others, 1983).

Summing the calculated fracture densities for all the fracture sets found along a core results in a fracture frequency that is actually for a volume rather than a length. Scott and others (1983) used a spherical unit volume of 1 m^3 as a standard, which required counting fractures along a 1.24 meter length of core. The same technique can be applied to calculating fracture frequency in an outcrop.

A potential problem exists in comparing fracture densities calculated for cores and those calculated for outcrops. At Yucca Mountain, north-facing slopes have more extensive cover than south-facing slopes, and on long traverses, talus zones preferentially cover zones with higher fracture densities. As a result, the fracture densities in Figure 4-4 are for well-exposed parts of south-facing traverses (Scott and others, 1983), and these values are substantially less than those calculated for core (Table 4-1).

4.4 Geologic Synthesis

The intense folding and thrusting of Mesozoic age that deformed the Paleozoic and Precambrian rocks exposed at Bare Mountain and the Calico Hills are reasonably expected to have deformed whatever Paleozoic and older rocks underlie the sequence of tuffaceous rocks at Yucca Mountain. This Mesozoic compression was replaced in Tertiary time by a deformation that at least at the surface looks to be the result of regional extension. Carr (1974) stated that some geologists believe the extensional features to be thin-skinned deformation and the result of regional shear stresses.

In the NTS area, Ekren and others (1968) reported two systems of normal faults. The older system consists of two sets, one trending to the northeast and the other to the northwest. The younger system has a single system of faults that trend north. No explanation was provided for the change in stress field to account for the change in orientation of the two fault systems. Nor was an explanation provided to explain the stress field that would allow for normal faults of the same age with potentially intersecting strikes.

Carr (1974), in his investigation of the stress-field orientation at NTS, stated that the northwest-trending Walker Lane has evidence of substantial right-lateral displacement and that a complementary set of southeast-trending faults with minor left-lateral displacement exists. In addition, the north-trending faults in the Yucca Mountain area were reported to have right-lateral slip, whereas the north-northwest-trending faults present northwest of Yucca Flat have oblique right-lateral displacement. To further complicate the

Table 4-1. Calculated fracture densities for tuff units in core from drill hole USW-GU3/G3 (data from Scott and others, 1983)

Unit	Degree of Welding	Fracture Density (Fractures/unit m^3)	Rock Type
Tiva Canyon	partially welded to nonwelded	9	
	densely welded	14	upper lithophysal zone
	densely welded	22	clinkstone
	densely welded	22	lower lithophysal zone
	densely welded	26	hackly zone
	densely welded	21	columnar zone
Underlying Tiva Canyon	nonwelded	<1	bedded tuff
Topopah Spring	partially welded	18	caprock zone
	densely welded	8.8	vitrophyre

picture, the strike-slip faults east of Yucca Flat probably had dip-slip displacement in the past (Carr, 1974).

Hydrofracture tests to determine the orientation and magnitude of the principal stresses at Yucca Mountain also yielded complex results. These tests were conducted in drill holes USW-G1, USW-G2, and UE25p-1. In each hydrofracture test, an interval of the borehole is isolated with packers, and the pressure is increased until the rock is fractured. The new fractures theoretically form perpendicular to the least horizontal stress. The orientation of any pre-existing fractures must be checked with a televiewer or downhole camera. Once the pressure to cause fracturing (breakdown pressure) and the pressure to keep the created fractures open are known, the principal horizontal stresses can be calculated by using

$$P_b = 3S_h - S_H + T - P_p \quad \text{(Haimson \& Fairhurst, 1967)} \qquad (4\text{-}2)$$

where, P_b = breakdown pressure (pressure to cause fracturing)

S_h = least horizontal principal stress (pressure required to keep fracture open)

S_H = maximum horizontal stress (to be calculated)

P_p = pore pressure

T = tensile strength (measured in lab; $T = 0$ for repeated tests on same interval)

Vertical stress (S_v) can be determined by calculating the pressure exerted by the overlying saturated and partially saturated column of rock.

The results of hydrofracture tests in both the unsaturated and saturated zones in drill hole USW-G2 (Stock and others, 1984) and in unspecified zones in USW-G1 (Healy and others, 1983) indicate that S_v is greater than S_H. This stress field is one of tension at the crest of Yucca Mountain, which is appropriate for basin and range faulting. To the east of Yucca Mountain at UE25p-1, which is 3.5 miles (5.6 kilometers) southeast of USWG-1 and 4.7 miles (7.5 kilometers) south-southeast of USW-G2, the stress field S_h approximately equals S_v, and S_H is substantially greater than S_v (Healy and others, 1983). The rocks at this borehole are in horizontal compression, even though a few kilometers to the northwest the rocks are in extension.

Orientations of faults at Yucca Mountain (Scott and others, 1983) are similar to those found elsewhere at NTS by Ekren and others (1968) and Carr (1974). Discrepancies exist in the offsets reported for the various fault orientations (Table 4-2) and the stress orientations determined in the Yucca Mountain area. These discrepancies may be the result of misinterpretation of the field data, different responses of certain faults to changes in the stress field, nonuniform response to a reorientation of the stress field because of large-scale inhomogeneities (e.g., uplifted blocks of Paleozoic rocks, caldera complexes), actual local differences in the stress field, or combinations of these reasons.

Table 4-2. Reported senses of displacement for fault orientations in NTS area

Fault Orientation	Ekren and others (1968)	Carr (1974)	Scott and others (1983)
NNE* to NE	dip slip	left lateral	dip slip
N	dip slip	right lateral	
NNW		oblique right lateral	right lateral
NW	dip slip	right lateral	right lateral

*locally may strike NNW

Normal faults at Yucca Mountain reportedly dip to the west at a steep angle. Based on gravity data, Snyder and Carr (1982) proposed a schematic cross section (B-B', Figure 4-5) that seems to indicate that the faults are the result of gravity settling into a caldera in the northern part of Crater Flat (Figure 4-6). This interpretation is not stated or implied in their report. The fact that the faults at Yucca Mountain are not arcuate and have the same orientations as the regional trends for other faults indicates that the faults did not form as a result of caldera collapse. Scott and others (1983) noted that the eastward dip of the layering in each fault block is steeper on the down-faulted blocks (Figure 4-7), and stated that this relationship may be the result of listric faulting (as described by Wernicke and Burchfiel, 1982; and Jackson and McKenzie, 1983). This structural style is characteristic of at least some areas of regional extension. With this type of faulting, the dip of the fault planes decreases with depth, and the faults either merge into a single low-angle to subhorizontal fault plane (Figure 4-8) or die out in ductile strata (Shelton, 1984). At Yucca Mountain, the depth to the flattening of the fault plane is postulated to be in excess of 0.6 mile (1 kilometer) (Scott and others, 1983).

Because of the complex history of faulting in this area, a detailed structural synthesis is not possible at this time. Some generalizations can be made about the age of faulting. According to Ekren and others (1968), volcanic ash dated at 29 million years (m.y.) old can be found in lacustrine limestone that has been preserved in downfaulted blocks. The widespread distribution of the limestone indicates that faulting had not yet occurred at the time of deposition of the limestone or volcanic ash. Northwest- and northeast-trending faults seem to be the oldest faults, in that these faults are contemporaneous with or slightly postdate a welded tuff dated at 26.5 m.y. (Ekren and others, 1968). At least locally, the northwest-trending faults originated more recently. Scott and others (1983) report that northwest-trending faults in the Yucca Mountain area are probably younger than the Tiva

Canyon Member (12.5 m.y. old) but do not cut the Rainier Mesa Member (11.3 m.y. old). Displacement along the north-trending faults generally began between 17 and 14 m.y. ago, although locally, significant offset did not occur until possibly 11 m.y. ago (Ekren and others, 1968).

In eastern Crater Flat, trenches were dug across two faults to obtain evidence for the age of last movement along these faults. The results were reported by Swadley and Hoover (1983). One fault zone contained basaltic ash that probably was washed into the zone while the fault was active. This ash dates at 1.1 m.y. An overlying unbroken soil horizon was estimated to be 27,000 to 35,000 years old. The second fault zone cuts into a soil horizon dated at 260,000 ($\pm$ 30,000) years, but does not cut a soil horizon dated at 40,000 ($\pm$ 10,000) years.

Seismic activity in the southern Great Basin indicates that some of the faults remain active. Rogers and others (1983) state that throughout this region the seismic activity primarily occurs along north-trending and northeast-trending faults, and recommend that despite aseismicity at Yucca Mountain, faults with these orientations be considered potentially active.

Faults that formed as a result of the volcanic activity in Crater Flat and possible activity associated with the postulated caldera underlying northern Yucca Mountain have not been reported at Yucca Mountain. Structures with these origins may be present at depth but as yet are undetected. Movement on faults of tectonic origin, both older than and contemporaneous to the volcanism, may have occurred as a result of volcanic activity.

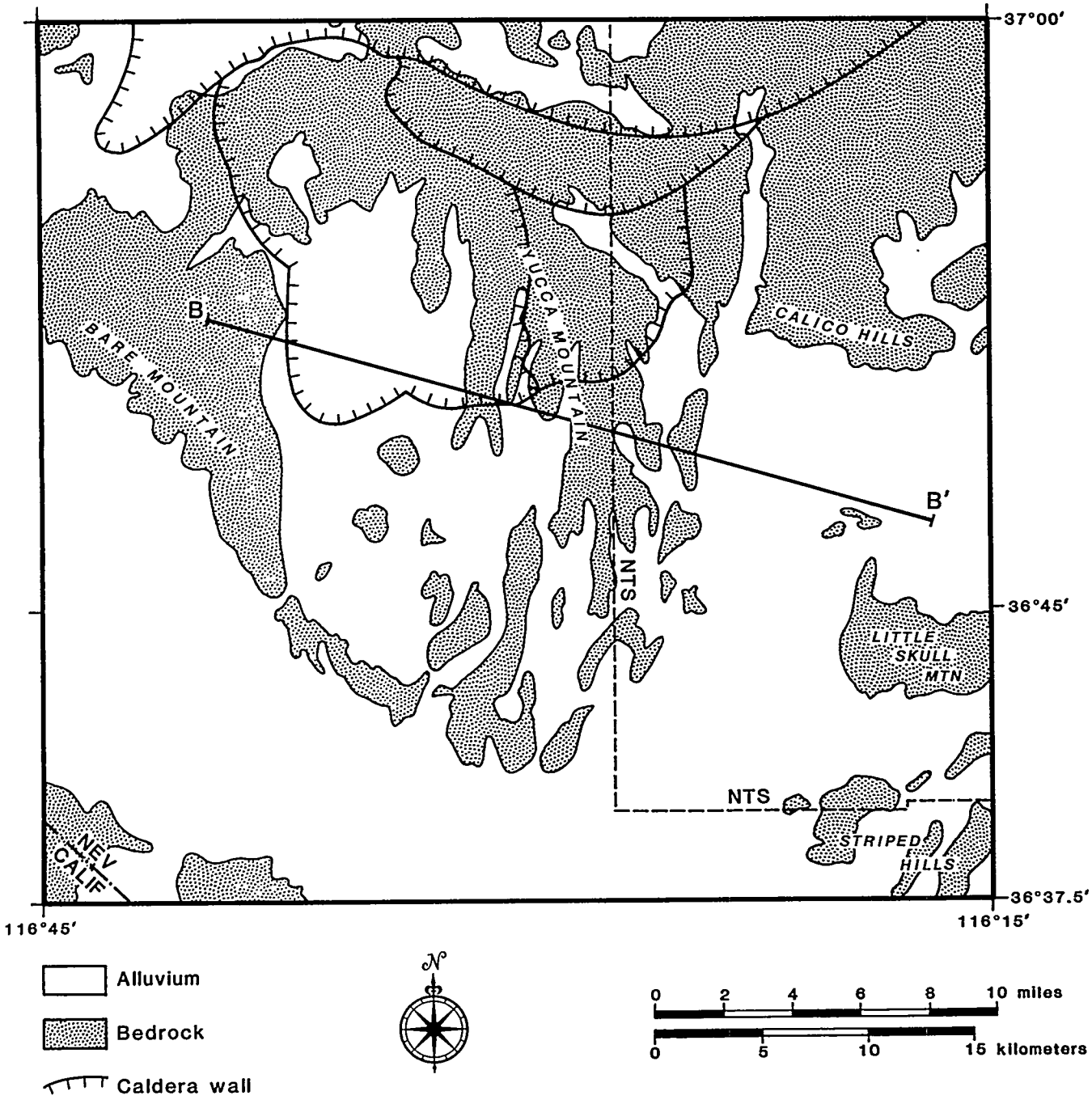

Figure 4-5. Location of cross section (B - B') in Figure 4-6 (after Snyder and Carr, 1982).

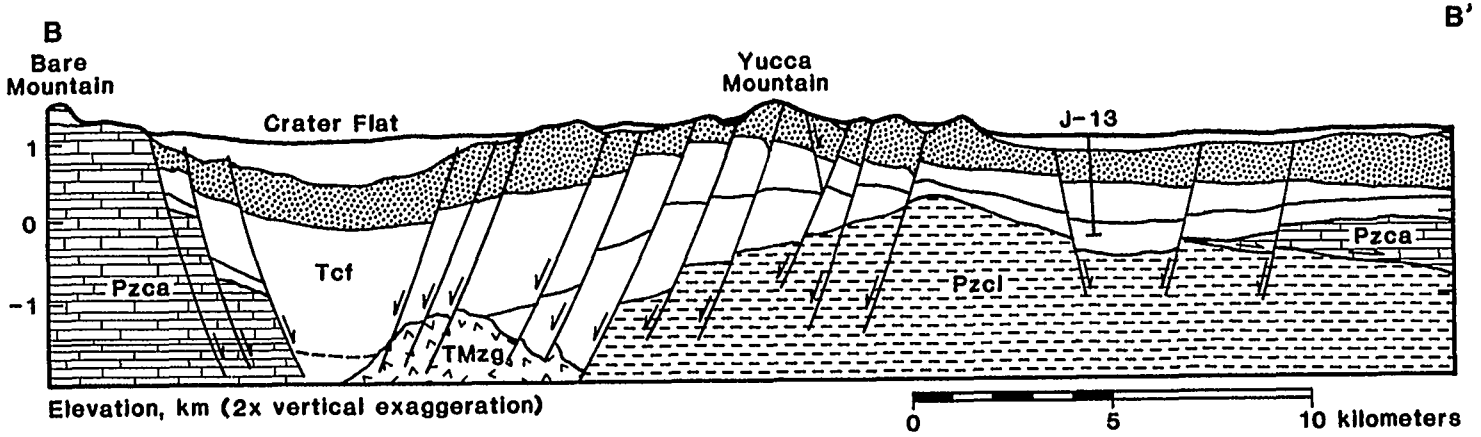

Figure 4-6. Schematic east-west structure section through Yucca Mountain based on gravity data. Pzca - lower and middle Paleozoic carbonate rocks; Pzcl - upper Paleozoic clastic rocks; TMzg - Mesozoic or Tertiary granite; Tcf - Crater Flat Tuff (after Snyder and Carr, 1982).

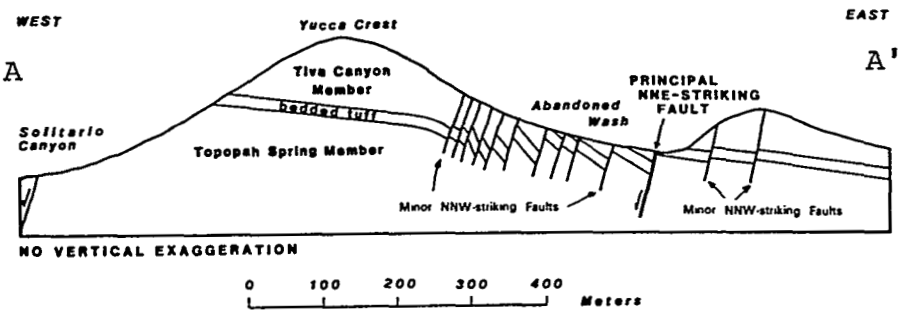

Figure 4-7. East-west structure section at Yucca Mountain based on field geology. See Figure 4-1 for location of section (A-A') (after Scott and others, 1983). From Mercer, Rao, and Marine, Role of the Unsaturated Zone in Radioactive and Hazardous Waste Disposal. Copyright 1983 Ann Arbor Science Publishers. Used with permission of the publisher.

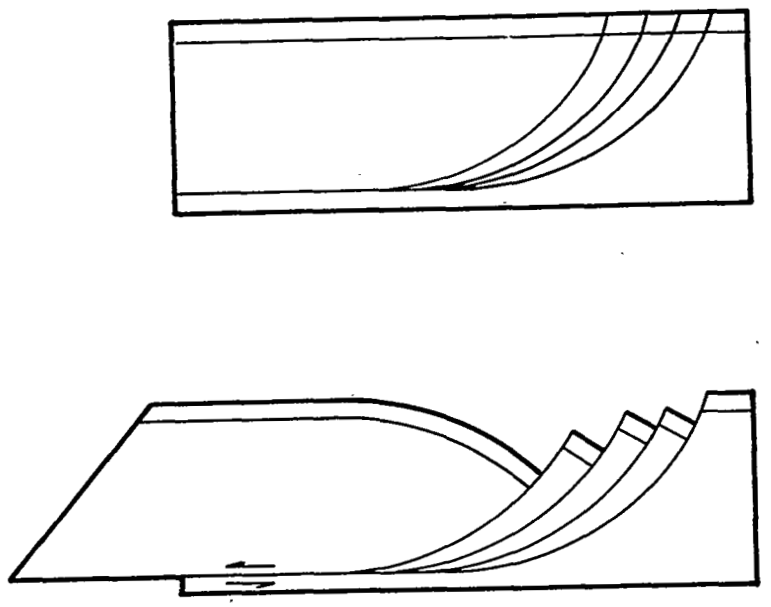

Figure 4-8. Schematic diagram of imbricate listric normal faults. Note that the dip of the marker bed is progressively steeper in the down-faulted blocks.

CHAPTER 5 - GEOCHEMISTRY

5.1 Ground-water Composition

5.1.1 Speculations on the chemistry of water in the unsaturated zone

At present, there are no available ground-water composition data for samples from the unsaturated zone at Yucca Mountain. According to the NNWSI Program Plan (LANL, 1984), samples will be taken during construction of the exploratory shaft. It has been suggested (Ogard and Kerrisk, 1984) that water in the unsaturated zone will be similar in composition to water sampled in the saturated zone of Yucca Mountain. According to this model, the probable composition of any water at Yucca Mountain can be bounded by the compositions of water from the following wells: USW-H3 (water below the repository), UE25p-1 (water in the Paleozoic aquifer), J-13 (water in the aquifer surrounding Yucca Mountain), and snow or rain (juvenile recharge) (Figure 5-1 and Table 5-1). This hypothesis is supported by data from four types of research: water chemistry studies of the saturated zone at Yucca Mountain; water chemistry studies of the unsaturated zone at Rainier Mesa in the NTS; experimental studies of tuff-water interactions; and theoretical calculations of mineral-water equilibria and reaction pathways. Ogard and Kerrisk (1984) suggest that because no saline water has been found in the tuff layers at Yucca Mountain and because the slow dissolution of volcanic glass does not lead to high concentrations of dissolved solids, water in the pores of the unsaturated zone is similar to that sampled in the wells listed above. The chemistry of waters in these wells is dominated by the reaction of vitric tuff and rain water and the production of secondary minerals. The approximate composition of water within the unsaturated zone, therefore, may lie between the compositions of rain water and the end-member water compositions represented by the wells listed above. The exact composition of pore fluid in any particular rock unit will depend upon the degree and nature of reactions with the surrounding wall rock, and thus may differ for different rock types and ground-water ages. For example, Ogard and Kerrisk (1984) suggest that the composition of water in the pores of unsaturated vitric tuff may differ from water in unsaturated devitrified tuff. Fluids in the latter rock may be higher in relative calcium content and lower in relative sodium contents than the waters described in Table 5-1. Water in equilibrium with zeolitic or vitric tuff should be similar to the water described in these tables. Kerrisk (1984a) suggests that water at Rainier Mesa provides a useful analog for the compositions of waters in fractures and matrix in the unsaturated zone at Yucca Mountain. The data obtained in the studies described above will be presented in more detail in the sections that follow.

5.1.2 Hydrochemical data from Yucca Mountain and Rainier Mesa

In this section the chemical compositions of water from Yucca Mountain, Rainier Mesa, Pahute Mesa, and the Amargosa Desert will be compared. Such a comparison is important for understanding the chemistry of pore fluids in the unsaturated zone because the waters from these areas may represent different stages in the hydrochemical evolution of ground water at Yucca Mountain.

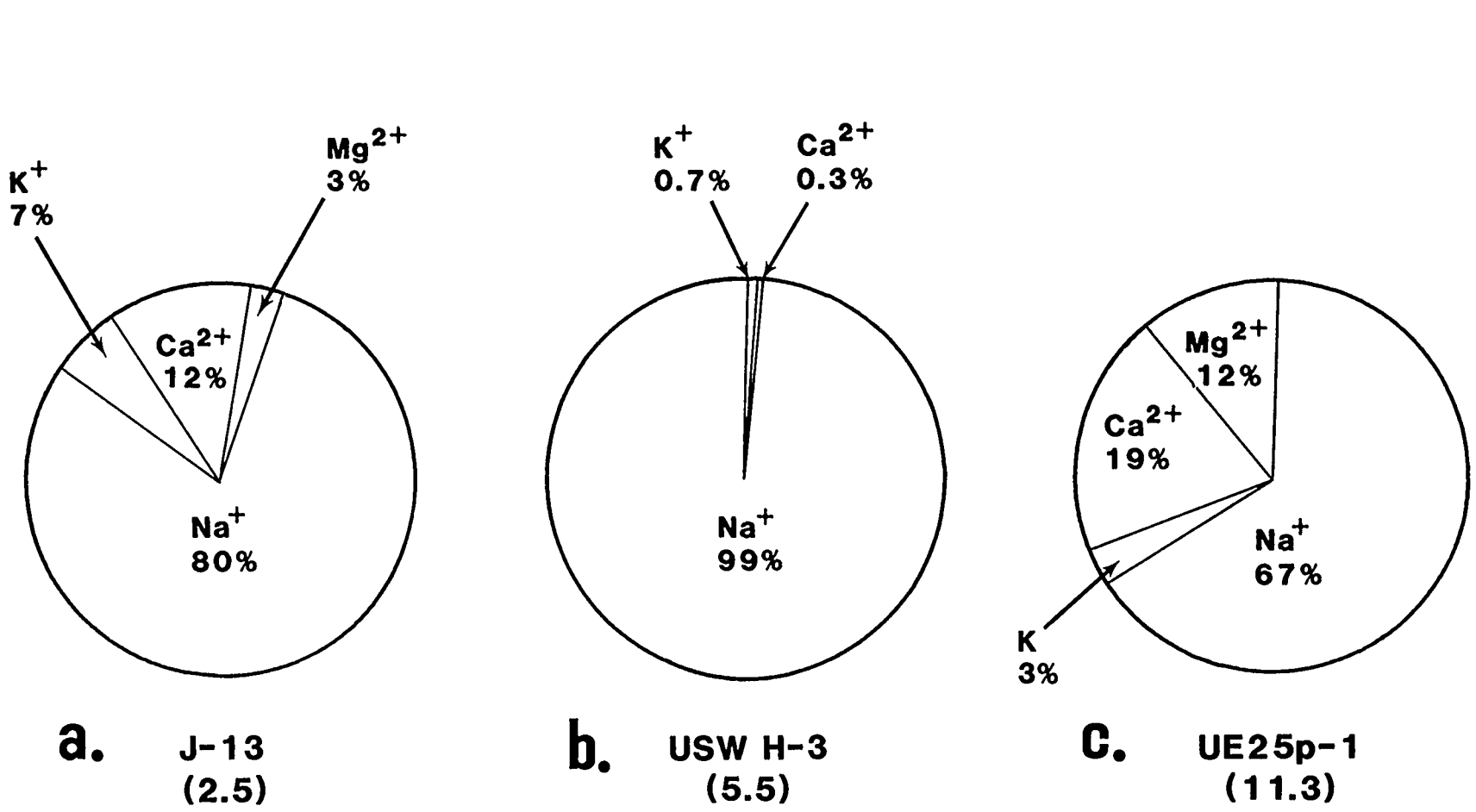

Figure 5-1a. Major cation concentration in well waters from Yucca Mountain: a. J-13 well, b. USW-H3 well, c. UE25p-1 well. Total concentrations are in millimoles/liter. See also Table 5-1.

MAJOR LIGAND CONCENTRATIONS IN YUCCA MOUNTAIN WATERS

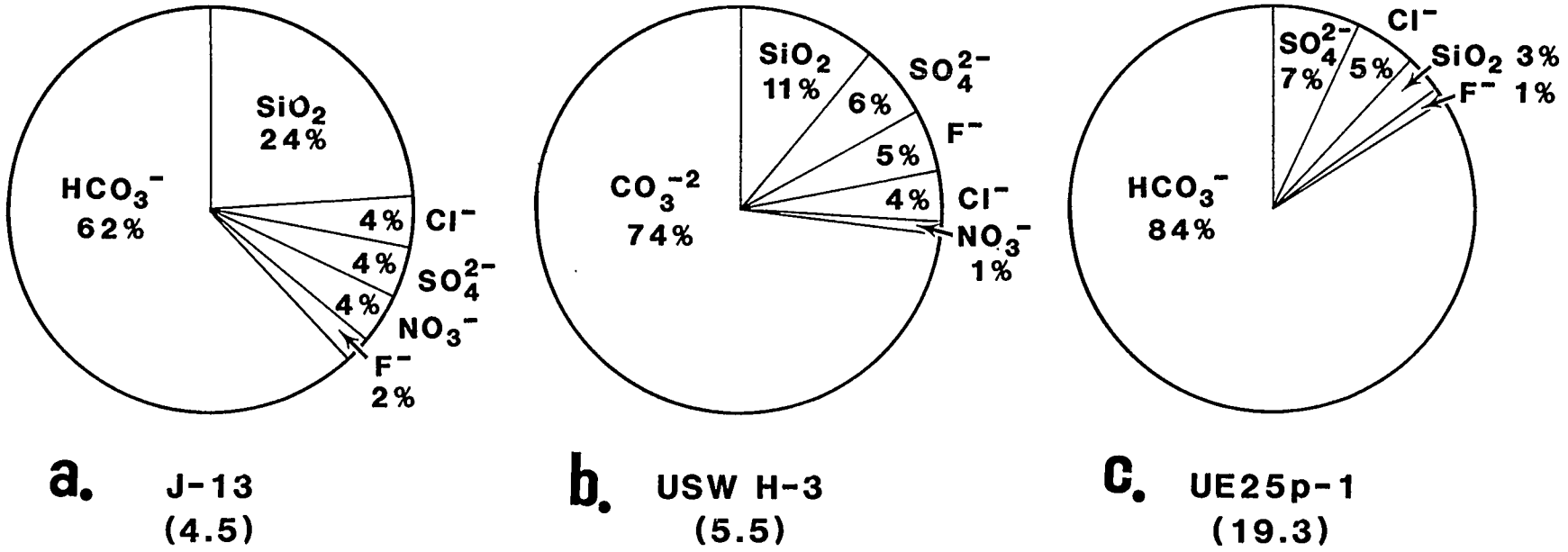

Figure 5-1b. Major ligand concentration in well waters from Yucca Mountain: a. J-13 well, b. USW-H3 well, c. UE25p-1 well. Concentrations are in millimoles/liter. See also Table 5-1.

Table 5-1. Water compositions (LANL, 1984; Ogard and Kerrisk, 1984)

	J-13	UE25p-1	USW-H3
Na^+ (mm/l)	1.96	7.43	5.39
K^+ (mm/l)	0.14	0.34	0.04
Ca^{2+} (mm/l)	0.29	2.19	0.02
Mg^{2+} (mm/l)	0.07	1.31	0.00
SiO_2(aq) (mm/l)	1.07	0.62	0.60
CO_3^{2-}(total)(mm/l)	2.81	16.1	4.04
Cl^- (mm/l)	0.18	1.04	0.23
SO_4^{2-} (mm/l)	0.19	1.34	0.32
F^- (mm/l)	0.11	0.18	0.28
pH	6.9	6.7	9.4
Eh (mV)	700	360	-143
TDS (mg/l)	130.4	504.22	189.3

Thus, after reaction with rock in the unsaturated zone, meteoric water may attain a composition similar to waters sampled in Rainier Mesa or Pahute Mesa. These sites may be recharge areas for Yucca Mountain (Waddell, 1982; Ogard and Kerrisk, 1984). The Amargosa Desert may receive discharge for flow from Yucca Mountain. The water composition of wells there may represent the final stage of hydrochemical evolution from a series of processes that are important in the area surrounding Yucca Mountain.

5.1.2.1 Yucca Mountain

Benson and others (1983) and Ogard and Kerrisk (1984) described the chemical and isotopic composition of waters from 10 wells in the Yucca Mountain area. Cation, anion, $\delta^{18}O$, δD, and ^{14}C ages are listed in Tables A5.1-1 to A5.1-6. The locations of the wells and lateral differences in the chemical and isotopic compositions among the wells are shown in Figures A5.1-1 to A5.1-4. The lateral heterogeneity in composition illustrated in these figures is due, in part, to differences in the mineral compositions of the permeable zones sampled. Figure A5.1-5 shows the vertical distribution of permeable intervals in the wells.

The water compositions described in Tables 5-1 and A5.1-1 to A5.1-6 belong to a sodium bicarbonate hydrochemical facies (Ogard and Kerrisk, 1984). Most of the waters are fresh; water from UE25p-1 is the most saline, with total dissolved solids of over 500 mg/l. With the exception of this latter well, these waters are similar in composition to the sodium potassium bicarbonate facies (Type II for water types at NTS) described by Winograd and Thordarson (1975) and Guzowski and others (1983). The chemistry of this water type is dominated by the leaching of potassium, sodium, and silica from vitric tuff. A more detailed discussion of the chemistry of this and other hydrochemical facies at NTS may be found in the two references cited above.

5.1.2.2 Rainier Mesa and Pahute Mesa

Rainier Mesa is an eroded volcanic plateau in the north-central part of the NTS, approximately 25 miles (40 km) northeast of Yucca Mountain. The structure, stratigraphy, and hydrology are reviewed by White and others (1980) and Guzowski and others (1983).

The stratigraphic units can be divided into three hydrogeologic units: (1) the upper welded and partly welded tuffs of the Timber Mountain and Belted Range Tuffs; (2) the friable vitric tuffs of the Paintbrush Tuff; and (3) lower zeolitized Miocene Tunnel Beds. Ground-water flow in the mesa is predominantly vertical through this sequence. Interstitial fluid flow predominates in the Paintbrush Tuff, whereas flow occurs primarily through fractures in the upper welded units (Benson, 1976; White and others, 1980). The Miocene Tunnel Beds are an aquitard, creating a perched water table 1,968 feet (600 meters) above the regional water table. Due to extensive zeolitization, interstitial hydraulic conductivity is very low. A system of poorly connected, partly saturated fractures exists within these units.

White and others (1980) and Guzowski and others (1983) compared the compositions of interstitial water and water from fractures at this site. Mean compositions of the two water types are presented in Table A5.1-5 and plotted in Figure 5-2. The general ranges of cationic compositions and total dissolved solids are similar in the two waters. Anionic compositions differ; water from fractures has higher bicarbonate concentrations, whereas interstitial water has higher SO_4^{2-} and Cl^- contents.

5.1.2.3 Amargosa Desert and Oasis Valley

As discussed above, the Amargosa Desert may be a discharge area for ground water from Yucca Mountain. Average compositions of waters from Oasis Valley and data from Well #9 in the Amargosa Desert are presented in Tables A5.1-5 and A5.1-7, respectively. Compositions of waters discharging in the west-central Amargosa Desert are described by Claassen (1983).

There is no evidence that water in the unsaturated zone at Yucca Mountain will be as saline as waters discharging in the Amargosa Desert. Waters discharging at Oasis Valley are the product of a complex series of geochemical reactions. This sequence includes (1) recharge at Pahute Mesa, (2) dissociation of soil-derived carbonic acid, (3) hydrolysis and incongruent dissolution of volcanic glass, (4) local dissolution of carbonates and sulfates, (5) precipitation of secondary phases, and (6) increase in total dissolved solids due to evapotranspiration. In Figure 5-2, the average composition of waters sampled along the probable flow path in the tuffaceous aquifer is compared to the composition of water exiting at the end of the flow path. The data are listed in Table A5.1-5. Details of the chemical reactions responsible for the compositions of these water are discussed by White (1979) and Guzowski and others (1983).

Based on geochemical data, Claassen (1983) suggests that ground water in the west-central Amargosa Desert was derived chiefly from snowmelt and was recharged primarily by subaerial flow along present-day stream channels and not by subsurface flow. This process and process (6) in the preceding para-

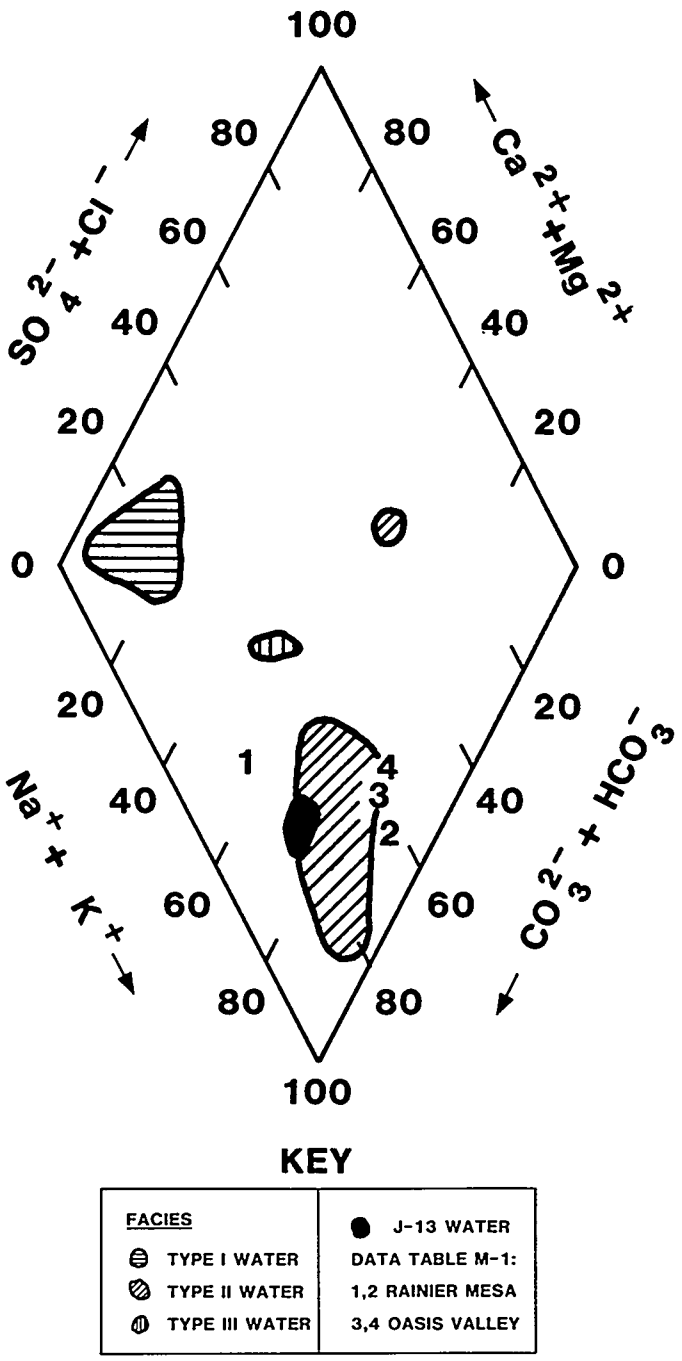

Figure 5-2. Compositions of waters from the vicinity of Yucca Mountain. Cross-hatched areas are composition fields for hydrochemical facies described by Winograd and Thordarson (1975) and Guzowski and others (1983). Field of J-13 well water composition is indicated by solid area. Waters from Rainier Mesa: 1. water from fractures; 2. interstitial waters. Water samples from Oasis Valley system: 3. water from tuff aquifer; 4: saline water from Amargosa Narrows.

graph are probably not important for water in the unsaturated zone at Yucca Mountain. Water chemistry data from the Amargosa Desert are included here, however, because they provide insights into the nature of hydrochemical reactions between tuff and ground water. The composition of water in Oasis Valley and Amargosa Desert is also important to understanding the behavior of radionuclides after they reach the accessible environment.

5.1.2.4 Summary of composition of ground water from Yucca Mountain and vicinity

The compositions of waters from many of the locations described in the preceding sections are compared in Figures 5-3 and 5-4. Figures 5-3a and b are ternary diagrams of relative sodium-potassium-calcium and relative sodium-potassium-magnesium contents respectively. The similarity of wells from Yucca Mountain and Pahute Mesa is evident in this figure. The solid area in Figure 5-3a represents compositions of water from Yucca Mountain and its western slopes (USW-H3, -H5, and -H6). Wells on the eastern slopes and washes of Yucca Mountain are represented by wells USW-H1, -H4, and -G4, J-13, and UE25b-1, and water from Pahute Mesa is represented by wells UE19e and U-20a-2. Wells on the exploration block, eastern slopes, and washes of Yucca Mountain exhibit increasing relative amounts of calcium in the order block → eastern slopes → washes. The carbonate aquifer well (UE25p-1) and the well from the Amargosa Desert (well #9) show the highest relative calcium content. The cross-hatched areas in Figure 5-3 represent the range of compositions of interstitial and fracture waters at Rainier Mesa (White and others, 1980; Ogard and Kerrisk, 1984).

Figure 5-4 shows additional relationships among the compositional variables of the wells described in Tables A5.1-1 to A5.1-5. Figure 5-4a shows the relationship between total sulfate content and total chloride content. A trend of increasing chloride and sulfate content is observed in water from Yucca Mountain and the west-central Amargosa Desert. The latter area is represented by data from relatively fresh water from wells in tuffaceous valley fill and more saline water from valley fill wells along the downstream reach of the Amargosa River (Claassen, 1983). Figure 5-4b shows relative fluoride content (F/(F + Cl)) as a function of relative sodium content (Na/(Na + Ca + K)). Ogard and Kerrisk (1984) suggest that although there is considerable scatter in the data, wells at Yucca Mountain and to the west have increasing relative sodium and fluoride contents. The increase in fluoride may be significant for radionuclide migration because of the high solubility of fluoride complexes. As the salinity of waters in the vicinity of Yucca Mountain increases due to reaction with the rock, then saturation with respect to both calcite ($CaCO_3$) and fluorite (CaF_2) increase.

5.1.2.5 Redox conditions

Ogard and Kerrisk (1984) suggest that the Eh within the devitrified Topopah Spring Member should be oxidizing (Eh > +400 mV). The fracture structure of this rock unit should allow oxygen to penetrate and equilibrate with water within this zone. In general, measured redox potentials of waters from Yucca Nountain have been oxidizing (e.g. Guzowski and others, 1983). The conceptual and analytical problems related to field measurements of Eh are well known (Stumm and Morgan, 1970; Lindberg and Runnells, 1984). The

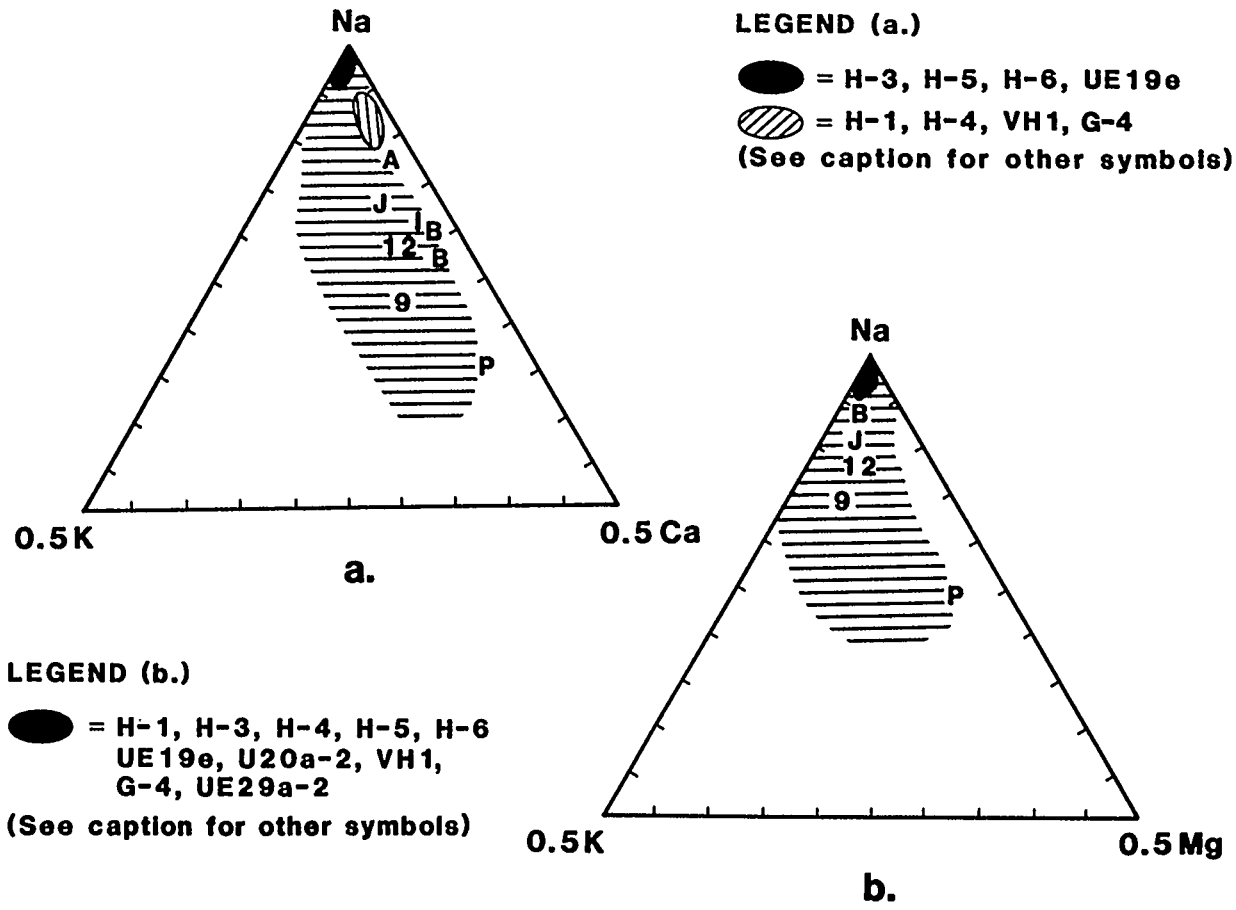

Figure 5-3. Ternary composition diagrams for Yucca Mountain vicinity water (after Ogard and Kerrisk, 1984). Well key: A = UE29a-2, B = UE25b-1 Bullfrog interval, I = UE25b-1 Integral sample, J = J-13, 12 = J-12, 9 = Well 9 in Amargosa Desert, P = UE25p-1. a. Relative Na-K-Mg in water. Solid area represents water from exploration block, slopes, and washes at Yucca Mountain (see text); b. Relative Na-K-Ca in waters. Cross hatched areas in both a and b are range of water compositions from Rainier Mesa (see text). Locations of other wells are plotted in Figure A5.1-1.

a.

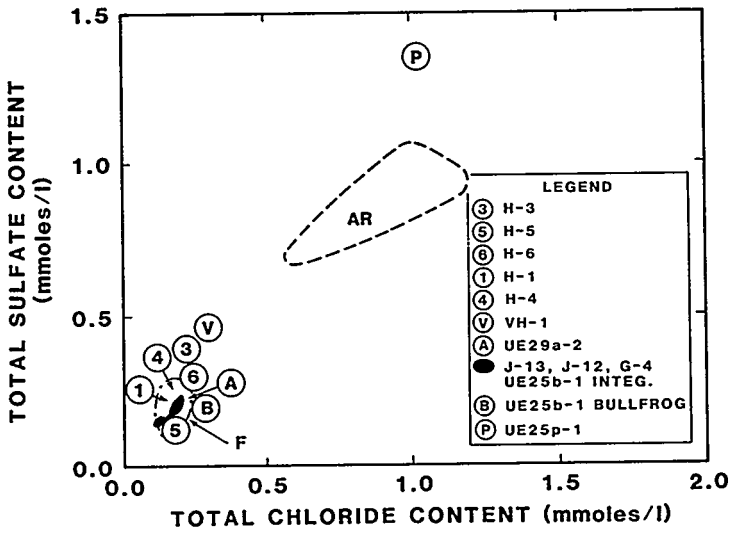

b.

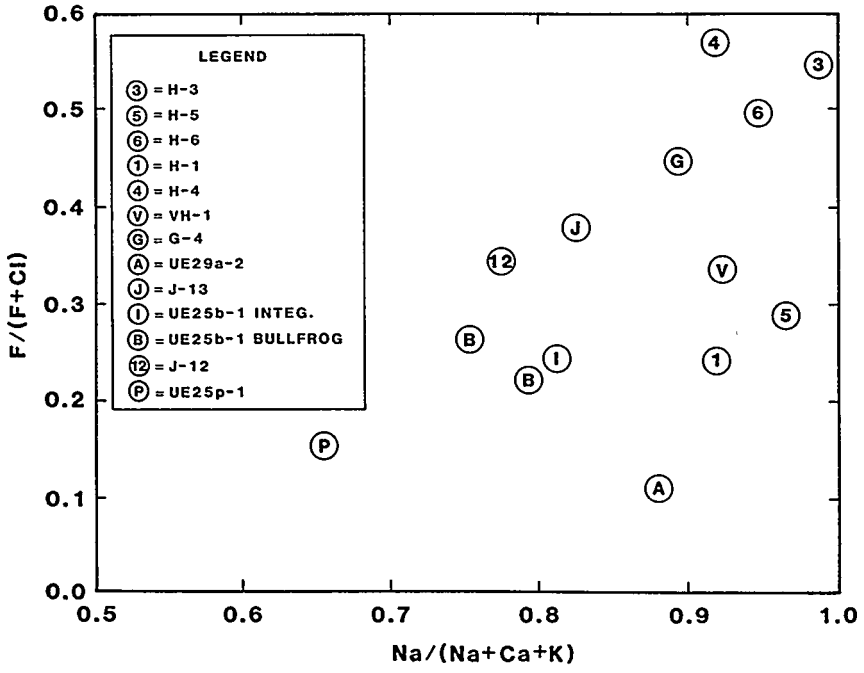

Figure 5-4. Relationships among compositional variables for water from the vicinity of Yucca Mountain (after Ogard and Kerrisk, 1984). a. Total sulfate content versus total chloride content. Dotted and dashed areas: F = range of compositions from wells in tuffaceous valley fill at Fortymile Canyon; AR = valley fill wells along downstream reach of Amargosa River (Claassen, 1983). b. Relative fluoride content versus relative sodium content.

particular problems associated with water sampling procedures and measurements of redox couples at Yucca Nountain have been discussed by Daniels and others (1982d). Redox potentials of waters in the saturated zone at Yucca Mountain are described in Tables 5-1 and A5.1-1 to A5.1-4.

Theoretically, the redox potential of ground water decreases as it migrates down through reactive soils and host rocks. The potential of the water is set primarily by reactions between oxygen-rich species (O_2, NO_3^-, MnO_2, $Fe(OH)_3$) and organic compounds in the soil zone. At Yucca Mountain, water from Well USW-H3 is the most reduced (Eh = -143 mV after pumping 1.5 gal/min for 2 months at a depth of 800 m). It contains no detectable oxygen, nitrate, detergent, or sulfide ion, but contains nitrite (NO_2^-) and iron. The absence of sulfide indicates that the water is not reducing enough to reduce sulfate ion. The absence of detergent indicates that the drilling fluid has been purged from the well. It has been suggested that the samples from Well USW-H3 were representative of water underlying the proposed repository horizon (LANL, 1984). The well is in the center of the Yucca Mountain block in a zone of low permeability. Wells outside or at the edges of the block (USW-H5, USW-H6, J-13) are more oxidizing (higher Eh, O_2, NO_3^-), suggesting that these areas are more actively recharged than the more stagnant waters observed in the block. Reducing conditions have also been observed in "thief samples" from wells USW-H1 and USW-H4 (negative Eh, no dissolved O_2). These data, however, have not yet been interpreted. At present, there are major uncertainties concerning the degree of equilibrium of the "thief sample" and the water in the particular zone sampled. The concentrations of organics reported in water samples from Yucca Mountain and vicinity are very low. Total organic content ranges from 0.15 mg/l (J-13) to 0.55 mg/l (UE25p-1).

Although the redox potential of ground water is set by conditions within the soil, it is buffered by redox couples of minerals within the rock units. Ogard and Kerrisk (1984) suggest that the dominant couples within Yucca Mountain tuffs are related to Fe-Ti oxide minerals (magnetite, ilmenite) and ferrous iron in sulfide minerals (pyrite) at depth. The presence of these minerals in sufficient quantity to reduce the entire waste inventory to insoluble forms would be a very favorable geochemical condition for this site. Vaniman and others (1984) suggested that a layer 3-6 meters thick below the entire area of the repository contains enough Fe^{2+} to achieve this condition for the inventory remaining after 1,000 years of storage. This calculation is based on the assumption of 0.16-0.33 percent by volume $FeTiO_3$ in the tuff and an assumed 70,000 MTHM repository loading of spent fuel containing Np, Pu, Tc, and U. The major uncertainty is whether or not the Fe^{2+} would be oxidized by the water and waste elements at a rapid enough rate to immobilize the radionuclides.

5.1.3 Rock-water interactions

The reaction of ground water with the tuff and other rock formations at Yucca Mountain controls the chemistry of pore fluids within the saturated and unsaturated zones. Previous attempts to estimate the composition of pore fluids within the unsaturated zone have been based both on experimental studies of tuff-water interactions and on theoretical calculations of mineral/water equilibria. These studies, as well as the stratigraphic distribution of minerals, suggest that the rock-water system in Yucca Mountain is probably not

at equilibrium. Although the fluid composition is controlled by reactions with the rock, not all of the observed solid phases are at equilibrium. Thermodynamic modeling of the system is useful, however, in describing changes that may occur as the free energy of the system decreases.

The mineral-water reactions that may influence the ground-water composition in pores in the rocks at Yucca Mountain have been summarized in Guzowski and others (1983). Table 5-2 summarizes many of these processes.

One way to determine whether these processes are important for the ground water at Yucca Mountain is to calculate saturation indices and activity-ratio diagrams for water samples. Such calculations have been carried out (LANL, 1984) and are summarized in Figures 5-5 and 5-6. Figure 5-5 shows the ratio of the ion activity product to equilibrium constant of calcite (saturation index) as a function of the saturation index for fluorite for water compositions from Yucca Mountain. Most of the waters are undersaturated with respect to calcite and fluorite. Waters from wells USW-H3 and UE25p-1 are saturated or near saturation with respect to calcite; UE25p-1 is saturated with respect to fluorite. In general, increasing saturation with respect to calcite is associated with higher degrees of saturation with respect to fluorite, magnesite ($FeCO_3$), and dolomite ($CaMg(CO_3)_2$) (Ogard and Kerrisk, 1984).

Figure 5-6 shows phase relations in the system Na-Si-Al at 25°C. Compositions of waters from the Yucca Mountain vicinity and mineral stability fields are plotted. These waters are supersaturated with cristobalite and near saturation with respect to pyrophyllite, Na-clinoptilolite, and kaolinite.

Kerrisk (1984a) has described the results of reaction-path calculations of ground-water chemistry and mineral formation at Rainier Mesa. Analyses of volcanic glass and integral ground-water samples from Yucca Mountain (see Figures 5-2 and 5-3) are similar to rock and water samples from Rainier Mesa. Based on these similarities, several researchers suggest that conclusions drawn from studies of rock-water interactions at Rainier Mesa will be applicable to Yucca Mountain (Ogard and Kerrisk, 1984). The main purpose of Kerrisk's study was to determine the extent to which equilibrium processes are sufficient to explain the ground-water and mineral composition at Rainier Mesa and Yucca Mountain. A number of important assumptions and approximations were made in these calculations: (1) formation constants for the zeolites present at NTS (clinoptilolite, heulandite, and mordenite) were estimated using the method proposed by Chen (1975); (2) equilibrium constraints were imposed at each stage of the reaction progress; and (3) the effects of slow kinetics (supersaturation and metastability) were simulated by suppressing the precipitation of selected phases. An initial water composition of pure water containing CO_2 (pH=4.5) was assumed. Experimentally determined cation leach rates were used, and aqueous silica activity was controlled by suppressing the precipitation of silica minerals. The results of these calculations are summarized below.

When cristobalite controls the aqueous silica activity, the mineral precipitates are cristobalite, smectite clays, clinoptilolite, and mordenite and are similar to those observed at Rainier Mesa. The aqueous phase pH, total dissolved silica and concentrations of Na, K, Ca, and Mg are all in the range observed at Rainier Mesa for calculations at 75°C and 125°C. Calculations at

Table 5-2. Processes important to ground-water chemistry at Yucca Mountain and NTS (Guzowski and others, 1983)

Process	Dissolved Constituent							
	Na^+	K^+	Ca^{2+}	Mg^{2+}	SO_4^{2-}	Cl^-	HCO_3^-	SiO_2
Dissolution of:								
vitric tuff	++	0	+	+		++	++	++
devitrified tuff	+	0	++	++		?	++	+
sulfates			++		++			
carbonates			++	++			++	
pyrite					++			
Precipitation of:								
montmorillonite		-	--	--				--
clinoptilolite	-	-	--	--				--
flourite			--					
calcite			--				--	
silica gel								--
Dissociation of carbonic acid							++	
Ion-exchange or fixation onto secondary minerals	+	--	--	--				
Evapotranspiration	++	++	++	++	++	++	++	++

Key: (++) = major source for this species; (+) = minor source for this species;
(O) = element is retained in solid phase during this process;
(?) = variable effect; (--) = sink for this species; (-) = minor sink.

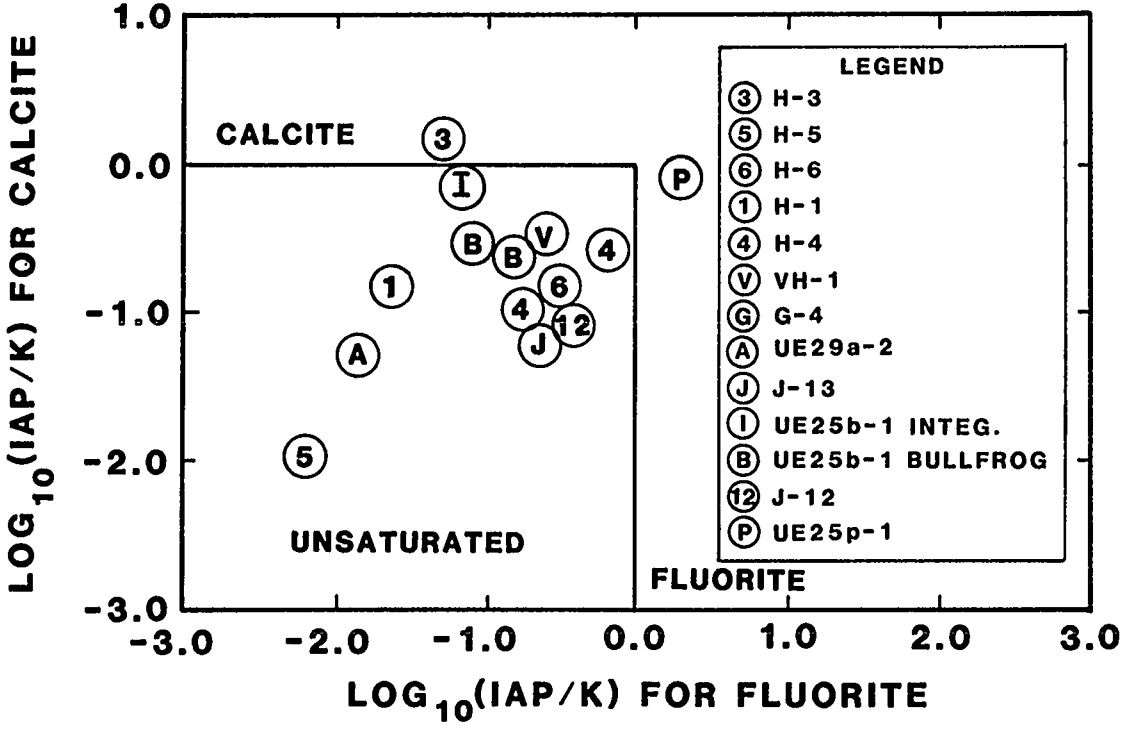

Figure 5-5. Saturation index ($\log_{10}$(IAP/K)) for calcite as a function of saturation index for fluorite for waters from Yucca Mountain (after Ogard and Kerrisk, 1984).

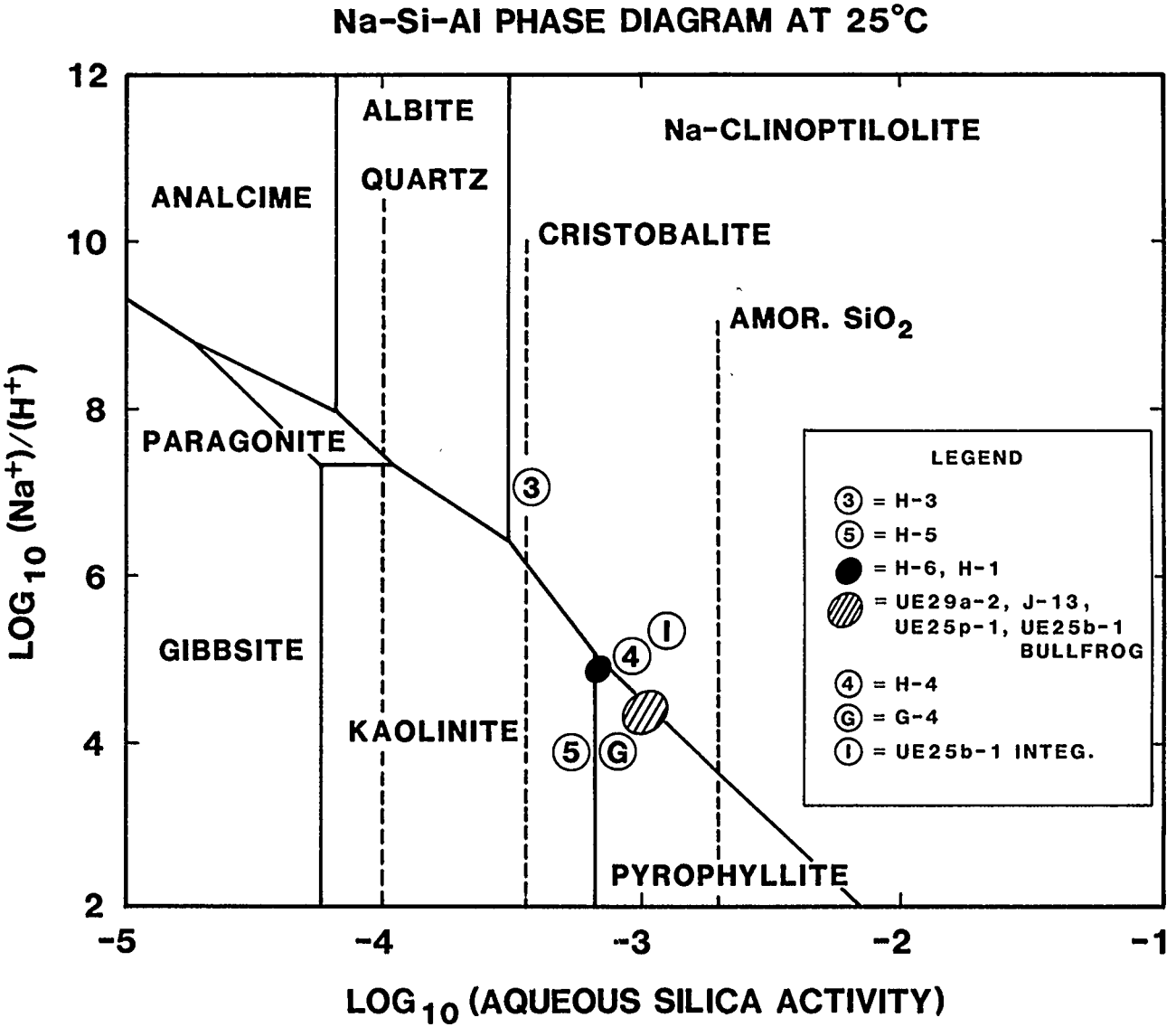

Figure 5-6. Activity diagrams for Na-Si-Al system at 25°C for waters from Yucca Mountain vicinity (LANL, 1984).

25°C and 175°C show poor agreement with observations in the field. These calculations correspond to the first stage of mineral alteration at NTS.

Field observations suggest that the next stages of mineral alteration involve the formation of a quartz, analcime, and illite assemblage followed by a quartz-albite and K-feldspar mixture. These transformations were simulated by allowing quartz to precipitate (lower SiO_2 activity). In Kerrisk's calculations, analcime would precipitate only if albite precipitation were suppressed. The relative stabilites of analcime and albite are probably functions of a number of additional variables such as temperature, pressure, and the activity of water. Agreement of calculated aqueous and mineral phase compositions with field observations was only fair in this case. Several other models for mineral diagenesis at Yucca Mountain have been proposed and were summarized by Guzowski and others (1983).

5.2 Radioelement Solubility and Speciation

5.2.1 Theoretical calculations

Solubility and speciation calculations for U, Pu, Am, Sr, Ra, and Tc have been carried out with the code EQ3/6 (Ogard and Kerrisk, 1984). Water compositions equivalent to those from wells J-13, UE25p-1 and USW-H3 were assumed (see Table 5-1). As discussed above, it has been suggested that these water compositions represent the extremes in water quality possible along flow paths from Yucca Mountain to the accessible environment. The results of the calculations are presented in Table 5-3 and Figures 5-7 to 5-12. The values for uranium and plutonium in J-13 water differ considerably from those published in previous Los Alamos reports (Daniels and others, 1982d; Wolfsberg and others, 1982). These differences are probably due to changes in the thermodynamic data base used in the EQ3/6 calculations.

5.2.2 Experimental solubility studies

Experimental studies of the solubility, dissolution, and radiolytic effects associated with colloidal $^{239}PuO_2$ have been described by Wolfsberg and Vaniman (1984). They found that Pu(V) undergoes both disproportionation and reduction and does not appear to reproportionate under the effects of alpha radiolysis. Colloidal Pu(IV) dissolves by oxidation to Pu(VI). An estimate of -57.1 for a log Ksp for colloidal PuO_2 was obtained by the disproportionation studies.

The results of actinide solubility measurements carried out at Lawrence Berkeley Laboratory have been described by Wolfsberg and Vaniman (1984), LANL (1984), and Crowe and Vaniman (1985). Initial studies have been carried out with $NaClO_4$ solution (0-1 M ionic strength, pH=7) to obtain data on actinide hydroxide formation without the presence of other complexing ligands. Oxidation state distributions of species in solution have been examined by adsorption spectrophotometry or extraction/coprecipitation methods. Solutions of $^{237}NpO_2^+$, $^{237}NpO_2^{2+}$, $^{243}Am^{3+}$, $^{242}Pu^{4+}$, $^{242}PuO_2^+$, and $^{242}PuO_2^{2+}$ have been studied. The experiments for Np suggested that the pentavalent species is the stable oxidation state in solution for both initial solutions studied (Np(V), Np(VI)). The measured neptunium solubility was $10^{-3.4}$M. A solubility of

Table 5-3. Waste-element solubilities in water from three Yucca Mountain wells (after Ogard and Kerrisk, 1984)

	Well J-13	Well UE-25p#1 (1298 to 1792 m)	Well H-3
Uranium			
Solubility (m/ℓ)	3.65×10^{-3}	1.74×10^{-3}	4.05×10^{-8}
Solid	Schoepite[a]	Rutherfordine[b]	Uraninite[c]
Primary aqueous species	$(UO_2)_2CO_3(OH)_3^-$ (98%)	$UO_2(CO_3)_2^{2-}$ (54%)	$UO_2(CO_3)_3^{4-}$ (86%)
	$UO_2(CO_3)_2^{2-}$ (1%)	$(UO_2)_2CO_3(OH)_3^-$ (31%)	$U(OH)_5^-$ (8%)
		$UO_2(CO_3)_3^{4-}$ (13%)	$UO_2(CO_3)_2^{2-}$ (7%)
		$UO_2CO_3^\circ$ (2%)	
Plutonium			
Solubility (m/ℓ)	1.79×10^{-6}	3.11×10^{-8}	1.33×10^{-5}
Solid	$Pu(OH)_4$[d]	$Pu(OH)_4$[d]	$Pu(OH)_4$[d]
Primary aqueous species	PuO_2^+ (71%)	$Pu(OH)_5^-$ (94%)	$Pu(OH)_5^-$ (100%)
	$PuO_2F_3^-$ (20%)	$Pu(OH)_4^\circ$ (6%)	
	$Pu(OH)_5^-$ (3%)		
	$PuO_2(CO_3)_2^{2-}$ (2%)		
	$PuO_2F_4^{2-}$ (2%)		
Americium			
Solubility (m/ℓ)	9.87×10^{-9}	2.16×10^{-8}	6.85×10^{-10}
Solid	$Am(OH)CO_3$	$Am(OH)CO_3$[e]	$Am(OH)CO_3$
Primary aqueous species	$AmCO_3^+$ (80%)	$AmCO_3^+$ (83%)	$Am(CO_3)_2^-$ (46%)
	$AmOH^{2+}$ (8%)	$Am(CO_3)_2^-$ (6%)	$Am(OH)_3^\circ$ (36%)
	AmF^{2+} (4%)	AmF^{2+} (4%)	$Am(OH)_2^+$ (12%)
	Am^{3+} (3%)	$AmSO_4^+$ (2%)	$AmCO_3^+$ (5%)
	$Am(CO_3)_2^-$ (3%)	$AmOH^{2+}$ (2%)	
		Am^{3+} (2%)	

Table 5-3. Waste-element solubilities in water from three Yucca Mountain wells (after Ogard and Kerrisk, 1984)--concluded

	Well J-13	Well UE-25p#1 (1298 to 1792 m)	Well H-3
Strontium			
Solubility (m/ℓ)	8.04×10^{-4}	5.27×10^{-4}	3.28×10^{-6}
Solid	Strontianite[f]	Strontianite[f]	Strontianite[f]
Primary aqueous species	Sr^{2+} (96%)	Sr^{2+} (86%)	Sr^{2+} (94%)
	$SrSO_4^\circ$ (4%)	$SrSO_4^\circ$ (14%)	$SrSO_4^\circ$ (6%)
Radium			
Solubility (m/ℓ)	3.39×10^{-7}	9.29×10^{-8}	2.94×10^{-7}
Solid	$RaSO_4$	$RaSO_4$	$RaSO_4$
Primary aqueous species	Ra^{2+} (99%)	Ra^{2+}(99%)	Ra^{2+} (99%)
Technetium			
Solubility (m/ℓ)	Large[g]	Large[g]	2.06×10^{-12}
Solid	--	--	Tc_3O_4
Primary aqueous species	TcO_4^- (100%)	TcO_4^- (100%)	TcO_4^- (91%)
			$TcO(OH)_2$ (9%)

[a] Schoepite is $UO_2(OH)_2 \cdot H_2O$.

[b] Rutherfordine is UO_2CO_3.

[c] Uraninite is UO_2.

[d] Also known as hydrous PuO_2; crystalline PuO_2 would give a much lower solubility but may not control solubility.

[e] $Am_2(CO_3)_3$ is less soluble under these conditions, but the thermodynamic data for this solid are uncertain.

[f] Strontianite is $SrCO_3$.

[g] Technetium would be very soluble (>1 m/ℓ) under these conditions.

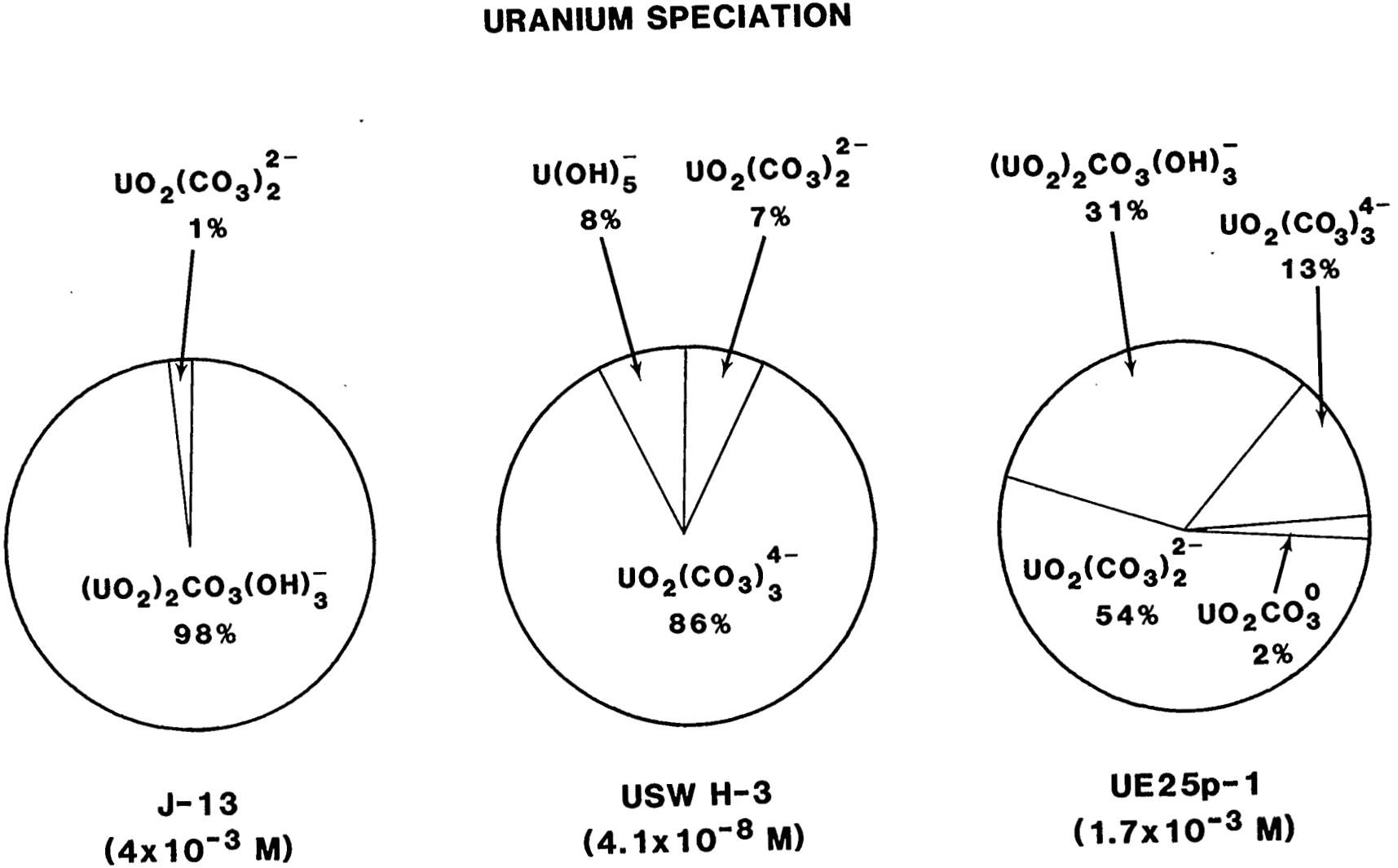

Figure 5-7. Speciation of uranium in waters from Yucca Mountain. Total concentration is in millimoles per liter. Percent of each species is shown (see Table 5-3).

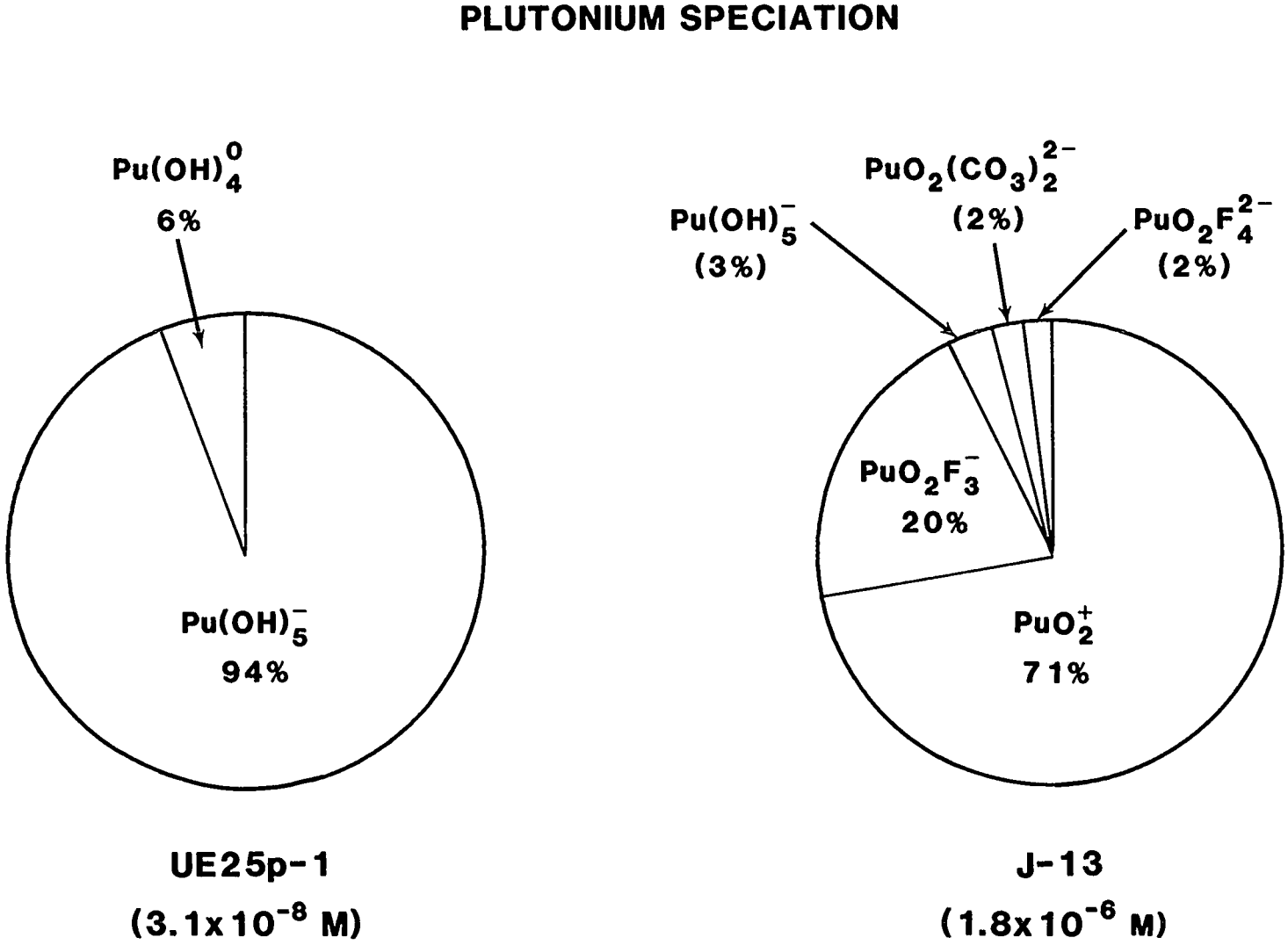

Figure 5-8. Speciation of plutonium in water from Yucca Mountain. Total concentration is in millimoles per liter. Percent of each species is shown (see Table 5-3).

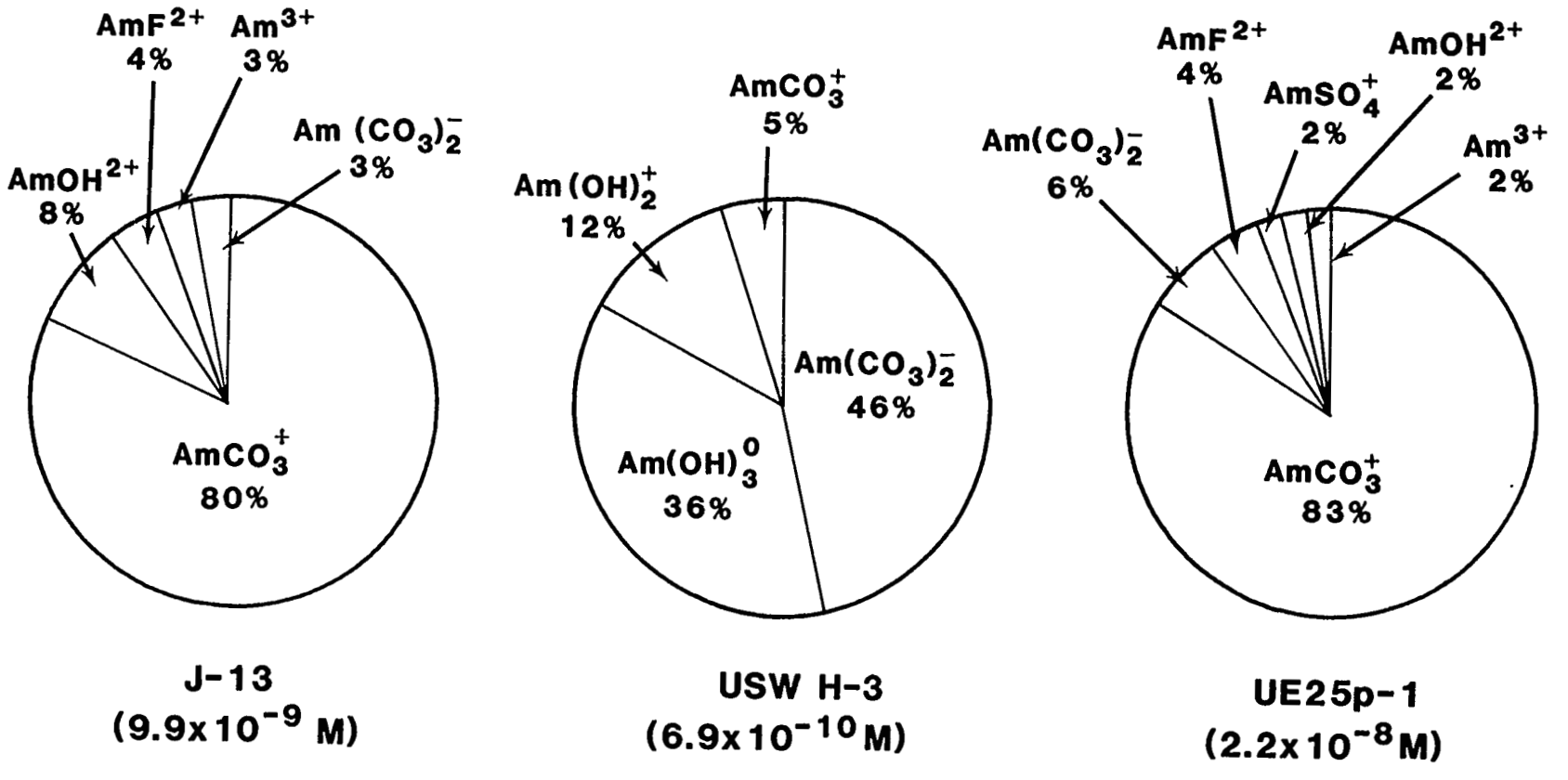

Figure 5-9. Speciation of americium in water from Yucca Mountain. Total concentration is in millimoles per liter. Percent of each species is shown (see Table 5-3).

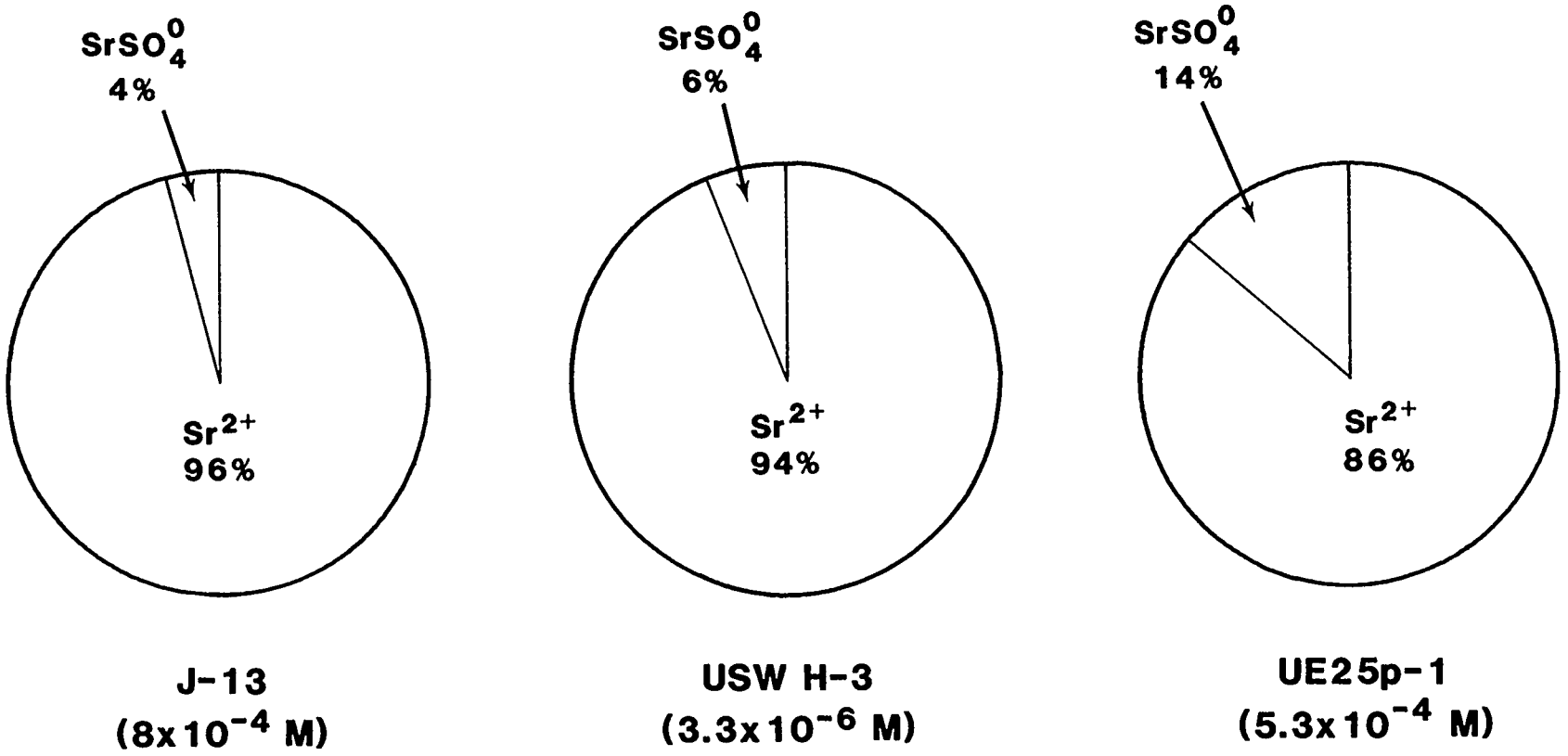

Figure 5-10. Speciation of strontium in water from Yucca Mountain. Total concentration is in millimoles per liter. Percent of each species is shown (see Table 5-3).

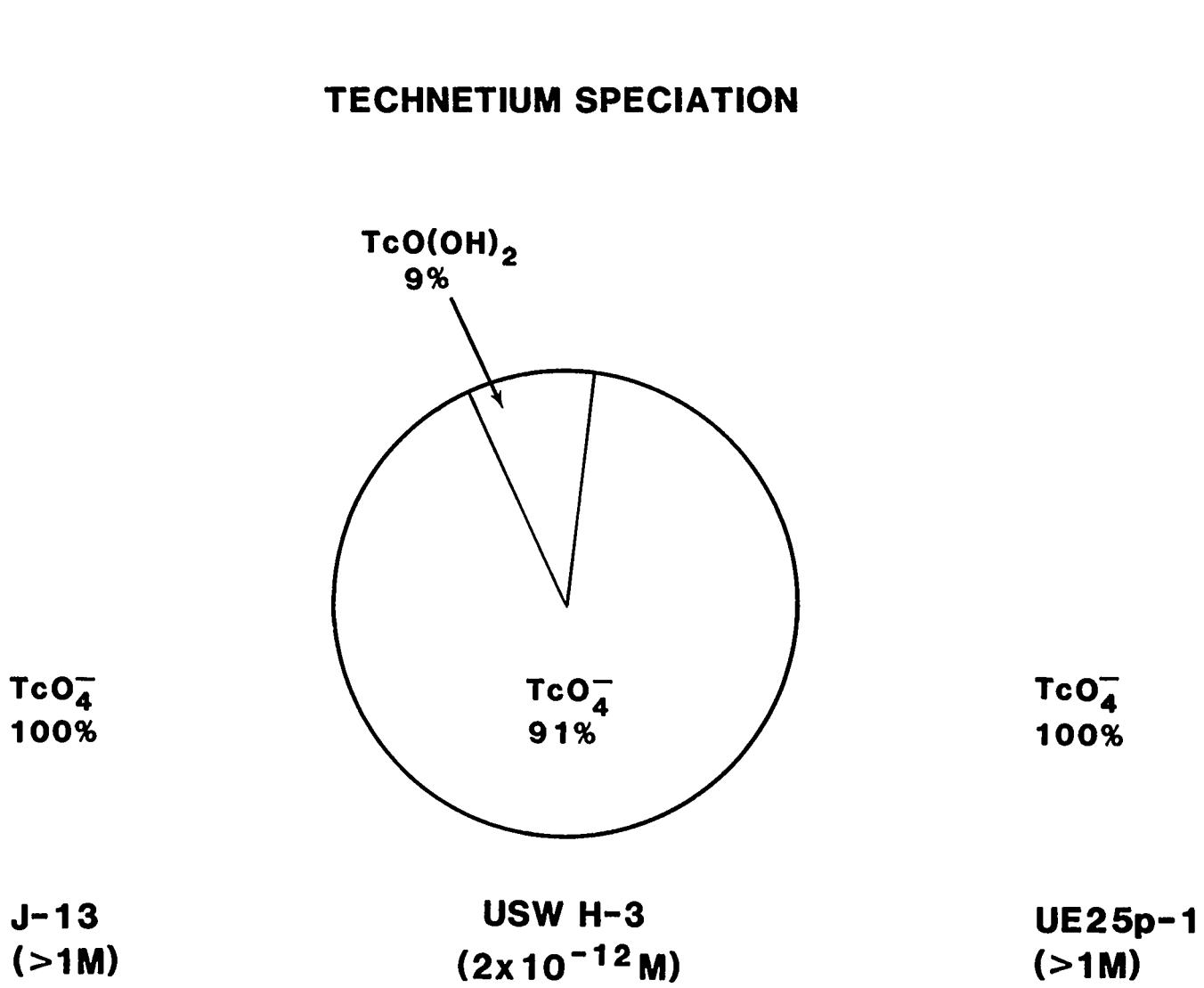

Figure 5-11. Speciation of technetium in water from Yucca Mountain. Total concentration is in millimoles per liter. Percent of each species is shown (see Table 5-3).

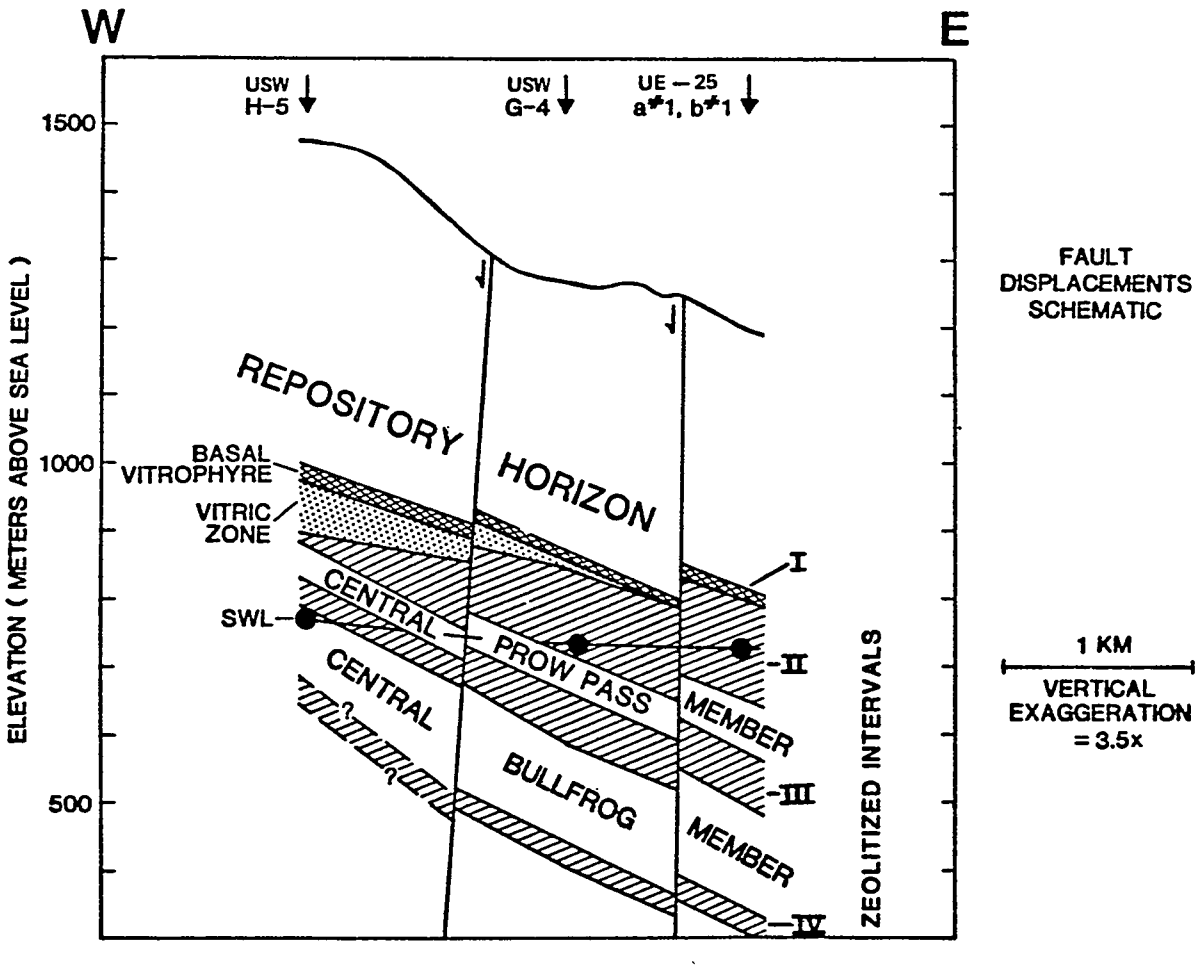

Figure 5-12. Sorptive stratigraphy of Yucca Mountain (Bryant and Vaniman, 1984).

$10^{-3.5}$ M was measured for Am^{3+}, which agrees well with previous experiments at PNL (Rai and others, 1983) with amorphous $Am(OH)_3$. Measured solubilities of Pu^{4+}, PuO_2^+ and PuO_2^{2+} were quite different. The solubility of solutions containing Pu^{4+} averaged $10^{-7.6}$M, which is within the range spanned by literature values for crystalline PuO_2 and amorphous $PuO_2 \cdot xH_2O$. The solubility measured in initial solutions of PuO_2+ was $10^{-8.5}$M, which is 7 orders of magnitude lower than previously reported solubilites for $PuO_2(OH)$. Finally, the solubility measured in solutions starting with PuO_2^{2+} was $10^{-6.9}$M, which agrees with solubilities measured for the homologs amorphous $NpO_2(OH)_2$ and $UO_2(OH)_2$. Future experiments at LBL will repeat these studies using J-13 water.

5.2.3 Sensitivity studies

Kerrisk (1984b) has carried out a sensitivity analysis to assess the importance of solubility in radionuclide release rates. Three models were compared: (1) a model in which the radionuclide dissolution rate was equal to the bulk congruent dissolution rate, (2) a model in which the dissolution rate of each radionuclide was set equal to the lesser of the bulk dissolution rate or the saturation-limited rate (solubility • volumetric flux), and (3) a model in which the dissolution rate was limited by diffusion into water flowing past the waste form and the solubility-limited saturation of the water at the solid/water interface. For conditions considered reasonable for a repository in the Topopah Spring Member, the calculations indicated that for spent fuel, releases of U, Pu, Am, and Sn were solubility-limited in the saturation-limited model and that U, Pu, Am, Sr, and Ra were solubility-limited in the diffusion model. For high level waste, Am and Sr were solubility-limited in the saturation model, whereas U, Pu, Am, and Sn were solubility-limited in the diffusion model.

The sensitivities of the results to the bulk fractional dissolution rate, waste element solubilities, and water recharge rate assumed in the calculation were also examined. For spent fuel, it was found that the results were very sensitive to the fractional dissolution rate and moderately sensitive to the solubilities and water recharge rate. For high-level waste the results were sensitive to the bulk fractional dissolution rate and insensitive to the other parameters. The results of the saturation-limited model were more sensitive to the above parameters than those of the solubility-limited model.

5.3 Sorption

5.3.1 Sorptive stratigraphy

The interval between the proposed host horizon and the water table at several locations at Yucca Mountain has been divided into ten sorptive intervals. These are described in detail by Bryant and others (1984) and are listed below:

- Repository Horizon (Host Rock)
- Zeolite Interval I
- Basal Vitrophyre of Topopah Spring Member

- Vitric Zone
- Zeolite Interval II
- Central Prow Pass Member
- Zeolite Interval III
- Central Bullfrog Member
- Zeolite Interval IV
- Deeper Petrologic Zone

These units are described in Figures 5-12 and 5-13. The water table has been observed as high as the Central Prow Pass Member (USW-G1) and as low as Zeolite Interval IV below the Central Bullfrog Member.

The petrologic zones described above do not correspond to the formal stratigraphic units defined for Yucca Mountain. This new classification was proposed after the discovery of significant differences in the degree of alteration between the southern and northern exploration blocks at Yucca Mountain. These are described in detail by Vaniman and others (1984) and are summarized below:

- Less alteration was observed within the southern exploration block than the northern block. In particular, the tuff of Calico Hills is unaltered vitric tuff in USW-GU3, whereas the same unit is heavily zeolitized in drill cores to the north.
- Clays are less abundant in cores from the southern block.
- Mordenite is virtually absent in cores from the southern block.
- The trend of Ca+Mg→K→Na zeolite zonation observed in the northern block is not well defined in the southern block. The most recent summary of exchangeable cation compositions of clinoptilolite at Yucca Mountain (Bryant and Vaniman, 1984) suggests that a western alkalic zeolite group (USW-G1, USW-H5, USW-G3) can be distinguished from an eastern calcic group (UE25a-1b/1H, UE25p-1, J-13). The former group exhibits a K→Na compositional trend with increasing depth whereas the latter group is characterized by a K→Ca+Mg trend. Two drill cores (USW-G4, USW-H4) are intermediate in location and zeolite composition. The differences in composition of the exchangeable cations can be crudely related to the Si/Al ratio of the clinoptilolite and perhaps to sorption potential.

5.3.2 Sorption data

Radioelement sorption data for tuff samples are summarized in Tables 5-4 and 5-5. Table 5-4 describes the relation between measured batch sorption ratios and sample mineralogy for four general tuff lithologic types. The mean, standard deviation, range, and type of frequency distribution assumed

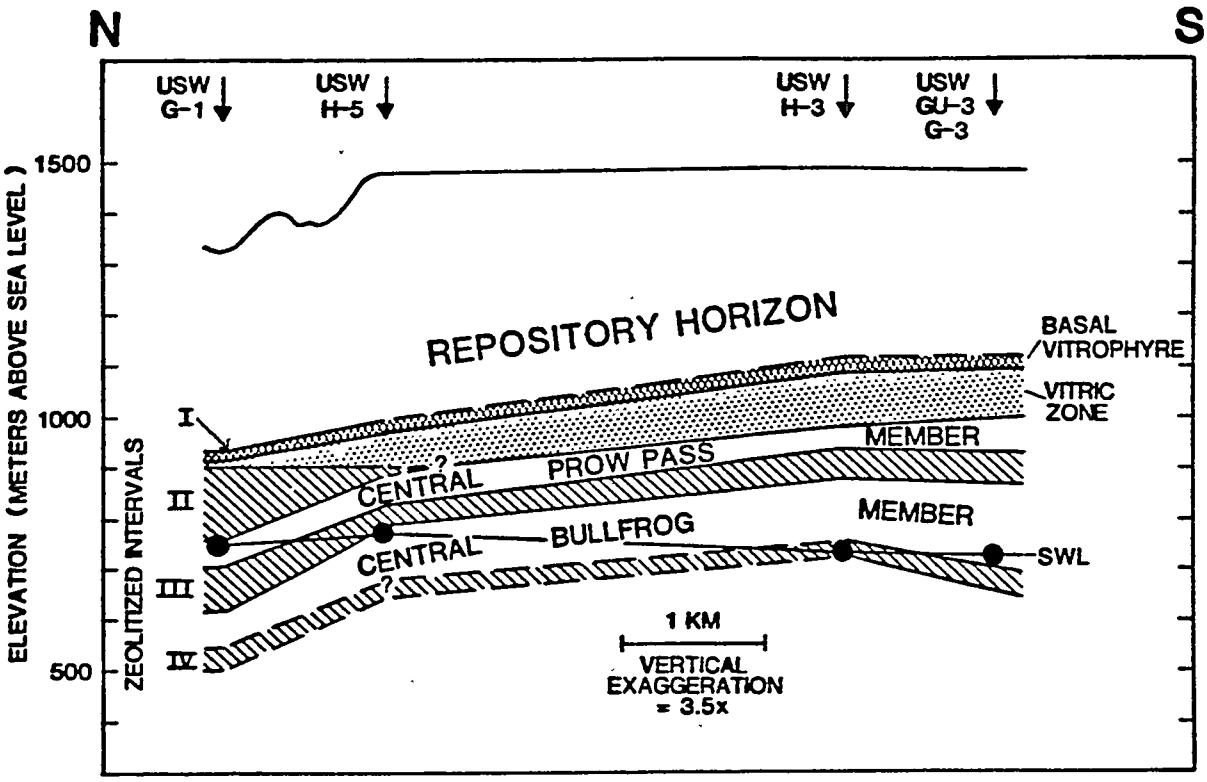

Figure 5-13. Sorptive stratigraphy of Yucca Mountain (Bryant and Vaniman, 1984).

Table 5-4. Comparison of sorption ratios for tuff lithologies (mℓ/gm)

Element	Devitrified tuff	Devitrified tuff with clay/glass	Vitric tuff ± clay	Zeolitized tuff
Am	2975 ± 1240 [a] 4, N [c] 1200:4000 [d]	[2.80 ± 0.93] [b] 4, L 130:13000	1430 ± 450 4, N 920:2000	[3.18 ± 0.32] 10, L 490:5500
Ba*	[3.00 ± 0.37] 17, L 340:1400	[2.92 ± 0.44] 29, L 140:10000	1155 ± 766 6, N 420:2100	[4.56 ± 0.60] 33, L 1170:250000
Ce	817 ± 427 13, N 297:1630	332 ± 293 5, N 82:730		[3.52 ± 0.72] 19, L 100: 59000
Cs*	596 ± 237 17, N 290:1100	[2.94 ± 0.45] 29, L 120:13300	[2.64 ± 0.67] 5, L 120:5800	[3.94 ± 0.40] 31, L 1160:42000
Eu*	1154 ± 614 15, N 68:2250	[3.04 ± 0.44] 29, L 90:5600	111 ± 68 4, N 38:190	[3.43 ± 0.45] 29, L 200:15000
Np	5.7 ± 0.8 5, N 4.9:7.0		2.1 ± 0.1 2, N 2.0:2.2	6.5 ± 3.5 6, N 4.0:11
Pu	224 ± 110 7, N 64:420	[2.24 ± 0.56] 4, L 90:1200	325 ± 85 4, N 210:410	[1.66 ± 0.32] 12, L 19:250

Table 5-4. Comparison of sorption ratios for tuff lithologies (mℓ/gm)--continued

Element	Devitrified tuff	Devitrified tuff with clay/glass	Vitric tuff + clay	Zeolitized tuff
Se	10.0 ± 7.1	[0.72 ± 0.46]	3.7 ± 3.1	5.7 ± 4.0
	2, N	5, L	3, N	5, N
	5:15	2:25	1:7	1.8:11
Sr	86 ± 50	111 ± 77	[1.85 ± 0.49]	[3.76 ± 0.68]
	16, N	26, N	5, L	34, L
	30:195	41:280	24:280	148:81000
Tc	0.40 ± 0.32	0	0.02 ± 0.02	0.01 ± 0.01
	7, N	1	6, N	3, N
	0:0.81	-	0:0.04	0:0.02
U	14 ± 26	3.4 ± 4.0	5 ± 10	6.2 ± 3.1
	4, N	8, N	4, N	7, N
	0:54	0:10	0:20	2.5:11

a mean ± standard deviation for assumed normal distribution
b [mean ± standard deviation] in $\log_{10}$ units for assumed lognormal distribution
c number of values, distribution assumed (N = normal; L = lognormal)
d minimum value : maximum value
* data for deionized water and water from well UE25p-1 are included in the means for vitric and zeolitized tuffs for Ba, Cs, and Eu.

Table 5-5. Summary of sorption data for stratigraphic sorption intervals

Sorption Interval	Element			
	Am	Ba, Ra	Cs	Eu
Host Rock	3350±354 2, N 3100:3600	575±332 2, N 340:810	515±163 2, N 400:630	84±23 2, N 68:100
Zeolite 1		3400	855	160000
Basal Vitrophyre	1110±269 2, N 920:1300	1585±690 4, N 640:2100	390±57 2, N 350:430	165±35 2, N 140:190
Vitric Zone	1750±354 2, N 1500:2000	357±250 3, N 82:570	108±58 3, N 45:160	[2.56±1.45] 3, L 38:17000
Zeolite 2	[3.18±0.32] 10, L 490:5500	[4.66±0.43] 23, L 6180:150000	[3.9±0.2] 19, L 3660:17000	[3.74±0.43] 21, L 1340:100000
Central Prow Pass	4700	[2.92±0.64] 11, L 162:1400	[2.81±0.41] 11, L 184:3650	878±598 9, N 110:1900
Zeolite 3	4300	[4.46±0.71] 15, L 1170:250000	[4.02±0.59] 12, L 1160:42000	[3.17±0.27] 12, L 779:5600
Central Bull Frog	372±309 2,N 153:590	[2.70±0.37] 16, L 140:3040	[2.75±0.36] 15, L 120:2020	[2.99±0.43] 12, L 340:5500
Zeolite 4		63000	7700	200
Deep Zone		7427±5685 10, N 1000:15000	[3.52±0.39] 10, L 1080:16000	[3.22±0.54] 9, L 440:15000

Table 5-5. Summary of sorption data for stratigraphic sorption intervals--(continued)

Sorption Interval	Element				
	Np	Pu	Sr	Tc	U
Host Rock	5.1±0.3 4, N 4.9:5.4	287±84 4, N 240:420	46±22 2, N 30:61	0.44±0.38 4, N 0:0.81	5.0±7.1 2, N 0:10
Zeolite 1			260		0 2 0:0
Basal Vitrophyre		365±64 2, N 320:418	121±112 2, N 42:200		0 2 0:0
Vitric Zone	2.1±0.1 4, N 2.0:2.2	285±106 2, N 210:360	22±11 3, N 10:32	0.03±0.02 5, N 0:0.04	10±14 2, N 0:20
Zeolite 2	6.5±3.5 6, N 4:11	[1.66±0.32] 12, L 19:250	[3.86±0.52] 24, L 1760:81000	0.01±0.01 3, N 0:0.02	7.2±3.3 3, N 5.3:11.0
Central Prow Pass	6.4	77	[1.73±0.34] 10, L 22:194		28±36 2, N 2.4:54
Zeolite 3	9	230	[3.50±0.88] 12, L 148:56000	0.18±0.04 2, N 0.15:0.21	6.0±3.8 3, N 2.5:10
Central Bull Frog		85±7 2, N 80:90	[1.94±0.29] 13, L 41:280		1.0±0.9 3,N 0:1.7
Zeolite 4			42000		
Deep Zone			[2.93±1.02] 11, L 68:13200		2.15±2.33 2, N 0.5:2.33

(normal or lognormal) in the descriptive calculations are listed for each element for each lithology. Sorption and desorption ratios for individual rock samples are listed in Appendix 5.2, Tables A.5.2-1a to A.5.2-1r. Descriptions of the samples are found in Appendix 5.3. The sorptive categories listed in Appendixes 5.2 and 5.3 were combined in Table 5-4 as follows:

Devitrified tuff	includes	Devitrified tuff (Table A.5.2-1d)
Devitrified tuff with clay/glass	includes	Devitrified tuff with clay (Table A.5.2-1g) Devitrified tuff with clay and minor glass (Table A.5.2-1d)
Vitric tuff ± clay	includes	Vitric tuff (Table A.5.2-1r) Clay-rich vitric tuff (Table A.5.2-1b) Smectite (Table A.5.2-1m)
Zeolitized tuff	includes	Zeolitized tuff (Table A.5.2-a)

Average sorption ratios for radioelements in each of the sorptive intervals described in Section 5.3.1 and Figures 5-12 and 5-13 are summarized in Table 5-5. Sorption and desorption ratios for individual rock samples are sorted by sorption interval in Appendix 5.2, Tables A.5.2-2a to A.5.2-2j.

The data included in Appendix 5 and summarized in Tables 5-4 and 5-5 were compiled from sorption data published by Los Alamos National Laboratory as of February 1985 (Daniels and others, 1982a, 1982b, 1982c, 1982d; Daniels, Erdal, and Vaniman, 1983; Ogard, Daniels, and Vaniman, 1983; Ogard, Wolfsberg, and Vaniman, 1983; Wolfsberg and others, 1981, 1982; Wolfsberg, Vaniman, and Ogard, 1983; Bryant and Vaniman, 1984; Wolfsberg and Vaniman, 1984; and Crowe and Vaniman, 1985). Classification of rock samples by sorption category was based on descriptions of the rock samples in the above reports. Classification by sorptive interval was based on the sample depth and descriptions of the sorption intervals given by Bryant and Vaniman (1984).

There are no sorption data measured under unsaturated conditions. Although several of the samples were taken from the unsaturated zone, the sorption experiments were conducted under saturated conditions. The data presented in the tables are for experiments carried out under oxidizing conditions with J-13 well water at room temperature, except where indicated otherwise.

Sorption data published in reports of Los Alamos National Laboratory (LANL) through December 1982 (Daniels and others, 1982d) were summarized by Guzowski and others (1983). The results of parametric studies of the effects of a number of experimental parameters were also reviewed in the latter report and will not be discussed here. The data from sorption experiments published in the LANL reports since December 1982 and presented at LANL (1984) are summarized below. These studies examined the dependence of measured sorption ratios on substrate mineralogy, water composition, tracer concentration, kinetic effects, controlled atmosphere, and experimental design. The following discussion is intended to be neither a comprehensive review nor a

critical evaluation of the Los Alamos research. For detailed descriptions of experimental methods and results, the reader is directed to the references listed in the text and bibliography.

5.3.2.1 Data for Ba, Ra, Se, U, Th, and Sn

A comparison of sorption ratios for barium and radium was made by Ogard, Wolfsberg, and Vaniman (1983). They concluded that barium is a reasonable analog for radium in sorption studies because measured sorption ratios for the two elements agreed to within a factor of two for all experiments. The data for barium and radium were combined in Table 5-5 but are listed separately in Appendix 5.

The average for all sorption ratios for selenium is 9 ± 8 mℓ/gm. No clear correlation between sorption ratio and sample mineralogy was observed (Ogard, Wolfsberg, and Vaniman, 1983).

Sorption ratios for uranium were measured for a variety of tuff lithologies under ambient conditions. Measured ratios were low, ranging form 0 to 54 with a mean of 4.3 mℓ/gm calculated from an assumed lognormal distribution. The standard deviation of the mean was ±0.48 log units.

Sorption ratios for thorium, measured in J-13 water under ambient conditions, ranged from 140 mℓ/gm (zeolitized tuff) to 1,212 mℓ/gm (devitrified tuff) (LANL, 1984).

Tin sorption and desorption ratios on devitrified, zeolitic, and devitrified tuff with minor calcite or glass were measured in J-13 and UE25p-1 waters. No clear trend in these data relate measured sorption ratio to mineralogy, water composition, or experimental design (LANL, 1984).

5.3.2.2 Data for additional minerals and tuff lithologies

The ability of minor minerals to enhance the sorptive ability of tuff was examined in several sets of experiments. Several general observations may be made:

- The sorptive ability of vitric tuff does not correlate significantly with the absolute glass content of a sample.
- Sorption of Cs, Ba, Pu, and Am, may be enhanced by the presence of clay, whereas the behavior of Sr is unaffected.
- The sorptive behavior of tuff from drill holes USW-G2 and -GU3 has been examined. These samples were rich in mordenite, glass, calcite, and analcime. Sorption ratios for Sr, Cs, and Ba in mordenite-rich samples in J-13 water were fairly high, whereas ratios for Am, Pu, Np, and Eu were low. The presence of calcite enhanced the sorption of Eu, Am, and Pu. Each of the zeolites examined affected the sorptive behavior of the tuff differently. Mordenite and clinoptilolite strongly sorb Cs and Ba to approximately the same extent, whereas the presence of analcime does not enhance the sorptive ability of tuff for Sr, Cs, or Ba. Mordenite

does not affect the sorptive behavior of devitrified tuff toward Sr, Pu, or Am.

5.3.2.3 Effects of water chemistry and atmosphere on sorption ratios

Changes in J-13 and UE25p-1 water composition when equilibrated with tuff samples were studied. Sample G4-1502 (zeolitized tuff) caused the greatest changes in J-13 water composition. Magnesium, strontium, potassium, calcium, and silica were removed from the water, whereas concentrations of sodium, fluorine, and chlorine and pH all increased as a result of the water/rock interaction (LANL, 1984).

Sorption ratios for Sr, Cs, Ba, and Eu on a zeolitized tuff (GU-3-1302) and on a vitric/devitrified tuff (G1-2233) in deionized, J-13, and UE25p-1 waters are compared in Table 5-6. With the exception of the Eu measurements, sorption ratios in the more saline UE25p-1 waters are lowest. A consistent effect related to mineralogy can be observed: sorption ratios for the vitric/devitrified tuff are lower. The lower sorption ratios in the more saline waters have been attributed to competition among radionuclides and major ions for the sorption sites (Crowe and Vaniman, 1985). The compositions of waters from J-13 and UE25p-1 are compared in Table 5-1 and Figure 5-1.

The effect of CO_2 on Np sorption rates has been examined for several tuffs by conducting sorption experiments under a controlled-CO_2 atmosphere at a buffered pH (7.0). No significant effect has been observed (LANL, 1984).

Sorption ratios measured under atmospheric and anoxic (N_2-controlled) conditions have been compared for a number of elements on devitrified and zeolitized tuff samples. The following elements exhibited no effect: Cs, Sr, Ba, Ce, Eu, Na, Se, Am. Sorption ratios for Mn and Sn were lower in the anoxic atmosphere by factors of 2 to 4. Rd values for Pu, Tc, U, and Np were higher in the anoxic atmosphere by factors of 2 to 10. At present, no adequate explanations of these trends are available.

5.3.2.4 Effect of tracer concentration on sorption

Neptunium sorption ratios have been measured over seven orders of magnitude change in tracer concentration. No significant concentration effect has been observed; the sorption ratio decreased by a factor of 2 over the concentration range (LANL, 1984).

Cesium exhibited non-linear sorption behavior over the concentration range 1.8×10^{-9} M to 1.3×10^{-3} M. The sorption ratio decreased from 1,130 mℓ/gm in the low concentration experiments to 19 mℓ/gm in the high concentration runs using the 75 to 500 μm size fraction of a devitrified tuff sample (G1-2840) (Daniels, Erdal, and Vaniman, 1982).

5.3.2.5 Effects of experimental design on sorption ratios

A sorption ratio of 160 mℓ/gm has been measured for plutonium in long term (more than two week) batch sorption tests using a vitric tuff sample (G1-1292). This R_d value would correspond to a retardation factor of several hundred in transport. In column tests with the same sample and a contact time

Table 5-6. Comparison of sorption and desorption ratios in Paleozoic, J-13, and deionized waters (after Crowe and Vaniman, 1985)

Core	Element	UE25p-1	J-13
		Sorption Ratios (mℓ/g)	
GU3-1301 (zeolitic)	Sr	10±2*	32±8
	Cs	45±5	160±60
	Ba	82±18	570±60
	Eu	> 17000	75±12
		Desorption Ratios (mℓ/g	
	Sr	32±1	90±20
	Cs	55±4	180±40
	Ba	140±30	660±100
	Eu	> 20000	110±40

Core	Element	UE25p-1	J-13	Deionized Water
		Sorption Ratios (mℓ/g)		
G1-2233 (vitric)	Sr	2000±330	48000±3000	> 56000
	Cs	7500±1100	13500±800	13000±1600
	Ba	41000±6300	250000±30000	55000±5300
	Eu	> 5600	900±200	810±100
		Desorption Ratios (mℓ/g)		
	Sr	3000±500	90000±40000	21000±12000
	Cs	8800±900	23000±6000	8700±3400
	Ba	59000±6000	240000±80000	34000±23000
	Eu	> 7800	5000±2000	1400±600

* Mean and standard deviation for 2 measurements

of a few hours, however, approximately 40 to 60 percent of the Pu in the feed solution showed little or no sorption (calculated retardation factor = 1.5). These results suggest that kinetic effects, colloid formation, or radioelement speciation reactions may be important under dynamic conditions and must be considered in transport modeling (Wolfsberg, Vaniman, and Ogard, 1983).

Horizontal and vertical shaking positions were compared in batch sorption tests. The horizontal position allowed more efficient mixing than the previously used vertical position, as indicated by a more rapid approach to steady-state conditions (Wolfsberg, Vaniman, and Ogard, 1983).

Long term (up to 9 months) Tc and Np sorption ratio measurements have been made for zeolitized, devitrified and glass-rich samples under atmospheric conditions. It was found that the loss of CO_2 to the atmosphere was a problem. No consistent time-dependent or mineralogy-dependent trends were observed (LANL, 1984).

Short-term (1 hour to 6 week) Am and Pu sorption experiments on a zeolitized tuff (G4-1502) have been carried out. Steady state was not obtained until after 2 to 3 days for both elements indicating some kinetic effects (Bryant and Vaniman, 1984).

Differences in sorption ratios between crushed-rock column and batch measurements have been examined for Sr, Cs, and Ba for 12 rock samples spanning lithologies ranging from vitrophyres to zeolitized tuff. No consistent trends have been observed. The majority of sample-element combinations showed rough equivalence for batch and column measurements; however, in other cases, column measurements or batch measurements were higher by factors ranging from 1 to 2. In only one reported case was the batch Rd measurement substantially larger (x11) than the column measurement (LANL, 1984).

A comparison of Rd values obtained from tuff wafers and crushed tuff has been made. Values for Sr and Ba for wafer experiments were higher than batch experiments, but no consistent trend was observed for Cs measurements (LANL, 1984).

5.4 Radionuclide Transport in the Unsaturated Zone

5.4.1 Effects of unsaturated media--general

In studies of radionuclide retardation in saturated tuff, the contributions of the various individual mechanisms discussed above are typically grouped into a single retardation constant R (Daniels and others, 1982a, 1982b, 1982c, 1982d). For the simulation of transport in unsaturated porous media, it is common to define a retardation constant that changes with the moisture content of the medium (Yeh and Luxmoore, 1982; Pin and Witten, 1983; Gureghian, 1983). The usual definition of the retardation constant for unsaturated flow is

$$R = 1 + \rho R_d/\theta, \qquad (1)$$

where R = Retardation constant,
R_d = Sorption ratio,

θ = Volume of water per unit volume of matrix, equal to the product of the porosity and fraction saturation,

and ρ = Bulk density of matrix.

When θ is equal to the porosity, the medium is saturated, and R from Equation 1 is equal to that determined in the experimental sorption studies conducted to date. Physically, R is the ratio of pore velocity to the contaminant migration velocity (Yeh and Tamura, 1982). The unsaturated convective-dispersion equation for linear retardation and no additional source or sink mechanisms is given by

$$\theta R\frac{\delta C}{\delta t} = - \nabla\bullet(UC) + \nabla\bullet(\theta\bar{D}\bullet\nabla C) - \lambda\theta RC - C\frac{\delta\theta}{\delta t} \qquad (2)$$

where C = Concentration,

$\bar{D}$ = Dispersion coefficient tensor,

U = Darcy velocity,

λ = Decay rate constant,

t = Time,

and $$\nabla = i\frac{\delta}{\delta x} + j\frac{\delta}{\delta y} + k\frac{\delta}{\delta z}$$

Equation 2 applies when contaminant transport occurs in the liquid phase only. If transport occurs in both the liquid and vapor phases, two equations similar to Equation 2 must be used. These equations are coupled through a term representing interchange between the two phases.

The application of Equations 1 and 2 implies that several important assumptions have been made concerning the effects of unsaturation. Equation 1 is strictly correct only when retardation is due to linear radionuclide/matrix interactions and when the total surface area of the solid (i.e., all active sites) is available to the radionuclide, independent of the degree of saturation. The condition that all active sites be available for interaction corresponds to porous media with very fine pores that remain saturated or porous media that are readily wetted and retain several monolayers of sorbed water. This bound water can serve as a radionuclide transport path from the bulk liquid phase to the active sorption/ion exchange sites. If the number of available active sites changes as the percent saturation changes or retardation is the result of a combination of mechanisms, then Equation 1 may not be applied <u>a priori</u>. Thus, the use of Equation 1 in transport calculation could result in underestimation of release rates, because if all possible sites are assumed to be always accessible and able to retard radionuclide migration, calculated release rates are the smallest possible values. On the other hand, use of a value of R with no correction for saturation content could result in overestimation of release rates. The error in the release rate could be substantial and would depend upon the magnitude of R, the retardation mechanism, and the degree of the change in saturation that occurs along the transport path.

5.4.2 Vapor phase transport

The presence of a vapor phase implies that a second radionuclide release path may exist. Under certain conditions, release rates of some radionuclides could conceivably be greater in the vapor phase than in the liquid phase. To date, reported research conducted as part of the Nevada Nuclear Waste Storage Investigations (NNWSI) has not addressed the problem of unsaturated radionuclide transport (Ogard and others, 1983a, 1983b; Wolfsberg and others, 1983). The possibility of vapor phase transport via diffusion and/or aerosol transport in fractures has been considered by Green and Evans (1983). Although the findings are inconclusive, it should be noted that they failed to consider the dominant transport mechanism, free and forced convection. Whether vapor phase transport represents an important release mechanism for a particular decay chain, as compared with liquid phase transport, depends upon the value of several parameters:

1. radionuclide vapor pressure.
2. radionuclide liquid phase mole fraction and activity coefficient,
3. percent saturation,
4. relative liquid and vapor phase transport rates,

and 5. liquid and vapor phase retardation.

The determination of the vapor phase concentration of a particular radionuclide is not straightforward, because of uncertainties about the chemical state of the liquid phase radionuclide and the large number of components that exist in the fluid. In order to perform a first-order analysis of vapor phase transport, it could be assumed that the liquid phase may be treated as an ideal solution (i.e., activity coefficient = 1). If the chemical state of the migrating species and an estimate of concentration are available, an upper bound on the vapor phase concentration may be calculated, because the vapor pressure of most "pure" radionuclides may be found in the literature. If the vapor phase concentration is negligible, as expected for most species, vapor phase transport effects need not be considered further for that species. If these preliminary calculations indicate a possible contribution of vapor phase transport, more rigorous calculations would be required, using estimates for all five parameters listed above. To date, this type of calculation does not appear to have been conducted. Because a first approximation may be generated with a minimum of effort, the calculations described should be conducted in the near future.

5.4.3 Matrix diffusion in fractured rock

For fractured welded tuff, the primary mode of radionuclide transport is the result of flow in the fractures. For retardation mechanisms such as sorption and ion exchange, the radionuclide may be retarded by interactions with the fracture surface and coating and also may migrate out of the fracture into the host rock. The transport of radionuclides from the fracture into the tuff matrix may be considered to be a three-step process: external or film-type mass transfer resistance at the fracture surface, molecular diffusion of radionuclides in the matrix, and possibly, configurational diffusion in zeolites and clays. For formations that are not highly fractured, the first two steps need not be considered, but configurational diffusion in zeolites and clays may still have a significant effect on

radionuclide migration. To assess the importance of each step for possible inclusion in a radionuclide transport model, the relative time scale for the step should be estimated and compared to the time scale of flow. If the time scale of a particular transport step is significantly shorter than the steps preceeding and following it, local equilibrium may be assumed, and kinetic effects associated with that particular mechanism ignored. When the flow time scale is longer than that of all matrix transport steps, the effects of matrix transport may be lumped into the retardation factor. In order to assess the relative rates of each of the three transport steps rigorously, the solution of three coupled partial differential equations describing convection/dispersion in the fracture, matrix duffusion, and configurational diffusion would be required.

The time scale for external or film mass transfer from the fracture to the fracture-matrix interface relative to diffusion in the matrix is a function of the fracture width, the effective matrix diffusivity, and a mass transfer coefficient. These parameters may be grouped into a dimensionless parameter, the Sherwood number:

$$N_{Sh} = kL/D_e \qquad (3)$$

where D_e = Effective diffusivity,
k = Mass transfer coefficient,
and L = Characteristic fracture width.

Mass transfer of a radionuclide from the bulk of the flow in the fracture into the matrix is a two-step process: external or film mass transfer followed by diffusion in the matrix. The slower of these two steps controls the overall mass transfer rate. The magnitude of the Sherwood number indicates the slower step. High Sherwood numbers imply that external mass transfer is faster and therefore can be neglected in determining the time scale of the process. It can result from a combination of high fluid velocity in the fracture, low matrix diffusivity, or low matrix porosity. Conversely, a low Sherwood number implies that the matrix diffusion step is faster than external mass transfer and can be neglected relative to the latter. When the fracture is unsaturated, less of the fracture surface area is wetted and in contact with radionuclide-containing fluid. Presuming that the matrix itself is still saturated, the effective Sherwood number will slightly decrease with decreasing saturation. The average fracture width has been determined for six tuff samples and was found to range between 57 and 252 μm (Ogard, 1983b). For a typical fracture width of 100 μm and diffusivity of 1×10^{-7} cm^2/s, the value of the mass transfer coefficient must be less than 0.001 cm/s for external resistance in the fracture to be of importance.

The effects of matrix diffusion in saturated welded tuff have been estimated using typical tuff physical properties and a theoretical diffusivity (Daniels and others, 1982c). Assuming that the characteristic matrix pore size is substantially greater than the kinetic diameter (i.e. effective molecular size) of the diffusing species, the effective diffusivity, D_e, may be related to the diffusion coefficient of the species in bulk solution (Satterfield, 1970) by

$$D_e = \varepsilon D_{AB}/\tau. \qquad (4)$$

The porosity, ε, is the fractional void volume of the matrix. The tortuosity factor, τ, accounts for pore constrictions, pore interconnections, pore direction, and dead-end pores. D_{AB} is the diffusion coefficient for the ion pair in solution. Sometimes the tortuosity factor defined in Equation 4 is written as τ^2/α, where α is a constriction factor and τ is a geometry parameter. Following regular practice (Satterfield, 1970), Equation 4 lumps these into a single constant. Typical values of the tortuosity factor are between 3 and 10 for a wide range of porous solids (Satterfield, 1970). For welded tuff, the effective matrix diffusivity is estimated to be 1.5×10^{-7} to 2.4×10^{-7} cm^2/s (Daniels and others, 1982d) if the tortuosity factor is assumed to be 10. The uncertainty associated with this value of the tortuosity factor is minor compared with the implied assumption that transient diffusion in tuff may be described by a unimodal pore model. The values given above serve as an upper bound for liquid phase matrix diffusion. If the matrix becomes unsaturated, the porosity ε is replaced by θ, and the value of the liquid phase effective diffusivity will decrease in direct proportion to the fractional moisture content. In the vapor phase portion of the matrix, if present, radionuclide diffusivities of volatile species will be substantially greater than the liquid phase values. Based on typical gas diffusivities (Hirschfelder and others, 1954) and the tuff physical properties reported by Daniels and others (1982c, 1982d), effective diffusivities in the vapor phase would be on the order of 10^{-5} to 10^{-2} cm^2/s. Of course, these larger effective diffusivities would be offset by a much-lower-concentration driving force in the vapor phase, as compared to the liquid phase.

Laboratory measurements of matrix diffusion in tuff samples have been reported by Walter (1982). The transport by diffusion of several species (NaBr, NaI, NaSCN) was studied in six tuff samples with porosities ranging from 0.194 to 0.405. Measurements were conducted by placing tuff samples between reservoirs of high and low tracer concentration. By measuring the change in concentration as a function of time, the diffusive flux and therefore, D_e, was calculated. Unfortunately, this type of experiment examines steady state behavior (even though the concentrations are changing, the time scale of the concentration change is much longer than the time scale for diffusion). By measuring steady-state diffusion only, the effects of dead-end pores and very small pores on the transport rate cannot be observed. Also, sorption and other retardation effects will lower the value of the transient effective diffusivity. In studies of diffusion in coal, which has a similar broad range of pore size, transient effective diffusivities were found to be one to two orders of magnitude smaller than steady-state values (Thimons and Kissell, 1973).

In addition to radionuclide diffusion in the matrix, configurational diffusion into zeolite crystals or clays contained in the tuff may affect the overall mass transfer rate. Zeolites are thought to contain a large fraction of retardation sites; however, as a result of the small pore diameters of zeolites, the large-pore potential excludes many radionuclides from entering the zeolite crystals. Due to the small pore size, many of the zeolite and clay pores will remain saturated under planned repository conditions (Breck, 1974; van Olphen, 1977). Rundberg (1984) has studied intracrystalline diffusion of Cs, Sr, and Ba in three tuff samples and compared them to published values for two natural zeolites. As expected, measured diffusi-

vities are much lower than free ion diffusion coefficients, because of the small pore size and resulting pore wall-ion interaction. Table 5-7 includes measured diffusion coefficients and the characteristic pore size. The values reported in Table 5-7 for the three tuff values represent upper bounds for the intracrystalline diffusion coefficients, because the rate of uptake by a particular crystal depends upon the crystal size. Rundberg obtained an upper bound on the crystal size of 1 μm using SEM techniques. These values of D_i will be substantially lower for radionuclides with larger effective sizes, such as high-molecular-weight free ions or radionuclides that form complexes. The ratio of the time scales for matrix diffusion to intracrystalline diffusion may be estimated if the two effective diffusivities, fracture spacing, crystal size, and retardation coefficients are known. The ratio of time scales for matrix diffusion to intracrystalline diffusion, α, is given by Smith (1984):

$$\alpha = \frac{D_i}{L_i^2 R_i} \quad \frac{L_M^2 R_M}{D_M}$$

where D_i = Effective intracrystalline diffusivity,
D_M = Effective matrix diffusivity,
L_i = Effective crystal radius,
L_M = Half-distance between fractures,
R_i = Retardation constant for the crystal,
R_M = Retardation constant for the matrix,
and α = Ratio of time scales.

Separate retardation constants are included because the effects of sorption or other retardation mechanisms are presumably different for the matrix and zeolite crystals. When α is greater than 100, matrix diffusion controls uptake and the pores in the zeolite are in equilibrium with the matrix. For this situation, intracrystalline diffusion may be ignored. When α is less than 0.01, intracrystalline diffusion will be much slower than matrix diffusion. Thus, for a step change in the radionuclide concentration in the fracture, a fairly rapid uptake by the matrix will be followed by a much slower uptake in the zeolite and clay particles. This phenomenon has implications for experimental sorption measurements. The end of the first rapid uptake due to matrix diffusion could be interpreted as the attainment of equilibrium. This would result in an underestimation of the retardation constant. For values of α between 0.01 and 100, the two transport steps are coupled, with neither one rate-controlling. As an approximation, the effects of retardation can be ignored. Using typical values of $D_M = 1 \times 10^{-7}$ cm^2/s, $D_i = 1 \times 10^{-15}$ cm^2/s, $L_M = 3$ cm (Scott and others, 1983), and $L_i = 0.5$ μm, a value of 36 is obtained for α.

Numerous studies of radionuclide transport in saturated fractures coupled with a single matrix diffusion step have been conducted and were reviewed by Guzowski and others (1983). Travis and others (1984a) have studied unsaturated flow in fractures coupled with migration of radionuclides into the matrix by diffusion. However, the effects of mass transfer resistance in zeolites and clays was not considered. The very low intracrystalline diffusion coefficients associated with the larger radionuclides may result in crystal uptakes at a rate that cannot be observed at the time scales of

Table 5-7. Intracrystalline diffusion coefficients for tuff and natural zeolites (Rundberg, 1984)

Sample	Pore Size (A)	D_i (cm^2/s) Cs	Sr	Ba
Clinoptilolite[1]	3.5*	$<2.3 \times 10^{-14}$	$<3.3 \times 10^{-15}$	$<2.8 \times 10^{-14}$
Montmorillonite[2]	5.6**	$<6.7 \times 10^{-15}$	$<1.1 \times 10^{-15}$	$<7.3 \times 10^{-15}$
Montmorillonite[3]	5.6**	$<7.8 \times 10^{-15}$	$<2.3 \times 10^{-15}$	$<7.3 \times 10^{-15}$
Chabazite	4.3*	4.9×10^{-13}	1.3×10^{-16}	1.3×10^{-13}
Mordenite	3.9*	5×10^{-15}	1.5×10^{-16}	4.5×10^{-15}

1. Highly zeolitized ash-fall tuff from Calico Hills.
2. Devitrified, partially welded tuff from Prow Pass.
3. Devitrified tuff from Prow Pass.

* Breck (1974).

** van Olphen (1977).

current experiments. This would have the net effect of underpredicting the retardation factor.

5.4.4 Transport modeling

Current hypotheses concerning transport in the unsaturated zone at Yucca Mountain are summarized below (Travis and others, 1984a, 1984b; LANL, 1984). It is believed that fracture flow in the unsaturated zone is unlikely, due to the high matric potential of tuff and the low infiltration rate at Yucca Mountain. Advection is dominated by the forces of gravity and capillary suction. Because of surface tension effects, water is preferentially drawn into the smallest available pores. This effect leads to greater constrictivity and lower permeability in the matrix. Matric potential data (see Figure 6-1, p. 143) suggest that at saturations below 50 percent, a pressure head in excess of 10 bars would be required to remove water from pores within the matrix. Advection and transport experiments in unsaturated tuff are not possible at present because of the difficulties in maintaining a pressure drop of such magnitude with available technology.

Calculations have been carried out with the computer code TRACR3D to simulate the transport of moisture in unsaturated, fractured porous rock (Travis and others, 1984a, 1984b; LANL, 1984). Some of the assumptions used in these calculations are illustrated in Figure 5-14. Given the conditions assumed in the simulations, the calculations suggest that significant fracture flow above the water table will occur only through highly-saturated tuff with

low matrix permeability. The effect of the degree of saturation on the depth of penetration of a slug of water in the rock can be seen by comparing Figures 5-15 and 5-16. Figure 5-15 shows that at a saturation level of 90 percent, a water slug will flow approximately 30 meters in a fracture 85 μm wide before it is held in place by surface potential, when the matrix diffusion coefficient for water, A, is 5×10^{-6} cm^2/s. If the rock matrix is less permeable ($A = 10^{-6}$ cm^2/s), the water slug will penetrate further into the rock (85 m). At a lower degree of saturation (Figure 5-16), the water slug will penetrate to a much shallower depth.

The analyses described above are based on an assumed infiltration rate of 8 mm/yr and the assertion that flux due to slug flow will be higher than that associated with film flow. Additional supporting evidence for these two important assumptions must be provided before these calculations can be interpreted to represent actual conditions at Yucca Mountain.

Calculations of radionuclide migration have been carried out using TRACR3D (Travis and others, 1984a, 1984b). The conceptual ground water flow path is illustrated in Figure 5-17. Upon leaving the repository, water flows through 50 m of the unsaturated, fractured, welded Topopah Springs Tuff, into 15 m of bedded tuff and then through 135 m of the zeolitized Calico Hills tuff layer. The water table lies within the fractured Calico Hills and Prow Pass tuff layers. The accessible environment is assumed to be located 10 km down the horizontal gradient along the water table. Concentration breakthrough curves for several radionuclides are shown for the Topopah Springs tuff layer (Figure 5-18), porous Calico Hills tuff (Figure 5-19), fractured Calico Hills tuff (Figure 5-20) and the 10 km horizontal transport path through saturated fractured tuff (Figure 5-21). These calculations indicate that none of the radionuclides studied will reach the accessible environment in less than 10,000 years if the assumptions inherent in the analyses are valid.

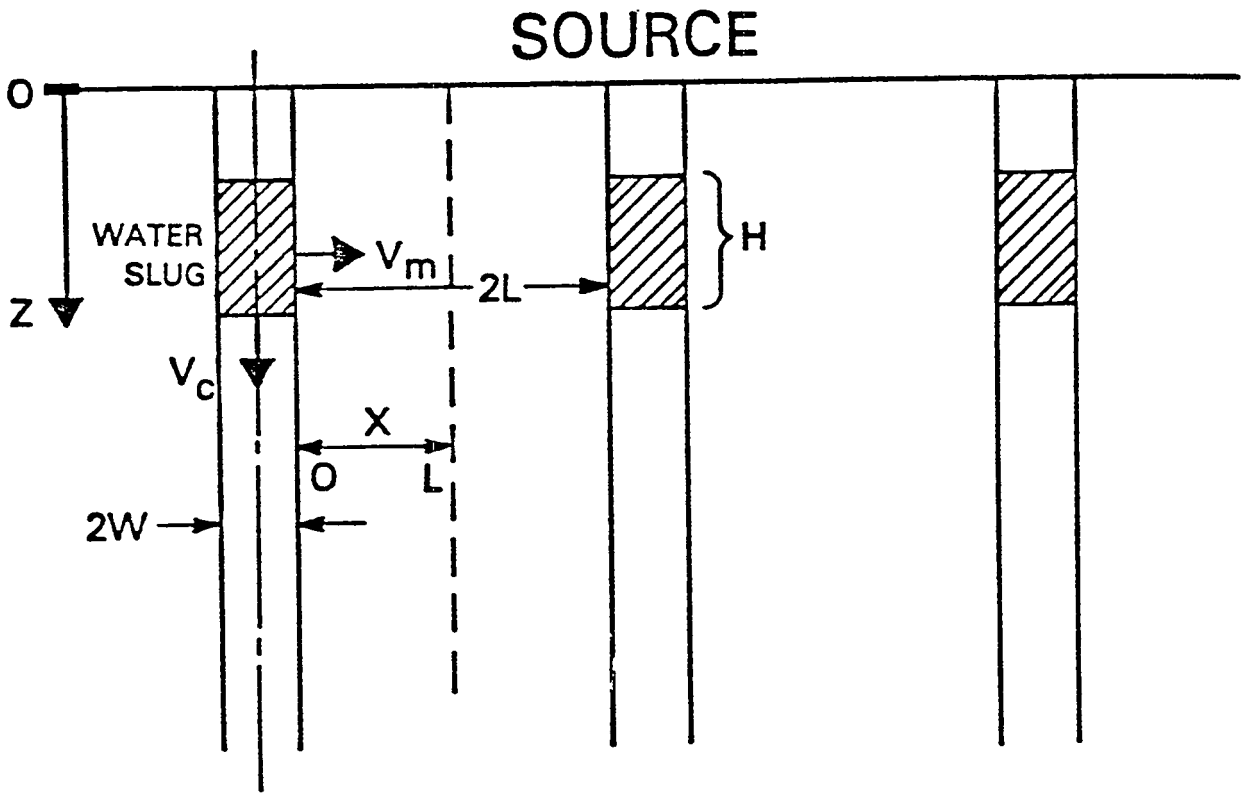

Figure 5-14. Scenario used for fracture flow analysis (Travis and others, 1984b).

2W = 10μ - 400 μ
2L = 10 cm
H = 100 - 2000 cm
V_m = f(A, saturation)
V_c = 0.008 - 3.2 cm/s

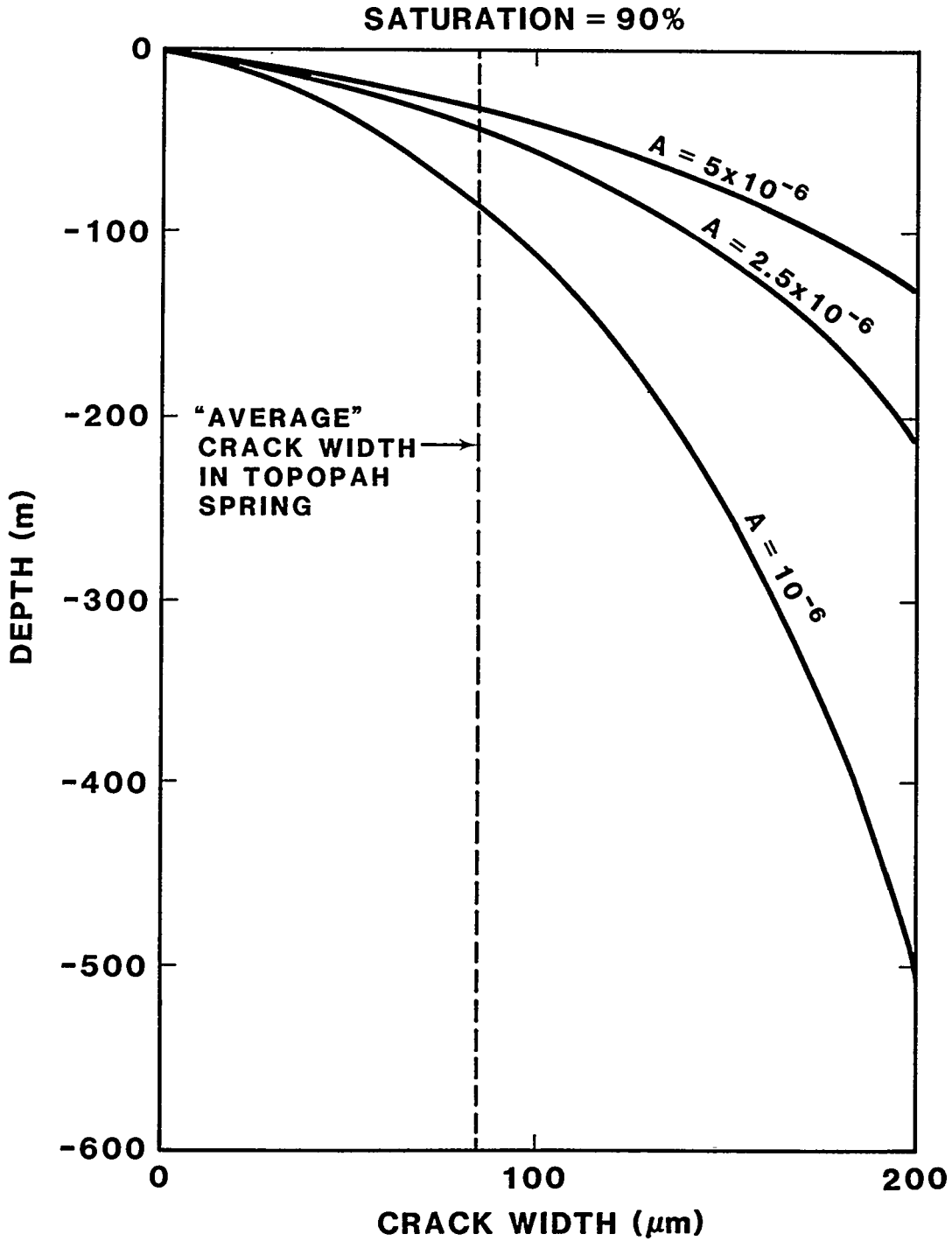

Figure 5-15. Depth reached by water slug as a function of crack width and diffusion coefficient A for matrix saturation of 90 percent (Travis and others, 1984b).

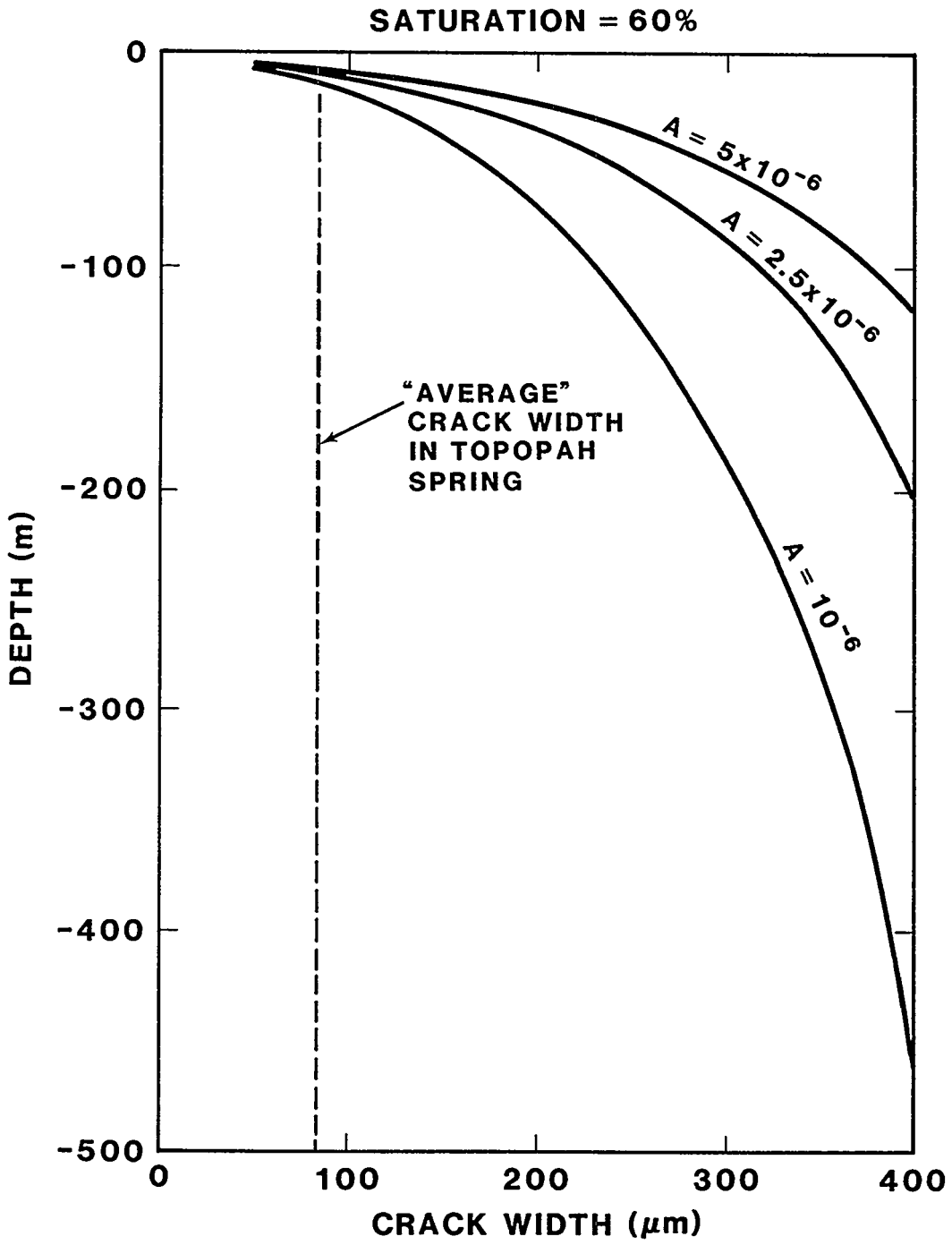

Figure 5-16. Depth reached by water slug as a function of crack width and diffusion coefficient A for matrix saturation of 60 percent (Travis and others, 1984b).

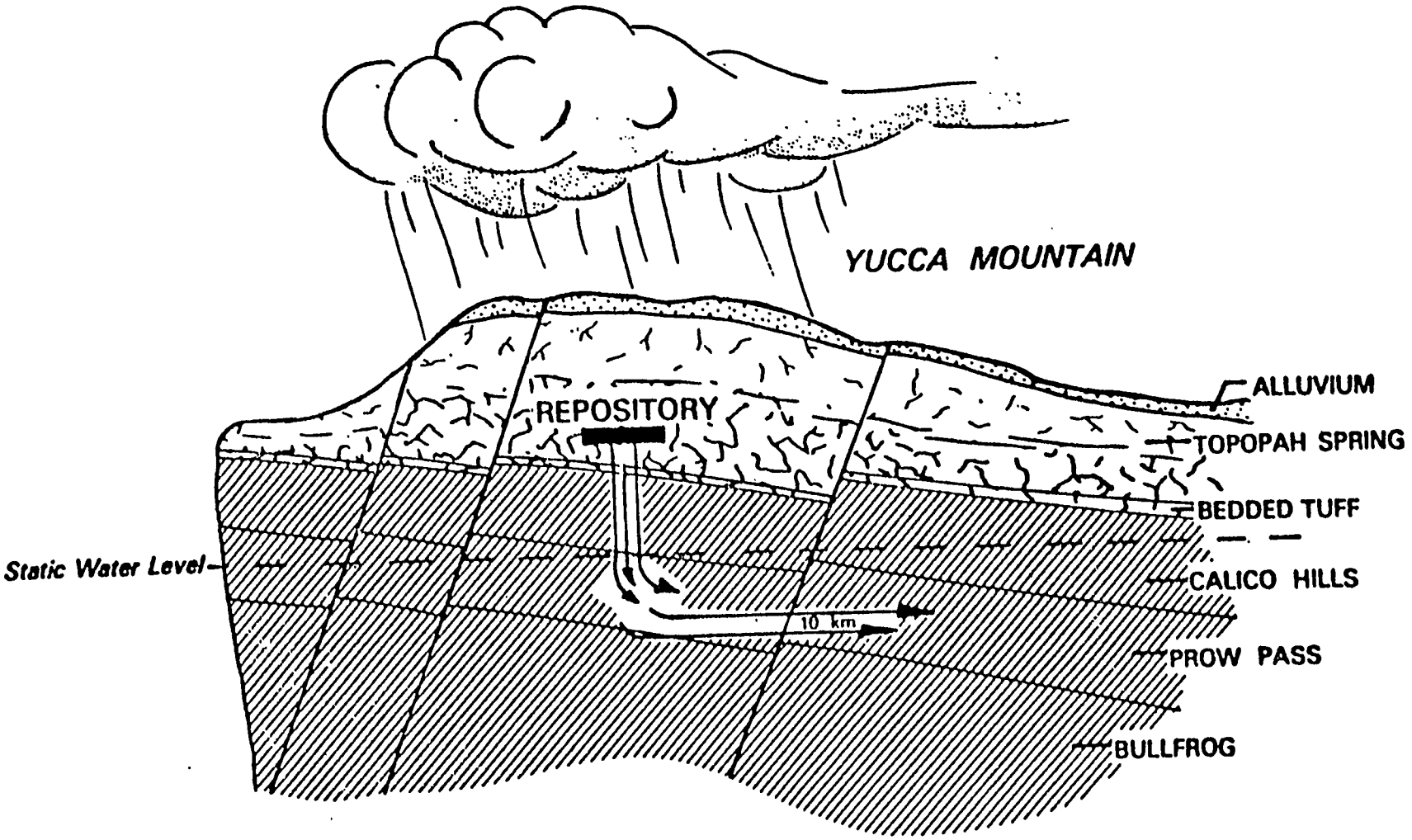

Figure 5-17. Conceptual radionuclide transport path for TRACR3D calculations (Travis and others, 1984a).

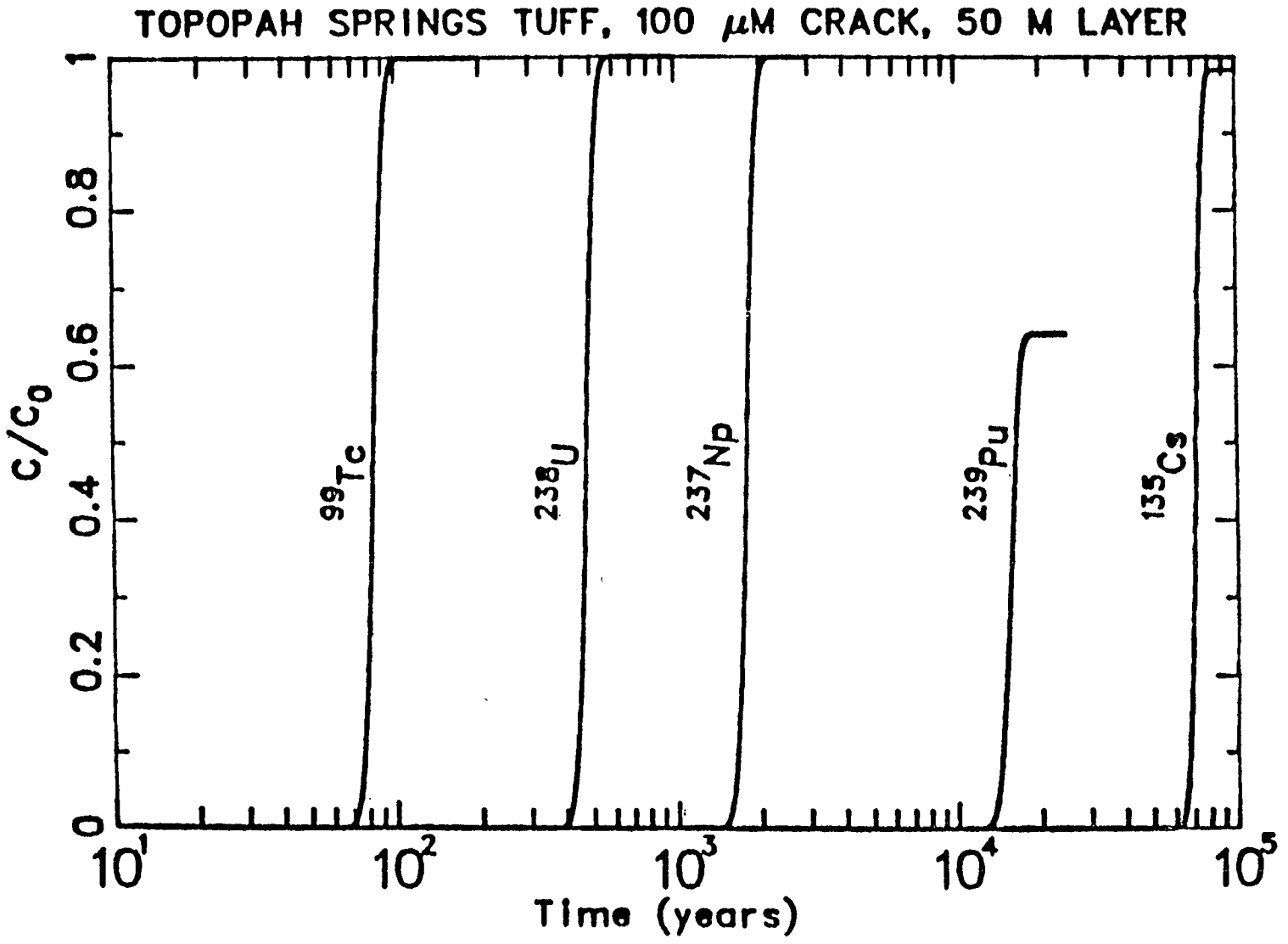

Figure 5-18. Concentration histories at the bottom of a 50 meter layer of Topopah Spring tuff for injection at the top of the layer in a 100 micron crack (Travis and others, 1984b).

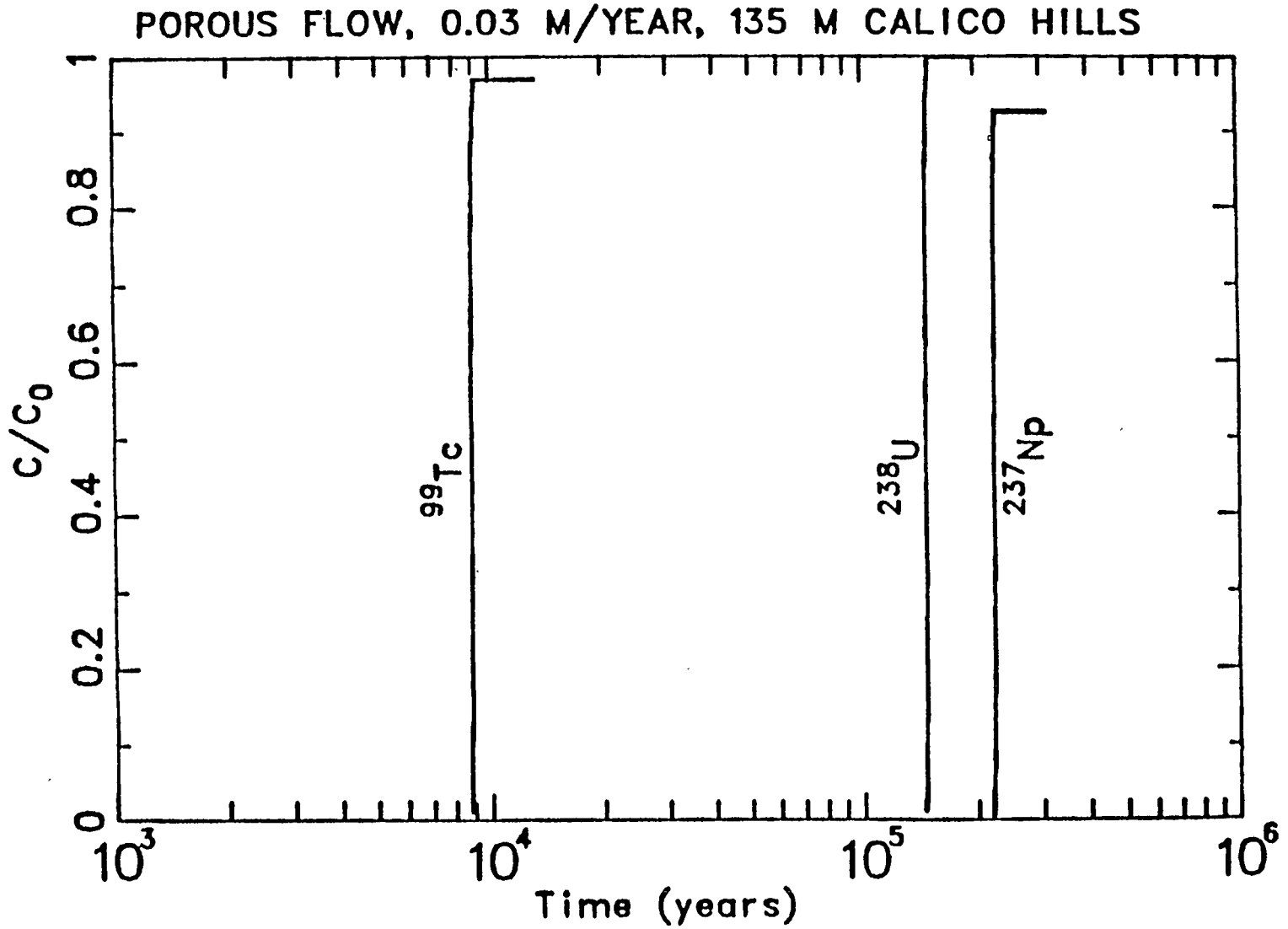

Figure 5-19. Concentration histories for ^{99}Tc, ^{238}U, and ^{237}Np at the bottom of the Calico Hills layer, assuming porous flow only (Travis and others, 1984b).

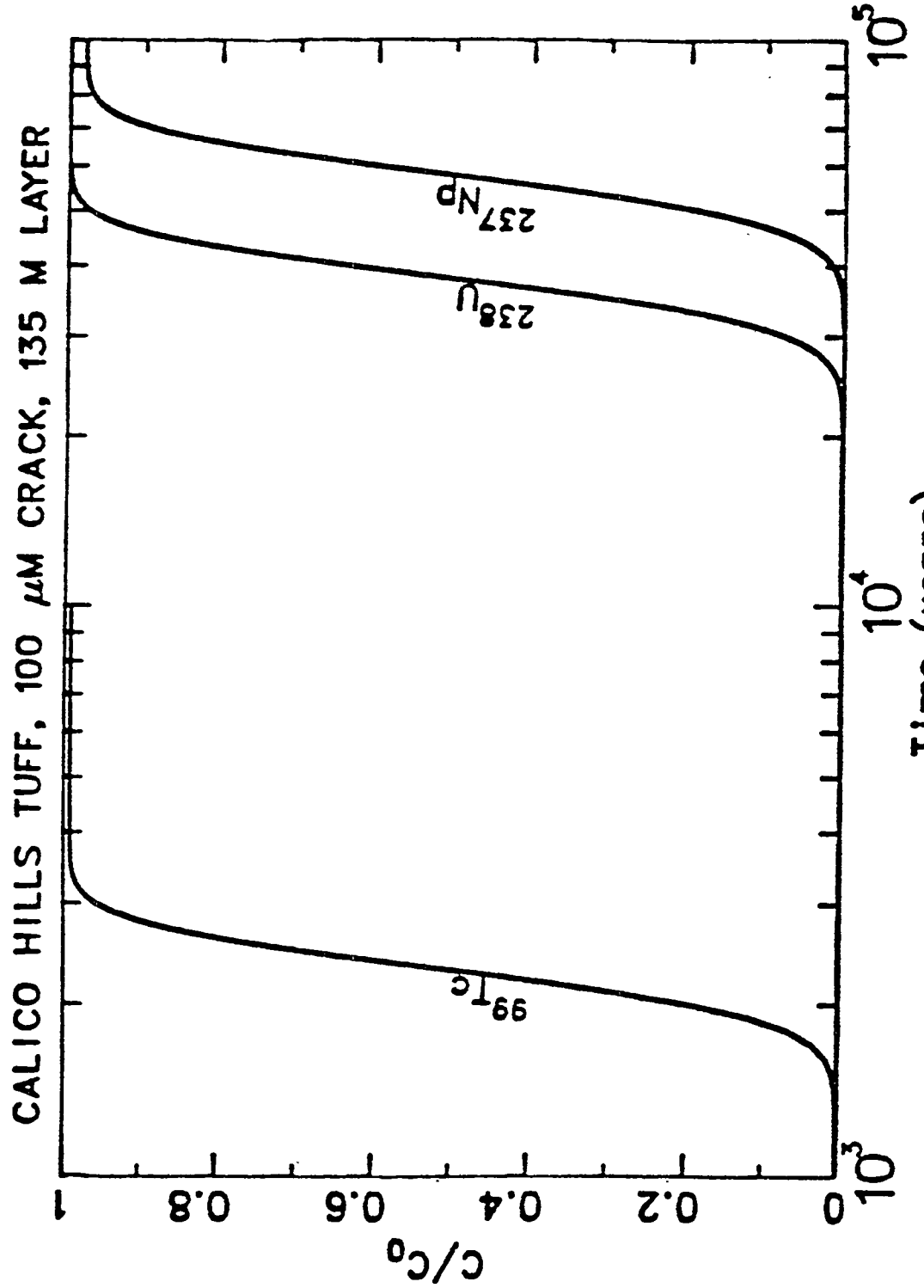

Figure 5-20. Concentration histories at the bottom of the 135 meter thick Calico Hills tuff layer for injection at the top of a layer in a 100 micron crack (Travis and others, 1984b).

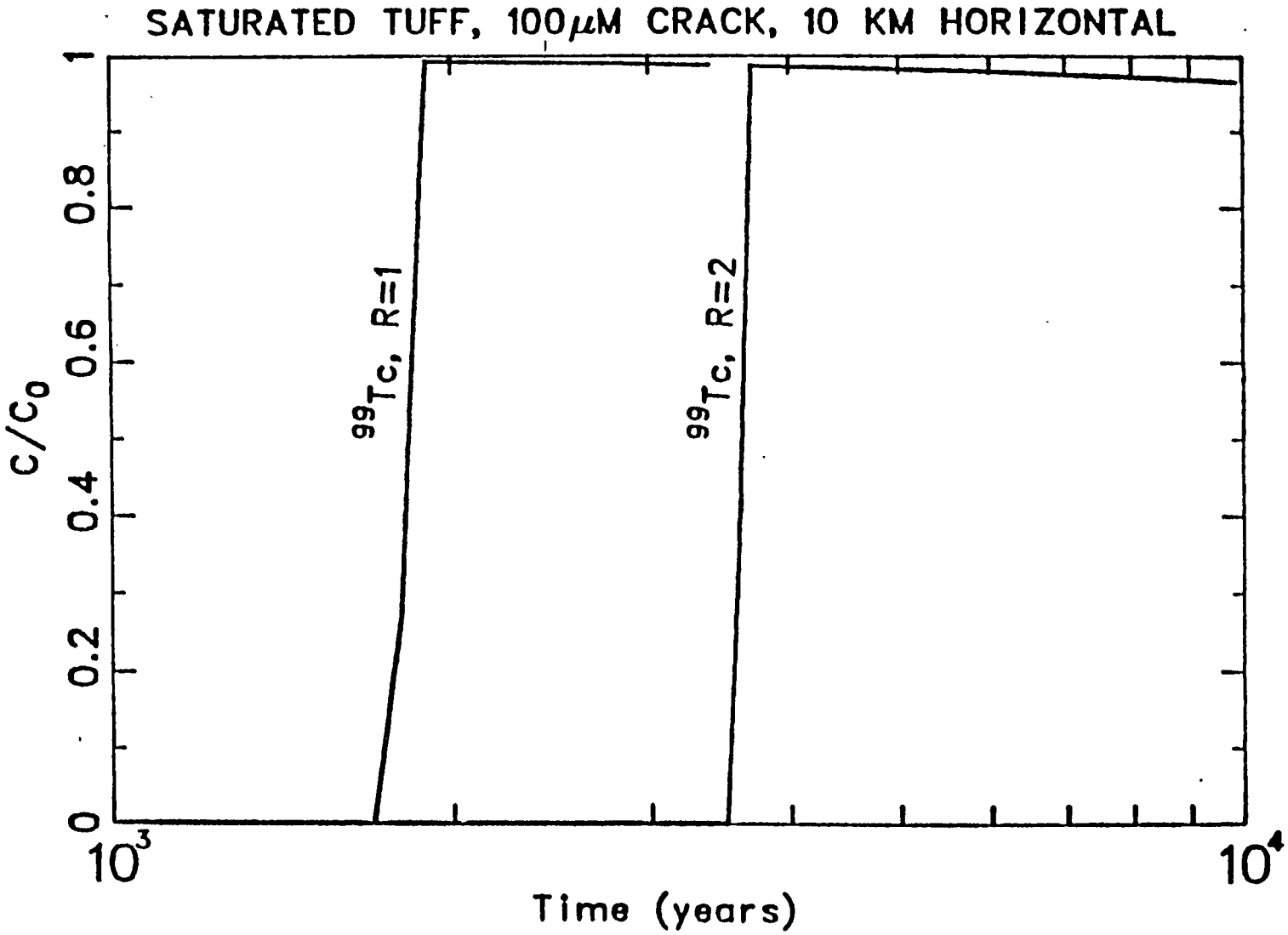

Figure 5-21. Concentration breakthrough curves for ^{99}Tc at 10 km horizontal distance for injection into the water table below the repository location. Curve R = 1 is for no retardation; curve R = 2 is with slight retardation (Travis and others, 1984b).

CHAPTER 6 - GROUND-WATER HYDROLOGY

This chapter presents the hydrologic characteristics of the unsaturated zone at Yucca Mountain. Most of the data, especially porosity and hydraulic conductivity, are from the Yucca Mountain area. Other data, such as fracture hydraulic conductivity, are obtained from other areas at the NTS. If no data are available for either Yucca Mountain or the NTS, then data were obtained for tuffs located elsewhere. In all cases, the intent was to construct a data base primarily from test wells located at or as near Yucca Mountain as possible. If a sufficient amount of a certain type data, such as porosity, was found for the Yucca Mountain area, then additional off-site data were not collected. However, if a certain type of data, such as fracture hydraulic conductivity, were lacking at Yucca Mountain, then additional data were obtained from tuffs located either within the NTS or elsewhere. The order of preference for obtaining data was Yucca Mountain, the NTS, and elsewhere.

The decision to study the unsaturated zone at Yucca Mountain has only recently been made by NNWSI. As a result, the unsaturated zone is currently being studied to evaluate its hydrologic characteristics. At this time many existing data have not been published, and so have not been included in this chapter.

This chapter is limited to sections on porosity, moisture content and saturation, and hydraulic conductivity. Many of the data presented in this chapter were obtained from several test wells located at or near Yucca Mountain (Figure 2-1).

6.1 Porosity

Porosity data appear to be the most abundant type of hydrologic data available for the Yucca Mountain area. Because porosity is used in thermo-mechanical, geohydrological, and geological modeling, it is reported in many types of literature. Porosity data with stratigraphy and lithology are tabulated below, as are moisture content and saturation data, which are discussed in Section 6.2.

6.1.1 Total matrix porosity

Matrix porosity data for several test wells (Table 6-1 through 6-6) have come from the thermo-mechanical, geological, and hydrological literature. Data for some test wells were obtained from more than one source.

Table 6-1 presents matrix porosity for rocks in the unsaturated zone of test well USW-H1. Rocks analyzed for porosity include the Yucca Mountain Member of the Paintbrush Tuff to the Bedded Tuff of Calico Hills, a total length 1,638 feet (500 meters). Rush and others (1983) obtained porosity estimates by calculation from measured dry bulk and grain density data. The data indicate a distinct porosity difference between welded and nonwelded tuffs. The nonwelded to partially welded tuffs typically have a porosity in excess of 0.40. The moderately to densely welded tuff has a porosity range between 0.10 and 0.28. Most porosities of the moderately to densely welded tuff range between 0.10 and 0.20.

Table 6-1. Porosity and saturation from USW-H1 (Rush and others, 1983)

Lithology	Depth (feet)	Depth (meters)	Porosity*	Saturation*	Moisture Content*
Paintbrush Tuff, Yucca Mountain Member					
Tuff, partially welded to nonwelded ash-flow; vitric	109.9	33.5	0.45	0.49	0.22
	111.9	34.1	0.43	0.55	0.23
Paintbrush Tuff, Pah Canyon Member					
Tuff, nonwelded ashflow; vitric	252.3	76.9	0.48	0.34	--
Paintbrush Tuff, Topopah Spring Member					
Tuff, moderately to densely welded ash-flow; devitrified	419.9	128.	0.22	0.45	0.10
	423.2	129.	0.24	0.49	0.11
	442.9	135.	0.21	0.44	0.093
	449.5	137.	0.19	0.57	0.11
	459.3	140.	0.16	0.58	0.10
	462.6	141.	0.17	0.57	0.094
	465.9	142.	0.17	0.54	0.090
	469.2	143.	0.15	0.57	0.085
	718.5	219.	0.17	0.73	0.13
	725.1	221.	0.28	0.42	0.12
	728.3	222.	0.18	0.68	0.12
	741.5	226.	--	--	0.12
	1,279.5	390.	0.16	0.70	0.11
	1,282.8	391.	0.16	0.74	0.11
	1,305.8	398.	0.14	0.72	0.10
	1,309.1	399.	0.10	0.80	0.082
	1,328.7	405.	0.12	0.82	0.10
	1,332.0	406.	0.11	0.76	0.084
Tuffaceous Beds of Calico Hills					
Tuff, nonwelded and zeolitized ash-flow	1,742.1	531.	0.47	0.96	0.46
	1,748.7	533.	0.44	0.96	0.42

Water level at 1,878 feet (572 meters), more or less.
*dimensionless.

Table 6-2. Porosity and saturation from USW-G1 (Lappin and others, 1982b)

Lithology	Depth (feet)	Depth (meters)	Porosity*	Saturation*
Paintbrush Tuff, Topopah Spring Member				
Tuff, nonwelded, vitric	263.5	80.3	0.27	0.93
Tuff, densely welded; devitrified, with or without lithophysae	751.8	229.1	0.18	0.94
	795.0	242.3	0.11	0.09
	810.0A	246.9A	0.10	0.90
	810.0B	246.9B	0.10	1.00
	890.3	271.4	0.11	1.00
	939.0A	286.2A	0.16	1.00
	939.0B	286.2B	0.12	0.83
	959.4	292.4	0.12	0.92
	1,017.6	310.2	0.13	1.08(sic)
	1,047.1	319.2	0.11	0.91
	1,100.1	335.3	0.15	0.93
	1,151.1	350.9	0.16	0.88
	1,210.7	369.0	0.11	0.82
	1,245.0	379.5	0.10	0.70
Tuff, densely welded vitric, the "basal vitophyre"	1,288.4	392.7	0.04	0.75
	1,330.0A	405.4A	0.03	0.33
	1,330.0B	405.4B	0.03	0.33
	1,330.0C	405.4C	0.04	0.50
	1,332.8	406.2	0.04	0.75
Tuff, partially welded to nonwelded	1,385.2	422.2	0.33	0.97
Bedded Tuff of Calico Hills				
Tuff, nonwelded ash-flow	1,469.9	448.0	0.37	0.97
	1,503.0	458.1	0.38	0.84
	1,505.0	458.7	0.31	0.94
	1,514.8	461.7	0.33	1.00
Tuff, nonwelded ash-flow	1,553.0	473.4	0.35	0.77

Table 6-2. Porosity and saturation from USW-G1--concluded

Lithology	Depth (feet)	Depth (meters)	Porosity*	Saturation*
Tuff, nonwelded ash-flow	1,571.2	478.9	0.39	0.97
	1,606.0A	489.5A	0.39	0.90
	1,606.0B	489.5B	0.31	0.52
	1,606.0C	489.5C	0.30	0.50
	1,606.0D	489.5D	0.32	0.75
	1,652.0A	503.5A	0.36	0.47
	1,652.0B	503.5B	0.33	0.94
	1,663.5	507.0	0.33	0.97
	1,667.0	508.1	0.35	0.97
Tuff, nonwelded ash-flow	1,705.5	519.8	0.33	0.94
	1,722.3	525.0	0.36	0.97
Tuff, bedded/reworked, including tuffaceous sandstone	1,784.5	543.9	0.24	1.00
Crater Flat Tuff, Prow Pass Member				
Tuff, partially welded ash-flow devitrified	1,832.0A	558.4A	0.35	0.94
	1,832.0B	558.4B	0.36	1.00
	1,847.0A	563.0A	0.36	0.97
	1,847.0B	563.0B	0.37	0.95

Water level at 1,850 feet (564 meters), more or less.
*dimensionless.

Table 6-3. Porosity and saturation from test well J-13 (Thordarson, 1983)

Lithology	Depth (feet)	Depth (meters)	Porosity*	Moisture Content*	Saturation*
Paintbrush Tuff, Tiva Canyon Member					
Tuff, ash-flow, partly welded, devitrified	530.5	161.7	0.081	0.058	0.716
	666.3	203.1	0.544	0.345	0.633
Tuff, ash-flow, zeolitized	669.0	203.9	0.319	0.256	0.802
Paintbrush Tuff, Topopah Spring Member					
Tuff, ash-flow, moderately welded, devitrified	792.3	241.5	0.167	0.159	0.955
	865.2-879.9	263.7-268.2	0.162	0.139	0.859
	915.0	278.9	0.110	0.093	0.846
	1,020.0	310.9	0.131	0.113	0.863
	1,093.8	333.4	0.279	0.225	0.912
	1,183.7	360.8	0.160	0.131	0.819
	1,283.5	391.2	0.123	0.097	0.790
Tuff, ash-flow, vitrophyre	1,332.0-1,336.0	406.0-407.2	0.037	0.024	0.644
Tuff, ash-flow, non to partly welded	1,407.5	429.0	0.116	0.090	0.769
	1,445.5	440.6	0.327	0.310	0.946

Water level at 926 feet (282 meters), more or less.
*dimensionless.

Table 6-4. Porosity and saturation from test well UE25a-1

Lithology	Depth (feet)	Depth (meters)	Porosity*	Moisture Content*	Saturation*
Paintbrush Tuff, Tiva Canyon Member					
Tuff, ashflow, densely welded	58	17.7	0.060	0.02	0.33
Tuff, ash-flow, densely welded, devitrified	102	31.1	0.073	0.05	0.69
	153	46.7	0.0614	0.03	0.50
Tuff, ash-flow, moderately welded	187	57.0	0.229	0.20	0.87
Tuff, ash-flow, partially welded, vitric	202	61.6	0.301	0.28	0.92
Tuff, ash-flow, non- to partially welded	212	64.6	0.527	0.42	0.80
Tuff, ash-flow, nonwelded	234	71.3	0.529	0.36	0.68
Tuff, ash-fall and reworked ash-fall, vitric	263	80.2	0.517	0.29	0.56
Paintbrush Tuff, Topopah Spring Member					
Tuff, ash-flow, nonwelded, vitric	273	83.2	0.274	0.17	0.62
Tuff, ash-flow, moderately to densely welded, devitrified	328	100.0	0.219	0.11	0.50
Tuff, ash-flow, densely welded, devitrified	360	109.8	0.133	0.05	0.37
	421	128.4	0.150	--	--
	471	143.6	0.186	--	--
	524	159.8	0.176	0.06	0.34
	569	173.5	0.177	0.03	0.17
	623	189.9	0.184	0.11	0.60
	660	201.2	0.075	0.06	0.79
	733	223.5	0.113	0.10	0.88
	772	235.4	0.133	0.09	0.68
	816	248.8	0.098	0.08	0.82
	866	264.0	0.0865	0.07	0.82
	921	280.8	0.100	0.03	0.30
	969	295.4	0.091	0.07	0.77
	1,010	307.9	0.118	0.10	0.87
	1,040	317.1	0.112	0.08	0.72
	1,112	339.0	0.087	0.05	0.58
Tuff, ash-flow, moderately to densely welded, devitrified	1,183	360.7	0.085	0.06	0.73
	1,249	380.8	0.0803	0.06	0.73
Tuff, ash-flow, moderately to densely welded, vitric	1,266	386.0	0.127	0.09	0.70
Tuff, ash-flow, vitrophyre	1,304	397.6	0.0628	0.02	0.31
Tuff, ash-flow, partially welded, vitric	1,324	403.7	0.303	0.27	0.89
Tuff, ash-flow, non- to partially welded, devitrified	1,338	407.9	0.277	0.24	0.87

Table 6-4. Porosity and saturation from test well UE25a-1--concluded

Lithology	Depth (feet)	Depth (meters)	Porosity*	Moisture Content*	Saturation*
Paintbrush Tuff, Topopah Spring Member					
Tuff, ash-flow, nonwelded	1,349	411.3	0.244	0.24	0.99
Tuff, ash-fall and reworked	1,361	414.9	0.234	0.22	0.94
Bedded Tuff of Calico Hills					
Tuff, ash-flow, nonwelded, devitrified	1,411	430.2	0.301	0.29	0.97
	1,464	446.3	0.281	0.26	0.93
	1,516	462.2	0.321	0.30	0.93

Water level at 1,540 feet (469 meters), more or less.
Geologic data from Spengler and others (1979).
Porosity data from Anderson (1981).
Moisture content and saturation calculated from Anderson (1981) density data.
*dimensionless.

Table 6-5. Porosity from test well UE25a-1

Lithology	Depth (feet)	Depth (meters)	Porosity*
Paintbrush Tuff, Topopah Spring Member			
Tuff, ash-flow, densely welded, devitrified	662.7	202.	0.140
	731.6	223.	0.102
	1,122.0	342.	0.089
	1,122.0	342.	0.060
Bedded Tuff of Calico Hills			
Tuff, ash-flow nonwelded, devitrified	1,364.8	416.	0.238
	1,364.8	416.	0.256
	1,548.6	472.	0.290
	1,48.6	472.	0.349
	1,19.2	524.	0.342

Water level at 1,540 feet (469 meters), more or less.
Lithology from Spengler and others (1979).
Porosity data from Moss and Haseman (1983a).
Porosity determined from the amount of water absorbed by a dry core sample.
*dimensionless.

Table 6-6. Porosity from test well USW-GU3 (Price and others, 1984)

Lithology	Depth (feet)	Depth (meters)	Porosity*
Paintbrush Tuff, Topopah Spring Member			
Tuff, moderately to densely welded, porphyritic	484.7	147.7	0.184 (3)
	519.4	158.3	0.160 (3)
	528.4	161.0	0.182 (3)
Tuff, densely welded, porphyritic	633.9	193.2	0.134 (1)
	634.4	193.4	0.124 (1)
Tuff, densely welded, aphanitic	760.9	231.9	0.140 (10)
Tuff, densely welded, porphyritic	853.4	260.1	0.128 (1)
	874.6	266.6	0.146 (1)
	1,050.4	320.1	0.118 (3)
	1,067.8	325.4	0.119 (4)
Tuff, densely welded, vitric	1,195.1	364.2	0.0745 (1)
	1,197.5	365.0	0.0820 (1)
Tuff, moderately to densely welded, porphyritic	1,280.6	390.3	0.139 (3)

Numbers in parenthesis indicate the number of samples for that particular depth.
*dimensionless.

Porosity data for test well USW-G1 are presented in Table 6-2. Rocks analyzed for porosity include the Topopah Spring Member of the Paintbrush Tuff to the Prow Pass Member of the Crater Flat Tuff, a length of 1,584 feet (483 meters) (Lappin and others, 1982b). Lappin and others (1982b) calculated porosities from measured dry bulk and grain densities. However, pore space less than 0.15 mm (5.9×10^{-3} inches) could not be measured because the crushing technique used prior to grain density measurements did not make rock particles smaller than 100 mesh (0.01 inch). Therefore, porosity estimates may be low. Porosity estimates are dependent on the degree of welding. The porosity estimates for the nonwelded tuff are high, ranging between 0.27 and 0.39. This is slightly less than the porosity of nonwelded tuff obtained from the USW-H1 test well. The porosity estimates for the partially welded tuff range between 0.33 and 0.37, which happens to be within the above-mentioned range for the nonwelded tuff, but lower than the porosity estimates for similar tuffs in the USW-H1 test well. The densely welded tuff has a porosity range between 0.10 and 0.18, which is within the porosity range for the data obtained from the USW H-1 test well. Porosity estimates for the vitrophyre are quite low, ranging between 0.03 and 0.04.

Porosity data from test well J-13 are presented in Table 6-3. Test well J-13 provides the main water supply for the Yucca Mountain area and is located in Jackass Flats, approximately four miles (6.4 kilometers) east of Yucca Mountain. Rocks in the unsaturated zone that were analyzed for porosity included the Tiva Canyon and Topopah Spring Members of the Paintbrush Tuff, covering 916 feet (279 meters) of core. Porosity was estimated by Thordarson (1983) from dry bulk and grain density measurements. The porosity estimates for moderately welded tuff range between 0.110 and 0.279. Only one of the seven porosity measurements for the moderately welded tuff exceeds 0.17. The vitrophyre has the lowest porosity, 0.037, which compares favorably with data from test well USW-G1. Nonwelded to partly welded tuff has a wide porosity range, 0.081 to 0.327; however, it is believed that the higher porosity estimate is representative of the nonwelded tuff. Zeolitized tuff has a high porosity that exceeds 0.30.

Porosity data for test well UE25a-1 are presented in Tables 6-4 and 6-5 (Anderson, 1981; Moss and Haseman, 1983a). The porosity data in Table 6-4 include the Tiva Canyon and Topopah Spring Members and a portion of the Bedded Tuff of Calico Hills. The porosity data in this table cover 1,458 feet (444 meters) of core and are based on density and volume measurements. The porosity data in Table 6-5 includes the Topopah Spring Member and the Bedded Tuff of Calico Hills. This table covers 1,056 feet (322 meters) of core and is based on measurements of the amount of water a core sample absorbs. The comparison of porosity for similar rock types from the two tables is favorable. Porosity data for the densely welded tuff of the Topopah Spring Member range between 0.075 and 0.186 in Table 6-4, and between 0.060 and 0.140 in Table 6-5. For the nonwelded bedded tuffs, the range is between 0.281 and 0.321 in Table 6-4, and between 0.238 and 0.349 in Table 6-5. It appears that the densely welded tuff of the Tiva Canyon Member has a porosity near the lower limit of the porosity range for the densely welded tuff of the Topopah Spring Member. The vitrophyre has the lowest porosity, 0.0628, which is consistent with the vitrophyre porosity from the other test wells. Nonwelded tuffs have a porosity range between 0.244 and 0.529; partially welded tuffs have a porosity of approximately 0.30; and moderately to densely welded tuffs have a porosity range between 0.085 and 0.127.

Matrix porosity data from test well USW-GU3 are presented in Table 6-6. The data represent only the Topopah Spring Member and cover approximately 800 feet (244 meters) of core. Porosity estimates range between 0.139 and 0.184 for moderately to densely welded tuffs and between 0.082 and 0.146 for densely welded tuffs.

Porosity data presented in Tables 6-1 through 6-6 indicate a definite relationship between the degree of welding and porosity. In general, densely welded tuffs have the lowest porosity and nonwelded tuffs have the highest porosity. This relationship has been observed by Scott and others (1983). Porosity ranges for the various degrees of welding are summarized below:

Nonwelded	0.24 - 0.54
Partially welded	0.30 - 0.37
Moderately welded	0.11 - 0.28
Densely welded	0.06 - 0.19
Vitrophyre	0.04 - 0.06
Ashfall	0.24 - 0.52

6.1.2 Effective matrix porosity

Some effective-matrix-porosity data are available from test well J-13 (Thordarson, 1983). Thordarson (1983) defines the effective matrix porosity as the ratio of interconnected pore space in the rock matrix to the total volume of rock. These data, which include both the Tiva Canyon and Topopah Spring Members, were determined by the water-saturation method and are presented in Table 6-7. Some of the data are from rocks located in the saturated zone. In all cases the effective porosity is less than 0.10 and much less than total matrix porosity. For instance, at depths between 800 and 1,200 feet (244 and 366 meters) the effective porosity for moderately welded tuff ranges between 0.027 and 0.068, while the total matrix porosity ranges between 0.160 and 0.225. This implies that only between 20 and 30 percent of the total matrix porosity is interconnected. Other types of tuff, except for the vitrophyre, appear to follow the same relationship. The vitrophyre appears to have an effective matrix porosity that is equivalent to the total matrix porosity, but more data are needed to confirm this.

The noneffective matrix porosity may consist of air or gas pockets within the tuff matrix or possibly pore space too small for water to enter within the testing period for the effective porosity. This may cause some underestimation of the effective matrix porosity. Also, true effective porosity includes dead-end or stagnant pore space. It is not clear whether these types of pores were measured during the effective porosity testing. Whether or not this type of pore space is included in the effective porosity estimates would have an effect on hydrodynamic dispersion, diffusion, and average pore velocity (Bear, 1972).

6.1.3 Fracture porosity

The literature does not appear to contain any data regarding the fracture porosity of tuffs. Fracture porosity, in this sense, would be defined as the ratio of the volume of fractures to the bulk volume of rock.

Table 6-7. Effective porosity from test well J-13 (Thordarson, 1983)

Lithology	Depth (feet)	Depth (meters)	Effective Porosity*
Paintbrush Tuff, Tiva Canyon Member			
Tuff, ash-flow, partly welded, devitrified	539.0	164.3	0.028
Tuff, ash-flow, zeolitized, faulted (?)	674.9	205.7	0.052
Tuff, ash-flow, zeolitized	680.1	203.3	0.037
Paintbrush Tuff, Topopah Spring Member			
Tuff, ash-flow, moderately welded, devitrified	800.9	244.1	0.027
	1,100.1	335.3	0.087
	1,192.9	363.6	0.068
Tuff, ash-flow, vitrophyre	1,341.9	409.0	0.054
Tuff, ash-flow, nonwelded to part welded	1,416.0	431.6	0.033

Water level at 926 feet (282 meters), more or less.

6.2 Saturation

This section presents data on moisture content and degree of saturation in the tuff units at the NTS. Tables for degree of saturation and moisture content for tuffs at Yucca Mountain are found in Section 6.1. In addition, this section presents data showing the relationship between degree of saturation and pressure head for tuffs, both on site and off site.

6.2.1 Matrix saturation

Matrix saturations and moisture contents for the various units of the Paintbrush Tuff and the Bedded Tuff of Calico Hills for test well USW-H1 (Table 6-1) are based on measured natural state, dry bulk, and grain densities. The degree of saturation within the Paintbrush Tuff ranges between 0.45 and 0.82, except for one measurement in a nonwelded unit. Saturation appears to increase with depth within the Paintbrush Tuff; however, because of porosity changes, moisture-content stays relatively constant. The degree of saturation within the Bedded Tuff of Calico Hills indicates that some parts of the unit may be saturated even though the depths at which the core samples were taken are more than 100 feet (30.5 meters) above the water table.

Degree-of-saturation data of core samples from test well USW-G1 (Table 6-2) are based on differences in measurements of original density, bulk

density, and grain density (Lappin and others, 1982b). Volumetric moisture content can be calculated from density data provided by Lappin and others (1982b). Degree of saturation within the densely welded tuffs of Paintbrush Tuff in the USW-G1 test well is quite different from those in the USW-H1 test well. In USW-G1, degrees of saturation are typically above 0.80. Some values of degree of saturation indicate that parts of the Paintbrush Tuff are saturated. The degree of saturation within the Bedded Tuff of Calico Hills ranges between 0.50 and 1.00. The data indicate that some portions of the Bedded Tuff of Calico Hills are completely saturated. Because of the higher porosity of the Bedded Tuff of Calico Hills relative to the Paintbrush Tuff, the Bedded Tuff of Calico Hills contains more moisture by volume than the Paintbrush Tuff. For the Bedded Tuff of Calico Hills, the degrees of saturation from the USW-G1 samples compare favorably with those from the USW-H1 samples.

Degree-of-saturation and moisture-content data from test well J-13 are presented in Table 6-3 for the Tiva Canyon and Topopah Spring Members of the Paintbrush Tuff. Thordarson (1983) calculated moisture content and degree of saturation from measured natural state, dry bulk, and grain densities. Degrees of saturation for the Topopah Spring Member range between 0.644 and 0.955. As in the other test wells, the Topopah Spring Member is near saturation at some depths. The range of saturations in the Topopah Spring Member in J-13 are compatible with those in USW-H1 and USW-G1. The three measured saturations in the Tiva Canyon Member are quite close to each other even though the porosities are quite different.

Degree of saturation in UE25a-1 from the Tiva Canyon and Topopah Spring Members and the Bedded Tuff of Calico Hills are presented in Table 6-4 (Anderson, 1981). At this site, the degree of saturation in the Topopah Spring Member has a wide range, between 0.17 and 0.99, but most values are greater than 0.50. Degree of saturation within the Bedded Tuff of Calico Hills agrees very well with the values from the other test wells. Within the Tiva Canyon Member, the degree of saturation ranges between 0.33 and 0.92. In all members at this test well, moisture contents appear to be higher at the bottom of the member than at the top. This may indicate downward movement of water, at least within a member.

6.2.2 Saturation characteristic curves

Several saturation characteristic curves are available for tuff. Some are available for NTS tuffs and others are available for off-site tuffs.

A characteristic curve of degree of saturation and matrix potential for a sample of Topopah Spring tuff taken from Fran Ridge is presented in Figure 6-1. The purpose for constructing this curve was to compare two methods for measuring saturation and matrix potential: mercury intrusion and pressure membranes (Mroz and others, 1983a). The solid line forms the characteristic curve determined from the mercury intrusion method and the vertical lines form the curve determined from the pressure membrane method. The comparison between the two methods is fairly good, as the small boxes attached to the vertical lines plot a shape similar to the solid line.

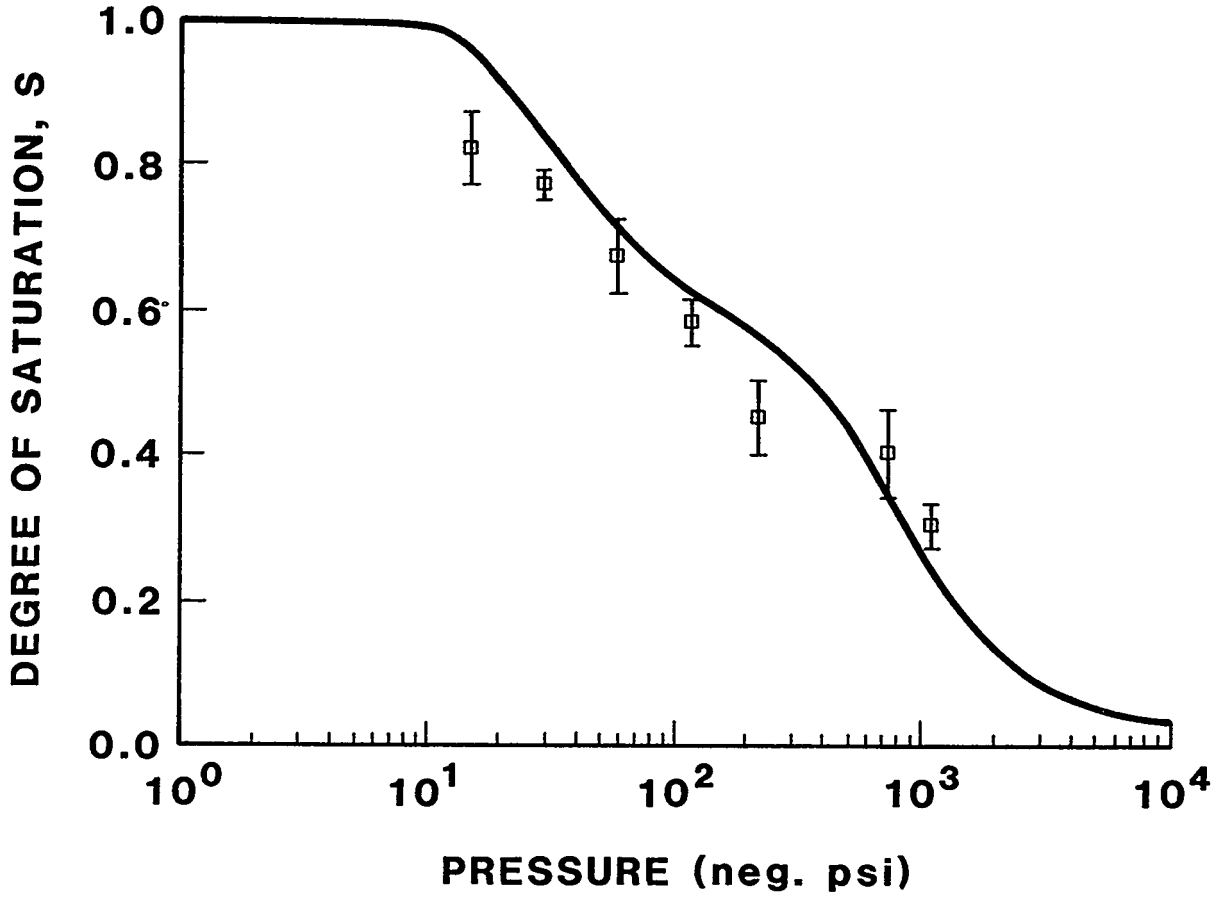

Figure 6-1. Saturation and matrix potential from the Topopah Spring Member of the Paintbrush Tuff (after Mroz and others, 1983a).

The saturation characteristic curve presented in Table 6-8 was used in a modeling study of water flow at Yucca Mountain. The measurement technique used to determine this curve was not described. The data in Table 6-8 would plot as a shape similar to the solid curve in Figure 6-1, but the data in Table 6-8 would generally fall below the curve.

Saturation characteristic curves with respect to matrix potential for crushed and solid Bandelier Tuff are tabulated in Tables 6-9 and 6-10. The data were obtained from volumetric pressure plate extraction and changes of weight of the sample (Abeele, 1979; Abeele and others, 1981). These two curves for Bandelier Tuff are generally steeper than the Mroz and others (1983a) and Travis and others (1984b) curves. The curves for the crushed and solid Bandelier Tuff are different from each other, in that when they are compared to each other they intersect at several points. The curve for solid Bandelier tuff changes from a saturation ratio of 1.00 to 0.02 within a matrix potential change of 260 feet (79.2 meters), while the crushed Bandelier Tuff saturation ratio changes from 1.00 to 0.223 within a matrix potential change of 65 feet (19.8 meters).

6.2.3 Temperature effects on saturation characteristic curves

Several authors have presented data and theoretical relationships describing temperature effects on saturation characteristic curves. Saturation (or moisture content) - matrix potential curves presented by Childs and Malstaff (1982) and Constantz (1983) indicate that for a constant matrix potential, saturation decreases as temperature increases. One model of the temperature dependence of this curve is based on proportioning the matrix potential portion of the curve with respect to the surface tension of water, which is temperature dependent. Several authors have found that this relationship generally underestimates the measured change in saturation with respect to temperature (Childs and Malstaff, 1982). Data and predictions by Constantz (1983) generally confirm this. Constantz (1983) indicated that the relationship appears valid only for saturations above 50 percent, but this may depend more on the soil tested than anything else. It appears that more work is necessary to adequately predict temperature effects on saturation characteristic curves.

6.3 Hydraulic Conductivity

This section presents data on the matrix hydraulic conductivity, the fracture hydraulic conductivity, and hydraulic conductivity characteristic curves for tuff. The data base for these items is fairly limited. It is expected that additional data will be available in the future for test wells USW-G4, -H6, -UZ1, and -H1 (Bentley, 1984; Craig and others, 1983; Department of Energy, 1984; Rush and others, 1983).

6.3.1 Matrix hydraulic conductivity

Matrix hydraulic conductivity data for test well UE25a-1 (Table 6-11) include the Tiva Canyon and Topopah Spring Members and the Bedded Tuff of Calico Hills. The table covers 1,558 feet (475 meters) of core. It can be seen that there is slightly more than three orders of magnitude difference between the lowest and highest value of hydraulic conductivity. Most of the

Table 6-8. Saturation characteristic curve (Travis and others, 1984b)

Saturation	Matrix (feet)	Matrix (meters)	Potential (psi)	Potential Pa
0.05	-1.676×10^{4}	-5.108×10^{3}	-7.252×10^{3}	-5.000×10^{7}
0.10	-3.352×10^{3}	-1.022×10^{3}	-1.450×10^{3}	-1.000×10^{7}
0.20	-2.011×10^{3}	-6.130×10^{2}	-8.702×10^{2}	-6.000×10^{6}
0.60	-3.352×10^{2}	-1.022×10^{2}	-1.450×10^{2}	-1.000×10^{6}
0.80	-3.352×10^{1}	-1.022×10^{1}	-1.450×10^{1}	-1.000×10^{5}
0.90	-3.352×10^{0}	-1.022×10^{0}	-1.450×10^{0}	-1.000×10^{4}
0.999	-1.676×10^{0}	-5.108×10^{-1}	-7.252×10^{-1}	-5.000×10^{3}
1.000	0.	0.	0.	0.

Matrix potential in feet (meters) of water at 68°F (20°C).

Table 6-9. Crushed Bandelier Tuff characteristic curves (Abeele and others, 1981)

Matrix (feet of water at 68°F)	Matrix (meters of water at 20°C)	Potential (psi)	Potential (kPa)	Saturation Ratio	Relative Permeability
0.00	0.00	-0.00	0	1.000	
-3.35	-1.02	-1.45	-10.	0.890	
-3.69	-1.12	-1.60	-11.	0.868	9.98×10^{-3}
-10.06	-3.06	-4.35	-30.	0.415	
-11.06	-3.37	-4.79	-33.	0.405	3.67×10^{-3}
-14.08	-4.29	-6.09	-42.	0.368	
-15.42	-4.70	-6.67	-46.	0.350	2.25×10^{-3}
-20.11	-6.13	-8.70	-60.	0.318	
-22.12	-6.74	-9.57	-60.	0.310	8.16×10^{-4}
-26.81	-8.17	-11.60	-80.	0.290	
-29.50	-8.99	-12.76	-88.	0.283	4.67×10^{-4}
-32.18	-9.81	-13.92	-96.	0.273	3.91×10^{-4}
-40.22	-12.26	-17.40	-120.	0.260	
-44.24	-13.49	-99.14	-132.	0.255	1.78×10^{-4}
-48.94	-14.92	-21.17	-146.	0.248	1.08×10^{-4}
-53.96	-16.45	-23.35	161.	0.240	8.71×10^{-5}
-59.33	-18.08	-25.67	-177.	0.230	5.67×10^{-5}
-65.36	-19.92	-28.28	-195.	0.223	5.58×10^{-5}

Table 6-10. Solid Bandelier Tuff characteristic curves (Abeele and others, 1981)

Matrix (feet of water at 68°F)	Matrix (meters of water at 20°C)	Potential (psi)	Potential (kPa)	Saturation Ratio	Relative Permeability
-0.34	-0.10	-0.15	-1.	0.883	3.91×10^{-2}
-4.36	-1.33	-1.89	-13.	0.817	2.55×10^{-2}
-6.70	-2.04	-2.90	-20.	0.750	1.70×10^{-2}
-8.38	-2.55	-3.63	-25.	0.683	1.19×10^{-2}
-9.72	-2.96	-4.21	-29.	0.617	7.66×10^{-3}
-11.06	-3.37	-4.79	-33.	0.550	5.11×10^{-3}
-12.07	-3.68	-5.22	-36.	0.483	3.28×10^{-3}
-13.74	-4.19	-5.95	-41.	0.417	1.91×10^{-3}
-16.09	-4.90	-6.96	-48.	0.350	9.79×10^{-4}
-20.11	-6.13	-8.70	-60.	0.283	4.68×10^{-4}
-27.48	-8.38	-11.89	-82.	0.217	1.83×10^{-4}
-38.55	-11.75	-16.68	-115.	0.150	5.53×10^{-5}
-67.03	-20.43	-29.01	-200.	0.083	9.79×10^{-6}
-261.44	-79.69	-113.13	-780.	0.017	5.96×10^{-7}

hydraulic conductivity measurements are within the 10^{-6} to 10^{-5} feet per day (approximately 10^{-12} to 4×10^{-11} meters per second) range. There does not appear to be a clear relationship between hydraulic conductivity and degree of welding.

Hydraulic conductivity data from test well J-13 (Table 6-12) include both the Tiva Canyon and the Topopah Spring Members and covers 877 feet (267 meters) of core. Some of the data come from core located in the saturated zone. The hydraulic conductivity data from this test well range over slightly more than four orders of magnitude. As with the UE25a-1 data, most hydraulic conductivity values are between 10^{-6} and 10^{-5} feet per day (approximately 10^{-12} to 4×10^{-11} meters per second). There does not seem to be any connection between hydraulic conductivity and degree of welding.

In addition to the tabulated data, test wells USW-GU3 and UE25b-1 each have one hydraulic conductivity measurement available (Duffy, 1983; Lobmeyer and others, 1983). The core sample from USW-GU3 comes from the Topopah Spring Member at a depth of 2,511.5 to 2,512.8 feet (765.5 to 765.9 meters) below land surface. The hydraulic conductivity for this sample is 4.1×10^{-6} feet per day (1.45×10^{-11} meters per second). The core sample from UE25b-1 comes from the densely welded tuff of Topopah Spring Member, approximately 741 feet (226 meters) below land surface. The horizontal and vertical hydraulic conductivities of the core sample are 2.7×10^{-6} and 5.2×10^{-2} feet per

Table 6-11. Hydraulic conductivity from test well UE25a-1

Lithology	Depth (feet)	Depth (meters)	k (micro-darcies)	K (10^{-6} feet/day)	K (10^{-12} meters/sec)
Paintbrush Tuff, Tiva Canyon Member					
Tuff, ash-flow, densely welded	58	17.7	0.186	.507	1.79
Tuff, ash-flow, densely welded, devitrified	102	31.1	2.90	7.90	27.9
	153	46.7	3.55-2.49	9.67-6.79	34.1-23.9
			3.45-2.58	9.40-7.03	33.2-24.8
Tuff, ash-flow, moderately welded	187	57.0	50.0	136.	481.
Tuff, ash-flow, partially welded, vitric	202	61.6	1.39	3.79	13.4
Paintbrush Tuff, Topopah Spring Member					
Tuff, ash-flow, moderately to densely welded, devitrified	328	100.0	52.7-25.3	144.-68.9	507.-.243
Tuff, ash-flow, densely welded, devitrified	421	128.4	1.91-1.57	5.20-4.28	18.4-15.1
	471	143.6	14.7-11.0	40.1-30.0	141.-.106
	524	159.8	610.-489.	1660.-1330.	5,860.-4,700.
	660	201.2	5.5-3.6	15.0-9.81	52.9-34.6
	733	223.5	3.42-1.23	9.32-3.35	32.9-11.8
	772	235.4	88.5-51.4	514.-140.	1,810.-494.
	816	248.8	0.80	2.18	7.69
	866	264.0	1.67	4.55	16.1
	921	280.8	1.15	3.13	11.1
	1,010	307.9	1.32	3.60	12.7
	1,040	317.1	14.2-13.5	38.7-36.8	137.-130.
	1,112	339.0	3.82-2.48	10.4-6.76	36.7-23.8
Tuff, ash-flow, moderately to densely welded, devitrified	1,183	360.7	12.5-3.3	34.1-8.99	120.1-31.7
	1,249	380.8	2.9	7.90	27.9
Tuff, ash-flow, moderately to densely welded, vitric	1,266	386.0	161.-26.2	439.-71.4	1,550.-252.0
Tuff, ash-flow, vitrophyre	1,304	397.6	8.10-3.58	22.1-9.76	77.9-34.4

Table 6-11. Hydraulic conductivity from test well UE25a-1--concluded

Lithology	Depth (feet)	Depth (meters)	k (micro-darcies)	K (10^{-6} feet/day)	K (10^{-12} meters/sec)
Tuff, ash-flow and reworked	1,361	414.9	51.9-40.6	141.-111.	499.-390.
Bedded Tuff of Calico Hills					
Tuff, ash-flow, nonwelded, devitrified	1,516	462.2	17.2-12.5	46.9-34.1	165.-120.

Lithology from Spengler and others (1979).
Permeability (k) data from Anderson (1981).
Hydraulic conductivity (K) data calculated from permeability (k) data for water at 68°F (20°C).

Table 6-12. Hydraulic conductivity from test well J-13 (Thordarson, 1983)

	Depth		Hydraulic Conductivity	
	(feet)	(meters)	(feet/day)	(meters/sec)
Paintbrush Tuff, Tiva Canyon Member				
Tuff, ash-flow, partly welded, devitrified	539.0	164.3	9.8×10^{-7}	3.5×10^{-12}
Tuff, ash-flow, zeolitized, faulted (?)	674.9	205.7	1.3×10^{-2}	4.6×10^{-8}
Tuff, ash-flow, zeolitized	680.1	207.3	6.6×10^{-6}	2.3×10^{-11}
Paintbrush Tuff, Topopah Spring Member				
Tuff, ash-flow, moderately welded, devitrified	800.9	244.1	9.8×10^{-6}	3.5×10^{-11}
	1000.1	335.3	$6.6.x10^{-4}$	2.3×10^{-9}
	1192.9	363.6	2.6×10^{-5}	9.3×10^{-11}
Tuff, ash-flow, vitrophyre	1341.9	409.0	2.6×10^{-6}	9.3×10^{-12}
Tuff, ash-flow, nonwelded to partially welded	1416.0	431.6	9.8×10^{-7}	3.5×10^{-12}

Water level at 926 feet (282 meters), more or less.
Hydraulic conductivity for water at 68°F (20°C).

day (9.6×10^{-12} and 1.9×10^{-12} meters per second), respectively. The ratio of the vertical to horizontal hydraulic conductivity does not appear to indicate any strong anisotropic tendencies for densely welded tuff. Hydraulic conductivity measurements from both test wells compare favorably with the hydraulic conductivities presented in Table 6-11 and Table 6-12.

Duffy and Raybold (1981) studied the impacts of changes in confining pressure on the hydraulic conductivity of various tuff samples taken from the saturated zone at test well USW-G1. Their results indicate that the hydraulic conductivity changed no more than a half an order of magnitude as confining pressure changed from 290 psi to 3900 psi (2 to 27 MPa). Their results further indicate that three types of behavior can occur as confining pressure is increased: (1) hydraulic conductivity does not change, (2) hydraulic conductivity decreases, or (3) hydraulic conductivity increases for a several-hundred-psi confining pressure change, then begins to decrease. It is not clear whether a strong relationship exists between hydraulic conductivity changes and confining pressure changes.

6.3.2 Fracture hydraulic conductivity

There do not seem to be many fracture hydraulic conductivity data at Yucca Mountain. The few data that do exist for Yucca Mountain and the NTS are presented in this section.

Fracture aperture data have been measured by Mroz and others (1983b) for core samples taken from test wells USW-G1 and USW-GU3. In Table 6-13, these aperture data have been converted to hydraulic conductivities by means of an analogy to flow between two parallel plates (Witherspoon and others, 1980). The hydraulic conductivities calculated from the aperture data are quite high, generally ranging between 10^3 and 10^4 feet per day (10^{-3} to 5×10^{-2} meters per second). Thus, the hydraulic conductivity of fractures can be as much as 10 orders of magnitude higher than that of the tuff matrix.

Some fracture hydraulic conductivity data are also available from tests performed on boreholes drilled in G-tunnel (Table 6-14). Because the test intervals included, for the most part, several fractures, the fracture hydraulic conductivities are averaged over the number of fractures tested. The average hydraulic conductivities from G-tunnel agree favorably with those from USW-G1 and USW-GU3.

6.3.3 Hydraulic conductivity characteristic curves

Two hydraulic conductivity characteristic curves for tuff are available in the literature. One has been used in a modeling study of recharge at Yucca Mountain. The other was developed from solid and crushed Bandelier Tuff. Hydraulic conductivity characteristic curves do not appear to exist for fractures.

The hydraulic conductivity characteristic curve that has been used in previous modeling studies is presented in Table 6-15 in terms of relative permeability. It includes relative permeability with respect to saturation for both air and water. The range of relative permeability for air covers approximately three orders of magnitude and the relative permeability for

Table 6-13. Fracture aperture and hydraulic conductivity from test well USW-G1 and USW-GU3 (Mroz and others, 1983b)

	Depth		Aperture		Hydraulic Conductivity	
	(feet)	(meters)	(feet)	(meters)	(feet/day)	(meters/sec)
USW-G1	103	31.4	4.95×10^{-4}	1.51×10^{-4}	5.22×10^{3}	1.84×10^{-2}
	753	229.5	1.87×10^{-4}	$.57 \times 10^{-4}$	7.44×10^{2}	2.62×10^{-3}
	1221	372.2	8.27×10^{-4}	2.52×10^{-4}	1.45×10^{4}	5.13×10^{-2}
USW-GU3	751	228.9	5.54×10^{-4}	1.69×10^{-4}	6.54×10^{3}	2.31×10^{-2}
	2114	644.3	8.20×10^{-4}	2.50×10^{-4}	1.43×10^{4}	5.05×10^{-2}
	2359	719.0	4.36×10^{-4}	1.33×10^{-4}	4.05×10^{3}	1.43×10^{-2}

Hydraulic conductivity calculated from aperture data for water at 68°F (20°C).

Table 6-14. Fracture hydraulic conductivity from G-Tunnel (Zimmerman and Vollendorf, 1982)

Test	Interval Length (feet)	(meters)	Approximate Number of Fractures	Average Fracture Hydraulic Conductivity (feet/day)	(meters/sec)
RM-P-1-1	1.50	0.46	5	1,658	0.00585
-2	1.50	0.46	3	1,936	0.00683
-3	1.50	0.46	2	2,996	0.01057
-4	1.50	0.46	4	3,529	0.01245
-5	4.00	1.22	8	3,183	0.01123
-6	1.50	0.46	2	5,451	0.01923
-7	1.50	0.46	1	1,236	0.00436
-8	1.50	0.46	1	1,324	0.00467
-9	1.50	0.46	1	96	0.00034
RM-P-2-1	1.50	0.46	2	62	0.00022
-2	1.50	0.46	2	--	--
-3	1.50	0.46	3	4,076	0.01438
-4	1.50	0.46	1	247	0.00087

Table 6-15. Relative permeability characteristic curve (Travis and others, 1984b)

Saturation	Relative Permeability	
	Air	Water
0.000	1.00	0.0
0.018	0.96	1.8×10^{-16}
0.036	0.93	8.2×10^{-12}
0.104	0.80	8.9×10^{-9}
0.171	0.69	1.0×10^{-7}
0.233	0.58	4.7×10^{-7}
0.370	0.40	7.3×10^{-6}
0.479	0.27	5.6×10^{-5}
0.562	0.19	2.45×10^{-4}
0.617	0.15	6.6×10^{-4}
0.754	0.06	7.0×10^{-3}
0.862	0.02	0.04
0.931	0.005	0.19
0.965	0.001	0.43
1.000	0.000	1.00

water covers approximately sixteen orders. These curves were used for modeling unsaturated ground-water flow and heat transport at Yucca Mountain (Travis and others, 1984b).

Relative permeability of water with respect to matrix potential or saturation for crushed Bandelier Tuff is presented in Table 6-9, which is discussed in Section 6.2. This curve is not as steep with respect to saturation as that presented in Table 6-15. Relative permeability for the crushed tuff curve presented in Table 6-9 changes less than five orders of magnitude for a change in saturation ratio from 1.00 to 0.2, while Travis and others' (1984b) curve (Table 6-15) changes slightly less than seven orders for the same change in saturation. After the relative permeabilities presented in Table 6-9 were measured, they were compared to a relative permeability calculated from a modified Millington-Quirk equation and a good comparison was obtained (Abeele, 1979; Abeele and others, 1981). The purpose of this comparison was to determine if an easier method than measurement could be used to obtain relative permeability data.

The relative permeability with respect to matrix potential and saturation for solid Bandelier Tuff is presented in Table 6-10. Because of the good correlation between measured and calculated relative permeabilities for the crushed tuff, the relative permeabilities on this table are calculated from the modified Millington-Quirk equation (Abeele and others, 1981). Because no

relative permeability measurements for the solid tuff samples were taken, it was impossible to compare measured and calculated relative permeabilities for the solid Bandelier Tuff. No calculations were performed to estimate relative permeability for air.

6.3.4 Temperature effects on hydraulic conductivity characteristic curves

It appears that very few data exist on the effects of temperature on hydraulic conductivity characteristic curves. There are enough data to give insight into the effects but not enough to make any quantifiable statements. Childs and Malstaff (1982) present hydraulic conductivity-moisture content curves for various temperatures. The curves show that for most water contents, hydraulic conductivity increases as temperature increases. For other moisture contents, hydraulic conductivity decreases slightly as temperature increases. These phenomena seem to indicate a temperature-dependent hydraulic conductivity beyond that which can be predicted because of temperature dependent density and viscosity effects as presented by Sophocleous (1979) and Milly (1982). In effect, either intrinsic permeability or relative permeability is also temperature dependent. That is, as temperatue increases, rock or soil particles increase in size, which in turn causes pore space to become rearranged or smaller. This may cause flow in the pores to change somewhat. There are no hard data to support this contention and additional data and research should be generated to confirm it.

CHAPTER 7 - THERMOMECHANICAL PROPERTIES

A knowledge of the thermal, mechanical, and thermomechanical properties of the host rock is essential for the design, construction, and performance assessment of an underground high-level waste repository. An extensive compilation of thermal/mechanical properties and other data for tuff was recently reported (Guzowski and others, 1983). These data were somewhat generic in that tuff data from all sites and locations (even outside Nevada) were included, and no attempt was made to focus on the unsaturated zone. Data presented in this chapter are primarily for the unsaturated zone. It was not feasible to restrict data reporting to the Yucca Mountain location, because a majority of the field experiments for rock mechanics data and geotechnical data have been (and are being) performed in the G-Tunnel complex at Rainier Mesa. Some data from the saturated zone are included out of necessity, because the literature does not always distinguish between the two. We have attempted to present all the available data from Yucca Mountain. For a formal definition of the properties discussed in the following sections, the reader is referred to Guzowski and others (1983).

7.1 Physical Properties

Density and porosity data are given in Tables 7-1 and 7-2. Data on the bulk density of as-received or oven-dried samples is tabulated along with the grain density. Appropriate notations are made to indicate the conditions of measurement, if reported in the original reference. Effective and total porosity data are reported in percent units. Some of the references (Lappin, 1980, 1981; Lappin and others, 1982b) indicate that the porosity was calculated from dry-bulk density and grain density data. It is possible that some of the other porosity data were similarly calculated rather than measured; however, the other references did not identify them as such.

7.2 Thermal/Thermomechanical Properties

Thermal conductivity, K_T, and specific heat capacity, C_p, are two thermal properties that control heat transfer by conduction. The thermal diffusivity, β, is a function of these two thermal properties and of bulk density, ρ_b. No diffusivity data are available for the tuffs at NTS; however, it can be calculated as follows:

$$\beta = \frac{K_T}{\rho_b C_p}$$

The product "$\rho_b C_p$" is the volumetric heat capacity of a material. The only available site-specific data on the heat capacity of NTS tuffs is reported as volumetric heat capacity (Zimmerman, 1982, 1983). Mineralogy, porosity, degree of saturation, pressure, and temperature can all affect the thermal conductivity of rocks. Models have been proposed to estimate the thermal conductivity of tuffs from their mineral contents and the conductivity of the minerals (Lappin, 1981; Lappin and others, 1982b). A list of conductivity values for tuff minerals is given in Guzowski and others (1983). An inverse relationship exists between porosity and thermal conductivity of

Table 7-1. Density, ρ (kg/m^3)

Unit/Location	ρ (Bulk)	p (Grain)	Reference
Calico Hills (zeolitized)	1620*	2270	Ogard and others (1983b)
Grouse Canyon Tuff, Rainier Mesa	2300	2600	Zimmerman (1982)
U12N.11 UG-1 Hole, Rainier Mesa	1620-1980 (n) 1280-1670 (d)	2300-2520	Butters and Gronseth (1980)
U12N.12 UG-1 Hole, Rainier Mesa	1790-2080 (n) 1380-1900 (d)	2360-2520	Butters and Gronseth (1980)
UE12N#12 Hole, Rainier Mesa	1670-2250 (n) 1240-2030 (d)	2310-2700	Cooley and others (1982)
U12N.14 UG-1 Hole, Rainier Mesa	1690-2170 (n) 1200-1940 (d)	2400-2730	Cooley and others (1982)
U12N.15 UG-1 Hole, Rainier Mesa	1820-2500 (n) 1460-2490 (d)	2320-2560	Cooley and others (1982)
U12N.15 UG-2 Hole, Rainier Mesa	1800-2120 (n) 1420-1840 (d)	2180-2610	Cooley and others (1982)
U12N.15 UG-3 Hole, Rainier Mesa	1930-1960 (n) 1600-1660 (d)	2330-2400	Cooley and others (1982)
Tiva Canyon Member, Yucca Mtn.	1190-2380	2310-2560	Scott and others (1983)
Topopah Spring Member, Yucca Mtn.		2370-2600	Price and others (1984)
	1870-2190		Snyder and Carr (1982)
Tuff Units Yucca Mtn.	1560-2330	2030-2620	Blacic and others (1982)
	1660-2400	2300-2640	Lappin (1980)
	2210-2390 (s) 1670-2310 (d) 1930-2330	2460-2700	Lappin (1981)

Table 7.1. Density, ρ (kg/m^3)--concluded

Unit/Location	ρ (Bulk)	ρ (Grain)	Reference
	1700-2410 (n)	2240-2750	Lappin and others (1982b)
	1470-2330		
	1510-2340 (d)	2240-2650	Moss and Haseman (1983b)

* At ambient conditions, partially saturated
n as received samples
d oven-dried samples
s saturated samples

Table 7-2. Porosity, ϕ (%)

Unit/Location	ϕ(Effective) Porosity	ϕ(Total) Porosity	Reference
Calico Hills (Zeolitized)		28.6	Ogard and others (1983b)
Grouse Canyon Tuff Rainier Mesa	16.0		Zimmerman (1982)
U12N.11 UG-1 Hole, Rainier Mesa		31.6-44.6	Butters and Gronseth (1980)
U12N.12 UG-1 Hole, Rainier Mesa		19.6-43.2	Butters and Gronseth (1980)
UE12N#12 Hole, Rainier Mesa		20.9-48.2	Cooley and others (1982)
U12N.14 UG-1 Hole, Rainier Mesa		4.6-49.9	Cooley and others (1982)
U12N.15 UG-1 Hole, Rainier Mesa		2.2-37.6	Cooley and others (1982)
U12N.15 UG-2 Hole, Rainier Mesa		26.5-38.6	Cooley and others (1982)
U12N.15 UG-3 Hole, Rainier Mesa		28.9-33.2	Cooley and others (1982)
G-Tunnel, Rainier Mesa		15.0 (welded) 45.0 (non-welded)	Zimmerman (1983)
Paintbrush Tuff Rainier Mesa		49.6±7.4	Benson (1976)
Tiva Canyon Member Yucca Mtn.	5.3-49.3*		Scott and others (1983)
Topopah Spring Member	7.5-18.4*		Price and others (1984)

Table 7-2. Porosity, ϕ (%)--concluded

Unit/Location	ϕ(Effective) Porosity	ϕ(Total) Porosity	Reference
Tuff Units Yucca Mtn.		1.7-30.0	Blacic and others (1982)
		13.0-24.0	Johnstone (1980)
		3.7-49.3(c)	Lappin (1980)
		9.0-32.0(c)	Lappin (1981)
		3.0-40.0(c)	Lappin and others (1982b)
		8.8-54.0	Olsson and Jones (1980)
		11.0-50.0	Tyler (1980)

*Reported as matrix porosity and clay content
c calculated, using $\phi = (1 - \rho_{dry\ bulk} / \rho_{grain})$

rocks. For example, Moss and others (1982) measured thermal conductivities of dehydrated samples of tuffs from Yucca Mountain. They found that at a given temperature (36°C), the conductivity showed a decrease from approximately 1.20 to 0.55 J/msK for samples with porosity increasing from 16.3 percent to 32.5 percent. Conductivity data for Yucca Mountain and Rainier Mesa tuffs in Table 7-3 are primarily for tuff units in the unsaturated zone.

The very limited amount of heat capacity data for NTS and vicinity is presented in Table 7-4. The heat capacity of saturated tuff is significantly higher than that of dehydrated tuff, with the unsaturated tuff having some intermediate heat capacity. For an assumed mineralogy, Guzowski and others (1983) show an increase in specific heat with increasing porosity for saturated tuffs.

The coefficient of expansion, α, is a thermomechanical property in that thermal processes (change in temperature) cause or tend to cause a mechanical effect (change in length or volume). Tuffs show great variation in α depending on their physical and mineralogical characteristics. Devitrified welded tuffs have increasing α's in the temperature range of 25-300°C. Nonwelded tuffs have α's that strongly depend on porosity and mineralogy (Lappin, 1980). Negative values of α (contraction upon heating) have been measured and are attributed to the presence of clays that dehydrate upon heating. The available data on α for the NTS tuffs are summarized in Table 7-5.

7.3 Mechanical Properties

The deformation behavior of a material prior to "failure" can be described in terms of its elastic constants. If the material is isotropic, only two independent elastic constants are needed to completely define its elastic deformation response. It is most common to determine the Young's modulus, E, and the Poisson's ratio, ν, of a material for engineering applications. Other elastic constants, in addition to E and ν, are the bulk modulus, shear modulus, and Lame's constants. If any two elastic constants are known, the others may be calculated from those two, provided that the material is isotropic. The level of stress at which failure in tension occurs represents the tensile strength of a material. Likewise, the level of stress at which failure occurs under a compressive load is a measure of the compressive strength. Rocks are different from metals in two important ways. First, the tensile strength of rock is generally one to two orders of magnitude lower than its compressive strength, whereas metals show nearly equal strength in tension and compression. Second, the confining pressure significantly affects the compressive strength of rocks.

Joints and fractures introduce nonlinearities in the behavior of rock masses that can dominate the mechanical response. It is, therefore, important to understand and account for these deviations from linear elastic behavior. Engineers and analysts frequently use "rock-mass" properties to account for the uncertainties due to discontinuities and other inhomogeneities. Clearly, the rock mass moduli and strength values are much lower than values obtained from laboratory-scale samples.

Table 7-3. Thermal Conductivity, K_T (J/msK)

Unit/Location	K_T (J/msK)	Temp. (°C)	Reference
	0.9 - 3.2		Sass and others (1979)
Grouse Canyon Tuff	1.49 (s) welded	<70	Zimmerman (1982)
	1.11 (d) welded	>120	
Rainier Mesa	1.80 (s) welded		Zimmerman (1983)
	1.44 (d) welded		
	1.30 (s) nonwelded		
	0.66 (d) nonwelded		
	1.20 - 1.26 (d) welded	37-150	Moss and others
	1.57 (w) welded	37	(1982)
Paintbrush Tuff Yucca Mtn.	0.5 - 1.5 (nonwelded)		Sinnock and others (1984)
	1.5 - 2.5 (densely welded)		
Tuff units Yucca Mtn.	0.55 - 1.25* (d)	36-151	Moss and others (1982)
	1.55 - 2.29 (s)welded	27	
	1.62 - 4.44	25 - 300	Lappin (1981)
	0.75 - 2.65	23 - 260	Lappin and others (1982b)
Yucca Mtn.	0.8 - 2.1 (welded tuff)		Lappin and others (1982a)

* The effect of porosity is much stronger than that of temperature. For instance, at 36°C, the conductivity ranges from 0.55 to 1.20. For a given dry sample, the change in conductivity between 36°C and 151°C is only a few percent (Moss and others, 1982).

s saturated
d dry
w wet

Table 7-4. Specific heat capacity, C_p (J/kgK)

Unit/Location	C_p (J/kgK)		Temp. (°C)	Reference
Grouse Canyon Tuff Rainier Mesa	1162* (s)		<70	Zimmerman (1982)
	710* (d)		>120	
G-Tunnel, Rainier Mesa	1116* (s)	welded		Zimmerman (1983)
	837* (d)	welded		
	2245* (s)	nonwelded		
	837* (d)	nonwelded		

*Divided the reported volumetric heat capacity by the reported bulk density to obtain specific heat capacity value.
s saturated
d dry

Table 7-5. Coefficient of thermal expansion, α (K^{-1})

Unit/Location	α (K^{-1})	Temp. (°C)	Reference
Calico Hills (Zeolitized)	-7×10^{-6}	25 - 75	Ogard and others (1983b)
Grouse Canyon Tuff Rainier Mesa	9.5×10^{-6}	<200	Zimmerman (1982)
Paintbrush Tuff Yucca Mtn.	-10×10^{-6} to 0 (nonwelded)		Sinnock and others (1984)
Topopah Spring Member Yucca Mtn.	$5 - 10 \times 10^{-6}$ (densely welded)		Sinnock and others (1984)
Tuff Units Yucca Mtn.	$4.0 - 9.9 \times 10^{-6}$	100 - 300	Johnstone (1980)
	-7.0 to 3.0×10^{-5}	25 - 500	Lappin (1980)
	$0.3 - 17.0 \times 10^{-6}$ (welded)	25 - 300	Smyth and Caporuscio, (1981)

The dynamic and static moduli for a given rock are often very different. It is not uncommon for the dynamic modulus to be an order of magnitude higher. Cheng and Johnston (1981) report ratios of static to dynamic bulk modulus for a number of rocks (including a tuff) as functions of pressure. For a majority (including tuff) of the rock types tested, this ratio is lowest at atmospheric pressure, increases with pressure, and approaches unity at high pressures. The differences between the low- and high-pressure results are attributed to cracks that are open at low pressures but are closed at high pressures. For Ammonia Tanks Tuff, the ratio varies from 0.15 at atmospheric pressure to 0.70 at a pressure of 2×10^8 Pa.

Olsson and Teufel (1980) performed triaxial compression tests on "jointed" (35° precuts) tuff with 4×10^7 Pa confining pressure at displacement rates between 10^{-6} cm/s to 10^{-3} cm/s. For a dry tuff, the coefficient of friction ranged from 0.62 to 0.66; and for wet tuff it ranged from 0.67 to 0.74. In each case, the coefficient of friction increased with decreasing displacement rate.

Data on Young's modulus of NTS tuffs measured using a variety of conditions and techniques are listed in Table 7-6. The dynamic Young's modulus of a given rock or rock type is typically higher than its corresponding static value. The dynamic technique in the laboratory generally consists of measuring the transit times of longitudinal and shear waves in a specimen, from which the moduli may be calculated. Olsson and Teufel (1980) report Young's modulus values of 2.7×10^{10} Pa for dry welded tuff specimens and 2.4×10^{10} Pa for wet specimens; this reduction of 11 percent is not considered significant except that a trend is noted. In attempting to provide a broader data base, Zimmerman and Vollendorf (1982) and Zimmerman and others (1984) have defined and measured the "modulus of deformation," which is indicative of the rock-mass Young's modulus. This modulus is found to be roughly 1/3 of the intact modulus. Price and others (1984) conducted a limited study of sample-size sensitivity and found that whereas the compressive strengths were similar, the Young's modulus of the larger sample was half that of the smaller samples. According to Price (1983), effective porosity is the best indicator of Young's modulus for tuffs.

The Poisson's ratio (ν) data show a maximum range of 0.05 to 0.39 (Table 7-7). For isotropic, elastic materials, ν must be greater than zero and less than 0.5.

Two types of tests are generally performed to estimate the compressive strength of rock. These are the uniaxial (unconfined) and triaxial compression tests. The stress-strain data from these tests is frequently also the basis for determining the elastic moduli. In general, the compressive strength increases with confining pressure. The strength of wet specimens (confined or unconfined) is lower than that of dry specimens (Olsson, 1982; Olsson and Teufel, 1980). Saturated specimen strengths were found by Price (1983) to be an average of 30 percent lower than the corresponding dry sample strengths, and this weakening due to presence of water is thought to be primarily chemical rather than mechanical. According to Price and others (1984), the uniaxial compressive strength showed little sensitivity to sample size.

Table 7-6. Young's modulus, E (Pa)

Unit/Location	E (Pa)	P_c (Pa)*	References
Calico Hills (zeolitized) Temp. 75°C	7.6×10^9	4.9×10^6	Ogard and others (1983b)
Tuff (welded) Ambient temperature NTS	2.7×10^{10} dry (intact) 2.4×10^{10} wet (intact)		Olsson and Teufel (1980)
G-Tunnel Ambient temperature NTS	$9.7\text{-}17.0 \times 10^9$ ** 2.8×10^{10} (intact)	$0\text{-}7.5 \times 10^6$	Zimmerman and others (1984)
Grouse Canyon Member Rainier Mesa	$32.4 \pm 11.8 \times 10^9$ (biaxial apparatus) $12.1 \pm 5.0 \times 10^9$ (borehole jack) 2.6×10^{10} $25.6 \pm 4.0 \times 10^9$ $2.1 - 3.0 \times 10^{10}$		Zimmerman and Vollendorf (1982) Zimmerman (1982) Johnstone (1980) Olson and Jones (1980)
Tuff units Rainier Mesa	$3.1 - 15.6 \times 10^9$		Cording (1967)
Paintbrush Tuff Ambient temperature Yucca Mtn.	$1.3 - 3.7 \times 10^{10}$ $3.6 - 4.3 \times 10^{10}$ (dynamic)	atmospheric	Price and others (1984)
Topopah Spring Member	$2.3 - 4.1 \times 10^{10}$		Price and others (1982a)
Calico Hills Tuff	$2.6 - 9.7 \times 10^9$		Price and Jones (1982)

Table 7-6. Young's Modulus, E (Pa)--concluded

Unit/Location	E (Pa)	P_c (Pa)	References
Bullfrog Member	$1.3 - 1.8 \times 10^{10}$	$0.5 - 2.4 \times 10^{7}$ ($0-5.0 \times 10^{6}$ pore pressure)	Olsson (1982)
200°C	$2.0 - 28.9 \times 10^{9}$		Price and others (1982b)
Tram Member	$5.2 - 22.5 \times 10^{9}$		Price and Nimick (1982)
Tuff units Yucca Mtn.	$6.4 - 47.9 \times 10^{9}$		Johnstone (1980)
	$0.4 - 73.0 \times 10^{9}$		Olsson and Jones (1980)
	$2.6 - 28.9 \times 10^{9}$		Price (1982)

* P_c is the confining pressure.
** "Modulus of deformation" is determined using a formula (see Zimmerman and others, 1984). This modulus can be thought of as a rock-mass Young's Modulus, which would typically be lower than the laboratory value obtained from small specimens.

Table 7-7. Poisson's ratio (ν)

Unit/Location	ν	Temp.(°C)	P_c (Pa)	Reference
Calico Hills (Zeolitized)	0.26	75	4.9×10^6	Ogard and others (1983b)
Grouse Canyon Tuff Rainier Mesa	0.21			Zimmerman (1982)
G-Tunnel, Rainier Mesa (welded tuff)	0.21 - 0.33	ambient	$0 - 7.5 \times 10^6$	Zimmerman and others (1984)
Tuff units Rainier Mesa	0.09 - 0.38			Cording (1967)
Topopah Spring Member Yucca Mtn.	0.13 - 0.30	ambient	atmospheric	Price and others (1984)
	0.15 - 0.33			Price and others (1982a)
Calico Hills Tuff	0.17 - 0.37			Price and Jones (1982)
Tuff Units Yucca Mtn.	0.05 - 0.31			Olsson and Jones (1980)
	0.08 - 0.39			Price (1982)
Bullfrog Member	0.08 - 0.16			Price and others (1982b)
Tram Member	0.09 - 0.38 (dyn)			Price and Nimick (1982)

dyn dynamic laboratory measurement

Results from analysis of tuff data by Price (1983) show that effective porosity is the "best indicator" of unconfined compressive strength. Listed in Table 7-8 are the compressive strength data reported for the various tuffs at NTS and vicinity. A linear relationship between the ultimate (compressive) strength and dynamic shear modulus is proposed by Lin (1983). For dry and 50 percent saturated Paintbrush Tuff from Area 12 (Rainier Mesa) at NTS, and up to confining pressures of 20 MPa, Lin (1983) estimated a constant slope of roughly 1.25×10^{-2} for a plot between strength and shear modulus.

Some tensile strength data are also available for the NTS tuffs; these are summarized in Table 7-9. Based on previously reported data (Blacic and others, 1982), Price (1983) determined the following empirical fit:

$$\text{Tensile strength in MPa} = 27.2 - \phi \times 0.847$$

Where ϕ is the effective porosity. According to tensile strength data for Yucca Mountain units from Blacic and others (1982), zeolitization appears to reduce the tensile strength.

7.4 Effect of Temperature on Rock Properties

A change in temperature, in general, is expected to produce a change in thermal and mechanical properties of a rock. The magnitude of this change, however, may or may not be significant. For repository applications, the temperature range of interest is 30°C to 250°C. Depending on the environment, some of these changes may be irreversible.

Hydrothermal conditions typical of the near-field environment of a tuff repository were imposed on test samples from the Topopah Spring, tuffaceous beds of Calico Hills, Bullfrog and Tram stratigraphic units (Wolfsberg and others, 1983). Significant permanent changes were observed in tensile strength, uniaxial compressive strength, and matrix permeability. The thermal properties, grain density, and porosity were apparently unchanged.

In his analysis of rock mechanics properties, Price (1983) found that strength is inversely related to temperature. Ash-fall tuffs with relatively high porosity (>25%) show a 30-40 percent decrease in strength in going from 23°C to 200°C. Strengths of lower-porosity tuffs appear to be unaffected by the same temperature variation.

The thermal conductivity of five tuffs from drill hole USW-G1 was measured in the temperature range of 36°C to 151°C (Moss and others, 1982). An increase of "several" percent was seen at the higher temperature. On the other hand, only a 5 percent increase was observed in the conductivity of dehydrated samples of welded tuff (Grouse Canyon Member, Rainier Mesa) for the same temperature range. Saturation and porosity appear to have a much greater effect on conductivity than does temperature. A decrease in conductivity occurs with porosity, and an increase occurs with saturation. Because the thermal conductivity of saturated or wet tuff is significantly higher than that of dry or dehydrated tuff, the conductivity would be expected to drop if vaporization (and hence dehydration) occurs at higher temperatures.

Table 7-8. Compressive strength (Pa)

Unit/Location	Compressive strength (Pa)	Reference
Tuff NTS	Welded, unconfined: dry, intact 1.58×10^8 wet, intact 1.12×10^8	Olsson and Teufel (1980)
Grouse Canyon Tuff, Rainier Mesa	Saturated: 1.10×10^8	Zimmerman (1982)
Tuff Units Rainier Mesa	Unconfined: $9.3 - 35.3 \times 10^6$	Cording (1967)
	Unconfined: $11.4 \pm 1.2 \times 10^7$	Johnstone (1980)
	Unconfined: $7.0 - 18.9 \times 10^7$	Olsson and Jones (1980)
Paintbrush Tuff (Pah Canyon, Yucca Mtn., and Upper Topopah Spring Members)	Nonwelded, unconfined: $<4.8 \times 10^7$	Sinnock and others (1984)
Topopah Spring Member Yucca Mtn.	Unconfined: $2.65 - 24.5 \times 10^7$	Price and others (1984)
	Densely welded: $4.8 - 13.8 \times 10^7$	Sinnock and others (1984)
	Confined (0.1 - 10 MPa) $4.5 - 17.7 \times 10^7$	Price and others (1982a)
	Unconfined: $5.5 - 13.8 \times 10^7$	Johnstone (1980)
	Confined (0.1 - 100 MPa) temp: 25 - 200°C $0.6 - 85.5 \times 10^7$	Olsson and Jones (1980)
	Unconfined: $1.4 - 15.3 \times 10^7$	Price (1982)
Calico Hills Tuff	Confined (0.1 - 20 MPa): $1.4 - 4.2 \times 10^7$	Price and Jones (1982)
Bullfrog Member, Crater Flat Tuff	Confined (5-20 MPa) at 200°C: dry $8.7 - 13.4 \times 10^7$ wet $7.0 - 8.6 \times 10^7$	Olsson (1982)
	$0.5 - 15.3 \times 10^7$	Price and others (1982b)

Table 7-8. Compressive strength (Pa)--concluded

Unit/Location	Compressive strength (Pa)	Reference
Tuff Units Yucca Mtn.	Unconfined: $3.0 - 24.2 \times 10^7$	Blacic and others (1982)
Silicic Tuffs Yucca Mtn.	Unconfined: $1.5 \times 10^7 - 1.5 \times 10^8$ Nonwelded 3×10^7 Densely welded, devitrified 1×10^8 Partially welded, devitrified 6×10^7	Lappin and others (1982a)

Table 7-9. Tensile strength

Unit Location	Tensile strength (Pa)	Reference
Grouse Canyon Tuff Rainier Mesa	4.0×10^6	Zimmerman (1982)
Ash-fall tuff Rainier Mesa	$2.1 - 3.3 \times 10^6$	Weisinger and others (1980)
Tuff Units Yucca Mtn.	$2.2 - 25.9 \times 10^6$	Blacic and others (1982)

Based on an evaluation of the data available to them, Guzowski and others (1983) believed that the specific heat capacity increases slightly with temperature. No new data were found to further substantiate or deny their suggestion.

7.5 In-situ Stresses

The in-situ state of stress will affect the behavior of the openings as well as serve as boundary condition data for modeling calculations. In particular, fracture behavior near the openings can be expected to be dominated by the magnitude of in-situ stress and ratios of principal stresses. Tyler and Vollendorf (1975) determined in-situ stresses from hydrofracture experiments near the southeast edge of Rainier Mesa. The minimum principal stress varied from 6.9×10^5 Pa at a depth of 280 feet (85 m) to 3.4×10^6 Pa at 1,434 feet (437 m) under the mesa top. Ellis and Swolfs (1983) observe that the in-situ horizontal principal stress components are not equal in the layered tuff units penetrated by the USW-G1 drill hole at Yucca Mountain. Further, the concentration of these stresses around the borehole are sufficient to locally exceed the "yield strength" of the rock. The yield strength is the value of stress at which a material begins to experience plastic flow. Ellis and Swolfs (1983) suspect that the minimum horizontal principal stress in the welded tuff units above the static water level at USW-G1 may be less than half that of the vertical stress. The in-situ state of stress was measured in welded tuff (Grouse Canyon Member of Rainier Mesa tuffs) in G-Tunnel. The principal stresses as measured by the overcoring technique are

$$\sigma_v = -8.1 \pm 1.5 \times 10^6 \text{ Pa}$$

$$\sigma_{h1} = -5.5 \pm 1.2 \times 10^6 \text{ Pa}$$

$$\sigma_{h2} = -0.3 \pm 1.4 \times 10^6 \text{ Pa}$$

where σ_v is the vertical stress, σ_{h1} is the maximum horizontal stress, and σ_{h2} is the minimum horizontal stress (Zimmerman and Vollendorf, 1982).

CHAPTER 8 - RECOMMENDATIONS FOR FUTURE WORK

This report is an extension of the "Repository site data report for tuff, Yucca Mountain, Nevada" (Guzowski and others, 1983), with emphasis on data derived from or applicable to the tuffs of the unsaturated zone. The recommendations made by Guzowski and others (1983), therefore, are still valid. The main purpose of this report is to provide an adequate data base for the NRC/SNLA risk assessment methodology being developed for unsaturated tuffs, using publicly available documents. Data on certain parameters may exist without yet being available in the open literature. The following recommendations are not intended to provide guidance to DOE for future site characterization programs but to highlight the major deficiencies in the available data.

Seismicity. Detailed seismic studies for the definition of the different seismic source zones and their delineation are needed. Seismic source zones are important parameters for the development of performance assessment and a seismic risk analysis.

Stratigraphy. Information on the subsurface distribution of the tuff units is limited to few drill hole locations. Detailed correlation from hole to hole is impossible. More subsurface data are needed to adequately model the site.

Lithology and mineralogy. Descriptions of lithology and mineralogy vary in thoroughness from drill hole to drill hole. A systematic description consisting of all needed parameters should be standardized for all drill hole samples.

The petrofabric of zeolitized tuffs should be studied, because the volume reductions of zeolites and smectites during dehydration vary along different crystallographic directions. Such variations could affect near-field groundwater flow modeling.

Structure. Active faults near the repository could disrupt the recharge pattern, and renewed movement along these faults could create barriers to flow and affect the unsaturated zone. For this reason, active faults and magnitude of movement along these faults should be identified.

If fault zones at Yucca Mountain are high permeability zones, one or more fault zones could provide a pathway for relatively rapid transport to the saturated zone. Fault attitude is important because fault zones that have surface traces near the repository may dip under the repository site. The attitude (depth, inclination, etc.) of faults and the nature of the fault zone within the Yucca Mountain area should be determined.

Most (or all) computer codes that deal with the movement of a liquid phase through fractured, unsaturated rock require fracture density in order to model water movement through the fractures. The discrepancy between fracture densities measured in outcrops and those in cores should be resolved. Are the differences the result of location or sampling technique?

In addition to reporting fracture density as fractures/volume, the orientation and spacing of each fracture set at each location should be reported, because most codes require fractures/length when dealing with fractures, even though fractures/volume may be more realistic.

Because fracture density is partially controlled by larger-scale structures, fracture density varies with location and rock type. As a result, areas with higher fracture density may allow more recharge than other areas. Additional data on the lateral and vertical distribution of fracture densities for each rock type, using a consistent sampling technique, are needed.

If water moves through fractures at Yucca Mountain, this movement needs to be modeled. In addition to fracture density, data on fracture aperture, fracture filling, the effective fracture porosity, and the relationship of these parameters to location, rock type, and fracture orientation are needed. Because aperture is not unique to a particular location, the statistical distribution of apertures will allow for sampling from the distribution that is in part weighted by the variability in fracture aperture.

At least one report has mentioned the possibility of renewed silicic volcanic activity. Certain disruptive scenarios could be postulated if the repository were underlain by a reactivated caldera rather than limestone basement. Whether the actual repository site is underlain at depth by a caldera, as suggested by gravity data or by Paleozoic (or Precambrian) rocks, should be determined.

Knowledge of the distribution of stresses in the area around Yucca Mountain could be used to predict future deformation. Fractures in an area of extension would tend to be more open than those in an area of compression. The distribution and relative magitude of stress orientations in the Yucca Mountain area should be determined to resolve the substantial variations noted in drill holes at the crest of Yucca Mountain (USW-G1 and USW-G2) and at UE25p-1.

Geochemistry. There are no reported analyses of the composition of water in the unsaturated zone. Although some information presented in Section 5.1 suggests that the composition of water above the water table could be similar to J-13 water, such a similarity is uncertain. This uncertainty is significant because ground-water chemistry exerts a strong influence on radionuclide sorption and speciation and mineral stability. The composition of water in rocks above the water table should be determined by methods such as direct sampling of pore fluids, bulk analyses of dry and partially saturated rocks, and computer modeling of rock/water interactions under conditions of cyclic drying and wetting.

Models of zeolite diagenesis and the thermal stabilities of secondary minerals are important to decisions concerning the location of the repository and the choice of a suitable backfill. Recently a model for the control of zeolite stability of silica activity has been proposed (Wolfsberg and Vaniman, 1984). This model depends on a large number of assumptions and in part on a reinterpretation of previously reported stratigraphic data. The model could lead to the adoption of nonconservative assumptions concerning the effect of temperature (or lack thereof) on zeolite stability. This theory should not

be adopted in place of the earlier more conservative model (Smyth and others, 1981) that describes zeolite stability as a function of temperature until more supporting evidence is obtained. The stratigraphic zonation of clinoptilolite, analcime, albite at Yucca Mountain should be reexamined in light of these two models.

The reversibility of dehydration and rehydration of zeolites and clays has not been extensively examined at low (25° to 30°C) temperatures. It is possible that changes in the mineral composition of the cores could be induced by drilling and sample storage. These changes might invalidate the sorption data obtained on these samples. This uncertainty in the sorption data could be minimized if it is demonstrated that any such changes (hydration or dehydration) are reversible or insignificant during drilling or storage.

Sensitivity studies reported at a recent workshop (LANL, 1984) suggested that radionuclides of Nb, Ni, and Zr in nuclear waste rank high in the list of toxic elements. There are no sorption data for these elements on site-specific materials. They should be included in future sorption studies.

Hydrology. In order to properly calibrate ground-water flow models and to model ground-water flow in the unsaturated zone at Yucca Mountain, some additional hydrologic data will be required.

Attempts to collect in-situ pressure-head data for air and liquid phases should be made. These data are necessary for setting initial conditions on modeling air and water flow in the unsaturated zone.

More characteristic-curve data for the various tuff units at Yucca Mountain should be obtained. These data should include relative air and liquid hydraulic conductivities versus pressure head and degree of saturation versus pressure head. These data are necessary to evaluate flow within a tuff unit and between tuff units. At present, characteristic curve data for the Yucca Mountain tuffs are almost nonexistent. Curve data presented in Chapter 6 come mostly from off-site tuffs.

A detailed description of the fracture network within the Yucca Mountain tuffs is needed. This information is needed to determine whether any preferential pathways for water movement exist. It is possible that fracture flow may dominate pore flow in the unsaturated zone.

More effective-porosity data are needed for the various tuffs. Currently data are limited to that obtained from one test well. These data are necessary for modeling flow and, in the future, for modeling contaminant transport. It has been shown in Chapter 6 that, for the most part, effective porosity is much less than total porosity.

A program to test the tuffs for dispersion parameters should be implemented. These data are necessary for modeling mass transport in the unsaturated zone. Dispersion data do not currently exist.

A more complete understanding of the recharge mechanism is needed. While several estimates of recharge are available, the dominant method of recharge

is not known. What is needed is to determine how much recharge enters the unsaturated zone by way of fractures and how much enters by way of pore space.

A detailed understanding of the flow mechanism in partially saturated fractures and the impacts that a porous medium may have on partially saturated fracture flow is needed. Some authors believe that partially saturated fracture flow occurs in slugs (Travis, 1984), while others believe it occurs as a thin film on the fracture surface (Evans, 1983). Data are needed to confirm whether either one or both of these phenomena occur. A mathematical model based on the data is needed.

Thermomechanical Property Data. An effort should be made to relate permeability to stress, because the stresses on the joints or fractures will not be constant. Fracture apertures are likely to vary with stress, which, in turn, can affect permeability. Some solutions are available in the literature for idealized crack (fracture) geometries; however, these may or may not be appropriate for applications to unsaturated tuff. Any relationships, analytical or empirical, that are developed should be validated against field or laboratory experiments.

The term "failure" is used to describe a number of situations in which the material (rock) no longer can support additional stress. There are different failure modes: plastic yielding, tensile cracking, compressive failure, and spalling are the main ones. These modes need to be analyzed for the specific mine design. Additional parameters, such as those associated with slip, may have to be determined for a proper predictive analysis. An understanding of the potential failure mechanisms is particularly significant for design, construction, and operational activities.

The strong dependence of nearly all thermal and mechanical properties on porosity makes it imperative to determine the porosity of the host rock with relatively high accuracy. Any uncertainty in the porosity data reflects similar or greater uncertainties in other properties. This uncertainty can be reduced to a large extent by obtaining a reliable estimate of the host rock porosity at the anticipated repository horizon.

APPENDIX 1.1

Potassium-Argon Dating on Volcanic Rocks Within the NTS Region

Table A.1.1-1. Rock name, mineral analyzed, analytical data, and age for specimen dated (after Kistler, 1978)

	Map No.[a]	Sample No.*	Ar^{40}/K^{40}	Age (m.y.)
Thirsty Canyon Tuff				
Labyrinth Canyon Member	1	N80A-S	0.000360	6.2
Spearhead Member	2	Age 11-S	0.000439	7.5
Tuff of caldera fill	3	Age 19-B	0.000552	9.4
Timber Mountain Tuff				
Ammonia Tanks Member	4	Age 17-B	0.000638	10.9
	5	Age 16-S (-80+100)	0.000630	10.8
		Age 16-S (-60+80	0.000634	10.8
	6	Age 12-B	0.000656	11.2
	7	Age 20-B	0.000665	11.4
	8	Age 5-B	0.000710	12.1
Tuff of Transvaal	9	Age 18-B	0.000646	11.0
Tuff of Cat Canyon				
Upper cooling unit	10	WJC138-S	0.000612	10.5
Ring fracture tuff	11	Age 7-B	0.000635	10.8
			0.000639	10.9
		Age 7-S	0.000620	10.6
			0.000641	10.9
Lower cooling unit				
(Upper part)	12	Age 22-S	0.000649	11.1
(Lower part)	13	Age 23-B	0.000687	11.7
		Age 23-S		
		(-100+115)	0.000651	11.1
		(-80+100)	0.000667	11.4
Rainier Mesa Member	14	Age 15-S	0.000609	10.4
Rhyolite lava	15	MC-336-B	0.000660	11.3
Paintbrush Tuff				
Tiva Canyon Member	16	Age 4-B	0.000727	12.4
	17	BC-308-B	0.000727	12.4
Topopah Spring Member	18	Age 2A-B	0.000724	13.2
Wahmonie Formation				
Rhyodacite lava	19	Age 9-B	0.000733	12.5
Ash fall	20	Age 8-B	0.000755	12.9

Table A.1.1-1. Rock name, mineral analyzed, analytical data, and age for specimen dated--concluded

	Map No.[a]	Sample No.*	Ar^{40}/K^{40}	Age (m.y.)
Rhyolite of Calico	21	Age 3-B	0.000787	13.4
Tuff of Redrock Valley	22	Age 13-S	0.000799	13.6
Biotite tuff	23	Age 6-B	0.001241	16.1
	24	Age 24-B	0.000881	15.0
Tuff of Trailer Pass	25	Age 25-B	0.001045	17.8
Tuff of White Blotch Spring	26	438-6-B	0.001241	21.1
		438-6-S	0.001285	21.9
Tuff of Belted Peak	27	163-3-B	0.001488	25.3
Tuff of Monotony	28	Age 26-B	0.001537	26.1
Dacite vitrophyre	29	644-3-B	0.001239	21.1

a See Figure A.1.1-1.
* Suffix letters: S, sanidine; B, biotite.

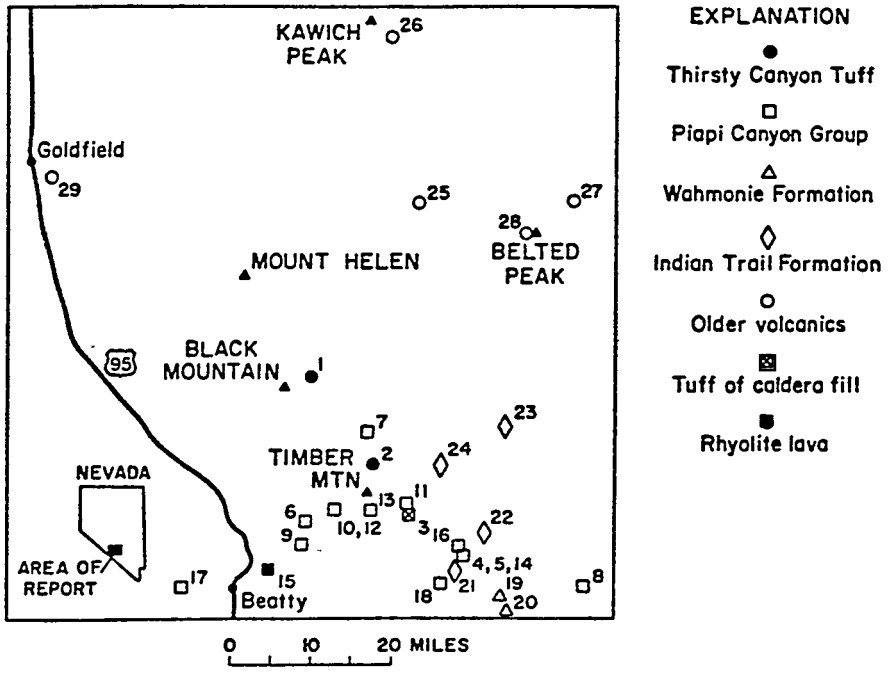

Figure A.1.1-1. Sketch map showing the localities sampled for potassium-argon dating (after Kistler, 1968).

APPENDIX 1.2

Location, Mineralization, and Production of Selected Mines and Prospects, Yucca Mountain and Vicinity

	Name(s) District	Location	Commodity	Status	Description
1.	Mammoth 1-5 Bare Mtn.	Sec 2 TIISR48E	Hg originally, now Ag, Au, Hg	Expl. 1980-1 incl. Flash Future, Effic, and Kenneth claims	Silica, cinnabar, alunite (plus Ag, Au?) along a N30°W trending belt of alunized, silicified copalized rhyolitic volcanics.
2.	Thompson Bare Mtn.	Sec 29 S/2 TIISR48E	Hg	Inactive since 1943	Disseminations, coatings and veinlets of cinnabar along shear zones in silicified rhyolite flows and tuffs. Hot spring sinter in area.
3.	Curly Wright (Calvin) (Lottie) Bare Mtn.	Sec 30 TIISR48E	Hg	Inactive	Pods and lenses of cinnabar disseminated in Tertiary rhyolitic flows and tuffs along NE-striking fault. Cinnabar associated with opal and chalcedony. Ore assay gave 1.4 lbs Hg/ton ore.
4.	Tip Top Group Earlybird Bare Mtn.	Sec 7 T128R48E	Hg	Inactive; 8 claims	Cinnabar and minor native mercury as disseminations and in 1-2" veins in zone striking NE and dipping vertical in Lone Mtn. dolomite of Silurian age. Average 6 lbs/ton, up to 6% Hg.
5.	Mary 1-4 Bare Mtn.	W/2 Sec 32 T125R48E	Fluorspar	Active in 1979; Mary and Star claims	Fluorspar in several irregular bodies, probably breccia pipes adjacent to NE-striking, 60°E dipping fault zone along east edge of Bare Mtn. Main ore body on hanging wall side of fault near flexure in fault. Ore consists of fluorite, quartz, calcite, dolomite and clay. Host rocks are Roberts Mtn. dolomite and Lone Mtn. dolomite of Silurian age.
6.	Lime Cap Bare Mtn.	9 mi. east of Beatty	Hg		

Production	References
Test loads, 1981	Knopf (1915); Personal comm.: 6/81 with Spicer by Bell and Larson (1982).
Small; 100 flasks to 1940	Bailey and Phoenix (1944); Holmes (1965); Cornwall and Kleinhampl (1961); Cornwall (1972b).
None. Estimated reserve of 200,000 lbs Hg at 1.4 lbs/ton of rock.	Cornwall and Kleinhampl (1961) Holmes (1965).
100 flasks, estimated 10,000 tons of ore remain	Bailey and Phoenix (1944); Cornwall (1972b); Holmes (1965); Cornwall and Kleinhampl (1961); Knopf (1915); Bare Mtn. Mining Corp. (1968); Anon. (1929).
13,000 tons of 40% CaF_2 or less	Papke (1979); Anon. (1974).
	Gallagher (1957).

	Name(s) District	Location	Commodity	Status	Description
7.	Harvey (Telluride) (Denver) Bare Mtn.	NW/4 Sec 18 T12SR48E	Hg, Au	Inactive, 10 unpatented claims	Cinnabar in small north-striking "pod" in shear zone between two Tertiary diabase dikes. Ore in Fluorspar Canyon Fm. - a Devonian dolomite. Deposit trends N35°E and dips 70°SW. Deposit near NE subsidence ring fracture of Bullfrog Hill caldera. Sample varied from 0.2 to 27.6 lbs Hg/ton.
8.	Docillion Bare Mtn.	?NE part of Bare Mtn.	Ag, Au		Quartz vein and stringer cutting limestone and schist. Some veins strike E-W and dip 45°S. Chalcopyrite disseminated in quartz. Malachite and azurite stain. Quartz veins faulted; locally cemented by gypsum. Ore high in Ag, low in Au.
9.	Thomas Group	3.5 mi. SE of Carrara	Au, Ag, Pb	4 claims; Clipper, Wild West, Mistletoe and Gate City	Lenses in limestone, N15E5NW; 2-4 feet wide x maximum length of 25 feet. Some high grade ore streaks. 6 samples assayed. Au: tr.-0.0402; Ag: 6.9-138.802, %Pb: tr.-19.3.
10.	Grochon Claim Bare Mtn.	E. flank Bare Mtn.	Au		High-grade Au ore in small irregular veins of quartz, showing no metal but assaying $84/ton in 1915.
11.	Big Dune Lee	Sec 23-27, 34-35 T15SR47E	Au, Cu		Specularite, siderite and trace of galena, some chalcocite, azurite, malachite and copper stains. Area of widely spaced quartz veins of pre-Cambrian hills. Virtually no associated alteration.

Production	References
80 flasks plus?	Bailey and Phoenix (1944); Cornwall and Kleinhampl (1964); Gianella (1940); Holmes (1965); Knopf (1915); Papke (1979).
	Ball (1905).
Some bullion produced by Mormons	Carper (1921).
	Knopf (1915).
	Baker and Hsu (1969); Ball (1907); Lincoln (1923).

	Name(s) District	Location	Commodity	Status	Description
12.	Treasure Hill Lee	Sec 23 T15SR47E Sec 24, 25 T15SR47E Sec 26 T15SR47E Sec 27 T15SR47E Sec 34 T15SR47E Sec 35 T15SR47E	Au, Cu, Ti		Quartz vein in pre-Cambrian rock.
13.	Lee Camp (incl.: Pumpkin, Squash, Oro, Oversight Fraction, Johnson Grass, Hayseed and Hidden Treasure) Lee	Sec 4,5,8,9 T28NR3E SBBM	Au	Inactive; Active in 1906-1922. Patent claims 180+ acres in DVNM	Quartz veins in sediments.
14.	Big Dune Amargosa Desert	Sec 17 T15SR48E	Ti, Fe	Inactive	Magnetite, rutile, titanite, zircon, hornblend, quartz in modern eolian dune. 4 samples assayed less than 0.5% TiO_2.
15.	Lucky Group Wahmonie	SW/4 Sec 15 T15SR50E	Cu	Inactive	Malachite in east-striking shear zone in quartzite. Traveable with width of 1-4' over 500' of strike.
16.	Rainstorm Group, Yucca Flat	Sec 15(?) T11SR53E	Pb, Ag, Au	Inactive	Vein, assays ran 31.5% Pb, 0.07 oz. Au/ton and 11.6 oz. Ag/ton.

Production	References
	Smith (1977); Cornwall (1972b)
	Smith (1977) Cornwall (1972b) Ball (1907) Hill (1912)
	Smith (1977) Cornwall (1972b)
	Smith (1977) Cornwall (1972b) Ball (1907) Hill (1912)
Little Hayseed: 1 carload shipped 1907 $150-200/ton. Pumpkin: $25/ton ore	Smith (1977); Norman and Stewart (1951); Tucker and Sampson (1938); Greene and Latscher (1981).
None	Beal (1962).
Trail shipment	Kral (1951)
80 tons conc. with 85% Pb, 25 oz. Ag/ton, 0.25 oz. Au/ton.	Kral (1951)

Name(s) District	Location	Commodity	Status	Description
17. Mine Mtn.	Sec 11, 14 T11SR52E	Pb,Ag,Hg	Inactive	Workings along high-angle normal faults trending N30°E in brecciated quartzite and dolomite of the Devils Gate Limestone in upper plate of a thrust fault. Spectrographic analysis shows 10%Pb, 0.5% Hg and 0.07% Ag.

Production

References

Cornwall (1972b); Anon (1969).

APPENDIX 2.1

Stratigraphic and Lithologic Descriptions of Drill Holes

Table A.2.1-1. Lithologic log of drill hole USW-G1. [Elev. 4,348.6 ft Color designations are from the Rock-Color Chart (Goddard and others, 1948)] (after Spengler and others, 1981)

Stratigraphic and lithologic description	Thickness of interval feet (meters)	Depth to bottom of interval feet (meters)
Alluvium, gravel, sand, silt, containing fragments of densely welded Tiva Canyon Member, and partially welded Yucca Member, a few fragments are partially coated with caliche	60 (18.3)	60 (18.3)
Paintbrush Tuff		
Yucca Mountain Member		
Tuff, ash-flow, grayish-orange-pink and pale-yellowish-brown, partially welded, vapor-phase crystallization; rare pumice, moderate-brown, reddish-brown, and white, vapor-phase, commonly 1-2 mm; rare phenocrysts	25 (7.6)	85 (25.9)
Tuff, ash-flow, pale-yellowish-brown and dark-yellowish-brown, nonwelded, vitric; rare pumice, grayish-orange-pink, and light-brown, vitric; rare phenocrysts; contains abundant glass shards	15 (4.6)	100 (30.5)
Tuff, bedded, reworked, white and pinkish-gray, poorly consolidated, vitric; pumice sparse, white, vitric; mixture of pumice and rhyolitic lithic fragments	35 (10.7)	135 (41.1)
Pah Canyon Member		
Tuff, ash-flow, grayish-orange-pink, nonwelded, vitric; pumice, white, vitric; contains sparse bronze biotite	45 (13.7)	180 (54.8)
Tuff, ash-flow, moderate-to-dark yellowish-brown, nonwelded, vitric; pumice, dark yellowish-brown, vitric; rare biotite	55 (16.8)	235 (71.6)

Table A.2.1-1. Lithologic log of drill hole USW-G1--continued

Stratigraphic and lithologic description	Thickness of interval feet (meters)	Depth to bottom of interval feet (meters)
Paintbrush Tuff--continued		
Topopah Spring Member		
Tuff, ash-flow, white and grayish-orange, nonwelded, vitric; pumice, white, vitric; conspicuous bronze biotite	10 (3.0)	245 (74.6)
Tuff, ash-flow, grayish-orange-pink to moderate-orange-pink, nonwelded, vitric; pumice yellowish-gray and white, vitric; sparse bronze biotite	5 (1.5)	250 (76.2)
Tuff, ash-flow, grayish-yellow to yellowish-gray, nonwelded, vitric; pumice, grayish-yellow and white, vitric; hornblende and pyroxene present	5 (1.5)	255 (77.7)
Tuff, ash-flow, very pale orange to light-brown, nonwelded, vitric; pumice, light-brown, vitric; hornblende and pyroxene present	15 (4.6)	270 (82.3)
Tuff, ash-flow (vitrophyre), moderate-reddish-brown, densely welded, glassy; 10-15 percent phenocrysts	10 (3.0)	280 (85.3)
Tuff, ash-flow, grayish-red, densely welded, vitric; pumice, pale-red to grayish-red, devitrified (some vapor phase), 2-10 mm; 5-10 percent phenocrysts (sanidine, plagioclase, hornblende and biotite) (quartz latitic caprock)	12.5 (3.8)	292.5 (89.1)
Tuff, ash-flow, grayish-red, densely welded, devitrified; pumice, brownish-gray and grayish-red, very light-gray to light-gray, mostly 5 mm to 3 cm, but as large as 5 cm; vapor-phase crystallization; 5-7 percent phenocrysts		

Table A.2.1-1. Lithologic log of drill hole USW-G1--continued

Stratigraphic and lithologic description	Thickness of interval feet (meters)	Depth to bottom of interval feet (meters)
Paintbrush Tuff--continued		
Topopah Spring Member--continued		
(predominantly plagioclase and sanidine); sparse light-gray rhyolitic lithic fragments; flattening and alignment of pumice fragments well developed	145.5 (44.3)	438.0 (133.5)
Tuff, ash-flow, light-gray to medium-light-gray, densely welded, devitrified; pumice white to light-gray and brownish-gray, devitrified, 5 mm to 6 cm; 2-3 percent phenocrysts (sanidine and plagioclase); sparse light-gray rhyolitic lithic fragments; unit contains 10-30 percent lithophysae, mostly 1-3 cm in diameter, but as large as 6 cm	18.5 (5.6)	456.5 (139.1)
Ash, brownish-gray, unconsolidated to poorly consolidated, contains minute pumice fragments and sanidine phenocrysts as well as tridymite and cristobalite	0.4 (0.1)	456.9 (139.2)
Tuff, ash-flow, light-gray to medium-light gray, densely welded, devitrified; pumice, white to light-gray and brownish-gray, devitrified, 5 mm to 6 cm; 2-3 percent phenocrysts (plagioclase and sanidine); sparse light-gray rhyolitic lithic fragments; unit contains 10-30 percent lithophysae, mostly 1-3 cm in diameter but as large as 6 cm	5.8 (1.8)	462.7 (141.0)
Tuff, ash-flow, light-gray to medium-light-gray, densely welded, devitrified; pumice, light-gray and light-brownish-gray, devitrified, 1-5 cm;1-2 percent phenocrysts, sparse light-gray rhyolitic lithic fragments	29.8 (9.1)	492.5 (150.1)

Table A.2.1-1. Lithologic Log of Drill Hole USW-G1--continued

Stratigraphic and lithologic description	Thickness of interval feet (meters)	Depth to bottom of interval feet (meters)
Paintbrush Tuff--continued		
Topopah Spring Member--continued		
Tuff, ash-flow, light-gray to medium-light-gray, densely welded, devitrified; pumice, white to light-gray and light-brownish-gray, devitrified, 5 mm to 6 cm; 2-3 percent phenocrysts (plagioclase and sanidine); rare light-gray rhyolitic lithic fragments; contains 20-30 percent lithophysae, mostly 1-3 cm in diameter, but as large as 6 cm; cavities are commonly lines with secondary minerals, predominantly feldspar	220.9 (67.3)	713.4 (217.4)
Tuff, ash-flow, brownish-gray, pale-reddish brown (mottled in places), densely welded, devitrified; pumice, light-brownish-gray and brownish-gray, sparse devitrified, less than 1 percent phenocrysts, rare dark-yellowish-brown and medium-light-gray volcanic lithic fragments, rare lithophysae, as large as 3 cm	58.6 (17.9)	772.0 (235.3)
Tuff, ash-flow, light-brownish-gray and very light-gray, densely welded, devitrified; pumice, brownish-gray and light-gray, devitrified, commonly 1-2 cm in length; less than 1 percent phenocrysts (sanidine and plagioclase); 5-15 percent lithophysae, ranging from 1-3 cm, commonly filled and spherical	17.3 (5.2)	789.3 (240.5)
Tuff, ash-flow, grayish-red and pale-reddish-brown (mottled), densely welded, devitrified; pumice, light-brownish-gray and very light gray, devitrified, commonly 1-2 cm; less than 1 percent phenocrysts; very light gray to medium-light-gray volcanic fragments, commonly 1-2 cm in length, occasional flattened lithophysae	25.5 (7.8)	814.8 (248.3)

Table A.2.1-1. Lithologic log of drill hole USW-G1--continued

Stratigraphic and lithologic description	Thickness of interval feet (meters)	Depth to bottom of interval feet (meters)
Paintbrush Tuff--continued		
Topopah Spring Member--continued		
Tuff, ash-flow, pale-red and pale-reddish-brown (mottled), densely welded, devitrified; pumice, grayish-red and pale-red, devitrified, commonly 1-2 cm; less than 1 percent phenocrysts (sanidine and plagioclase); unit contains 5-20 percent lithophysae, mostly 2-3 cm in diameter, but as large as 5 cm, usually completely filled with secondary mineralization; conspicuous increase in light-gray to dark-gray rhyolitic lithic fragments as large as 4 cm (notable accumulation of lithic fragments from 840 to 841.2 ft or 256 to 256.4 m)	151.7 (46.2)	966.5 (294.5)
Tuff, ash-flow, pale-red and pale-reddish-brown (mottled), densely welded, devitrified; pumice, grayish-red and pale-red, devitrified, commonly 1-2 cm; less than 1 percent phenocrysts; unit contains 20-30 percent lithophysae, commonly 1-2 cm in diameter, but as large as 4 cm, nearly spherical, some flattened, commonly completely filled with secondary minerals; sparse light-gray rhyolitic lithic fragments; core contains numerous very thin (less than 0.5 mm) silica veinlets from 988.3 to 993.5 ft (301.2 to 302.8 m)	30.5 (9.3)	997.0 (303.8)
Tuff, ash-flow, grayish-red to moderate-yellowish-brown (mottled), densely welded, devitrified; pumice, grayish-red and medium-gray, devitrified, 1-3 cm, pumice foliation well developed; less than 1 percent phenocrysts; sparse light-gray to medium-gray rhyolitic lithic fragments, commonly 1-3 cm in diameter; 5-15 percent lithophysae, as large as 4 cm, cavities filled with argillic material in upper half of unit, open in lower half; interval from 1,100.6 to 1,107.0 ft		

Table A.2.1-1. Lithologic log of drill hole USW-G1--continued

Stratigraphic and lithologic description	Thickness of interval feet (meters)	Depth to bottom of interval feet (meters)
Paintbrush Tuff--continued		
Topopah Spring Member--continued		
(335.4 to 337.4 m) contains numerous silica veinlets	202.2 (61.6)	1,199.2 (365.4)
Tuff, ash-flow, grayish-red to moderate-yellowish-brown (mottled), densely welded, devitrified; pumice grayish-red, devitrified, commonly 1-3 cm in length, foliation of pumice fragments well developed; less than 1 percent phenocrysts; occasional lithophysal cavities; sparse medium-gray rhyolitic lithic fragments, commonly 2-4 cm in length; lower 1.5-2.0 ft (0.5-0.6 m) of unit appears slightly altered	87.8 (26.8)	1,287.0 (392.2)
Tuff, ash-flow, dark-gray to black (vitrophyre), densely welded, glassy; pumice, black, vitric, commonly 5 mm to 2 cm; 1-2 percent phenocrysts (predominantly sanidine); 1-2 percent rhyolitic lithic fragments, pale-red and gray; concentrated in upper 3 ft (0.9 m) of unit	55.4 (16.9)	1,342.4 (409.1)
Tuff, ash-flow, dark-gray, moderately welded, vitric; pumice, light-brown to moderate-brown, vitric, 0.5 to 3 cm; less than 1 percent phenocrysts (sanidine and plagioclase); rare pale-red and light-gray volcanic lithic fragments, 5 mm to 2 cm; groundmass composed of abundant black glass shards	18.1 (5.5)	1,360.5 (414.6)
Tuff, ash-flow, medium-dark-gray, grades downward to dark-yellowish-brown, partially welded to nonwelded, decreases in welding downward, vitric; pumice, light-brown to moderate-brown, vitric, commonly 1-4 cm in length, as large as 8 cm; less than 1 percent		

Table A.2.1-1. Lithologic Log of Drill Hole USW-G1--continued

Stratigraphic and lithologic description	Thickness of interval feet (meters)	Depth to bottom of interval feet (meters)
Paintbrush Tuff--continued		
Topopah Spring Member--continued		
phenocrysts; sparse pale-reddish-brown and medium-gray volcanic lithic fragments, 1-2 cm in diameter; abundant glass shards	33.8 (10.3)	1,394.3 (424.9)
Tuff, ash-flow, light-brown and light-brownish-gray, nonwelded, devitrified (slightly silicified, slightly zeolitized); pumice, light-brownish-gray and pale-red, devitrified (some zeolitized), 1-3 cm; less than 1 percent phenocrysts; sparse grayish-red volcanic lithic fragments, 5 mm to 1 cm; unit contains abundance of grayish-red volcanic lithic fragments, 5 mm to 1 cm; unit contains abundance of grayish-red, pale-red, and medium-dark-gray volcanic cobbles ranging in size from 4 to 6 cm from 1,399.0 to 1,399.9 ft (426.4 to 426.7 m)	9.6 (2.9)	1,403.9 (247.8)
Tuff, bedded, reworked, light-brownish-gray, light-gray, and pale-reddish-brown; individual beds range in thickness from 0.1 to 2.5 ft; (30 cm to 0.8 m) pumice fragments well rounded, generally 5 mm to 1 cm; pale-red beds occasionally silicified; pumice-rich bed from 1,416.0 to 1,417.5 ft (431.6 to 432.0 m)	21.6 (6.6)	1,425.5 (434.4)
Tuffaceous beds of Calico Hills (informal unit)		
Tuff, ash-flow, light-brown, moderate-orange-pink, and light-olive-gray, nonwelded, devitrified (zeolitized and slightly argillic); pumice, pinkish-gray, yellowish-gray, dusky-yellow, moderate-orange-pink, and light-red, zeolitized, slightly argillic, commonly 5 mm to 2 cm, as large as 3.5 cm; 2-3 percent phenocrysts (sanidine, quartz, and sparse medium-light-gray, grayish-red, and plagioclase); dark-reddish-brown volcanic		

Table A.2.1-1. Lithologic Log of Drill Hole USW-G1--continued

Stratigraphic and lithologic description	Thickness of interval feet (meters)	Depth to bottom of interval feet (meters)
Tuffaceous beds of Calico Hills (informal unit)--continued		
lithic fragments, commonly 5-30 mm in length, as large as 6 cm; unit shows a gradational downward increase to 4-7 percent lithic fragments 2-3 cm in length from 1,468.0 to 1,482.0 (447.4 to 451.7 m) ft; apparent increase in zeolitization from 1,520.9 to 1,540.9 ft (463.5 to 469.6 m)	113.7 (34.7)	1,539.2 (469.1)
Tuff, bedded, reworked, moderate-orange-pink to moderate-yellow-green, slightly indurated; 70-80 percent pumice fragments, zeolitized; abundant grayish-red volcanic lithic fragments, 5 mm to 1 cm	1.7 (0.5)	1,540.9 (469.6)
Tuff, ash-flow, grayish-orange, nonwelded, zeolitized; pumice, very pale orange, grayish-yellow to moderate greenish-yellow, devitrified, zeolitized, commonly 5 mm to 2 cm; less than 1 percent phenocrysts; sparse grayish-red and black volcanic lithic fragments, commonly 2-3 mm, but as large as 2-5 cm	16.2 (4.9)	1,557.1 (474.5)
Tuff, bedded, reworked, and air-fall, moderate-orange-pink; pumice, white to moderate-orange-pink, 10-80 percent zeolitized, 1-10 mm; notable concentration of grayish-brown volcanic lithic fragments, commonly less than 2 mm	1.4 (0.4)	1,558.5 (474.9)
Tuff, ash-flow, light-brown to grayish-orange, nonwelded to partially welded, devitrified and zeolitized (slightly argillic); pumice, grayish-yellow to yellowish-gray and grayish-pink, zeolitized, commonly 1-3 cm in length; less than 1 percent phenocrysts (sanidine and plagioclase); sparse grayish-brown volcanic		

Table A.2.1-1. Lithologic log of drill hole USW-G1--continued

Stratigraphic and lithologic description	Thickness of interval feet (meters)	Depth to bottom of interval feet (meters)
Tuffaceous beds of Calico Hills (informal unit)--continued		
lithic fragments, commonly less than 2.0 mm, but as large as 1.0 cm	11.8 (3.6)	1,570.3 (478.5)
Tuff, reworked, brownish-gray to olive-gray, zeolitized; pumice, 2 mm to 1 cm, subrounded, conspicuous brownish-gray volcanic lithic fragments, 1-5 mm	0.4 (0.1)	1,570.7 (478.6)
Tuff, ash-flow, light-red to moderate-reddish-brown, grayish-orange-pink, and light-brown (mottled grayish-black in places), nonwelded, zeolitized and slightly argillic; pumice, dusky-yellow, yellowish-gray, pale-yellowish-orange, grayish-orange-pink, grayish-orange, and very pale-orange, commonly 5-10 mm, but as large as 6 cm, grayish-orange-pink pumice commonly argillic; less than 1 percent phenocrysts, rare grayish-brown volcanic lithic fragments, commonly less than 1.0 cm in size	122.1 (37.2)	1,692.8 (515.8)
Tuff, bedded, reworked and air-fall, moderate-reddish-brown, moderate-orange-pink, pale-olive, and yellowish-gray, zeolitized; pumice, commonly pale-greenish-yellow and grayish-orange-pink, 1-20 mm, subrounded, content within individual beds ranges from 5 to 80 percent; beds ranges in thickness from 1 to 10 cm; grayish-brown volcanic lithic fragments are conspicuous in some beds, commonly less than 2 mm	2.8 (0.9)	1,695.6 (516.7)
Tuff, ash-flow, pale-olive, light-brown, and grayish-orange-pink, nonwelded, zeolitized; pumice, very pale orange, grayish-pink, yellowish-gray, commonly less than 1 cm, but as large as 4 cm; less than 1 percent phenocrysts; sparse grayish-brown volcanic lithic		

Table A.2.1-1. Lithologic log of drill hole USW-G1--concluded

Stratigraphic and lithologic description	Thickness of interval feet (meters)	Depth to bottom of interval feet (meters)
Tuffaceous beds of Calico Hills (informal unit)--continued		
fragments, commonly less than 1 cm, increase in size and abundance near base of unit, as large as 3 cm near base	40.8 (12.4)	1,736.4 (529.1)
Tuff, bedded, reworked, air-fall, and tuffaceous sandstone, pale-yellowish-brown, pale-olive, yellowish-gray, pale-greenish-yellow, moderate-greenish-yellow, and pale-reddish-brown, varying degrees of zeolitization and silicification; pumice, white, grayish-yellow, and pale-greenish-yellow, zeolitized; beds contain varying amounts of brownish-gray volcanic lithic fragments, commonly less than 1 cm; individual beds commonly 1-3 ft (0.3-0.9 m) thick, some as thin as 2 cm, lower 2 ft (0.6 m) of interval extremely zeolitic	65.1 (19.9)	1,801.5 (549.0)
Crater Flat Tuff		

Table A.2.1-2. Lithologic log of drill hole USW-G2. [Cuttings at 0-289.7 ft (0-88.3 m); core at 289.7 ft (88.3 m) to TD; color designations from Rock-Color Chart (Goddard and others, 1948)] (after Maldonado and Koether, 1983)

Stratigraphic and lithologic description	Thickness of interval feet (meters)	Depth to bottom of interval feet (meters)
Paintbrush Tuff		
Tiva Canyon Member		
Tuff, ash-flow, pale-brown glassy, densely welded, welded, vitric; pumice, black, vitric; contains approximately 10-15 percent sanidine and plagioclase phenocrysts (quartz latitic caprock)	45.0 (13.7)	45.0 (13.7)
Tuff, ash-flow, pale-red, densely welded, devitrified; pumice, very light gray, devitrified; contains approximately 10-15 percent feldspar sanidine, plagioclase, and bronze biotite (quartz latitic caprock)	60.0. (18.3)	105.0 (32.0)
Tuff, ash-flow, pale-red, and light-brownish-gray, densely welded, devitrified; pumice, medium-dark-gray, devitrified; approximately 2 percent sanidine and plagioclase biotite phenocrysts; lithophysae common	25.0 (7.6)	130.0 (39.6)
Tuff, ash-flow, pale-red and light-brownish-gray, densely welded, devitrified; pumice, medium-dark-gray, devitrified; as large as 1 cm; approximately 2 percent sanidine and plagioclase biotite phenocrysts; lithophysal zone, approximately 10-15 percent lithophysae	10.0 (3.1)	140.0 (42.7)
Tuff, ash-flow, pale-red and light-brownish-gray, densely welded, devitrified; pumice, medium-dark-gray, devitrified, as large as 4 cm; contains approximately 2 percent sanidine, plagioclase, and biotite phenocrysts	60.0 (18.2)	200.0 (60.9)

Table A.2.1-2. Lithologic log of drill hole USW-G2--continued

Stratigraphic and lithologic description	Thickness of interval feet (meters)	Depth to bottom of interval feet (meters)
Paintbrush Tuff--continued		
Tiva Canyon Member--continued		
Tuff, ash-flow, grayish-pink, and grayish-orange-pink, moderately to partially welded, devitrified, partly argillic; pumice, medium-light-gray, vapor phase, as large as 3 cm, approximately 1 percent sanidine and plagioclase phenocrysts	20.0 (6.2)	220.0 (67.1)
Tuff, ash-flow, grayish-pink, and moderate-orange-pink, nonwelded, partly argillized; pumice, medium-gray and grayish-orange-pink, argillized, as large as 2 cm	5.0 (1.5)	225.0 (68.6)
Bedded tuff Tuff, ash-fall, bedded, reworked, partly argillized, white, light-gray, grayish-pink, moderate-pink, and grayish-orange-pink, laminated to massive beds; contains pumice and volcanic lithics, subangular to rounded	20.0 (6.1)	245.0 (74.7)
Yucca Mountain Member		
Tuff, ash-flow, pinkish-gray and light-brownish-gray, nonwelded vitric; pumice, white, vitric, as large as 3 cm; sparse sanidine, plagioclase, and biotite phenocrysts	5.0 (1.5)	250.0 (76.2)
Tuff, ash-flow, light-gray, partially welded, partly devitrified and partly vitric; pumice, light-gray, vapor phase, as large as 3 cm; sparse sanidine and plagioclase phenocrysts	10.0 (3.1)	260.0 (79.3)
Tuff, ash-flow, light-gray to light-brownish-gray, moderately to densely welded, devitrified; pumice, light-gray, devitrified, as large as 3 cm; sparse sanidine and plagioclase phenocrysts; manganese oxide speckles common,		

Table A.2.1-2. Lithologic log of drill hole USW-G2--continued

Stratigraphic and lithologic description	Thickness of interval meters feet (meters)	Depth to bottom of interval feet (meters)
Paintbrush Tuff--continued		
Yucca Mountain Member--continued		
as large as 3 mm, disseminated, and along fractures	29.7 (9.0)	289.7 (88.3)
Tuff, ash-flow, light-brownish-gray, moderately to densely welded, devitrified; pumice, gray, devitrified, as large as 4 cm; sparse sanidine and plagioclase phenocrysts; manganese speckles, oxide speckles, as large as 3 mm; disseminated and along fractures; occasional fractures coated with calcite	37.0 (11.3)	326.7 (99.6)
Tuff, ash-flow, grayish-orange to pale-yellowish-orange, moderately welded grading to partially welded toward base, devitrified; pumice in upper part is devitrified, argillic in lower part; manganese oxide speckles common, disseminated and, along fractures, black mottled interval toward bottom 2 ft. (0.6 m); possible fault at about 333.3 ft. (101.6 m)	9.7 (2.9)	336.4 (102.5)
Tuff, ash-flow, light-gray to very light gray, nonwelded, vitric; less than 1 percent sanidine and plagioclase phenocrysts; pumice, pink to pinkish-gray, argillic, abundant glass shards	4.6 (1.4)	341.0 (103.9)
Tuff, reworked, bedded, very light gray to light-gray, individual beds range from 3 to 25 cm in thickness; composed predominantly of subangular to rounded pumice, argillized	2.5 (0.8)	343.5 (104.7)
Tuff, ash-flow, bedded, with some ash-fall, grayish-pink to grayish-orange-pink, nonwelded, vitric and partly argillized; pumice, white to grayish-pink, vitric and partly argillized, as		

Table A.2.1-2. Lithologic log of drill hole USW-G2--continued

Stratigraphic and lithologic description	Thickness of interval feet (meters)	Depth to bottom of interval feet (meters)
Paintbrush Tuff--continued		
Yucca Mountain Member--continued		
large as 4 cm; approximately 1 percent quartz, sanidine, and plagioclase phenocrysts; volcanic lithics common,as large as 6 cm increasing toward base, occasional black, vitric pumice toward base	144.5 (44.0)	488.0 (148.7)
Tuff, reworked, bedded, pinkish-gray and very pale orange; contains pumice argillic, 2-7 cm, subangular to rounded, and moderate-brown to pale-yellowish-brown volcanic lithics, as large as 3 cm, subrounded to rounded	10.0 (3.1)	498.0 (151.8)
Pah Canyon Member		
Tuff, ash-flow, grayish-orange-pink and light-brown, nonwelded, vitric; pumice, grayish-orange-pink, vitric, as large as 8 cm; biotite phenocrysts common	39.8 (12.1)	537.8 (163.9)
Tuff ash-flow, light- to very light gray, non-welded to partially welded vitric; partly zeolitized and argillized; pumice, grayish-orange-pink, vitric, as large as 8 cm; biotite phenocrysts common in matrix and pumice; occasional pale-brown volcanic lithics	27.6 (30.8)	565.4 (203.1)
Tuff, ash-flow, grayish-orange-pink, partially to moderately welded, partly zeolitized; pumice,pale-brown to grayish-orange-pink, zeolitized (?), as large as 7 cm (vapor phase at 171.2-178.5 and 202.6-203.1 m); contains approximately 5 percent biotite, sanidine and plagioclase phenocrysts; moderate-brown and medium-light-gray volcanic lithics common, as large as 3 cm	101.0 (30.8)	666.4 (203.1)

Table A.2.1-2. Lithologic log of drill hole USW-G2--continued

Stratigraphic and lithologic description	Thickness of interval feet (meters)	Depth to bottom of interval feet (meters)
Paintbrush Tuff--continued		
Pah Canyon Member--continued		
Tuff, ash-flow, moderate-orange-pink, and grayish-orange-pink, partially welded to nonwelded, partly zeolitized and argillized; pumice, light-brown, zeolitized (?), as large as 3 cm; contains approximately 5 percent biotite, sanidine, and plagioclase phenocrysts; occasional moderate-brown volcanic lithics, as large as 3 cm	12.1 (3.7)	678.5 (206.8)
Tuff, ash-flow, white to grayish-orange-pink, nonwelded, vitric; pumice, grayish-orange-pink, vitric, as large as 5 cm; contains approximately 5 percent biotite, plagioclase and sanidine phenocrysts; moderate-brown volcanic lithics common	52.2 (15.9)	730.7 (222.7)
Tuff, reworked, bedded, and some ash-fall, grayish-orange-pink, very light pink, and light-brown individual beds range from 1 cm to massive; contains abundant pumice and volcanic lithics; 3-cm-thick silicified zone at 730.7 ft.(222.7 m); 3-cm-thick silicified ash-fall bed, moderate-reddish-brown at 755.0 ft. (230.1 m)	28.7 (8.8)	759.4 (231.5)
Topopah Spring Member		
Tuff, ash-flow, light-gray to medium-light-gray, nonwelded, vitric; pumice blocks as large as 8 cm, light-gray to medium-light-gray, vitric	2.4 (0.7)	761.8 (232.2)
Tuff, ash-flow, moderate-brown, moderately welded, devitrified; pumice, grayish-orange-pink, argillic, as large as 3 cm	5.2 (1.6)	767.0 (233.8)

Table A.2.1-2. Lithologic log of drill hole USW-G2--continued

Stratigraphic and lithologic description	Thickness of interval feet (meters)	Depth to bottom of interval feet (meters)
Paintbrush Tuff--continued		
Topopah Spring Member--continued		
Tuff, ash-flow (vitrophyre), grayish-red to black, densely welded, glassy; as much as 20 percent phenocrysts of biotite, sanidine, and plagioclase; black vitrophyre appears to be in fault contact with grayish-red vitrophyre at 770.0 ft. (234.7 m)	3.9 (1.1)	770.9 (234.9)
Tuff, ash-flow, grayish-red, densely welded, devitrified; pumice, light-brownish-gray, mostly vapor phase, as large as 7 cm; contains approximately 15 percent bronze biotite, sanidine, and plagioclase phenocrysts; fractures commonly contain quartz and calcite; cavities in pumice occasionally contain quartz, along with vapor-phase crystallization material	135.5 (41.4)	906.4 (276.3)
Tuff, ash-flow, light-gray to brownish-gray (partly mottled), densely welded, devitrified; pumice, devitrified, light-gray and moderate-brown, devitrified, as large as 10 cm; approximately 2 percent phenocrysts of sanidine and plagioclase, sparse light-gray volcanic lithics, lithics in upper part as large as 10 cm; lithophysae as much as 60 percent, and average approximately 30 percent, cavities commonly filled or coated predominantly with calcite, with some quartz; breccia (fault) at 925.6 ft (282.1 m)	34.6 (10.5)	941.0 (286.8)
Tuff, ash-flow, light-brown (mottled in places), densely welded, devitrified; pumice, light-gray, devitrified, as large as 6 cm; 1-2 percent sanidine and plagioclase phenocrysts; occasional light-gray volcanic lithics; lithophysae as much as about 90 percent, and average approximately 50 percent, as large as 10 cm, commonly spheroidal, cavities coated		

Table A.2.1-2. Lithologic log of drill hole USW-G2--continued

Stratigraphic and lithologic description	Thickness of interval feet (meters)	Depth to bottom of interval feet (meters)
Paintbrush Tuff--continued		
Topopah Spring Member--continued		
with quartz and feldspar, and less calcite than above subunit	124.0 (37.8)	1,065.0 (324.6)
Tuff, ash-flow, pale-yellowish-brown, densely welded, devitrified; pumice, light-gray, devitrified, as large as 3 cm; approximately 3 percent sanidine and plagioclase phenocrysts; lithophysae as much as 50 percent and average approximately 30 percent	33.4 (10.2)	1,098.4 (334.8)
Tuff, ash-flow, light-brown and light-brownish-gray (mottled), densely welded, devitrified; pumice, light-gray, devitrified; as large as 2 cm; approximately 2 percent sanidine and plagioclase; phenocrysts occasional light-gray volcanic lithics; lithophysae as much as 80 percent and average approximately 60 percent, as large as 7 cm, cavities commonly coated with quartz, and feldspar, and occasionally calcite, commonly spheroidal but occasionally flattened; brecciated zones at 1,165.7, 1136.9 and 1,239.6 ft (353.3, 364.5, and 377.8 m); brecciated zone (fault) healed with calcite at 1,248.1 ft (380.4 m)	151.0 (46.0)	1,249.4 (380.8)
Tuff, ash-flow, pale-red, densely welded, devitrified; pumice, light-gray, devitrified, as large as 1 cm; approximately 2 percent sanidine and plagioclase phenocrysts; lithophysae as much as 13 percent and average approximately 5 percent, as large as 2 cm	22.1 (6.8)	1,271.5 (387.6)
Tuff, ash-flow, light-brown, pale-red, and medium-light-gray (mottled), densely welded, devitrified; pumice, light-gray, as large as 4 cm; light-gray volcanic lithics are common;		

Table A.2.1-2. Lithologic log of drill hole USW-G2--continued

Stratigraphic and lithologic description	Thickness of interval feet (meters)	Depth to bottom of interval feet (meters)
Paintbrush Tuff--continued		
Topopah Spring Member--continued		
approximately 2 percent sanidine and plagioclase phenocrysts; lithophysae as much as 82 percent and average approximately 40 percent, commonly spheroidal, with cavities coated with quartz and feldspar; slickensides at 1,278.0 and 1,300.0-1,307.2 ft (389.5 and 396.2-398.4 m); brecciated zones at 1,307.2-1,308.8 ft (398.4-398.9 m)	43.5 (12.6)	1,315.0 (400.2)
Tuff, ash-flow, light-brown, pale-red, and medium-light-gray (mottled), densely welded, devitrified; pumice, light-gray, devitrified, as large as 6 cm, occasional light-gray volcanic lithics as large as 7 cm; approximately 2 percent sanidine and plagioclase phenocrysts; lithophysae as much as 75 percent, and average approximately 40 percent, the lithophysae (mottled areas) are spheroidal, usually coated with quartz and feldspar, and occasionally with calcite; brecciated zones at 1,466.9 and 1,472.8 ft (447.1 and 448.9 m)	178.0 (54.9)	1,493.0 (455.1)
Tuff, ash-flow, pale-red, and light-brown, densely welded, devitrified; pumice, light-brown to moderate-brown, devitrified, as large as 2 cm; approximately 2 percent sanidine and plagioclase phenocrysts; lithophysae as much as 56 percent and average approximately 20 percent, commonly flattened, and coated with quartz and feldspar; light-gray volcanic lithics common; brecciated zone at 1,552.6 ft (473.2 m)	111.0 (33.8)	1,604.0 (488.9)
Tuff, ash-flow, pale-red and pale-yellowish-brown, densely welded,devitrified; pumice, moderate-brown, as large as 3 cm, devitrified; approximately 3 percent sanidine and plagio-		

Table A.2.1-2. Lithologic log of drill hole USW-G2--continued

Stratigraphic and lithologic description	Thickness of interval feet (meters)	Depth to bottom of interval feet (meters)
Paintbrush Tuff--continued		
Topopah Spring Member--continued		
clase phenocrysts; occasional light-gray volcanic lithics; sparse lithophysae	30.0 (9.1)	1,634.0 (498.0)
Tuff, ash-flow, grayish-black to black (vitrophyre), light-brown in upper meter, densely welded, glassy; pumice, grayish-black, vitric, as large as 5 cm; sparse sanidine and plagioclase phenocrysts; pale-brown and medium-gray volcanic lithics common toward base, as large as 4 cm	30.3 (9.3)	1,664.3 (507.3)
Tuff, ash-flow, grayish-black (vitrophyre), moderately to densely welded, vitric; pumice, light-brown, partly vitric and partly devitrified, as large as 5 cm; sparse sanidine and plagioclase phenocrysts; light-gray volcanic lithics common, as large as 4 cm	4.7 (1.4)	1,669.0 (508.7)
Tuff, ash-flow, light-brown, with irregular zones of black, moderately welded, vitric to devitrified; pumice, moderate-brown, devitrified, as large as 4 cm; sparse sanidine and plagioclase phenocrysts; light-gray and grayish-brown volcanic lithics common, as large as 4 cm	12.0 (3.7)	1,681.0 (512.4)
Tuff, ash-flow, light-brown, and grayish-orange-pink, partially to nonwelded, devitrified; pumice, pale-brown and grayish-orange-pink, devitrified, as large as 3 cm; 1-2 percent sanidine and plagioclase phenocrysts; light-gray and grayish-brown volcanic lithics common, as large as 4 cm; some silicification and zeolitization of matrix and pumice toward base	20.0 (6.1)	1,701.0 (518.5)

Table A.2.1-2. Lithologic log of drill hole USW-G2--continued

Stratigraphic and lithologic description	Thickness of interval feet (meters)	Depth to bottom of interval feet (meters)
Paintbrush Tuff--continued		
Topopah Spring Member--continued		
Tuff, bedded, reworked, pale-pink to grayish-orange-pink, zeolitized thin-bedded to massive; pumice, pale-pink to pale-greenish-yellow, subrounded to rounded; medium-light-gray and grayish-brown, subrounded to rounded volcanic lithics, increse toward base; large blocks at base, as large as 24 cm	56.0 (17.0)	1,757.0 (535.5)
Tuffaceous beds of Calico Hills		
Tuff, ash-flow, grayish-orange-pink, nonwelded, devitrified, zeolitized; pumice, very pale orange, partly vitric and partly argillized and zeolitized, as large as 5 cm; 1 percent quartz sanidine and plagioclase phenocrysts; abundant brown volcanic lithics, as large as 1 cm	51.3 (15.7)	1,808.3 (551.2)
Tuff, bedded, reworked, moderate-yellowish-brown, thin grayish-orange-pink, air-fall intercalated with the bedded tuff; pumice fragments, pale-greenish-yellow, and zeolitized, rounded, as large as 2 cm; grayish-brown volcanic lithics, as large as 2 mm; beds dip approximately 4°	0.7 (0.2)	1,809.0 (551.4)
Tuff, ash-flow, grayish-orange-pink, nonwelded, devitrified, zeolitized; pumice, pale-yellowish-orange, zeolitized, partly argillized, as large as 5 cm; approximately 5 percent phenocrysts (quartz, sanidine, and plagioclase); grayish-brown volcanic lithics common, as large as 1 cm	15.7 (4.8)	1,824.7 (556.2)
Tuff, bedded, reworked, and ash-fall, grayish-orange-pink; pumice lithics, pale-greenish-		

Table A.2.1-2. Lithologic log of drill hole USW-G2--continued

Stratigraphic and lithologic description	Thickness of interval meters feet (meters)	Depth to bottom of interval feet (meters)
Tuffaceous beds of Calico Hills--continued		
yellow, zeolitized, as large as 1 mm, rounded and grayish-brown volcanic lithics, as large as 1 mm, rounded, beds dip approximately 1°	0.5 (0.1)	1,825.2 (556.3)
Tuff, ash-flow, grayish-orange-pink, nonwelded devitrified, zeolitized; pumice, very pale orange, zeolitized and argillized, as large as 2 cm; approximately 1 percent quartz, sanidine and plagioclase phenocrysts; grayish-brown volcanic lithics common, as large as 2 cm	65.3 (19.9)	1,890.5 (576.2)
Tuff, ash-fall, grayish-orange-pink, very fine grained, argillized, contains approximately 1 percent quartz, and feldspar phenocrysts	0.2 (0.1)	1,890.7 (576.3)
Tuff, ash-flow, grayish-orange-pink to moderate-orange-pink, nonwelded, divitrified, zeolitized; pumice, grayish-pink and very pale orange, zeolitized, as large as 5 cm; approximately 2 percent quartz, sanidine, and plagioclase phenocrysts; grayish-brown volcanic lithics common, as much as 2 cm	69.3 (21.1)	1,960.0 (597.4)
Tuff, bedded, reworked, with a 1 cm ash-fall at base, moderate-orange-pink; pumice lithics, moderate-reddish-orange, zeolitized, as large as 2 cm, rounded flattened; grayish-brown volcanic lithics common, as large as 1 cm, rounded; beds dip approximately 2°	0.5 (0.2)	1,960.5 (597.6)
Tuff, ash-flow, moderate-orange-pink, nonwelded, zeolitized; pumice, grayish-pink, zeolitized, as large as 5 cm; 2 percent quartz sanidine and plagioclase phenocrysts; grayish-brown volcanic lithics common, as large as 2 cm	38.5 (11.7)	1,999.0 (609.3)

Table A.2.1-2. Lithologic log of drill hole USW-G2--continued

Stratigraphic and lithologic description	Thickness of interval feet (meters)	Depth to bottom of interval feet (meters)
Tuffaceous beds of Calico Hills--continued		
Tuff, bedded, reworked with some ash-fall, pinkish-gray, and pale-yellowish brown; ash-fall occurs in upper 1.6 ft (0.5 m); concentration of grayish-brown and light-gray volcanic lithics and zeolitized pumice fragments occur toward base of unit; slickensides at 2,005.7 and 2,009.0 ft (611.3 and 612.3 m)	11.7 (3.6)	2,010.7 (612.9)
Tuff, ash-flow, grayish-pink and very pale orange, nonwelded, zeolitized; pumice, white and very pale orange, zeolitized, as large as 3 cm; 5 percent quartz, sanidine, plagioclase, and biotite phenocrysts; grayish-brown and light-gray volcanic lithics common, as large as 5 cm	110.9 (33.8)	2,121.6 (646.7)
Tuff, ash-fall, grayish-orange-pink, argillized, and partly zeolitized; conspicuous biotite phenocrysts and occasional quartz, sanidine, and plagioclase phenocrysts; banding present, dipping approximately 60°	1.4 (0.4)	2,123.0 (647.1)
Tuff, ash-flow, grayish-pink to grayish-orange-pink, and yellowish-gray, nonwelded, zeolitized; pumice, white and pale-greenish-yellow, zeolitized and argillized, as large as 3 cm; approximately 5 percent phenocrysts, consisting of quartz (some resorbed), sanidine, plagioclase, and biotite; conspicuous reddish-brown and light-gray lithics as large as 7 cm, tuff lithics, approximately 12 cm toward top of unit	109.0 (33.2)	2,232.0 (680.3)
Tuff, bedded, reworked, and ash-fall, pale-greenish-yellow, grayish-orange-pink and very light gray; individual beds range from about 1 cm to 2 m and consist of rounded reddish-		

Table A.2.1-2. Lithologic log of drill hole USW-G2--continued

Stratigraphic and lithologic description	Thickness of interval feet (meters)	Depth to bottom of interval feet (meters)
Tuffaceous beds of Calico Hills--continued brown and light-gray volcanic lithics and pale-greenish-yellow pumice, zeolitized; thin (1 cm) ash-fall toward base; beds dip approximately 1°	10.0 (3.1)	2,242.0 (683.4)
Tuff, ash-flow, pale-yellowish-orange, nonwelded argillized and zeolitized; pumice, white, argillized, as large as 3 cm; approximately 5 percent phenocrysts consisting of quartz (some resorbed), sanidine, plagioclase, and biotite; reddish-brown volcanic lithics common, as large as 2 cm	36.3 (11.0)	2,278.3 (694.4)
Tuff, bedded, reworked, pale purple and grayish-orange-pink, zeolitized, and argillized; conspicuous biotite phenocrysts; reddish-brown volcanic lithics, as large as 10 cm	4.4 (1.4)	2,282.7 (695.8)
Tuff, ash-flow, very pale orange, nonwelded, devitrified, zeolitized; pumice, argillized, as large as 2 cm; approximately 5 percent phenocrysts consisting of quartz (some resorbed), sanidine, plagioclase and biotite; reddish-brown volcanic lithics common, and tuff lithics as large as 10 cm toward top of subunit	21.9 (6.6)	2,304.6 (702.4)
Tuff, bedded, reworked, very pale orange; blocks of tuff and pale purple ash-fall tuff common; banding (lamination) present at 2,305.6-2,306.2 ft (702.7-702.9 m)	2.4 (0.8)	2,307.0 (703.2)
Tuff, ash-flow, very pale orange, nonwelded, devitrified, zeolitized; pumice, white, argillized, as large as 2 cm; approximately 5 percent phenocrysts consisting of quartz (some resorbed), sanidine, plagioclase, and biotite;		

Table A.2.1-2. Lithologic log of drill hole USW-G2--continued

Stratigraphic and lithologic description	Thickness of interval feet (meters)	Depth to bottom of interval feet (meters)
Tuffaceous beds of Calico Hills--continued reddish-brown volcanic lithics common, as large as 3 cm	30.8 (9.4)	2,337.8 (712.6)
Tuff, bedded, reworked, very pale orange and pale-yellowish-brown; individual beds range from 1 cm to 10 cm, and consist of reddish-brown and light-gray volcanic lithics, rounded, as large as 2 cm, and pumice lithics, pale-greenish-yellow, zeolitized, as large as 1 cm; beds dip approximately 7°	3.8 (1.1)	2,341.6 (713.7)
Tuff, ash-flow, moderate-orange-pink, nonwelded, devitrified, zeolitized; pumice white, argillized as large as 7 cm, biotite in pumice more common; 5-10 percent quartz phenocrysts of quartz (some resorbed), sanidine, plagioclase, and biotite (more biotite that above subunit); reddish-brown volcanic lithics common, as large as 2 cm	21.8 (6.7)	2,363.4 (720.4)
Tuff, reworked, massive, yellowish-gray; contains pumice, pale-greenish-yellow, zeolitized, as large as 1 cm, subrounded to rounded, and subrounded to rounded reddish-brown volcanic lithics, as large as 1 cm	2.2 (0.6)	2,365.6 (721.0)
Tuff, ash-flow, moderate-orange-pink, nonwelded, devitrified, zeolitized; pumice, white, argillized, as large as 4 cm; 5-10 percent phenocrysts of quartz (some resorbed), sanidine, plagioclase, and biotite; reddish-brown volcanic lithics common, as large as 2 cm	8.4 (2.6)	2,374.0 (723.6)
Tuff, reworked, contains subrounded to rounded pumice, pale-greenish-yellow, zeolitized, as		

Table A.2.1-2. Lithologic log of drill hole USW-G2--continued

Stratigraphic and lithologic description	Thickness of interval feet (meters)	Depth to bottom of interval feet (meters)
Tuffaceous beds of Calico Hills--continued		
large as 5 mm, reddish-brown volcanic lithics, as large as 5 mm	0.3 (0.1)	2,374.3 (723.7)
Tuff, ash-flow, moderate-orange-pink, nonwelded, devitrified, zeolitized; pumice, white, argillized, as large as 4 cm; 5-10 percent phenocrysts of quartz (some resorbed), sanidine, plagioclase, and biotite; reddish-brown volcanic lithics common as large as 2 cm	5.1 (1.5)	2,379.4 (725.2)
Tuff, reworked, massive, yellowish-gray; contains pumice lithics, zeolitized, pale-greenish-yellow, as large as 5 mm, and subrounded to rounded reddish-brown volcanic lithics as large as 5 mm	0.6 (0.2)	2,380.0 (725.4)
Tuff, ash-flow, moderate-orange-pink, nonwelded, devitrified, zeolitized; pumice, white, argillized, as large as 5 cm; 5-10 percent phenocrysts of quartz (some resorbed), sanidine, plagioclase and biotite, reddish-brown volcanic lithics common, as large as 1 cm	4.0 (1.2)	2,384.0 (726.6)
Tuff, reworked, massive, very pale orange, contains pumice lithics, pale-greenish-yellow, zeolitized, as large as 1 cm, and reddish-brown volcanic lithics, as large as 1 cm, subrounded to rounded	1.2 (0.4)	2,385.2 (727.0)
Tuff, ash-flow, grayish-orange-pink to moderate-orange-pink, nonwelded, devitrified, zeolitized; pumice, grayish-pink to grayish-orange-pink, argillized and zeolitized, as large as 5 cm; contains 5-10 percent phenocrysts of quartz (some resorbed), sanidine,		

Table A.2.1-2. Lithologic log of drill hole USW-G2--concluded

Stratigraphic and lithologic description	Thickness of interval feet (meters)	Depth to bottom of interval feet (meters)
Tuffaceous beds of Calico Hills--continued		
plagioclase, and biotite; reddish-brown volcanic lithics commons, as large as 2 cm	191.3 (58.3)	2,576.5 (785.3)
Tuff, bedded, reworked, light-brown, grayish-pink, and very light gray; individual beds range from 1 cm to 1.5 m and contains pumice, pale-greenish-yellow, zeolitized, as large as 2 cm, and reddish-brown and light-gray volcanic lithics as large as 1 cm, beds dip approximately 2°	11.4 (3.5)	2,587.9 (788.8)
Tuff, ash-flow, pale-red, and grayish-orange-pink, nonwelded to partially welded, devitrified, zeolitized; pumice, white, grayish-pink, argillized and zeolitized, biotite in pumice very common, as large as 3 cm; approximately 15-25 percent phenocrysts of quartz (some resorbed), sanidine, plagioclase and biotite; reddish-brown volcanic lithics, as large as 5 cm; healed fracture toward base, dipping approximately 55°, slickensides at approximately 2,703.9 ft (824.1 m)	116.1 (35.4)	2,704.0 (824.2)
Crater Flat Tuff		

Table A.2.1-3. Lithologic log of drill hole USW-G4 (after Richard W. Spengler, U.S. Geological Survey, written communication, 1982, by Bentley, 1984)

Stratigraphic and lithologic description	Thickness of interval feet (meters)	Depth to bottom of interval feet (meters)
Alluvium	22.0 (6.7)	22.0 (6.7)
Paintbrush Tuff Tiva Canyon Member Tuff, ash-flow, grayish-red, densely welded, devitrified; pumice, grayish-red, medium gray, devitrified; 2 percent phenocrysts (sanidine): rare very-light-gray rhyolitic lithic fragments; occasional lithophysal cavities (open and flattened), in upper 39.4 ft (12 m)	57.4 (17.5)	79.4 (24.2)
Tuff, ash-flow, pale-brown, pale-red, moderately to densely welded, devitrified; pumice, pale-red, brownish gray, devitrified with sparse to abundant moderate reddish-orange pumice altered to smectite (swelling) clay; less than 2 to 4 percent phenocrysts (sanidine and plagioclase); rare very-light-gray to medium-light-gray rhyolitic lithic fragments, commonly less than 5 mm in size	38.7 (11.8)	118.1 (36.0)
Tuff, ash-flow, dark-yellowish-orange, partially-to-nonwelded, vitric; pumice, grayish-orange-pink, vitric and argillic (?); 1 to 2 percent phenocrysts (sanidine and plagioclase); abundant black and very yellowish-orange glass shards	20.0 (6.1)	138.1 (42.1)
Bedded tuff, ash-fall, light-brown, moderately indurated, vitric, abundant moderate-orange pink pumice (vitric, argillic) and black glass shards; 7.9 ft (2.4 m) of core lost, of which part may be from subsequent unit	9.8 (3.0)	147.9 (45.1)

Table A.2.1-3. Lithologic log of drill hole USW-G4--continued

Stratigraphic and lithologic description	Thickness of interval feet (meters)	Depth to bottom of interval feet (meters)
Paintbrush Tuff--continued		
Yucca Mountain Member		
Bedded tuff, ash-fall, bedded, reworked, pale-yellowish-brown, light-olive-gray, light-brown, slightly indurated, vitric, beds predominantly composed of light-olive-gray vitric pumice and black glass shards, rare light brownish-gray rhyolitic fragments, bedding planes indistinct (graduation); thickness of beds commonly 30-610 mm	20.3 (6.2)	168.2 (51.3)
Pah Canyon Member		
Tuff, ash-flow, light-brown, nonwelded, vitric, pumice, yellowish-gray, light olive-gray, dusky-yellow, vitric, commonly 10-30 mm in size; 5 percent phenocrysts (sanidine and biotite); rare light-red volcanic-lithic fragments	19.7 (6.0)	187.9 (57.3)
Bedded tuff, reworked, light-brown, poorly consolidated, vitric, well-sorted, predominantly composed of grayish-orange, vitric pumice, less than 1 mm in size; sanidine and biotite present; light-red volcanic-lithic fragments present, less than 1 mm in size; fault plane at 60.5 m, crushed zone on one side of plane, magnitude of offset unknown; inclination of plane is 55°	11.5 (3.5)	199.4 (60.8)
Tuff, ash-fall (?), yellowish-gray to light-olive-gray, vitric, poorly consolidated, poorly sorted, predominantly composed of white yellowish-gray to light olive-gray pumice fragments, commonly 10-20 mm in size, black vitrophyric lithic fragments commonly 5-15 mm, as large as 50 mm; minor constituents of sanidine and biotite; in upper 3 ft (0.9 m) reddish-orange clay; fault plane at 202.1 ft (61.6 m), truncation of pumice fragments, magnitude of offset unknown; plane dips 76°	28.5 (8.7)	227.9 (69.5)

Table A.2.1-3. Lithologic log of drill hole USW-G4--continued

Stratigraphic and lithologic description	Thickness of interval feet (meters)	Depth to bottom of interval feet (meters)
Paintbrush Tuff--continued		
Topopah Spring Member		
Tuff, ash-flow, moderate-reddish-brown, non-welded (poorly consolidated), vitric; pumice moderate-reddish-brown, yellowish-gray, light-olive-gray,vitric; 1 percent phenocrysts (sanidine and biotite); rare grayish-red volcanic-lithic fragments (lower contact gradational)	5.2 (1.6)	233.1 (71.1)
Tuff, ash-fall, light-gray to medium light gray, pale-reddish-brown, fused(?), moderately indurated, almost entirely composed of light-gray, medium light-gray and light brownish-gray pumice, vitric, commonly less than 10 mm in size, rare grayish-red volcanic-lithic fragments	5.6 (1.7)	238.7 (72.8)
Tuff, ash-flow, light-brownish gray to dark-reddish brown and black, partially to densely welded, devitrified (some vapor phase crystallization); pumice blackish-red, yellowish-gray, devitrified and vapor-phase crystallization, commonly varying in size from 5 to 40 mm, 5-20 percent phenocrysts (sanidine, plagioclase, bronze biotite); rare very-light gray rhyolitic-lithic fragments; upper 3.9 ft (1.2 m) vitrophyre, perlitic	45.6 (13.9)	284.3 (86.7)
Tuff, ash-flow, grayish-red, densely welded, devitrified and vapor phase; pumice, pale-red, light-brown, grayish-red, light-gray, medium light-gray, yellowish-gray, extremely large grayish pumice, vapor phase, distinctive foliation of pumice, commonly 10-60 mm, 3-5 percent phenocrysts (sanidine, plagioclase, biotite); rare very-light-gray rhyolitic-lithic fragments, commonly 10-20 mm in size	115.8 (35.3)	400.1 (122.0)

Table A.2.1-3. Lithologic log of drill hole USW-G4--continued

Stratigraphic and lithologic description	Thickness of interval feet (meters)	Depth to bottom of interval feet (meters)
Paintbrush Tuff--continued		
Topopah Spring Member--continued		
Tuff, ash-flow, pale-red, light brownish-gray, densely welded, devitrified; pumice, mixture of very-light-gray, light-gray and brownish-gray, devitrified, commonly 5 to 50 mm in size, brownish-gray pumice commonly the larger size, devitrified and some vapor phase; 1 to 4 percent phenocrysts (sanidine and plagioclase); lithophysal cavities, abundant at top, sparse at base; spherical and flattened parallel to axis of core, commonly open; commonly 20-40 mm in size, as large as 60 mm	50.9 (15.5)	451.0 (137.5)
Tuff, ash-flow, pale-red to grayish-red moderate-brown (mottled), densely welded, devitrified; pumice, pale-red, grayish-red, devitrified; less than 2 percent phenocrysts (sanidine and plagioclase); rare light-gray rhyolitic-lithic fragments; abundant (more than 30 percent) lithophysal cavities, commonly open, cavities sub-rounded and flattened; in upper 49.9 ft (15.2 m), cavities are commonly less than 20 mm in size, commonly lined with feldspar, quartz; below 49.9 ft (15.2 m), cavities commonly 10-60 mm in size, with pale-red alteration rims; due to hole problems, no core was collected from 452.1-460.0 ft (137.8-140.2 m), and only 1.3 m of core was recovered from 460.0 - 475.1 ft (140.2-144.8 m), using a globe basket (lower contact gradational)	163.1 (49.7)	614.1 (187.2)
Tuff, ash-flow, pale-brown, light-brown, grayish-red, and pale-red (mottled), moderately to densely welded, devitrified; pumice, pale-red, light-brown, light-gray, devitrified, commonly 5-30 mm, as large as 60 mm in length; 1 to 2 percent phenocrysts (sanidine and plagioclase); rare very-light-gray and light-gray rhyolitic-lithic fragments increasing toward base; lithophysae common, mostly flat-		

Table A.2.1-3. Lithologic log of drill hole USW-G4--continued

Stratigraphic and lithologic description	Thickness of interval feet (meters)	Depth to bottom of interval feet (meters)
Paintbrush Tuff--continued Topopah Spring Member--continued tened cavities with large alteration rims; fracturing and broken core intervals common (lower contact gradational)	498.4 (151.9)	1,112.5 (339.1)
Tuff, ash-flow, light brown, dark-yellowish-brown to dark-yellowish-orange, moderately to densely welded, devitrified, but partially vitric, argillic and zeolitic(?), (altered vitrophyre in lower 23 ft or 7 m); pumice light brown, dusky-yellowish-brown, pale-yellowish-orange, dark-yellowish-orange, devitrified vitric (lower 23 ft or 7 m), commonly 8-50 mm; 1 percent phenocrysts of sanidine and plagioclase; sparse very-light-gray rhyolitic-lithic fragments, commonly range from 5 mm to as large as 84 mm; two fault zones with moderate to intense alteration [smectite (?)] along nearly vertical fault planes at 1,314-1,315 ft (400.5-400.9 m), and 1,318.3-1,320.0 ft (401.8-402.3 m); 2 ft (0.6 m) or more of displacement along second fault zone, as indicated by core sample at 1,318.6 ft (401.9 m)	204.1 (62.2)	1,316.6 (401.3)
Tuff, ash-flow, dark-gray to black, densely welded, vitrophyre; pumice, black, glassy, 1 to 2 percent phenocrysts (sanidine and plagioclase); sparse very-light-gray rhyolitic-lithic fragments, commonly 4 to 18 mm, occasionally as large as 30 mm; moderate-olive-brown with light-brown pumice fragments; moderately altered from 1,318.6-1,319.6 ft (401.9 to 402.2 m); interval contains several near-vertical, silica-coated, fractures (conchoidal microfractures common) (lower contact gradational)	28.9 (8.8)	1,345.5 (410.1)

Table A.2.1-3. Lithologic log of drill hole USW-G4--continued

Stratigraphic and lithologic description	Thickness of interval feet (meters)	Depth to bottom of interval feet (meters)
Paintbrush Tuff--continued		
Topopah Spring Member--continued		
Tuff, ash-flow, light brown to black, vitric, nonwelded to moderately welded (welding decreases downward); pumice, light phenocrysts of sanidine and plagioclase; abundant black glass shards near top and base; rare very-light-gray, brownish-gray and pale-red rhyolitic-lithic fragments, commonly from less than 1.5 mm to as large as 60 mm	32.1 (9.8)	1,377.6 (419.9)
Tuff, ash-flow, light-brown and grayish-orange-pink, partially welded, zeolitized; pumice, light-brownish and pale-yellowish-orange, zeolitic, commonly less than 10 mm in size; 1 percent phenocrysts of sanidine and plagioclase; abundant (3 to 30 percent of rock) brownish-gray, grayish-red, greenish-gray, rhyolitic- and vitrophyric-lithic fragments vary from 5 to 80 mm, many fragments greater than 20 mm in length (lower contact gradational)	10.2 (3.1)	1,387.8 (423.0)
Tuff, ash-flow, grayish-orange-pink, nonwelded, partly vitric and partly zeolitic (interval from 1,388.8-1,390.5 ft or 423.3-423.8 m) dominantly vitric; pumice, very-pink-orange, grayish-orange-pink, and moderate-yellow, mainly zeolitic, some vitric, commonly range in size from 3 to 20 mm, as large as 42 mm; sparse (2 to 3 percent) volcanic-lithic fragments, grayish-brown, brownish-gray, medium-light gray, rhyolitic and vitrophyric, commonly less than 10 mm in size, a few as large as 40 mm, fault plane cutting core from 1,405.9-1,406.0 ft (428.5-428.6 m); fault about 20 mm thick; contains silicified breccia, inclined about 72° relative to core axis	19.0 (5.8)	1,406.8 (428.8)
Bedded tuff, reworked, ash-fall, light-brown, pale-red and light-gray, moderately indurated, zeolitic; dominantly made up of pumice frag-		

Table A.2.1-3. Lithologic log of drill hole USW-G4--continued

Stratigraphic and lithologic description	Thickness of interval feet (meters)	Depth to bottom of interval feet (meters)
Paintbrush Tuff--continued Topopah Spring Member--continued ments, white to light-gray, and light-brownish-gray, zeolitic, subrounded, commonly less than 5 mm in size; beds are 430 and 370 mm thick	2.6 (0.8)	1,409.4 (429.6)
Tuffaceous beds of Calico Hills (informal usage) Tuff, ash-flow, moderate-orange-pink, moderate-reddish-orange, and light brown, nonwelded, vitric (slightly zeolitic); pumice grayish-orange, very-pale-orange, yellowish-gray, and medium-light-gray, dominantly vitric; commonly range from 5 to 50 mm, as large as 110 mm (larger pumice fragments occur in upper 4 ft (1.2 m) of unit); 3 to 4 percent phenocrysts (quartz, sanidine, plagioclase, biotite); sparse grayish-red rhyolitic and grayish-black to medium gray, slightly altered, vitrophyre lithic fragments, commonly range in size from 3 to 35 mm; greater concentration of lithic fragments in lower 6.6 ft (2.0 m) of unit	15.1 (4.6)	1,424.5 (434.2)
Tuff, bedded, reworked, moderate-orange-pink, pale-red, and grayish-orange-pink, moderately to highly indurated, zeolitic; dominantly composed of pumice, grayish-orange-pink and grayish-orange, zeolitic, subrounded, commonly less than 5 mm; abundant grayish-red rhyolitic-lithic fragments, commonly less than 2 mm in size; individual beds range from 30-240 mm	1.6 (0.5)	1,426.1 (434.7)
Tuff, ash-flow, grayish-orange, grayish-orange-pink, and moderate reddish-orange, nonwelded, zeolitic; pumice, very-pale-orange, grayish-orange-pink, moderate-orange-pink, and yellowish-gray zeolitic; commonly range from 3 to 35 mm, as large as 50° mm; 1 percent phenocrysts (quartz, sanidine, plagioclase); rare medium-dark-gray and brownish-gray		

Table A.2.1-3. Lithologic log of drill hole USW-G4--continued

Stratigraphic and lithologic description	Thickness of interval feet (meters)	Depth to bottom of interval feet (meters)
Tuffaceous beds of Calico Hills (informal usage)--continued		
rhyolitic-lithic fragments, commonly less than 5 mm, occasionally as large as 50 mm; larger fragments are commonly slightly altered vitrophyric fragments	20.7 (6.3)	1,446.8 (441.0)
Tuff, reworked, ash-fall, bedded, light brown, pale-red, grayish-orange-pink, and moderate-orange-pink, moderately indurated, zeolitic, and, in places, silicified; dominantly composed of pumice fragments having similar colors as those listed above, pumice commonly less than 10 mm in size, zeolitic; subordinate amounts of brownish-gray and medium-gray rhyolitic-lithic fragments, less than 10 mm in size; individual beds less than 670 mm thick, where well-defined, bedding planes are inclined 5° to 6°	9.5 (2.9)	1,456.3 (443.9)
Tuff, ash-flow, moderate-orange-pink, grayish-orange-pink, light brown, grayish-orange, and dusky-yellow, nonwelded zeolitic; pumice, very-pale-orange, pale-red, moderate pink, grayish-orange-pink, yellowish-gray, grayish-yellow, grayish-orange, zeolitic, commonly range from 20 to 45 mm; 1 percent phenocrysts (quartz, sanidine, plagioclase, biotite); rare-to-sparse moderate-brown and grayish-red rhyolitic-lithic fragments, commonly less than 20 mm in size; lower 11.2 ft (3.4 m) of unit indicates a slight increase in content of lithic fragments; fault plane with slickensides present from 1,556.5-1,557.2 ft (474.4-474.6 m), inclined 77°	104.3 (31.8)	1,560.6 (475.7)
Tuff, ash-fall and reworked, moderate-orange-pink and grayish-orange, moderately indurated, zeolitic; dominantly composed of pumice, grayish-yellow, grayish-orange-pink, dusky-yellow, and very-pale-orange, zeolitic, commonly less than 20 mm in size, subangular to		

Table A.2.1-3. Lithologic log of drill hole USW-G4--continued

Stratigraphic and lithologic description	Thickness of interval feet (meters)	Depth to bottom of interval feet (meters)
Tuffaceous beds of Calico Hills (informal usage)--continued		
subrounded, poorly sorted; subordinate quantities (10-20 percent) of volcanic lithic fragments, grayish-red, dark gray, and medium-light-gray, subangular to subrounded, poorly sorted, range in size from 1 to 23 mm; lower 1.6 ft (0.5 m) of unit contains some of lithic fragments; individual beds range in thickness from 60-300 mm	3.3 (1.0)	1,563.9 (476.7)
Tuff, ash-flow, grayish-orange, light brown, and moderate-reddish-orange, and occasionally dark-yellowish-brown, nonwelded zeolitic; pumice, very-pale-orange, grayish-yellow, dusky-yellow,moderate-greenish-yellow, zeolitic, commonly range in size from 2 to 310 mm, as large as 570 mm; 1 to 2 percent phenocrysts (quartz, sanidine, plagioclase, biotite); sparse (1-2 percent) rhyolitic-lithic fragments, brownish-gray and brownish-black, commonly less than 5 mm in size; ash-fall parting, 10 mm thick, present at 1,607 ft (489.8 m), inclined 7°; fault plane present from 1,631.3-1,631.6 ft (497.2-497.3 m), slightly off-set, inclined 77°; ash-fall parting, 63 mm thick present from 1,662.2-1,662.5 ft (506.6-506.7 m); shear fractures with slickensides present from 1,633.9-1,634.3 ft (498.0-498.1 m) and 1,671.0-1.671.3 ft (509.3-509.4 m); ash-fall tuff, 140 mm thick at 1,663.1 ft (506.9 m)	141.4 (43.1)	1,705.3 (519.8)
Bedded tuff, ash-fall, reworked (tuffaceous sandstone) grayish-yellow, yellowish-gray, light brown, greenish-gray, moderate-reddish-brown, dusky-yellow, pale-yellowish-brown, grayish-yellow, zeolitic (in places, silicified) moderately to well indurated; pumice, moderate-orange-pink, grayish-pink, very-pale-orange, pale-greenish-yellow, and grayish-yellow, zeolitic, commonly less than 5 mm in size, sparse		

Table A.2.1-3. Lithologic log of drill hole USW-G4--concluded

Stratigraphic and lithologic description	Thickness of interval feet (meters)	Depth to bottom of interval feet (meters)
Tuffaceous beds of Calico Hills (informal usage)--continued to abundant brownish-black, brownish-gray and medium-gray rhyolitic-lithic fragments, commonly less than 5 mm in size; individual beds as much as 4.9 ft (1.5 m) thick; numerous silicified beds are present from 1,705.5-1,708.1 ft (519.8-520.6 m); basal part of unit from 1,758.9 - 1,761.6 ft (536.1-536.9 m), consists of tuffaceous sandstone, pale- to dark-yellowish-brown, well-sorted, abundant biotite; individual beds range from 5-85 mm	56.1 (17.1)	1,761.4 (536.9)
Crater Flat Tuff		

Table A.2.1-4. Generalized lithologic log of drill hole USW-H1 (modified from Richard Spengler, U.S. Geological Survey, written communication, 1981, by Rush and others, 1983]

Stratigraphic and lithologic description	Thickness of interval feet (meters)	Depth to bottom of interval feet (meters)
Paintbrush Tuff		
Tiva Canyon Member		
Tuff, ash-flow, brown, partially welded to non-welded; pumice and glass shards	27 (8.1)	27 (8.1)
Tuff, bedded, light gray to white, vitric	2 (0.6)	29 (8.7)
Yucca Mountain Member		
Tuff, ash-flow, light gray and light brown, partially welded to nonwelded, vitric; glass shards	20 (6.1)	49 (14.8)
Tuff, bedded, vitric	9 (2.7)	58 (17.5)
Pah Canyon Member		
Tuff, ash-flow, pale-brown, nonwelded, vitric; pumice	27 (8.2)	85 (25.7)
Topopah Spring Member		
Tuff, ash-flow, light brown and red, moderately to densely welded and devitrified; lithophysae and devitrified pumice	369 (112.5)	454 (138.2)
Tuff, bedded	5 (1.5)	459 (139.7)
Tuffaceous beds of Calico Hills		
Tuff, ash-flow, pink, nonwelded and zeolitized; pumice and volcanic lithic fragments common	90 (27.4)	549 (167.1)
Tuff, bedded, pink, slightly indurated, zeolitized	17 (5.2)	566 (172.3)
Crater Flat Tuff		

Table A.2.1-5. Lithologic log of drill hole USW-H5
(after Bentley and others, 1983)

Stratigraphic and lithologic description	Thickness of interval feet (meters)	Depth to bottom of interval feet (meters)
Paintbrush Tuff		
Tiva Canyon Member		
Tuff, ash-flow, brownish-gray, densely welded, devitrified (probable vapor-phase crystallization from 35.1-40.0 ft or 10.7-12.2 meters)	40.0 (12.2)	40.0 (12.2)
Tuff, ash-flow, light-brownish-gray and light gray, densely welded, devitrified (probable lithophysal zone); 5 percent phenocrysts of sanidine and plagioclase	170.0 (51.8)	210.0 (64.0)
Tuff, ash-flow, light-brownish-gray to brownish gray, densely welded, devitrified; pumice, light gray, devitrified; less than 1 percent phenocrysts	150.0 (45.7)	360.0 (109.7)
Tuff, ash-flow, dark-yellowish-brown, moderately welded, devitrified; pumice, dark-yellowish brown, devitrified; 2 percent phenocrysts (sanidine and plagioclase); rare grayish-red volcanic lithic fragments	30.2 (9.2)	390.2 (118.9)
Tuff, ash-flow, pale-yellowish-brown, partially welded, devitrified; pumice, pale-yellowish brown and brownish gray; 2 percent phenocrysts (sanidine and plagioclase); interval from 400.0-409.8 ft (121.9-124.9 m) contains grayish-orange, argillic pumice fragments	20.0 (6.1)	410.2 (124.9)
Tuff, ash-flow, grayish-orange, nonwelded, vitric; pumice, light-brown, argillic; less than 1 percent phenocrysts; abundant black and light-brown glass shards	75.1 (22.9)	485.3 (147.8)

Table A.2.1-5. Lithologic log of drill hole USW-H5--continued

Stratigraphic and lithologic description	Thickness of interval feet (meters)	Depth to bottom of interval feet (meters)
Paintbrush Tuff--continued		
Tiva Canyon Member--continued		
Tuff, bedded, bedded/ash-fall(?), moderate-reddish orange vitric, abundant grayish pink and white vitric pumice	5.2 (1.6)	490.5 (149.4)
Pah Canyon Member		
Tuff, ash-flow, moderate-orange-pink, dusky yellow, nonwelded, vitric; pumice, dusky yellow, vitric; 5 percent phenocrysts (sanidine, plagioclase, biotite)	44.9 (13.7)	535.4 (163.1)
Tuff, bedded(?), ash-fall grayish-pink, vitric	6.9 (2.1)	542.3 (165.2)
Topopah Spring Member		
Tuff, ash-flow, moderate-red, nonwelded, vitric; pumice, dominantly moderate-red; sparse bronze biotite	25.9 (7.9)	568.2 (173.1)
Tuff, ash-flow, moderate-red, densely welded, (vitrophyre)	2.0 (0.6)	570.2 (173.7)
Tuff, ash-flow, grayish-red, densely welded, devitrified; 10 percent phenocrysts [sanidine, plagioclase, bronze biotite; (caprock)]	20.0 (6.1)	590.2 (179.8)
Tuff, ash-flow, pale brown, moderately welded, vapor phase; pumice, dominantly light gray, vapor phase; 5 to 10 percent phenocrysts (sanidine, plagioclase, biotite)	93.8 (28.6)	684.0 (208.5)
Tuff, ash-flow, grayish-red and medium-light gray (mottled), densely welded, devitrified; pumice, very light gray to white, devitrified, some vapor-phase crystallization; less than 2		

Table A.2.1-5. Lithologic log of drill hole USW-H5--continued

Stratigraphic and lithologic description	Thickness of interval feet (meters)	Depth to bottom of interval feet) (meters)
Paintbrush Tuff--continued		
Topopah Spring Member--continued		
percent phenocrysts (sanidine and plagioclase); probable lithophysal zone	715.9 (218.2)	1,399.9 (426.7)
Tuff, ash-flow, light-brown and brownish-gray (mottled), densely welded, devitrified; less than 2 percent phenocrysts	182.1 (55.5)	1,582.0 (482.2)
Tuff, ash-flow, black, densely welded (vitrophyre)	72.8 (22.2)	1,654.8 (504.4)
Tuff, ash-flow, black and pale yellowish-brown, moderately to partially welded, vitric; pumice, light brown, vitric; less than 3 percent phenocrysts (sanidine and plagioclase); most of bit-cutting samples composed of black glass shards (sidewall sample collected at 1,666.7 ft or 508 m)	44.3 (13.5)	1,699.1 (517.9)
Tuff, ash-fall, bedded, yellowish-gray, vitric; pale reddish-brown volcanic lithic fragments; bedding identified in television-camera log	11.2 (3.4)	1,710.3 (521.2)
Tuffaceous beds of Calico Hills		
Tuff, ash-flow, very-pale-orange, white and moderate-orange-pink, non-to-partially welded, vitric; pumice, white, vitric; less than 5 percent phenocrysts (sanidine, plagioclase, quartz, biotite); black, glassy lithic fragments are common; in television-camera log, top of a lithic-rich zone was recognized at 1,733 ft (528.2 m), and bedding planes were recognized at 1,745.2 ft (531.9 m), 1,748.1 ft (532.8 m), 1,754.0 ft (534.6 m), 1,760.0 ft (535.2 m), 1,775.0 ft (541.0 m), and 1,799.0 ft (548.3 m); sidewall samples collected at		

Table A.2.1-5. Lithologic log of drill hole USW-H5--concluded

Stratigraphic and lithologic description	Thickness of interval feet (meters)	Depth to bottom of interval feet (meters)
Tuffaceous beds of Calico Hills--continued		
1,762.2 ft (537.1 m), 1,800 ft (548.6 m), 1,852.1 ft (564.5 m), and 1,875.1 (571.5 m)	170.0 51.8	1,880.3 573.0
Tuff, bedded, reworked, ash-fall(?), yellowish-gray zeolitic; subequal proportions of phenocrysts and subrounded pumice fragments; in television-camera log, a coarse pumice ash-fall was identified at 1,881 ft (573.3 m), and bedding planes were recognized at 1,880.0 ft (573.0 m), 1,881.0 ft (573.3 m), 1,885.9 ft (574.8 m), 1,892.2 ft (576.7 m), 1,894.1 ft (577.3 m), 1,895.1 ft (577.6 m), 1,899.0 ft (578.8 m), 1,904.0 ft (580.3 m), 1,908.2 ft (581.6 m), 1,911.2 ft (582.5 m), 1,913.2 ft (583.1 m), 1,921.0 ft (585.5 m), and 1,935.1 ft (589.8 m); sidewall sample collected at 1,917.1 ft (584.3 m) contains about 25 percent phenocrysts of sanidine plagioclase, quartz, and biotite in a zeolitic groundmass	65.0 (19.8)	1,945.3 (592.8)
Crater Flat Tuff		

Table A.2.1-6. Lithologic log of drill hole USW-H6 (after Craig and others, 1983)

Stratigraphic and lithologic description	Thickness of interval feet (meters)	Depth to bottom of interval feet (meters)
Alluvium of Quaternary age, boulders, gravel, sand; predominantly composed of densely welded Tiva Canyon Member of the Paintbrush Tuff, a few fragments are partly coated with caliche.	29.9 (9.1)	29.9 (9.1)
Paintbrush Tuff		
Tiva Canyon Member		
Tuff, ash-flow, brownish-gray, grayish-red, densely welded, devitrified; less than 2 percent phenocrysts (sanidine)	160.0 (48.8)	189.9 (57.9)
Tuff, ash-flow, dusky-yellowish-brown, moderately welded(?); vitric (vitrophyre); abundant black glass shards	10.2 (3.1)	200.1 (61.0)
Tuff, ash-flow, light-brown and dark-yellowish-orange, partially welded, vitric (partially argillic; less than 2 percent phenocrysts; abundant black and dark-yellowish-orange glass shards)	60.0 (18.3)	260.1 (79.3)
Tuff, bedded, ash-fall, white, vitric	9.8 (3.0)	269.9 (82.3)
Pah Canyon Member		
Tuff, ash-flow, moderate-orange-pink, nonwelded, vitric; pumice, very-pale-orange, vitric; conspicuous biotite (ash-fall may be present from 290.0-299.9 ft or 88.4-91.4 m)	29.9 (9.1)	299.8 (91.5)
Topopah Spring Member		
Tuff, ash-flow, light-brown, nonwelded, vitric; mostly light-brown, vitric pumice; pale-reddish-brown and black vitrophyric lithic fragments(?)	29.9 (9.1)	329.7 (100.6)

Table A.2.1-6. Lithologic log of drill hole USW-H6--continued

Stratigraphic and lithologic description	Thickness of interval feet (meters)	Depth to bottom of interval feet (meters)
Paintbrush Tuff--continued		
Topopah Spring Member--continued		
Tuff, ash-flow, moderate-reddish-brown, (densely welded, vitrophyre)	2.0 (0.6)	331.7 (101.2)
Tuff, ash-flow, grayish-red, densely welded, devitrified; 10 percent(?) phenocrysts (abundant bronze biotite)	7.9 (2.4)	339.6 (103.6)
Tuff, ash-flow, grayish-red, moderately welded, vapor phase; pumice, grayish-red(?), vapor phase (bit cuttings very fine grained)	80.0 (24.4)	419.6 (128.0)
Tuff, ash-flow, light-brown-gray to very-light-gray, densely welded, devitrified; possible lithophysal zone(?)	230.0 (70.1)	649.6 (198.1)
Tuff, ash-flow, light-brown and grayish-red (mottled) densely welded, devitrified; less than 1 percent phenocrysts; conspicuous mottled appearance of bit cuttings between 880.0 and 1,180.2 ft (268.2 and 359.7 m)suggesting a possible lithophysal zone(?)	567.0 (172.8)	1,216.6 (370.9)
Tuff, ash-flow, black, vitrophyre; upper part of subunit altered to light brown and moderate brown; may be zeolites(?)	89.0 (27.4)	1,305.6 (398.3)
Tuff, ash-flow, grayish-brown to moderate-yellowish-brown, partially welded to non-welded, vitric, abundant black glass shards; base identified in television camera videotape observations	36.1 (11.0)	1,341.7 (409.3)

Table A.2.1-6. Lithologic log of drill hole USW-H6--continued

Stratigraphic and lithologic description	Thickness of interval feet (meters)	Depth to bottom of interval feet (meters)
Paintbrush Tuff--continued		
Topopah Spring Member--continued		
Tuff, ash-fall, bedded, reworked, light-olive-gray, moderate brown, light brownish-gray, vitric, slightly to moderately indurated(?); predominantly composed of pumice; sparse brownish-gray, medium-light-gray, and medium-dark-gray vitrophyric lithic fragments; beds range in thickness from 30-37 mm; beds dip 7-10°	30.2 (9.2)	1,371.9 (418.5)
Tuffaceous beds of Calico Hills		
Tuff, ash-flow, moderate-reddish-orange, light-brown, non-to-partially welded, vitric; pumice, grayish-orange-pink, light-gray, very-light-gray, yellowish-gray, vitric, particles range in size from 3 mm to 60 mm; less than 2 percent phenocrysts (sanidine); sparse brownish-gray rhyolitic lithic fragments and light gray to black vitrophyre lithic fragments. [Bedded tuff interval from 1,418.0 - 1,418.7 ft (432.2-432.4 m), moderate-pink to grayish-orange-pink, moderately indurated, vitric, dominantly pumice fragments, rare brownish-gray, rhyolitic lithic fragments]. [Television camera videotape observations suggest the base of the interval is 1,458 ft (444.4 m)]	81.7 (24.9)	1,453.6 (443.4)
Tuff, bedded, reworked, moderate-orange-pink, grayish-yellow, pale-yellowish-brown; dominantly zeolitic and argillic pumice fragments; lower 3 m well sorted	45.9 (14.0)	1,499.5 (457.4)
Crater Flat Tuff		

Table A.2.1-7. Lithologic log of drill hole UE25a-1 (after Spengler and others, 1979)

Stratigraphic and lithologic description	Thickness of interval feet (meters)	Depth to bottom of interval feet (meters)
Alluvium, gravel, sand, silt consisting of ash-flow and ash-fall tuff debris	30.0 (9.1)	30.0 (9.1)
Paintbrush Tuff		
Tiva Canyon Member		
Tuff, ash-flow, grayish-red, densely welded; white to dark-gray pumice, devitrified, some vapor phase; 1-2 percent phenocrysts (sanidine, quartz, biotite)	11.0 (3.4)	65.0 (19.8)
Tuff, ash-flow, grayish-red, densely welded; white to dark-gray pumice, devitrified; 1 percent sanidine, quartz, phenocrysts (contains sparse lithophysal)	7.0 (2.1)	72.0 (22.0)
Tuff, ash-flow, grayish-red, densely welded; blackish-red pumice, devitrified; 1 percent sanidine, quartz, phenocrysts	18.0 (5.5)	90.0 (27.4)
Tuff, ash-flow, grayish-red pumice, densely welded, devitrified; grayish-pink to pale-red pumice, devitrified, 5 mm, some as large as 4 cm; 1 percent phenocrysts	14.0 (4.3)	104.0 (31.7)
Tuff, ash-flow, grayish-red, densely welded, devitrified; light-gray to blackish-red pumice, devitrified (some vapor phase); 1-3 percent phenocrysts	10.0 (3.0)	114.0 (34.8)
Tuff, ash-flow, grayish-red, densely welded, devitrified; medium-light-gray to dark-gray pumice, devitrified (sparse vapor phase), 1-5 mm; 3 percent phenocrysts; sparse rhyolitic lithic fragments. Interval contains a zone from 152.0 to 164.6 ft (46.3-50.2 m)		

Table A.2.1-7. Lithologic log of drill hole UE25a-1--continued

Stratigraphic and lithologic description	Thickness of interval feet (meters)	Depth to bottom of interval feet (meters)
Paintbrush Tuff--continued		
Tiva Canyon Member--continued		
where several large pumice fragments have been altered to red-brown clay	59.0 (18.0)	173.0 (52.7)
Tuff, ash-flow, grayish-red, pale-red, light-brownish-gray, and medium-gray, moderately welded; pumice, vapor phase crystallization; 1-2 percent phenocrysts; 2-3 percent volcanic lithic fragments	22.0 (6.7)	195.0 (59.4)
Tuff, ash-flow, moderate-yellow-brown, partially welded, vitric, partly argillized; white to yellow-brown pumice, argillized; 1 percent phenocrysts, black and red volcanic lithic fragments; contains yellow-brown glass shards	12.0 (3.7)	207.0 (63.1)
Tuff, ash-flow, moderate-yellow-brown, nonwelded to partially welded; grayish-orange-pink to pale-brown pumice, argillized; 1 percent sanidine and quartz penocrysts; contains abundant yellow glass shards	10.0 (3.0)	217.0 (66.1)
Tuff, reworked ash-fall, bedded, very light gray to light-gray, poorly consolidated; pumice, white to light-gray, argillized; less than 1 percent phenocrysts, sparse biotite, 1-3 percent pale-red volcanic lithic fragments	1.2 (0.4)	218.2 (66.5)
Tuff, ash-flow, pale-red, nonwelded; white to gray pumice, argillized, as large as 5 cm; 1-2 percent phenocrysts; minor glass shards and bronze biotite	18.0 (5.5)	235.0 (71.6)

Table A.2.1-7. Lithologic log of drill hole UE25a-1--continued

Stratigraphic and lithologic description	Thickness of interval feet (meters)	Depth to bottom of interval feet (meters)
Paintbrush Tuff--continued		
Tiva Canyon Member--continued		
Tuff, ash-flow, yellow brown to pale-red-brown pumice, vitric, slightly argillized; 3-8 percent phenocrysts, minor bronze biotite; rare red volcanic lithic fragments; sparse black glass shards	4.5 (1.4)	239.0 (73.0)
Tuff, ash-fall and reworked ash-fall, grayish-orange, thick-bedded, friable to partially indurated; white to light-brown pumice, vitric (some pumice altered to clay); 1-3 percent phenocrysts (quartz, sanidine, biotite,); 1-2 percent red-brown volcanic lithic fragments	30.5 (9.3)	270.0 (82.3)
Topopah Spring Member		
Tuff, ash flow, pale-yellowish-brown, non-welded; 90 percent pale-yellowish-brown to grayish-orange pumice, vitric, blocky, 10 mm; less than 1 percent phenocrysts, 2-4 percent dark-gray to red-brown volcanic lithic fragments, lower 1.0 ft (0.3 m) grades into moderately welded glassy zone	5.6 (1.7)	275.6 (84.0)
Tuff, ash-flow, grayish red, densely welded (quartz latitic caprock); vitric, contains 15-20 percent phenocrysts of sanidine, plagioclase, biotite, and hornblende	13.4 (4.1)	289.0 (88.1)
Tuff, ash-flow, grayish-red, moderately welded; moderate-red to grayish-red, vapor phase pumice; 5-8 percent phenocrysts, sparse biotite	5.0 (1.5)	294.0 (89.6)
Tuff, ash-flow, grayish-red, moderately to densely welded, devitrified; pumice, grayish-red and white, vapor phase; 3-5 percent		

Table A.2.1-7. Lithologic log of drill hole UE25a-1--continued

Stratigraphic and lithologic description	Thickness of interval feet (meters)	Depth to bottom of interval feet (meters)
Paintbrush Tuff--continued Topopah Spring Member--continued phenocrysts; contains highly fractured and granulated zones at 301.4, 316.3-318.5, and 319.2-326.6 ft (91.9 and 92.9, 96.4-97.1, and 97.3-99.6 m) (zone of brecciation, with a slight indication of clay at 298.0-328.0 ft (90.8-100.0 m)	52.0 (15.8)	346.0 (105.5)
Tuff, ash-flow, pale-red to grayish-red, densely welded, devitrified; very light gray to dark-gray and pale-red pumice, devitrified (subordinate vapor-phase crystallization), as large as 5 cm in length; 8-10 percent phenocrysts	62.0 (18.9)	408.0 (124.4)
Tuff, ash-flow, grayish-red, densely welded, devitrified; light-gray to pale-red pumice as large as 25 mm; contains lithophysae as large as 25 mm in diameter lined with quartz and feldspars (zone of highly broken and granulated core at 409.6-426.0 ft (124.8-129.8 m), slight indication of swelling clay)	30.0 (9.1)	438.0 (133.5)
Tuff, ash-flow, medium-light-gray, densely welded, devitrified; very light gray to medium-light gray and pale-brown pumice, devitrified; 1 percent quartz and sanidine phenocrysts	19.0 (5.8)	457.0 (139.3)
Tuff, ash-flow, grayish-red, densely welded, devitrified; pale-red and very light gray to medium-gray pumice, devitrified (some vapor phase crystallization); 1 percent phenocrysts; contains abundant lithophysae, as much as 5 cm in diameter, lined with quartz and feldspars (two highly granulated zones with a slight		

Table A.2.1-7. Lithologic log of drill hole UE25a-1--continued

Stratigraphic and lithologic description	Thickness of interval feet (meters)	Depth to bottom of interval feet (meters)
Paintbrush Tuff--continued		
Topopah Spring Member--continued		
indication of clay at 581-521.0 and 525.0-529.0 ft (157.9-158.8 and 160.0-161.2 m)	174.0 (53.0)	631.0 (192.3)
Tuff, ash-flow, very light gray to medium-light and grayish-red-purple and grayish-orange-pink (mottled), densely welded, devitrified; very light gray and pale-red pumice, devitrified; less than 1 percent phenocrysts, rare biotite; sparse lithophysae; sparse light-gray rhyolitic lithic fragments; highly granulated zone with a slight indication of clay at 665.8-672.4 and 708.9-718.4 ft (202.9-205.0 and 216.1-219.9 m) (highly brecciated at 718.4 ft (219.0 m))	87.4 (26.6)	718.4 (219.0)
Tuff, ash-flow, moderate-brown, densely welded, devitrified; grayish-orange-pink pumice, devitrified, 1 mm-1 cm: 1 percent phenocrysts; sparse medium-gray rhyolitic lithic fragments	16.6 (5.1)	735.0 (224.0)
Tuff, ash-flow, moderate-brown and pale-red-brown (mottled), densely welded, devitrified; medium-light-gray to medium-gray pumice, devitrified, 1-10 mm; 1 percent phenocrysts; minor light-gray rhyolitic lithic fragments	5.3 (1.6)	740.0 (225.6)
Tuff, ash-flow, moderate-brown (pale-red-purple along fractures), densely welded, devitrified; moderate-brown to pale-red-purple pumice; 1 percent phenocrysts; sparse moderate-orange-pink and very light gray volcanic lithic fragments; some lithophysae, as much as 8 cm in diameter, rich in biotite, some lithophysae filled with clay and (or) zeolites	55.7 (17.0)	796.0 (242.6)

Table A.2.1-7. Lithologic log of drill hole UE25a-1--continued

Stratigraphic and lithologic description	Thickness of interval feet (meters)	Depth to bottom of interval feet (meters)
Paintbrush Tuff--continued		
Topopah Spring Member--continued		
Tuff, ash-flow, brownish-gray, partially to moderately welded, devitrified; light-gray pumice, less than 10 mm, vapor phase crystallization and devitrified (predominantly vapor phase); 1 percent phenocrysts	1.5 (0.5)	797.5 (243.1)
Tuff, ash-flow, moderate-brown and grayish-red-purple (mottled), densely welded; light-gray and moderate-brown pumice, 1-5 mm, devitrified; 1 percent phenocrysts; contains some grayish-red-purple lithophysae, as much as 10 cm in diameter, some cavities lined with quartz, others partially filled with clay and (or) zeolites	11.7 (3.6)	809.2 (246.6)
Tuff, ash-flow, grayish-red-purple, partially to moderately welded; grayish-red-purple pumice, 1-20 mm, devitrified and vapor phase crystallization; 1 percent phenocrysts; (interval appears partially brecciated)	1.0 (0.3)	810.2 (247.0)
Tuff, ash-flow, moderate-brown and medium-light-gray (slightly mottled), densely welded, devitrified; medium-light-gray pumice, devitrified, 1-20 mm; 1 percent phenocrysts; contains sparse medium-light-gray lithophysae; increase in light-gray rhyolitic lithic fragments as much as 10 cm in length	102.1 (31.1)	912.3 (278.1)
Tuff, ash-flow, pale-brown and light-brown (mottled), densely welded, devitrified; light-gray pumice, devitrified, 1-20 mm; 1 percent phenocrysts; 3-4 percent light-gray rhyolitic lithic fragments, as large as 3 cm in length; rare lithophysae, yellow brown, as much as 4 cm in diameter	26.3 (8.0)	938.6 (286.1)

Table A.2.1-7. Lithologic log of drill hole UE25a-1--continued

Stratigraphic and lithologic description	Thickness of interval feet (meters)	Depth to bottom of interval feet (meters)
Paintbrush Tuff--continued		
Topopah Spring Member--continued		
Tuff, ash-flow, pale-brown and moderate-brown (mottled), densely welded, devitrified; light-gray and light-brown pumice, devitrified, as large as 1 cm; 1 percent phenocrysts; 3-4 percent light-gray rhyolitic lithic fragments, 1-5 mm; 5-10 percent lithophysae, pale yellowish brown, as much as 10 cm in diameter	13.4 (4.1)	952.0 (290.2)
Tuff, ash-flow, pale-brown and moderate-brown (mottled), densely welded, devitrified; light-gray and light-brown pumice, devitrified, 1-10 mm; contains 20-30 percent lithophysae, pale yellowish brown, slightly argillized; 3-4 percent light-gray rhyolitic lithic fragments, commonly 1-2 cm in length, as large as 4 cm	124.0 (37.8)	1,076.0 (328.0)
Tuff, ash-flow, pale-brown to moderate-brown (mottled), densely welded, devitrified; light-gray to moderate-brown pumice, devitrified, 1-20 mm; 1 percent phenocrysts (sanidine and quartz); 4-5 percent rhyolitic lithic fragments, 1-5 mm, as large as 5 cm; rare lithophysae, pale yellowish brown, less than 5 cm in diameter; highly granulated zone with slight amount of clay at 1,118.0-1,123.5 ft (340.8-342.4 m)	53.0 (16.2)	1,129.0 (344.1)
Tuff, ash-flow, light-brown and pale-brown (mottled), densely welded, devitrified; brown to gray pumice, devitrified, 1-10 mm; 1 percent sanidine and quartz phenocrysts; 5-10 percent light-gray rhyolitic ash flow and reworked lithic fragments, 5-20 mm	34.0 (10.4)	1,163.0 (354.5)

Table A.2.1-7. Lithologic log of drill hole UE25a-1--continued

Stratigraphic and lithologic description	Thickness of interval feet (meters)	Depth to bottom of interval feet (meters)
Paintbrush Tuff--continued		
Topopah Spring Member--continued		
Tuff, ash-flow, pale-brown, moderately to densely welded, devitrified; pale-brown pumice (outer rims are moderate orange pink), devitrified (some vapor phase crystallization); 1 percent phenocrysts of sanidine and quartz; 2-4 percent light-gray rhyolitic and tuffaceous lithic fragments	71.6 (21.8)	1,234.6 (376.3)
Tuff, ash-flow, moderate-yellowish brown, moderately to densely welded, devitrified; pale-brown to moderate-brown pumice, devitrified (occasional vapor phase), 2-30 mm; rare light-gray rhyolitic lithic fragments, 1-5 mm, as large as 3 cm	27.4 (8.4)	1,262.0 (384.7)
Tuff, ash-flow, dark-yellowish-brown to yellowish-orange (altered), moderately to densely welded, vitric, partially argillized, pale-reddish-brown pumice, 1-10 mm; 2-3 percent volcanic lithic fragments; contains abundant black glass shards in dark-yellowish-brown altered zones	11.0 (3.4)	1,273.0 (388.0)
Tuff, ash-flow, black, vitrophyre, glassy conchoidal fracturing; contains abundant fractures; moderate-yellowish-brown clay gouge along some fractures [clay zone from 1,295.3 to 1,296.2 ft (394.8 to 395.1 m)]	44.2 (13.5)	1,317.2 (401.5)
Tuff, ash-flow, light-brown, partially welded, vitric; moderate-brown pumice, devitrified or partially vitric, 1-20 mm; less than 1 percent phenocrysts (sanidine, quartz); abundant moderate-yellow glass shards; 2-3 percent moderate-dark-gray volcanic lithic fragments, less than 5 mm	7.4 (2.3)	1,324.6 (403.7)

Table A.2.1-7. Lithologic log of drill hole UE25a-1--continued

Stratigraphic and lithologic description	Thickness of interval feet (meters)	Depth to bottom of interval feet (meters)
Paintbrush Tuff--continued		
Topopah Spring Member--continued		
Tuff, ash-flow, grayish-orange-pink to light-brown, nonwelded to partially welded, devitrified; pale brown pumice, partially devitrified, less than 1 cm; less than 1 percent phenocrysts (sanidine, quartz); 2-3 percent dark-medium-gray volcanic lithic fragments; sparse dark-brown glass shards	15.4 (4.7)	1,340.0 (408.4)
Tuff, ash-flow, grayish-orange-pink, nonwelded; devitrified grayish-orange-pink pumice, contains volcanic lithic fragments as much as 6 cm in size	10.1 (3.1)	1,350.1 (411.5)
Tuff, ash-flow, grayish-orange-pink to light-brown, nonwelded; grayish-orange-pink pumice, devitrified, 3-15 mm; 1 percent phenocrysts; 4-5 percent dark-brown rhyolitic lithic fragments as much as 20 mm	9.9 (3.0)	1,360.0 (414.5)
Tuff, ash-fall and reworked, slightly indurated, upper 15 cm contains lithic fragments as much as 2 cm in diameter, grading downward in size and abundance	3.9 (1.2)	1,363.9 (415.7)
Tuffaceous beds of Calico Hills		
Tuff, ash-flow, light-brown to moderate-brown, moderate-reddish-orange, and pale-reddish-brown, nonwelded, devitrified; pumice, devitrified to slightly zeolitized, 5-40 mm; less than 1 percent phenocrysts (sanidine, plagioclase, quartz, biotite); less than 1 percent dark-reddish-brown volcanic lithic fragments; ash-flow tuff intercalated with thin ash-fall and bedded tuffs (slightly argillized and zeolitized) at 1,383.5-1,386.3, 1,492.0-1,508.0,1,582.4-1,585.5,		

Table A.2.1-7. Lithologic log of drill hole UE25a-1--concluded

Stratigraphic and lithologic description	Thickness of interval feet (meters)	Depth to bottom of interval feet (meters)
Tuffaceous beds of Calico Hills--continued 1,762.6-1,764.0, and 1,775.1-1,775.9 ft (421.7-422.5, 454.8-459.6, 482.3-483.3, 537.2-537.7, and 541.0-541.3 m)	425.1 (129.6)	1,789.0 (545.3)
Tuff, bedded and reworked, pale-brown, moderate-red, light-red, moderate-orange-pink, yelowish-gray, moderate-greenish-yellow, and pale-olive, moderately to highly indurated; occasionally silicified; inter-bedded ash flow, air fall, reworked and tuffaceous sandstone; thickness of beds ranges from 0.05 to 3.0 ft (0.02 to 0.9 m); white to gray and yellow pumice, slightly argillized and zeolitized; volcanic lithic fragments vary from 2-20 percent (iron stained from 1,819.4 to 1,832.0 ft (554.6 to 558.4 m))	46.7 (14.2)	1,835.7 (559.5)
Crater Flat Tuff		

Table A.2.1-8. Lithologic log of drill hole UE25a-4 (after Springler and Rosenbaum, 1980)

Stratigraphic and lithologic description	Thickness of interval feet (meters)	Depth to bottom of interval feet (meters)
Alluvium, gravel, sand, and silt consisting of ash-flow and ash-fall tuff debris	30.0 (9.1)	30.0 (9.1)
Paintbrush Tuff		
Tiva Canyon Member		
Tuff, ash-flow, pale-red, moderately to densely welded; pumice, light-gray and pale red, devitrified, 1 percent sanidine phenocrysts	91.0 (27.7)	121.0 (36.8)
Tuff, ash-flow, grayish-orange to moderate-yellow-brown and pale-yellowish-brown, partially welded to nonwelded, vitric; pumice, pale-red and grayish-orange-pink, 1 mm-3 cm, vitric, increase in size and abundance downward, some altered to clay; abundant black and moderate-brown glass shards, increase in abundance downward, less than 1 percent phenocrysts (lower 5 ft. or 1.5 m friable)	29.7 (9.1)	150.7 (45.9)
Tuff, bedded/reworked, moderate-reddish-orange, friable; pumice, grayish-orange-pink, 1-2 mm, altered to clay; 1 percent phenocrysts, subrounded; sparse red-brown volcanic lithic fragments, well rounded	1.0 (0.3)	151.7 (46.2)
Tuff, bedded/reworked, pale-red, friable; pumice, grayish-orange-pink to moderate-orange-pink, 1-5 mm, altered to clay, some vitric; less than 1 percent phenocrysts; sparse black volcanic glass shards, rare pale-red volcanic lithic fragments	1.0 (0.3)	152.7 (46.5)
Yucca Mountain Member		
Tuff, ash-flow, yellowish-gray, nonwelded, vitric; pumice, grayish-orange-pink, 1-3 mm,		

Table A.2.1-8. Lithologic log of drill hole UE25a-4--continued

Stratigraphic and lithologic description	Thickness of interval feet (meters)	Depth to bottom of interval feet (meters)
Paintbrush Tuff		
Yucca Mountain Member--continued		
vitric; abundant yellowish-gray glass shards, sparse pale-red volcanic lithic fragments; core slightly altered and friable from 170 to 173.0 ft (51.8 - 52.7 m), clay (plastic) from 173.0 to 177.2 ft (52.7 - 54.0 m)	26.5 (8.1)	179.2 (54.6)
Tuff, air-fall/reworked, bedded, light-olive-gray, friable (unconsolidated), vitric; abundant colorless glass shards, rare pale-red volcanic lithic fragments	11.8 (3.6)	191.0 (58.2)
Pah Canyon Member		
Tuff, ash-flow, moderate brown to red-brown, nonwelded, vitric, friable to unconsolidated (slightly altered to clay); pumice, very pale orange and light gray, less than 2 mm, vitric (some clay); sparse red-brown volcanic lithic fragments; unit grades into underlying unit	30.5 (9.3)	221.5 (67.5)
Tuff, ash-flow, moderate- to dark-yellowish-brown, nonwelded (friable), slightly argillic; pumice; light-olive-brown, vitric (slightly argillic), 1 mm-5 cm, less than 1 percent phenocrysts, rare biotite, sparse pale-red volcanic lithic fragments, sparse black glass shards	46.7 (14.2)	268.2 (81.7)
Tuff, ash-flow, grayish-orange, nonwelded, friable, argillic; pumice, white, vitric (slightly argillic), 1-5 mm; less than 1 percent phenocrysts sparse pale-red volcanic lithic fragments, sparse black glass shards	6.5 (2.0)	274.7 (83.7)
Tuff, reworked, bedded, grayish-orange to dark-yellowish-brown, friable; pumice, white vitric		

Table A.2.1-8. Lithologic log of drill hole UE25a-4--continued

Stratigraphic and lithologic description	Thickness of interval feet (meters)	Depth to bottom of interval feet (meters)
Paintbrush Tuff--continued		
Pah Canyon Member--continued		
(slightly altered to clay), conspicuous black glass shards; 1-2 percent phenocrysts, sparse pale-red volcanic lithic fragments [altered to clay from 275 to 280.0 ft (83.8 - 85.3 m), moderate red from 279.0 to 280.0 ft (85.0 - 85.3 m)]	5.3 (1.6)	280.0 (85.3)
Topopah Spring Member		
Tuff, ash-flow, moderate-reddish-brown to moderate-brown and grayish-orange, nonwelded, vitric, friable to poorly indurated, slightly argillic; pumice, grayish orange pink and white, vitric (some altered to clays), conspicuous black glass fragments, less than 1 percent phenocrysts	30.0 (9.1)	310.0 (94.4)
Tuff, ash-flow, light-gray, nonwelded to partially welded, vitric, greater than 90 percent pumice, light-gray, less than 1 percent phenocrysts	6.8 (2.1)	316.8 (96.5)
Tuff, ash-flow, vitrophyre, black and grayish-red, perlitic, densely welded, contains abundant calcite veinlets (randomly oriented), 5-7 percent phenocrysts (quartz, feldspar)	3.2 (1.0)	320.0 (97.5)
Tuff, ash-flow, grayish-brown to moderate red, densely welded, devitrified; pumice, grayish-red, devitrified, 2-5 mm; 7-10 percent phenocrysts (rare biotite, pyroxene, hornblende); abundant, thin (1 mm) calcite veinlets, randomly oriented [quartz latitic caprock highly crushed interval from 332.1 to 346.9 ft (101.2 - 105.7 m)]	26.9 (8.2)	346.9 (105.7)

Table A.2.1-8. Lithologic log of drill hole UE25a-4--concluded

Stratigraphic and lithologic description	Thickness of interval feet (meters)	Depth to bottom of interval feet (meters)
Paintbrush Tuff--continued		
Topopah Spring Member--continued		
Tuff, ash-flow, pale-red to grayish-red moderately to densely welded, devitrified (some vapor phase); pumice, pale-red to grayish-red and light-gray, devitrified (some vapor phase), 2 mm - 2 cm, 3-7 percent phenocrysts; crushed intervals 346.9-365.5, 369.5-372.0, and 414-416 ft (105.7 - 111.4, 112.6 - 113.4 and 126.2 - 126.8 m); predominantly vapor phase from 363.1 to 367.5 ft and 431.9 to 433.7 ft (110.6 to 112.0 m and 131.6 to 132.2 m)	153.1 (46.7)	500.0 (152.4)
TD		500.0 (152.4)

Table A.2.1-9. Lithologic log of drill hole UE25a-5 (after Spengler and Rosenbaum, 1980)

Stratigraphic and lithologic description	Thickness of interval feet (meters)	Depth to bottom of interval feet (meters)
Alluvium/colluvium, gravel, sand, silt consisting of ash-flow and air-fall tuff debris	90.0 (27.4)	90.0 (27.4)
Paintbrush Tuff		
Tiva Canyon Member		
Tuff, ash-flow, pale-red to grayish-red, densely welded, devitrified, 2-3 cm; 1-2 percent phenocrysts (quartz, sanidine); less than 1 percent pale-red volcanic lithic fragments	38.0 (11.6)	128.0 (39.0)
Tuff, ash-flow, moderate-yellow-brown, nonwelded to partially welded, vitric; grayish-orange and pale-red pumice, 2-10 mm, altered to clay, less than 1 percent phenocrysts, abundant glass shards	10.6 (3.2)	138.6 (42.2)
Core from 138.6 to 153 ft (42.2 to 46.6 m) lost	14.4 (4.4)	153.0 (46.6)
Yucca Mountain Member		
Tuff, ash-flow, very pale orange to pale-yellowish-brown, vitric; pumice, white to grayish-pink, less than 1 mm, slightly argillic, less than 1 percent phenocrysts; contains colorless to light-gray glass shards	14.0 (4.3)	167.0 (50.9)
Tuff, bedded/reworked, pale-reddish-brown and very light gray, moderately indurated, vitric; pumice, grayish-orange-pink, vitric, less than 5 mm; less than 1 percent phenocrysts, less than 1 percent pale-red volcanic lithic fragments	18.3 (5.6)	185.3 (56.5)

Table A.2.1-9. Lithologic log of drill hole UE25a-5--continued

Stratigraphic and lithologic description	Thickness of interval feet (meters)	Depth to bottom of interval feet (meters)
Paintbrush Tuff--continued		
Pah Canyon Member		
Tuff, ash-flow, pale-red to pale-reddish-brown, nonwelded, vitric; pumice, light-olive-gray, pale-olive, and pale-red, vitric (slightly argillic), as large as 5 cm; less than 1 percent phenocrysts, rare bronze biotite; unit becomes progressively more argillic downhole, intensely argillic and friable from 210 to 228.0 ft (64 to 69.5 m)	44.3 (13.5)	229.6 (70.0)
Tuff, ash-fall and reworked bedded, light-olive-gray to greenish-gray and pale-yellowish-brown (mottled), friable, thick-bedded; pumice, white to greenish-gray, vitric (some argillic, less than 1 percent phenocrysts; conspicuous bronze biotite, less than 1 percent pale-red volcanic lithic fragments, altered to moderate-red clay (plastic) from 234.7 to 236.0 ft (71.5 to 71.9 m)	7.5 (2.3)	237.1 (72.3)
Topopah Spring Member		
Tuff, ash-flow, grayish-orange, nonwelded, vitric; pumice, very light gray, vitric, 1-2 percent phenocrysts, abundant black and moderate-reddish-brown glass fragments; 1 percent pale-red volcanic lithic fragments	30.9 (9.4)	268.0 (81.7)
Tuff, ash-flow, light-bluish-gray and greenish-gray, nonwelded (extremely friable and poorly consolidated) to moderately welded, vitric, consists almost entirely of light-bluish-gray pumice fragments, vitric, 1mm-1.5cm	9.0 (2.7)	277.0 (84.4)
Tuff, ash-flow, grayish-red and black (mottled), densely welded, vitrophyre; pumice, moderate-reddish-brown, vitric,		

Table A.2.1-9. Lithologic log of drill hole UE25a--concluded

Stratigraphic and lithologic description	Thickness of interval feet (meters)	Depth to bottom of interval feet (meters)
Paintbrush Tuff--continued		
Topopah Spring Member--continued		
10-15 percent phenocrysts (feldspar, quartz), perlitic	2.0 (0.6)	279.0 (85.0)
Tuff, ash-flow, grayish-brown, densely welded, devitrified, contains 15-20 percent phenocrysts of sanidine, plagioclase, hornblende, biotite, pyroxene; pumice, grayish-red, devitrified and vapor phase (quartz latitic caprock)	30.6 (9.3)	309.6 (94.3)
Tuff, ash-flow, grayish-red, moderately to densely welded, devitrified; pumice, white to pale-red and light-gray, 2 mm-1 cm, as large as 7 cm, vapor phase and devitrified; 5-7 percent phenocrysts; sparse, light-gray volcanic lithic fragments, as large as 3 cm, predominantly vapor phase from 323 to 329.8 ft (98.4 to 100.5 m)	132.8 (40.5)	442.4 (134.8)
Tuff, ash-flow, light-gray to moderate-light-gray and grayish-red (mottled), densely welded, devitrified; pumice, light-gray to white and pale-red, devitrified (some vapor phase), 2 mm-5 cm contains lithophysae, generally 2-4 cm in diameter, as large as 6 cm in diameter, lines with quartz, feldspar; groundmass contains 1-2 percent phenocrysts (predominantly sanidine)	36.3 (11.1)	478.7 (145.3)
Tuff, ash-flow, grayish-red-purple, densely welded, devitrified; pumice, white to light-gray, devitrified, 1 mm-1 cm; less than 1 percent phenocrysts, sparse, pale-red and light-gray volcanic lithic fragments, 1-3 cm	8.3 (2.5)	487.0 (148.4)
TD		487.0 (148.4)

Table A.2.1-10. Lithologic log of drill hole UE25a-6 (after Spengler and Rosenbaum, 1980)

Stratigraphic and lithologic description	Thickness of interval feet (meters)	Depth to bottom of interval feet (meters)
Alluvium (no samples recovered)	20.0 (6.1)	20.0 (6.1)
Paintbrush Tuff		
Tiva Canyon Member		
Tuff, ash-flow, light-gray to pale-red, devitrified, densely welded; pumice, light-gray and pale-red, devitrified, less than 1 percent phenocrysts	60.0 (18.3)	80.0 (24.4)
Tuff, ash-flow pale-red, moderately welded, devitrified; pumice, light-gray and pale-red vapor phase, as large as 8 cm, 1-3 percent phenocrysts	3.5 (1.1)	83.5 (25.5)
Tuff, ash-flow, pale-red, densely welded, devitrified; pumice, pale-red and light-gray, devitrified, 2 mm-2 cm, 1-2 percent phenocrysts (predominantly sanidine)	19.5 (5.9)	103.0 (31.4)
Tuff, ash-flow, pale-red to grayish-red, partially to moderately welded, devitrified; pumice, grayish-red and moderate-reddish-orange, 5 mm-3 cm, 1-2 percent altered to moderate-reddish-orange clay; less than 1 percent phenocrysts, sparse, pale-red volcanic lithic fragments	20.1 (6.1)	123.1 (37.5)
Tuff, ash-flow, pale-red to moderate-brown and moderate-yellowish-brown, nonwelded to partially welded, vitric; pumice, grayish-red, argillite 2-10 mm; 1-2 percent phenocrysts, abundant glass shards	21.1 (6.4)	144.2 (43.9)
Tuff, bedded/reworked, pale-yellowish-brown, poorly consolidated (friable), moderately		

Table A.2.1-10. Lithologic log of drill hole UE25a-6--continued

Stratigraphic and lithologic description	Thickness of interval feet (meters)	Depth to bottom of interval feet (meters)
Paintbrush Tuff--continued		
Tiva Canyon Member--continued		
argillic, poorly bedded, sparse, pale-red volcanic lithic fragments	5.1 (1.6)	149.3 (45.5)
Yucca Mountain Member		
Tuff, ash-flow, grayish-orange-pink to grayish-orange, and yellowish-gray, non-welded, vitric; pumice, grayish-orange-pink to white, vitric, 1-4 mm, less than 1 percent phenocrysts, sparse, pale-red volcanic lithic fragments, abundant glass shards	20.0 (6.1)	169.3 (51.6)
Tuff, bedded/reworked, very light gray to light-gray, unconsolidated, poorly bedded, vitric; mixture of pale-red volcanic fragments and white to light-gray vitric pumice	2.7 (0.8)	172.0 (52.4)
Tuff, bedded/reworked, moderate-yellowish-brown; poorly consolidated to unconsolidated, predominantly sand-size granules and volcanic lithic fragments, subrounded to well rounded, very little pumice	2.4 (0.7)	174.4 (53.1)
Tuff, bedded/reworked, grayish-orange-pink, poorly consolidated, predominantly grayish-orange-pink and white vitric pumice, subrounded to well rounded; abundant black and pale-red volcanic lithic fragments	10.0 (3.0)	184.4 (56.1)
Tuff, ash-fall, very light gray, vitric; pumice, predominantly very light gray, vitric; sparse red-brown volcanic lithic fragments, conspicuous bronze biotite	3.8 (1.2)	188.2 (57.3)

Table A.2.1-10. Lithologic log of drill hole UE25a-6--continued

Stratigraphic and lithologic description	Thickness of interval feet (meters)	Depth to bottom of interval feet (meters)
Paintbrush Tuff--continued		
Pah Canyon Member		
Tuff, ash-flow, grayish-orange-pink, nonwelded; pumice, white and yellowish-gray, vitric, 2-8 mm; 2-4 percent phenocrysts, some glass shards, sparse pale-red volcanic lithic fragments	13.6 (4.1)	201.8 (61.4)
Tuff, bedded/reworked, grayish-orange-pink, unconsolidated, abundant subrounded volcanic lithic fragments; some white to light-gray and moderate-orange-pink, vitric pumice [core from 208.1 to 227.0 ft (63.4 to 69.1 m) lost]	25.2 (7.7)	227.0 (69.1)
Topopah Spring Member		
Tuff, ash-flow, grayish-orange-pink to moderate-brown, nonwelded, vitric; pumice, very light gray, vitric (some argillic), 5 mm-2 cm; 2-3 percent phenocrysts (conspicuous pale-bronze biotite), abundant glass shards; abundant pale-red volcanic lithic fragments, 2 mm-1.5 cm	10.6 (3.2)	237.6 (72.3)
Tuff, ash-flow, pale-red and medium-light-gray, nonwelded to partially welded, vitric, consists of 90 percent pale-red and medium-light-gray vitric pumice, 1 mm-2 cm; sparse pale-red volcanic lithic fragments	4.1 (1.2)	241.7 (73.5)
Tuff, ash-flow, vitrophyre, moderate-reddish-brown and black, vitric, densely welded, 20-30 percent phenocrysts (quartz, feldspar)	4.3 (1.3)	246.0 (74.8)
Tuff, ash-flow, grayish-red, densely welded, devitrified; pumice, moderate-orange-pink and grayish-red, devitrified, 1 mm-1 cm, 15-		

Table A.2.1-10. Lithologic log of drill hole UE25a-6--concluded

Stratigraphic and lithologic description	Thickness of interval feet (meters)	Depth to bottom of interval feet (meters)
Paintbrush Tuff--continued		
Topopah Spring Member--continued		
20 percent phenocrysts (conspicuous biotite) (quartz latitic caprock)	17.5 (5.3)	263.5 (80.1)
Tuff, ash-flow pale-red, densely welded, devitrified; pumice, pale-red and very light gray, devitrified (some vapor phase), 2 mm-9 cm; 5-7 percent phenocrysts	136.1 (41.5)	399.6 (121.6)
Tuff, ash-flow, light-brownish-gray to very light gray, densely welded, devitrified; pumice, very light gray and grayish-red, devitrified, 2 mm-7 cm, contains abundant lithophysae, very light gray, 1-6 cm in diameter, lines with quartz and feldspar	100.4 (30.6)	500.0 (152.2)
TD		500.0 (152.2)

Table A.2.1-11. Lithologic log of drill hole UE25a-7 [Thickness and depth adjusted for inclination of drill hole] (after Spengler and Rosenbaum, 1980)

Stratigraphic and lithologic description	Thickness of interval feet (meters)	Depth to bottom of interval feet (meters)
Alluvium/colluvium, boulders, gravel, and sand consisting of ash-flow and bedded tuff, nonwelded to densely welded, vitric to devitrified. Cored interval from 80 to 153 feet consists of colluvium of cobble- to boulder-size tuff fragments of variable lithology and orientation. Caliche coatings are common	137.5 (41.9)	137.5 (41.9)
Paintbrush Tuff		
Tiva Canyon Member		
Tuff, ash-flow, grayish-red and medium-gray, densely welded, devitrified; pumice, light-gray and light-brownish-gray, devitrified, 1 mm-1 cm; 1 percent phenocrysts (sanidine), upper 2.6 ft (0.8 m) contains sparse (less than 1 percent) lithophysae as large as 3 cm in diameter; interval from 142.7 to 152.0 ft (43.5 to 46.3 m) contains abundant spherulites commonly 5 mmin diameter, some as large as 2 cm	14.5 (4.4)	152.0 (46.3)
Tuff, ash-flow, pale-yellowish-brown, moderately welded, devitrified; pumice, light-brown and grayish-red, 1 mm-1 cm, dominantly vapor phase, slightly argillic; less than 1 percent phenocrysts; less than 1 percent pale-reddish-brown and light-gray volcanic lithic fragments	3.9 (1.2)	155.9 (47.5)
Tuff, ash-flow, pale-brown to grayish-orange partially welded to nonwelded, vitric; pumice, pale-red and grayish-orange, commonly 2.6 mm, as large as 1 cm, argillic; less than 1 percent phenocrysts, mainly sanidine; size and abundance of pumice increases downwards; abundance of black glass shards increases		

Table A.2.1-11. Lithologic log of drill hole UE25a-7--continued

Stratigraphic and lithologic description	Thickness of interval feet (meters)	Depth to bottom of interval feet (meters)
Paintbrush Tuff--continued		
Tiva Canyon Member--continued		
toward base of unit	14.9 (4.5)	170.8 (52.0)
Tuff, bedded/reworked, pale-yellowish-brown (upper 0.5 ft), pale-reddish-brown, slightly indurated, argillic; over 80 percent pumice, white to pale-yellowish-orange, argillic; 3-5 percent pale-reddish-brown and black volcanic lithic fragments	3.7 (1.1)	174.5 (53.1)
Yucca Mountain Member		
Tuff, ash-flow, grayish-orange, and yellowish-gray, nonwelded, vitric; pumice, grayish-orange-pink, vitric (some argillic), 1-2 percent, 1-3 mm, as large as 1 cm; abundant, colorless and black glass shards, rare phenocrysts	16.9 (5.2)	194.4 (58.3)
Tuff, reworked/bedded, pale-yellowish-brown and light-olive-gray, moderately indurated, thick-bedded; over 50 percent pumice, white to light-gray and light-olive-gray, vitric, slightly argillic abundant well-rounded phenocrysts of quartz and feldspar, abundant grayish-red and black volcanic lithic fragments, as large as 1 cm	5.5 (1.7)	197.9 (60.0)
Pah Canyon Member		
Tuff, ash-flow, moderate-orange-pink to grayish-orange-pink, nonwelded, vitric; pumice, yellowish-gray and pinkish-gray, greater than 30 percent, 5 mm-5 cm, vitric, slightly argillic, less than 1 percent phenocrysts, conspicuous black biotite, sparse pale-red volcanic lithic fragments; unit grades downward into underlying unit	28.9 (8.8)	226.8 (68.8)

Table A.2.1-11. Lithologic log of drill hole UE25a-7--continued

Stratigraphic and lithologic description	Thickness of interval feet (meters)	Depth to bottom of interval feet (meters)
Paintbrush Tuff--continued		
Pah Canyon Member--continued		
Tuff, ash-flow, grayish-orange-pink to light-brown, nonwelded, vitric; pumice, grayish-orange, 5 mm, as large as 5 cm, vitric, less than 1 percent phenocrysts, sparse, pale-red volcanic lithic fragments, grades into underlying unit	10.5 (3.2)	237.3 (72.0)
Tuff, ash-flow, grayish-pink, nonwelded, vitric; pumice, grayish-pink, as large as 5 cm, vitric; less than 1 percent phenocrysts (rare biotite), sparse, pale-red volcanic lithic fragments	1.6 (0.5)	238.9 (72.5)
Tuff, bedded/reworked, grayish-orange-pink, slightly indurated, poorly sorted; 50 percent pumice, grayish-orange-pink, subrounded to subangular, slightly argillic, 2-5 mm, conspicuous amount of black glass fragments and pale-red volcanic lithic fragments, interval from 243.6 to 244.9 ft (74.2 to 74.6 m) is stained light red, argillic	6.2 (1.9)	245.1 (74.4)
Topopah Spring Member		
Tuff, ash-flow, grayish-orange-pink to very pale orange, nonwelded, vitric; pumice, white to grayish-orange-pink; pumice, white to grayish-orange-pink, vitric and argillic, 5-30 mm; 2-3 percent phenocrysts (quartz, sanidine); conspicuous hornblende and bronze biotite; conspicuous pale-red and moderate-red volcanic lithic fragments	22.4 (6.8)	267.5 (81.2)
Tuff, ash-flow, light-gray and pale-yellowish-brown, nonwelded to partially welded, vitric; pumice, greater than 60 percent, light-gray and pale-yellowish-brown		

Table A.2.1-11. Lithologic log of drill hole UE25a-7--concluded

Stratigraphic and lithologic description	Thickness of interval feet (meters)	Depth to bottom of interval feet (meters)
Paintbrush Tuff-continued		
Topopah Spring Member--continued		
and moderate-reddish-orange, vitric, 2-20 mm, conspicuous black and moderate-reddish-brown glass fragments, minor pale-red volcanic lithic fragments, sparse biotite	6.2 (1.9)	273.7 (83.1)
Tuff, ash-flow, dark-reddish-brown to black, vitrophyre, densely welded, 15-20 percent phenocrysts, predominantly sanidine, sparse biotite	3.1 (0.9)	276.8 (84.0)
Tuff, ash-flow, pale-red to grayish-brown, densely welded, devitrified, 10 percent phenocrysts (sanidine, biotite, pyroxene); sparse moderate-reddish-brown pumice (quartz latitic caprock)	13.5 (4.1)	280.3 (88.1)
Tuff, ash-flow, pale-red to grayish-red and light-gray, moderately to densely welded, devitrified; pumice, white to medium-gray and blackish-red, 1 mm-4 cm, as large as 7 cm, vapor phase and devitrified; 3-5 percent phenocrysts (feldspar, hornblende, quartz, biotite, magnetite) light-gray volcanic lithic fragments, rhyolitic, 1-2 cm [conspicuous vapor phase from 338.0 to 354.5 ft (103 to 108 m)]	140.0 (42.7)	430.3 (130.8)
Tuff, ash-flow, pale-red, densely welded, devitrified; pumice, white to medium-gray and pale red, 2 mm-7 cm, vapor phase and devitrified, contains as much as 30 percent lithophysae, 2-5 cm in diameter, lined with quartz and feldspar; 2-3 percent sanidine	19.1 (5.8)	499.4 (136.6)
TD		449.4 (136.6)

Table A.2.1-12. Lithologic log for test well UE-25b-1 [Color designations are from the Rock Color Chart (Goddard and others, 1948); modified from R. W. Spengler, U.S. Geological Survey, written communication 1983, and oral communication 1983 by Lobmeyer and others, 1983]

Stratigraphic and lithologic description	Thickness of interval feet (meters)	Depth to bottom of interval feet (meters)
Alluvium		
Gravel, composed of fragments of Tiva Canyon and Yucca Mountain Members of Paintbrush Tuff, subangular to subrounded, few fragments coated with caliche	149.9 (45.7)	149.9 (45.7)
Paintbrush Tuff		
Tiva Canyon Member		
Tuff, ash-flow, grayish-red, densely welded; grayish-red pumice; 1-2 percent phenocrysts	60.0 (18.3)	209.9 (64.0)
Tuff, ash-flow, light-brown, partially to nonwelded; pale-yellowish-brown pumice, vitric, less than 1 percent phenocrysts	29.9 (9.1)	239.8 (73.1)
Pah Canyon Member		
Tuff, ash-flow, moderate-reddish-orange, pale-reddish-brown, nonwelded, vitric, grayish-orange pumice, vitric, less than 1 percent phenocrysts	20.0 (6.1)	259.8 (79.2)
Tuff, bedded/reworked, grayish-yellow, vitric and devitrified, rich in pumice	15.1 (4.6)	274.9 (83.8)
Topopah Spring Member		
Tuff, ash-flow, grayish-red, densely welded (vitrophyre)	4.9 (1.5)	279.8 (85.3)
Tuff, ash-flow, grayish-red, densely welded, devitrified; blackish-red pumice, devitrified; 10 percent phenocrysts (quartz,		

Table A.2.1-12. Lithologic log for test well UE-25b-1--continued

Stratigraphic and lithologic description	Thickness of interval feet (meters)	Depth to bottom of interval feet (meters)
Paintbrush Tuff--continued		
Topopah Spring Member--continued		
sanidine, plagioclase, biotite, pyroxene) (quartz latitic caprock)	10.1 (3.1)	289.9 (88.4)
Tuff, ash-flow, grayish-red, light-brown, densely welded, devitrified; moderate-reddish-orange pumice, devitrified; 2-3 percent phenocrysts; core samples collected from 540-556.1, 560-584, 584-599.1, 730-736.9, 736.9-740.2, 740.2-745.1 ft (164.6-169.5, 170.7-178.0, 178.0-182.6, 222.5-224.6, 224.6-225.6, and 225.6-227.1 m); samples collected from 560-584 ft (170.7-178.0 m) occur in a lithophysal zone	1,005.0 (306.3)	1,294.9 (394.7)
Tuff, ash-flow, black, densely welded, vitric (vitrophyre)	35.1 (10.7)	1,330.0 (405.4)
Tuff, ash-flow, light-brown, moderately to partially welded, vitric; moderate-brown pumice, vitric; abundant black glass shards	20.0 (6.1)	1,350.0 (411.5)
Tuff, bedded/reworked, dark-yellowish-orange, altered, abundant medium-dark-gray rhyolite lithic fragments	35.1 (10.7)	1,385.1 (422.2)
Tuffaceous beds of Calico Hills (informal usage)		
Tuff, ash-flow, light-brown, grayish-orange, yellowish-orange, and yellowish-gray, non-welded, zeolitized; pumice, grayish-yellow and yellowish-gray, zeolitized; commonly 1-3 cm; 1-3 percent phenocrysts; about 5 percent brownish-gray and medium-gray volcanic lithic fragments, rhyolitic; commonly 1-4 cm [core collected from 1,570 to		

Table A.2.1-12. Lithologic log for test well UE-25b-1--concluded

Stratigraphic and lithologic description	Thickness of interval feet (meters)	Depth to bottom of interval feet (meters)
Tuffaceous beds of Calico Hills--continued		
1,591 ft (478.5 to 484.9 m), recovered 21 ft (6.4 m)]	455.1 (138.7)	1840.2 (560.8)
Tuff, bedded, ash-fall(?), identified on density log and downhole television camera	28.9 (8.8)	1869.1 (569.7)
Crater Flat Tuff		

APPENDIX 2.2

Isopach Maps for the Paintbrush Tuff and the Bedded Tuff of Calico Hills

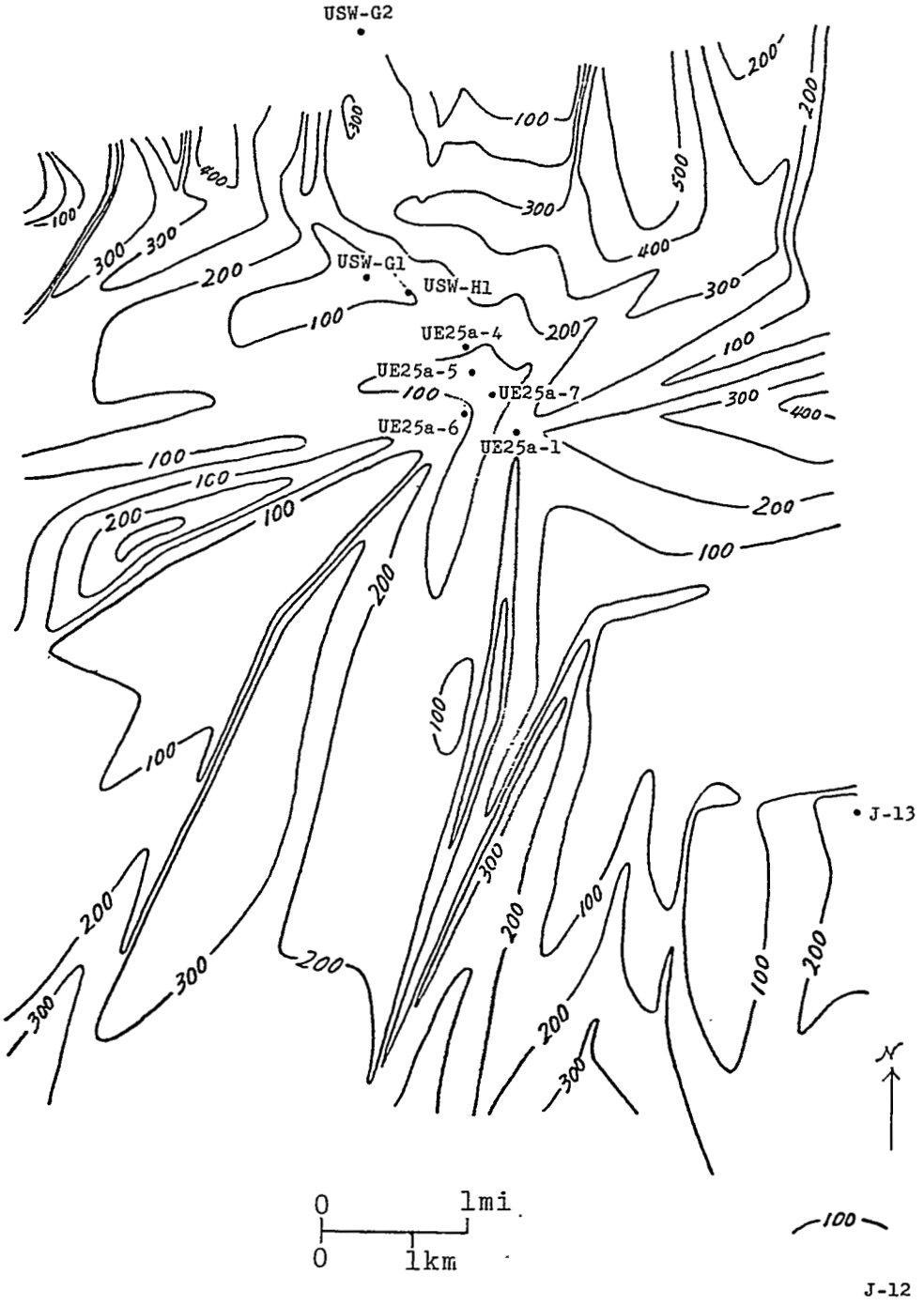

Figure A.2.2-1. Isopach map, Tiva Canyon Member.

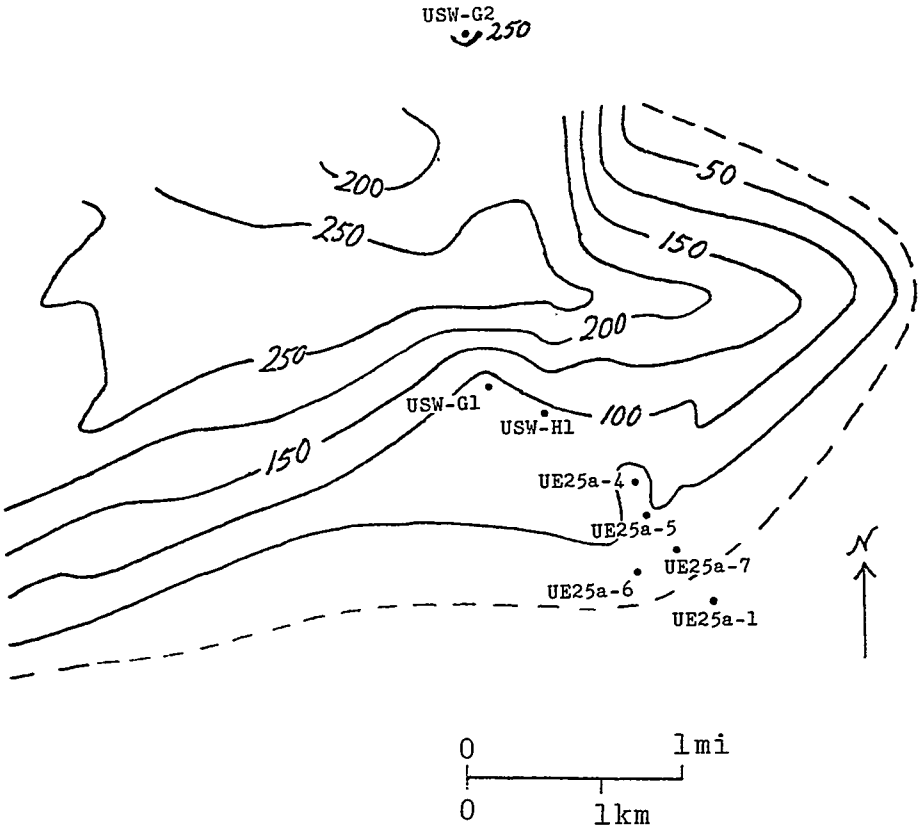

Figure A.2.2-2. Isopach map, Yucca Mountain Member. Dotted line is the inferred limit of the Yucca Mountain Member.

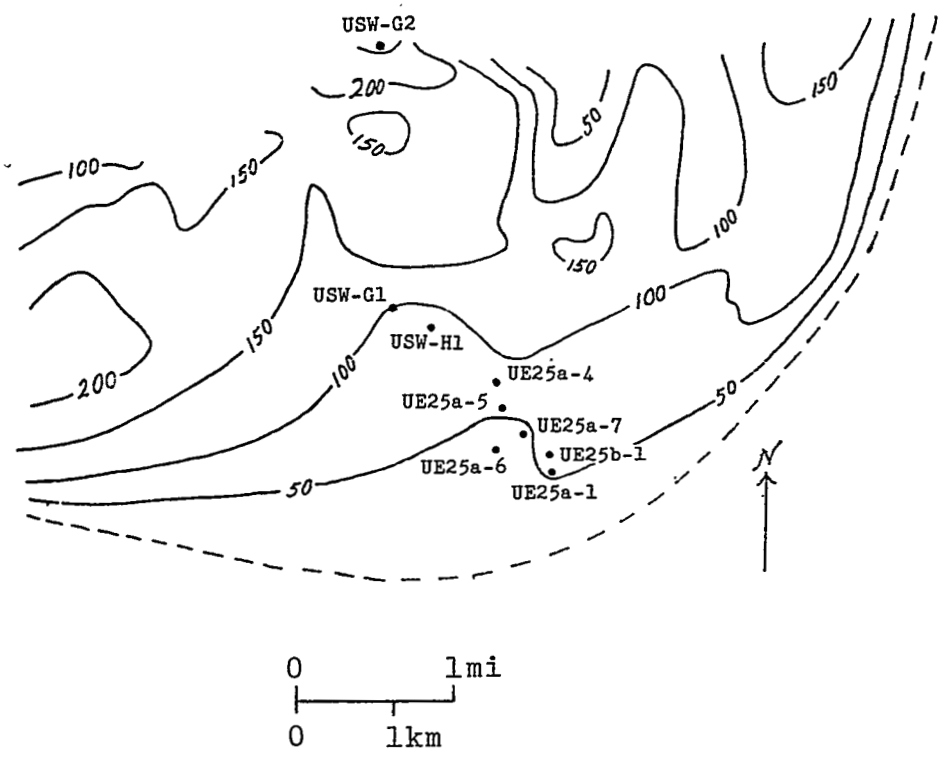

Figure A.2.2-3. Isopach map, Pah Canyon Member. Dotted line is the inferred limit of the Pah Canyon Member.

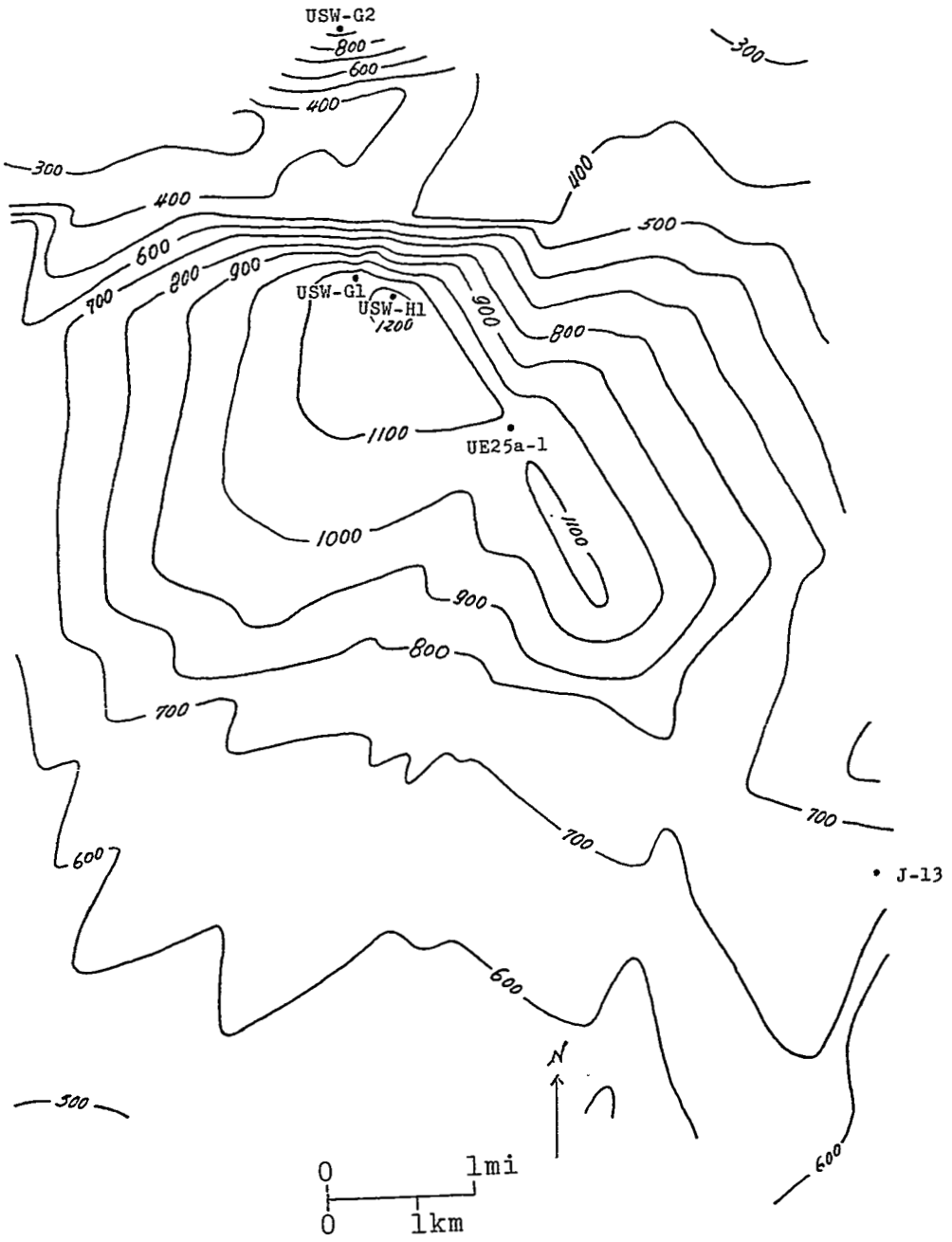

Figure A.2.2-4. Isopach map, Topopah Spring Member.

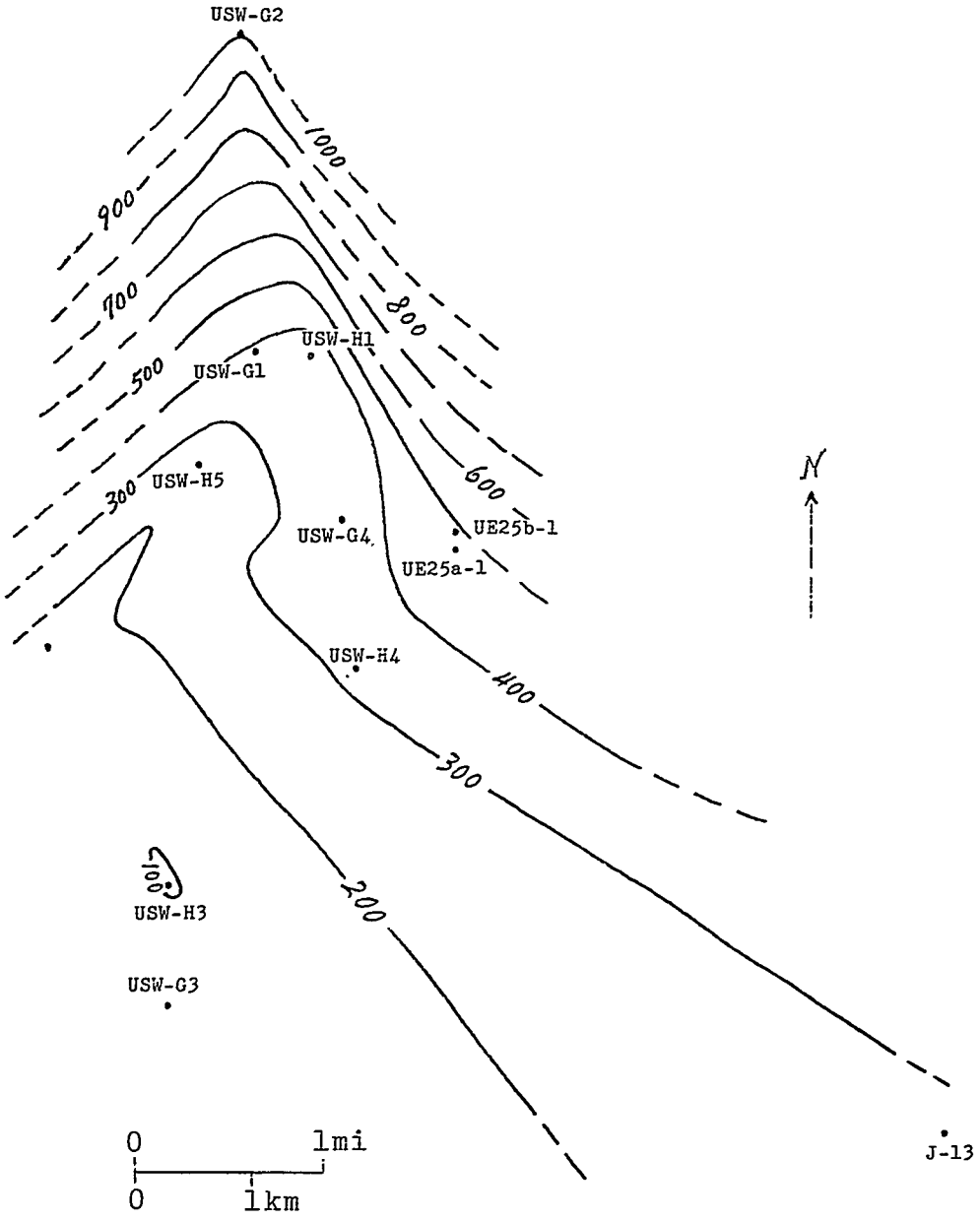

Figure A.2.2-5. Isopach map, Bedded Tuff of Calico Hills.

APPENDIX 3.1

Mineral Abundance in Drill Holes

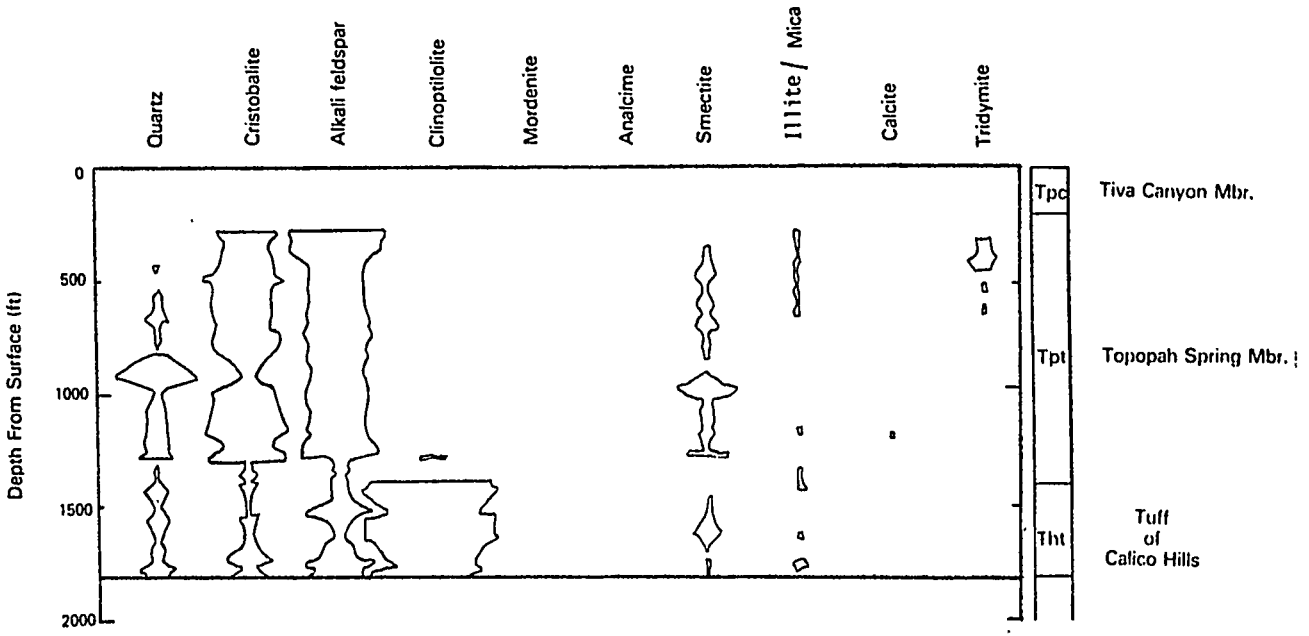

Figure A3.1-1. Mineral abundance in drill hole USW-G1. Mineral identification and estimates of abundance are by X-ray diffraction techniques (Bish and others, 1981).

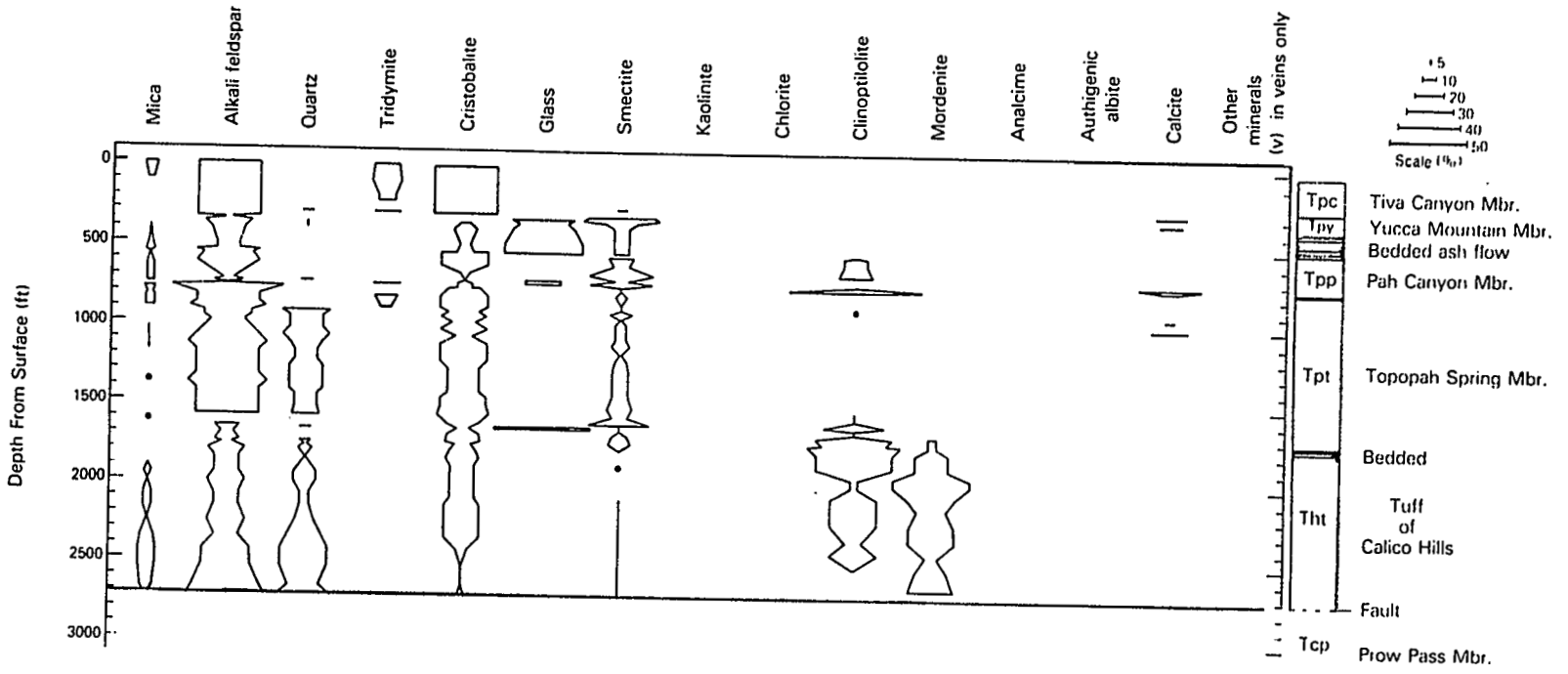

Figure A3.1-2. Mineral and glass abundance in drill hole USW-G2, determined by X-ray diffraction. Occurrences of authigenic albite and of barite were determined by optical examination and are not quantitative. The scale in the upper right corner of this figure can be used to estimate relative volume percentages. All data are listed in Table A3.2-2 (after Caporuscio and others, 1982).

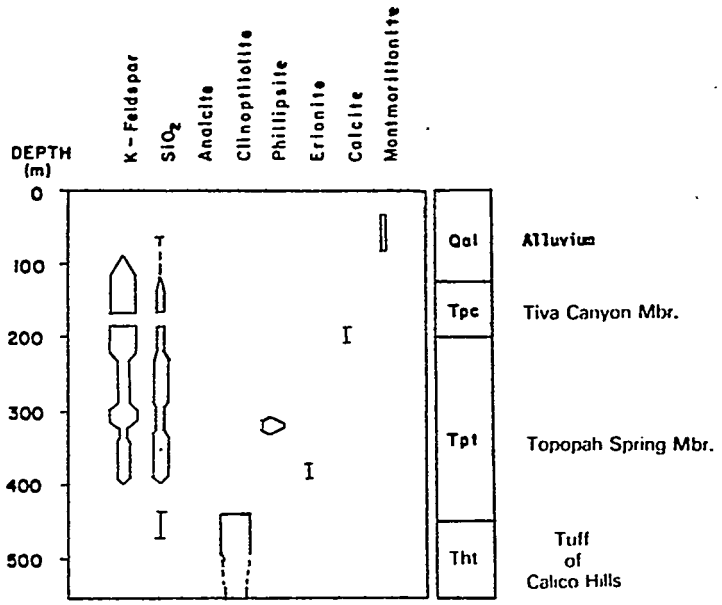

Figure A.3.1-3. Distribution of authigenic minerals in the section penetrated by drill hole J-13. Width of a column is qualitative representation of the abundance of a particular authigenic phase (from Heiken and Bevier, 1979)

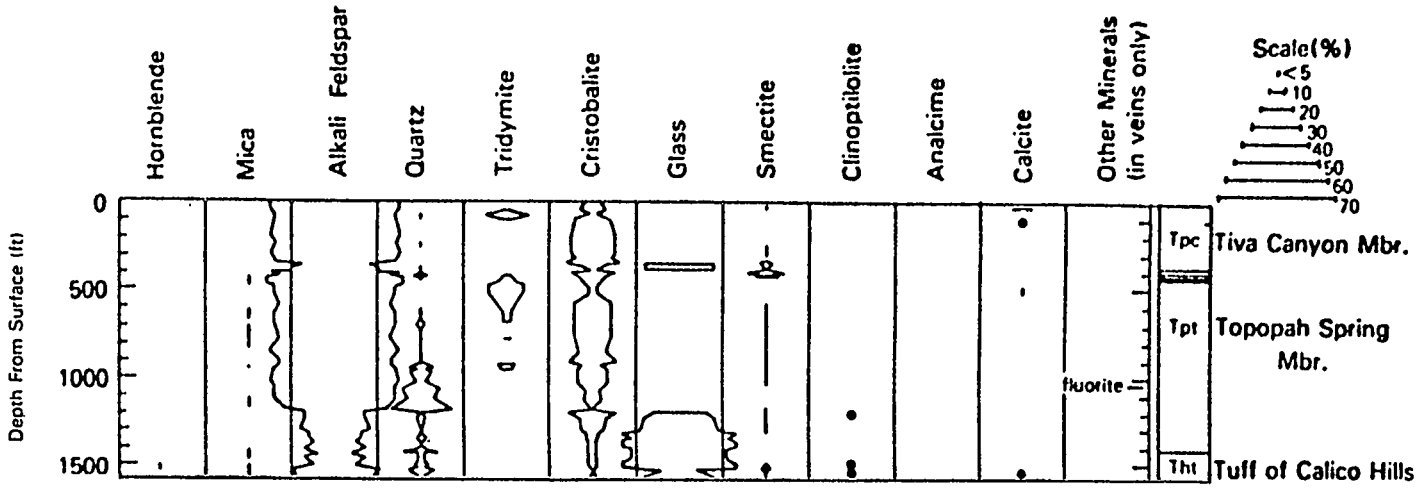

Figure A3.1-4. Mineral abundance in drill hole USW-GU3/G3. Mineral abundances determined by X-ray diffraction techniques (Bish and others, 1983).

APPENDIX 3.2

X-Ray Diffraction Analysis of Selected Core Samples

Table A3.2-1. X-ray diffraction analyses of Topopah Spring Member in drill hole USW-G1 (after Bish and others, 1981)

Depth of Sample	Montmorillonite	Illite Muscovite	Clinoptilolite	Quartz	Cristobalite/Opal	Alkali Feldspar	Calcite	Glass	Tridymite	Comment
292	–	2–5	–	–	30–40	40–70	–	–	–	
352	–	Tr	–	–	20–30	40–70	–	–	5–10	
399	Tr	Tr?	–	–	25–40	40–70	–	–	10–15	
450A	10–20	Tr?	–	–	Tr	30–40	–	–	40–60	Lithophysal linings
450B	2–5	Tr	–	Tr	30–40	25–40	–	–	10–20	Bulk
504A	5–10	–	–	10-20	2–5	20–30	–	–	40–60	Lithophysal linings
504B	5–10	–	–	20-40	2–5	20–30	–	–	30–50	Lithophysal linings
504C	5–10	Tr	–	–	40–60	30–40	–	–	5–10	Bulk possible contam.
553A	2–5	–	–	2–5	30–50	30–40	–	–	–	Bulk
553B	10–15	–	–	10-20	10–20	30–40	–	–	20–30	Cavity lining contam.
619A	5–10	–	Tr	20–40	5–10	20–30	–	–	30–40	Lithophysal lining; Str. contam.
619B	5–10	–	–	5–10	30–50	30–40	–	–	Tr	Bulk
673	2–5	Tr	–	10–20	25–45	30–45	–	–	Tr?	
722A	10–15	–	–	Tr	25–45	30–40	–	–	–	Bulk
722B	10–15	–	15–25	Tr?	20–40	10–20	–	–	–	Fracture lining contam. v. slight
757A	Tr	–	–	2-5	30–50	30–50	–	–	–	Bulk
757B	x	x	–	x	x	–	–	–	x?	Fracture lining contam.

Table A3.2-1. X-ray diffraction analyses of Topopah Spring Member in drill hole USW-G1--concluded

Depth of Sample	Montmorillonite	Illite Muscovite	Clinoptilolite	Quartz	Cristobalite/Opal	Alkali Feldspar	Calcite	Glass	Tridymite	Comment
819	2-5	-	-	2-5	30-50	30-40	-	-	Tr?	
874	Tr	-	-	25-40	10-15	30-45	-	-	-	
936A	2-5	-	-	20-40	Tr	5-10	30-50	-	-	Vein(?)
936B	Tr	-	-	35-60	5-10	20-40	-	-	-	Bulk
995A	5-10	-	-	20-40	-	20-30	-	-	20-35	Cavity lining contam.
995B	30-40	Tr	-	2-5	30-50	25-40	-	-	-	Bulk
1063	2-5	-	-	10-15	30-50	25-40	-	-	-	
1104A	10-15	-	-		10-15	20-30	-	-	20-30	Fracture lining contam.
1104B	5-10	-	-	10-20	30-50	25-40	-	-	-	Bulk
1123	5-10	-	-	10-20	30-45	25-40	-	-	-	
1179	2-5	Tr	-	10-20	40-60	30-50	Tr	-	-	
1191	5-10	Tr	-	10-20	30-60	20-40	Tr	-	-	
1240	2-5	-	-	10-20	20-30	30-50	-	-	-	
1274	-	-	-	10-20	30-50	30-50	-	-	-	
1281A	5-10	Tr	-	2-5	50-80	10-20	-	-	-	Cavity lining
1281B	2-5	-	-	15-25	30-60	30-50	-	-	-	Bulk
1286	20-30	-	10-20	Tr	25-40	10-20	-	-	-	
1292	Tr	-	-	-	5-10	5-10	-	80-90	-	
1319	-	-	-	Tr	Tr	2-5	-	80-95	-	
1341	-	-	-	Tr	2-5	2-5	-	80-90	-	
1357	Tr	Tr	-	Tr	5-15	5-10	-	75-90	-	
1392	Tr	-	5-10	Tr	Tr	Tr	-	80-95	-	
1400	Tr	Tr	60-90	5-10	5-10	5-15	-	-	-	
1436	-	Tr	65-85	10-20	2-5	5-10	-	-	-	
1492	Tr	-	50-80	2-5	2-5	5-10	-	-	-	
1539	Tr	-	30-50	5-10	2-5	30-50	-	-	-	
1561	Tr	-	60-85	10-20	2-10	10-20	-	-	-	
1639	10-20	Tr	60-90	2-5	2-5	2-5	-	-	-	
1693	Tr	-	40-70	5-10	5-15	15-25	-	-	-	
1748	-	-	40-60	5-10	20-30	15-30	-	-	-	
1774	Tr	Tr	30-70	10-20	2-5	20-30	-	-		
1784	Tr?	5-10	15-30	15-30	5-10	30-50	-	-	-	
1799	Tr	Tr	40-70	5-10	15-25	5-10	-	-	-	

Table A3.2-2. X-Ray diffraction analyses of tuffs from drill hole USW-G2 (Wt.%) (after Caporuscio and others, 1982)

Depth (m)	Smectite	Mica	Clinoptilolite	Mordenite	Quartz	Cristobalite	Alkali Feld spar	Calcite	Other
3.0		5-10				30-50	30-50		10-20[b]
30.5		<5				30-50	30-50		10-25[b]
61.0						30-50	30-50		5-15[b]
70.1						30-50	30-50		5-15[b]
82.3	2-10					30-50	30-50	15-30	
92.7					5-10	30-50	30-50		10-20[b]
100.9	30-50						30-50	10-20	
103.0	40-60						5-10		30-50[c]
109.1	15-30				Tr.	5-10	20-40		20-40[c]
120.4	5-15	<2			<5	10-20	15-30		30-50[c]
152.7	5-20	<3				5-10	10-20		40-60[c]
166.7	5-15	<5				5-15	10-20		40-60[c]
167.0		<5	5-10		20-40	30-50			
171.0	10-20	<3	10-20			20-40	25-40		
191.1	5-15	<5		10-20		20-40	30-50		
205.7	30-50	<5	15-30			5-10	15-30		
220.4	5-15	<5				<5	5-10	30-50	15-30[c]
226.5	30-50	<5	<5		5-15	5-15	10-20	5-15	15-30[c]
232.3	2-5		75-90			5-15	<5		10-20[b]
234.7	<2	5-10				15-30	60-80		
250.5	5-10	<5				20-40	30-50		10-20[b]
260.6	<5	2-5				20-40	30-50		5-15[b]
273.7	<2	2-5	<5			20-40	40-60		5-10[b]
280.7	10-20				20-40	15-30	20-40	5-10	
289.9	<2				15-30	20-40	20-40		
299.9	2-10				15-30	10-20	15-30	15-30	
314.6	2-10	<2			15-30	20-40	20-40		
326.7	2-10	<2			20-40	5-15	30-50		
345.3	5-15	<2			15-30	20-40	40-60		
359.1	<5	<2			10-25	20-40	30-50		
376.1	2-10				10-25	20-40	30-50		
390.4	5-15				15-30	15-30	30-50		

Table A3.2-2. X-Ray diffraction analyses of tuffs from drill hole USW-G2 (Wt.%)--concluded

Depth (m)	Smectite	Mica	Clinoptilolite	Mordenite	Quartz	Cristobalite	Alkali Feldspar	Calcite	Other
405.7	5-15				15-30	20-40	30-50		
421.2	5-15	2			15-30	15-30	40-60		
432.8	5-15				15-30	20-40	30-50		
445.3	5-15				10-20	30-50	30-50		
468.2	10-20		5		10-20	30-50	30-50		
483.1	5-15		5		10-25	20-40	30-50		
498.0	30-50	2	30-50			15-30			
507.2	2		2		5-10	5-10	10-20		50-70[c]
515.4	5-15		40-60	5-10		15-25	5-15		
531.9	10-20		30-50	5-10	5-10	15-30	10-20		
534.0	5-15		50-70	5-10	5	5-15	5-10		
548.0	2		40-60	15-30	5-15	10-20	15-30		
563.3			40-60	15-30	Tr.	15-30	10-20		
578.8	2	2	40-60	15-30	5-10	10-20	10-20		
595.0		5	5-10	40-60	10-20	10-20	10-20		
609.9		2	5-10	40-60	10-20	10-20	15-30		
633.4	5	5	20-40	20-40	5-10	10-20	10-20		
657.8	5	5	20-40	15-30	5-10	15-30	10-20		
685.2	5	2	20-40	20-40	5-15	15-30	15-30		
717.2	2	2-10	5-15	20-40	15-30	15-30	10-20		
740.7	5	5-15	20-40	5-15	20-40	0-10	20-40		
770.5	5	5-15	5	15-30	20-40	5	20-40		
812.9	5	5-10		20-40	15-30	5	30-50		

b Fluorite

c Todorokite $(Mn^{+2}, Ca, Mg)\ Mn_3^{+4}\ O_7 \cdot H_2O$

Table A3.2-3. X-Ray diffraction analyses of tuff samples in Topopah Spring Member from drill hole UE25a-1 (% sample) (after Carroll and others, 1981)

Depth (m)	Depth (ft)	Smectite	Mica	Clino-ptilolite	Morden-ite	Quartz	Cristo-balite	Alkali Feldspar	Glass	Tridymite
84	277	~5	5–15	–	–	–	–	15–30	55–80	–
102	335	<5	5–15	–	–	–	5–20	50–70	–	5–15
137	450	5–15	–	–	–	5–10	5–20	40–60	–	–
143	469	5–15	–	–	–	5–10	5–20	40–60	–	–
Clay Fraction 10±10% illite randomly interstratified with montmorillonite										
206	667	5–10	–	–	–	40–50	5–15	40–50	–	–
Clay Fraction 35±10% illite randomly interstratified with montmorillonite										
223	733	5–10	<5	–	–	40–50	5–15	40–50	–	–
227	744	5–10	<5	–	–	30–40	5–20	40–60	–	–
255	836	5–10	–	–	–	40–60	–	40–60	–	–
258	848	5–10	–	–	–	40–60	–	40–60	–	–
268	879	5–15	<5	–	–	40–60	–	40–60	–	–
272	894	5–10	–	–	–	40–60	–	40–60	–	–
286	937	<5	–	–	–	40–60	–	40–60	–	–
308	1012	<5	~5	–	–	40–60	–	40–60	–	–
323	1061	<5	–	10	–	50–60	–	30–50	–	–
339	1112	5–15	5–10	–	–	40–60	–	40–60	–	–
351	1153	5–15	–	–	–	40–60	–	35–55	–	–
364	1195	5–10	–	–	–	40–60	–	40–60	–	–
385	1264	5–10	~5	5–10	–	40–60	5–15	30–50	–	–
390	1279	10–20	–	10	–	10	10–20	5–15	50–80	
Clay Fraction 20±10% illite randomly interstratified with montmorillonite										
403	1324	5–15	–	60–80	~	5–10	–	5–10	–	–
Clay Fraction 25±10% illite randomly interstratified with montmorillonite										
414	1358	~5	–	60–80	5–10	5–15	–	5–10	–	–
421	1382	~5	–	50–70	30–50	–	–	–	–	–

APPENDIX 3.3

Lithology and Mineral Zones in Selected Drill Holes

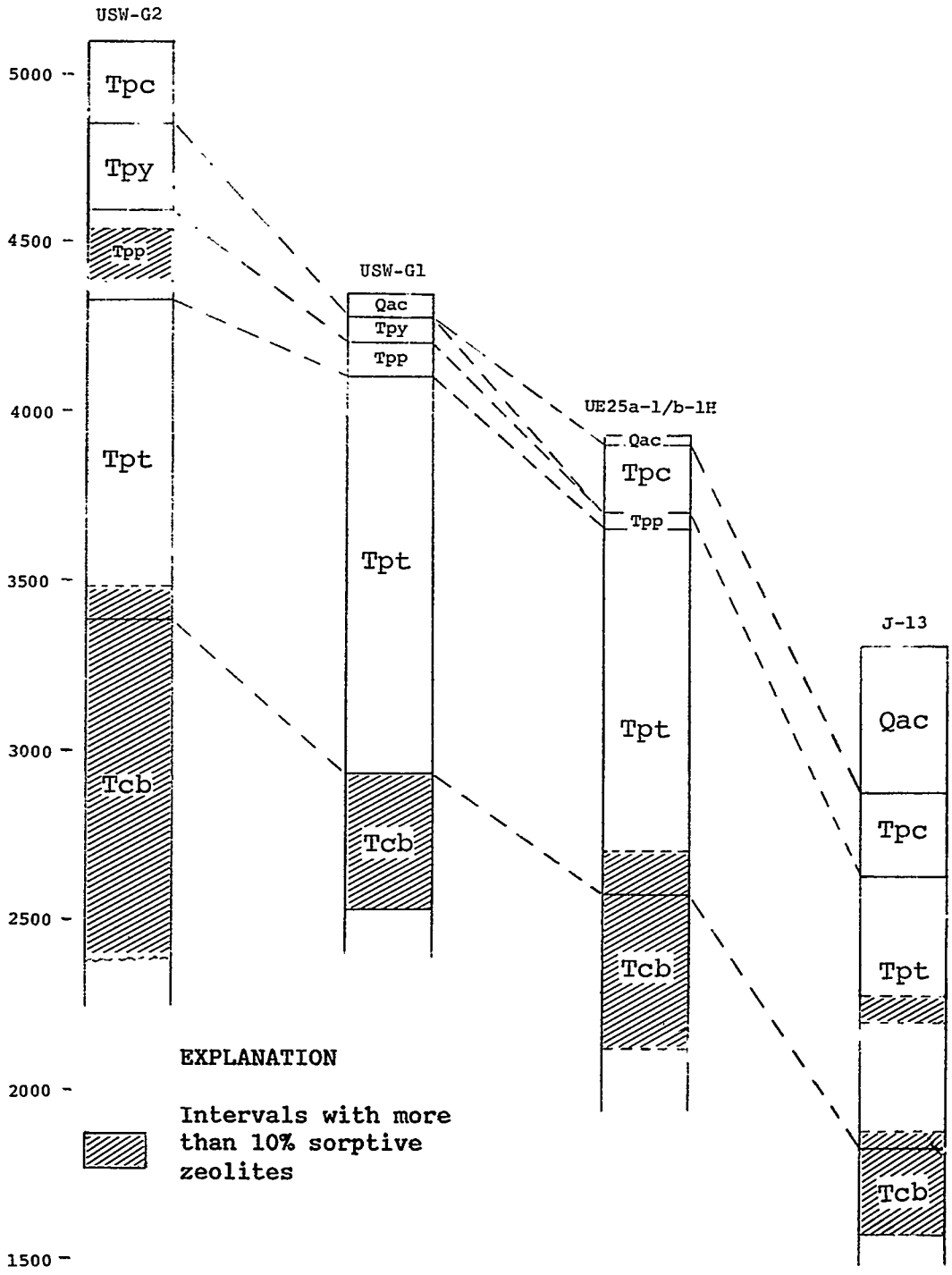

Figure A3.3-1. Comparative stratigraphy and the occurrence of sorptive zeolites in selected drill holes at Yucca Mountain (after Bish and others, 1982).

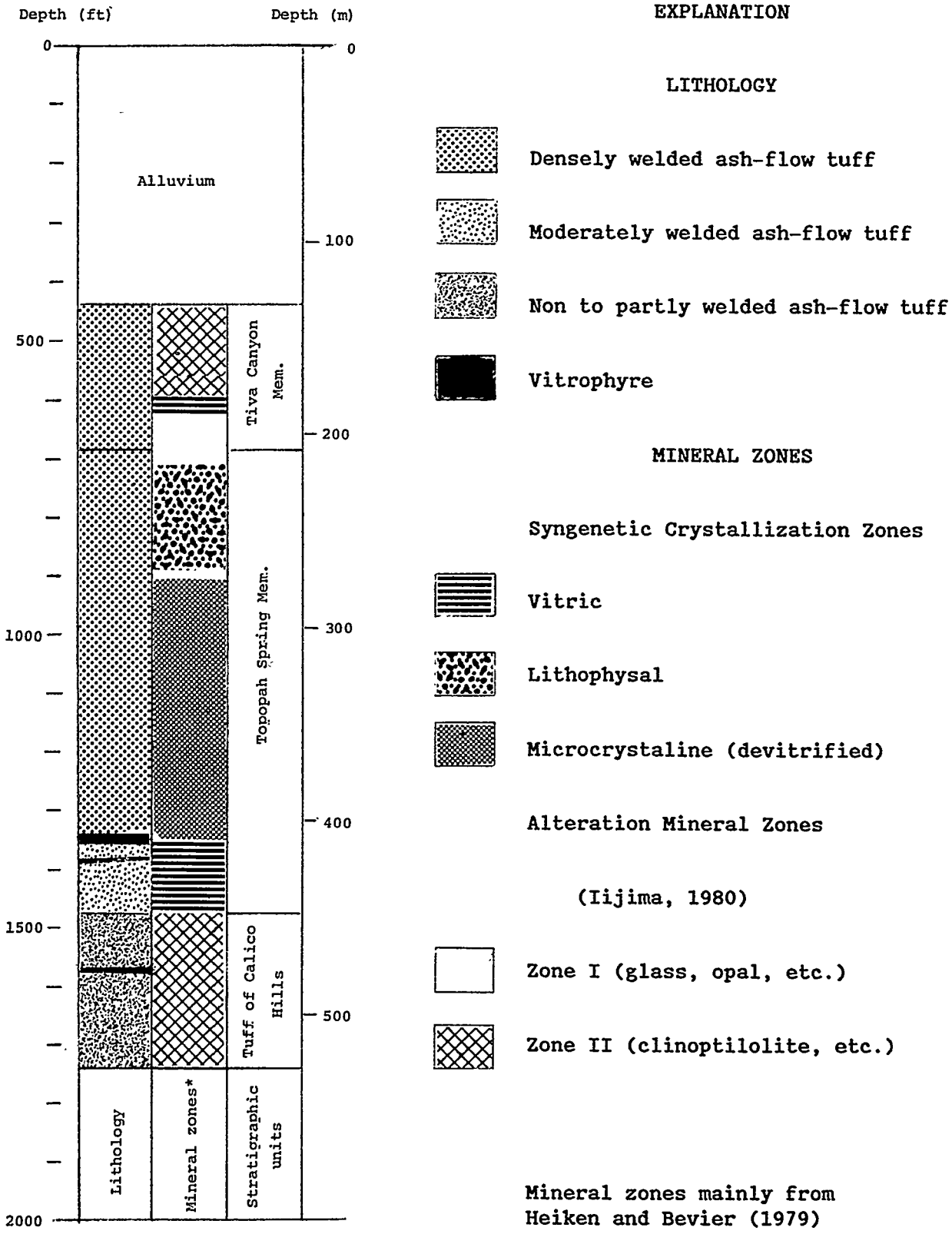

Figure A3.3-2. Summary diagram of lithology and mineral zones in drill hole J-13 (Bish and others, 1982).

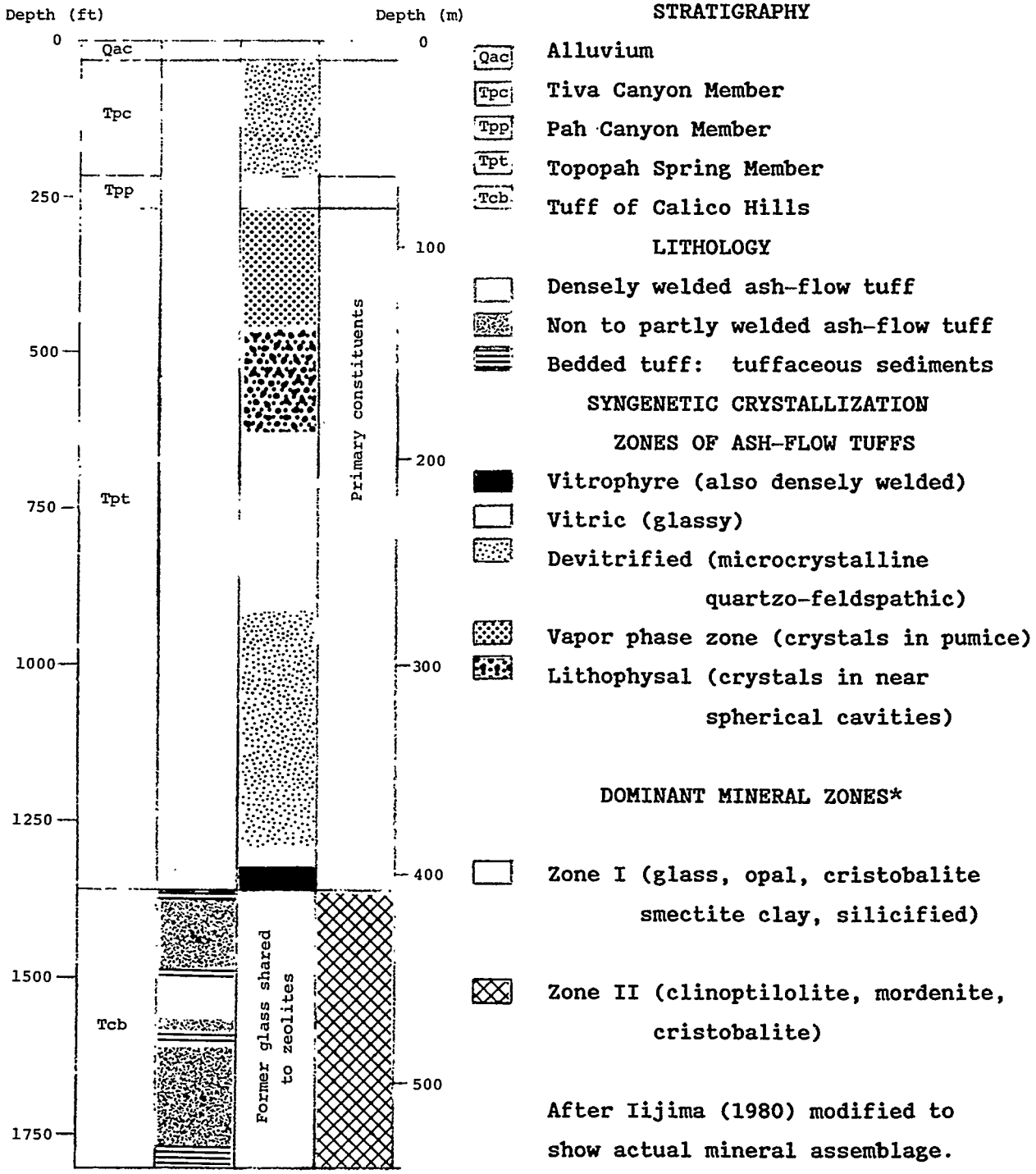

Figure A.3.3-3. Summary diagram of lithology, mineral zones in drill holes UE25a-1 and UE25b-1H (after Bish and others, 1982).

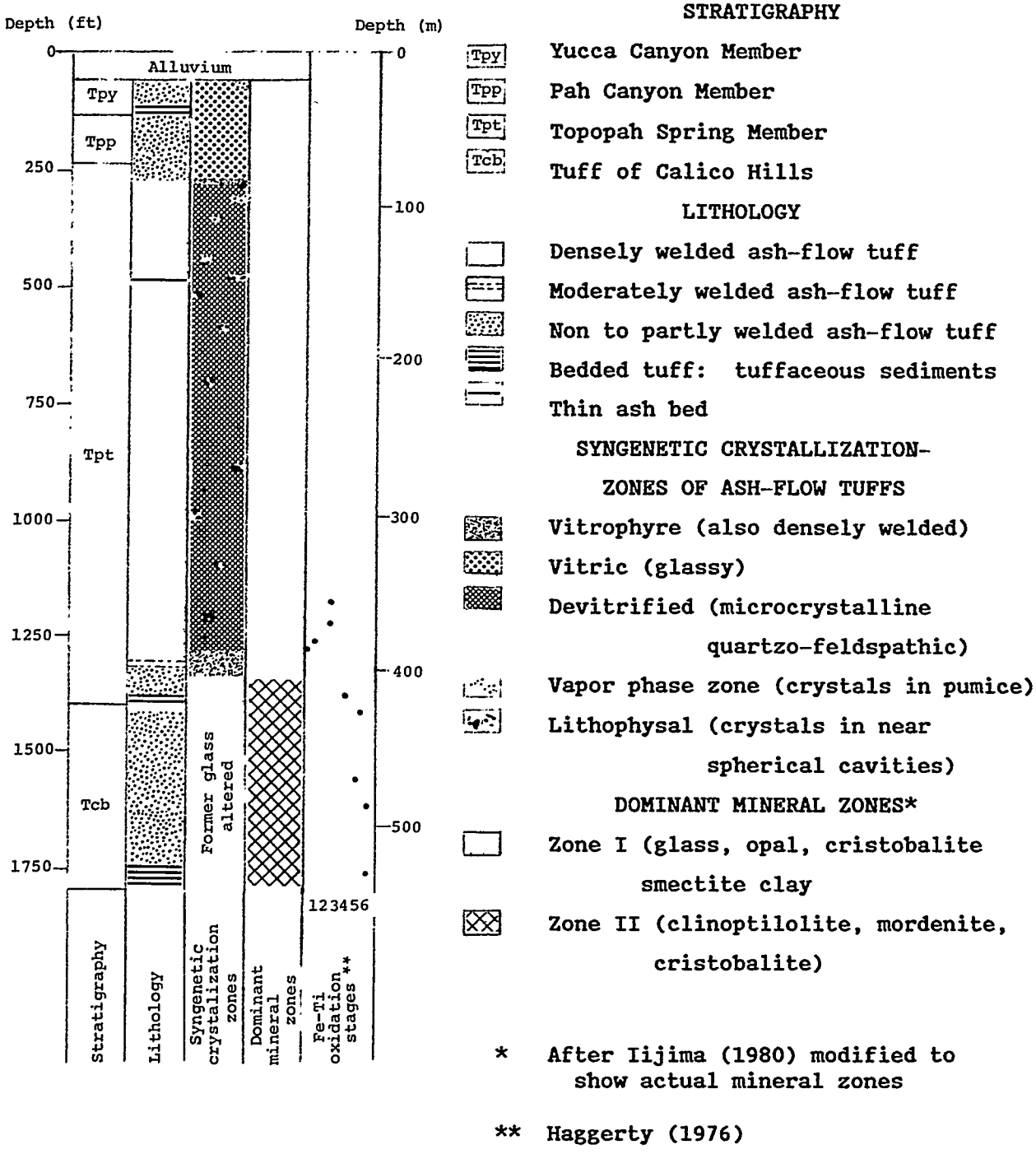

Figure A.3.3-4. Summary diagram of lithology, mineral zones, and Fe-Ti oxidation stages in drill hole USW-G1 (after Bish and others, 1982).

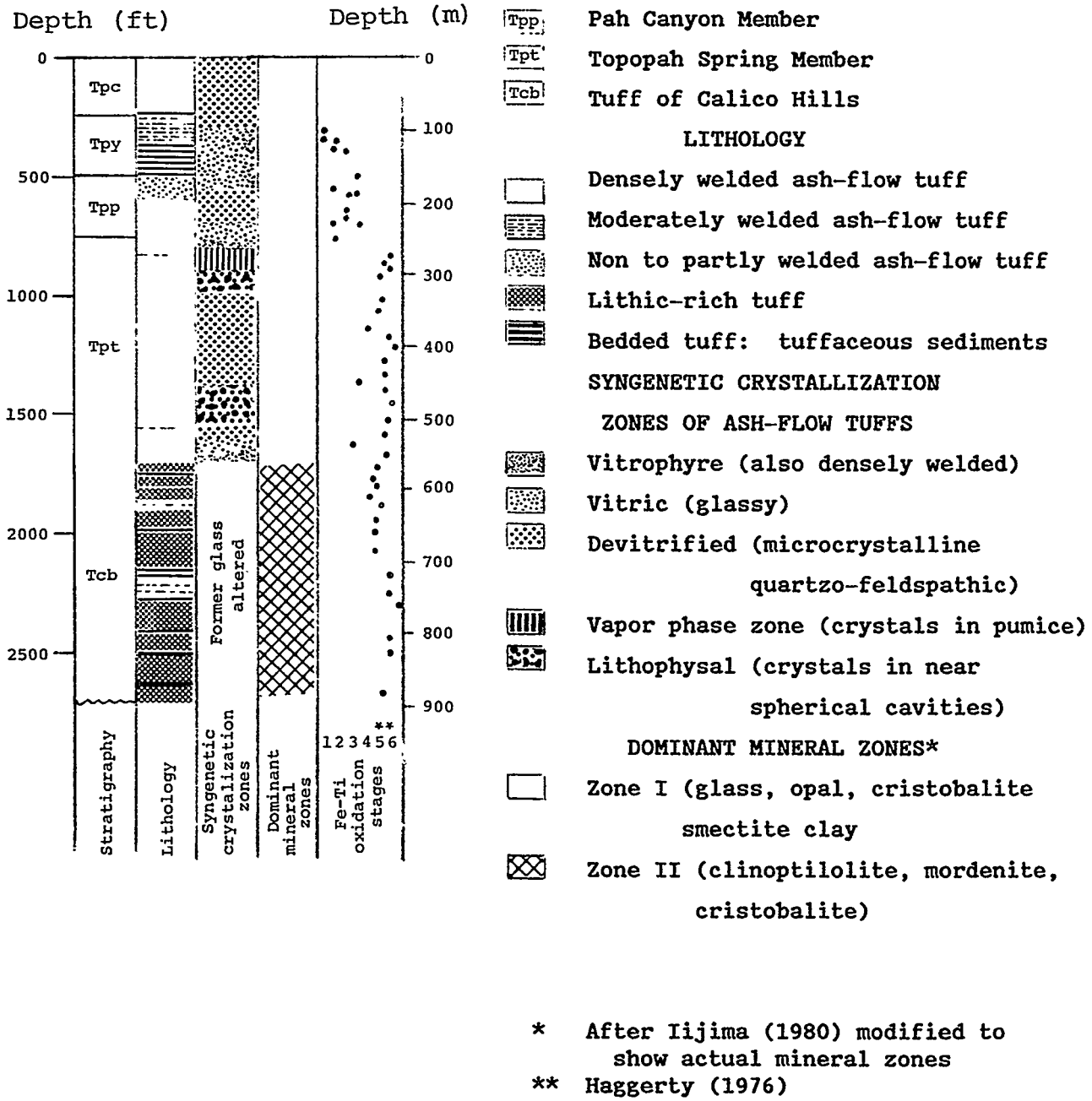

Figure A3.3-5. Summary diagram of lithology, mineral zones, and Fe-Ti oxidation stages in drill hole USW-G2 (after Bish and others, 1982).

APPENDIX 3.4

Zeolite Zone Mineralogy for Alkali and Calcic Zeolite Series (after Iijima [1980] by Smyth [1982])

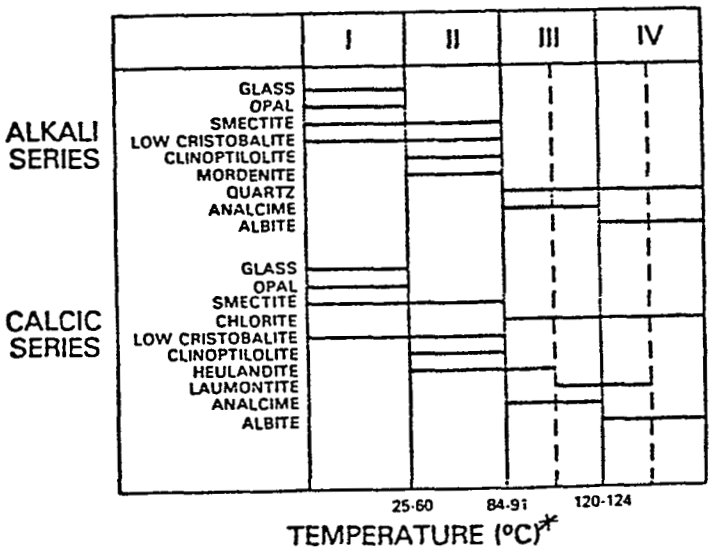

*Approximate temperatures of boundaries between zones at bottom of figure are given for marine tuffs with high concentration of Na^+ in pore fluid (Iijima and Ohwa, 1980).

APPENDIX 5.1

Compositions of Ground Waters from Yucca Mountain and Vicinity

Table A5.1-1. Elemental concentrations in ground waters from the vicinity of Yucca Mountain ((Ogard and Kerrisk, 1984)

Well No.	Field pH	Concentration[a] (mg/ℓ) Ca	Mg	Na	K	Li	Fe	Mn	Al	Si
USW VH-1[b]	7.5	10	1.5	80	1.9	0.090				23
USW H-6	7.4	5.5	0.22	74	2.1	0.10	0.12	0.04	0.12	20.0
USW H-3	9.4	0.8	0.01	124	1.5	0.22	0.13	0.01	0.51	16.9
USW H-5	7.1	1.1	0.03	54	2.3	0.04	0.01	N.D.	0.17	17.4
USW G-4	7.1	9.2	0.15	56	2.5	0.08	0.04	0.02	0.02	19.6
USW H-1[b]	7.5	6.2	<0.1	51	1.6	0.04				19
USW H-4	7.4	10.8	0.19	84	2.6	0.16	0.03	0.005	0.04	25.9
UE-25b#1[c]	7.7	19.7	0.68	56	3.3	0.28	0.04	0.004	0.03	31.5
UE-25b#1[d]	7.2	18.4	0.68	46	2.5	0.30	0.69	0.36	0.04	28.7
UE-25b#1[e]	7.3	17.9	0.66	37	3.0	0.17	0.08	0.07	0.06	28.8
J-13	6.9	11.5	1.76	45	5.3	0.06	0.04	0.001	0.03	30.0
UE-29a#2	7.0	11.1	0.34	51	1.2	0.10	0.05	0.03	0.04	25.8
J-12[b]	7.1	14	2.1	38	5.1					25
UE-25p#1	6.7	87.8	31.9	171	13.4	0.32	<0.1	<0.1	0.1	30

a. Ionic or molecular species are not listed; concentration is based on the element.
b. Data from Benson and others (1983).
c. Integral water sample.
d. Bullfrog zone, 4th day.
e. Bullfrog zone, 28th day.

Table A5.1-2. Anion concentrations and other measurements for ground waters from the vicinity of Yucca Mountain (Ogard and Kerrisk, 1984)

Well No.	Concentration (mg/ℓ) F^-	Cl^-	SO_4^{2-}	HCO_3^-	NO_2^-	NO_3^-	O_2	Detergent	Eh[a]
USW VH-1[b]	2.7	10	45	165					
USW H-6	4.1	7.7	27.5		N.D.[c]	5.3	5.6		395
USW H-3	5.4	8.3	31.2		<0.10	0.2	<0.1	<0.02	-143
USW H-5	1.3	5.7	14.6		N.D.	8.6	6.3	<0.005	353
USW G-4	2.4	5.5	15.7		N.D.	5.5	6.4		402
USW H-1[b]	1.0	5.8	19	122					
USW H-4	4.5	6.2	23.9		N.D.	4.7	5.8	>2	216
UE-25b#1[d]	1.2	7.1	20.6		N.D.	0.6	1.8		220
UE-25b#1[e]	1.5	9.8	21.0		0.5	2.2	<0.1	2.7	-18
UE-25b#1[f]	1.2	6.6	20.3		N.D.	4.5	1.8	0.02	160
J-13	2.1	6.4	18.1		N.D.	10.1	5.7	N.D.	
UE-29a#2	0.56	8.3	22.7		N.D.	18.7	5.7		305
J-12[b]	2.1	7.3	22	119					
UE-25p#1	3.5	37	129		N.D.	<0.1		<0.2	360

a. mV vs. H_2 electrode.
b. Data from Benson and others (1983).
c. Not detected.
d. Integral water sample.
e. Bullfrog zone, 4th day.
f. Bullfrog zone, 28th day.

Table A5.1-3. Compositions of ground waters from Yucca Mountain wells "thief samples" (Ogard and Kerrisk, 1984)

Well No. Depth (m)	pH	Concentration (mg/ℓ) Ca	Mg	Na	K	Li	Fe	Mn	Al	Si
USW H-1										
610	7.2	3.5	0.20	106	6.4	0.07	0.02	0.11	0.02	3.6
915	7.0	5.2	0.09	153	1.4	0.09	0.14	0.08	0.03	11.5
1220	8.0	1.7	0.07	166	1.4	0.11	0.03	0.04	0.02	12.9
1800	7.6	6.2	0.15	120	2.2	0.14	0.21	0.15	0.02	16.1
USW H-4										
628	8.7	8.0	0.35	114	4.1	0.26	0.05	0.09	0.04	11.3
683	8.6	7.3	0.21	107	3.5	0.34	0.12	0.10	0.04	26.4
721	8.6	8.3	0.23	109	3.4	0.40	0.20	0.08	0.06	26.5
792	8.4	12.4	0.25	105	3.2	0.38	0.86	0.13	0.05	26.3
869	9.6	3.9	0.14	99	3.8	0.33	0.01	<0.01	0.06	26.4
908	8.6	12.8	0.25	92	3.5	0.27	<0.05	0.08	0.08	25.9
1036	8.7	11.4	0.22	93	3.2	0.26	0.16	0.08	0.09	25.4
1187	8.6	7.7	0.16	98	3.3	0.21	<0.05	0.09	0.06	26.0
USW H-1[a] integral	7.5	6.2	<0.1	51	1.6	0.04				19
USW H-4 integral	7.4	10.8	0.19	84	2.6	0.16	0.03	0.005	0.04	25.9

a. Data from Benson and others (1983).

Table A5.1-4. Compositions of ground waters from Yucca Mountain wells "thief samples" (Ogard and Kerrisk, 1984)

Well No. Depth (m)	Concentration (mg/ℓ)								Alkalinity (meq/ℓ)
	F^-	Cl^-	SO_4^{2-}	NO_2^-	NO_3^-	O_2	S^{2-}	Eh[a]	
USW H-1									
610	12.7	24.6	13.9	N.D.	N.D.	3.4	N.D.	270	3.49
915	17.7	8.3	34.4	N.D.	N.D.	1.3	6.4×10^{-2}	-40	5.86
1220	13.1	8.4	60.9	N.D.	N.D.	1.2	6.4×10^{-5}	-25	5.90
1800	16.8	9.5	50.0	N.D.	N.D.	<1.2	3.2×10^{-2}	-150	4.25
USW H-4									
628	5.4	7.6	32.0	N.D.	N.D.	0.1	6.4×10^{-1}	-160	2.96
683	4.2	7.8	24.4	N.D.	N.D.	<0.1	32	-158	2.69
721	3.3	7.3	25.0	N.D.	N.D.	0.1	33	-190	2.75
792	3.0	7.6	24.8	N.D.	N.D.	<0.1	6	-177	2.70
869	4.4	8.8	27.6	<0.1	0.2	<0.1	6	-191	2.23
908	2.8	7.3	25.5	N.D.	1.3	<0.1	6.4×10^{-2}	-160	2.46
1036	2.9	7.1	24.2	N.D.	<0.5	<0.1	6	-171	2.53
1181	2.7	7.0	24.1	N.D.	<0.5	<0.1	6	-159	2.42
USW H-1[b] integral	1.0	5.8	19						2.00
USW H-4 integral	4.5	6.2	23.9	N.D.	4.7	5.8	N.D.	216	2.82

a. mV vs. H_2 electrode.
b. Data from Benson and others (1983).

Table A5.1-5. Composition of waters from Rainier Mesa and Oasis Valley, Nevada (mmoles/liter) (Guzowski and others, 1983)

	Rainier Mesa (1)	(2)	Oasis Valley (3)	(4)
Na	1.18	2.13	6.10	12.62
K	0.14	0.07	0.17	0.26
Ca	0.41	0.09	0.45	0.95
Mg	0.11	0.02	0.07	0.23
HCO_3	1.81	1.34	3.68	7.20
SO_4	0.15	0.35	1.12	2.60
Cl	0.22	0.45	1.27	2.82
F	0.01	--	0.24	0.33
SiO_2	1.04	0.81	0.90	1.12
pH	7.50	7.96	7.95	7.88
$\frac{Na}{Ca+Mg}$	2.27	19.36	11.73	10.69
$\frac{HCO_3}{Cl+SO_4}$	4.89	1.68	1.54	1.33

(1) Mean of 10 analyses of fracture waters from Rainier Mesa that have had little contact with zeolitized tunnel beds (from Table 2 in White and others, 1980).

(2) Mean of 7 analyses of interstitial waters in contact with zeolitized tuffs (analyses 13-19 in Table 1 in White and others, 1980).

(3) Average composition of water in Tertiary rhyolitic tuff aquifer in Oasis Valley (from Tables 2 and 7 in White, 1979).

(4) Water composition at Amargosa Narrows representing "end stage" of evolution of water in Oasis Valley (from Tables 2 and 7 in White, 1979).

Table A5.1-6. Isotopic composition of water samples obtained from wells in the Yucca Mountain area (Benson and others, 1983)

Site designation	Land-surface altitude (m)	Approximate well depth (m)	Approximate depth to water (m)	Interval sampled (m)[a]	Collection date	δD o/oo SMOW[b]	$\delta^{18}O$ o/oo SMOW[c]	$\delta^{13}C$ o/oo PDB[d]	^{14}C, percent modern	^{14}C apparent age (yr B.P.)[e]	HTO[f]
UE-25b#1	1,200.4	1,220	470	---	08/07/81	- 99.5	-13.4	-10.7	----	------	----
UE-25b#1				---	09/01/81	-101	-13.4	-10.4	16.7	14,400	<200
UE-25b#1				(863- 875)	07/20/82	- 99.5	-13.5	- 8.6	18.9	13,400	2
UE-29a#2	1,215.1	422	29	---	01/08/82	- 93.5	-12.8	-12.6	62.3	3,800	37
UE-29a#2				---	01/15/82	- 93.0	-12.8	-13.1	60.0	4,100	37
USW G-4	1,270.0	915	541	---	12/09/82	-103	-13.8	- 9.1	22.0	12,160	---
USW H-1	1,302.2	1,829	572	(572- 687)	10/20/80	-103	-13.4	-----	19.9	13,000	<20
USW H-1				(687-1,829)	12/08/80	-101	-13.5	-11.4	23.9	12,000	<20
USW H-4	1,249.0	1,220	519	---	05/17/82	-104	-14.0	- 7.4	11.8	17,200	<10
USW H-5	1,477.8	1,220	704	---	07/03/82	-102	-13.6	-10.3	18.2	13,700	<200
USW H-5				---	07/26/82	-102	-13.6	-10.3	21.4	12,400	<200
USW H-6	1,306.1	1,220	526	---	10/16/82	-106	-13.8	- 7.5	16.3	14,600	<10
USW VH-1	954.5	762	184	---	02/06/81	----	-----	-----	----	------	---
USW VH-1				---	02/08/81	----	-----	-----	----	------	---
USW VH-1				---	02/11/81	-108	-14.2	- 8.5	12.2	17,000	<20
J-12	953.5	347	225	---	03/26/71	- 97.5	-12.8	- 7.9	32.2	9,100	<220
J-13	1,011.3	1,063	282	---	03/26/71	- 97.5	-13.0	- 7.3	29.2	9,900	<220

a. - indicates entire well bore pumped.
b. δD reported in parts per thousand, % relative to SMOW, standard mean ocean water.
c. $\delta^{18}O$ reported in % relative to SMOW.
d. $\delta^{13}C$ reported in % relative to PDB, Peedee belemaite.
e. ^{14}C age reported in years before present.
f. HTO, tritium reported in picocuries per liter.

Table A5.1-7. Elemental concentration in ground water from Pahute Mesa wells and a well in the Amargosa Desert (Ogard and Kerrisk, 1984)

Well No.	pH	Concentration (mg/ℓ) Ca	Mg	Na	K	Li	Fe	Mn	Al	Si
UE-19e	7.7	0.4	0.1	38	0.9	0.04	<0.01	0.07	<0.01	30
U-20a-2	7.9	5.9	0.2	55	2.2	0.05	<0.01	<0.01	0.02	21
#9[a]	8.1	20.0	2.7	42	9.0					13

	Concentration (mg/ℓ) F^-	Cl^-	SO_4^{2-}	NO_3^-	HCO_3^-
UE-19e	0.7	4.6	8.0	2.8	81
U-20a-2	2.8	10	28	0.7	110
#9[a]		7.5	26.7		

a. Well #9 is located in Amargosa Desert.

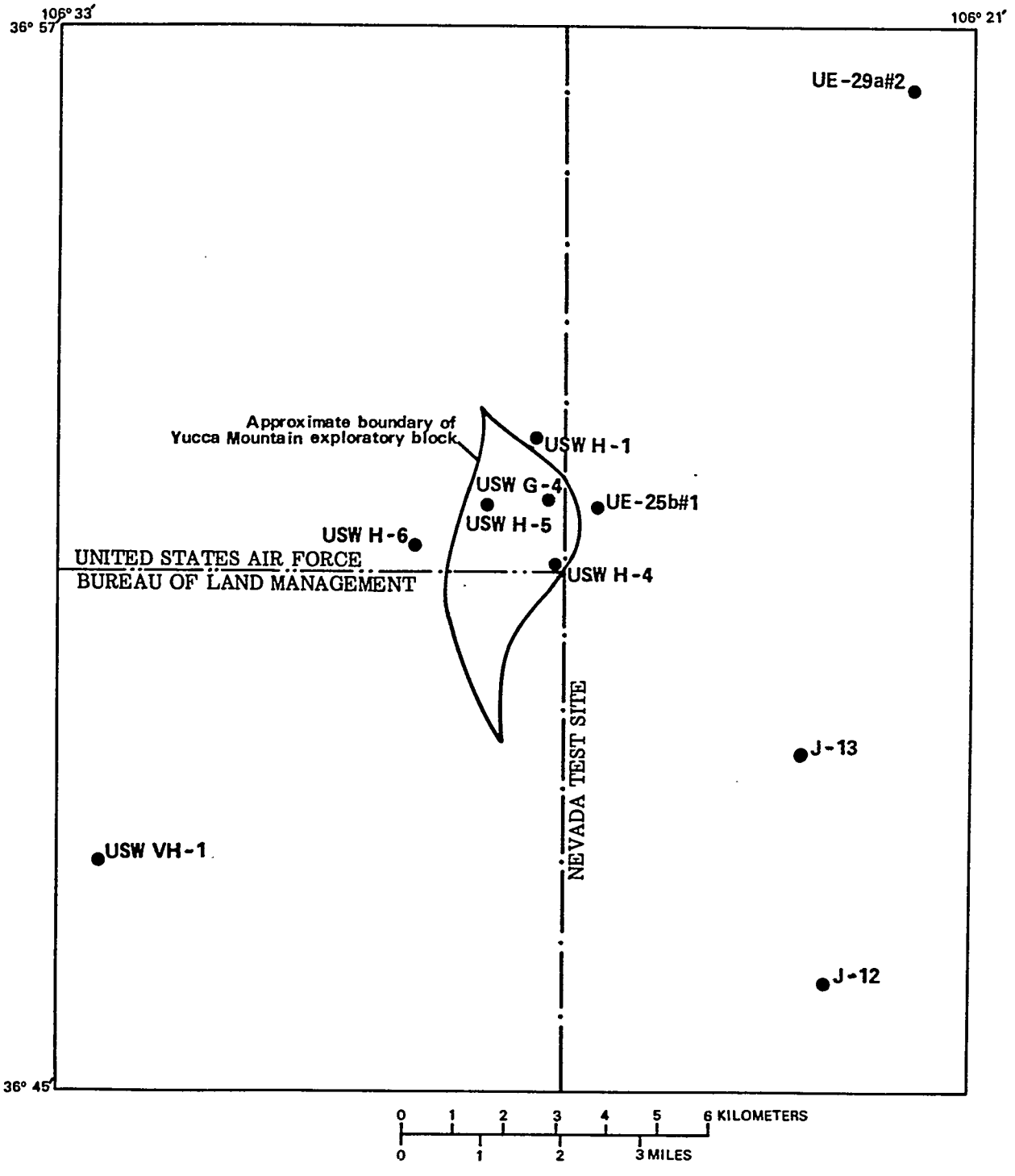

Figure A5.1-1. Selected drill-hole locations on and near the Yucca Mountain exploratory block (Benson and others, 1983).

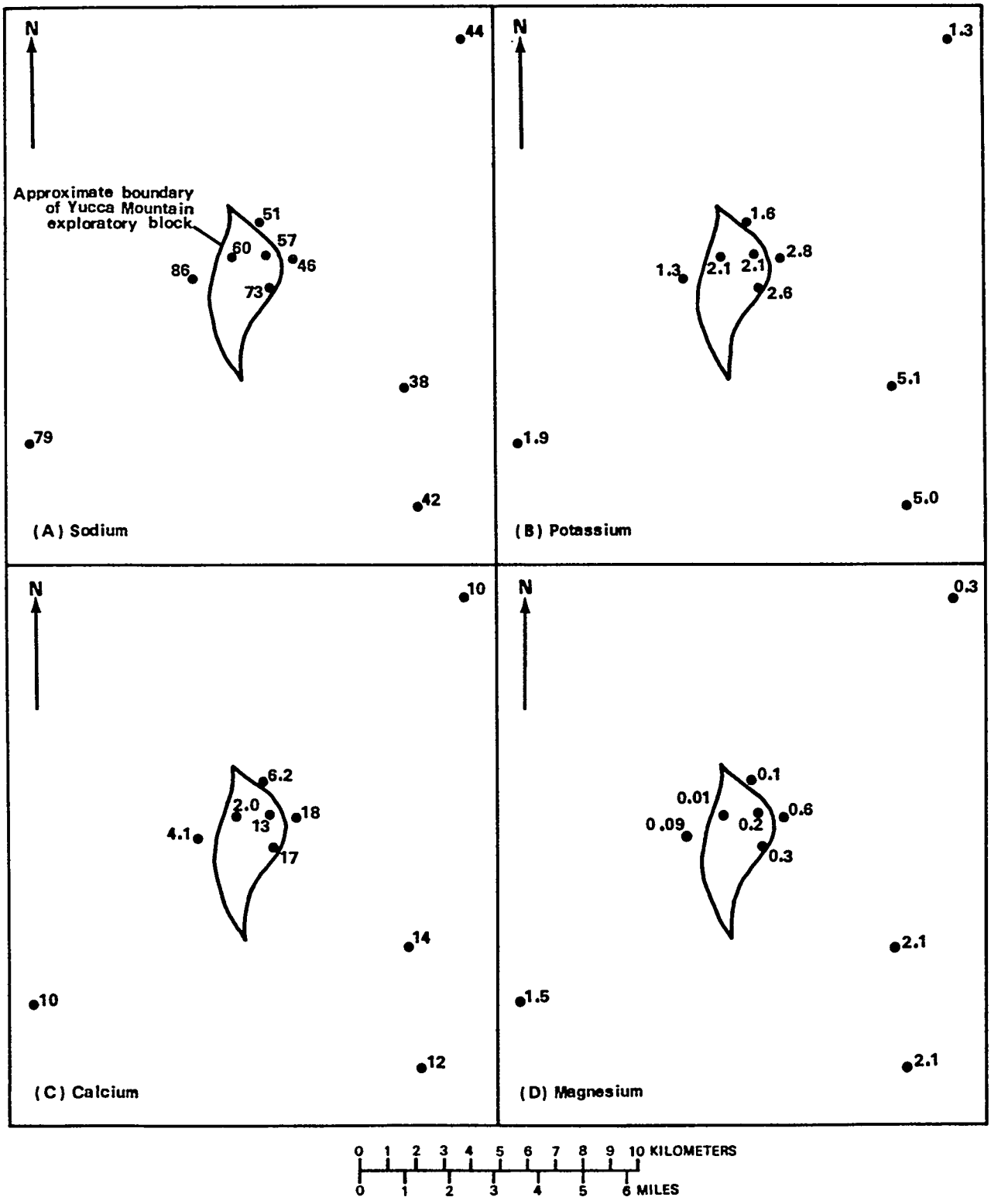

Figure A5.1-2. Sodium, potassium, calcium, and magnesium concentrations, in milligrams/liter, in ground water from the Yucca Mountain area (Benson and others, 1983).

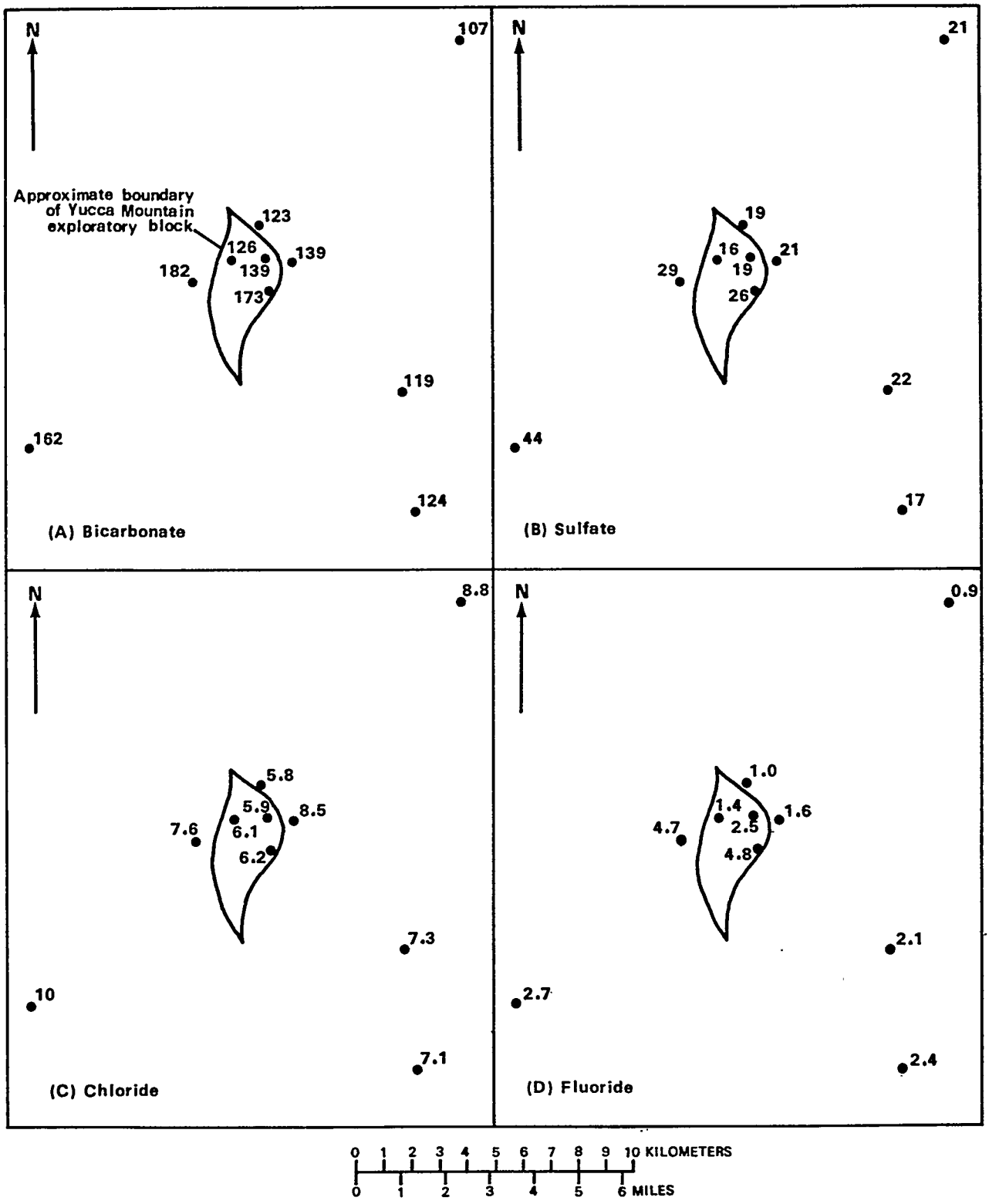

Figure A5.1-3. Bicarbonate, sulfate, chloride, and fluoride concentrations, in milligrams/liter, in ground water from the Yucca Mountain area (Benson and others, 1983.

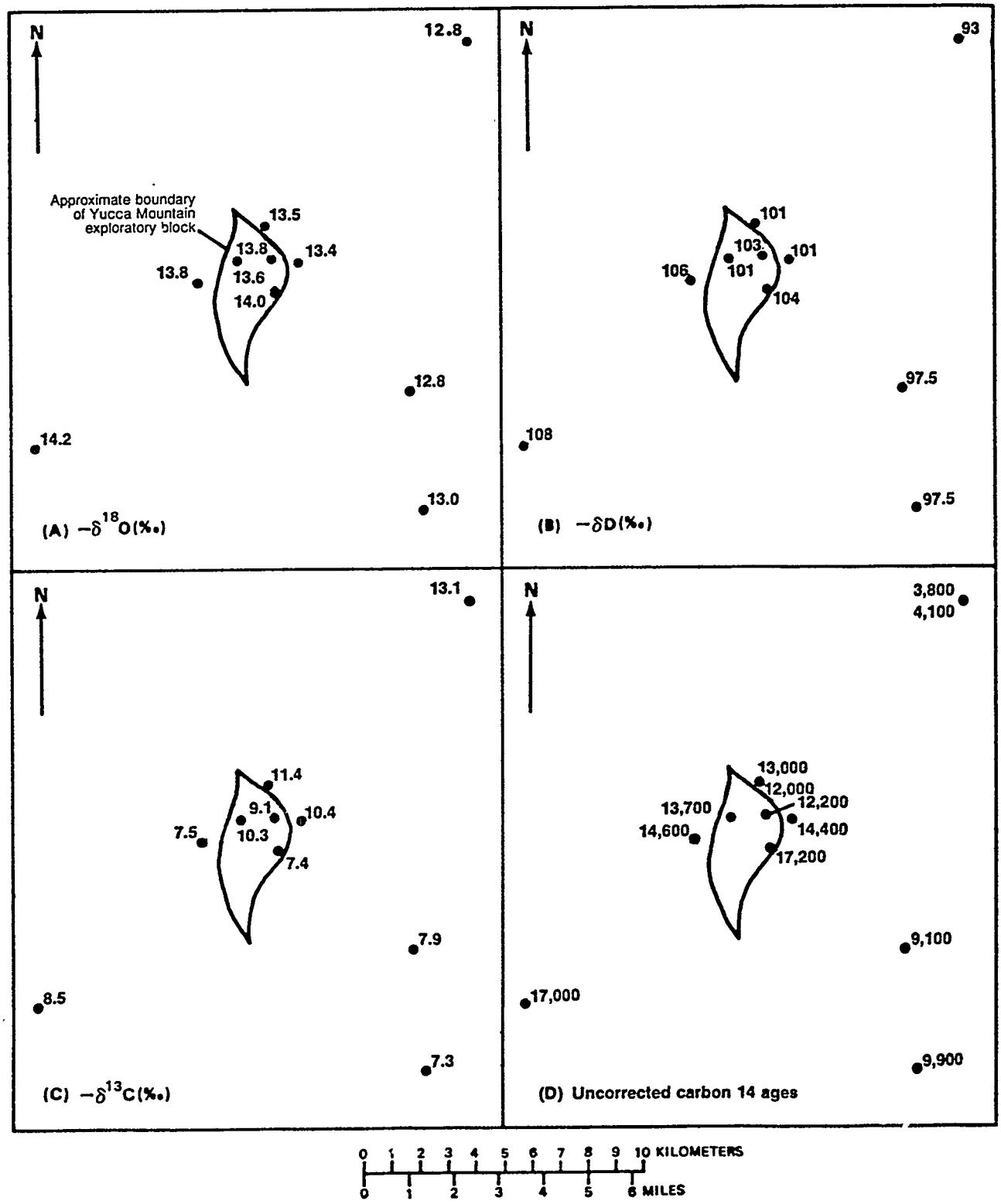

Figure A5.1-4. Del oxygen-18 ($\delta^{18}O$), δD, $\delta^{13}C$, and uncorrected ^{14}C ages for ground water from the Yucca Mountain area (Benson and others, 1983).

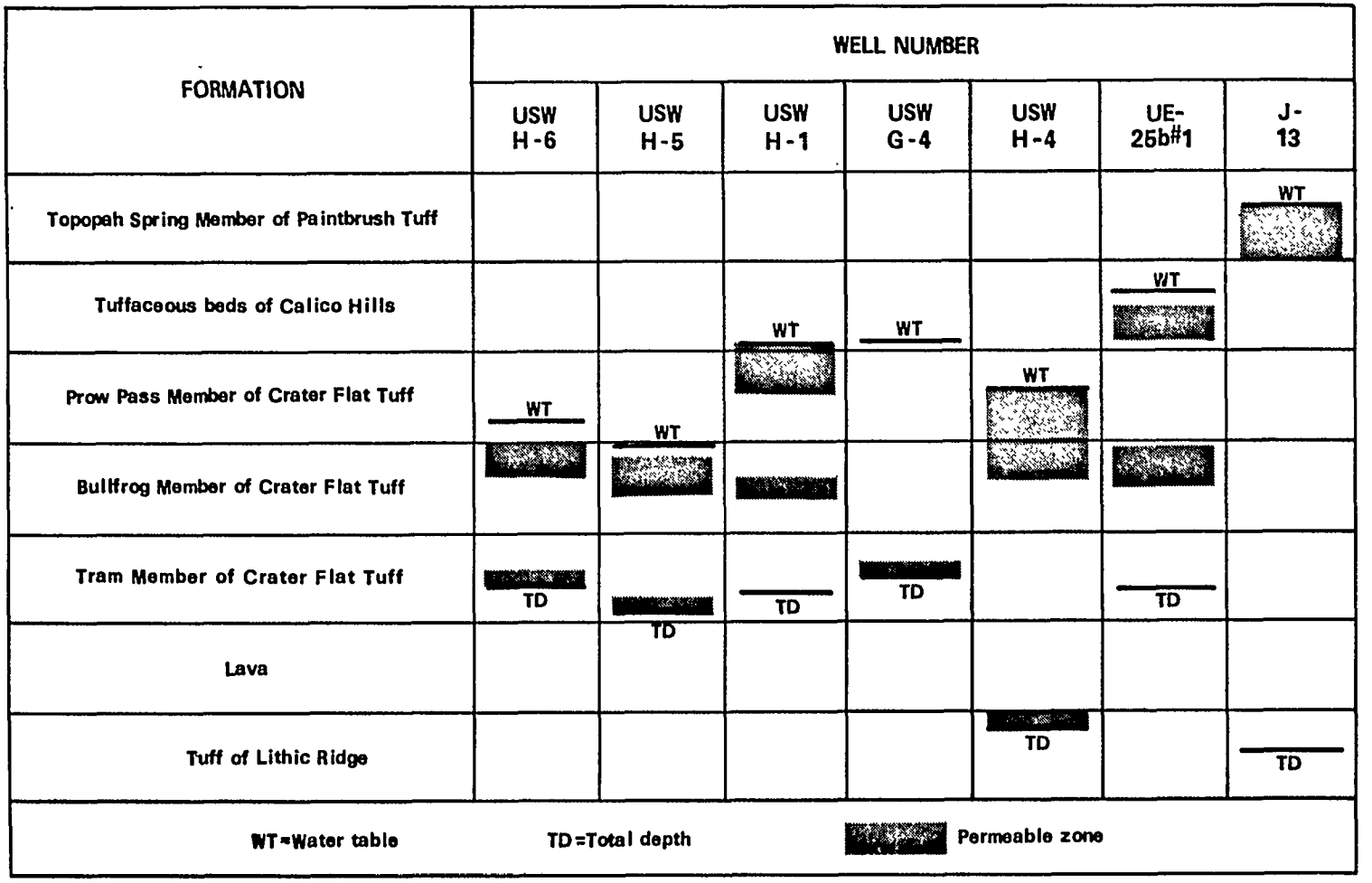

Figure A5.1-5. Vertical distribution of permeable zones in selected wells in the Yucca Mountain area (Benson and others, 1983).

APPENDIX 5.2

Sorption Data for Tuff Samples from Yucca Mountain and Vicinity

Contents

Note: In the tables, the symbol * indicates that the analysis was not used in the calculation of summary statistics in Tables 5.4 and 5.5.

Table A.5.2-1a
Sorption Data For Sorptive Categories
Zeolitized Tuff

Sample	Average Sorption Ratio (ml/g)	Repli-cations	Std. Dev. (ml/g)	Contact Time (days)	Average Desorption Ratio (ml/g)	Repli-cations	Std. Dev. (ml/g)	Contact Time (days)	Particle Size (μm)	Soln-Solid Ratio (ml/g)	Tracer Feed Concentration (Molar)	Source
** ELEMENT: Am												
G4-1502	490	2	20	.04					75 - 500	NG	1.3E-8	10006-5
G4-1502	715	2	5	.16					75 - 500	NG	1.3E-8	10006-5
G4-1502	1100	2	60	1					75 - 500	NG	1.3E-8	10006-5
G4-1502	1200	2	5	2					75 - 500	NG	1.3E-8	10006-5
G4-1502	1450	2	50	3					75 - 500	NG	1.3E-8	10006-5
G4-1502	1900	2	20	7					75 - 500	NG	1.3E-8	10006-5
G4-1502	1550	2	10	21					75 - 500	NG	1.3E-8	10006-5
G4-1502	1400	2	5	42					75 - 500	NG	1.3E-8	10006-5
YM-38	5500	3	1000	49	9500	3	1300	49	0 - 500	NG	NG	9328-30
YM-38	4600	2	1100	14	7100	2	1200	14	75 - 500	NG	1E-10	9328-21
** ELEMENT: Ba												
G1-1436	150000	2	24000	42					75 - 500	NG	NG	9846-18
G1-1436	150000	NG	24000	14	340000	NG	90000	14	75 - 500	NG	NG	9328-21
G1-1854	56000	2	8000	18	195000	2	77782		0 - 75	NG	1E-7	9328-29
G1-1854	34000	2	0	18					75 - 500	NG	1E-7	9328-29
G1-1854	45000	NG	7000	14	150000	NG	40000	14	75 - 500	NG	NG	9328-21
G1-2233	250000	NG	30000	14	240000	NG	80000	14	75 - 500	NG	NG	9328-21
G1-2233	41000*	2	6300	42	59000	2	6000	42	75 - 500	NG	7E-8	10154-13
G1-2233	55000*	2	5300	42	34000	2	23000	42	75 - 500	NG	5E-8	10154-13
G1-2289	140000	2	30000	21					0 - 38	NG	1E-7	9328-28
G1-2289	51000	2	3000	21					38 - 106	NG	1E-7	9328-28
G1-2289	80000	2	10000	21					106 - 500	NG	1E-7	9328-28
G1-2289	66000	2	9000	42					75 - 500	NG	NG	9846-18
G1-2289	66000	NG	9000	14					75 - 500	NG	NG	9328-21
G1-2333	1860	2	40	18	1650	2	71		0 - 75	NG	3E-7	9328-29
G1-2333	1170	2	30	18					75 - 500	NG	3E-7	9328-29
G1-2333	1500	NG	200	14	1460	NG	130	14	75 - 500	NG	NG	9328-21
G1-2698	63000	NG	5000	14	190000	NG	80000	14	75 - 500	NG	NG	9328-21
G1-3116	12000	NG	4000	14	160000	NG	80000	14	75 - 500	NG	NG	9328-21
YM-38	11000	1	561	21					0 - 75	5:1	NG	9328-XLII
YM-38	81500	1	2934	21					0 - 75	30:1	6E-7	9328-XLII
YM-38	9020	1	469	42					0 - 75	5:1	NG	9328-XLII

Table A.5.2-1a
Sorption Data For Sorptive Categories
Zeolitized Tuff

Sample	Average Sorption Ratio (ml/g)	Repli-cations	Std. Dev. (ml/g)	Contact Time (days)	Average Desorption Ratio (ml/g)	Repli-cations	Std. Dev. (ml/g)	Contact Time (days)	Particle Size (μm)	Soln-Solid Ratio (ml/g)	Tracer Feed Concentration (Molar)	Source
YM-38	16000	1	544	42					0 - 75	10:1	NG	9328-XLII
YM-38	78900	1	2919	42					0 - 75	30:1	NG	9328-XLII
YM-38	7410	1	378	21					75 - 500	5:1	NG	9328-XLII
YM-38	48000	1	3456	21					75 - 500	10:1	NG	9328-XLII
YM-38	54200	1	1680	21					75 - 500	30:1	NG	9328-XLII
YM-38	6180	1	254	42					75 - 500	5:1	NG	9328-XLII
YM-38	23200	1	905	42					75 - 500	10:1	NG	9328-XLII
YM-38	49200	1	1870	42					75 - 500	30:1	NG	9328-XLII
YM-38	66000	3	13000	49	260000	3	NG	49	0 - 500	NG	NG	9328-30
YM-38	130000	2	60000	21					0 - 38	NG	4E-7	9328-28
YM-38	110000	2	9000	21					38 - 106	NG	4E-7	9328-28
YM-38	80000	2	23000	21					106 - 500	NG	4E-7	9328-28
YM-38	100000	NG	10000	14	260000	NG	NG	14	75 - 500	NG	NG	9328-21
YM-42	94000	NG	14000	14	90000	NG	30000	14	75 - 500	NG	NG	9328-21
** ELEMENT: Ce												
G1-1436	59000	NG	7000	14	6700	NG	600	14	75 - 500	NG	NG	9328-21
G1-2233	1400	NG	300	14	20000	NG	13000	14	75 - 500	NG	NG	9328-21
G1-2698	240	NG	30	14	2000	NG	400	14	75 - 500	NG	NG	9328-21
G1-3116	100	NG	10	14	3000	NG	1000	14	75 - 500	NG	NG	9328-21
YM-38	1330	1	230	21					0 - 75	5:1	NG	9328-XLII
YM-38	6390	1	837	21					0 - 75	10:1	NG	9328-XLII
YM-38	9070	1	544	21					0 - 75	30:1	NG	9328-XLII
YM-38	1140	1	233	42					0 - 75	5:1	NG	9328-XLII
YM-38	5460	1	835	42					0 - 75	10:1	NG	9328-XLII
YM-38	9190	1	763	42					0 - 75	30:1	NG	9328-XLII
YM-38	2560	1	440	21					75 - 500	5:1	NG	9328-XLII
YM-38	7230	1	940	21					75 - 500	10:1	NG	9328-XLII
YM-38	16000	1	928	21					75 - 500	30:1	NG	9328-XLII
YM-38	1600	1	309	42					75 - 500	5:1	NG	9328-XLII
YM-38	6050	1	926	42					75 - 500	10:1	NG	9328-XLII
YM-38	11600	1	1311	42					75 - 500	30:1	NG	9328-XLII
YM-38	820	3	100	49	2640	3	NG	49	0 - 500	NG	NG	9328-30
YM-38	760	NG	140	14	2600	NG	NG	14	75 - 500	NG	NG	9328-21

Table A.5.2-1a
Sorption Data For Sorptive Categories
Zeolitized Tuff

Sample	Average Sorption Ratio (ml/g)	Repli-cations	Std. Dev. (ml/g)	Contact Time (days)	Average Desorption Ratio (ml/g)	Repli-cations	Std. Dev. (ml/g)	Contact Time (days)	Particle Size (μm)	Soln-Solid Ratio (ml/g)	Tracer Feed Concentration (Molar)	Source
YM-42	49000	NG	7000	14	44000	NG	5000	14	75 - 500	NG	NG	9328-21
** ELEMENT: Cs												
G1-1436	7800	NG	500	14	24000	NG	2000	14	75 - 500	NG	NG	9328-21
G1-1854	13000	NG	2000	14	14000	NG	2000	14	75 - 500	NG	NG	9328-21
G1-2233	13500	NG	800	14	23000	NG	6000	14	75 - 500	NG	NG	9328-21
G1-2233	7500	2	1100	42	8800	2	900	42	75 - 500	NG	2E-9	10154-13
G1-2233	13000	2	1600	42	8700	2	3400	42	75 - 500	NG	2E-9	10154-13
G1-2289	35000	2	8000	21					0 - 38	NG	4E-9	9328-28
G1-2289	31000	2	3000	21					38 - 106	NG	4E-9	9328-28
G1-2289	42000	2	30000	21					106 - 500	NG	4E-9	9328-28
G1-2289	37000	NG	13000	14					75 - 500	NG	NG	9328-21
G1-2333	1600	2	100	18	1350	2	71		0 - 75	NG	5E-9	9328-29
G1-2333	1160	2	40	18					75 - 500	NG	5E-9	9328-29
G1-2333	1400	NG	130	14	1230	NG	100	14	75 - 500	NG	NG	9328-21
G1-2698	7700	NG	400	14	17000	NG	1100	14	75 - 500	NG	NG	9328-21
G1-3116	6600	NG	500	14	11000	NG	3000	14	75 - 500	NG	NG	9328-21
YM-38	5970	1	698	21					0 - 75	5:1	NG	9328-XLII
YM-38	5760	1	432	21					0 - 75	10:1	NG	9328-XLII
YM-38	7980	1	271	21					0 - 75	30:1	NG	9328-XLII
YM-38	5100	1	622	42					0 - 75	5:1	NG	9328-XLII
YM-38	5120	1	312	42					0 - 75	10:1	NG	9328-XLII
YM-38	3660	1	388	21					75 - 500	5:1	2E-9	9328-XLII
YM-38	5750	1	403	21					75 - 500	10:1	NG	9328-XLII
YM-38	5540	1	177	21					75 - 500	30:1	NG	9328-XLII
YM-38	5110	1	925	42					75 - 500	5:1	NG	9328-XLII
YM-38	7280	1	510	42					75 - 500	10:1	NG	9328-XLII
YM-38	6270	1	270	42					75 - 500	30:1	NG	9328-XLII
YM-38	8600	3	1700	49	13000	3	NG	49	0 - 500	NG	NG	9328-30
YM-38	15000	2	4000	21					0 - 38	NG	4E-9	9328-28
YM-38	16000	2	900	21					38 - 106	NG	4E-9	9328-28
YM-38	14200	2	200	21					106 - 500	NG	4E-9	9328-28
YM-38	13000	NG	2000	14	13000	NG	NG	14	75 - 500	NG	NG	9328-21
YM-42	17000	NG	1000	14	21000	NG	2000	14	75 - 500	NG	NG	9328-21

Table A.5.2-1a
Sorption Data For Sorptive Categories
Zeolitized Tuff

Sample	Average Sorption Ratio (ml/g)	Repli-cations	Std. Dev. (ml/g)	Contact Time (days)	Average Desorption Ratio (ml/g)	Repli-cations	Std. Dev. (ml/g)	Contact Time (days)	Particle Size (μm)	Soln-Solid Ratio (ml/g)	Tracer Feed Concentration (Molar)	Source
** ELEMENT: Eu												
G1-1436	30000*	NG	2000	14	5300	NG	600	14	75 - 500	NG	NG	9328-21
G1-1854	100000*	2	NG	14					0 - 75	NG	NG	9328-29
G1-1854	14000	2	NG	14					75 - 500	NG	NG	9328-29
G1-1854	15000	NG	NG	14	4800	NG	700	14	75 - 500	NG	NG	9328-21
G1-2233	900	NG	200	14	5000	NG	2000	14	75 - 500	NG	NG	9328-21
G1-2233	5600*	2	NG	42	7800	2	NG	42	75 - 500	NG	3E-8	10154-13
G1-2233	810*	2	100	42	1400	2	600	42	75 - 500	NG	1E-8	10154-13
G1-2289	1500	2	100	21					0 - 38	NG	2E-8	9328-28
G1-2289	779	2	1	21					38 - 106	NG	2E-8	9328-28
G1-2289	815	2	3	21					106 - 500	NG	2E-8	9328-28
G1-2289	797	NG	10	14					75 - 500	NG	NG	9328-21
G1-2333	2600	2	600	18	6100	2	6930		0 - 75	NG	3E-8	9328-29
G1-2333	2200	2	800	18					75 - 500	NG	3E-8	9328-29
G1-2333	2300	NG	400	14	9900	NG	1200	14	75 - 500	NG	NG	9328-21
G1-2698	200	NG	30	14					75 - 500	NG	NG	9328-21
G1-3116	760	NG	60	14	8000	NG	3000	14	75 - 500	NG	NG	9328-21
YM-38	2700	1	478	21					0 - 75	5:1	NG	9328-XLII
YM-38	9070	1	1197	21					0 - 75	10:1	NG	9328-XLII
YM-38	9700	1	524	21					0 - 75	30:1	NG	9328-XLII
YM-38	2160	1	397	42					0 - 75	5:1	NG	9328-XLII
YM-38	4330	1	407	42					0 - 75	10:1	NG	9328-XLII
YM-38	6000	1	342	42					0 - 75	30:1	NG	9328-XLII
YM-38	3060	1	50	21					75 - 500	5:1	6E-9	9328-XLII
YM-38	6780	1	766	21					75 - 500	10:1	NG	9328-XLII
YM-38	10400	1	510	21					75 - 500	30:1	NG	9328-XLII
YM-38	2500	1	443	42					75 - 500	5:1	NG	9328-XLII
YM-38	6330	1	709	42					75 - 500	10:1	NG	9328-XLII
YM-38	8810	1	652	42					75 - 500	30:1	NG	9328-XLII
YM-38	3000	3	1000	49	7300	3	NG	49	0 - 500	NG	NG	9328-30
YM-38	2600	2	400	21					0 - 38	NG	7E-8	9328-28
YM-38	1340	2	10	21					38 - 106	NG	7E-8	9328-28
YM-38	1400	2	100	21					106 - 500	NG	7E-8	9328-28

Table A.5.2-1a
Sorption Data For Sorptive Categories
Zeolitized Tuff

Sample	Average Sorption Ratio (ml/g)	Repli-cations	Std. Dev. (ml/g)	Contact Time (days)	Average Desorption Ratio (ml/g)	Repli-cations	Std. Dev. (ml/g)	Contact Time (days)	Particle Size (μm)	Soln-Solid Ratio (ml/g)	Tracer Feed Concentration (Molar)	Source
YM-38	1600	NG	200	14	7300	NG	NG	14	75 - 500	NG	NG	9328-21
YM-42	52000 *	NG	4000	14	64000	NG	3000	14	75 - 500	NG	NG	9328-21
** ELEMENT: Mn												
G1-2233	6000	3	400	49	9300	3	NG	49	0 - 500	NG	NG	9328-30
** ELEMENT: Na												
G1-2233	141	3	4	49	160	3	10	49	0 - 500	NG	NG	9328-30
** ELEMENT: Np												
G4-1502	4	2	.5	42					75 - 500	NG	1E-10	10006-IV
G4-1502	4	2	1	42	11	2	2	42	75 - 500	NG	1E-10	10032-2
G4-1502	4.3	2	1	91					75 - 500	NG	1E-10	10032-2
G4-1502	4.8	2	1	183					75 - 500	NG	1E-10	10154-XI
YM-38	11	3	1	49	23	3	3	49	0 - 500	NG	NG	9328-30
YM-38	11.0	2	.7	14	24	2	2	14	75 - 500	NG	1E-10	9328-21
** ELEMENT: Pu												
G4-1502	19	2	1	.04					75 - 500	NG	1.3E-8	10006-5
G4-1502	22	2	1.2	.16					75 - 500	NG	1.3E-8	10006-5
G4-1502	27	2	1	1					75 - 500	NG	1.3E-8	10006-5
G4-1502	34	2	2.3	2					75 - 500	NG	1.3E-8	10006-5
G4-1502	34	2	2.9	3					75 - 500	NG	1.3E-8	10006-5
G4-1502	36	2	1	7					75 - 500	NG	1.3E-8	10006-5
G4-1502	34	2	1	21					75 - 500	NG	1.3E-8	10006-5
G4-1502	43	2	1	42					75 - 500	NG	1.3E-8	10006-5
G4-1502	57	2	3	42					75 - 500	NG	2E-7	10006-IV
G4-1502	59	2	3.4	42	230	2	34	42	75 - 500	NG	1.5E-7	10032-2
YM-38	250	3	90	49	2000	3	500	49	0 - 500	NG	NG	9328-30
YM-38	140	2	30	14	1600	2	300	14	75 - 500	NG	1E-10	9328-21

Table A.5.2-1a
Sorption Data For Sorptive Categories
Zeolitized Tuff

Sample	Average Sorption Ratio (ml/g)	Replications	Std. Dev. (ml/g)	Contact Time (days)	Average Desorption Ratio (ml/g)	Replications	Std. Dev. (ml/g)	Contact Time (days)	Particle Size (μm)	Soln-Solid Ratio (ml/g)	Tracer Feed Concentration (Molar)	Source
** ELEMENT: Ra												
G1-1436	100000	2	30000	42					75 - 500	NG	NG	9846-18
G1-2289	46000	2	20000	42					75 - 500	NG	NG	9846-18
G1-2289	50000	2	20000	42					75 - 500	NG	3.6E-7	9846-13
** ELEMENT: Se												
G1-2233	11	3	2	49	46	3	5	49	0 - 500	NG	NG	9328-30
G1-2233	1.8	2	.1	42					75 - 500	NG	1.8E-11	10154-X
G1-2289	9	2	1	42					75 - 500	NG	1E-10	9846-18
G1-3116	3.1	2	.1	42					75 - 500	NG	1.8E-11	10154-X
GU-3-1937	3.6	2	.1	42					75 - 500	NG	1.8E-11	10154-X
** ELEMENT: Sn												
G1-2233	460	3	130	49	580	3	70	49	0 - 500	NG	NG	9328-30
G4-1502	215	2	56	42					75 - 500	NG	3E-8	10154-X
** ELEMENT: Sr												
G1-1436	36000	NG	3000	14	87000	NG	12000	14	75 - 500	NG	NG	9328-21
G1-1854	81000	2	11000	18	54500	2	23335		0 - 75	NG	3E-8	9328-29
G1-1854	15000	2	100	18					0 - 75	NG	NG	9328-29
G1-1854	38000	2	6000	18					75 - 500	NG	3E-8	9328-29
G1-1854	10700	2	700	18					75 - 500	NG	NG	9328-29
G1-1854	60000	NG	14000	14	72000	NG	13000	14	75 - 500	NG	NG	9328-21
G1-2233	48000	NG	3000	14	90000	NG	40000	14	75 - 500	NG	NG	9328-21
G1-2233	2000*	2	330	42	3000	2	500	42	75 - 500	NG	3E-8	10154-13
G1-2233	56000*	2	NG	42	21000	2	12000	42	75 - 500	NG	3E-8	10154-13
G1-2289	14000	2	3000	21					0 - 38	NG	3E-8	9328-28
G1-2289	6380	2	40	21					38 - 106	NG	3E-8	9328-28
G1-2289	8100	2	300	21					106 - 500	NG	3E-8	9328-28
G1-2289	7300	NG	500	14					75 - 500	NG	NG	9328-21
G1-2333	218	2	2	18	160	2	0		0 - 75	NG	1E-6	9328-29
G1-2333	148	2	4	18					75 - 500	NG	1E-6	9328-29
G1-2333	180	NG	20	14	140	NG	13	14	75 - 500	NG	NG	9328-21
G1-2698	42000	NG	3000	14	210000	NG	50000	14	75 - 500	NG	NG	9328-21

Table A.5.2-1a
Sorption Data For Sorptive Categories
Zeolitized Tuff

Sample	Average Sorption Ratio (ml/g)	Replications	Std. Dev. (ml/g)	Contact Time (days)	Average Desorption Ratio (ml/g)	Replications	Std. Dev. (ml/g)	Contact Time (days)	Particle Size (μm)	Soln-Solid Ratio (ml/g)	Tracer Feed Concentration (Molar)	Source
G1-3116	2400	NG	17	14	24000	NG	13000	14	75 - 500	NG	NG	9328-21
YM-38	2770	1	150	21					0 - 75	5:1	NG	9328-XLII
YM-38	2790	1	95	21					0 - 75	10:1	NG	9328-XLII
YM-38	3610	1	79	21					0 - 75	30:1	NG	9328-XLII
YM-38	2370	1	152	42					0 - 75	5:1	NG	9328-XLII
YM-38	2410	1	82	42					0 - 75	10:1	NG	9328-XLII
YM-38	3700	1	89	42					0 - 75	30:1	NG	9328-XLII
YM-38	2040	1	100	21					75 - 500	5:1	NG	9328-XLII
YM-38	2840	1	94	21					75 - 500	10:1	NG	9328-XLII
YM-38	2770	1	58	21					75 - 500	30:1	NG	9328-XLII
YM-38	1760	1	97	42					75 - 500	5:1	NG	9328-XLII
YM-38	3080	1	117	42					75 - 500	10:1	NG	9328-XLII
YM-38	2050	1	53	42					75 - 500	30:1	NG	9328-XLII
YM-38	11900	3	3200	49	21700	3	NG	49	0 - 500	NG	NG	9328-30
YM-38	17000	2	3000	21					0 - 38	NG	4E-7	9328-28
YM-38	20000	2	400	21					38 - 106	NG	4E-7	9328-28
YM-38	17600	2	0	21					106 - 500	NG	4E-7	9328-28
YM-38	17000	NG	2000	14	22000	NG	NG	14	75 - 500	NG	NG	9328-21
YM-42	3900	NG	600	14	4100	NG	1000	14	75 - 500	NG	NG	9328-21
** ELEMENT: Tc												
G4-1502	.02	2	.02	42					75 - 500	NG	8E-10	10154-XI
G4-1502	.01	2	.05	91					75 - 500	NG	8E-10	10154-XI
G4-1502	0	2	NG	91					75 - 500	NG	8E-10	10154-XI
** ELEMENT: Th												
G1-2233	344	NG	55	12					NG - NG	NG	1.07E-7	10032-13
G1-2289	143	NG	2	12					NG - NG	NG	5.86E-8	10032-13
** ELEMENT: U												
G1-1436	11	2	1	42					75 - 500	NG	NG	9846-18

Table A.5.2-1a
Sorption Data For Sorptive Categories
Zeolitized Tuff

Sample	Average Sorption Ratio (ml/g)	Replications	Std. Dev. (ml/g)	Contact Time (days)	Average Desorption Ratio (ml/g)	Replications	Std. Dev. (ml/g)	Contact Time (days)	Particle Size (μm)	Soln-Solid Ratio (ml/g)	Tracer Feed Concentration (Molar)	Source
G1-2233	5.5	2	.4	42					75 - 500	NG	2.7E-6	10154-X
G1-2289	2.5	2	.1	42					75 - 500	NG	5.E-6	9846-15
G1-3116	3.8	2	.1	42					75 - 500	NG	2.7E-6	10154-X
GU-3-1937	10	2	.1	42					75 - 500	NG	2.7E-6	10154-X
YM-38	5.3	3	.2	49	15	3	1	49	0 - 500	NG	NG	9328-30
YM-38	5.3	2	.2	14	14.8	2	1.	14	75 - 500	NG	1E-10	9328-21

Table A.5.2-1b
Sorption Data For Sorptive Categories
Clay-Rich Vitric Tuff

Sample	Average Sorption Ratio (ml/g)	Repli-cations	Std. Dev. (ml/g)	Contact Time (days)	Average Desorption Ratio (ml/g)	Repli-cations	Std. Dev. (ml/g)	Contact Time (days)	Particle Size (μm)	Soln-Solid Ratio (ml/g)	Tracer Feed Concentration (Molar)	Source
** ELEMENT: Am												
GU-3-1301	2000	2	40	42					75 - 500	NG	NG	9846-18
GU-3-1301					1500	2	5	NG	75 - 500	NG	NG	9846-17
GU-3-1301	1500	2	120	42	3500	2	320	NG	75 - 500	NG	NG	9846-17
** ELEMENT: Ba												
GU-3-1301	570	2	60	42					75 - 500	NG	NG	9793-5
GU-3-1301	420	2	50	42					75 - 500	NG	NG	9793-5
GU-3-1301					660	2	100	42	0 - 500	NG	NG	9846-16
GU-3-1301					690	2	100	42	0 - 500	NG	NG	9846-16
GU-3-1301	82 *	2	18	42	140	2	30	42	75 - 500	NG	8E-8	10154-13
YM-5	1100	NG	200	14	1200	NG	120	14	75 - 500	NG	NG	9328-21
** ELEMENT: Ce												
YM-5	450000	NG	240000	14	310000	NG	30000	14	75 - 500	NG	NG	9328-21
** ELEMENT: Cs												
GU-3-1301	160	2	35	42					75 - 500	NG	NG	9793-5
GU-3-1301	120	2	15	42					75 - 500	NG	NG	9793-5
GU-3-1301					180	2	40	42	0 - 500	NG	NG	9846-16
GU-3-1301					180	2	30	42	0 - 500	NG	NG	9846-16
GU-3-1301	45 *	2	5	42	55	2	4	42	75 - 500	NG	4E-9	10154-13
YM-5	5800	NG	800	14	8900	NG	600	14	75 - 500	NG	NG	9328-21
** ELEMENT: Eu												
GU-3-1301	75	2	12	42					75 - 500	NG	NG	9793-5
GU-3-1301	38	2	7	42					75 - 500	NG	NG	9793-5
GU-3-1301					110	2	40	42	0 - 500	NG	NG	9846-16
GU-3-1301					90	2	40	42	0 - 500	NG	NG	9846-16
GU-3-1301	17000 *	2	NG	42	20000	2	NG	42	75 - 500	NG	1E-7	10154-13
YM-5	230000 *	NG	40000	14	36000	NG	14000	14	75 - 500	NG	NG	9328-21

Table A.5.2-1b
Sorption Data For Sorptive Categories
Clay-Rich Vitric Tuff

Sample	Average Sorption Ratio (ml/g)	Repli-cations	Std. Dev. (ml/g)	Contact Time (days)	Average Desorption Ratio (ml/g)	Repli-cations	Std. Dev. (ml/g)	Contact Time (days)	Particle Size (μm)	Soln-Solid Ratio (ml/g)	Tracer Feed Concentration (Molar)	Source
** ELEMENT: Np												
GU-3-1301	2.2	2	1	91	25	2	2	42	75 - 500	NG	6E-11	10032-2
GU-3-1301	2	2	1	91					75 - 500	NG	6E-11	10032-2
GU-3-1301	2.1	4	1	91					75 - 500	NG	6E-11	10154-XI
GU-3-1301	2.2	2	1	183					75 - 500	NG	6E-11	10154-XI
** ELEMENT: Pu												
GU-3-1301	210	2	30	42					75 - 500	NG	NG	9846-18
GU-3-1301					580	2	20	NG	75 - 500	NG	NG	9846-17
GU-3-1301	360	2	20	42	2100	2	330	NG	75 - 500	NG	NG	9846-17
** ELEMENT: Se												
GU-3-1301	7	2	2	42					75 - 500	NG	1E-10	9846-18
** ELEMENT: Sn												
GU-3-1301	168	2	8	42					75 - 500	NG	2E-8	10154-X
** ELEMENT: Sr												
GU-3-1301	32	2	8	42					75 - 500	NG	NG	9793-5
GU-3-1301	24	2	1	42					75 - 500	NG	NG	9793-5
GU-3-1301					90	2	20	42	0 - 500	NG	NG	9846-16
GU-3-1301					60	2	30	42	0 - 500	NG	NG	9846-16
GU-3-1301	10*	2	2	42	32	2	1	42	75 - 500	NG	1E-6	10154-13
YM-5	280	NG	80	14	320	NG	30	14	75 - 500	NG	NG	9328-21
** ELEMENT: Tc												
GU-3-1301	.03	2	.004	42					75 - 500	NG	NG	9793-5
GU-3-1301	.04	2	.01	42					75 - 500	NG	NG	9793-5
GU-3-1301	.04	2	.02	42					75 - 500	NG	7E-10	10032-2
GU-3-1301	.03	2	.03	91					75 - 500	NG	7E-10	10154-XI
GU-3-1301	0	2	.004	91					75 - 500	NG	7E-10	10154-XI
** ELEMENT: U												
GU-3-1301	0	2	NG	42					75 - 500	NG	5.E-6	9846-15

Table A.5.2-1c
Sorption Data For Sorptive Categories
Glass-Rich Clay

Sample	Average Sorption Ratio (ml/g)	Repli-cations	Std. Dev. (ml/g)	Contact Time (days)	Average Desorption Ratio (ml/g)	Repli-cations	Std. Dev. (ml/g)	Contact Time (days)	Particle Size (μm)	Soln-Solid Ratio (ml/g)	Tracer Feed Concentration (Molar)	Source
** ELEMENT: Ba												
JA-8	435	NG	15	14	480	NG	50	14	75 - 500	NG	NG	9328-21
** ELEMENT: Cs												
JA-8	2700	NG	400	14	4600	NG	400	14	75 - 500	NG	NG	9328-21
** ELEMENT: Eu												
JA-8	2100	NG	300	14	10000	NG	3000	14	75 - 500	NG	NG	9328-21
** ELEMENT: Sr												
JA-8	270	NG	5	14	311	NG	3	14	75 - 500	NG	NG	9328-21

Table A.5.2-1d
Sorption Data For Sorptive Categories
Devitrified Tuff

Sample	Average Sorption Ratio (ml/g)	Repli-cations	Std. Dev. (ml/g)	Contact Time (days)	Average Desorption Ratio (ml/g)	Repli-cations	Std. Dev. (ml/g)	Contact Time (days)	Particle Size (μm)	Soln-Solid Ratio (ml/g)	Tracer Feed Concentration (Molar)	Source
** ELEMENT: Am												
GU-3-433	3100	2	200	42					75 - 500	NG	NG	9846-18
GU-3-433					7800	2	1700	NG	75 - 500	NG	NG	9846-17
GU-3-433	3600	2	150	42	11000	2	3300	NG	75 - 500	NG	NG	9846-17
YM-22	4000	3	1200	49	4700	3	1000	49	0 - 500	NG	NG	9328-30
YM-22	1200	2	130	14	2500	2	400	14	75 - 500	NG	1E-10	9328-21
** ELEMENT: Ba												
GU-3-433	810	2	100	42					75 - 500	NG	NG	9793-5
GU-3-433	340	2	50	42					75 - 500	NG	NG	9793-5
GU-3-433					470	2	10	42	0 - 500	NG	NG	9846-16
GU-3-433					460	2	50	42	0 - 500	NG	NG	9846-16
YM-22	980	3	80	49	1000	3	210	49	0 - 500	NG	NG	9328-30
YM-22	1490	1	27	21					0 - 75	5:1	NG	9328-XLI
YM-22	1360	1	19	21					0 - 75	10:1	NG	9328-XLI
YM-22	1010	1	11	21					0 - 75	30:1	NG	9328-XLI
YM-22	1280	1	23	42					0 - 75	5:1	NG	9328-XLI
YM-22	1820	1	27	42					0 - 75	10:1	NG	9328-XLI
YM-22	1850	1	20	42					0 - 75	30:1	NG	9328-XLI
YM-22	601	1	13	21					75 - 500	5:1	NG	9328-XLI
YM-22	530	1	10	21					75 - 500	10:1	NG	9328-XLI
YM-22	412	1	8	21					75 - 500	30:1	NG	9328-XLI
YM-22	805	1	14	42					75 - 500	5:1	NG	9328-XLI
YM-22	605	1	8	42					75 - 500	10:1	NG	9328-XLI
YM-22	568	1	7	42					75 - 500	30:1	NG	9328-XLI
YM-22	900	NG	30	14	830	NG	100	14	75 - 500	NG	NG	9328-21
YM-46	14000	NG	6000	14	21000	NG	3000	14	75 - 500	NG	NG	9328-21
** ELEMENT: Ca												
YM-22	1300	3	100	49	6100	3	700	49	0 - 500	NG	NG	9328-30
YM-22	459	1	39	21					0 - 75	5:1	NG	9328-XLI
YM-22	500	1	29	21					0 - 75	10:1	NG	9328-XLI
YM-22	1050	1	47	21					0 - 75	30:1	NG	9328-XLI
YM-22	297	1	26	42					0 - 75	5:1	NG	9328-XLI

Table A.5.2-1d
Sorption Data For Sorptive Categories
Devitrified Tuff

Sample	Average Sorption Ratio (ml/g)	Repli-cations	Std. Dev. (ml/g)	Contact Time (days)	Average Desorption Ratio (ml/g)	Repli-cations	Std. Dev. (ml/g)	Contact Time (days)	Particle Size (μm)	Soln-Solid Ratio (ml/g)	Tracer Feed Concentration (Molar)	Source
YM-22	748	1	54	42					0 - 75	10:1	NG	9328-XLI
YM-22	303	1	20	21					75 - 500	5:1	NG	9328-XLI
YM-22	508	1	27	21					75 - 500	10:1	NG	9328-XLI
YM-22	1000	1	46	21					75 - 500	30:1	NG	9328-XLI
YM-22	524	1	50	42					75 - 500	5:1	NG	9328-XLI
YM-22	1040	1	96	42					75 - 500	10:1	NG	9328-XLI
YM-22	1630	1	109	42					75 - 500	30:1	NG	9328-XLI
YM-22	1270	NG	40	14	6500	NG	800	14	75 - 500	NG	NG	9328-21
YM-46	310000 *	NG	110000	14	300000	NG	50000	14	75 - 500	NG	NG	9328-21
** ELEMENT: Cs												
GU-3-433	630	2	20	42					75 - 500	NG	NG	9793-5
GU-3-433	400	2	40	42					75 - 500	NG	NG	9793-5
GU-3-433					530	2	50	42	0 - 500	NG	NG	9846-16
GU-3-433					510	2	20	42	0 - 500	NG	NG	9846-16
YM-22	340	3	60	49	420	3	400	30	0 - 500	NG	NG	9328-30
YM-22	827	1	39	21					0 - 75	5:1	NG	9328-XLI
YM-22	755	1	22	21					0 - 75	10:1	NG	9328-XLI
YM-22	749	1	16	21					0 - 75	30:1	NG	9328-XLI
YM-22	740	1	34	42					0 - 75	5:1	NG	9328-XLI
YM-22	857	1	26	42					0 - 75	10:1	NG	9328-XLI
YM-22	1100	1	24	42					0 - 75	30:1	NG	9328-XLI
YM-22	363	1	12	21					75 - 500	5:1	NG	9328-XLI
YM-22	336	1	8	21					75 - 500	10:1	NG	9328-XLI
YM-22	368	1	8	21					75 - 500	30:1	NG	9328-XLI
YM-22	565	1	23	42					75 - 500	5:1	NG	9328-XLI
YM-22	457	1	12	42					75 - 500	10:1	NG	9328-XLI
YM-22	522	1	11	42					75 - 500	30:1	NG	9328-XLI
YM-22	290	NG	30	14	365	NG	7	14	75 - 500	NG	NG	9328-21
YM-46	840	NG	6	14	1800	NG	300	14	75 - 500	NG	NG	9328-21
** ELEMENT: Eu												
GU-3-433	100	2	14	42					75 - 500	NG	NG	9793-5
GU-3-433	68	2	14	42					75 - 500	NG	NG	9793-5

Table A.5.2-1d
Sorption Data For Sorptive Categories
Devitrified Tuff

Sample	Average Sorption Ratio (ml/g)	Repli-cations	Std. Dev. (ml/g)	Contact Time (days)	Average Desorption Ratio (ml/g)	Repli-cations	Std. Dev. (ml/g)	Contact Time (days)	Particle Size (μm)	Soln-Solid Ratio (ml/g)	Tracer Feed Concentration (Molar)	Source
GU-3-433					120	2	20	42	0 - 500	NG	NG	9846-16
GU-3-433					150	2	20	42	0 - 500	NG	NG	9846-16
YM-22	1400	3	100	49	3600	3	NG	49	0 - 500	NG	NG	9328-30
YM-22	926	1	NG	21					0 - 75	5:1	NG	9328-XLI
YM-22	1270	1	NG	21					0 - 75	10:1	NG	9328-XLI
YM-22	1640	1	NG	21					0 - 75	30:1	NG	9328-XLI
YM-22	749	1	59	42					0 - 75	5:1	NG	9328-XLI
YM-22	2250	1	140	42					0 - 75	10:1	NG	9328-XLI
YM-22	794	1	NG	21					75 - 500	5:1	NG	9328-XLI
YM-22	909	1	NG	21					75 - 500	10:1	NG	9328-XLI
YM-22	1600	1	NG	21					75 - 500	30:1	NG	9328-XLI
YM-22	910	1	63	42					75 - 500	5:1	NG	9328-XLI
YM-22	1300	1	64	42					75 - 500	10:1	NG	9328-XLI
YM-22	2010	1	70	42					75 - 500	30:1	NG	9328-XLI
YM-22	1390	NG	110	14	3500	NG	200	14	75 - 500	NG	NG	9328-21
YM-46	307000*	NG	110000	14	31000	NG	2000	14	75 - 500	NG	NG	9328-21
** ELEMENT: Np												
GU-3-916	4.9*	2	.1	42					75 - 500	NG	6E-11	10006-IV
GU-3-916	4.9	2	1	42	33	2	1	42	75 - 500	NG	6E-11	10032-2
GU-3-916	5.3	2	1.0	91					75 - 500	NG	6E-11	10032-2
GU-3-916	5.4	2	1	183					75 - 500	NG	6E-11	10154-XI
YM-22	5.9	3	.6	49	33	3	5	49	0 - 500	NG	NG	9328-30
YM-22	7.0	2	1.0	14	33	2	5	14	75 - 500	NG	1E-10	9328-21
** ELEMENT: Pu												
GU-3-433	420	2	80	42					75 - 500	NG	NG	9846-18
GU-3-433					890	2	100	NG	75 - 500	NG	NG	9846-17
GU-3-433	240	2	2	42	960	2	80	NG	75 - 500	NG	NG	9846-17
GU-3-916	240	2	25	42					75 - 500	NG	1E-7	10006-IV
GU-3-916	250	2	25	42	680	2	40	42	75 - 500	NG	1E-7	10032-2
YM-22	140	3	40	49	1400	3	100	49	0 - 500	NG	NG	9328-30

Table A.5.2-1d
Sorption Data For Sorptive Categories
Devitrified Tuff

Sample	Average Sorption Ratio (ml/g)	Repli-cations	Std. Dev. (ml/g)	Contact Time (days)	Average Desorption Ratio (ml/g)	Repli-cations	Std. Dev. (ml/g)	Contact Time (days)	Particle Size (μm)	Soln-Solid Ratio (ml/g)	Tracer Feed Concentration (Molar)	Source
YM-22	220	3	50	49	1600	3	300	49	0 - 500	NG	NG	9328-30
YM-22	64	2	20	14	1330	2	140	14	75 - 500	NG	1E-10	9328-21
** ELEMENT: Se												
GU-3-1531	5	2	1	42					0 - 500	NG	NG	9846-18
GU-3-433	15	2	3	42					75 - 500	NG	1E-10	9846-18
** ELEMENT: Sr												
GU-3-433	61	2	6	42					75 - 500	NG	NG	9793-5
GU-3-433	30	2	2	42					75 - 500	NG	NG	9793-5
GU-3-433					44	2	5	42	0 - 500	NG	NG	9846-16
GU-3-433					34	2	2	42	0 - 500	NG	NG	9846-16
YM-22	56	3	4	49	63	3	4	49	0 - 500	NG	NG	9328-30
YM-22	122	1	2	21					0 - 75	5:1	NG	9328-XLI
YM-22	80.3	1	2	21					0 - 75	10:1	NG	9328-XLI
YM-22	67.4	1	1.4	21					0 - 75	30:1	NG	9328-XLI
YM-22	129	1	3	42					0 - 75	5:1	NG	9328-XLI
YM-22	99.4	1	2	42					0 - 75	10:1	NG	9328-XLI
YM-22	97.9	1	2.2	42					0 - 75	30:1	NG	9328-XLI
YM-22	63	1	1.2	21					75 - 500	5:1	NG	9328-XLI
YM-22	44.9	1	1	21					75 - 500	10:1	NG	9328-XLI
YM-22	195	1	4	21					75 - 500	30:1	NG	9328-XLI
YM-22	32.5	1	1.17	42					75 - 500	5:1	NG	9328-XLI
YM-22	59.4	1	.89	42					75 - 500	30:1	NG	9328-XLI
YM-22	53	NG	4	14	59	NG	2	14	75 - 500	NG	NG	9328-21
YM-46	190	NG	60	14	260	NG	20	14	75 - 500	NG	NG	9328-21
** ELEMENT: Tc												
GU-3-433	0	2	NG	42					75 - 500	NG	NG	9793-5
GU-3-433	.07	2	.02	42					75 - 500	NG	NG	9793-5
GU-3-916	.72	2	.2	42					75 - 500	NG	6E-10	10032-2
GU-3-916	.81	2	.5	91					75 - 500	NG	6E-10	10032-2

Table A.5.2-1d
Sorption Data For Sorptive Categories
Devitrified Tuff

Sample	Average Sorption Ratio (ml/g)	Repli-cations	Std. Dev. (ml/g)	Contact Time (days)	Average Desorption Ratio (ml/g)	Repli-cations	Std. Dev. (ml/g)	Contact Time (days)	Particle Size (μm)	Soln-Solid Ratio (ml/g)	Tracer Feed Concentration (Molar)	Source
GU-3-916	.62	2	.2	183					75 - 500	NG	6E-10	10154-XI
YM-22	.3	3	.1	49	1.2	3	.3	49	0 - 500	NG	NG	9328-30
YM-22	.3	NG	.14	14	1.2	NG	.30	14	75 - 500	NG	NG	9328-21
** ELEMENT: U												
GU-3-1531	54	2	9	42					0 - 500	NG	NG	9846-18
GU-3-433	0	2	NG	42					75 - 500	NG	5.E-6	9846-15
YM-22	1.8	3	.2	49	5.3	3	1.9	49	0 - 500	NG	NG	9328-30
YM-22	1.8	2	0.2	14	5	2	2	14	75 - 500	NG	1E-10	9328-21

Table A.5.2-1e
Sorption Data For Sorptive Categories
Devitrified Tuff With Clay and Zeolites

Sample	Average Sorption Ratio (ml/g)	Repli-cations	Std. Dev. (ml/g)	Contact Time (days)	Average Desorption Ratio (ml/g)	Repli-cations	Std. Dev. (ml/g)	Contact Time (days)	Particle Size (μm)	Soln-Solid Ratio (ml/g)	Tracer Feed Concentration (Molar)	Source
** ELEMENT: Ba												
YM-30	3400	NG	1500	14	3100	NG	600	14	75 - 500	NG	NG	9328-21
** ELEMENT: Ce												
YM-30	230000	NG	100000	14	170000	NG	15000	14	75 - 500	NG	NG	9328-21
** ELEMENT: Cs												
YM-30	855	NG	5	14	1500	NG	100	14	75 - 500	NG	NG	9328-21
** ELEMENT: Eu												
YM-30	160000	NG	50000	14	11000	NG	700	14	75 - 500	NG	NG	9328-21
** ELEMENT: Sr												
YM-30	260	NG	80	14	210	NG	30	14	75 - 500	NG	NG	9328-21

Table A.5.2-1f
Sorption Data For Sorptive Categories
Devitrified Tuff With Glass, Clay, and Zeolite

Sample	Average Sorption Ratio (ml/g)	Replications	Std. Dev. (ml/g)	Contact Time (days)	Average Desorption Ratio (ml/g)	Replications	Std. Dev. (ml/g)	Contact Time (days)	Particle Size (μm)	Soln-Solid Ratio (ml/g)	Tracer Feed Concentration (Molar)	Source
** ELEMENT: Am												
JA-18	180	2	30	14	1100	2	300	14	75 - 500	NG	1E-10	9328-21
** ELEMENT: Ba												
JA-18	38000	NG	18000	14	280000	NG	50000	14	75 - 500	NG	NG	9328-21
** ELEMENT: Ce												
JA-18	2800	NG	1400	14	1600	NG	500	14	75 - 500	NG	NG	9328-21
** ELEMENT: Cs												
JA-18	16000	NG	1000	14	17500	NG	700	14	75 - 500	NG	NG	9328-21
** ELEMENT: Eu												
JA-18	1400	NG	200	14	2400	NG	300	14	75 - 500	NG	NG	9328-21
** ELEMENT: Pu												
JA-18	120	2	20	14	350	2	140	14	75 - 500	NG	1E-10	9328-21
** ELEMENT: Sr												
JA-18	17000	NG	3000	14	15000	NG	2000	14	75 - 500	NG	NG	9328-21
** ELEMENT: U												
JA-18	2.5	2	.4	14	9.4	2	1.4	14	75 - 500	NG	1E-10	9328-21

Table A.5.2-1g
Sorption Data For Sorptive Categories
Devitrified Tuff With Clay

Sample	Average Sorption Ratio (ml/g)	Replications	Std. Dev. (ml/g)	Contact Time (days)	Average Desorption Ratio (ml/g)	Replications	Std. Dev. (ml/g)	Contact Time (days)	Particle Size (μm)	Soln-Solid Ratio (ml/g)	Tracer Feed Concentration (Molar)	Source
** ELEMENT: Am												
JA-32	130	2	30	14	2200	2	600	14	75 - 500	NG	1E-10	9328-21
YM-54	590	3	210	49	600	3	50	49	0 - 500	NG	NG	9328-30
YM-54	153	2	6	14	550	2	80	14	75 - 500	NG	1E-10	9328-21
** ELEMENT: Ba												
G1-1982	10000	2	0	18					0 - 38	NG	4E-6	9328-28
G1-1982	760	2	90	18					38 - 75	NG	4E-6	9328-28
G1-1982	670	2	100	18					75 - 250	NG	4E-6	9328-28
G1-1982	740	2	40	18					250 - 500	NG	4E-6	9328-28
G1-1982	700	NG	50	14	2780	NG	120	14	75 - 500	NG	NG	9328-21
G1-2363	890	2	30	21					0 - 38	NG	1E-7	9328-28
G1-2363	250	2	10	21					38 - 106	NG	1E-7	9328-28
G1-2363	220	2	10	21					106 - 500	NG	1E-7	9328-28
G1-2363	235	2	9	42					106 - 500	NG	NG	9846-18
G1-2363	235	NG	9	14	820	NG	20	14	75 - 500	NG	NG	9328-21
G1-2410	3040	1	NG	14					0 - 75	NG	2E-7	9328-29
G1-2410	1780	1	NG	14					75 - 500	NG	2E-7	9328-29
G1-2410					1760	NG	150	14	75 - 500	NG		9328-21
G1-2476	500	2	20	18					0 - 75	NG	1E-7	9328-29
G1-2476	385	2	10	18					75 - 500	NG	1E-7	9328-29
G1-2476	385	NG	11	14					75 - 500	NG	NG	9328-21
G1-2840	2500	2	200	18					0 - 75	NG	2E-7	9328-29
G1-2840	2070	2	70	18					75 - 500	NG	2E-7	9328-29
G1-2840	2070	NG	70	14	2500	NG	200	14	75 - 500	NG	NG	9328-21
G1-2854	4000	2	2000	18					0 - 75	NG	1E-7	9328-29
G1-2854	1000	2	50	18					75 - 500	NG	1E-7	9328-29
G1-2854	1000	NG	50	14	1330	NG	0	14	75 - 500	NG	NG	9328-21
JA-32	380	NG	30	14	490	NG	40	14	75 - 500	NG	NG	9328-21
YM-45	1200	NG	100	14	1310	NG	60	14	75 - 500	NG	NG	9328-21
YM-54	620	3	80	49	660	3	20	49	0 - 500	NG	NG	9328-30
YM-54	1670	2	60	21					0 - 38	NG	3E-7	9328-28
YM-54	474	2	3	21					38 - 106	NG	3E-7	9328-28
YM-54	140	2	7	21					106 - 500	NG	3E-7	9328-28

Table A.5.2-1g
Sorption Data For Sorptive Categories
Devitrified Tuff With Clay

Sample	Average Sorption Ratio (ml/g)	Repli-cations	Std. Dev. (ml/g)	Contact Time (days)	Average Desorption Ratio (ml/g)	Repli-cations	Std. Dev. (ml/g)	Contact Time (days)	Particle Size (μm)	Soln-Solid Ratio (ml/g)	Tracer Feed Concentration (Molar)	Source
YM-54	400	NG	150	14	660	NG	20	14	75 - 500	NG	NG	9328-21
** ELEMENT: Ce												
G1-1982	560	NG	40	14	7000	NG	900	14	75 - 500	NG	NG	9328-21
G1-2363					130000	NG	6000	14	75 - 500	NG	NG	9328-21
JA-32	82	NG	14	14	530	NG	120	14	75 - 500	NG	NG	9328-21
YM-45	730	NG	100	14	5800	NG	600	14	75 - 500	NG	NG	9328-21
YM-54	140	3	40	49	1000	3	200	49	0 - 500	NG	NG	9328-30
YM-54	150	NG	40	14	1000	NG	200	14	75 - 500	NG	NG	9328-21
** ELEMENT: Cs												
G1-1982	3650	2	200	18					0 - 38	NG	3E-9	9328-28
G1-1982	1250	2	50	18					38 - 75	NG	3E-9	9328-28
G1-1982	1000	2	70	18					75 - 250	NG	3E-9	9328-28
G1-1982	1200	2	0	18					250 - 500	NG	3E-9	9328-28
G1-1982	1120	NG	110	14	2300	NG	200	14	75 - 500	NG	NG	9328-21
G1-2363	1300	2	100	21					0 - 38	NG	4E-9	9328-28
G1-2363	540	2	20	21					38 - 106	NG	4E-9	9328-28
G1-2363	400	2	20	21					106 - 500	NG	4E-9	9328-28
G1-2363	470	NG	40	14	1200	NG	30	14	75 - 500	NG	NG	9328-21
G1-2410	2020	2	20	18					0 - 75	NG	4E-9	9328-29
G1-2410	1250	2	50	18					75 - 500	NG	4E-9	9328-29
G1-2410	1250	NG	50	14	1120	NG	100	14	75 - 500	NG	NG	9328-21
G1-2476	870	2	50	18					0 - 75	NG	5E-9	9328-29
G1-2476	700	2	40	18					75 - 500	NG	5E-9	9328-29
G1-2476	700	NG	40	14	1520	NG	0	14	75 - 500	NG	NG	9328-21
G1-2840	2600	2	200	18					0 - 75	NG	5E-9	9328-29
G1-2840	2200	2	200	18					75 - 500	NG	5E-9	9328-29
G1-2840	2200	NG	200	14	2300	NG	130	14	75 - 500	NG	NG	9328-21
G1-2854	1100	2	600	18					0 - 75	NG	5E-9	9328-29
G1-2854	1080	2	120	18					75 - 500	NG	5E-9	9328-29
G1-2854	1080	NG	120	14	1160	NG	20	14	75 - 500	NG	NG	9328-21
JA-32	123	NG	4	14	175	NG	11	14	75 - 500	NG	NG	9328-21
YM-45	520	NG	90	14	620	NG	110	14	75 - 500	NG	NG	9328-21

Table A.5.2-1g
Sorption Data For Sorptive Categories
Devitrified Tuff With Clay

Sample	Average Sorption Ratio (ml/g)	Repli-cations	Std. Dev. (ml/g)	Contact Time (days)	Average Desorption Ratio (ml/g)	Repli-cations	Std. Dev. (ml/g)	Contact Time (days)	Particle Size (μm)	Soln-Solid Ratio (ml/g)	Tracer Feed Concentration (Molar)	Source
YM-54	250	3	20	49	310	3	20	49	0 - 500	NG	NG	9328-30
YM-54	910	2	30	21					0 - 38	NG	3E-9	9328-28
YM-54	187	2	1	21					38 - 106	NG	3E-9	9328-28
YM-54	120	2	10	21					106 - 500	NG	3E-9	9328-28
YM-54	180	NG	40	14	310	NG	20	14	75 - 500	NG	NG	9328-21
** ELEMENT: Eu												
G1-1982	1900	2	700	18					0 - 38	NG	1E-7	9328-28
G1-1982	710	2	180	18					38 - 75	NG	1E-7	9328-28
G1-1982	960	2	300	18					75 - 250	NG	1E-7	9328-28
G1-1982	980	2	120	18					250 - 500	NG	1E-7	9328-28
G1-1982	970	NG	150	14	6370	NG	130	14	75 - 500	NG	NG	9328-21
G1-2363	5500	2	100	21					0 - 38	NG	5E-8	9328-28
G1-2363	786	2	8	21					38 - 106	NG	5E-8	9328-28
G1-2363	680	2	100	21					106 - 500	NG	5E-8	9328-28
G1-2363	730	NG	50	14	6100	NG	300	14	75 - 500	NG	NG	9328-21
G1-2410	420	2	30	18					0 - 75	NG	2E-8	9328-29
G1-2410	440	2	80	18					75 - 500	NG	2E-8	9328-29
G1-2410	440	NG	80	14	6000	NG	3000	14	75 - 500	NG	NG	9328-21
G1-2476	4800	2	300	18					0 - 75	NG	6E-8	9328-29
G1-2476	3200	2	100	18					75 - 500	NG	6E-8	9328-29
G1-2476	3200	NG	100	14					75 - 500	NG	NG	9328-21
G1-2840	5600	2	600	18					0 - 75	NG	3E-8	9328-29
G1-2840	4900	2	400	18					75 - 500	NG	3E-8	9328-29
G1-2840	4900	NG	400	14	9000	NG	1100	14	75 - 500	NG	NG	9328-21
G1-2854	1800	2	800	18					0 - 75	NG	2E-8	9328-29
G1-2854	1300	2	200	18					75 - 500	NG	2E-8	9328-29
G1-2854	1300	NG	200	14	5000	NG	200	14	75 - 500	NG	NG	9328-21
JA-32	90	NG	20	14	850	NG	130	14	75 - 500	NG	NG	9328-21
YM-45	1600	NG	200	14	7300	NG	900	14	75 - 500	NG	NG	9328-21
YM-54	510	3	80	49	1800	3	100	49	0 - 500	NG	NG	9328-30
YM-54	1600	2	10	21					0 - 38	NG	4E-8	9328-28
YM-54	340	2	80	21					38 - 106	NG	4E-8	9328-28
YM-54	470	2	20	21					106 - 500	NG	4E-8	9328-28

Table A.5.2-1g
Sorption Data For Sorptive Categories
Devitrified Tuff With Clay

Sample	Average Sorption Ratio (ml/g)	Replications	Std. Dev. (ml/g)	Contact Time (days)	Average Desorption Ratio (ml/g)	Replications	Std. Dev. (ml/g)	Contact Time (days)	Particle Size (μm)	Soln-Solid Ratio (ml/g)	Tracer Feed Concentration (Molar)	Source
YM-54	470	NG	40	14	1840	NG	110	14	75 - 500	NG	NG	9328-21
** ELEMENT: Pu												
JA-32	110	2	0	14					75 - 500	NG	1E-10	9328-21
YM-54	90	3	20	49	720	3	5	49	0 - 500	NG	NG	9328-30
YM-54	80	2	20	14	720	2	40	14	75 - 500	NG	1E-10	9328-21
** ELEMENT: Ra												
G1-2363	540	2	60	42					106 - 500	NG	NG	9846-18
** ELEMENT: Se												
G1-1982	2.6	2	.1	42					75 - 500	NG	1.8E-11	10154-X
G1-2363	25	2	5	42					75 - 500	NG	1E-10	9846-18
G1-2840	3.1	2	.2	42					75 - 500	NG	1.8E-11	10154-X
GU-3-855	10	2	4	42					0 - 500	NG	NG	9846-18
** ELEMENT: Sn												
G1-2840	283	2	160	42					75 - 500	NG	2E-8	10154-X
** ELEMENT: Sr												
G1-1982	1200 *	2	0	18					0 - 38	NG	2E-7	9328-28
G1-1982	63	2	4	18					38 - 75	NG	2E-7	9328-28
G1-1982	51	2	2	18					75 - 250	NG	2E-7	9328-28
G1-1982	59	2	7	18					250 - 500	NG	2E-7	9328-28
G1-1982	55	NG	4	14	322	NG	8	14	75 - 500	NG	NG	9328-21
G1-2363	170	2	10	21					0 - 38	NG	5E-7	9328-28
G1-2363	70	2	10	21					38 - 106	NG	5E-7	9328-28
G1-2363	60	2	2	21					106 - 500	NG	5E-7	9328-28
G1-2363	64	NG	3	14	150	NG	6	14	75 - 500	NG	NG	9328-21
G1-2410	280	2	4	18	245	2	7		0 - 75	NG	4E-7	9328-29
G1-2410	169	2	1	18					75 - 500	NG	4E-7	9328-29
G1-2410					140	NG	14	14	75 - 500	NG		9328-21
G1-2476	50	2	1	18					0 - 75	NG	9E-7	9328-29
G1-2476	41	2	1	18					75 - 500	NG	9E-7	9328-29

Table A.5.2-1g
Sorption Data For Sorptive Categories
Devitrified Tuff With Clay

Sample	Average Sorption Ratio (ml/g)	Repli-cations	Std. Dev. (ml/g)	Contact Time (days)	Average Desorption Ratio (ml/g)	Repli-cations	Std. Dev. (ml/g)	Contact Time (days)	Particle Size (μm)	Soln-Solid Ratio (ml/g)	Tracer Feed Concentration (Molar)	Source
G1-2476	41	NG	1	14	200	NG	4	14	75 - 500	NG	NG	9328-21
G1-2840	170	2	1	18					0 - 75	NG	1E-6	9328-29
G1-2840	160	2	1	18					75 - 500	NG	1E-6	9328-29
G1-2840	160	NG	1	14	150	NG	4	14	75 - 500	NG	NG	9328-21
G1-2854	90	2	30	18					0 - 75	NG	5E-7	9328-29
G1-2854	94	2	1	18					75 - 500	NG	5E-7	9328-29
G1-2854					96	NG	1	14	75 - 500	NG		9328-21
JA-32	57	NG	3	14	53	NG	3	14	75 - 500	NG	NG	9328-21
YM-45	194	NG	14	14	210	NG	20	14	75 - 500	NG	NG	9328-21
YM-54	90	3	4	49	94	3	9	49	0 - 500	NG	NG	9328-30
YM-54	276	2	2	21					0 - 38	NG	6E-7	9328-28
YM-54	56.5	2	.4	21					38 - 106	NG	6E-7	9328-28
YM-54	47	2	10	21					106 - 500	NG	6E-7	9328-28
YM-54	62	NG	12	14	97	NG	9	14	75 - 500	NG	NG	9328-21
** ELEMENT: Th												
G1-2363	1213	NG	193	12					NG - NG	NG	6.52E-8	10032-13
** ELEMENT: U												
G1-1982	2.4	2	.1	42					75 - 500	NG	2.7E-6	10154-X
G1-2363	0	2	NG	42					75 - 500	NG	5.E-6	9846-15
G1-2840	.5	2	.1	42					75 - 500	NG	2.7E-6	10154-X
GU-3-855	10	2	.1	42					0 - 500	NG	NG	9846-18
JA-32	2.2	2	.9	14	8	2	2	14	75 - 500	NG	1E-10	9328-21
YM-54	1.7	3	.2	49	13	3	3	49	0 - 500	NG	NG	9328-30
YM-54	1.3	2	.3	14	12	2	8	14	75 - 500	NG	1E-10	9328-21

Table A.5.2-1h
Sorption Data For Sorptive Categories
Devitrified Tuff With Vapor

Sample	Average Sorption Ratio (ml/g)	Repli-cations	Std. Dev. (ml/g)	Contact Time (days)	Average Desorption Ratio (ml/g)	Repli-cations	Std. Dev. (ml/g)	Contact Time (days)	Particle Size (μm)	Soln-Solid Ratio (ml/g)	Tracer Feed Concentration (Molar)	Source
** ELEMENT: Am												
G1-1883	4700	2	300	14	7200	2	900	14	75 - 500	NG	1E-10	9328-21
** ELEMENT: Ba												
G1-1883	500	2	300	21					0 - 38	NG	7E-6	9328-28
G1-1883	204	2	5	21					38 - 106	NG	7E-6	9328-28
G1-1883	162	2	1	21					106 - 500	NG	7E-6	9328-28
G1-1883	182	NG	12	14	440	NG	10	14	75 - 500	NG	NG	9328-21
** ELEMENT: Ce												
G1-1883	140	NG	20	14	2200	NG	100	14	75 - 500	NG	NG	9328-21
** ELEMENT: Cs												
G1-1883	500	2	200	21					0 - 38	NG	4E-9	9328-28
G1-1883	190	2	10	21					38 - 106	NG	4E-9	9328-28
G1-1883	184	2	3	21					106 - 500	NG	4E-9	9328-28
G1-1883	187	NG	3	14	430	NG	4	14	75 - 500	NG	NG	9328-21
** ELEMENT: Eu												
G1-1883	510	2	200	21					0 - 38	NG	3E-8	9328-28
G1-1883	110	2	10	21					38 - 106	NG	3E-8	9328-28
G1-1883	160	2	10	21					106 - 500	NG	3E-8	9328-28
G1-1883					1350	NG	50	14	75 - 500	NG	NG	9328-21
** ELEMENT: Np												
G1-1883	6.4	2	.6	14	36	2	10	14	75 - 500	NG	1E-10	9328-21
** ELEMENT: Pu												
G1-1883	77	2	11	14	890	2	60	14	75 - 500	NG	1E-10	9328-21
** ELEMENT: Sr												
G1-1883	50	2	30	21					0 - 38	NG	3E-7	9328-28
G1-1883	22	2	1	21					38 - 106	NG	3E-7	9328-28
G1-1883	22	2	1	21					106 - 500	NG	3E-7	9328-28
G1-1883	22	NG	.2	14	59	NG	1	14	75 - 500	NG	NG	9328-21

Table A.5.2-1i
Sorption Data For Sorptive Categories
Zeolitic Tuff With Glass

Sample	Average Sorption Ratio (ml/g)	Repli-cations	Std. Dev. (ml/g)	Contact Time (days)	Average Desorption Ratio (ml/g)	Repli-cations	Std. Dev. (ml/g)	Contact Time (days)	Particle Size (μm)	Soln-Solid Ratio (ml/g)	Tracer Feed Concentration (Molar)	Source
** ELEMENT: Am												
YM-49	4300	2	1400	14	3400	2	400	14	75 - 500	NG	1E-10	9328-21
** ELEMENT: Ba												
YM-48	18000	NG	6000	14	34000	NG	7000	14	75 - 500	NG	NG	9328-21
YM-49	42000	NG	8000	14	65000	NG	7000	14	75 - 500	NG	NG	9328-21
** ELEMENT: Ce												
YM-48	1400	NG	500	14	128000	NG	300	14	75 - 500	NG	NG	9328-21
YM-49	550	NG	100	14	1040	NG	40	14	75 - 500	NG	NG	9328-21
** ELEMENT: Cs												
YM-48	9000	NG	4000	14	27000	NG	4000	14	75 - 500	NG	NG	9328-21
YM-49	36000	NG	3000	14	39000	NG	1000	14	75 - 500	NG	NG	9328-21
** ELEMENT: Eu												
YM-48	2200	NG	500	14	8100	NG	1200	14	75 - 500	NG	NG	9328-21
YM-49	1200	NG	100	14	2100	NG	500	14	75 - 500	NG	NG	9328-21
** ELEMENT: Np												
YM-49	9	2	3	14	12	2	4	14	75 - 500	NG	1E-10	9328-21
** ELEMENT: Pu												
YM-49	230	2	50	14	720	2	90	14	75 - 500	NG	1E-10	9328-21
** ELEMENT: Sr												
YM-48	2100	NG	400	14	2700	NG	200	14	75 - 500	NG	NG	9328-21
YM-49	3200	NG	300	14	4400	NG	100	14	75 - 500	NG	NG	9328-21
** ELEMENT: Tc												
YM-48	.15	NG	.02	14	1.6	NG	.2	14	75 - 500	NG	NG	9328-21
YM-49	.21	NG	.02	14	2.0	NG	.3	14	75 - 500	NG	NG	9328-21

Table A.5.2-1j
Sorption Data For Sorptive Categories
Analcime-Rich Tuff

Sample	Average Sorption Ratio (ml/g)	Repli-cations	Std. Dev. (ml/g)	Contact Time (days)	Average Desorption Ratio (ml/g)	Repli-cations	Std. Dev. (ml/g)	Contact Time (days)	Particle Size (μm)	Soln-Solid Ratio (ml/g)	Tracer Feed Concentration (Molar)	Source
** ELEMENT: Ba												
JA-26	800	NG	300	14	450	NG	13	14	75 - 500	NG	NG	9328-21
JA-28	820	NG	50	14	1160	NG	20	14	75 - 500	NG	NG	9328-21
** ELEMENT: Cs												
JA-26	1500	NG	600	14	1580	NG	90	14	75 - 500	NG	NG	9328-21
JA-28	1640	NG	210	14	2400	NG	100	14	75 - 500	NG	NG	9328-21
** ELEMENT: Eu												
JA-26					2900	NG	200	14	75 - 500	NG	NG	9328-21
JA-28	2100	NG	1000	14	12300	NG	500	14	75 - 500	NG	NG	9328-21
** ELEMENT: Sr												
JA-26	95	NG	35	14	39	NG	3	14	75 - 500	NG	NG	9328-21
JA-28	94	NG	20	14	114	NG	3	14	75 - 500	NG	NG	9328-21

Table A.5.2-1k
Sorption Data For Sorptive Categories
Devitrified Tuff With Calcite

Sample	Average Sorption Ratio (ml/g)	Repli-cations	Std. Dev. (ml/g)	Contact Time (days)	Average Desorption Ratio (ml/g)	Repli-cations	Std. Dev. (ml/g)	Contact Time (days)	Particle Size (μm)	Soln-Solid Ratio (ml/g)	Tracer Feed Concentration (Molar)	Source
** ELEMENT: Ba												
G1-2901	1600	NG	200	14	1980	NG	30	14	75 - 500	NG	NG	9328-21
** ELEMENT: Ce												
G1-2901	42000	NG	3000	14	39000	NG	1000	14	75 - 500	NG	NG	9328-21
** ELEMENT: Cs												
G1-2901	1290	NG	110	14	1380	NG	30	14	75 - 500	NG	NG	9328-21
** ELEMENT: Eu												
G1-2901	160000	NG	50000	14	210000	NG	50000	14	75 - 500	NG	NG	9328-21
** ELEMENT: Sn												
G1-2901	22000	2	5000	42					75 - 500	NG	1E-7	10154-X
** ELEMENT: Sr												
G1-2901	68	NG	1	14	67	NG	1	14	75 - 500	NG	NG	9328-21

Table A.5.2-11
Sorption Data For Sorptive Categories
Clay-Rich Devitrified Samples With Zeolites

Sample	Average Sorption Ratio (ml/g)	Repli-cations	Std. Dev. (ml/g)	Contact Time (days)	Average Desorption Ratio (ml/g)	Repli-cations	Std. Dev. (ml/g)	Contact Time (days)	Particle Size (μm)	Soln-Solid Ratio (ml/g)	Tracer Feed Concentration (Molar)	Source
** ELEMENT: Am												
JA-37	28000	2	10000	14	32000	2	10000	14	75 - 500	NG	1E-10	9328-21
** ELEMENT: Ba												
JA-37	760	NG	150	14	920	NG	40	14	75 - 500	NG	NG	9328-21
** ELEMENT: Cs												
JA-37	610	NG	40	14	850	NG	50	14	75 - 500	NG	NG	9328-21
** ELEMENT: Eu												
JA-37	6000	NG	800	14	11000	NG	2000	14	75 - 500	NG	NG	9328-21
** ELEMENT: Np												
JA-37	28	2	7	14	170	2	50	14	75 - 500	NG	1E-10	9328-21
** ELEMENT: Pu												
JA-37	400	2	70	14	1400	2	300	14	75 - 500	NG	1E-10	9328-21
** ELEMENT: Sr												
JA-37	287	NG	14	14	312	NG	9	14	75 - 500	NG	NG	9328-21
** ELEMENT: U												
JA-37	4.6	2	.3	14	9.9	2	.4	14	75 - 500	NG	1E-10	9328-21

Table A.5.2-1m
Sorption Data For Sorptive Categories
Smectite-Rich Tuff

Sample	Average Sorption Ratio (ml/g)	Repli-cations	Std. Dev. (ml/g)	Contact Time (days)	Average Desorption Ratio (ml/g)	Repli-cations	Std. Dev. (ml/g)	Contact Time (days)	Particle Size (μm)	Soln-Solid Ratio (ml/g)	Tracer Feed Concentration (Molar)	Source
** ELEMENT: Ba												
G1-3658	15000	2	4000	21					0 - 38	NG	9E-6	9328-28
G1-3658	9600	2	600	21					38 - 106	NG	9E-6	9328-28
G1-3658	13000	2	1000	21					106 - 500	NG	9E-6	9328-28
G1-3658	13500	NG	500	14	10000	NG	4000	14	75 - 500	NG	NG	9328-21
** ELEMENT: Ce												
G1-3658	1000	NG	200	14	9000	NG	4000	14	75 - 500	NG	NG	9328-21
** ELEMENT: Cs												
G1-3658	16000	2	2000	21					0 - 38	NG	7E-9	9328-28
G1-3658	6600	2	500	21					38 - 106	NG	7E-9	9328-28
G1-3658	4980	2	70	21					106 - 500	NG	7E-9	9328-28
G1-3658	4950	NG	50	14	12000	NG	2000	14	75 - 500	NG	NG	9328-21
** ELEMENT: Eu												
G1-3658	15000	2	600	21					0 - 38	NG	4E-7	9328-28
G1-3658	440	2	30	21					38 - 106	NG	4E-7	9328-28
G1-3658	530	2	40	21					106 - 500	NG	4E-7	9328-28
G1-3658	530	NG	40	14	9000	NG	3000	14	75 - 500	NG	NG	9328-21
** ELEMENT: Sr												
G1-3658	13000	2	3000	21					0 - 38	NG	3E-7	9328-28
G1-3658	13000	2	1000	21					38 - 106	NG	3E-7	9328-28
G1-3658	13200	2	200	21					106 - 500	NG	3E-7	9328-28
G1-3658	13000	NG	0	14	12000	NG	3000	14	75 - 500	NG	NG	9328-21

Table R.5.2-1n
Sorption Data For Sorptive Categories
Devitrified Tuff With Clay and Minor Glass

Sample	Average Sorption Ratio (ml/g)	Repli-cations	Std. Dev. (ml/g)	Contact Time (days)	Average Desorption Ratio (ml/g)	Repli-cations	Std. Dev. (ml/g)	Contact Time (days)	Particle Size (μm)	Soln-Solid Ratio (ml/g)	Tracer Feed Concentration (Molar)	Source
** ELEMENT: Am												
G2-547	13000	2	110	42					75 - 500	NG	NG	9846-18
G2-547					17000	2	1400	NG	75 - 500	NG	NG	9846-17
G2-547	13000	2	110	NG					NG - NG	NG	NG	9793-6
** ELEMENT: Ba												
G2-547					2900	2	170	42	0 - 500	NG	NG	9793-4
G2-547	3490	2	30	42					75 - 500	NG	NG	9846-18
** ELEMENT: Cs												
G2-547					8900	2	550	42	0 - 500	NG	NG	9793-4
G2-547	13300	2	1500	42					75 - 500	NG	NG	9846-18
** ELEMENT: Eu												
G2-547					1700	2	630	42	0 - 500	NG	NG	9793-4
G2-547	390	2	30	42					75 - 500	NG	NG	9846-18
** ELEMENT: Pu												
G2-547	1200 *	2	200	42					75 - 500	NG	NG	9846-18
G2-547	1200	2	120	42	1200	2	80	NG	75 - 500	NG	NG	9846-17
** ELEMENT: Se												
G2-547	2	2	2	42					75 - 500	NG	1E-10	9846-18
** ELEMENT: Sr												
G2-547					206	2	11	42	0 - 500	NG	NG	9793-4
G2-547	265	2	10	42					75 - 500	NG	NG	9846-18
** ELEMENT: Tc												
G2-547	0	2	NG	42	0	2	NG	42	0 - 500	NG	NG	9793-4
** ELEMENT: U												
G2-547	9.4	2	.1	42					75 - 500	NG	5.E-6	9846-15

Table A.5.2-1o
Sorption Data For Sorptive Categories
Calcite-Rich Vitric Tuff With Clay

Sample	Average Sorption Ratio (ml/g)	Repli-cations	Std. Dev. (ml/g)	Contact Time (days)	Average Desorption Ratio (ml/g)	Repli-cations	Std. Dev. (ml/g)	Contact Time (days)	Particle Size (μm)	Soln-Solid Ratio (ml/g)	Tracer Feed Concentration (Molar)	Source
** ELEMENT: Am												
G2-723	890000	2	50000	42					75 - 500	NG	NG	9846-18
G2-723					2800000	2	NG	NG	75 - 500	NG	NG	9846-17
G2-723	890000	2	49000	NG					NG - NG	NG	NG	9793-6
** ELEMENT: Ba												
G2-723	3500	2	430	42	4210	2	10	42	0 - 500	NG	NG	9793-4
G2-723	3500	2	400	42					75 - 500	NG	NG	9846-18
** ELEMENT: Cs												
G2-723	4080	2	550	42	4280	2	4	42	0 - 500	NG	NG	9793-4
G2-723	4100	2	600	42					75 - 500	NG	NG	9846-18
** ELEMENT: Eu												
G2-723					10000	2	NG	42	0 - 500	NG	NG	9793-4
G2-723	10000		NG	42					75 - 500	NG	NG	9846-18
** ELEMENT: Pu												
G2-723	4500	2	NG	42					75 - 500	NG	NG	9846-18
G2-723					4700	2	NG	NG	75 - 500	NG	NG	9846-17
G2-723	10000	2	NG	NG					NG - NG	NG	NG	9793-6
** ELEMENT: Se												
G2-723	19	2	2	42					75 - 500	NG	1E-10	9846-18
** ELEMENT: Sr												
G2-723					330	2	4	42	0 - 500	NG	NG	9793-4
G2-723	290	2	40	42					75 - 500	NG	NG	9846-18
** ELEMENT: Tc												
G2-723	0	2	NG	42	0	2	NG	42	0 - 500	NG	NG	9793-4
** ELEMENT: U												
G2-723	2.4	2	.6	42					75 - 500	NG	5.E-6	9846-15

Table A.5.2-1p
Sorption Data For Sorptive Categories
Devitrified Tuff With Mordenite

Sample	Average Sorption Ratio (ml/g)	Replications	Std. Dev. (ml/g)	Contact Time (days)	Average Desorption Ratio (ml/g)	Replications	Std. Dev. (ml/g)	Contact Time (days)	Particle Size (μm)	Soln-Solid Ratio (ml/g)	Tracer Feed Concentration (Molar)	Source
** ELEMENT: Am												
G2-1952	1800	2	70	42					75 - 500	NG	NG	9846-18
G2-1952					3900	2	100	NG	75 - 500	NG	NG	9846-17
G2-1952	1600	2	100	42	7600	2	500	NG	75 - 500	NG	NG	9846-17
** ELEMENT: Ba												
G2-1952	25000	2	3700	42	40000	2	6000	42	0 - 500	NG	NG	9793-4
G2-1952	25000	2	4000	42					75 - 500	NG	NG	9846-18
** ELEMENT: Cs												
G2-1952					46000	2	1400	42	0 - 500	NG	NG	9793-4
G2-1952	63300	2	1100	42					75 - 500	NG	NG	9846-18
** ELEMENT: Eu												
G2-1952					1600	2	200	42	0 - 500	NG	NG	9793-4
G2-1952	89	2	14	42					75 - 500	NG	NG	9846-18
** ELEMENT: Np												
G2-1952	2.7	2	.1	42	15	2	2	NG	75 - 500	NG	NG	9846-17
** ELEMENT: Pu												
G2-1952	76	2	4	42					75 - 500	NG	NG	9846-18
G2-1952					420	2	40	NG	75 - 500	NG	NG	9846-17
G2-1952	56	2	1	42	280	2	30	NG	75 - 500	NG	NG	9846-17
G2-1952	83	2	6	NG					NG - NG	NG	NG	9793-6
G2-1952	59	2	2	NG					NG - NG	NG	NG	9793-6
** ELEMENT: Se												
G2-1952	2	2	1	42					75 - 500	NG	1E-10	9846-18
** ELEMENT: Sr												
G2-1952					4200	2	180	42	0 - 500	NG	NG	9793-4
G2-1952	2200	2	400	42					75 - 500	NG	NG	9846-18
** ELEMENT: Tc												
G2-1952	0	2	NG	42	0	2	NG	42	0 - 500	NG	NG	9793-4
** ELEMENT: U												
G2-1952	0	2	NG	42					75 - 500	NG	5.E-6	9846-15

Table A.5.2-1q
Sorption Data For Sorptive Categories
Devitrified Tuff With Analcime and Clay

Sample	Average Sorption Ratio (ml/g)	Replications	Std. Dev. (ml/g)	Contact Time (days)	Average Desorption Ratio (ml/g)	Replications	Std. Dev. (ml/g)	Contact Time (days)	Particle Size (μm)	Soln-Solid Ratio (ml/g)	Tracer Feed Concentration (Molar)	Source
** ELEMENT: Am												
G2-3933	6600	2	400	42					75 - 500	NG	NG	9846-18
G2-3933					11500	2	500	NG	75 - 500	NG	NG	9846-17
G2-3933	6600	2	370	NG					NG - NG	NG	NG	9793-6
** ELEMENT: Ba												
G2-3933					1100	2	200	42	0 - 500	NG	NG	9793-4
G2-3933	1700	2	500	42					75 - 500	NG	NG	9846-18
** ELEMENT: Cs												
G2-3933					1400	2	350	42	0 - 500	NG	NG	9793-4
G2-3933	2500	2	1000	42					75 - 500	NG	NG	9846-18
** ELEMENT: Eu												
G2-3933					3000	2	1100	42	0 - 500	NG	NG	9793-4
G2-3933	1500	2	700	42					75 - 500	NG	NG	9846-18
** ELEMENT: Pu												
G2-3933	1600	2	30	42					75 - 500	NG	NG	9846-18
G2-3933					490	2	160	NG	75 - 500	NG	NG	9846-17
G2-3933	1600	2	50	NG					NG - NG	NG	NG	9793-6
** ELEMENT: Se												
G2-3933	0	2	1	42					75 - 500	NG	1E-10	9846-18
** ELEMENT: Sr												
G2-3933					140	2	24	42	0 - 500	NG	NG	9793-4
G2-3933	240	2	60	42					75 - 500	NG	NG	9846-18
** ELEMENT: Tc												
G2-3933					0	2	NG	42	0 - 500	NG	NG	9793-4
G2-3933	.1	2	.06	42					75 - 500	NG	NG	9846-18
** ELEMENT: U												
G2-3933	0	2	NG	42					75 - 500	NG	5.E-6	9846-15

Table A.5.2-1r
Sorption Data For Sorptive Categories
Vitric Tuff

Sample	Average Sorption Ratio (ml/g)	Repli-cations	Std. Dev. (ml/g)	Contact Time (days)	Average Desorption Ratio (ml/g)	Repli-cations	Std. Dev. (ml/g)	Contact Time (days)	Particle Size (μm)	Soln-Solid Ratio (ml/g)	Tracer Feed Concentration (Molar)	Source
** ELEMENT: Am												
GU-3-1203	920	2	60	42					75 - 500	NG	NG	9846-18
GU-3-1203					1200	2	200	NG	75 - 500	NG	NG	9846-17
GU-3-1203	1300	2	110	42	1400	2	460	NG	75 - 500	NG	NG	9846-17
** ELEMENT: Ba												
G1-1292	2100	2	300	42					75 - 500	NG	NG	9846-18
G1-1292	2100	NG	300	14	1500	NG	100	14	75 - 500	NG	NG	9328-21
GU-3-1203	640	2	40	42	720	2	30	42	75 - 500	NG	4E-8	10006-IV
** ELEMENT: Ca												
G1-1292	66	NG	8	14	600	NG	200	14	75 - 500	NG	NG	9328-21
** ELEMENT: Cs												
G1-1292	430	NG	28	14	510	NG	20	14	75 - 500	NG	NG	9328-21
GU-3-1203	350	2	30	42	340	2	10	42	75 - 500	NG	4E-9	10006-IV
** ELEMENT: Eu												
G1-1292	140	NG	14	14	600	NG	70	14	75 - 500	NG	NG	9328-21
GU-3-1203	190	2	2	42	650	2	50	42	75 - 500	NG	9E-8	10006-IV
** ELEMENT: Pu												
GU-3-1203	410	2	70	42					75 - 500	NG	NG	9846-18
GU-3-1203					900	2	20	NG	75 - 500	NG	NG	9846-17
GU-3-1203	320	2	20	42	930	2	10	NG	75 - 500	NG	NG	9846-17
** ELEMENT: Ra												
G1-1292	1500	2	100	42					75 - 500	NG	NG	9846-18
** ELEMENT: Se												
GU-3-1203	1	2	1	42					75 - 500	NG	1E-10	9846-18
GU-3-1436	3	2	0	42					0 - 500	NG	NG	9846-18

Table A.5.2-1r
Sorption Data For Sorptive Categories
Vitric Tuff

Sample	Average Sorption Ratio (ml/g)	Repli-cations	Std. Dev. (ml/g)	Contact Time (days)	Average Desorption Ratio (ml/g)	Repli-cations	Std. Dev. (ml/g)	Contact Time (days)	Particle Size (μm)	Soln-Solid Ratio (ml/g)	Tracer Feed Concentration (Molar)	Source
** ELEMENT: Sr												
G1-1292	200	NG	6	14	120	NG	5	14	75 - 500	NG	NG	9328-21
GU-3-1203	42	2	1	42	47	2	1	42	75 - 500	NG	1E-6	10006-IV
** ELEMENT: Tc												
GU-3-1203	0	2	NG	42					75 - 500	NG	1E-11	10006-IV
** ELEMENT: Th												
G1-1292	478	NG	63	12					NG - NG	NG	5.39E-8	10032-13
** ELEMENT: U												
G1-1292	0	2	NG	42					75 - 500	NG	5.E-6	9846-15
GU-3-1203	0	2	NG	42					75 - 500	NG	5.E-6	9846-15
GU-3-1436	20	2	2	42					0 - 500	NG	NG	9846-18

Table A.5.2-2a
Sorption Data For Sorptive Intervals
Host Rock

Sample	Average Sorption Ratio (ml/g)	Repli-cations	Std. Dev. (ml/g)	Contact Time (days)	Average Desorption Ratio (ml/g)	Repli-cations	Std. Dev. (ml/g)	Contact Time (days)	Particle Size (μm)	Soln-Solid Ratio (ml/g)	Tracer Feed Concentration (Molar)	Source
** ELEMENT: Am												
GU-3-433	3100	2	200	42					75 - 500	NG	NG	9846-18
GU-3-433					7800	2	1700	NG	75 - 500	NG	NG	9846-17
GU-3-433	3600	2	150	42	11000	2	3300	NG	75 - 500	NG	NG	9846-17
** ELEMENT: Ba												
GU-3-433	810	2	100	42					75 - 500	NG	NG	9793-5
GU-3-433	340	2	50	42					75 - 500	NG	NG	9793-5
GU-3-433					470	2	10	42	0 - 500	NG	NG	9846-16
GU-3-433					460	2	50	42	0 - 500	NG	NG	9846-16
** ELEMENT: Cs												
GU-3-433	630	2	20	42					75 - 500	NG	NG	9793-5
GU-3-433	400	2	40	42					75 - 500	NG	NG	9793-5
GU-3-433					530	2	50	42	0 - 500	NG	NG	9846-16
GU-3-433					510	2	20	42	0 - 500	NG	NG	9846-16
** ELEMENT: Eu												
GU-3-433	100	2	14	42					75 - 500	NG	NG	9793-5
GU-3-433	68	2	14	42					75 - 500	NG	NG	9793-5
GU-3-433					120	2	20	42	0 - 500	NG	NG	9846-16
GU-3-433					150	2	20	42	0 - 500	NG	NG	9846-16
** ELEMENT: Np												
GU-3-916	4.9	2	.1	42					75 - 500	NG	6E-11	10006-IV
GU-3-916	4.9	2	1	42	33	2	1	42	75 - 500	NG	6E-11	10032-2
GU-3-916	5.3	2	1.0	91					75 - 500	NG	6E-11	10032-2
GU-3-916	5.4	?	1	183					75 - 500	NG	6E-11	10154-XI
** ELEMENT: Pu												
GU-3-433	420	2	80	42					75 - 500	NG	NG	9846-18
GU-3-433					890	2	100	NG	75 - 500	NG	NG	9846-17

Table A.5.2-2a
Sorption Data For Sorptive Intervals
Host Rock

Sample	Average Sorption Ratio (ml/g)	Replications	Std. Dev. (ml/g)	Contact Time (days)	Average Desorption Ratio (ml/g)	Replications	Std. Dev. (ml/g)	Contact Time (days)	Particle Size (μm)	Soln-Solid Ratio (ml/g)	Tracer Feed Concentration (Molar)	Source
GU-3-433	240	2	2	42	960	2	80	NG	75 - 500	NG	NG	9846-17
GU-3-916	240	2	25	42					75 - 500	NG	1E-7	10006-IV
GU-3-916	250	2	25	42	680	2	40	42	75 - 500	NG	1E-7	10032-2
** ELEMENT: Se												
GU-3-433	15	2	3	42					75 - 500	NG	1E-10	9846-18
GU-3-855	10	2	4	42					0 - 500	NG	NG	9846-18
** ELEMENT: Sr												
GU-3-433	61	2	6	42					75 - 500	NG	NG	9793-5
GU-3-433	30	2	2	42					75 - 500	NG	NG	9793-5
GU-3-433					44	2	5	42	0 - 500	NG	NG	9846-16
GU-3-433					34	2	2	42	0 - 500	NG	NG	9846-16
** ELEMENT: Tc												
GU-3-433	0	2	NG	42					75 - 500	NG	NG	9793-5
GU-3-433	.07	2	.02	42					75 - 500	NG	NG	9793-5
GU-3-916	.72	2	.2	42					75 - 500	NG	6E-10	10032-2
GU-3-916	.81	2	.5	91					75 - 500	NG	6E-10	10032-2
GU-3-916	.62	2	.2	183					75 - 500	NG	6E-10	10154-XI
** ELEMENT: U												
GU-3-433	0	2	NG	42					75 - 500	NG	5.E-6	9846-15
GU-3-855	10	2	.1	42					0 - 500	NG	NG	9846-18

Table A.5.2-2b
Sorption Data For Sorptive Intervals
Zeolite 1

Sample	Average Sorption Ratio (ml/g)	Repli-cations	Std. Dev. (ml/g)	Contact Time (days)	Average Desorption Ratio (ml/g)	Repli-cations	Std. Dev. (ml/g)	Contact Time (days)	Particle Size (μm)	Soln-Solid Ratio (ml/g)	Tracer Feed Concentration (Molar)	Source
** ELEMENT: Ba												
YM-30	3400	NG	1500	14	3100	NG	600	14	75 - 500	NG	NG	9328-21
** ELEMENT: Ce												
YM-30	230000	NG	100000	14	170000	NG	15000	14	75 - 500	NG	NG	9328-21
** ELEMENT: Cs												
YM-30	855	NG	5	14	1500	NG	100	14	75 - 500	NG	NG	9328-21
** ELEMENT: Eu												
YM-30	160000	NG	50000	14	11000	NG	700	14	75 - 500	NG	NG	9328-21
** ELEMENT: Sr												
YM-30	260	NG	80	14	210	NG	30	14	75 - 500	NG	NG	9328-21

Table A.5.2-2c
Sorption Data For Sorptive Intervals
Basal Vitrophyre

Sample	Average Sorption Ratio (ml/g)	Repli-cations	Std. Dev. (ml/g)	Contact Time (days)	Average Desorption Ratio (ml/g)	Repli-cations	Std. Dev. (ml/g)	Contact Time (days)	Particle Size (μm)	Soln-Solid Ratio (ml/g)	Tracer Feed Concentration (Molar)	Source
** ELEMENT: Am												
GU-3-1203	920	2	60	42					75 - 500	NG	NG	9846-18
GU-3-1203					1200	2	200	NG	75 - 500	NG	NG	9846-17
GU-3-1203	1300	2	110	42	1400	2	460	NG	75 - 500	NG	NG	9846-17
** ELEMENT: Ba												
G1-1292	2100	2	300	42					75 - 500	NG	NG	9846-18
G1-1292	2100	NG	300	14	1500	NG	100	14	75 - 500	NG	NG	9328-21
GU-3-1203	640	2	40	42	720	2	30	42	75 - 500	NG	4E-8	10006-IV
** ELEMENT: Ce												
G1-1292	66	NG	8	14	600	NG	200	14	75 - 500	NG	NG	9328-21
** ELEMENT: Cs												
G1-1292	430	NG	28	14	510	NG	20	14	75 - 500	NG	NG	9328-21
GU-3-1203	350	2	30	42	340	2	10	42	75 - 500	NG	4E-9	10006-IV
** ELEMENT: Eu												
G1-1292	140	NG	14	14	600	NG	70	14	75 - 500	NG	NG	9328-21
GU-3-1203	190	2	2	42	650	2	50	42	75 - 500	NG	9E-8	10006-IV
** ELEMENT: Pu												
GU-3-1203	410	2	70	42					75 - 500	NG	NG	9846-18
GU-3-1203					900	2	20	NG	75 - 500	NG	NG	9846-17
GU-3-1203	320	2	20	42	930	2	10	NG	75 - 500	NG	NG	9846-17
** ELEMENT: Ra												
G1-1292	1500	2	100	42					75 - 500	NG	NG	9846-18
** ELEMENT: Se												
GU-3-1203	1	2	1	42					75 - 500	NG	1E-10	9846-18
** ELEMENT: Sr												
G1-1292	200	NG	6	14	120	NG	5	14	75 - 500	NG	NG	9328-21
GU-3-1203	42	2	1	42	47	2	1	42	75 - 500	NG	1E-6	10006-IV
** ELEMENT: Tc												
GU-3-1203	0	2	NG	42					75 - 500	NG	1E-11	10006-IV
** ELEMENT: Th												
G1-1292	478	NG	63	12					NG - NG	NG	5.39E-8	10032-13
** ELEMENT: U												
G1-1292	0	2	NG	42					75 - 500	NG	5.E-6	9846-15
GU-3-1203	0	2	NG	42					75 - 500	NG	5.E-6	9846-15

Table A.5.2-2d
Sorption Data For Sorptive Intervals
Vitric Zone

Sample	Average Sorption Ratio (ml/g)	Repli-cations	Std. Dev. (ml/g)	Contact Time (days)	Average Desorption Ratio (ml/g)	Repli-cations	Std. Dev. (ml/g)	Contact Time (days)	Particle Size (μm)	Soln-Solid Ratio (ml/g)	Tracer Feed Concentration (Molar)	Source
** ELEMENT: Am												
GU-3-1301	2000	2	40	42					75 - 500	NG	NG	9846-18
GU-3-1301					1500	2	5	NG	75 - 500	NG	NG	9846-17
GU-3-1301	1500	2	120	42	3500	2	320	NG	75 - 500	NG	NG	9846-17
** ELEMENT: Ba												
GU-3-1301	570	2	60	42					75 - 500	NG	NG	9793-5
GU-3-1301	420	2	50	42					75 - 500	NG	NG	9793-5
GU-3-1301					660	2	100	42	0 - 500	NG	NG	9846-16
GU-3-1301					690	2	100	42	0 - 500	NG	NG	9846-16
GU-3-1301	82	2	18	42	140	2	30	42	75 - 500	NG	8E-8	10154-13
** ELEMENT: Cs												
GU-3-1301	160	2	35	42					75 - 500	NG	NG	9793-5
GU-3-1301	120	2	15	42					75 - 500	NG	NG	9793-5
GU-3-1301					180	2	40	42	0 - 500	NG	NG	9846-16
GU-3-1301					180	2	30	42	0 - 500	NG	NG	9846-16
GU-3-1301	45	2	5	42	55	2	4	42	75 - 500	NG	4E-9	10154-13
** ELEMENT: Eu												
GU-3-1301	75	2	12	42					75 - 500	NG	NG	9793-5
GU-3-1301	38	2	7	42					75 - 500	NG	NG	9793-5
GU-3-1301					110	2	40	42	0 - 500	NG	NG	9846-16
GU-3-1301					90	2	40	42	0 - 500	NG	NG	9846-16
GU-3-1301	17000	2	NG	42	20000	2	NG	42	75 - 500	NG	1E-7	10154-13
** ELEMENT: Np												
GU-3-1301	2.2	2	1	91	25	2	2	42	75 - 500	NG	6E-11	10032-2
GU-3-1301	2	2	1	91					75 - 500	NG	6E-11	10032-2
GU-3-1301	2.1	4	1	91					75 - 500	NG	6E-11	10154-XI
GU-3-1301	2.2	2	1	183					75 - 500	NG	6E-11	10154-XI

Table A.5.2-2d
Sorption Data For Sorptive Intervals
Vitric Zone

Sample	Average Sorption Ratio (ml/g)	Repli-cations	Std. Dev. (ml/g)	Contact Time (days)	Average Desorption Ratio (ml/g)	Repli-cations	Std. Dev. (ml/g)	Contact Time (days)	Particle Size (μm)	Soln-Solid Ratio (ml/g)	Tracer Feed Concentration (Molar)	Source
** ELEMENT: Pu												
GU-3-1301	210	2	30	42					75 - 500	NG	NG	9846-18
GU-3-1301					580	2	20	NG	75 - 500	NG	NG	9846-17
GU-3-1301	360	2	20	42	2100	2	330	NG	75 - 500	NG	NG	9846-17
** ELEMENT: Se												
GU-3-1301	7	2	2	42					75 - 500	NG	1E-10	9846-18
GU-3-1436	3	2	0	42					0 - 500	NG	NG	9846-18
** ELEMENT: Sn												
GU-3-1301	168	2	8	42					75 - 500	NG	2E-8	10154-X
** ELEMENT: Sr												
GU-3-1301	32	2	8	42					75 - 500	NG	NG	9793-5
GU-3-1301	24	2	1	42					75 - 500	NG	NG	9793-5
GU-3-1301					90	2	20	42	0 - 500	NG	NG	9846-16
GU-3-1301					60	2	30	42	0 - 500	NG	NG	9846-16
GU-3-1301	10	2	2	42	32	2	1	42	75 - 500	NG	1E-6	10154-13
** ELEMENT: Tc												
GU-3-1301	.03	2	.004	42					75 - 500	NG	NG	9793-5
GU-3-1301	.04	2	.01	42					75 - 500	NG	NG	9793-5
GU-3-1301	.04	2	.02	42					75 - 500	NG	7E-10	10154-XI
GU-3-1301	.03	2	.03	91					75 - 500	NG	7E-10	10154-XI
GU-3-1301	0	2	.004	91					75 - 500	NG	7E-10	10154-XI
** ELEMENT: U												
GU-3-1301	0	2	NG	42					75 - 500	NG	5.E-6	9846-15
GU-3-1436	20	2	2	42					0 - 500	NG	NG	9846-18

Table A.5.2-2a
Sorption Data For Sorptive Intervals
Zeolite 2

Sample	Average Sorption Ratio (ml/g)	Replications	Std. Dev. (ml/g)	Contact Time (days)	Average Desorption Ratio (ml/g)	Replications	Std. Dev. (ml/g)	Contact Time (days)	Particle Size (μm)	Soln-Solid Ratio (ml/g)	Tracer Feed Concentration (Molar)	Source
** ELEMENT: Am												
G4-1502	490	2	20	.04					75 - 500	NG	1.3E-8	10006-5
G4-1502	715	2	5	.16					75 - 500	NG	1.3E-8	10006-5
G4-1502	1100	2	60	1					75 - 500	NG	1.3E-8	10006-5
G4-1502	1200	2	5	2					75 - 500	NG	1.3E-8	10006-5
G4-1502	1450	2	50	3					75 - 500	NG	1.3E-8	10006-5
G4-1502	1900	2	20	7					75 - 500	NG	1.3E-8	10006-5
G4-1502	1550	2	10	21					75 - 500	NG	1.3E-8	10006-5
G4-1502	1400	2	5	42					75 - 500	NG	1.3E-8	10006-5
YM-38	5500	3	1000	49	9500	3	1300	49	0 - 500	NG	NG	9328-30
YM-38	4600	2	1100	14	7100	2	1200	14	75 - 500	NG	1E-10	9328-21
** ELEMENT: Ba												
G1-1436	150000	2	24000	42					75 - 500	NG	NG	9846-18
G1-1436	150000	NG	24000	14	340000	NG	90000	14	75 - 500	NG	NG	9328-21
G1-1854	56000	2	8000	18	195000	2	77782		0 - 75	NG	1E-7	9328-29
G1-1854	34000	2	0	18					75 - 500	NG	1E-7	9328-29
G1-1854	45000	NG	7000	14	150000	NG	40000	14	75 - 500	NG	NG	9328-21
YM-38	11000	1	561	21					0 - 75	5:1	NG	9328-XLII
YM-38	81500	1	2934	21					0 - 75	30:1	6E-7	9328-XLII
YM-38	9020	1	469	42					0 - 75	5:1	NG	9328-XLII
YM-38	16000	1	544	42					0 - 75	10:1	NG	9328-XLII
YM-38	78900	1	2919	42					0 - 75	30:1	NG	9328-XLII
YM-38	7410	1	378	21					75 - 500	5:1	NG	9328-XLII
YM-38	48000	1	3456	21					75 - 500	10:1	NG	9328-XLII
YM-38	54200	1	1680	21					75 - 500	30:1	NG	9328-XLII
YM-38	6180	1	254	42					75 - 500	5:1	NG	9328-XLII
YM-38	23200	1	905	42					75 - 500	10:1	NG	9328-XLII
YM-38	49200	1	1870	42					75 - 500	30:1	NG	9328-XLII
YM-38	66000	3	13000	49	260000	3	NG	49	0 - 500	NG	NG	9328-30
YM-38	130000	2	60000	21					0 - 38	NG	4E-7	9328-28
YM-38	110000	2	9000	21					38 - 106	NG	4E-7	9328-28
YM-38	80000	2	23000	21					106 - 500	NG	4E-7	9328-28
YM-38	100000	NG	10000	14	260000	NG	NG	14	75 - 500	NG	NG	9328-21

Table A.5.2-2e
Sorption Data For Sorptive Intervals
Zeolite 2

Sample	Average Sorption Ratio (ml/g)	Repli-cations	Std. Dev. (ml/g)	Contact Time (days)	Average Desorption Ratio (ml/g)	Repli-cations	Std. Dev. (ml/g)	Contact Time (days)	Particle Size (μm)	Soln-Solid Ratio (ml/g)	Tracer Feed Concentration (Molar)	Source
YM-42	94000	NG	14000	14	90000	NG	30000	14	75 - 500	NG	NG	9328-21
** ELEMENT: Ca												
G1-1436	59000	NG	7000	14	6700	NG	600	14	75 - 500	NG	NG	9328-21
YM-38	1330	1	230	21					0 - 75	5:1	NG	9328-XLII
YM-38	6390	1	837	21					0 - 75	10:1	NG	9328-XLII
YM-38	9070	1	544	21					0 - 75	30:1	NG	9328-XLII
YM-38	1140	1	233	42					0 - 75	5:1	NG	9328-XLII
YM-38	5460	1	835	42					0 - 75	10:1	NG	9328-XLII
YM-38	9190	1	763	42					0 - 75	30:1	NG	9328-XLII
YM-38	2560	1	440	21					75 - 500	5:1	NG	9328-XLII
YM-38	7230	1	940	21					75 - 500	10:1	NG	9328-XLII
YM-38	16000	1	928	21					75 - 500	30:1	NG	9328-XLII
YM-38	1600	1	309	42					75 - 500	5:1	NG	9328-XLII
YM-38	6050	1	926	42					75 - 500	10:1	NG	9328-XLII
YM-38	11600	1	1311	42					75 - 500	30:1	NG	9328-XLII
YM-38	820	3	100	49	2640	3	NG	49	0 - 500	NG	NG	9328-30
YM-38	760	NG	140	14	2600	NG	NG	14	75 - 500	NG	NG	9328-21
YM-42	49000	NG	7000	14	44000	NG	5000	14	75 - 500	NG	NG	9328-21
** ELEMENT: Cs												
G1-1436	7800	NG	500	14	24000	NG	2000	14	75 - 500	NG	NG	9328-21
G1-1854	13000	NG	2000	14	14000	NG	2000	14	75 - 500	NG	NG	9328-21
YM-38	5970	1	698	21					0 - 75	5:1	NG	9328-XLII
YM-38	5760	1	432	21					0 - 75	10:1	NG	9328-XLII
YM-38	7980	1	271	21					0 - 75	30:1	NG	9328-XLII
YM-38	5100	1	622	42					0 - 75	5:1	NG	9328-XLII
YM-38	5120	1	312	42					0 - 75	10:1	NG	9328-XLII
YM-38	3660	1	388	21					75 - 500	5:1	2E-9	9328-XLII
YM-38	5750	1	403	21					75 - 500	10:1	NG	9328-XLII
YM-38	5540	1	177	21					75 - 500	30:1	NG	9328-XLII
YM-38	5110	1	925	42					75 - 500	5:1	NG	9328-XLII
YM-38	7280	1	510	42					75 - 500	10:1	NG	9328-XLII
YM-38	6270	1	270	42					75 - 500	30:1	NG	9328-XLII

Table A.5.2-2e
Sorption Data For Sorptive Intervals
Zeolite 2

Sample	Average Sorption Ratio (ml/g)	Repli-cations	Std. Dev. (ml/g)	Contact Time (days)	Average Desorption Ratio (ml/g)	Repli-cations	Std. Dev. (ml/g)	Contact Time (days)	Particle Size (μm)	Soln-Solid Ratio (ml/g)	Tracer Feed Concentration (Molar)	Source
YM-38	8600	3	1700	49	13000	3	NG	49	0 - 500	NG	NG	9328-30
YM-38	15000	2	4000	21					0 - 38	NG	4E-9	9328-28
YM-38	16000	2	900	21					38 - 106	NG	4E-9	9328-28
YM-38	14200	2	200	21					106 - 500	NG	4E-9	9328-28
YM-38	13000	NG	2000	14	13000	NG	NG	14	75 - 500	NG	NG	9328-21
YM-42	17000	NG	1000	14	21000	NG	2000	14	75 - 500	NG	NG	9328-21
** ELEMENT: Eu												
G1-1436	30000	NG	2000	14	5300	NG	600	14	75 - 500	NG	NG	9328-21
G1-1854	100000*	2	NG	14					0 - 75	NG	NG	9328-29
G1-1854	14000	2	NG	14					75 - 500	NG	NG	9328-29
G1-1854	15000	NG	NG	14	4800	NG	700	14	75 - 500	NG	NG	9328-21
YM-38	2700	1	478	21					0 - 75	5:1	NG	9328-XLII
YM-38	9070	1	1197	21					0 - 75	10:1	NG	9328-XLII
YM-38	9700	1	524	21					0 - 75	30:1	NG	9328-XLII
YM-38	2160	1	397	42					0 - 75	5:1	NG	9328-XLII
YM-38	4330	1	407	42					0 - 75	10:1	NG	9328-XLII
YM-38	6000	1	342	42					0 - 75	30:1	NG	9328-XLII
YM-38	3060	1	50	21					75 - 500	5:1	6E-9	9328-XLII
YM-38	6780	1	766	21					75 - 500	10:1	NG	9328-XLII
YM-38	10400	1	510	21					75 - 500	30:1	NG	9328-XLII
YM-38	2500	1	443	42					75 - 500	5:1	NG	9328-XLII
YM-38	6330	1	709	42					75 - 500	10:1	NG	9328-XLII
YM-38	8810	1	652	42					75 - 500	30:1	NG	9328-XLII
YM-38	3000	3	1000	49	7300	3	NG	49	0 - 500	NG	NG	9328-30
YM-38	2600	2	400	21					0 - 38	NG	7E-8	9328-28
YM-38	1340	2	10	21					38 - 106	NG	7E-8	9328-28
YM-38	1400	2	100	21					106 - 500	NG	7E-8	9328-28
YM-38	1600	NG	200	14	7300	NG	NG	14	75 - 500	NG	NG	9328-21
YM-42	52000	NG	4000	14	64000	NG	3000	14	75 - 500	NG	NG	9328-21
** ELEMENT: Np												
G4-1502	4	2	.5	42					75 - 500	NG	1E-10	10006-IV
G4-1502	4	2	1	42	11	2	2	42	75 - 500	NG	1E-10	10032-2

Table A.5.2-2a
Sorption Data For Sorptive Intervals
Zeolite 2

Sample	Average Sorption Ratio (ml/g)	Repli-cations	Std. Dev. (ml/g)	Contact Time (days)	Average Desorption Ratio (ml/g)	Repli-cations	Std. Dev. (ml/g)	Contact Time (days)	Particle Size (μm)	Soln-Solid Ratio (ml/g)	Tracer Feed Concentration (Molar)	Source
G4-1502	4.3	2	1	91					75 - 500	NG	1E-10	10154-XI
G4-1502	4.8	2	1	183					75 - 500	NG	1E-10	10154-XI
YM-38	11	3	1	49	23	3	3	49	0 - 500	NG	NG	9328-30
YM-38	11.0	2	.7	14	24	2	2	14	75 - 500	NG	1E-10	9328-21
** ELEMENT: Pu												
G4-1502	19	2	1	.04					75 - 500	NG	1.3E-8	10006-5
G4-1502	22	2	1.2	.16					75 - 500	NG	1.3E-8	10006-5
G4-1502	27	2	1	1					75 - 500	NG	1.3E-8	10006-5
G4-1502	34	2	2.3	2					75 - 500	NG	1.3E-8	10006-5
G4-1502	34	2	2.9	3					75 - 500	NG	1.3E-8	10006-5
G4-1502	36	2	1	7					75 - 500	NG	1.3E-8	10006-5
G4-1502	34	2	1	21					75 - 500	NG	1.3E-8	10006-5
G4-1502	43	2	1	42					75 - 500	NG	1.3E-8	10006-5
G4-1502	57	2	3	42					75 - 500	NG	2E-7	10006-IV
G4-1502	59	2	3.4	42	230	2	34	42	75 - 500	NG	1.5E-7	10032-2
YM-38	250	3	90	49	2000	3	500	49	0 - 500	NG	NG	9328-30
YM-38	140	2	30	14	1600	2	300	14	75 - 500	NG	1E-10	9328-21
** ELEMENT: Ra												
G1-1436	100000	2	30000	42					75 - 500	NG	NG	9846-18
** ELEMENT: Sn												
G4-1502	215	2	56	42					75 - 500	NG	3E-8	10154-X
** ELEMENT: Sr												
G1-1436	36000	NG	3000	14	87000	NG	12000	14	75 - 500	NG	NG	9328-21
G1-1854	81000	2	11000	18	54500	2	23335		0 - 75	NG	3E-8	9328-29
G1-1854	15000	2	100	18					0 - 75	NG	NG	9328-29
G1-1854	38000	2	6000	18					75 - 500	NG	3E-8	9328-29
G1-1854	10700	2	700	18					75 - 500	NG	NG	9328-29
G1-1854	60000	NG	14000	14	72000	NG	13000	14	75 - 500	NG	NG	9328-21

Table A.5.2-2e
Sorption Data For Sorptive Intervals
Zeolite 2

Sample	Average Sorption Ratio (ml/g)	Repli-cations	Std. Dev. (ml/g)	Contact Time (days)	Average Desorption Ratio (ml/g)	Repli-cations	Std. Dev. (ml/g)	Contact Time (days)	Particle Size (μm)	Soln-Solid Ratio (ml/g)	Tracer Feed Concentration (Molar)	Source
YM-38	2770	1	150	21					0 - 75	5:1	NG	9328-XLII
YM-38	2790	1	95	21					0 - 75	10:1	NG	9328-XLII
YM-38	3610	1	79	21					0 - 75	30:1	NG	9328-XLII
YM-38	2370	1	152	42					0 - 75	5:1	NG	9328-XLII
YM-38	2410	1	82	42					0 - 75	10:1	NG	9328-XLII
YM-38	3700	1	89	42					0 - 75	30:1	NG	9328-XLII
YM-38	2040	1	100	21					75 - 500	5:1	NG	9328-XLII
YM-38	2840	1	94	21					75 - 500	10:1	NG	9328-XLII
YM-38	2770	1	58	21					75 - 500	30:1	NG	9328-XLII
YM-38	1760	1	97	42					75 - 500	5:1	NG	9328-XLII
YM-38	3080	1	117	42					75 - 500	10:1	NG	9328-XLII
YM-38	2050	1	53	42					75 - 500	30:1	NG	9328-XLII
YM-38	11900	3	3200	49	21700	3	NG	49	0 - 500	NG	NG	9328-30
YM-38	17000	2	3000	21					0 - 38	NG	4E-7	9328-28
YM-38	20000	2	400	21					38 - 106	NG	4E-7	9328-28
YM-38	17600	2	0	21					106 - 500	NG	4E-7	9328-28
YM-38	17000	NG	2000	14	22000	NG	NG	14	75 - 500	NG	NG	9328-21
YM-42	3900	NG	600	14	4100	NG	1000	14	75 - 500	NG	NG	9328-21
** ELEMENT: Tc												
G4-1502	.02	2	.02	42					75 - 500	NG	8E-10	10154-XI
G4-1502	.01	2	.05	91					75 - 500	NG	8E-10	10154-XI
G4-1502	0	2	NG	91					75 - 500	NG	8E-10	10154-XI
** ELEMENT: U												
G1-1436	11	2	1	42					75 - 500	NG	5.E-6	9846-15
YM-38	5.3	3	.2	49	15	3	1	49	0 - 500	NG	NG	9328-30
YM-38	5.3	2	.2	14	14.8	2	1.	14	75 - 500	NG	1E-10	9328-21

Table A.5.2-2f
Sorption Data For Sorptive Intervals
Central Prow Pass

Sample	Average Sorption Ratio (ml/g)	Repli-cations	Std. Dev. (ml/g)	Contact Time (days)	Average Desorption Ratio (ml/g)	Repli-cations	Std. Dev. (ml/g)	Contact Time (days)	Particle Size (μm)	Soln-Solid Ratio (ml/g)	Tracer Feed Concentration (Molar)	Source
** ELEMENT: Am												
G1-1883	4700	2	300	14	7200	2	900	14	75 - 500	NG	1E-10	9328-21
** ELEMENT: Ba												
G1-1883	500	2	300	21					0 - 38	NG	7E-6	9328-28
G1-1883	204	2	5	21					38 - 106	NG	7E-6	9328-28
G1-1883	162	2	1	21					106 - 500	NG	7E-6	9328-28
G1-1883	182	NG	12	14	440	NG	10	14	75 - 500	NG	NG	9328-21
G1-1982	10000	2	0	18					0 - 38	NG	4E-6	9328-28
G1-1982	760	2	90	18					38 - 75	NG	4E-6	9328-28
G1-1982	670	2	100	18					75 - 250	NG	4E-6	9328-28
G1-1982	740	2	40	18					250 - 500	NG	4E-6	9328-28
G1-1982	700	NG	50	14	2780	NG	120	14	75 - 500	NG	NG	9328-21
YM-45	1200	NG	100	14	1310	NG	60	14	75 - 500	NG	NG	9328-21
YM-46	14000	NG	6000	14	21000	NG	3000	14	75 - 500	NG	NG	9328-21
** ELEMENT: Ce												
G1-1883	140	NG	20	14	2200	NG	100	14	75 - 500	NG	NG	9328-21
G1-1982	560	NG	40	14	7000	NG	900	14	75 - 500	NG	NG	9328-21
YM-45	730	NG	100	14	5800	NG	600	14	75 - 500	NG	NG	9328-21
YM-46	310000	NG	110000	14	300000	NG	50000	14	75 - 500	NG	NG	9328-21
** ELEMENT: Cs												
G1-1883	500	2	200	21					0 - 38	NG	4E-9	9328-28
G1-1883	190	2	10	21					38 - 106	NG	4E-9	9328-28
G1-1883	184	2	3	21					106 - 500	NG	4E-9	9328-28
G1-1883	187	NG	3	14	430	NG	4	14	75 - 500	NG	NG	9328-21
G1-1982	3650	2	200	18					0 - 38	NG	3E-9	9328-28
G1-1982	1250	2	50	18					38 - 75	NG	3E-9	9328-28
G1-1982	1000	2	70	18					75 - 250	NG	3E-9	9328-28
G1-1982	1200	2	0	18					250 - 500	NG	3E-9	9328-28
G1-1982	1120	NG	110	14	2300	NG	200	14	75 - 500	NG	NG	9328-21
YM-45	520	NG	90	14	620	NG	110	14	75 - 500	NG	NG	9328-21
YM-46	840	NG	6	14	1800	NG	300	14	75 - 500	NG	NG	9328-21

Table A.5.2-2f
Sorption Data For Sorptive Intervals
Central Prow Pass

Sample	Average Sorption Ratio (ml/g)	Repli-cations	Std. Dev. (ml/g)	Contact Time (days)	Average Desorption Ratio (ml/g)	Repli-cations	Std. Dev. (ml/g)	Contact Time (days)	Particle Size (μm)	Soln-Solid Ratio (ml/g)	Tracer Feed Concentration (Molar)	Source
** ELEMENT: Eu												
G1-1883	510	2	200	21					0 - 38	NG	3E-8	9328-28
G1-1883	110	2	10	21					38 - 106	NG	3E-8	9328-28
G1-1883	160	2	10	21					106 - 500	NG	3E-8	9328-28
G1-1883					1350	NG	50	14	75 - 500	NG	NG	9328-21
G1-1982	1900	2	700	18					0 - 38	NG	1E-7	9328-28
G1-1982	710	2	180	18					38 - 75	NG	1E-7	9328-28
G1-1982	960	2	300	18					75 - 250	NG	1E-7	9328-28
G1-1982	980	2	120	18					250 - 500	NG	1E-7	9328-28
G1-1982	970	NG	150	14	6370	NG	130	14	75 - 500	NG	NG	9328-21
YM-45	1600	NG	200	14	7300	NG	900	14	75 - 500	NG	NG	9328-21
YM-46	307000*	NG	110000	14	31000	NG	2000	14	75 - 500	NG	NG	9328-21
** ELEMENT: Np												
G1-1883	6.4	2	.6	14	36	2	10	14	75 - 500	NG	1E-10	9328-21
** ELEMENT: Pu												
G1-1883	77	2	11	14	890	2	60	14	75 - 500	NG	1E-10	9328-21
** ELEMENT: Se												
G1-1982	2.6	2	.1	42					75 - 500	NG	1.8E-11	10154-X
GU-3-1531	5	2	1	42					0 - 500	NG	NG	9846-18
** ELEMENT: Sr												
G1-1883	50	2	30	21					0 - 38	NG	3E-7	9328-28
G1-1883	22	2	1	21					38 - 106	NG	3E-7	9328-28
G1-1883	22	2	1	21					106 - 500	NG	3E-7	9328-28
G1-1883	22	NG	.2	14	59	NG	1	14	75 - 500	NG	NG	9328-21
G1-1982	1200*	2	0	18					0 - 38	NG	2E-7	9328-28
G1-1982	63	2	4	18					38 - 75	NG	2E-7	9328-28
G1-1982	51	2	2	18					75 - 250	NG	2E-7	9328-28
G1-1982	59	2	7	18					250 - 500	NG	2E-7	9328-28
G1-1982	55	NG	4	14	322	NG	8	14	75 - 500	NG	NG	9328-21
YM-45	194	NG	14	14	210	NG	20	14	75 - 500	NG	NG	9328-21
YM-46	190	NG	60	14	260	NG	20	14	75 - 500	NG	NG	9328-21
** ELEMENT: U												
G1-1982	2.4	2	.1	42					75 - 500	NG	2.7E-6	10154-X
GU-3-1531	54	2	9	42					0 - 500	NG	NG	9846-18

Table A.5.2-2g
Sorption Data For Sorptive Intervals
Zeolite 3

Sample	Average Sorption Ratio (ml/g)	Repli-cations	Std. Dev. (ml/g)	Contact Time (days)	Average Desorption Ratio (ml/g)	Repli-cations	Std. Dev. (ml/g)	Contact Time (days)	Particle Size (μm)	Soln-Solid Ratio (ml/g)	Tracer Feed Concentration (Molar)	Source
** ELEMENT: Am												
YM-49	4300	2	1400	14	3400	2	400	14	75 - 500	NG	1E-10	9328-21
** ELEMENT: Ba												
G1-2233	250000	NG	30000	14	240000	NG	80000	14	75 - 500	NG	NG	9328-21
G1-2233	41000	2	6300	42	59000	2	6000	42	75 - 500	NG	7E-8	10154-13
G1-2233	55000	2	5300	42	34000	2	23000	42	75 - 500	NG	5E-8	10154-13
G1-2289	140000	2	30000	21					0 - 38	NG	1E-7	9328-28
G1-2289	51000	2	3000	21					38 - 106	NG	1E-7	9328-28
G1-2289	80000	2	10000	21					106 - 500	NG	1E-7	9328-28
G1-2289	66000	2	9000	42					75 - 500	NG	NG	9846-18
G1-2289	66000	NG	9000	14					75 - 500	NG	NG	9328-21
G1-2333	1860	2	40	18	1650	2	71		0 - 75	NG	3E-7	9328-29
G1-2333	1170	2	30	18					75 - 500	NG	3E-7	9328-29
G1-2333	1500	NG	200	14	1460	NG	130	14	75 - 500	NG	NG	9328-21
YM-48	18000	NG	6000	14	34000	NG	7000	14	75 - 500	NG	NG	9328-21
YM-49	42000	NG	8000	14	65000	NG	7000	14	75 - 500	NG	NG	9328-21
** ELEMENT: Ce												
G1-2233	1400	NG	300	14	20000	NG	13000	14	75 - 500	NG	NG	9328-21
YM-48	1400	NG	500	14	128000	NG	300	14	75 - 500	NG	NG	9328-21
YM-49	550	NG	100	14	1040	NG	40	14	75 - 500	NG	NG	9328-21
** ELEMENT: Cs												
G1-2233	13500	NG	800	14	23000	NG	6000	14	75 - 500	NG	NG	9328-21
G1-2233	7500	2	1100	42	8800	2	900	42	75 - 500	NG	2E-9	10154-13
G1-2233	13000	2	1600	42	8700	2	3400	42	75 - 500	NG	2E-9	10154-13
G1-2289	35000	2	8000	21					0 - 38	NG	4E-9	9328-28
G1-2289	31000	2	3000	21					38 - 106	NG	4E-9	9328-28
G1-2289	42000	2	30000	21					106 - 500	NG	4E-9	9328-28
G1-2289	37000	NG	13000	14					75 - 500	NG	NG	9328-21
G1-2333	1600	2	100	18	1350	2	71		0 - 75	NG	5E-9	9328-29
G1-2333	1160	2	40	18					75 - 500	NG	5E-9	9328-29
G1-2333	1400	NG	130	14	1230	NG	100	14	75 - 500	NG	NG	9328-21

Table A.5.2-2g
Sorption Data For Sorptive Intervals
Zeolite 3

Sample	Average Sorption Ratio (ml/g)	Repli-cations	Std. Dev. (ml/g)	Contact Time (days)	Average Desorption Ratio (ml/g)	Repli-cations	Std. Dev. (ml/g)	Contact Time (days)	Particle Size (μm)	Soln-Solid Ratio (ml/g)	Tracer Feed Concentration (Molar)	Source
YM-48	9000	NG	4000	14	27000	NG	4000	14	75 - 500	NG	NG	9328-21
YM-49	36000	NG	3000	14	39000	NG	1000	14	75 - 500	NG	NG	9328-21
** ELEMENT: Eu												
G1-2233	900	NG	200	14	5000	NG	2000	14	75 - 500	NG	NG	9328-21
G1-2233	5600	2	NG	42	7800	2	NG	42	75 - 500	NG	3E-8	10154-13
G1-2233	810	2	100	42	1400	2	600	42	75 - 500	NG	1E-8	10154-13
G1-2289	1500	2	100	21					0 - 38	NG	2E-8	9328-28
G1-2289	779	2	1	21					38 - 106	NG	2E-8	9328-28
G1-2289	815	2	3	21					106 - 500	NG	2E-8	9328-28
G1-2289	797	NG	10	14					75 - 500	NG	NG	9328-21
G1-2333	2600	2	600	18	6100	2	6930		0 - 75	NG	3E-8	9328-29
G1-2333	2200	2	800	18					75 - 500	NG	3E-8	9328-29
G1-2333	2300	NG	400	14	9900	NG	1200	14	75 - 500	NG	NG	9328-21
YM-48	2200	NG	500	14	8100	NG	1200	14	75 - 500	NG	NG	9328-21
YM-49	1200	NG	100	14	2100	NG	500	14	75 - 500	NG	NG	9328-21
** ELEMENT: Mn												
G1-2233	6000	3	400	49	9300	3	NG	49	0 - 500	NG	NG	9328-30
** ELEMENT: Na												
G1-2233	141	3	4	49	160	3	10	49	0 - 500	NG	NG	9328-30
** ELEMENT: Np												
YM-49	9	2	3	14	12	2	4	14	75 - 500	NG	1E-10	9328-21
** ELEMENT: Pu												
YM-49	230	2	50	14	720	2	90	14	75 - 500	NG	1E-10	9328-21
** ELEMENT: Ra												
G1-2289	46000	2	20000	42					75 - 500	NG	NG	9846-18
G1-2289	50000	2	20000	42					75 - 500	NG	3.6E-7	9846-13

Table A.5.2-2g
Sorption Data For Sorptive Intervals
Zeolite 3

Sample	Average Sorption Ratio (ml/g)	Repli-cations	Std. Dev. (ml/g)	Contact Time (days)	Average Desorption Ratio (ml/g)	Repli-cations	Std. Dev. (ml/g)	Contact Time (days)	Particle Size (μm)	Soln-Solid Ratio (ml/g)	Tracer Feed Concentration (Molar)	Source
** ELEMENT: Sa												
G1-2233	11	3	2	49	46	3	5	49	0 - 500	NG	NG	9328-30
G1-2233	1.8	2	.1	42					75 - 500	NG	1.8E-11	10154-X
G1-2289	9	2	1	42					75 - 500	NG	1E-10	9846-18
GU-3-1937	3.6	2	.1	42					75 - 500	NG	1.8E-11	10154-X
** ELEMENT: Sn												
G1-2233	460	3	130	49	580	3	70	49	0 - 500	NG	NG	9328-30
** ELEMENT: Sr												
G1-2233	48000	NG	3000	14	90000	NG	40000	14	75 - 500	NG	NG	9328-21
G1-2233	2000	2	330	42	3000	2	500	42	75 - 500	NG	3E-8	10154-13
G1-2233	56000	2	NG	42	21000	2	12000	42	75 - 500	NG	3E-8	10154-13
G1-2289	14000	2	3000	21					0 - 38	NG	3E-8	9328-28
G1-2289	6380	2	40	21					38 - 106	NG	3E-8	9328-28
G1-2289	8100	2	300	21					106 - 500	NG	3E-8	9328-28
G1-2289	7300	NG	500	14					75 - 500	NG	NG	9328-21
G1-2333	218	2	2	18	160	2	0		0 - 75	NG	1E-6	9328-29
G1-2333	148	2	4	18					75 - 500	NG	1E-6	9328-29
G1-2333	180	NG	20	14	140	NG	13	14	75 - 500	NG	NG	9328-21
YM-48	2100	NG	400	14	2700	NG	200	14	75 - 500	NG	NG	9328-21
YM-49	3200	NG	300	14	4400	NG	100	14	75 - 500	NG	NG	9328-21
** ELEMENT: Tc												
YM-48	.15	NG	.02	14	1.6	NG	.2	14	75 - 500	NG	NG	9328-21
YM-49	.21	NG	.02	14	2.0	NG	.3	14	75 - 500	NG	NG	9328-21
** ELEMENT: Th												
G1-2233	344	NG	55	12					NG - NG	NG	1.07E-7	10032-13
G1-2289	143	NG	2	12					NG - NG	NG	5.86E-8	10032-13
** ELEMENT: U												
G1-2233	5.5	2	.4	42					75 - 500	NG	2.7E-6	10154-X
G1-2289	2.5	2	.1	42					75 - 500	NG	5.E-6	9846-15
GU-3-1937	10	2	.1	42					75 - 500	NG	2.7E-6	10154-X

Table A.5.2-2h
Sorption Data For Sorptive Intervals
Central Bull Frog

Sample	Average Sorption Ratio (ml/g)	Repli-cations	Std. Dev. (ml/g)	Contact Time (days)	Average Desorption Ratio (ml/g)	Repli-cations	Std. Dev. (ml/g)	Contact Time (days)	Particle Size (μm)	Soln-Solid Ratio (ml/g)	Tracer Feed Concentration (Molar)	Source
** ELEMENT: Am												
YM-54	590	3	210	49	600	3	50	49	0 - 500	NG	NG	9328-30
YM-54	153	2	6	14	550	2	80	14	75 - 500	NG	1E-10	9328-21
** ELEMENT: Ba												
G1-2363	890	2	30	21					0 - 38	NG	1E-7	9328-28
G1-2363	250	2	10	21					38 - 106	NG	1E-7	9328-28
G1-2363	220	2	10	21					106 - 500	NG	1E-7	9328-28
G1-2363	235	2	9	42					106 - 500	NG	NG	9846-18
G1-2363	235	NG	9	14	820	NG	20	14	75 - 500	NG	NG	9328-21
G1-2410	3040	1	NG	14					0 - 75	NG	2E-7	9328-29
G1-2410	1780	1	NG	14					75 - 500	NG	2E-7	9328-29
G1-2410					1760	NG	150	14	75 - 500	NG	NG	9328-21
G1-2476	500	2	20	18					0 - 75	NG	1E-7	9328-29
G1-2476	385	2	10	18					75 - 500	NG	1E-7	9328-29
G1-2476	385	NG	11	14					75 - 500	NG	NG	9328-21
YM-54	620	3	80	49	660	3	20	49	0 - 500	NG	NG	9328-30
YM-54	1670	2	60	21					0 - 38	NG	3E-7	9328-28
YM-54	474	2	3	21					38 - 106	NG	3E-7	9328-28
YM-54	140	2	7	21					106 - 500	NG	3E-7	9328-28
YM-54	400	NG	150	14	660	NG	20	14	75 - 500	NG	NG	9328-21
** ELEMENT: Ce												
G1-2363					130000	NG	6000	14	75 - 500	NG	NG	9328-21
YM-54	140	3	40	49	1000	3	200	49	0 - 500	NG	NG	9328-30
YM-54	150	NG	40	14	1000	NG	200	14	75 - 500	NG	NG	9328-21
** ELEMENT: Cs												
G1-2363	1300	2	100	21					0 - 38	NG	4E-9	9328-28
G1-2363	540	2	20	21					38 - 106	NG	4E-9	9328-28
G1-2363	400	2	20	21					106 - 500	NG	4E-9	9328-28
G1-2363	470	NG	40	14	1200	NG	30	14	75 - 500	NG	NG	9328-21
G1-2410	2020	2	20	18					0 - 75	NG	4E-9	9328-29
G1-2410	1250	2	50	18					75 - 500	NG	4E-9	9328-29

Table A.5.2-2h
Sorption Data For Sorptive Intervals
Central Bull Frog

Sample	Average Sorption Ratio (ml/g)	Repli-cations	Std. Dev. (ml/g)	Contact Time (days)	Average Desorption Ratio (ml/g)	Repli-cations	Std. Dev. (ml/g)	Contact Time (days)	Particle Size (μm)	Soln-Solid Ratio (ml/g)	Tracer Feed Concentration (Molar)	Source
G1-2410	1250	NG	50	14	1120	NG	100	14	75 - 500	NG	NG	9328-21
G1-2476	870	2	50	18					0 - 75	NG	5E-9	9328-29
G1-2476	700	2	40	18					75 - 500	NG	5E-9	9328-29
G1-2476	700	NG	40	14	1520	NG	0	14	75 - 500	NG	NG	9328-21
YM-54	250	3	20	49	310	3	20	49	0 - 500	NG	NG	9328-30
YM-54	910	2	30	21					0 - 38	NG	3E-9	9328-28
YM-54	187	2	1	21					38 - 106	NG	3E-9	9328-28
YM-54	120	2	10	21					106 - 500	NG	3E-9	9328-28
YM-54	180	NG	40	14	310	NG	20	14	75 - 500	NG	NG	9328-21
** ELEMENT: Eu												
G1-2363	5500	2	100	21					0 - 38	NG	5E-8	9328-28
G1-2363	786	2	8	21					38 - 106	NG	5E-8	9328-28
G1-2363	680	2	100	21					106 - 500	NG	5E-8	9328-28
G1-2363	730	NG	50	14	6100	NG	300	14	75 - 500	NG	NG	9328-21
G1-2410	420	2	30	18					0 - 75	NG	2E-8	9328-29
G1-2410	440	2	80	18					75 - 500	NG	2E-8	9328-29
G1-2410					6000	NG	3000	14	75 - 500	NG	NG	9328-21
G1-2476	4800	2	300	18					0 - 75	NG	6E-8	9328-29
G1-2476	3200	2	100	18					75 - 500	NG	6E-8	9328-29
G1-2476									75 - 500	NG	NG	9328-21
YM-54	510	3	80	49	1800	3	100	49	0 - 500	NG	NG	9328-30
YM-54	1600	2	10	21					0 - 38	NG	4E-8	9328-28
YM-54	340	2	80	21					38 - 106	NG	4E-8	9328-28
YM-54	470	2	20	21					106 - 500	NG	4E-8	9328-28
YM-54					1840	NG	110	14	75 - 500	NG	NG	9328-21
** ELEMENT: Pu												
YM-54	90	3	20	49	720	3	5	49	0 - 500	NG	NG	9328-30
YM-54	80	2	20	14	720	2	40	14	75 - 500	NG	1E-10	9328-21
** ELEMENT: Ra												
G1-2363	540	2	60	42					106 - 500	NG	NG	9846-18

Table A.5.2-2h
Sorption Data For Sorptive Intervals
Central Bull Frog

Sample	Average Sorption Ratio (ml/g)	Repli-cations	Std. Dev. (ml/g)	Contact Time (days)	Average Desorption Ratio (ml/g)	Repli-cations	Std. Dev. (ml/g)	Contact Time (days)	Particle Size (μm)	Soln-Solid Ratio (ml/g)	Tracer Feed Concentration (Molar)	Source
** ELEMENT: Se												
G1-2363	25	2	5	42					75 - 500	NG	1E-10	9846-18
** ELEMENT: Sr												
G1-2363	170	2	10	21					0 - 38	NG	5E-7	9328-28
G1-2363	70	2	10	21					38 - 106	NG	5E-7	9328-28
G1-2363	60	2	2	21					106 - 500	NG	5E-7	9328-28
G1-2363	64	NG	3	14	150	NG	6	14	75 - 500	NG	NG	9328-21
G1-2410	280	2	4	18	245	2	7		0 - 75	NG	4E-7	9328-29
G1-2410	169	2	1	18					75 - 500	NG	4E-7	9328-29
G1-2410					140	NG	14	14	75 - 500	NG	NG	9328-21
G1-2476	50	2	1	18					0 - 75	NG	9E-7	9328-29
G1-2476	41	2	1	18					75 - 500	NG	9E-7	9328-29
G1-2476					200	NG	4	14	75 - 500	NG	NG	9328-21
YM-54	90	3	4	49	94	3	9	49	0 - 500	NG	NG	9328-30
YM-54	276	2	2	21					0 - 38	NG	6E-7	9328-28
YM-54	56.5	2	.4	21					38 - 106	NG	6E-7	9328-28
YM-54	47	2	10	21					106 - 500	NG	6E-7	9328-28
YM-54	62	NG	12	14	97	NG	9	14	75 - 500	NG	NG	9328-21
** ELEMENT: Th												
G1-2363	1213	NG	193	12					NG - NG	NG	6.52E-8	10032-13
** ELEMENT: U												
G1-2363	0	2	NG	42					75 - 500	NG	5.E-6	9846-15
YM-54	1.7	3	.2	49	13	3	3	49	0 - 500	NG	NG	9328-30
YM-54	1.3	2	.3	14	12	2	8	14	75 - 500	NG	1E-10	9328-21

Table A.5.2-2i
Sorption Data For Sorptive Intervals
Zeolite 4

Sample	Average Sorption Ratio (ml/g)	Repli-cations	Std. Dev. (ml/g)	Contact Time (days)	Average Desorption Ratio (ml/g)	Repli-cations	Std. Dev. (ml/g)	Contact Time (days)	Particle Size (μm)	Soln-Solid Ratio (ml/g)	Tracer Feed Concentration (Molar)	Source
** ELEMENT: Ba												
G1-2698	63000	NG	5000	14	190000	NG	80000	14	75 - 500	NG	NG	9328-21
** ELEMENT: Ce												
G1-2698	240	NG	30	14	2000	NG	400	14	75 - 500	NG	NG	9328-21
** ELEMENT: Cs												
G1-2698	7700	NG	400	14	17000	NG	1100	14	75 - 500	NG	NG	9328-21
** ELEMENT: Eu												
G1-2698	200	NG	30	14					75 - 500	NG	NG	9328-21
** ELEMENT: Sr												
G1-2698	42000	NG	3000	14	210000	NG	50000	14	75 - 500	NG	NG	9328-21

Table A.5.2-2j
Sorption Data For Sorptive Intervals
Deep Zone

Sample	Average Sorption Ratio (ml/g)	Repli-cations	Std. Dev. (ml/g)	Contact Time (days)	Average Desorption Ratio (ml/g)	Repli-cations	Std. Dev. (ml/g)	Contact Time (days)	Particle Size (μm)	Soln-Solid Ratio (ml/g)	Tracer Feed Concentration (Molar)	Source
** ELEMENT: Eu												
G1-2840	5600	2	600	18					0 - 75	NG	3E-8	9328-29
G1-2840	4900	2	400	18					75 - 500	NG	3E-8	9328-29
G1-2840					9000	NG	1100	14	75 - 500	NG	NG	9328-21
G1-2854	1800	2	800	18					0 - 75	NG	2E-8	9328-29
G1-2854	1300	2	200	18					75 - 500	NG	2E-8	9328-29
G1-2854					5000	NG	200	14	75 - 500	NG	NG	9328-21
G1-2901	160000*	NG	50000	14	210000	NG	50000	14	75 - 500	NG	NG	9328-21
G1-3116	760	NG	60	14	8000	NG	3000	14	75 - 500	NG	NG	9328-21
G1-3658	15000	2	600	21					0 - 38	NG	4E-7	9328-28
G1-3658	440	2	30	21					38 - 106	NG	4E-7	9328-28
G1-3658	530	2	40	21					106 - 500	NG	4E-7	9328-28
G1-3658	530	NG	40	14	9000	NG	3000	14	75 - 500	NG	NG	9328-21
** ELEMENT: Se												
G1-2840	3.1	2	.2	42					75 - 500	NG	1.8E-11	10154-X
G1-3116	3.1	2	.1	42					75 - 500	NG	1.8E-11	10154-X
** ELEMENT: Sn												
G1-2840	283	2	160	42					75 - 500	NG	2E-8	10154-X
G1-2901	22000	2	5000	42					75 - 500	NG	1E-7	10154-X
** ELEMENT: Sr												
G1-2840	170	2	1	18					0 - 75	NG	1E-6	9328-29
G1-2840	160	2	1	18					75 - 500	NG	1E-6	9328-29
G1-2840	160	NG	1	14	150	NG	4	14	75 - 500	NG	NG	9328-21
G1-2854	90	2	30	18					0 - 75	NG	5E-7	9328-29
G1-2854	94	2	1	18					75 - 500	NG	5E-7	9328-29
G1-2854					96	NG	1	14	75 - 500	NG	NG	9328-21
G1-2901	68	NG	1	14	67	NG	1	14	75 - 500	NG	NG	9328-21
G1-3116	2400	NG	17	14	24000	NG	13000	14	75 - 500	NG	NG	9328-21
G1-3658	13000	2	3000	21					0 - 38	NG	3E-7	9328-28
G1-3658	13000	2	1000	21					38 - 106	NG	3E-7	9328-28
G1-3658	13200	2	200	21					106 - 500	NG	3E-7	9328-28
G1-3658	13000	NG	0	14	12000	NG	3000	14	75 - 500	NG	NG	9328-21
** ELEMENT: U												
G1-2840	.5	2	.1	42					75 - 500	NG	2.7E-6	10154-X
G1-3116	3.8	2	.1	42					75 - 500	NG	2.7E-6	10154-X

Table A.5.2-2j
Sorption Data For Sorptive Intervals
Deep Zone

Sample	Average Sorption Ratio (ml/g)	Repli-cations	Std. Dev. (ml/g)	Contact Time (days)	Average Desorption Ratio (ml/g)	Repli-cations	Std. Dev. (ml/g)	Contact Time (days)	Particle Size (μm)	Soln-Solid Ratio (ml/g)	Tracer Feed Concentration (Molar)	Source
** ELEMENT: Ba												
G1-2840	2500	2	200	18					0 - 75	NG	2E-7	9328-29
G1-2840	2070	2	70	18					75 - 500	NG	2E-7	9328-29
G1-2840					2500	NG	200	14	75 - 500	NG	NG	9328-21
G1-2854	4000	2	2000	18					0 - 75	NG	1E-7	9328-29
G1-2854	1000	2	50	18					75 - 500	NG	1E-7	9328-29
G1-2854					1330	NG	0	14	75 - 500	NG	NG	9328-21
G1-2901	1600	NG	200	14	1980	NG	30	14	75 - 500	NG	NG	9328-21
G1-3116	12000	NG	4000	14	160000	NG	80000	14	75 - 500	NG	NG	9328-21
G1-3658	15000	2	4000	21					0 - 38	NG	9E-6	9328-28
G1-3658	9600	2	600	21					38 - 106	NG	9E-6	9328-28
G1-3658	13000	2	1000	21					106 - 500	NG	9E-6	9328-28
G1-3658	13500	NG	500	14	10000	NG	4000	14	75 - 500	NG	NG	9328-21
** ELEMENT: Ce												
G1-2901	42000	NG	3000	14	39000	NG	1000	14	75 - 500	NG	NG	9328-21
G1-3116	100	NG	10	14	3000	NG	1000	14	75 - 500	NG	NG	9328-21
G1-3658	1000	NG	200	14	9000	NG	4000	14	75 - 500	NG	NG	9328-21
** ELEMENT: Cs												
G1-2840	2600	2	200	18					0 - 75	NG	5E-9	9328-29
G1-2840	2200	2	200	18					75 - 500	NG	5E-9	9328-29
G1-2840					2300	NG	130	14	75 - 500	NG	NG	9328-21
G1-2854	1100	2	600	18					0 - 75	NG	5E-9	9328-29
G1-2854	1080	2	120	18					75 - 500	NG	5E-9	9328-29
G1-2854					1160	NG	20	14	75 - 500	NG	NG	9328-21
G1-2901	1290	NG	110	14	1380	NG	30	14	75 - 500	NG	NG	9328-21
G1-3116	6600	NG	500	14	11000	NG	3000	14	75 - 500	NG	NG	9328-21
G1-3658	16000	2	2000	21					0 - 38	NG	7E-9	9328-28
G1-3658	6600	2	500	21					38 - 106	NG	7E-9	9328-28
G1-3658	4980	2	70	21					106 - 500	NG	7E-9	9328-28
G1-3658	4950	NG	50	14	12000	NG	2000	14	75 - 500	NG	NG	9328-21

APPENDIX 5.3

Descriptions of Tuff Samples Used in Sorption Experiments

Sample No.	Drill Hole	Depth (ft.)	Sorption Category	Source*	Sorption Interval	Source*	Sat.**
Formation: Pah							
G2-547	USWG-2	547	Dv/Clay/Glass	9846-PR			U
G2-723	USWG-2	723	Calcite/Glass/Clay	9846-PR			U
Formation: Tiva Canyon							
YM-5	UE25A-1	251	Glass/Clay	9328-MS			U
Formation: Topopah Spring							
JA-18	J-13	1420	Dv/Glass/Clay/Z	9328-MS			S
JA-8	J-13	606	Clay/Glass	9328-MS			U
YM-30	UE25A-1	1264	Dv/Clay/Z	9328-MS	Zeolite 1	10006,9707	U
YM-22	UE25A-1	848	Dv	9328-MS			U
G1-1292	USWG-1	1292	Glass	9328-MS	Basal Vitrophyre	9328,10006	U
GU-3-1203	USWG3/GU3	1203	Glass	9846-PR	Basal Vitrophyre	10006,9707	U
GU-3-1301	USWG3/GU3	1301	Glass/Clay	9846-PR	Vitric	10006,9707	U
GU-3-433	USWG3/GU3	433	Dv	9846-PR	Host Rock	10006,9707	U
GU-3-855	USWG3/GU3	855	Dv/Clay	9846-PR	Host Rock	10006,9707	U
GU-3-916	USWG3/GU3	916	Dv	10006-PR	Host Rock	10006,9707	U
Formation: Calico Hills							
YM-38	UE25A-1	1504	Zeolite	9328-MS	Zeolite 2	10006,9707	U
YM-42	UE25A-1	1824	Zeolite	9328-MS	Zeolite 2	10006,9707	S
G1-1436	USWG-1	1436	Zeolite	9328-MS	Zeolite 2	10006,9707	U
G2-1952	USWG-2	1952	Dv/Mordenite	9846-PR			S
G4-1502	USWG-4	1502	Zeolite	10006-PR	Zeolite 2	10006	U
GU-3-1436	USWG3/GU3	1436	Glass	9846-PR	Vitric	10006,9707	U
GU-3-1531	USWG3/GU3	1531	Dv	9846-PR	C.Prow Pass	10006,9707	U
Formation: Prow Pass							
JA-26	J-13	1995	Analcime	9328-MS			S
YM-45	UE25A-1	1930	Dv/Clay	9328-MS	C.Prow Pass	10006,9707	S
YM-46	UE25A-1	2002	Dv	9328-MS	C.Prow Pass	10006,9707	S
YM-48	UE25A-1	2114	Zeolite/Glass	9328-MS	Zeolite 3	10006,9707	S
YM-49	UE25A-1	2221	Zeolite/Glass	9328-MS	Zeolite 3	10006,9707	S
G1-1982	USW G-1	1982	Dv/Clay	9328-MS	C.Prow Pass	10006,9707	S

Sample No.	Drill Hole	Depth (ft.)	Sorption Category	Source*	Sorption Interval	Source*	Sat.**
G1-1854	USWG-1	1854	Zeolite	9328-MS	Zeolite 2	10006,9707	U
G1-1883	USWG-1	1883	Dv/Vapor	9328-MS	C.Prow Pass	10006,9707	S
GU-3-1937	USWG3/GU3	1937	Zeolite	10154-PR	Zeolite 3	10006-PR	U
Formation: Bull Frog							
JA-28	J-13	2001	Analcime	8747-MS			S
JA-32	J-13	2533	Dv/Clay	9328-MS			S
YM-54	UE25A-1	2491	Dv/Clay	9328-MS	C.Bull Frog	10006,9707	S
G1-2334	USW G-1	2334	Zeolite ?				S
G1-2233	USWG-1	2233	Zeolite	9328-MS	Zeolite 3	10006,9707	S
G1-2289	USWG-1	2289	Zeolite	9328-MS	Zeolite 3	10006,9707	S
G1-2333	USWG-1	2333	Zeolite	9328-MS	Zeolite 3	10006,9707	S
G1-2363	USWG-1	2363	Dv/Clay	9328-MS	C.Bull Frog	10006,9707	S
G1-2410	USWG-1	2410	Dv/Clay	9328-MS	C.Bull Frog	10006,9707	S
G1-2476	USWG-1	2476	Dv/Clay	9328-MS	C.Bull Frog		S
Formation: Tram							
JA-37	J-13	3497	Clay/Dv/Z	9328-MS			S
G1-2698	USWG-1	2698	Zeolite	9328-MS	Zeolite 4		S
G1-2840	USWG-1	2840	Dv/Clay	9328-MS	Deep Zone		S
G1-2854	USWG-1	2854	Dv/Clay	9328-MS	Deep Zone		S
G1-2901	USWG-1	2901	Dv/Calcite	9328-MS	Deep Zone		S
G1-3116	USWG-1	3116	Zeolite	9328-MS	Deep Zone		S
Formation: Tram/bedded							
G2-3933	USWG-2	3933	Dv/Analcime/Clay	9846-PR			S
Formation: Flow Breccia							
G1-3658	USWG-1	3658	Smectite	9328-MS	Deep Zone	10006	S

* Sources for data used to identify sorption category or interval:
8747-MS: Wolfsberg and others, 1981
9328-MS: Daniels and others, 1982d
9707: Vaniman and others, 1984
9846: Ogard and others, 1983b
10006: Bryant and Vaniman, 1984

** Saturation is classified by heights of water table and sample in drill core (Robison, 1984)
U: Unsaturated zone--above water table
S: Saturated zone--below water table

REFERENCES

Abeele, W. V., 1979, Determination of hydraulic conductivity in crushed Bandelier Tuff: Los Alamos Sci. Lab., LA-8147-MS, 5 p.

Abeele, W. V., Wheeler, M. L., and Burton, B. W., 1981, Geohydrology of Bandelier Tuff: Los Alamos Nat. Lab., LA-8962-MS, 50 p.

Alietti, A., 1972, Polymorphism and crystal chemistry of heulandites and clinoptilolites: Amer. Mineralogist, v. 57, p. 1437-1451.

Anderson, L. A., 1981, Rock property analysis of core samples from the Yucca Mountain UE25a-1 borehole, Nevada Test Site, Nevada: U.S. Geol. Survey Open-File Rept. 81-1338, 36 p.

Anderson, R. E., 1968, Possible relationship between type of volcanic center and magnitude of hydrothermal alteration in southern Nevada (Abs.): Geol. Soc. America Special Paper 101, p. 383-384.

Anderson, R. E., and Ekren, E. B., 1968, Widespread miocene igneous rocks of intermediate composition, southern Nye County, Nevada, in Nevada Test Site: Geol. Soc. America, Mem. 110, p. 57-63.

Anderson, R. E., Ekren, E. B., and Healey, D. L., 1965, Possible buried mineralized areas in Nye and Esmeralda Counties, Nevada: U.S. Geol. Survey Prof. Paper 525-D, p. D144-D150.

Anonymous, 1929, Preliminary report of the Tiptop Group of claims, Fluorine Mining District: Nevada Bur. Mines Geol., Nye County file 228, item 9.

Anonymous, 1969, NTS History steeped in fact and fiction, in NTS News: REECO Pub., v. 12, n. 16.

Anonymous, 1974, Fluoride mine on Mary 1-4 claims: Nevada Bur. Mines Geol., Nye County File 228, Item 7.

Armstrong, R. L., 1970, Geochronology of Tertiary igneous rocks, eastern Nevada and vicinity U.S.A., Geoch. et Cosmoch. Acta, v. 34, p. 203-232.

Bailey, E. H., and Phoenix, D. H., 1944, Quicksilver deposits in Nevada: Nevada Univ. Bull., v. 38, n. 5, 206 p.; also Nevada Bur. Mines Geol. Bull. 41.

Baker, A., III and Hsu, L., 1969, Lee (Big Dunes) district: Nevada Bur. Mines Geol., Nye County file 237, item 1.

Ball, S. H., 1905, Notes on ore deposits of southwestern Nevada and eastern California: U.S. Geol. Survey Bull. 285, Ser. A, Econ. Geol. 73, p. 53-73.

Ball, S. H., 1907, A geological reconnaissance in southwestern Nevada and eastern California: U.S. Geol. Survey Bull. 308, p. 176-182.

Bare Mountain Mining Corporation, 1968, Description of mercury property: Nevada Bur. Mines Geol., Nye County file 228, item 5.

Beal, L. H., 1962, Investigation of titanium occurrences in Nevada: Nevada Bur. Mines Geol., Rept. 3, 42 p.

Bear, J., 1972, Dynamics of fluids in porous media: New York, American Elsevier Publishing, 764 p.

Bell, E. J., and Larson, L. T., 1982, Overview of energy and mineral resources for the Nevada Nuclear Waste Storage Investigations: Nevada Test Site, Nye County, Nevada: NVO-250, Las Vegas, NV, U.S. Dept. of Energy.

Benson, L. V., 1976, Mass transport in vitric tuffs of Rainier Mesa, Nye County, Nevada: Water Resources Center, Desert Res. Inst., Rept. NVO-1253-10, 41 p.

Benson, L. V., Robinson, J. H., Blankennagel, R. K., and Ogard, A. E., 1983, Chemical composition of ground water and the locations of permeable zones in the Yucca Mountain area, Nevada: U.S. Geol. Survey Open-File Rept. 83-854, 19 p.

Bentley, C. B., 1984, Geohydrologic data for test well USW G-4, Yucca Mountain area, Nye County, Nevada: U. S. Geol. Survey Open-File Rept. 84-063, 48 p.

Bentley, C. B., Robison, J. H., and Spengler, R. W., 1983, Geohydrologic data for test well USW H-5, Yucca Mountain area, Nye County, Nevada: U.S. Geol. Survey Open-File Rept. 83-853, 34 p.

Bertram, S. G., and Everett, J. J., 1982, NNWSI environmental characterization prior to the exploratory shaft: Proc. 1982 NWTS Prog. Inf. Meetings, Las Vegas, Nevada, p. 125-128.

Best, M. G., and Brimhall, W. H., 1974, Late Cenozoic alkali basaltic magmas in the western Colorado Plateau and the Basin and Range transition zone, U.S.A., and their bearing on mantle dynamics: Geol. Soc. America Bull., v. 85, p. 1677-1690.

Best, M. G., and Hamblin, W. K., 1978, Origin of the northern Basin and Range province: Implications from the geology of its eastern boun- dary," in Cenozoic tectonics and regional geophysics of the western Cordillera: Geol. Soc. America, Mem. 152, p. 313-340.

Birkeland, P. W., and Larson, E. E., 1978, Putnam's Geology: Oxford Univ. Press, New York, NY, 659 p.

Bish, D. L., 1982, The effect of composition on the dehydration of clinoptilolites and heulandite (abs.): 6th Int. Zeolite Conf., Reno, Nevada, July 10 - 15, 1983.

Bish, D. L., 1984, Effects of composition on the thermal expansion/contraction of clinoptilolite: Los Alamos Nat. Lab., LA-UR-84-451, 32 p.

Bish, D. L., and Semarge, R. E., 1982, Mineralogic variations in a silicic tuff sequence: Evidence of diagenetic and hydrothermal reactions (abs.): 19th Ann. Clay Minerals Soc. Mtg., August 9 - 13, 1982.

Bish, D. L., Broxton, D. E., Byers, F. M., Jr., Caporuscio, F. A., Carlos, B. A., Gooley, R. C., Levy, S. S., Semarge, R. E., and Vaniman, D. T., 1983a, Mineralogy and petrology of tuff, in Research and development related to the Nevada Nuclear Waste Storage Investigations: Los Alamos Nat. Lab., LA-9793-PR, p. 36-40.

Bish, D. L., Caporuscio, F. A., Copp, J. F., Crowe, B. M., Purson, J. D., Smyth, J. R., and Warren, R. G., 1981, Preliminary stratigraphic and petrologic characterization of core samples from Yucca Mountain, Nevada: Los Alamos Nat. Lab., LA-8840-MS, 66p.

Bish, D. L., Vaniman, D. T., Byers, F. M., Jr., and Broxton, D. E., 1982, Summary of the mineralogy--petrology of tuffs of Yucca Mountain and the thermal stability of secondary phases in tuffs: Las Alamos Nat. Lab., LA-9321-MS, 50 p.

Bish, D. L., Vaniman, D. T., Rundberg, R. S., Wolfsberg, K., Daniels, W. R., and Broxton, D. E., 1983b, Natural sorptive barriers in Yucca Mountain, Nevada, for long-term isolation of high-level waste: Los Alamos Nat. Lab., LA-UR-83-758, 19 p.

Blacic, J., Carter, J., Halleck, P., Johnson P., Shankland, T., Anderson, R., Spicochi, K., and Heller, A., 1982, Effects of long-term exposure of tuffs to high-level nuclear waste repository conditions: Los Alamos Nat. Lab., LA-9174-PR, 26 p.

Boles, J. R., 1971, Synthesis of analcime from natural heulandite and clinoptilolite: Amer. Mineralogist, v. 56, p. 1724-1734.

Boles, J. R., 1972, Composition, optical properties, cell dimensions, and thermal stability of some heulandite group zeolites: Amer. Mineralogist, v. 57, p. 1463-1493.

Breck, D. W., 1974, Zeolite molecular sieves: J. Wiley and Sons, New York.

Breger, I., Chandler, J. C., and Zubovic, P., 1970, An infrared study of water in heulandite and clinoptilolite: Amer. Mineralogist, v. 55, p. 825-840.

Broecker, W. S., and Kaufman, A., 1965, Radiocarbon chronology of Lake Lahontan and Lake Bonneville, 2, Great Basin: Geol. Soc. America Bull., v. 76, p. 537-566.

Bryant, E. A., and Vaniman, D. T., 1984, Research and development related to the Nevada Nuclear Waste Storage Investigations, July 1 - September 30, 1983: Los Alamos Nat. Lab., LA-10006-PR, 100 p.

Butters, S. W., and Gronseth, J. M., 1980, Material properties of Nevada Test Site tuff and grout: Terra Tek, Inc., DNA-5379F, 110 p.

Byers, F. M., Jr. and Barnes, H., 1967, Geologic map of the Paiute Ridge Quadrangle, Nye and Lincoln Counties, Nevada: U.S. Geol. Survey, Geol. Quad. Map, GQ-577.

Byers, F. M., Jr. and Warren, R. G., 1983, Revised volcanic stratigraphy of drill hole J-13, Fortymile Wash, Nevada, based on petrographic modes and chemistry of phenocrysts: Los Alamos Nat. Lab., LA-9652-MS, 23 p.

Byers, F. M., Jr., Carr, W. J., Christiansen, R. L., Lipman, P. W., Orkild, P. P., and Quinlivan, W. D., 1976a, Geologic map of the Timber Mountain Caldera area, Nye County, Nevada: U.S. Geol. Survey, Misc. Inv. Ser. Map I-891.

Byers, F. M., Jr., Carr, W. J., Orkild, P. P., Quinlivan, W. D., and Sargent, K. A., 1976b, Volcanic suites and related cauldrons of Timber Mountain--Oasis Valley caldera complex, southern Nevada: U.S. Geol. Survey, Prof. Paper 919, 70 p.

Byers, F. M., Jr., Orkild, P. P., Carr, W. J., and Christiansen, R. L., 1964, Timber Mountain caldera, Nevada Test Site and vicinity - A preliminary report (abs.): Geol. Soc. America, Spec. Paper 76, p. 267.

Byers, F. M., Jr., Orkild, P. P., Carr, W. J., and Quinlivan, W. D., 1968, Timber Mountain Tuff, southern Nevada, and its relation to cauldron subsidence: Geol. Soc. America, Mem. 110, p. 87-97.

Caporuscio, F., Vaniman, D., Bish, D., Broxton, D., Arney, B., Heiken, G., Byers, F., Gooley, R., and Semarge, R., 1982, Petrologic studies of core from drill hole USW-G2, and UE256-1H, Yucca Mountain, Nevada: Los Alamos Nat. Lab., LA-9255-MS.

Carper, A. F., 1921, Report on Thomas Group. Diamond Queen Mining District, Nye County, Nevada: Nevada Bur. Mines Geol., Nye County file 228, item 3.

Carr, W. J., 1974, Summary of tectonic and structural evidence for stress orientation at the Nevada Test Site: U.S. Geol. Survey Open-File Rept. 74-176, 53 p.

Carr, W. J., 1979, Possible paleoseismic belt in Nevada Test Site region (abs.): U.S. Geol. Survey Prof. Paper 1150, p. 82.

Carr, W. J., 1982a, Structural setting and rate of tectonic activity in the Yucca Mountain region, southwestern Great Basin, Nevada and California: Proc. 1982 NWTS Program Inf. Meetings, Las Vegas, Nevada, p. 107-108.

Carr, W. J., 1982b, Volcano-tectonic history of Crater Flat, southwestern Nevada, as suggested by new evidence from drill hole USW-VH-1 and vicinity: U.S. Geol. Survey Open-File Rept. 82-457, 23 p.

Carr, W. J., and Quinlivan, W. D., 1968, Structure of Timber Mountain--resurgent dome, in Nevada Test Site: Geol. Soc. America, Mem. 110, p. 99-108.

Carr, W. J., and Rogers, A. M., 1982, Tectonics, seismicity, volcanism, and erosion rates in the southeastern Great Basin: U.S. Geol. Survey Circ. 847, p. 7-10.

Carroll, P. I, Capruscio, F. A. and Bish, D. L., 1981, Further description of the petrology of the Topopah Spring Member of the Paintbrush Tuff in drill holes UE25a-1 and USW-G1, Yucca Mountain, Nevada: Los Alamos Nat. Lab., LA-9000-MS.

Chen, C., 1975, A method of estimation of standard free energies of formation of silicate minerals at 298.15 K: Amer. Jour. Science, v. 275, 801-817.

Cheng, C. H., and Johnston, D. H., 1981, Dynamic and static moduli: Geophys. Res. Letters, v. 8, p. 39-42.

Childs, S. W., and Malstaff, G., 1982, Final report: Heat and mass transfer in unsaturated porous media: Pacific Northwest Lab., PNL-4036, 101 p. plus 1 appendix.

Christiansen, R. L., and Lipman, P. W., 1965, Geologic map of the Topopah Spring NW quadrangle, Nye County, Nevada: U.S. Geol. Survey, Geol. Quad. Map GQ-444.

Christiansen, R. L., Lipman, P. W., Carr, W. J., Byers, F. M., Jr., Orkild, P. P., and Sargent, K. A., 1977, Timber Mountain-Oasis Valley caldera complex of southern Nevada: Geol. Soc. America Bull., v. 88, p. 943-959.

Claassen, H. C., 1983, Sources and mechanisms of recharge for ground water in the west-central Amargosa Desert, Nevada--a geochemical investigation: U. S. Geol. Survey Open-file Rept. 83-542.

Constantz, J., 1983, Laboratory analysis of water retention in unsaturated zone materials at high temperature, in Role of the unsaturated zone in radioactive and hazardous waste disposal: Ann Arbor, MI, Ann Arbor Science, p. 147-164.

Cook, E. F., 1965, Stratigraphy of Tertiary volcanic rocks in eastern Nevada: Nevada Bur. Mines Geol., Rept. 11, 61 p.

Cooley, C. H., Smith, R. H., and Schatz, J. F., 1982, Properties of tuffs, grouts and other materials: Terra Tek, Inc., DNA-5986F, 212 p.

Cording, E. J., 1967, Stability during construction of three large underground openings in rock: Unpub. Ph.D. thesis, Univ. of Illinois, 259 p.

Cornwall, H. R., 1972a, Geologic map of southern Nye County, Nevada: Nevada Bur. Mines Geol. Bull. 77, Plate 1.

Cornwall, H. R., 1972b, Geology and mineral deposits of southern Nye County, Nevada: Nevada Bur. Mines Geol. Bull. 77, 49 p., Maps.

Cornwall, H. R., and Kleinhampl, F. J., 1961, Geology of the Bare Mountain Quadrangle: U.S. Geol. Survey, Geol. Quad. Map, GQ-157.

Craig, R. W., Reed, R. L., and Spengler, R. W., 1983, Geohydrologic data for test well USW H-6, Yucca Mountain area, Nye County, Nevada: U. S. Geol. Survey Open-File Rept. 83-856, 35 p.

Crowe, B. M., and Carr, W. J., 1980, Preliminary assessment of the risk of volcanism at a proposed nuclear waste repository in the southern Great Basin: U.S. Geol. Survey Open-File Rept. 80-357, 15 p.

Crowe, B. M., and Sargent, K. A., 1979, Major-element geochemistry of the Silent Canyon-Black Mountain peralkaline volcanic centers, northwestern Nevada Test Site: Application to an assessment of renewed volcanism: U.S. Geol. Survey Open-File Rept. 79-926, 27 p.

Crowe, B. M., and Vaniman, D. T., 1985, Research and development related to the Nevada Nuclear Waste Storage Investigations, January 1 - March 31, 1984: Los Alamos Nat. Lab., LA-10154-PR, 124 p.

Daniels, J. J., and Scott, J. H.., 1980, Borehole geophysical measurements for hole UE25a-3, Nevada Test Site, Nuclear Isolation Program: U.S. Geol. Survey Open-File Rept. 80-126.

Daniels, J. J., Scott, J. H. and Hagsrum, J. T., 1981, Interpretation of geophysical well log measurement in drill holes UE25a-4, -5, -6, and -7, Yucca Mountain, Nevada Test Site: US. Geol. Survey Open-File Rept. 81-615, 29 p.

Daniels, W. R., and others, 1982a, Research and development related to the Nevada Nuclear Waste Storage Investigations, July 1 - September 30, 1981: Los Alamos Nat. Lab., LA-9095-PR, 78 p.

Daniels, W. R., and others, 1982b, Research and development related to the Nevada Nuclear Waste Storage Investigations, October 1 - December 31, 1981: Los Alamos Nat. Lab., LA-9225-PR, 97 p.

Daniels, W. R., and others, 1982c, Research and development related to the Nevada Nuclear Waste Storage Investigations, Jan. 1 - March 31, 1982: Los Alamos Nat. Lab., LA-9327-PR, 42 p.

Daniels, W. R., and others, 1982d, Summary report on the geochemistry of Yucca Mountain and environs: Los Alamos Nat. Lab., LA-9328-MS, 364 p.

Daniels, W. R., and others, 1983, Laboratory and field studies related to the Radionuclide Migration Project, October 1, 1981 - September 30, 1982: Los Alamos Nat. Lab., LA-9691-PR, 65 p.

Daniels, W. R., and others, 1984, Laboratory and field studies related to the Radionuclide Migration Project, October 1, 1982 - September 30, 1983: Los Alamos Nat. Lab., LA-10121-PR, 35 p.

Daniels, W. R., Erdal, B. R., and Vaniman, D. T., 1983, Research and development related to the Nevada Nuclear Waste Storage Investigations, July 1 - September 30, 1982: Los Alamos Nat. Lab., LA-9577-PR.

Deer, W. A., Howie, R. A., and Zussman, J., 1971, An introduction to the rock-forming minerals: New York, NY, John Wiley, 528 p.

Department of Energy, 1984, NWPA environmental assessment (draft): Nevada Nuclear Waste Storage Investigations Project, Waste Management Project Office, Nevada Operations Office, Las Vegas, NV.

Dudley, W. W., Jr. and Erdal, B. R., 1982, Site characterization for evaluation of potential nuclear waste isolation at Yucca Mountain, Nevada": Proc. 1982 NWTS Prog. Inf. Meetings, Las Vegas, Nevada, p. 10-12.

Duffy, C., 1983, Matrix permeability and porosity of unsaturated tuffs, in Research and development related to the Nevada Nuclear Waste Storage Investigations, October 1 - December 31, 1982: Los Alamos Nat. Lab., LA-9666-PR, p. 20-21.

Duffy, C. J., and Raybold, N. A., 1981, Tuff permeability measurements, in Research and development related to the Nevada Nuclear Waste Storage Investigations, April 1 - June 30, 1981: Los Alamos Nat. Lab., LA-8959-PR, p. 38-45.

Eardley, A. J., 1951, Structural geology of North America: Harper and Brothers, New York, NY, 624 p.

Ekren, E. B., 1968, Geologic setting of Nevada Test Site and Nellis Air Force Range, in Nevada Test Site: Geol. Soc. America, Mem. 110, p. 11-19.

Ekren, E. B., and Sargent, K. A., 1965, Geologic map of the Skull Mountain Quadrangle, Nye County, Nevada: U.S. Geol. Survey, Geol. Quad. Map CQ-387.

Ekren, E. B., Anderson, R. E., Rogers, C. L., and Noble, D. C., 1971, Geology of the northern Nellis Air Force Base Bombing and Gunnery Range, Nye County, Nevada: U.S. Geol. Survey Prof. Paper 651, 91 p.

Ekren, E. B., Rogers, C. L., Anderson, R. E., and Orkild, P. P., 1968, Age of basin and range normal faults in Nevada Test Site and Nellis Air Force Range, Nevada, in Nevada Test Site: Geol. Soc. America, Mem. 110, p. 247-250.

Elevatorski, E. A., 1973, Nevada industrial minerals: MINOBRAS, 62 p.

Ellis, W. L., and Swolfs, H. S., 1983, Preliminary assessment of in-situ geomechanical characterizations in drill hole USW-G1, Yucca Mountain, Nevada: U. S. Geol. Survey Open-file Rept. 83-401, 18 p.

Fenneman, N. M., 1931, Physiography of the western United States: McGraw-Hill, New York, NY, 534 p.

Fisher, R. V., 1961, Proposed classification of volcaniclastic sediments and rocks: Geol. Soc. America Bull., v. 72, p. 1409-1414.

French, D. E., and Freeman, K. J., 1979, Tertiary volcanic stratigraphy and reservoir characteristics of Trap Spring field, Nye County, Nevada, in RMAG-UGA-1979 Basin and Range symposium: Las Vegas, Oct. 7-11, 1979 Proc., p. 487-502.

Gallagher, M. J., 1957-69, Nevada mines, mills and smelters in operation: Nevada State Inspector of Mines Report.

Garside, L. G., 1973, Radioactive mineral occurrences in Nevada: Nevada Bur. Mines Geol. Bull. 81, 121 p.

Garside, L. G., 1979, Radioactive mineral occurrences in Nevada--An update to Bulletin 81: Nevada Bur. Mines Geol. Open-File Rept. 79-2.

Garside, L. G., and Papki, K. G., 1980, A preliminary first-stage study of Nevada coal resources: Nevada Bur. Mines Geol. Open-File Rept. 80-5.

Geotechnical Engineers, Inc., 1979, Preliminary study of radioactive waste disposal in the vadose zone: submitted to Lawrence Livermore Nat. Lab., LLL Proj. Rept. 77393.

Gianella, V. P., 1940, Report on the Harvey mercury property near Beatty, Nevada: Nevada Bur. Mines Geol., Nye County file 228, item 4.

Gibbons, A. B., Hinrichs, E. N., Hansen, W. R., and Lemke, R. W., 1963, Geology of the Rainier Mesa Quadrangle, Nye County, Nevada: U.S. Geol. Survey, Geol. Quad. Map GQ-215.

Gildersleeve, B., 1962, Magnesite and brucite in the United States: U.S. Geol. Survey, Min. Inv. Res. Map, MR-27.

Gilluly, J., Waters, A. C., and Woodford, A. O., 1959, Principles of geology: W. H. Freeman and Co., 2nd ed., 534 p.

Goddard, E. N., Trask, P. D., De Ford, R. K., Rove, O. N., Singewald, J. T., Jr., and Overbeck, R. M., 1948, Rock Color Chart, Geol. Soc. America, Boulder, CO.

Gordon, M., Jr. and Poole, F. G., 1968, Mississippian-Pennsylvanian boundary in southwest Nevada and southeastern California, in Nevada Test Site: Geol. Soc. America, Mem. 110, p. 157-168.

Green, R. T., and Evans, D. D., 1983, Radionuclide transport as a vapor through unsaturated fractured rock - a preliminary assessment, NRC-04-81-224 Contract Report.

Greene, L. W., and Latscher, J. A., 1981, Historic resources study: A history of mining in Death Valley National Monument: U.S. Dept. Interior, National Park Service, v. I and II, pts. 1 and 2 each, 786 p.

Greene-Kelly, R., 1957, The montmorillonite minerals, in The differential thermal investigation of clays: Mineralogical Soc. (Clay Min. Group), London, p. 140-164.

Grim, R. E., 1968, Clay mineralogy (2nd ed.): McGraw Hill, 596 p.

Gureghian, A. E., 1983, TRIPM: A two-dimensional finite-element model for the simultaneous transport of water and reacting solutes through saturated and unsaturated media: Batelle Office of Nuclear Waste Isolation, ONWI-465, 150 p.

Guzowski, R. V., Nimick, F. B., Siegel, M. D., and Finley, N. C., 1983, Repository site data report for tuff: Yucca Mountain, Nevada: Sandia Nat. Labs., NUREG/CR-2937, SAND82-2105, 312 p.

Hagstrum, J. T., Daniels, J. J., and Scott, J. H., 1980, Analysis of the magnetic susceptibility well log in drill hole UE25a-5, Yucca Mountain, Nevada Test Site: U.S. Geol. Survey Open-File Rept. 80-1263, 33 p.

Haimson, B. C., and Fairhurst, C., 1967, Initiation and extension of hydraulic fractures in rock: Soc. Petroleum Engineers Jour., v. 7, p. 310-318.

Hall, R. B., 1978, World nonbauxite aluminum resources - alunite: U.S. Geol. Survey Prof. Paper 1076-A, 35 p.

Harris, H. D., 1959, Late Mesozoic positive area in western Utah: Amer. Assoc. Petroleum Geologists, v. 43, p. 2636-2652.

Hausel, W. D., and Nash, W. P., 1977, Petrology of Tertiary and Quaternary volcanic rocks, Washington County, southeastern Utah: Geol. Soc. America Bull., v. 88, p. 1831-1842.

Healy, J., Stock, J., Svitek, J., and Hickman, S., 1983, Hydrofrac stress measurements on Yucca Mountain, Nevada: Amer. Geophys. Union Trans., v. 64, p. 320.

Heiken, G. H., and Bevier, M. L., 1979, Petrology of tuff units from the J-13 drill site, Jackass Flats, Nevada: Los Alamos Sci. Lab., LA-7563-MS, 55 p.

Heikes, V. C., 1931, Gold, silver, copper, lead, and zinc in Nevada--mine report, in Mineral Resources of the U.S., 1928: U.S. Dept. Commerce, Bur. of Mines, pt. 1, p. 441-478.

Hill, J. M., 1912, The mining districts of the western U.S.: U.S. Geol. Survey Bull. 507, 309 p.

Hirschfelder, J. O., Curtiss, C. F., and Bird, R. B., 1954, Molecular Theory of Gases and Liquids, Wiley, New York.

Hoffman, U., and Endell, J., 1939, Die Abhangigkert des Kationenaustausches und der Quelling bei Montmorillonite von der Vorerhitzung (Auszug): Zeitschr. Angewandte Chemie, v. 25, p. 708.

Holmes, G. H., Jr., 1965, Mercury in Nevada, in Mercury potential of the United States: U.S. Bur. Mines, I. C. 8252, p. 215-300.

Honda, S., and Muffler, L. J. P., 1970, Hydrothermal alteration in core from research drill hole Y-1, Upper Geyser Basin, Yellowstone National Park, Wyoming: Amer. Mineralogist, v. 55, p. 1714-1737.

Horton, R. C., 1964, Mineral fuels--coal, in Mineral and water resources of Nevada: Nevada Bur. Mines Geol., Bull. 65, p. 51-53.

Iijima, A., 1975, Effect of pore water to clinoptilolite-analcime-albite reaction series: Jour. Fac. Sci. Univ. Tokyo, Sec. II, n. 19, p. 133-147.

Iijima, A., 1980, Geology of natural zeolites and zeolitic rocks, in Proc. Fifth Int. Conf. Zeolites: Heyden, London, p. 103-118.

Iijima, A., and Ohwa, I., 1980, Zeolitic burial diagenesis in Creta-Tertiary geophysical deposits of central Hokkaido, Japan: Proc. 5th Int. Conf. Zeolites, p. 139-148.

Jackson, J., and McKenzie, D., 1983, The geometrical evolution of normal fault systems: Jour. Structural Geol., v. 5, p. 471-482.

Johnstone, J. K., 1980, In-situ tuff water migration/heater experiment: experimental plan: Sandia Nat. Labs., SAND79-1276, 177 p.

Johnstone, J. K., and Wolfsberg, K. (eds), 1980, Evaluation of tuff as a medium for nuclear waste repository, interim report on the properties of tuff: Sandia Nat. Labs., SAND80-1464, 142 p.

Judson, S., Deffeyes, K. S., and Hargraves, R. B., 1976, Physical geology: Prentice-Hall, 560 p.

Kane, M. F., Webring, M. W., and Bhattachargya, B. K., 1981, A preliminary analysis of gravity and aeromagnetic surveys of the Timber Mountain area, southern Nevada: U.S. Geol. Survey Open-File Rept. 81-189, 40 p.

Kerrisk, J., 1984a, Reaction-path calculations of groundwater chemistry and mineral formation at Rainier Mesa, Nevada: Los Alamos Nat. Lab., LA-9912-MS, 40 p.

Kerrisk, J., 1984b, Solubility limits on radionuclide dissolution at a Yucca Mountain Repository: Los Alamos Nat. Lab., LA-9995-MS, 54 p.

Kistler, R. W., 1968, Potassium-argon age of volcanic rocks in Nye and Esmeralda Counties, Nevada, in Nevada Test Site: Geol. Soc. America, Mem. 110, p. 251-262.

Knopf, A., 1915, Some cinnabar deposits in western Nevada: U.S. Geol. Survey Bull. 620-D, p. 59-68.

Kral, V. E., 1951, Mineral resources of Nye County, Nevada: Univ. Nevada Bull., v. 45, n. 3, Geol. Mining Ser. 50, 223 p.

Lachenbruch, A. H., 1981, Temperature effects of varying phase composition during the steady vertical flow of moisture in unsaturated, stratified sediments: U.S. Geol. Survey Open-File Rept. 81-1220, 11 p.

LANL, 1984, DOE presentation viewgraphs from the NNWSI/NRC geochemistry workshop, July 10 - 12, 1984, Los Alamos Nat. Lab.

Lappin, A. R., 1980, Preliminary thermal expansion screening data for tuffs: Sandia Nat. Labs., SAND78-1147, 40 p.

Lappin, A. R., 1981, Thermal conductivity of silicic tuffs: Predictive formalism and comparison with preliminary experimental results: Sandia Nat. Labs., SAND80-0769, 51 p.

Lappin, A. R., Price, R. H., Thomas, R. K., Koski, J. A., and van Buskirk, R. G., 1982a, Thermal and mechanical stratigraphy of silicic tuffs at Yucca Mountain, Nye County, Nevada (abs.): Geol. Soc. of America, Programs with Abstracts, v. 14, p. 319.

Lappin, A. R., VanBuskirk, R. G., Enniss, D. O., Butters, S. W., Prater, F. M., Muller, C. B., and Bergosh, J. L., 1982b, Thermal conductivity, bulk properties, and thermal stratigraphy of silicic tuffs from the upper portion of hole USW-G1, Yucca Mountain, Nye County, Nevada: Sandia Nat. Labs., SAND81-1873, 48 p.

Leeman, W. P., and Rogers, J. J. W., 1970, Late Cenozoic alkali-olivine basalts of the Basin-Range province, U.S.A.: Contr. Mineral. and Petrol., v. 25, p. 1-25.

Leet, L. D., and Judson, S., 1971, Physical geology: Prentice-Hall, 4th ed., 887 p.

Levy, S. S., 1983, Studies of altered vitrophyre for the prediction of nuclear waste repository-induced thermal alteration at Yucca Mountain, Nevada: Los Alamos Nat. Lab., LA-UR-3402, 7 p.

Levy, S. S., 1984. Petrology of samples from drill holes USW H-3, H-4, and H-5, Yucca Mountain, Nevada: Los Alamos Nat. Lab., LA-7706-MS, 77 p.

Lin, W., 1983, Correlation of ultrasonic velocity and rock strength: Lawrence Livermore Nat. Lab., UCID-19658, 20 p.

Lincoln, F. C., 1923, Mining districts and mineral resources of Nevada: Nevada Newsletter Pub. Co., Reno, 295 p.

Lindberg, R. D., and Runnells, D. D., 1984, Ground water redox reactions: an analysis of equilibrium state applied to Eh measurements and geochemical modeling: Science, v. 225, p. 925-927.

Liou, J. G., 1971, Analcime equilibria: Litho, v. 4, p. 389-402.

Lipman, P. W., and McKay, E. J., 1965, Geologic map of the Topopah Spring SW quadrangle, Nye County, Nevada: U.S. Geol. Survey, Geol. Quad. Map GQ-439, scale 1:24,000.

Lipman, P. W., Christiansen, R. L., and O'Conner, J. T., 1966a, A compositionally zoned ash-flow sheet in southern Nevada: U.S. Geol. Survey Prof. Paper 524-F, 47 p.

Lipman, P. W., Quinlivan, W. D., Carr, W. J., and Anderson, R. E., 1966b, Geologic map of the Thirsty Canyon SE quadrangle, Nye County, Nevada: U.S. Geol. Survey, Geol. Quad. Map, GQ-489.

Lobmeyer, D. H., Whitfield, Jr., M. S., Lahoud, R. G., and Bruckheimer, L., 1983, Geohydrologic data for test well UE-25b#1, Nevada Test Site, Nye County, Nevada: U.S. Geol. Survey Open-File Rept. 83-855, 48 p.

Locke, A., Billingsley, P. R., and Mayo, E. B., 1940, Sierra Nevada tectonic pattern: Geol. Soc. America Bull., v. 51, p. 513-540.

Longwell, C. R., 1960, Possible explanation of diverse structural patterns in southern Nevada: Amer. Journ. Sci., v. 258-A, p. 192-203.

Longwell, C. R., Pampeyan, E. H., and Bowyer, B., 1965, Geologic map of Clark County, Nevada: Nevada Bur. Mines Bull. 62, Plate 1.

Lovering, T. G., 1954, Radioactive deposits of Nevada: U.S. Geol. Survey Bull. 1009-C, 106 p.

Luft, S. J., 1964, Mafic lavas of Dome Mountain, Timber Mountain caldera, southern Nevada: U.S. Geol. Survey Prof. Paper 501-D, p. D14-D21.

Mackenzie, R. C., 1964, Hydration characteristics of montmorillonite: Ber. Deut. Keram. Ges., v. 41, p. 696-707.

Mackin, J. H., 1960, Structural significance of Tertiary volcanic rocks in southwestern Utah: Amer. Journ. Sci., V. 258, p. 21-131.

Maldonado, F., 1977, Summary of the geology and physical properties of the Climax Stock, Nevada Test Site: U.S. Geol. Survey Open-File Rept. 77-1977, 27 p.

Maldonado, F., 1981, Geology of the Twinridge pluton area, Nevada Test Site, Nevada: U.S. Geol. Survey Open-File Rept. 81-156, 13 p.

Maldonado, F., and Koether, S. L., 1983, Stratigraphy, structure, and some petrographic features of Tertiary volcanic rocks in the USW G-2 drill hole, Yucca Mountain, Nye County, Nevada: U.S. Geol. Survey Open-File Rept. 83-732, 83 p.

Mariner, R. H., and Surdam, R. C., 1970, Alkalinity and formation of zeolites in saline alkaline lakes: Science, v. 170, p. 977-980.

Marvin, R. F., Byers, F. M., Jr., Mehnert, H. H., Orkild, P. P., and Stern, T. W., 1970, Radiometric ages and stratigraphic sequence of volcanic and plutonic rocks, southern Nye and western Lincoln Counties, Nevada: Geol. Soc. America Bull., v. 81, p. 2657-2676.

McKay, E. J., 1963, Hydrothermal alteration in the Calico Hills, Jackass Flats quadrangle, Nevada Test Site: U.S. Geol. Survey, Tech Letter NTS-43, 6 p.

Mehringer, P. J., Jr., 1965, Late Pleistocene vegetation in the Mohave Desert of southern Nevada: Journ. Arizona Acad. Sci., v. 3, p. 172-188.

Mehringer, P. J., Jr., 1967, Pollen analysis of the Tule Springs area, Nevada, in Pleistocene Studies in Southern Nevada: Nevada State Museum Anthropological Paper n. 13, p. 129-200.

Meyers, J. S., 1962, Evaporation from the 17 Western States: U.S. Geol. Survey Prof. Paper 272-D, p. 71-91.

Mifflin, M. D., and Wheat, M., 1979, Pluvial lakes and estimated climates of Nevada: Nev. Bur. Mines Geol. Bull. 94.

Miller, R. R., 1948, The Cyprinodont fishes of the Death Valley system of eastern California and southwestern Nevada: Museum of Zoology, Univ. Michigan, Misc. Pub. 68, 155 p.

Milly, P. C. D., 1982, Moisture and heat transport in hysteretic, inhomogeneous porous media: a matric head-based formulation and a numerical model: Water Resources Research, v. 18, p. 489-498.

Moss, M., and Haseman, G. M., 1983a, A proposed model for the thermal conductivity of dry and water-saturated tuff: Sandia Nat. Labs., SAND83-0535C, 9 p.

Moss, M., and Haseman, G. M., 1983b, A proposed model for the thermal conductivity of dry and water-saturated tuff: 7th Internat. Symposium on the scientific basis for nuclear waste management, Material Res. Soc. Annual Meeting, Nov. 14-17, 1983, Boston, MA, p. 967-974.

Moss, M., Koski, J. A., Haseman, G. M., and Tormey, T. V., 1982, The effects of composition, porosity, bedding-plane orientation, water content and a joint on the thermal conductivity of tuff: Sandia Nat. Labs., SAND82-1164, 28 p.

Mroz, E. J., Rundberg, R. S., and Mitchell, A. J., 1983a, Matric potential determinations, in Research and development related to the Nevada Nuclear Waste Storage Investigations, April 1 - June 30, 1983: Los Alamos Nat. Lab., LA-9846-PR, p. 42-43.

Mroz, E. J., Rundberg, R. S., and Mitchell, A. J., 1983b, Fracture-flow experiments, in Research and development related to the Nevada Nuclear Waste Storage Investigations, April 1 - June 30, 1983: Los Alamos Nat. Lab., LA-9846-PR, p. 43.

Naeser, C. W., and Maldonado, F., 1981, Fission-track dating of the Climax and Gold Meadows stocks, Nye County, Nevada: U.S. Geol. Survey Prof. Paper 1199-E, p. 45-47.

NNWSI, 1981, Nevada Nuclear Waste Storage Investigations, Quarterly Report, April through June 1981: U.S. Dept. Energy, Nevada Operations Office Rept. NVO-196-26.

Nolan, T. B., 1943, The Basin and Range province in Utah, Nevada and California: U.S. Geol. Survey Prof. Paper 197-D, p. 141-196.

Norman, L. A., Jr. and Stewart, R. M., 1951, Mines and mineral resources of Inyo County: California Journ. Mines, v. 47, n. 1, p. 18-223.

Norrish, K., 1972, Forces between clay particles: Int. Clay Conf. 1972, Preprints v. 2, p. 271.

Ogard, A. E., and Kerrisk, J. F., 1984, Groundwater chemistry along flow paths between a proposed repository site and the accessible environment, Los Alamos Nat. Lab., LA-10188-MS, 48 p.

Ogard, A. E., Daniels, W. R., and Vaniman, D. T., 1983a, Research and development related to the Nevada Nuclear Waste Storage Investigations, October 1 - December, 1982: Los Alamos Nat. Lab., LA-9666-PR, 53 p.

Ogard, A. E., Wolfsberg, K., Daniels, W. R., Kerrisk, J., Rundberg, R. S. and Thomas, K. W., 1984, Retardation of radionuclides by rock units along the path to the accessible environment, in Scientific basis for nuclear waste management VII: North-Holland, New York, NY, p. 329-336.

Ogard, A. E., Wolfsberg, K., and Vaniman, D. T., 1983b, Research and development related to the Nevada Nuclear Waste Storage Investigations, April 1 - June 30, 1983: Los Alamos Nat. Lab., LA-9846-PR, 105 p.

Olsson, W. A., 1982, Effects of elevated temperature and pore pressure on the mechanical behavior of Bullfrog Tuff: Sandia Nat. Labs., SAND81-1664, 17 p.

Olsson, W. A., and Jones, A. K., 1980, Rock mechanics properties of volcanic tuffs from the Nevada Test Site: Sandia Nat. Labs., SAND80-1453, 45 p.

Olsson, W. A., and Teufel, L. W., 1980, Effects of water on the mechanical properties of intact and jointed welded tuff (abs.): Geophs. Union Trans., v. 61, n. 17. p. 372.

Ore, H. T., and Warren, C. N., 1971, Late Pleistocene-early Holocene geomorphic history of Lake Mojave, California: Geol. Soc. America Bull., v. 82, p. 2553-2562.

Orkild, P. P., 1965, Paintbrush Tuff and Timber Mountain Tuff of Nye County, Nevada, in Changes in stratigraphic nomenclature by the U.S. Geological Survey: U.S. Geol. Survey Bull. 1224-A, p. A44-A51.

Orkild, P. P., Sargent, K. A., and Snyder, R. P., 1969, Geologic map of Pahute Mesa, Nevada Test Site and vicinity, Nye County, Nevada: U.S. Geol. Survey, Misc. Geol. Inv., Map 1-567.

Papke, K. G., 1970, Montmorillonite, bentonite, and fuller's earth deposits in Nevada: Nevada Bur. Mines Geol. Bull. 76.

Papke, K. G., 1979, Fluorspar in Nevada: Nevada Bur. Mines Geol. Bull. 93, 77 p.

Pettijohn, F. J., 1975, Sedimentary rocks (3rd ed.): New York, Harper and Row, 628 p.

Pin, F. G., and Witten, A. J., 1983, Numerical simulation of unsaturated flows and seepage of contaminants from subgrade mill tailings disposal area: Nuclear Regulatory Commission, NUREG/CR-3398.

Plummer, C. C., and McGeary, D., 1979, Physical geology: Wm. C. Brown Co., Pub., 462 p.

Price, R. H., 1982, Uniaxial compression of volcanic tuff: (abstr.): Eos, v. 63, no. 18, p. 440-441.

Price, R. H., 1983, Analysis of rock mechanics properties of volcanic tuff units from Yucca Mountain, Nevada Test Site: Sandia Nat. Labs., SAND 82-1315.

Price, R. H., and Jones, A. K., 1982, Uniaxial and triaxial compression test series on Calico Hills Tuff: Sandia Nat. Labs., SAND82-1314, 43 p.

Price, R. H., and Nimick, K. G., 1982, Uniaxial compressive test series on Tram Tuff: Sandia Nat. Labs., SAND82-1055, 33 p.

Price, R. H., Jones, A. R., and Nimick, K. G., 1982b, Uniaxial compressive test series on Bullfrog Tuff; Sandia Nat. Labs., SAND82-0481, 39 p.

Price, R. H., Nimick, K. G., and Zirzow, J. A., 1982a, Uniaxial and triaxial compression test series on Topopah Spring Tuff: Sandia Nat. Labs., SAND82-1723, 37 p.

Price, R. H., Spence, S. J., and Jones, A. K., 1984, Uniaxial compression test series on Topopah Spring tuff from USW-GU3, Yucca Mountain, southern Nevada: Sandia Nat. Labs., SAND83-1646, 61 p.

Quiring, R. F., 1965, Annual precipitation amount as a function of elevation in Nevada south of 38 1/2 degree latitude: Las Vegas, Nev., U.S. Weather Bur. Res. Sta., 14 p.

Rai, D., Strickert, R. G., Moore, D. A., and Ryan, J. L., 1983, Am(III) hydrolysis constants and solubility of Am(III) hydroxide: Radiochim. Acta, v. 33, p. 201-206.

Ratte, J. C., and Steven, T. A., 1967, Ash-flows and related volcanic rocks associated with the Creede caldera, San Juan Mountains, Colorado: U.S. Geol. Survey Prof. Paper 524-H, 58 p.

Robison, J. H., 1984, Ground-water level data and preliminary potentiometric-surface maps, Yucca Mountain and vicinity, Nye County, Nevada: U. S. Geol. Survey, Water-Resources Invest. Rept. 84-4197, 8p.

Rogers, A. M., Harmsen, S. C., Carr, W. J., and Spence, W., 1983, Southern Great Basin seismological data report for 1981 and preliminary data analysis: U.S. Geol. Survey Open-File Rept. 83-669, 263 p.

Rogers, A. M., Perkins, D. M., and McKeown, F. A., 1976, A catalog of seismicity with 400 km of the Nevada Test Site: U.S. Geol. Survey Open-File Rept. 76-832.

Rogers, A. M., Perkins, D. M., and McKeown, F. A., 1977, A preliminary assessment of the seismic hazard of the Nevada Test Site region: Seismol. Soc. Amer. Bull., v. 69, p. 1587-1606.

Ross, C. S., and Hendricks, S. B., 1945, Minerals of the montmorillonite group: U. S. Geol. Survey, Prof. Paper 205B, p. 23-80.

Ross, C. S., and Smith, R. L., 1961, Ash-flow tuffs: Their origin, geologic relations, and identification: U.S. Geol. Survey Prof. Paper 366, 81 p.

Rundberg, R. S., 1984, Kinetics of the adsorption of radionuclides on tuff from Yucca Mountain, in Scientific basis for nuclear waste management VII: North-Holland, New York, NY, p. 827-834.

Rush, F. E., Thordarson, W., and Bruckheimer, L., 1983, Geohydrologic and drill hole data for test well USW H-1, adjacent to Nevada Test Site, Nye County Nevada: U.S. Geol. Survey Open-File Rept. 83-141, 38 p.

Rytuba, J. J., and Conrad, W. K., 1981, Petrochemical characteristics of volcanic rocks associated with uranium deposits in the McDermitt caldera complex, in Uranium in volcanic and volcanoclastic rocks: Amer. Assoc. Petroleum. Geologists, Studies in Geology n. 13, p. 63-72.

Saha, P., 1959, Geochemical and X-ray investigation of natural and synthetic analcites: Amer. Mineralogist, v. 44, p. 300-313.

Sass, J. H., Kennelly, Jr., J. P., Wendt, W. E., Moses, Jr., T. H., and Ziagos, J. P., 1979, In-situ determination of heat flow in unconsolidated sediments, U.S. Geol. Survey Open File Rept. 79-595.

Sass, J. H., and Lachenbruch, A. H., 1982, Preliminary interpretation of thermal data from Nevada Test Site: U.S. Geol. Survey Open-File Rept. 82-973, 30 p.

Satterfield, C. N., 1970, Mass transfer in heterogeneous catalysis: MIT Press, Cambridge, MA.

Schlenker, J. L., Pluth, J. J., and Smith, J. V., 1979a, Position of cations and molecules in zeolites with the mordenite-type framework, VIII. Dehydrated sodium-exchanged mordenite: Mat. Research Bull., v. 14, p. 751-758.

Schlenker, J. L., Pluth, J. J., and Smith, J. V., 1979b, Position of cations and molecules in zeolites with the mordenite-type framework, IX. Dehydrated H-mordenite via acid exchange: Mat. Research Bull., v. 14, p. 849-856.

Schmid, R., 1981, Descriptive nomenclature and classificaton of pyroclastic deposits and fragments: Recommendations of the IUGS Subcommission on the systematics of igneous rocks: Geology, v. 9, p. 41-43.

Schumm, S. A., 1963, The disparity between present rate of denudation and orogeny: U.S. Geol. Survey Prof. Paper 454-H, 13 p.

Scott, R. B., Spengler, R. W., Diehl, S., Lappin, A. R., and Chornack, M. P., 1983, Geologic character of tuffs in the unsaturated zone at Yucca Mountain, southern Nevada, in Role of the unsaturated zone in radioactive and hazardous waste disposal: Ann Arbor, MI, Ann Arbor Sci. Publishers, p. 289-335

Seyfert, C. K., and Sirkin, L. A., 1973, Earth history and plate tectonics, an introduction to historical geology: Harper and Row, Publishers, 504 p.

Shelton, J. W., 1984, Listric normal faults: An illustrated summary: Amer. Assoc. Petroleum Geologists, Bull., v. 68, p. 801-815.

Sheridan, M. F., 1970, Fumarolic mounds and ridges of the Bishop Tuff, California: Geol. Soc. America Bull., v. 81, p. 851-868.

Sheridan, M. F., and Burt, D. M., 1979, A model for the genesis of uranium lithophile element deposits related to rhyolitic volcanism (abs.): Geol. Soc. America, Programs with Abstracts, v. 11, p. 515.

Sinnock, S., 1982, Geology of the Nevada Test Site and nearby areas, southern Nevada: Sandia Nat. Labs. SAND82-2207, 57 p.

Sinnock, S., and Easterling, R. G., 1982, Empirically determined uncertainty in potassium-argon ages for young basalts from Crater Flat, Nye County, Nevada: Sandia Nat. Labs., SAND-1711.

Sinnock, S., Fernandez, J. A., and Twenhofel, W. S., 1984, Attributes and associated favorability graphs for the NNWSI area-to-location screening activity: Sandia Nat. Labs., SAND82-0838, 188 p.

Smith, C., and Ross, H. P., 1979, Interpretation of resistivity and induced polarization profiles with severe topographic effects, Yucca Mountain Area, Nevada Test Site: Res. Inst. Univ. Utah, Rept. ESL-21, 20 p.

Smith, D. M., 1984, Sorption and diffusion in bidisperse porous cylinders: Industrial and Engineering Chemistry Fundamentals, 23, 265-7.

Smith, G. I., 1968, Late-Quaternary geologic and climatic history of Searles Lake, southeastern California, in Means of correlation of Quaternary Successions: Proc. VII Congress Int. Assoc. Quaternary Res. v. 8, Univ. Utah Press, p. 293-310.

Smith, G. I., 1979, Subsurface stratigraphy and geochemistry of late Quarternary evaporites, Searles Lake, California: U.S. Geol. Survey Prof. Paper 1943, pp. 112-116.

Smith, R. L., 1960a, Ash flows: Geol. Soc. America Bull. v. 71, p. 795-842.

Smith, R. L., 1960b, Zones and zonal variation in welded ash flow: U.S. Geol. Survey Prof. Paper 354F, p. F149-F159.

Smith, R. L., and Bailey, R. A., 1968, Resurgent cauldrons: Geol. Soc. America, Mem. 116, p. 613-662.

Smith, R. M., 1977, Map showing mineral exploration potential in the Death Valley quadrangle, California and Nevada: U.S. Geol. Survey, Misc. Field Inv. Map MF-873, 1:250,000 Scale.

Smyth, J. R., 1982, Zeolite stability constraints on radioactive waste isolation in zeolite-bearing volcanic rocks: Jour. Geology, v. 90, p. 195-201.

Smyth, J. R., and Caporuscio, F. A., 1981, Review of the thermal stability and cation exchange properties of the zeolite minerals clinoptilolite, mordenite, and analcine: Applications to radioactive waste isolation in silica tuff: Los Alamos Nat. Lab. LA-8841-MS, 30 p.

Smyth, J. R., Crowe, B. M., and Halleck, P. M., 1978, Evaluation of the concept of terminal storage of radioactive waste in silicic pyroclastic rocks: Los Alamos Sci. Lab., LA-UR-1580, 32 p.

Snyder, C. T., and Langbein, W. B., 1962, The Pleistocene lake in Spring Valley, Nevada and its climate implications: Journ. Geophys. Res., v. 67, p. 2365-2394.

Snyder, D. B., and Carr, W. J., 1982, Preliminary results of gravity investigations at Yucca Mountain and vicinity, southern Nye County, Nevada: U.S. Geol. Survey Open-File Rept. 82-701, 36 p.

Snyder, D. B., and Oliver, H. W., 1981, Preliminary results of gravity investigations of the Calico Hills, Nevada Test Site, Nye County, Nevada: U.S. Geol. Survey Open-File Rept. 81-101, 42 p.

Snyder, W. S., Dickinson, W. R., and Silberman, M. L., 1976, Tectonic implications of space-time patterns of Cenozoic magmatism in the western United States: Earth and Planetary Sci. Letters, v. 32, p. 91-106.

Sophocleous, M., 1979, Analysis of water and heat flow in unsaturated-saturated porous media: Water Resources Research, v. 15, p. 1195-1206.

Spaulding, W. G., 1977, Late Quaternary vegetational change in the Sheep Range, southern Nevada: Journ. Arizona Acad. Sci., v. 12, p. 3-8.

Spaulding, W. G., 1980, The changing vegetation of a southern Nevada mountain range: Unpub. Ph.D. Thesis, Univ. Arizona, Tucson.

Spengler, R. W., and Rosenbaum, J. G., 1980, Preliminary interpretations of geologic results obtained from boreholes UE25a-4, -5, -6, and -7. Yucca Mountain, Nevada Test Site: U.S. Geol. Survey Open-File Rept. 80-929, 33 p.

Spengler, R. W., Byers, F. M., Jr., and Warner, J. B., 1981, Stratigraphy and structure of volcanic rocks in drill hole USW-G1, Yucca Mountain, Nye County, Nevada: U.S. Geol. Survey Open-File Rept. 81-1349, 50 p.

Spengler, R. W., Muller, D. C., and Livermore, R. B., 1979, Preliminary report on the geology and geophysics of drill hole UE25a-1, Yucca Mountain, Nevada Test Site: U.S. Geol. Survey Open-File Rept. 79-1244, 43 p.

Stewart, J. H., 1980, Geology of Nevada: Nevada Bur. Mines Geol., Spec. Pub. 4, 136 p.

Stewart, J. H., and Carlson, J. E., 1976, Cenozoic rocks of Nevada: Nevada Bur. Mines Geol., Map 52, 5 p., 4 Maps.

Stewart, J. H., and Carlson, J. E., 1978, Generalized maps showing distribution, lithology, and age of Cenozoic igneous rocks, in the western United States, in Cenozoic tectonics and regional geophysics of the western Cordillera: Geol. Soc. America, Mem. 152, p. 263-264.

Stewart, J. H., Moore, W. J., and Zietz, Z., 1977, East-west patterns of Cenozoic igneous rocks, aeromagnetic anomolies and mineral deposits, Nevada and Utah: Geol. Soc. America Bull., v. 88, p. 67-77.

Stock, J. M., Healy, J. H., and Hickman, S. H., 1984, Report on the televiewer log and stress measurements in corehole USW G-2, Nevada Test Site, October - November, 1982: U. S. Geol. Survey Open-file Rept. 84-172, 52 p.

Stumm, W., and Morgan, J. J., 1970, Aquatic chemistry, an introduction emphasizing chemical equilibria in natural waters: John Wiley, New York, NY, 583 p.

Suppe, J., Powell, C., and Berry, R., 1975, Regional topography, seismicity, Quaternary volcanism, and the present-day tectonics of the western United States: Am. Journ. Sci., v. 275-A, p. 397-436.

Swadley, W. C., and Hoover, D. L., 1983, Geology of faults exposed in trenches in Crater Flat, Nye County, Nevada: U. S. Geol. Survey Open-file Rept. 83-608, 15 p.

Sykes, M. L., Heiken, G. H., and Smyth, J. R., 1979, Mineralogy of tuff units from UE 25a-1 drill site, Yucca Mountain, Nevada: Los Alamos Sci. Lab., LA-8136-MS, 76 p.

Tien, Pei-lin, Leavens, P. B., and Nelen, J. A., 1975, Swinefordite, a dioctohedral-trioctohedral Li-rich member of smectite group from Kings Mountain, North Carolina: Amer. Mineralogist, v. 60, p. 540-547.

Thimons, E. D., and Kissell, F. N., 1973, Diffusion of gases through coal: Fuel, v. 52, p. 274-280.

Thordarson, W., 1983, Geohydrologic data and test results from well J-13, Nevada Test Site, Nye County, Nevada: U.S. Geol. Survey, Water-Resources Inv. 83-4171, 57 p.

Travis, B. J., Hodson, S. W., Nuttall, H. E., Cook, T. L., and Rundberg, R. S., 1984a, Numerical simulation of flow and transport in fractured tuff, in Scientific basis for nuclear waste management VII: North-Holland, New York, NY, p 1039-1046.

Travis, B. J., Hodson, S. W., Nuttall, H. E., Cook, T. L., and Rundberg, R. S., 1984b, Preliminary estimates of water flow and radionuclide transport in Yucca Mountain: Los Alamos Nat. Lab., LA-UR-84-40.

Treher, E. N., and Raybold, N. A., 1982, Elution of radionuclides through columns of crushed rock from the Nevada Test Site: Los Alamos Nat. Lab., LA-9329-MS, 136 p.

Tschanz, C. M., and Pampeyan, E. M., 1970, Geologic map of Lincoln County, Nevada: Nevada Bur. Mines Geol. Bull. 73, Plate 2.

Tucker, W. B., and Sampson, R. J., 1938, Mineral resources of the Inyo County: California Jour. Mines Geol., v. 34, n. 4, p. 368-590.

Tyler, L. D., 1980, Thermal/mechanical modeling for a tuff repository, in Proceedings of workshop on thermomechanical-hydrochemical modeling for a hardrock waste repository: Lawrence Berkeley Nat. Lab. LBL-11204, p. 62-69.

Tyler, L. D., and Langkopf, B. S., 1980, Mine design working group, in Evaluation of tuff as a medium for a nuclear waste repository: Sandia Nat. Labs., SAND80-1464, p., 85-96.

Tyler, L. D., and Vollendorf, W. C., 1975, Mined-back experiment to observe hydraulic fractures formed during in-situ stress measurements: Sandia Nat. Labs., SAND75-5367, 6 p.

U.S. Geological Survey, 1974, Summary of tectonic and structural evidence for stress orientation at the Nevada Test Site: U.S. Geol. Survey Open-File Rept. 76-176, 55 p.

Van Devender, T. R., 1977, Holocene woodlands in the southwestern desert: Science, v. 198, p. 189-192.

Van Devender, T. R., and Spaulding, W. G., 1979, Development of vegetation of climate in the southwestern United States: Science, v. 204, p. 701-710.

Vaniman, D., and Crowe, B., 1981, Geology and petrology of the basalts of Crater Flat: Applications to volcanic risk assessment for the Nevada Nuclear Waste Storage Investigation: Los Alamos Nat. Lab., LA-8845-MS, 68 p.

Vaniman, D., Bish, D., Broxton, D., Byers, F., Heiken, G., Carlos, B., Semarge, E., Caporuscio, F., and Gooley, R., 1984, Variation in authigenic mineralogy and soptive zeolite abundance at Yucca Mountain, Nevada, based on studies of drill cores USW GU-3 and G-3: Los Alamos Nat. Lab., LA-9707-MS, 71 p.

Vaniman, D., Crowe, B. M., Gladney, E., Carr, W. J., and Fleck, R. J., 1980, Geology and petrology of the Crater Flat and related volcanic fields, south-central Great Basin, Nevada (abs): Geol. Soc. America, Programs with Abstracts, v. 12, n. 7, p. 540.

van Olphen, H., 1977, An introduction to clay colloid chemistry: John Wiley and Sons, New York.

Waddell, R., 1982, Two-dimensional, steady-state model of groundwater flow, Nevada Test Site and vicinity, Nevada-California: U. S. Geol. Survey, Water Res. Invest. 82-4085.

Wallace, A. B., and Roper, M. W., 1981, Geology and uranium deposits along the northeastern margin, McDermitt caldera complex, Oregon: in Uranium in volcanic and volcaniclastic rocks: Amer. Assoc. Petroleum Geologists, Studies in Geology n. 13, p. 73-79.

Walter, G. R., 1982, Theoretical and experimental determination of matrix diffusion and related solute transport properties: Los Alamos Nat. Lab., LA-9471-MS, 137 p.

Weedfall, R. O., 1963, An approach to the development of isohyetal maps for the Nevada and California deserts: Las Vegas, Nev., U.S. Weather Bur. Res. Sta., 17 p.

Weide, D. L., and Weide, M. L., 1977, Time, space, and intensity in Great Basin paleoecological models, in Models and Great Basin prehistory: Desert Res. Inst., Publ. in Social Sci., n. 12, p. 79-111.

Weisinger, R., Costin, L. S., and Lutz, T. S., 1980, K_{IC} and J-resistence-curve measurements on Nevada Tuff: Experimental Mechanics, v. 20, p. 68-72.

Wells, P. V., 1979, An equable glacio-pluvial in the West: Pleni-glacial evidence of increased precipitation on a gradient from the Great Basin to the Sonoran and Chihuahuan desert: Quaternary Res. v. 12, p. 311-325.

Wells, P. V., and Berger, R., 1967, Late Pleistocene history of coniferous woodland in the Mojave Desert: Science, v. 155, p. 1640-1647.

Wells, P. V., and Jorgensen, C. D., 1964, Pleistocene wood rat middens and climatic change in Mohave Desert, A record of juniper woodlands: Science, v. 143, p. 1171-1174.

Wernicke, B., and Burchfiel, B. C., 1982, Modes of extensional tectonics: Jour. Structural Geol., v. 4, p. 105-115.

White, A. F., 1979, Geochemistry of ground water associated with tuffaceous rocks, Oasis Valley, Nevada: U. S. Geol. Survey, Prof. Paper 712-E, 26 p.

White, A. F., and others, 1980, The effect of dissolution of volcanic glass on the water chemistry in a tuffaceous aquifer, Rainier Mesa, Nevada: U. S. Geol. Survey, Water-supply Paper 1535-Q, 34 p.

Williams, H., Turner, F. J., and Gilbert, C. M., 1954, Petrography: San Francisco, W. H. Freeman and Co., 406 p.

Winograd, I. J., 1974, Radioactive waste storage in the arid zone: Amer. Geophys. Union Trans. v. 55, p. 884-897.

Winograd, I. J., and Doty, G. C., 1980, Paleohydrology of the southern Great Basin, with special reference to water table fluctuation beneath the Nevada Test Site during late Pleistocene: U.S. Geol. Survey Open-File Rept. 80-569, 91 p.

Winograd, I. J. and Thordarson, W., 1975, Hydrogeologic and hydrochemical framework, south-central Great Basin, Nevada-California, with special reference to the Nevada Test Site: U.S. Geol. Survey Prof. Paper 712-C, 126 p.

Witherspoon, P. A., Wang, J. S. Y., Iwai, K., and Gale, J.E., 1980, Validity of cubic law for fluid flow in a deformable rock fracture: Water Resources Research, v. 16, p. 1016-1024.

Wolfsberg, K., and others, 1981, Sorption-desorption studies on tuff: III. A continuation of studies with samples from Jackass Flats, Nevada: Los Alamos Nat. Lab., LA-8747-MS, 364 p.

Wolfsberg, K., and others, 1982, Research and development related to the Nevada Nuclear Waste Storage Investigations, April 1 - June 30, 1982: Los Alamos Nat. Lab., LA-9484-PR, 59 p.

Wolfsberg, K., and Vaniman, D. T., 1984, Research and development related to the Nevada Nuclear Waste Storage Investigations, October 1 - December 31, 1983: Los Alamos Nat. Lab., LA-10032-PR, 76 p.

Wolfsberg, K., Vaniman, D. T., and Ogard, A. E., 1983, Research and development related to the Nevada Nuclear Waste Storage Investigations, January 1 - March 31, 1983: Los Alamos Nat. Lab., LA-9793-PR, 52 p.

Wollenberg, H. A., Yang, J. S. Y., and Korbin, G., 1982, An appraisal of nuclear waste isolation in the vadose zone in arid and semi-arid regions: Lawrence Berkeley Nat. Lab., NUREG/CR-3158, LBL-15010, 126 p.

Wollenberg, H. A., Yang, J. S. Y., and Korbin, G., 1983, Nuclear waste isolation in the unsaturated zone of arid regions, in Role of the unsaturated zone in radioactive and hazardous waste disposal: Ann Arbor, MI, Ann Arbor Science, p. 195-210.

Yeh, G. T., and Luxmoore, R. J., 1982, Chemical transport in macropore-mesopore media under partially saturated conditions: Proceedings of the Symposium on Unsaturated Flow and Transport Modelling, 267-282.

Yeh, G. T., and Tamura, T., 1982, Geohydrochemical consideration in land disposal of low-level wastes: Nuclear Science and Engineering, p. 206-219.

Zimmerman, R. M., 1982, Conceptual design of field experiments for welded tuff rock-mechanics program: Sandia Nat. Labs., SAND81-1768, 26 p.

Zimmerman, R. M., 1983, First phase of small diameter heater experiments in tuff: Proc. 24th U.S. Symposium on Rock Mechanics, June 1983, Texas A&M Univ., p. 271-282.

Zimmerman, R. M., and Vollendorf, W. C., 1982, Geotechnical field measurements, G-tunnel, Nevada Test Site: Sandia Nat. Labs. SAND 81-1971, 29 p.

Zimmerman, R. M., Board, M. P., Hardin, E. L., and Voegele, M. D., 1984, Ambient temperature testing of the G-Tunnel heated block: Proc. 25th U.S. Symposium on Rock Mechanics, June 25-27, Northwestern Univ., p. 281-295.

DISTRIBUTION:

U.S. Government Printing Office
Receiving Branch (Attn: NRC Stock)
8610 Cherry Lane
Laurel, MD 20707

1512	K. L. Erickson	
1540	W. C. Luth	
1542	W. A. Olsson	
6310	T. O. Hunter	
	Attn:	F. W. Bingham
		L. W. Scully
		S. Sinnock
		J. R. Tillerson
6330	W. D. Weart	
	Attn:	D. R. Anderson
		A. R. Lappin
		M. L. Merritt
		L. D. Tyler
6400	A. W. Snyder	
6430	N. R. Ortiz	
	Attn:	L. O. Cropp
6431	R. M. Cranwell	
	R. L. Hunter	
	M. D. Siegel (30)	
3141	S. A. Landenberger (5)	
3151	W. L. Garner	
8024	M. A. Pound	

NRC FORM 335 (2-84) NRCM 1102, 3201, 3202

U.S. NUCLEAR REGULATORY COMMISSION

BIBLIOGRAPHIC DATA SHEET

INSTRUCTIONS ON THE REVERSE

1 REPORT NUMBER (Assigned by TIDC, add Vol No., if any)

NUREG/CR-4110
SAND84-2668

TLE AND SUBTITLE

Repository Site Data Report for Unsaturated Tuff, Yucca Mountain, Nevada

3 LEAVE BLANK

4 DATE REPORT COMPLETED

MONTH	YEAR
August	1985

5. AUTHOR(S)

Pei-Lin Tien, M. D. Siegel, C. D. Updegraff, K. K. Wahi, and R. V. Guzowski

6. DATE REPORT ISSUED

MONTH	YEAR
November	1985

7. PERFORMING ORGANIZATION NAME AND MAILING ADDRESS (Include Zip Code)

Sandia National Laboratories
Albuquerque, NM 87185
951 9245
Subcontractors:
Science Applications International Corporation
705 Marquette Avenue, NW
Suite 1200
Albuquerque, NM 87102
and
Remote Sensing System, Inc.
2101 San Pedro Boulevard, NE
Suite A
Albuquerque, NM 87110

8. PROJECT/TASK/WORK UNIT NUMBER

9. FIN OR GRANT NUMBER

A-1158

10 SPONSORING ORGANIZATION NAME AND MAILING ADDRESS (Include Zip Code)

Division of Waste Management
Office of Nuclear Material Safety and Safeguards
U.S. Nuclear Regulatory Commission
Washington, DC 20555

11a TYPE OF REPORT

Formal Report

b PERIOD COVERED (Inclusive dates)

3/84 - 9/85

12 SUPPLEMENTARY NOTES

13. ABSTRACT (200 words or less)

The U. S. Department of Energy is currently considering the thick sequences of unsaturated, fractured tuff at Yucca Mountain, on the southwestern boundary of the Nevada Test Site, as a possible candidate host rock for a nuclear-waste repository. Yucca Mountain is in one of the most arid areas in the United States. The site is within the south-central part of the Great Basin section of the Basin and Range physiographic province and is located near a number of silicic calderas of Tertiary age. Although localized zones of seismic activity are common throughout the province, and faults are present at Yucca Mountain, the site itself is basically aseismic.

No data are available on the composition of ground water in the unsaturated zone at Yucca Mountain. It has been suggested that the composition is bounded by the compositions of water from wells USW-H3, UE25p-1, J-13, and snow or rain. There are relatively few data available from Yucca Mountain on the moisture content and saturation, hydraulic conductivity, and characteristic curves of the unsaturated zone. The available literature on thermomechanical properties of tuff does not always distinguish between data from the saturated zone and data from the unsaturated zone. Geochemical, hydrologic, and thermomechanical data available on the unsaturated tuffs of Yucca Mountain are tabulated in this report. Where the data are very sparse, they have been supplemented by data from the saturated zone or from areas other than Yucca Mountain.

14 DOCUMENT ANALYSIS – a KEYWORDS/DESCRIPTORS

Tuff, Yucca Mountain, unsaturated zone, geologic setting, ground-water flow, geochemistry, thermomechanical properties

IDENTIFIERS/OPEN-ENDED TERMS

15 AVAILABILITY STATEMENT

Unlimited

16 SECURITY CLASSIFICATION

(This page) Unclassified

(This report) Unclassified

17 NUMBER OF PAGES

18 PRICE